Transductional Retargeting of Human Adenovirus Type 5 to αvβ6 Integrin for Cancer Gene Therapy

Lynda Coughlan

A thesis submitted for the degree of Doctor of Philosophy

July 2009

Centre for Tumour Biology/Molecular Oncology and Imaging
Barts and the London School of Medicine and Dentistry
Queen Mary University of London

Doras feasa fiafraí

Seanfhocal Gaeilge

Declaration

I hereby declare that the work presented in this thesis is original and is my own. Experiments were conducted jointly at the Centres for Tumour Biology/Molecular Oncology and Imaging, Barts and the London School of Medicine and Dentistry, Queen Mary University of London, and within the Gene and Viral Therapy Group at the Institut Català d'Oncologia, Barcelona, Spain. Work undertaken by others in contribution to this thesis has been clearly stated. All external sources have been properly acknowledged.

_____

Lynda Coughlan

Dedication

This thesis is dedicated to my mother who has been an inspiration to me in every way throughout my life, and for Dave, for a million and one reasons.

Acknowledgements

Firstly, I would like to thank my supervisors Gareth Thomas and Ian Hart for giving me a fantastic project to work on, for giving me unlimited scientific freedom and finances and finally, for graciously enduring my fiesty and often willful nature! To Ian, thank you for always keeping me on my toes, for testing me and pushing me to be better. Thank you for everything you say and everything you don't say. You have been, and I suspect always will be, the biggest influence on my scientific career. A special mention must go to John Marshall for the project idea and for his unending belief in αvβ6. Prof. Lemoine, thank you for turning a blind eye to my not-so-silent invasion of Molecular Oncology! A big thank you to Georges Vassaux for his constant support and words of encouragement and for his door being always open whenever I needed to discuss the ups and downs of my experiments/PhD/life etc. A massive, massive thank you to Iain McNeish for his generosity, for welcoming me wholeheartedly into his team and for always making me feel like I belonged there. Also, a special thank you to Pilar Martin-Duque for her positive energy, motivating words and encouragement.

Thank you to Sabari Vallath, Sarah Williams, Linda Hammond, Jennelle Francis, Jerome Burnet, Vipul Bhakta and Keyur Trivedi, for taking the time to teach me techniques and assisting me with experiments and/or analysis, without ever asking anything in return. To Pam and Katie for being there with a smile, always ready to listen. Thanks to Daniel Öberg, Simon Hughes, Amelie Morin and Karsten Friedrich for solving many of my cloning problems and for our many drunken discussions about molecular biology techniques! Thank you to all my friends in the lab who have kept me entertained and sane over the last three years! Firstly, Sabari for being trustworthy, dependable and always willing to help others, you have been a true friend to me. To Andrew, for brightening up every day in the lab, for always making me laugh and for our many wild nights out to de-stress!!! To Amelie, for how easy it is to be friends with you, for all our interesting conversations and adventures abroad! Karwan, for your dedication to science, thank you for all our laughs and diva moments! To the team McNeish girls, Maggie, AM, Sarah, Katrina and Carin, for all the tea and chats (or red wine and whinging!). For Katrina and Virginie, thank you for sharing your dreams and secrets with me, and for always listening to mine.

To Ramon Alemany, thank you for your intelligence, integrity and honesty as a scientist and, as a person. Thanks to Manel Cascalló, the man who knows everything about everything, thank you for your patience and perfectionist attitude to everything you do.

Thank you to you both and everyone in your team, Sònia Guedan, Juan José Rojas, Jordi Martínez-Quintanilla, Eduardo Laborda, Cristina Puig, Marta Giménez, Miguel Camacho, Raúl Gil, Francisca Alcayaga and Alena Gros, for your wonderful passion for science, your fiery latino lab meetings (!) and for welcoming me and showing me the real Barcelona. For mis chiquitas, Alena, Sonia, Marta and Cristina, gràcies de tot cor per rebrem amb els braços oberts. I will treasure my memories of summers at ICO as long as I live.

A very special thank you to Andy Baker, for your knowledge and for your infectious enthusiasm for science, for your time, energy and interest in my project and for inspiring me with many scientific ideas during our much valued email discussions.

To Dave, for giving me the freedom and support to follow my dreams, for keeping me sane and being the only reason to make me leave work and go home! To Ciara, my oldest and closest friend, for always being there and never changing. Thank you for understanding when I have missed some of the biggest events in your life, yet you still consider me to be a valuable friend. And finally, to my parents and my family, for always supporting me (often financially!), for understanding my never ending student status and for accepting a very detached and forgetful Lynda in the last few months! And for my mother who has always shown us that education can be fun, thank you for teaching me, inspiring me and making me believe that I can do anything I put my mind to.

Abbreviations

5' FOA	Fluoro-orotic acid
Ad5	Human Adenovirus Type 5
ALT	Alanine transaminase
Amp	Ampicillin
AST	Aspartate transaminase
BAC	Bacterial artificial chromosome
BCA	Bicinchoninic acid
BCC	Basal cell carcinoma
BSA	Bovine serum albumin
C4BP	Complement 4-binding protein
CAR	Coxsackie and Adenovirus Receptor
CAV-1/2	Canine Adenovirus -1/2
CAV9	Coxsackievirus A9
Chl	Chloramphenicol
cDNA	Complementary deoxyribonucleic acid
CPE	Cytopathic effect
CRAd	Conditionally replicating adenovirus
DAPI	4',6-diamidino-2-phenylindole
DMEM	Dulbecco's modification of Eagle's medium
DMSO	Dimethyl sulphoxide
DNA	Deoxyribonucleic acid
DTT	1,4-Dithioreitol
EC_{50}	Effective concentration (50% effect)
ECM	Extracellular Matrix
EDTA	Ethylene diamino tetraacetic acid
EGFP	Enhanced green fluorescent protein
EMT	Epithelial to mesenchymal transition
FACS	Fluorescence activated cell sorting
FITC	Fluorescein isothiocyanate
FIX	Factor IX (Human)
FMDV	Foot and Mouth Disease Virus
FVII	Factor VII (Human)
FX	Factor X (Human)
GM-CSF	Granulocyte macrophage-colony stimulating factor (Human)
H&E	Haematoxylin and Eosin
HIS	Histidine
HIV	Human Immunodeficiency Virus
hNIS	Sodium iodide symporter (Human)
HNSCC	Head and neck squamous cell carcinoma
HPLC	High performance liquid chromatography
HSPG	Heparan sulphate proteoglycan
IC_{50}	Inhibitory concentration (50% effect)

IFN	Interferon
IgG	Immunoglobulin G
IL	Interleukin
IPTG	Isopropyl thiogalactopyranoside
Kan	Kanamycin
KC	Kupffer cell
KGM	Keratinocyte growth medium
LAP	Latency associated peptide
LPS	Lipopolysaccharide
LRP	Low density lipoprotein related receptor
MAPK	Mitogen activated protein kinase
MCS	Multi cloning site
MIP	Macrophage inflammatory protein
MMP	Matrix metalloprotease
MTT	3-2,5-diphenyltetrazolium bromide
Ni-NTA	Nickel-nitrilotriacetic acid
OD	Optical density
OSCC	Oral squamous cell carcinoma
PBS	Phosphate buffered saline
PCR	Polymerase chain reaction
PKR	Protein kinase receptor (dsRNA)
qPCR	Quantitative polymerase chain reaction
RANTES	Regulated upon activation, normal T cell expressed and secreted
RGD	Arginine-glycine-aspartate
RGDLXXL	Arginine-glycine-aspartate-leucine-X-X-leucine
RNA	Ribonucleic acid
RPMI	Roswell Park Memorial Institute
SDS-PAGE	Sodium dodecyl sulphate polyacrylamide gel electrophoresis
SOEing	Splicing by overlap extension
SR-A	Scavenging receptor A
TAYT	Threonine-alanine-tyrosine-threonine
TCID	Tissue culture infectious dose
TGF-β	Transforming growth factor β
TLR	Toll like receptor
TNF	Tumour necrosis factor
uPA	Urokinase plasminogen activator
URA3	Orotidine-5’-phosphate (OMP) decarboxylase
UV	Ultraviolet
VP1	Viral protein
YAC	Yeast artificial chromosome
ZO-1	Zona Occludens-1

Abstract

A key impediment to successful cancer therapy with adenoviral vectors is the inefficient transduction of malignant tissue *in vivo*. Compounding this problem is the lack of cancer-specific targets, coupled with a shortage of corresponding high efficiency ligands, permitting selective retargeting. The epithelial specific integrin αvβ6 represents an attractive target for directed therapy since generally it is not expressed on normal epithelium, but is upregulated in numerous carcinomas where it plays a role in tumour progression. We previously have characterised a high affinity, αvβ6-selective peptide (A20FMDV2), derived from VP1 of Foot and Mouth Disease Virus. In an attempt to subvert the tropism of Ad5 to αvβ6, A20FMDV2 was incorporated genetically into the HI loop of the Ad5 fibre protein to generate Ad5-EGFP$_{A20}$. Furthermore, the native CAR-binding and putative FIX/C4BP-binding capacity of Ad5-EGFP$_{A20}$ was ablated to generate Ad5-477*dl*TAYT$_{A20}$. *In vitro*, these A20-retargeted vectors displayed up to 50-fold increases in CAR-independent transduction, and up to 480-fold increased cytotoxicity on a panel of αvβ6-positive human carcinoma lines compared with Ad5-EGFP$_{WT}$.

In vivo, both Ad5-EGFP$_{A20}$ and Ad5-477*dl*TAYT$_{A20}$ improved tumour targeting (~2-fold/3-fold) following systemic delivery in immunodeficient mice, when compared with Ad5-EGFP$_{WT}$. Furthermore, ~5-fold fewer Ad5-EGFP$_{A20}$/Ad5-477*dl*TAYT$_{A20}$ genomes were detected in the liver, which correlated with reduced serum transaminase levels and minimal E1A expression. Warfarin pre-treatment, to deplete coagulation factors, did not improve tumour uptake significantly with either virus, but did further reduce liver sequestration and hepatic toxicity. The unexpected reduction in liver tropism and toxicity we observed was supported by similar results obtained in immunocompetent mice. Furthermore, in immunocompetent mice, Ad5-EGFP$_{WT}$ induced dramatic elevations in serum cytokines/chemokines in addition to inducing acute thrombocytopenia. These effects were attenuated substantially in Ad5-EGFP$_{A20}$/Ad5-477*dl*TAYT$_{A20}$ treated cohorts. In summary, we have found that *in vivo* retargeting Ad5 to αvβ6 in a murine model results in improved tumour delivery, limited hepatotropism/toxicity and a reduced induction of anti-viral innate immune responses.

TABLE OF CONTENTS

LIST OF TABLES

LIST OF FIGURES

1.INTRODUCTION

2. MATERIALS AND METHODS

3. RESULTS

4. RESULTS

5.RESULTS

6.RESULTS

CHAPTER 1. Introduction

*Section.*1.1 Introduction

Cancer is the second leading cause of death worldwide, and is estimated at approximately ~22% of all deaths in the UK (Bray *et al.*, 2002). The global burden of cancer has remained largely unchanged for the past three decades despite significant advances in diagnosis, reductive surgery and therapeutic intervention. Furthermore, conventional chemo- and radiotherapies remain ineffective in treating tumour metastases, fail to prolong survival following late diagnosis, and are associated with adverse side effects. Therefore, it is clear that innovative approaches to treatment are required. Virotherapy or viral gene therapy of cancer represents such a strategy.

Viruses are obligate intracellular parasites, which have evolved to behave as biological delivery vehicles, capable of self-amplification and lateral propagation. The potential for exploiting these intrinsic properties make viruses a natural choice of vector for gene therapy applications, including the therapy of cancer. In recent years, increased knowledge of the pathogenesis of cancer, and the molecular networks underlying malignant transformation, has prompted the development of rationally designed therapeutics, accelerating the manipulation of viruses for therapeutic effect.

The exploitation of viruses for the treatment of cancer is not a novel concept, in fact, several reports of spontaneous tumour regression during/following an acute viral infection, have been documented over the past century (Bierman *et al.*, 1953; Bluming & Ziegler, 1971; Pasquinucci, 1971; Pelner *et al.*, 1958; Taqi *et al.*, 1981; Taylor, 1953; Zygiert, 1971). These observations led to the initiation of a clinical trial at the National Cancer Institute during the 1950s, using a Human Adenovirus Type-5 (Ad5) for the treatment of cancer (Huebner *et al.*, 1956). Although the trial was largely unsuccessful, with tumour progression following initially promising regression, it did serve to highlight the relative safety, and lack of significant toxicity associated with Ad5 *in vivo*. However, the use of Ad5 in clinical trials has been associated previously with adverse effects and severe outcome. In 1998, the field suffered substantial negative publicity following the death of 18 year old Jesse Gelsinger, a patient enrolled in a trial using adenovirus to deliver a corrective gene for an ornithine transcarbamylase (OTC) deficiency. His death was attributed to a massive inflammatory response; a cytokine cascade induced by widespread systemic dissemination of the virus, which resulted in respiratory distress, coagulopathy and multi organ failure (Raper *et al.*, 2003). Consequently, this tragic event has highlighted the importance of designing vectors which display reduced immunogenicity and toxicity *in vivo*.

The ultimate goal of virotherapy is to generate a non-toxic, self-localising and self-amplifying agent, which is capable of selectively eradicating malignant tissue. The modification of adenoviral tropism determinants represents a strategy for achieving selective delivery. Modifications to structural proteins aim to confer a new or expanded tropism, permitting vectors to be customised for a broad range of targeting applications. Native receptor detargeting when used in combination with retargeting strategies, can restrict delivery, and minimise non-specific sequestration at off target locations. However, it is becoming increasingly clear that achieving this is not as simple as originally envisaged, and several major challenges remain to be addressed before virotherapy can fulfil its promise. One such challenge is the distinct lack of cancer specific markers which would be suitable for selective retargeting of Ad5 to tumours *in vivo*. Compounding this is the lack of high efficiency targeting ligands capable of interacting with those identified markers to facilitate high efficiency retargeting to tumours, and to disseminated metastases.

The epithelial specific integrin, αvβ6, is not normally expressed on normal adult epithelia but is upregulated significantly during epithelial remodelling events, which include wound healing, embryogenesis and carcinogenesis (Breuss *et al.*, 1995). It is overexpressed in a broad range of carcinomas, and has been independently identified as a prognostic indicator in breast, lung, ovarian, cervical and colorectal carcinomas (Ahmed *et al.*, 2002b; Bates *et al.*, 2005; Elayadi *et al.*, 2007; Hazelbag *et al.*, 2007). Additionally, work in our laboratory has identified that >90% oral squamous cell (OSCC) carcinomas express αvβ6 to high levels, and that its expression is associated with invasion and metastasis *in vivo* (Nystrom *et al.*, 2006; Thomas *et al.*, 2001a; Thomas *et al.*, 2001b; Van Aarsen *et al.*, 2008). Therefore, the restricted expression profile of αvβ6 *in vivo*, coupled with its cell surface localisation, make it a very accessible and attractive cancer-specific target. Moreover, we already possess a suitable high-affinity targeting ligand capable of selective delivery to αvβ6, which has been characterised extensively both *in vitro* and *in vivo*. This ligand was initially identified by extensive functional analysis of a panel of linear peptides, which were rationally selected from known αvβ6 ligands (DiCara *et al.*, 2007). A candidate peptide, A20FMDV2, derived from Foot and Mouth Disease Virus, was chosen for its very high affinity and specificity for αvβ6. The resolution of the crystal structure of the Ad5 knob domain by X-ray crystallography identified the HI loop region as being suitable for heterologous peptide incorporation (Xia *et al.*, 1994). Thus, the focus of this study was to genetically incorporate the targeting ligand, A20FMDV2, into the HI loop of the Ad5 fibre in an attempt to redirect the tropism of Ad5 to αvβ6.

Section.1.2 Molecular Genetics of Adenoviruses

Adenoviruses (Ad) are dsDNA viruses which were first isolated from human adenoid lymphoid tissue in 1953 (Hilleman & Werner, 1954; Rowe *et al.*, 1953). Clinical symptoms of adenoviral infection include acute respiratory infection, epidemic conjunctivitis and infantile gastroenteritis (Grandien *et al.*, 1987; Louie *et al.*, 2008; Yolken *et al.*, 1982). The family *Adenoviridae* consists of five genera, most importantly the genus *Mastadenovirus* and genus *Aviadenovirus*, which infect mammals and birds respectively. There are 52 different serotypes of human adenoviruses, divided into subgroups A-G, which can be distinguished on the basis of their serological cross-reactivity, haemagglutinating properties and phylogenetic sequence similarity (Crawford-Miksza & Schnurr, 1996; Fauquet *et al.*, 2005; Rosen, 1960). Additionally, the grouping correlates with their oncogenic potential and ability to form tumours in rodents, a characteristic which is associated with abortive infection. Subgroup C contains serotypes Ad2 and Ad5, which have been studied extensively, and have no oncogenic potential in humans. Therefore, these serotypes are used widely in experimental gene therapy applications.

Section.1.2.1 Adenoviral Structure

Adenoviruses are non-enveloped, icosahedral virions which contain a linear, monopartite, dsDNA genome approximately 36kbp in size (*Figure.*1.1). Adenovirus contains at least 13 structural proteins, assigned with a numbering order from II-X, including; IIIa, Mu, TP, IVa2, a protease which is putatively associated with interior of the icosahedron vertices, and L1-52K, which has been proposed to act as a scaffolding protein during viral assembly (Christensen *et al.*, 2008; Hasson *et al.*, 1992; Hasson *et al.*, 1989; Russell, 2009; Silvestry *et al.*, 2009). A nucleoprotein core complex surrounds the genome. This complex consists of a core-penton bridging protein (V), histone-like protein (VII), Mu protein and a Terminal Protein (TP), which is covalently attached to the 5' region of the genome (Rekosh *et al.*, 1977; Robinson *et al.*, 1973). Together, adenoviral structural proteins are responsible for stabilisation of the genome and the encapsidation of the nucleoprotein core complex.

The icosahedral capsid structure is composed of seven polypeptides; the trimeric hexon (II), which is complexed with three minor hexon polyproteins (VI, VIII and IX) which provide stabilisation, the penton (III) and penton associated protein (IIIa) which bridge the hexon-penton, and the receptor binding fibre (IV) protein (Everitt *et al.*, 1975; Everitt *et al.*, 1973). The fibre protein (IV) is composed of three domains; the tail at the

N-terminus, the rod-like shaft and the globular knob domain at the C-terminus. The fibre shaft is comprised of a 15 amino acid polylysine motif (KKTK), repeated 22 times in Ad5 (Chroboczek *et al.*, 1995; van Raaij *et al.*, 1999). The fibre exists as a glycosylated homotrimer, non-covalently complexed to the pentameric penton base protein (III) at the N-terminus (Mautner & Pereira, 1971). This complex is also known as the penton capsomere. These trimeric complexes are embedded at the 12 vertices of the icosahedron structure, extending as protrusions on the external viral surface (van Oostrum & Burnett, 1985; Xia *et al.*, 1994).

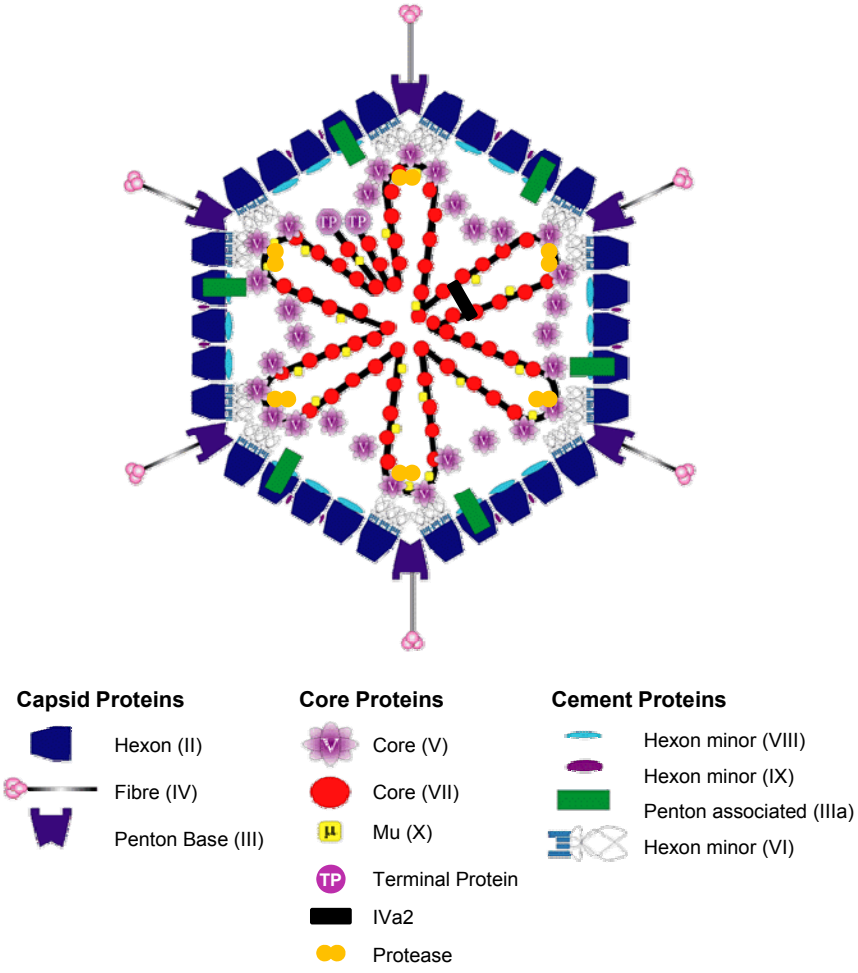

***Figure.*1.1 Adenovirus Structure.** Schematic representation of the major and minor structural proteins of adenovirus and the nucleoprotein core with terminal protein (TP) covalently attached at each end of the dsDNA genome. Figure adapted from (Russell, 2000; 2009).

*Section.*1.2.2 Adenoviral Entry

The classical two-step Ad5 entry pathway in epithelial cells is initiated by a docking process in which the distal knob of the fibre binds to target cells via the 46kDa, transmembrane Coxsackie and Adenovirus Receptor, CAR (Bergelson *et al.*, 1997; Bergelson *et al.*, 1998; Kirby *et al.*, 2000; Roelvink *et al.*, 1998; Roelvink *et al.*, 1999; Santis *et al.*, 1999; Tomko *et al.*, 1997). CAR, a member of the immunoglobulin

superfamily has two extracellular Ig-like domains (D1 and D2) and functions as a tight junction protein forming homodimeric adhesions between polarised epithelial cells and the cardiac intercalated disc (Cohen *et al.*, 2001; Shaw *et al.*, 2004; van Raaij *et al.*, 2000). Additionally, in associaton with tight junction protein Zona Occludens (ZO-1), it can function as a barrier to the paracellular movement of macromolecules and ions (Cohen *et al.*, 2001). Importantly, the localisation of CAR means that it is not initially accessible as a receptor for viral entry, unless membrane integrity is compromised. Therefore, it may seem paradoxical for a virus to utilise an occluded receptor for primary attachment. However, Ad5 appears to have exploited the location of CAR to facilitate maximal spread, as progeny virions have been shown to be released from the basolateral surface of infected cells (Cohen *et al.*, 2001; Walters *et al.*, 2002). This phenomenon and its role in viral release and spread, is discussed further detail in *Section*.1.2.6.

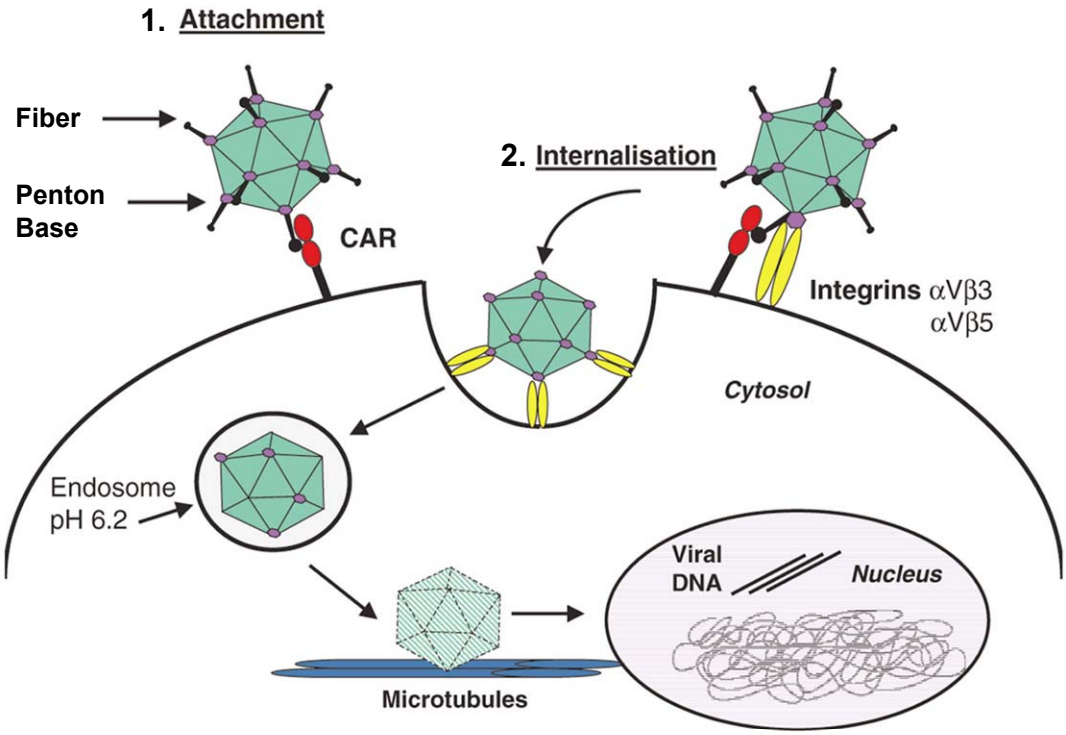

***Figure*.1.2 Classical Two-Step Entry Pathway of Adenovirus. (1)** Adenovirus attachment is mediated by the distal knob domain of the fibre. The flexible fibre binds to the 46kDa transmembrane protein, the Coxsackie and Adenovirus Receptor, CAR. **(2)** The RGD motif in the penton base of the Ad particle triggers internalisation via αvβ3/αvβ5 integrins. Partial disassembly of the capsid is induced by acidification of the endosome following clathrin-mediated endocytosis. Endosomal escape is modulated through the action of protein VI, after which the nucleocapsid core is translocated to the nucleus along the microtubule network. Further capsid dissociation permits the viral DNA to enter the nucleus for subsequent transcription and replication. Figure adapted from (Horwood *et al.*, 2002).

Fibre-CAR binding is followed by the interaction of an Arg-Gly-Asp (RGD) motif in the penton base to αvβ3/αvβ5 integrins, which subsequently triggers viral internalisation (Wickham *et al.*, 1993). It is thought that the Ad5 penton-integrin interaction results in integrin clustering which activates signalling pathways, such as phosphoinositide-3-OH kinase (PI3K), p38 MAPK and ERK1/2, inducing downstream effects resulting in the polymerisation and reorganisation of actin filaments (Bhat & Fan, 2002; Li *et al.*, 1998a; Li *et al.*, 1998b; Shayakhmetov *et al.*, 2005a; Suomalainen *et al.*, 2001; Tibbles *et al.*, 2002). Recent data have also shown that Ad5 binding to CAR leads to the activation of ERK1/2 (p44/42 MAPK) which promotes the dimerisation and clustering of CAR, in addition to increasing the activation status of -β1 and -β3 integrins (Farmer *et al.*, 2009). Viral internalisation is mediated via clathrin-mediated endocytosis (Meier *et al.*, 2002; Wang *et al.*, 1998), followed by partial capsid disassembly upon acidification of the endosome (Greber *et al.*, 1993). Endosomal escape is modulated by the lytic action of protein VI, after which the nucleocapsid is translocated to the perinuclear envelope along the microtubule network (Dales & Chardonnet, 1973; Suomalainen *et al.*, 1999; Wiethoff *et al.*, 2005). Transport to the nuclear pore complex involves the microtubule-dependent motor, cytoplasmic dynein which permits Ad attachment to microtubules (Kelkar *et al.*, 2004; Leopold *et al.*, 2000). The capsid undergoes its final dissociation event at the nuclear pore complex (Greber *et al.*, 1997), allowing the core DNA to extrude into the nucleus for subsequent transcription and replication (*Figure.*1.2).

However, it is now clear that the process of infection by Ad5 is more complex than previously assumed, and it involves various receptors and co-receptors other than CAR and αvβ3/αvβ5 integrins. Heparan sulphate proteoglycans (HSPGs) have been shown to permit binding of Ad5 in the absence of CAR in A549 and CHO-K1 cells (Dechecchi *et al.*, 2001; Dechecchi *et al.*, 2000). The KKTK motif of the fibre shaft was once thought to be responsible for promoting infection through HSPGs (Dechecchi *et al.*, 2000; Smith *et al.*, 2003b). However, it is now widely believed that the KKTK motif serves only to confer structural flexibility to the fibre (Nicklin *et al.*, 2005; van Raaij *et al.*, 1999). Alternatively, vascular cell adhesion molecule 1 (VCAM-1) or MHC class I have also been proposed to facilitate low affinity Ad5 interactions, although evidence which supports the latter interaction has been challenged (Chu *et al.*, 2001; Davison *et al.*, 1999; Hong *et al.*, 1997; McDonald *et al.*, 1999). Furthermore, additional integrins, αvβ1, α3β1, α5β1 and αMβ2 have also been shown to permit the internalisation of adenoviruses (Davison *et al.*, 1997; Davison *et al.*, 2001; Huang *et al.*, 1996; Li *et al.*, 2001; Salone *et al.*, 2003).

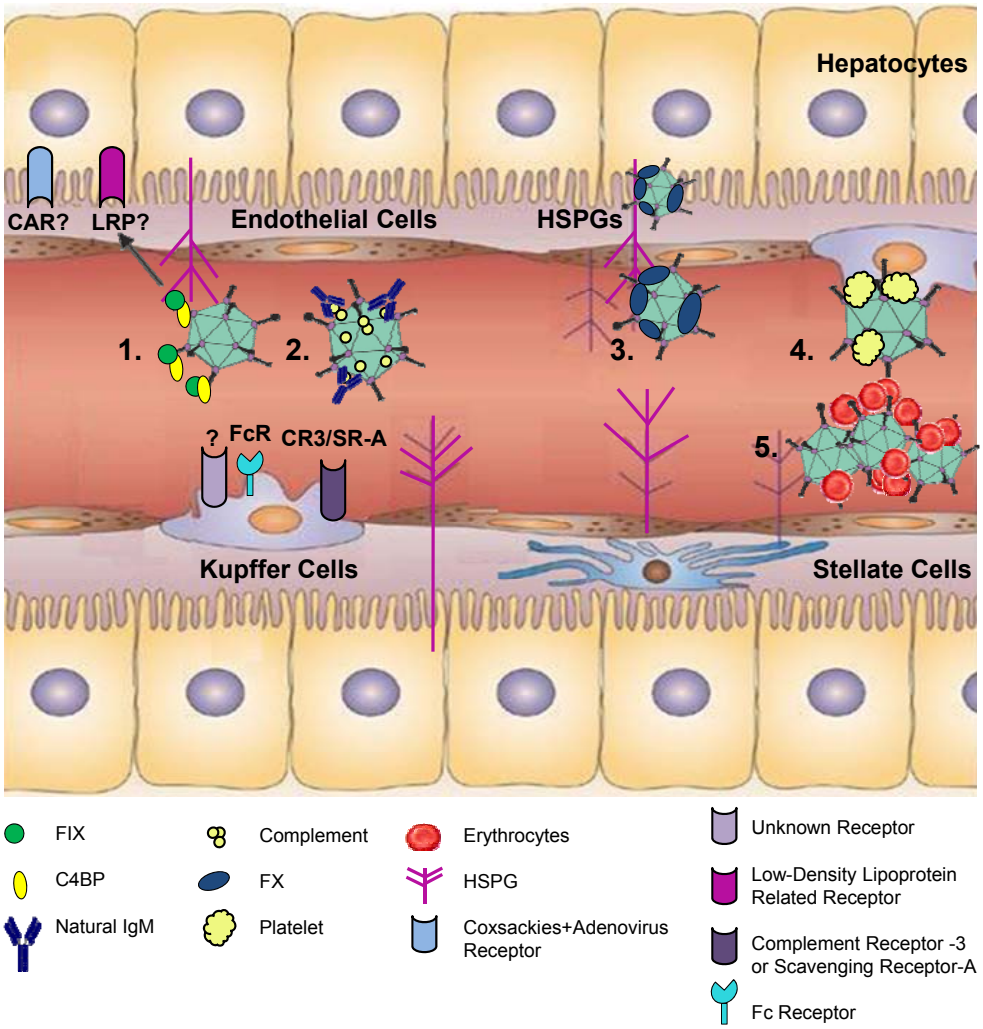

***Figure.*1.3 Ad5 Interactions with Blood Components *In Vivo*. (1)** FIX/C4BP binding to the fibre knob mediates hepatocyte entry via HSPGs or LRP. Additionally, FIX/C4BP binding to the fiber directs Kupffer cell uptake by an unknown mechanism (Shayakhmetov *et al*., 2005b). **(2)** Opsonisation of Ad5 with natural IgM and/or complement directs Kupffer cell uptake through complement receptor-3 (CR3), Fc Receptor or through scavenging receptor SR-A (Haisma *et al*., 2009; Xu *et al*., 2008). **(3)** FX binding to Ad5 hexon promotes hepatocyte entry through HSPGs (Waddington *et al*., 2008). **(4)** Adenovirus binding to platelets enhances uptake by Kupffer cells (Stone *et al*., 2007b). **(5)** Ad5 binds to CAR on erythrocytes causing trapping of virus in the circulation. Figure adapted from (Prudencio *et al*., 2006).

More recently, a number of "bridging interactions" have been identified which have particular relevance *in vivo*, especially following systemic delivery of Ad5 in mice (*Figure*.1.3). It has now been shown by several groups that direct interactions between the Ad5 capsid and vitamin K-dependent coagulation factors, including FX, FIX, FVII, Protein C, in addition to Complement 4-Binding protein (C4BP), can modulate viral entry through HSPGs or low-density lipoprotein receptor-related protein, LRP (Alba *et al*., 2009; Kalyuzhniy *et al*., 2008; Shayakhmetov *et al*., 2005b; Vigant *et al*., 2008; Waddington *et al*., 2008; Waddington *et al*., 2007). These interactions play a critical role in directing off-target hepatocyte transduction *in vivo*. Additionally, coagulation

factor "bridging" has been shown to be involved in the enhanced infection of various tumour cells both *in vitro* and *in vivo* (Coughlan *et al.*, 2009; Gimenez-Alejandre *et al.*, 2008; Liu *et al.*, 2009; Parker *et al.*, 2007; Parker *et al.*, 2006; Shayakhmetov *et al.*, 2005b). However, Ad5 also has been shown to interact with various other components within the circulation, such as natural IgM and complement, platelets and erythrocytes. Opsonisation of Ad5 by IgM and complement, or binding to platelets to promote the formation of Ad5-platelet-leukocyte aggregates, are mechanisms proposed to play a role in Kupffer cell scavenging (Stone *et al.*, 2007b; Xu *et al.*, 2008). Moreover, Ad5 interactions with CAR-expressing erythrocytes in mice have been shown to preclude efficient tumour transduction *in vivo* by trapping virus in the circulation (Carlisle *et al.*, 2009).

*Section.*1.2.3 Adenoviral Genome Organisation

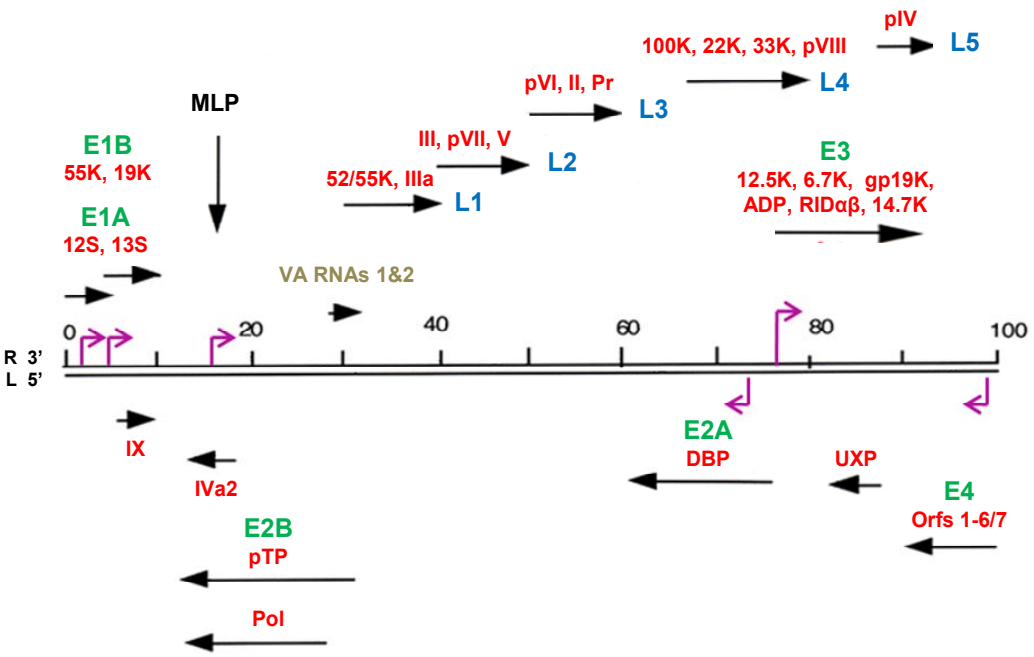

***Figure.*1.4 Overview of the Transcription Profile of Ad5.** Early gene transcripts are shown in green, late transcripts in blue and gene products in red. The Virus Associated (VA) RNAs are in brown. Black arrows indicate the direction of transcription, purple arrows indicate promoter regions. Rightward (R) and Leftward (L) strands are transcribed by 5'-3' directional reading. The genes have been mapped by superimposing an arbitrary scale of 100 map units. Abbreviations are as follows; MLP = Major Late Promoter, Pr = Protease (adenain), ADP = Adenovirus Death Protein, RID = Receptor Internalisation and Destruction, ORF = Open Reading Frame, UXP = U exon protein (Tollefson *et al.*, 2007), DBP = DNA Binding Protein, TP = Terminal Protein and Pol = Polymerase. All gene products listed numerically can be found in *Fig.*1.1. Figure adapted from (Russell, 2000; Wold & Gooding, 1991).

The Adenoviral genome is complex and contains terminally redundant sequences with inverted terminal repeats (ITR), each with an identical origin of replication and a

terminal protein (TP) covalently attached at the 5' end (Rekosh *et al.*, 1977; Robinson *et al.*, 1973). A terminal, cis-acting packaging signal, required for successful encapsidation of the Ad5 genome, is situated at the left end of the viral DNA (Grable & Hearing, 1992). Viral genome transcription is defined by two main transcription events, Early and Late. Viral mRNAs are transcribed by a cellular RNA polymerase II from five early transcription units (E1-E4), two delayed early units (IX and IVa2) and one late (L1-5) transcription unit (*Figure*.1.4). The viral genome also contains two virus-associated genes (VA) which are transcribed by host RNA polymerase III. Adenoviral gene transcription can give rise to differential mRNA transcripts through the use of alternate polyadenylation sites or by the generation of multiple splice variants (Berget *et al.*, 1977; Berget & Sharp, 1977; Chow *et al.*, 1977).

Section.1.2.4 Activation of Early Transcription

Early proteins have a range of functions which include; subversion of the host cell cycle in order to facilitate optimal conditions for viral replication (E1A, E1B and E4 region), the synthesis of viral gene products essential for replication (E2 region) and immune evasion from innate anti-viral responses (E3 region). Prior to, and independently of viral replication, the Immediate Early (IE) E1A mRNA transcripts, 12S and 13S, are spliced and exported to the cytoplasm where they are translated and their corresponding proteins phosphorylated extensively (Mal *et al.*, 1996; Whalen *et al.*, 1997). These are then transported back to the nucleus where they are required as trans-acting transcriptional activators of downstream Early (E) genes, and as regulators of cell cycle (Berk, 1986a; b; Berk *et al.*, 1979; Jones & Shenk, 1979).

The conserved regions of E1A proteins (CR1-3) can activate transcription through their ability to interact with a range of cellular transcription factors and regulatory proteins (Branton & Rowe, 1985; Harlow *et al.*, 1986; Yee & Branton, 1985). However, in addition to these functions, E1A proteins promote cell cycle progression, creating a cellular environment conducive for viral replication. The CR1 and CR2 domains within E1A (12S and 13S) can bind directly to members of the cellular retinoblastoma (pRb) tumour suppressor family (ie. pRb, p107 and p130) preventing them from forming complexes with the transcriptional activator, E2F (Bandara & La Thangue, 1991; Whyte *et al.*, 1989). Dissociated, or free E2F, activates several genes associated with cell cycle progression.

Innate cellular tumour suppressor mechanisms (p53) respond to the unscheduled induction of proliferation effected by E1A, by activating pro-apoptotic pathways

(Debbas & White, 1993; Lowe & Ruley, 1993). The virus therefore employs E1B proteins, E1B-55kDa and E1B-19kDa, to act synergistically with E1A and counteract the accumulation of pro-apoptotic p53. The adenoviral E1B-55kDa protein, in conjunction with E4-Orf6 and cellular ubiquitination proteins, antagonises the ability of p53 to induce apoptosis by inducing its degradation (Harada *et al.*, 2002; Querido *et al.*, 2001a; Querido *et al.*, 1997; Querido *et al.*, 2001b). E1B-19kDa functions similarly to cellular anti-apoptotic Bcl-2, binding both Bax and Bak and inhibiting the induction of apoptosis (Rao *et al.*, 1992; White *et al.*, 1991; White *et al.*, 1992).

*Section.*1.2.5 Adenoviral Replication and Transition to Late Gene Transcription

As is the case with most DNA viruses, adenoviral replication takes place in the nucleus. Both strands of DNA, rightward (R) and leftward (L), are transcribed by 5'-3' directional reading. The E2 proteins which facilitate viral replication include; the terminal protein (TP), a precursor of which primes synthesis of the viral genome, the DNA polymerase, which possesses an intrinsic 3'-5' exonuclease activity, and finally the DNA-binding protein (DBP), which permits elongation. These proteins act in concert with various cellular factors, such as nuclear factors NFI/NFIII which provide stabilisation, enhancing viral DNA replication, and NFII which facilitates successful DNA elongation (Bosher *et al.*, 1990; Chen *et al.*, 1990; Mul *et al.*, 1990; Nagata *et al.*, 1983). The E4 open reading frame (ORF) encodes two proteins, Orf3 and Orf6, which have also been shown to play a role in viral replication. These proteins use complementary functions to interfere with various facets of the cellular DNA repair response, including inhibition of concatemer formation and ubiqitination of the dsDNA break repair complex, Mre11 (Evans & Hearing, 2003; 2005; Stracker *et al.*, 2002).

Once critical levels of E2 gene products accumulate, genome replication is initiated in two stages, displacement replication and single strand replication, also called Type I and Type II replication, respectively (Lechner & Kelly, 1977). Displacement replication occurs when synthesis is initiated at the ITR of either strand of DNA. Synthesis proceeds continuously to the end of the genome without lagging strand synthesis, displacing the complementary single strand (*Figure*.1.5). This results in a duplex of nascent dsDNA, plus the single displaced strand which is capable of panhandle formation, as a result of its self-complementary termini. In single strand replication, this panhandle structure is again primed by the terminal protein and replication is reinitiated, resulting in the formation of another duplex DNA genome (Lechner & Kelly, 1977).

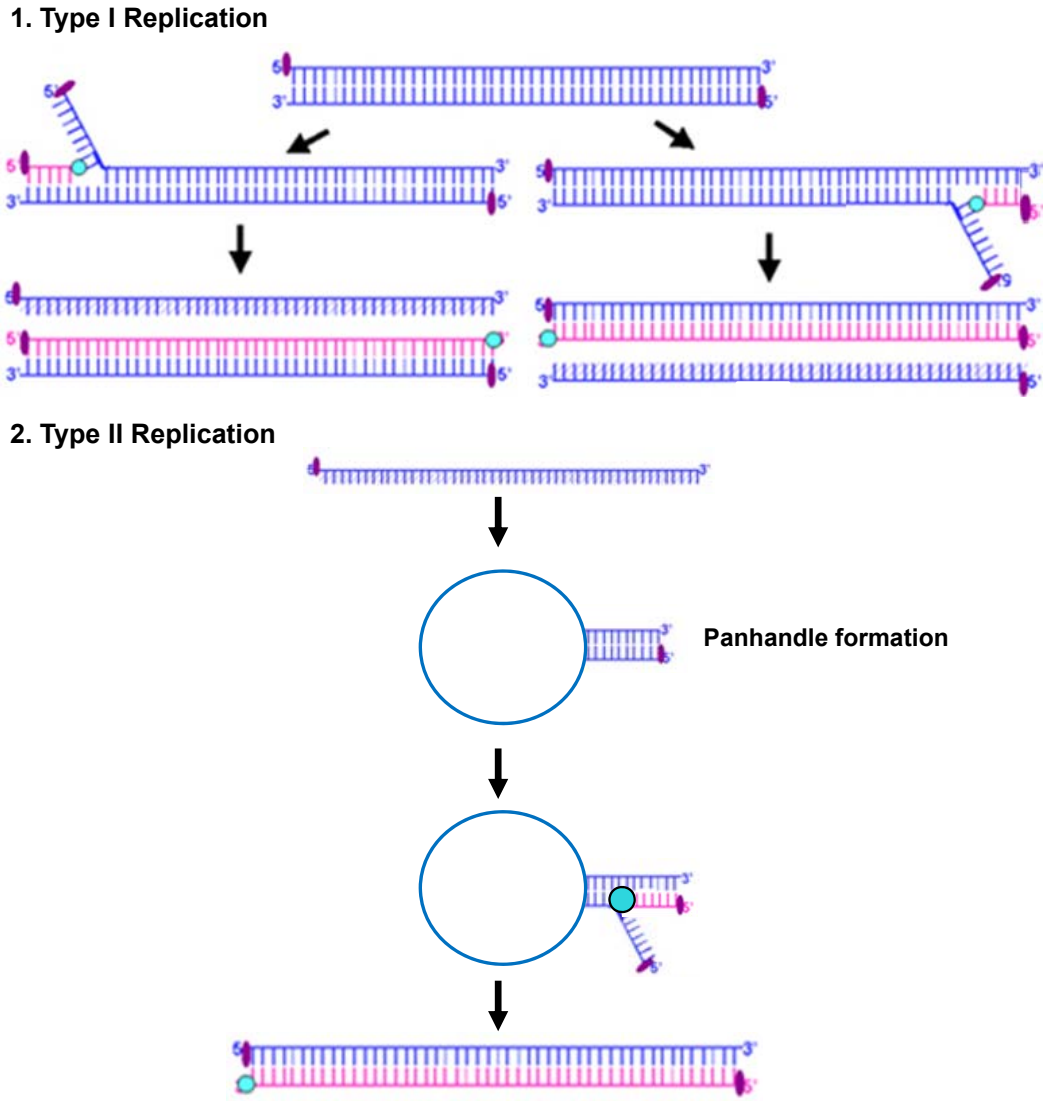

***Figure*.1.5 Overview of the Adenoviral Replication Strategy (1)** Type I replication, or displacement replication, is initiated at the ITR of the dsDNA genome. Replication is primed by the terminal protein and is continuous without lagging strand synthesis. In this process a DNA duplex is created from the template of one strand of DNA, whereas the remaining strand of DNA is displaced. **(2)** Type II replication is the strategy of replication used for the synthesis of duplex DNA from the displaced single strand. Single stranded DNA is circularised via the complementary ITR, resulting in a panhandle structure. This panhandle structure can once again be primed for replication by the terminal protein, resulting in duplex DNA. (Figure is adapted from www.pathmicro.med.sc.edu/mhunt/dna1.htm).

Concomitant with the onset of DNA replication, Late phase expression from the major late promoter (MLP) is activated by E1A, and transcripts are processed by differential poly (A) utilisation (L1-5), and post-transcriptional splicing to generate at least 18 mRNAs. Host cell transcription factors, MAZ and Sp1, in concert with E1A, can activate transcription from the MLP, independently of viral replication (Parks & Shenk, 1997). Additionally, a product of the delayed early transcription unit, IVa2, has been shown to contribute to the induction of expression from the MLP (Lutz & Kedinger, 1996). Following the processing of late viral mRNAs, an E1B-55kDa/E4-Orf6 complex is

responsible for their nuclear export and cytoplasmic accumulation, where they are translated into the proteins required for assembly of progeny virions (Babiss *et al.*, 1985; Sarnow *et al.*, 1984). This complex also prevents the translocation of host mRNAs to the cytoplasm, in addition to targeting host proteins, p53 and Mre11, for ubiqitin-mediated degradation (Cheng *et al.*, 2007; Evans & Hearing, 2005).

The accumulation of dsRNA within adenovirally infected cells triggers the induction of an antiviral state (Maran & Mathews, 1988). This IFN-induced response involves the activation of the Protein Kinase R (PKR) pathway, which is stimulated by the presence of dsRNA in the cytoplasm. Upon its activation, PKR autophosphorylates and then subsequently phosphorylates eukaryotic initiation factor 2α (eIF2α), inactivating it and resulting in the inhibition of cellular mRNA translation. The preferential and sustained translation of viral mRNAs can overcome this shutdown in protein synthesis by several means. Firstly, the activation of PKR is counteracted by the virally encoded VA genes, which bind PKR directly, regulating its autophosphorylation and function (Katze *et al.*, 1987). Additionally, the inactivation of another cellular initiation factor (eIF-4F) late after infection is exploited to ensure the preferential translation of viral mRNAs. This factor, eIF-4F, possesses an inherent helicase activity which is required for host mRNA translation. This function becomes redundant in the translation of viral mRNAs due to the presence of the identical 200nt tripartite leader sequence at their 5' end, which permits ribosomal shunting from the 5' cap to the start codon, without the requirement for helicase activity. Additionally, the L4-100K protein is also responsible for blocking the translation of host mRNAs and ensuring the preferential translation of viral mRNAs which contain the tri-partite leader sequence (Cuesta *et al.*, 2000; 2004; Hayes *et al.*, 1990; Xi *et al.*, 2004). Thus, efficient viral translation is successfully achieved through the co-ordinated action of these multiple viral gene products.

Section.1.2.6 Virion Assembly and Release

The late genes predominantly encode structural and scaffolding proteins, and virion assembly is initiated by the formation of an empty capsid, after which a viral DNA molecule enters mediated by the cis-acting packaging sequence (Hearing *et al.*, 1987; Sundquist *et al.*, 1973). Monomeric hexon proteins polymerise into trimeric capsomers, assisted by the L4-100K chaperone protein (Cepko & Sharp, 1982; Hong *et al.*, 2005). Penton-fibre capsomers are joined following their independent assembly (Horwitz *et al.*, 1969). Structural proteins accumulate in the nucleus where they are incorporated into the virus capsid structure. Encapsidation of the genome is polar and is facilitated by the L1-52/55kDa protein, IVa2 and pVII (Ewing *et al.*, 2007; Gustin & Imperiale, 1998;

Hasson *et al.*, 1989; Perez-Romero *et al.*, 2006; Tyler *et al.*, 2007). The L3-encoded proteinase cleaves several structural precursors including; VI, VII, VIII and the TP, to generate mature derivatives which result in infectious particle formation. This proteinase activity is dependent on the presence of DNA, in addition to the formation of a heterodimer complex with the 11aa, C-terminal peptide from pVI (Ding *et al.*, 1996; Honkavuori *et al.*, 2004; Mangel *et al.*, 1993).

Virion release is facilitated by disruptions to the cytoskeleton induced by L3 proteinase, in addition to the action of an E3-encoded gene, the adenovirus death protein (ADP) which has a cytolytic effect of unknown mechanism. Recent evidence has uncovered an interaction between ADP and MAD2B, a mitotic checkpoint protein, which may contribute to cell death (Tollefson *et al.*, 1996; Ying & Wold, 2003; Yun *et al.*, 2005). Furthermore, Ad5 displays a unique means of exploiting CAR to promote efficient lateral spread. Ad5 fibre is produced in excess quantities during the viral lifecycle and it has been shown that fibre can competitively disrupt CAR:CAR homodimer formation (Walters *et al.*, 2002), as a result of the superior affinity of the knob domain for CAR (Freimuth *et al.*, 1999; van Raaij *et al.*, 2000). In further support of this, crystallographic analyses revealed that the interface bridging the fibre knob:CAR interaction, overlaps with the CAR:CAR homodimeric interface (van Raaij *et al.*, 2000). The dissociation constant (K_d) for binding of the Ad5 fibre domain to soluble CAR has been calculated by SPR to be ~14.8nM (Kirby *et al.*, 2000). Interestingly, the affinity for CAR homodimer formation was determined to be ~16uM, almost 1000-fold lower than the affinity of the Ad5 fibre for CAR (van Raaij *et al.*, 2000). Therefore, the fibre of Ad5 can serve to function in the spread of virion progeny to neighbouring cells, through the disruption of CAR-mediated tight junction adhesions.

Section.1.3 Oncolytic Adenoviruses; Transcriptional Retargeting Strategies

Achieving tumour selectivity and maximising efficacy are major goals for viral therapy applications. Replication selective, oncolytic adenoviruses possess the capacity for restricted oncolysis. Transcriptional selectivity can be achieved by two means; genetic complementation, or through the use of tumour-specific promoters to drive viral replication. Complementation strategies are dependent on an existing understanding of the underlying interactions between viral and cellular molecular networks. These approaches are typified by the genetic modification or deletion of viral effectors whose functions are essential for productive infection in normal cells, but are redundant in tumour cells. Thus, the viral defect results in the attenuation of viral replication in normal cells, but this defect is compensated for in transformed tissue, allowing replication to progress unaffected. These effects can also be achieved by exploiting the state of transcriptional dysfunction within the tumour cell environment, by placing critical viral genes under the control of heterogenous tumour-specific promoter responsive elements. In theory, these conditionally replicating agents have the potential for expansive transgene expression as a result of their ability to self-amplify and propagate throughout the tumour. However, this often is limited by the numerous physical and biological barriers imposed by the cellular heterogeneity of the tumour, and by its micro-environment.

Section.1.3.1 Complementation of Viral Genetic Defects

The design of conditionally replicating adenoviruses (CRAds) exploits the fact that tumours frequently possess dysfunctional, or non-functional, pRb or p53 tumour suppressor proteins (Sherr & McCormick, 2002). The critical and synergistic role for E1A and E1B-55kDa, in the coercion and deregulation of these growth-regulatory networks, is therefore rendered dispensable in the neoplastic context. The first generation CRAd developed was ONYX-015 (*dl*1520), which featured a non-functional E1B-55kDa protein. It was thought initially that productive infection of ONYX-015 was only possible in p53 deficient cells (Bischoff *et al.*, 1996). However, replication of E1B-55K mutants in tumour cells is no longer thought to be due to p53 deficiency, and this property is now attributed to the unique ability of some tumour cells to compensate for the lack of E1B-55K-mediated late viral mRNA export (O'Shea *et al.*, 2004). Subsequent approaches to generate tumour-selective CRAds, were achieved by the introduction of a 24 base pair deletion (Δ24) within a conserved region (CR2) of the E1A gene (Fueyo *et al.*, 2000). This modification inhibits CR2-mediated binding to the

tumour suppressor, pRb (Whyte *et al*., 1989), effectively limiting the replicative capacity of the virus to pRb defective cell types (Jelsma *et al.*, 1989; Moran *et al.*, 1986; Whyte *et al.*, 1989).

Section.1.3.2 Placement of Tumour Selective Promoters

CRAds have also been developed so that replicative function is under the control of tumour activated promoters, and therefore restricted to neoplastic cell conditions. The fundamental principle of this approach is the absolute requirement of E1A for replication, and effects are achieved by substitution of the endogenous viral E1A promoter with selective tumour-associated promoters upstream of, and driving E1A expression. Various tumour-associated promoter elements, suitable for such applications, have been described previously. These have included the use of promoter elements from E2F (Tsukuda *et al.*, 2002), prostate-specific antigen promoter (Pang *et al.*, 1997), telomerase (Hernandez-Alcoceba *et al.*, 2000; Huang *et al.*, 2003), the COX-2 promoter (Bauerschmitz *et al.*, 2006) and hypoxia inducible factor (HIF) responsive elements (Cho *et al.*, 2004; Post & Van Meir, 2003). Additionally, these responsive elements can be combined with complementation mutations, such as Δ24, or with insulators to prevent leaky transcription, and further enhance selectivity (Cascallo *et al.*, 2007; Guse *et al.*, 2009; Majem *et al.*, 2006; Suzuki *et al.*, 2001).

Section.1.4 Oncolytic Adenoviruses; Transductional Retargeting Strategies

Applications which aim to treat metastatic disease favour the systemic delivery of Ad-based therapeutic agents. This requires restrictions to viral tropism determinants, in order to achieve selective delivery to malignant tissue. These restrictions require retargeting modifications, in which the natural tropism is redirected to a cancer-specific marker, in addition to detargeting modifications, in which the native receptor interactions of the vector are ablated. Thus, efficient transductional retargeting has the potential to subvert viral infection to defined tissues. However, efficient delivery also requires the evasion of various components which constitute the circulatory system, in addition to overcoming the inherent biological and physical barriers within the tumour, once selective delivery has been achieved.

The Coxsackie and Adenovirus Receptor (CAR) is the critical determinant of adenoviral tropism *in vitro*, therefore it has long been considered to determine tumour transduction *in vivo*. However, in recent years its relevance in directing the tropism and biodistribution of Ad5 following systemic delivery has become controversial, and is currently the subject of much scrutiny. Nonetheless, several studies have reported the low expression of CAR in carcinoma lines, tumour explants and pathological specimens (Anders *et al.*, 2009; Jee *et al.*, 2002; Matsumoto *et al.*, 2005; Mikami *et al.*, 2001; Rauen *et al.*, 2002; Sachs *et al.*, 2002). Downregulation of CAR is thought to correlate with tumour progression and advanced disease states (Matsumoto *et al.*, 2005; Mikami *et al.*, 2001; Vincent *et al.*, 2009), and low level CAR expression may render tumour cells somewhat refractory to adenoviral infection *in vivo*, or at least impair intratumoural spread (Douglas *et al.*, 2001; Li *et al.*, 1999a; Li *et al.*, 1999b).

A further impediment to generating successfully retargeted Ads is the lack of cancer-specific targets. This is in addition to the distinct lack of corresponding ligands which could permit high efficiency retargeting. The incorporation of many targeting entities is limited by the incompatibility between the inserted ligand and the Ad fibre at the level of intracellular trafficking, and post-translational modification (Belousova *et al.*, 2008; Magnusson *et al.*, 2002). However, with the aim of improving tumour delivery *in vivo*, various retargeting strategies have been described for adenoviruses which include; chemical conjugate strategies, based on the conjugation of an adapter molecule to crosslink the vector to a cellular target receptor, (ii) capsid protein substitution or “pseudotyping”, between divergent strains or species of viruses which exhibit differential tropisms, or (iii) the genetic incorporation of heterogenous binding ligands to

redirect the tropism (*Figure*.1.6). However, the vast majority of these current retargeting strategies are designed to broadly enhance the tropism of Ad5, and do not display inherent tumour selectivity.

The off-target sequestration of Ad5 in the liver also remains a major obstacle to achieving high efficiency, tumour-specific delivery following systemic delivery. The redundancy of CAR in directing the innate hepatotropism of Ad5 has been demonstrated in recent years (Alemany & Curiel, 2001; Leissner *et al.*, 2001; Martin *et al.*, 2003; Mizuguchi *et al.*, 2002; Nicol *et al.*, 2004; Smith *et al.*, 2002) and it is now known that various coagulation factors, FVII, FIX, Protein C, but predominantly FX, direct the accumulation of Ad5 in the liver (Alba *et al.*, 2009; Kalyuzhniy *et al.*, 2008; Parker *et al.*, 2006; Waddington *et al.*, 2008; Waddington *et al.*, 2007). It is evident that high affinity, tumour-specific retargeting strategies should be combined not only with native receptor (CAR) detargeting, but with liver avoidance strategies, in order to permit maximal vector efficacy at the lowest possible dose (Glasgow *et al.*, 2006).

Section.1.4.1 Transductional Retargeting by Chemical Conjugation of Ligands

Adapter based transductional retargeting is achieved by cross-linking extraneous targeting entities to the virus, either by covalent or non-covalent interactions (Mathis *et al.*, 2005). Additionally, various conjugate-based strategies can be combined to create multi-component targeting systems (Barnett *et al.*, 2002; Glasgow *et al.*, 2006; Myhre *et al.*, 2009). Adapters can consist of chemically conjugated Ab fragments, genetically fused variable fragments (scFv) or bispecific diabodies (scFv-scFv), and recombinant fusion proteins (Belousova *et al.*, 2008; Miller *et al.*, 1998; Myhre *et al.*, 2009; Nettelbeck *et al.*, 2001; Yoshioka *et al.*, 2008).

Bispecific “adenobodies” possess dual selectivity; firstly for the target receptor, and secondarily for the virus itself (Watkins *et al.*, 1997). This can be exploited so that these bivalent moieties simultaneously bind native Ad receptor tropism determinants, and thus facilitate ablation of native tropism, whilst in conjunction redirecting the transductional capacity of the vector. Similarly, with this concept in mind, Ab-sCAR ectodomain fusion proteins have also been assessed and have demonstrated enhanced *in vitro* retargeting to CD40 and Epidermal Growth Factor (EGF) in a CAR-independent manner (Dmitriev *et al.*, 2000; Pereboev *et al.*, 2002). Successful retargeting *in vivo* has also been achieved using each of these strategies. Reynolds and colleagues demonstrated enhanced targeting to lung tissue which overexpressed angiotensin-converting enzyme (ACE) using a bispecific anti-knob, anti-ACE diabody

(Reynolds *et al.*, 2000). Additionally, efficient tumour targeting was achieved following intravenous delivery of Ad5 conjugated to a bifunctional sCAR-anti carcinoembryonic antigen (CEA) scFv fusion complex (Li *et al.*, 2007). Both studies demonstrated efficient retargeting which was accompanied by dramatic reductions in liver transduction. More recently, Ad5 has been successfully retargeted to Human Epidermal Growth Factor (Her2) *in vitro* using non-immunoglobulin based Affibodies™, a novel form of artificial protein ligand (Belousova *et al.*, 2008; Henning *et al.*, 2002; Magnusson *et al.*, 2007; Myhre *et al.*, 2009). However, performance *in vivo* has not been assessed for these vectors.

Applications for adapter-ligand based complexes currently are limited, as they do not meet the requirements for applications in human gene therapy, a result of their low yield, and often heterogenous viral populations. They do, however, provide valuable evidence that such retargeting strategies can enhance gene delivery in a CAR-independent fashion, and perhaps further pharmacoanalysis and confirmation of complex stability may enhance their clinical status in the future (Glasgow *et al.*, 2006).

Section.1.4.2 Transductional Retargeting by Genetic Pseudotyping

There are over 50 distinct human adenoviruses, all of which exhibit differential tropisms, mediated primarily by the interaction of the fibre protein with diverse cell surface receptors (Shayakhmetov *et al.*, 2003). Genetic pseudotyping of adenoviruses therefore represents a logical and natural approach to transductional retargeting allowing the expansion, or subversion of viral tropism. The vectors most commonly used for gene therapy applications are subgroup C Adenoviruses (ie. Ad5 and Ad2), which use CAR as their primary receptor (Bergelson *et al.*, 1997). The high fidelity of structural integrity, and the conserved homology of fibre tail domains amongst diverse Ad species, permits genetic engineering with minimal perturbations to the trimeric fibre (Barnett *et al.*, 2002; Tarassishin *et al.*, 2000). Whole fibre replacement strategies mostly focus on the substitution of the Ad5 fibre with fibres derived from subgroup B adenoviruses (ie. Ad3, Ad11 and Ad35) for which the primary receptor is CD46 (Gaggar *et al.*, 2003; Liu *et al.*, 2009; Rea *et al.*, 2001; Segerman *et al.*, 2003; Stone *et al.*, 2007a; Stone *et al.*, 2007b). Pseudotyped vectors based on Ad5/3 have demonstrated enhanced gene transfer to a broad range of cell types (Kanerva *et al.*, 2002a; Ulasov *et al.*, 2007; Von Seggern *et al.*, 2000). Additionally, the overexpression of CD46 in many human cancers has prompted the investigation of Ad5/11 and Ad5/35-based vectors for potential tumour targeting applications (Liu *et al.*, 2009; Shayakhmetov *et al.*, 2002; Stone *et al.*, 2007a; Stone *et al.*, 2005). Vectors

pseudotyped with fibres from subgroup D adenoviruses (ie. Ad17, Ad19, Ad24, Ad30, Ad33, Ad37, Ad43 and Ad47) which can use sialic acid and/or αv integrins as receptors, often in addition to CAR, are also currently undergoing investigation for various applications (Arnberg *et al.*, 2000a; Arnberg *et al.*, 2000b; Chiu *et al.*, 2001; Diaconu *et al.*, 2009; Hsu *et al.*, 2005; Parker *et al.*, 2007; Roelvink *et al.*, 1998; Waddington *et al.*, 2007).

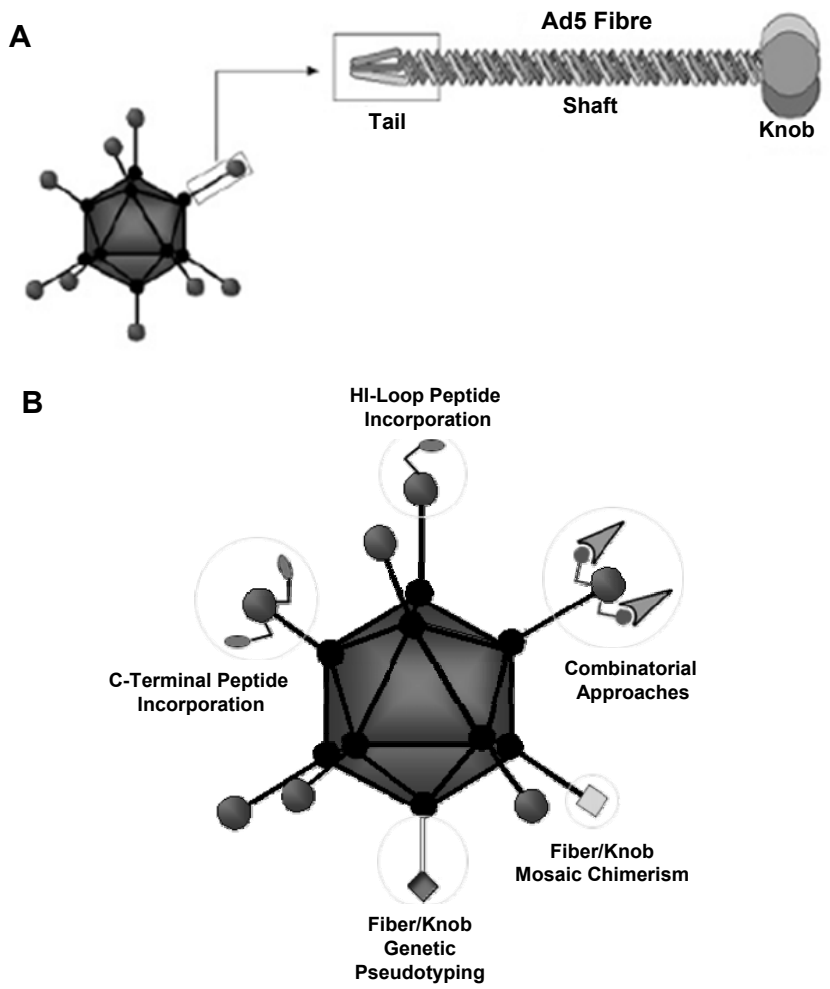

***Figure.*1.6 Tranductional Retargeting by Adenoviral Fibre Modification (A)** Schematic overview of the structure of the fibre protein. **(B)** Outline of fibre retargeting strategies from top, clockwise, genetic incorporation of targeting peptides into the HI-loop, combinatorial approaches whereby chemical conjugates are attached by cross-linking targeting molecules to the fibre surface, substitution of the knob/fibre with that of another serotype whilst additionally retaining the original fibre, genetic pseudotype switching of knob/fibre with that of another serotype, and the genetic incorporation of targeting peptides into the C-terminus of the knob domain. Figure adapted from (Curiel, 1999)

Novel xenotyping strategies involve the substitution of Ad5 knob proteins with those of non-human adenoviruses such as canine adenovirus (CAV-1 and CAV-2), and ovine atadenovirus type 7 (OAdV7), the prototype member of genus *Atadenovirus* (Nakayama *et al.*, 2006; Stoff-Khalili *et al.*, 2005). Additionally, a successful fibre

mosaic virus has been constructed by incorporating the trimeric σ1 spike protein from Reovirus into Ad5 (Tsuruta *et al.*, 2005). This approach was made technically possible by the high degree of structural similarity between the receptor-binding determinants of these two distinct viral families. The generation of this mosaic virus resulted in CAR-independent infectivity enhancement conferred by reoviral tropism determinants, junction adhesion molecule (JAM-1) and sialic acid (Barton *et al.*, 2001; Chappell *et al.*, 1997). However, it is worth considering that genetic pseudotyping of tropism determinants has been shown to alter the intracellular trafficking of Ads, and can often result in reduced infectivity as a result of inefficient endosomal escape, retarded nuclear translocation or retention of virus in late endosomal or lysosomal compartments (Miyazawa *et al.*, 2001; Miyazawa *et al.*, 1999). This may impact their use for gene therapy applications.

Section.1.4.3 Transductional Retargeting by Genetic Incorporation of Ligands

The genetic incorporation of retargeting ligands results in one-component Ad vectors, which are capable of multiple rounds of amplification due to their inherent ability to self-assemble and self-replicate (Mathis *et al.*, 2005). However, the criteria which define the success of this approach are based predominantly on retention of the structural integrity of the fibre. Trimerisation of the fibre is a requisite for capsid assembly which cannot be compromised, and therefore insertions must not disrupt the innate molecular interactions required for adequate assembly (Campos *et al.*, 2004; Krasnykh *et al.*, 2001). Additionally, the heterologous ligand must retain its targeting capacity without the necessity for any major cytosolic post-translational modifications. This is because of the nature of Ad5 fibre translation and virion assembly, both of which take place under non-reducing conditions, in the cytosol and nucleus, respectively.

Several studies have highlighted a number of potential sites suitable for the incorporation of heterologous binding ligands. Capsid sites which can tolerate the insertion of large peptides include the C-terminus of the fibre, the HI loop of the fibre, the penton base, the hypervariable regions of hexon and the minor hexon protein, IX (Belousova *et al.*, 2002; Campos *et al.*, 2004; Dmitriev *et al.*, 1998; Krasnykh *et al.*, 1998; Kurachi *et al.*, 2007a; Le *et al.*, 2004; Le *et al.*, 2005; Meulenbroek *et al.*, 2004). The distal carboxy terminus of the fibre protein was first used for the genetic incorporation of gastrin releasing peptide (Michael *et al.*, 1995). Further studies followed suit with the incorporation of a heparan-binding polylysine motif (pK7), and an arginine-glycine-aspartic acid (RGD) motif, both of which were successful in enhancing the *in vitro* infection of a panel of CAR deficient cell lines (Wickham *et al.*, 1996;

Wickham *et al.*, 1997). However, attempts to incorporate peptides at this site are limited to the inclusion of up to 27aa, due to disruptions to the trimerising capacity of the fibre (Hong & Engler, 1996).

The resolution of the crystal structure of the Ad5 knob domain by X-ray crystallography identified the HI loop region as a region suitable for peptide incorporation (Xia *et al.*, 1994). The rationale for this was that the loop was exposed on the surface of the fibre knob structure, had no involvement in the native tropism of Ad5, was innately flexible, and its length varied greatly between Ad serotypes. To date, the HI loop has been shown to tolerate insertions of up to 83aa, with minimal detrimental effects on structural integrity (Belousova *et al.*, 2002). Insertions range from rationally selected motifs, such as RGD-4C or TAT peptide from HIV-1, to various candidate peptides screened using phage display, including ligands for human transferrin receptor, vascular endothelial cells, and peptides with enhanced homing to the kidney (Denby *et al.*, 2007; Dmitriev *et al.*, 1998; Kurachi *et al.*, 2007b; Nicklin *et al.*, 2001; Nicklin *et al.*, 2004; Wickham *et al.*, 1997; Xia *et al.*, 2000). Strategies featuring dual incorporation of peptides within the C-terminus in conjunction with the HI loop also have demonstrated enhanced infectivity in both CAR- and CAR+ cell lines (Koizumi *et al.*, 2003; Wu *et al.*, 2002).

Additionally, the identification of a number of hypervariable regions within the solvent-exposed loops on the hexon surface highlighted the potential of this capsid protein as an alternative site for the genetic incorporation of peptides (Crawford-Miksza & Schnurr, 1996; Kalyuzhniy *et al.*, 2008; Vigant *et al.*, 2008). This is a particularly attractive approach as the Ad5 hexon has been shown to be one of the major antigenic determinants for neutralising antibody responses (Sumida *et al.*, 2005). Therefore insertions within the HVRs may result in the occlusion of antigenic target sites, permitting escape from neutralisation, or alternatively, presentation of antigenic peptides at these sites could be exploited for vaccine based strategies (Crompton *et al.*, 1994; McConnell *et al.*, 2006). Additionally, the insertion of targeting ligands into the hexon could, in theory, impair binding of FX and therefore reduce hepatotropism of Ad5 *in vivo* (Kalyuzhniy *et al.*, 2008; Vigant *et al.*, 2008).

*Section.*1.5 Oncolytic Adenoviruses; Transductional Detargeting Strategies

It is now clear that factors other than direct receptor-mediated interactions, contribute to the *in vivo* biodistribution of systemically delivered Ads. This is supported by various studies which have demonstrated that ablating native Ad5 tropism determinants (CAR and/or αv- integrins) have little, or no effect on the tropism of Ad5 *in vivo* (Alemany & Curiel, 2001; Fechner *et al.*, 1999; Leissner *et al.*, 2001; Martin *et al.*, 2003; Mizuguchi *et al.*, 2002; Nicol *et al.*, 2004; Smith *et al.*, 2002). However, the importance of CAR-binding ablating strategies has once again become a worthy consideration when contemplating the design of therapeutic Ads. This is based on recent research which has uncovered implications for Ad5-CAR interactions with erythrocytes *in vitro* and *in vivo* (Carlisle *et al.*, 2009; Nicol *et al.*, 2004; Seiradake *et al.*, 2009). This finding has particular relevance for the translation of Ad-based treatments to the clinical setting.

A prominent role for receptor-independent bridging interactions in mediating the *in vivo* tropism of Ad5 has been uncovered in recent years. The intravenous delivery of Ad5 is associated with acute hepatotoxicity which limits the therapeutic efficacy (Engler *et al.*, 2004; Lieber *et al.*, 1997). The mechanism underlying its innate hepatotropism is now known to result from a direct interaction between the hexon and vitamin K-dependent coagulation factor, FX (Alba *et al.*, 2009; Kalyuzhniy *et al.*, 2008; Waddington *et al.*, 2008). This interaction permits engagement with HSPGs or low density lipoprotein receptor on the surface of hepatocytes, facilitating viral entry via an indirect bridging mechanism (Parker *et al.*, 2006; Shayakhmetov *et al.*, 2005b; Waddington *et al.*, 2008; Waddington *et al.*, 2007). Therefore, modifications which ablate or disrupt this FX-hexon interaction would have utility in minimising sequestration at non-target sites, and would greatly improve the selectivity of delivery.

*Section.*1.5.1 Transductional Detargeting by Ablation of Native Tropism

Ablation of CAR-binding determinants was once considered an essential strategy for refining the broad tropism of Ad5 *in vivo*. This was based on the assumption that the classical, two-step entry pathway for Ad5, via CAR and αvβ3/αvβ5, was also relevant *in vivo*. However, subsequent studies highlighted the redundancy of CAR in directing the tropism of Ad5 following systemic delivery (Alemany & Curiel, 2001; Fechner *et al.*, 1999; Leissner *et al.*, 2001; Martin *et al.*, 2003; Mizuguchi *et al.*, 2002; Nicol *et al.*, 2004; Smith *et al.*, 2002). Although the tissue distribution of CAR in humans has not been well characterised, it has been shown to be expressed in cardiac/skeletal muscle,

and on the surface of human erythrocytes (Carlisle *et al.*, 2009; Seiradake *et al.*, 2009; Shaw *et al.*, 2004). Furthermore, CAR mRNA has been detected in the heart, testis, small intestine, pancreas, prostate, liver, kidney and brain (Tomko *et al.*, 1997; Zhang & Bergelson, 2005). Therefore, it is important to consider that the localisation of CAR in humans may impact the selectivity/toxicity of targeted delivery and serves to further highlight the necessity for developing CAR-independent retargeting strategies.

Murine CAR displays high amino acid sequence homology to human CAR, with more than 90% homology within the cytoplasmic and extracellular domains (Bergelson *et al.*, 1998; Tomko *et al.*, 1997). Expression of CAR in mice is most abundant in the liver, kidney, lung and in the heart, where it has been shown to regulate atrioventricular conduction, through associations with connexion-45, β-catenin and ZO-1 (Cohen *et al.*, 2001; Kallewaard *et al.*, 2009; Lim *et al.*, 2008; Lisewski *et al.*, 2008; Shaw *et al.*, 2004). It has also been shown to play a role in murine develoment (Dorner *et al.*, 2005; Hotta *et al.*, 2003). Ad5 can agglutinate human, but not murine, erythrocytes via a CAR-binding interaction (Carlisle *et al.*, 2009; Seiradake *et al.*, 2009). *In vivo* this interaction was shown to impair the extravasation of Ad5 into tumour xenografts when using transgenic mice expressing CAR on the surface of their erythrocytes, or mice transplanted with washed human erythrocytes (Carlisle *et al.*, 2009). This factor has particular relevance when choosing suitable animal models in which to study the effects of systemically delivered therapeutic Ads. Alternatively, the use of CAR-binding ablated vectors which are also unable to agglutinate human erythrocytes, could represent an alternative means to improve the translational relevance of *in vivo* studies which are performed in murine models. Furthermore, Ad5 binding to CAR has been identified as a key event leading to the activation of pro-inflammatory cytokine transcription in respiratory epithelial cells *in vitro* (Tamanini *et al.*, 2006), and has been associated with the induction of cytokine transcription *in vivo* (Schoggins *et al.*, 2005).

The precise molecular determinants for CAR binding have been described previously (Kirby *et al.*, 1999; 2000; Roelvink *et al.*, 1999; Santis *et al.*, 1999). The fibre of Ad5 exists as a homotrimer, and the topological arrangement of the knob monomer is as an eight-stranded antiparallel β sandwich, with interspersing loop regions (Xia *et al.*, 1995). The loop regions vary from 8-55aa residues and are named AB, CD, DE, DG, GH, HI and IJ (see *Appendix I*). Residues, Ser408 and Pro409 in the AB loop, Tyr477 in the DG loop and Leu485 in β-strand F, have been identified as the critical epitopes involved in a high affinity interaction with CAR (Kirby *et al.*, 2000). Substitution mutations at these sites, S408E, P409A, Y477A and L485K, have been shown to effectively abolish the interaction with CAR (Kirby *et al.*, 2000; Leissner *et al.*, 2001).

Interestingly, CAR-binding mutations, S408E and P409A, have also been shown to prevent the agglutination of human and rat erythrocytes (Nicol *et al.*, 2004).

Following on from the original hypothesis that ablating the native receptor binding determinants of Ad5 would refine its broad tissue biodistribution, several studies reported the generation of vectors featuring a mutation in the penton RGD motif, or penton mutants which were combined with CAR-binding ablations (Einfeld *et al.*, 2001; Koizumi *et al.*, 2006; Mizuguchi *et al.*, 2002; Nicol *et al.*, 2004; Smith *et al.*, 2003a). The latter modifications (CAR- and αv-binding ablation) were sufficient to reduce liver tropism to some extent following systemic delivery, although this remains controversial. However, efficient retargeting with these vectors has not been reported.

Finally, the KKTK motif within the shaft of the Ad5 fibre has been proposed to promote direct binding to HSPGs, although this has never been verified experimentally (Dechecchi *et al.*, 2001; Dechecchi *et al.*, 2000). Hepatocytes express high levels of HSPGs (Lyon *et al.*, 1994), thus it was thought that HSPG-mediated entry could contribute to the dramatic liver transduction observed following systemic delivery of Ad5. Subsequently, various studies described significant hepatocyte detargeting in mice, rats and non-human primates as a result of introducing fibre shaft mutations, KKTK to GAGA, which were in some cases accompanied by CAR-binding mutations (Bayo-Puxan *et al.*, 2006; Kritz *et al.*, 2007; Nicol *et al.*, 2004; Smith *et al.*, 2003a; Smith *et al.*, 2003b). In contrast with this, when shaft-chimeric Ad5 viruses featuring long Ad31, or Ad41 shaft domains (lacking the KKTK motif) were generated, the liver accumulation, transduction and levels of pro-inflammatory cytokines produced were identical to Ad5 (Di Paolo *et al.*, 2007). These data suggest that the KKTK motif itself is not responsible for a direct, receptor-mediated interaction with HSPGs. It now is believed that the shaft mutation confers rigidity/instability to the fibre, impairing the flexibility required for efficient receptor interactions (Nicklin *et al.*, 2005; Wu *et al.*, 2003). Thus, the mechanism underlying the reduced liver tropism of these vectors is now thought to be due to the inefficient endocytosis, viral trafficking or endosomal escape of these vectors (Di Paolo *et al.*, 2009b; Kritz *et al.*, 2007). Furthermore, transduction cannot be rescued by ligand-directed retargeting; the incorporation of RGD-4C, or the endothelial targeting peptide QPEHSST, into the HI loop of the KKTK mutant vectors failed to demonstrate efficient retargeting (Bayo-Puxan *et al.*, 2006; Kritz *et al.*, 2007).

*Section.*1.5.2 Transductional Detargeting by Ablation of "Bridging" Interactions

Recent research has demonstrated a fundamental role for serum/coagulation factors, C4BP, FVII, FIX, protein C and predominantly FX, in directing the hepatocyte transduction of Ad5 following systemic delivery (Alba *et al.*, 2009; Kalyuzhniy *et al.*, 2008; Parker *et al.*, 2006; Shayakhmetov *et al.*, 2005b; Vigant *et al.*, 2008; Waddington *et al.*, 2008; Waddington *et al.*, 2007). Surface Plasmon Resonance (SPR) analysis was used to confirm the direct interaction between the hypervariable regions (HRV) of the Ad5 hexon and the Gla domain of FX (Waddington *et al.*, 2008). This interaction was further supported the ablation of hepatocyte transduction when using an Ad5 vector in which the HRVs were switched for those of Ad48, a serotype D adenovirus which fails to bind FX and does not display hepatocyte transduction *in vivo* (Waddington *et al.*, 2008). Additionally, other studies have shown that the insertion of various peptides into hexon hypervariable region -5 (HRV5) of Ad5 also lead to reductions in liver transgene expression (Kalyuzhniy *et al.*, 2008; Vigant *et al.*, 2008).

The critical domains and epitopes responsible for the hexon-FX interaction have recently been mapped to hexon HRV-5 and HRV-7 (Alba *et al.*, 2009). Again, switching HRV5 or HRV7 with the corresponding domains derived from a non-FX interacting serotype Ad26, impaired FX binding both *in vitro* and *in vivo*, although the HRV5 substitution was shown to prevent adequate virion assembly. Cryo-electron microscopy and structural modelling were used to predict putative interacting residues between the Ad5 hexon and FX. Several key residues mapping to HRV5 (T270P and E271G) and HRV7 (I421G, T423N, E424S, L426Y and E451Q) were identified and subsequently mutated. A single amino acid residue, E451, was found to be conserved among FX-binding Ad serotypes, but to be absent from non-binders. Accordingly, a point mutation at this site, E451Q, was sufficient to ablate FX-mediated infectivity enhancement *in vitro* and *in vivo*.

Additionally, Shayakhmetov and colleagues previously described an Ad5 mutant, Ad*mut*, featuring a set of mutations in the fibre knob domain which ablated binding to coagulation factors FIX/C4BP (Shayakhmetov *et al.*, 2005b). The Y477A-*dl*TAYT$_{FLAG}$ modification was sufficient to reduce the hepatotropism of Ad5 *in vivo*. Furthermore, this construct displayed reduced hepatotoxicity and a failure to co-localise with Kupffer cells. However, a mechanism to explain this phenotype was never proposed and remains uncharacterised to date.

Alternative strategies which can be exploited to shield the Ad5 hexon from FX binding *in vivo*, involve coating the Ad5 particle in synthetic polymers, such as polyethylene glycol or the multivalent copolymer poly-[N-(2-hydroxypropyl) methacrylamide]. Originally, this approach was designed to permit efficient retargeting and impair native receptor utilisation whilst simultaneously allowing the evasion of neutralising antibody and innate inflammatory responses (Chillon *et al.*, 1998; De Geest *et al.*, 2005; Fisher *et al.*, 2001; O'Riordan *et al.*, 1999; Wortmann *et al.*, 2008). However, more recently, these strategies have proven useful in reducing the liver tropism and hepatotoxicity associated with intravenous delivery of Ad5, in addition to demonstrating selective retargeting *in vivo* (Eto *et al.*, 2008; Green *et al.*, 2008; Kreppel *et al.*, 2005; Morrison *et al.*, 2008; Stevenson *et al.*, 2007).

Section.1.6 Other Limitations of Adenoviral Gene Therapy

Systemic delivery modalities are preferential for the treatment of many diseases, especially disseminated cancers. However, intravenous delivery of Ad5 in murine models is dose limiting, and is characterised by significant liver accumulation and hepatocyte transduction, which can result in acute toxicity and the induction of potent anti-viral immune effectors (Engler *et al.*, 2004; Lieber *et al.*, 1997). Viral capsid proteins also possess distinct antigenic determinants capable of eliciting cellular and humoral immune responses (Gahery-Segard *et al.*, 1998; Gahery-Segard *et al.*, 1997; Onion *et al.*, 2007; Roberts *et al.*, 2006; Sumida *et al.*, 2005; Willcox & Mautner, 1976; Youil *et al.*, 2002). Furthermore, pre-existing immunity and high Ad5 seroprevalance in humans represent major challenges to successful therapeutic interventions (Parker *et al.*, 2009; Sprangers *et al.*, 2003; Stallwood *et al.*, 2000; Sumida *et al.*, 2005).

It is clear that a multitude of factors encountered in the circulation impede the delivery of Ad5 to target tissues *in vivo*. However, once successful tumour-selective delivery has been achieved, further challenges remain. Both the innate and adaptive immune responses contribute significantly to the clearance of virus from the tumour, resulting in limited efficacy. Furthermore, current *in vivo* models for studying the anti-tumoural efficacy of Ad5-based vectors do not accurately reflect the clinical scenario in patients, in that they are immunodeficient, naïve of pre-existing immunity and are non-permissive for viral replication. However, the widespread use of immunocompetent animal models (ie. Syrian hamsters or Cotton rats) which are permissive, or semi-permissive for Ad5 replication, is limited by the shortage of suitable reagents, the unavailability of multiple syngeneic tumour cell lines, in addition to the distinct lack of transgenic models which display genetic homogeneity (Thomas *et al.*, 2006b; Toth *et al.*, 2007). Additionally, the inherent physical and biological barriers imposed by the heterogenous nature of solid tumours also impedes adequate viral replication, lysis, intra-tumoural spread, transgene expression and, therefore, the potency of oncolytic strategies.

Section.1.6.1 The Innate Immune Response

Systemic delivery of Ads induces acute inflammation, which is characterised by the activation of multiple innate immune effectors. In mice, the innate response to Ad5 is biphasic (Lieber *et al.*, 1997; Liu & Muruve, 2003; Liu *et al.*, 2003). The first phase, induced independently of viral gene expression, peaks between 1 and 6hrs post-infection and is followed by a secondary peak 5 to 7 days post-infection, when the

response is directed primarily against transgene expression (Lieber *et al.*, 1997; Liu & Muruve, 2003; Liu *et al.*, 2003). Recent evidence has implicated receptor binding determinants (CAR/integrins) in the potent activation of cytokines and chemokines (Di Paolo *et al.*, 2009a; Liu *et al.*, 2003; Schoggins *et al.*, 2005; Shayakhmetov *et al.*, 2004b; Tamanini *et al.*, 2006; Tibbles *et al.*, 2002). These interactions can induce various signal transduction pathways including p38 mitogen activated kinase (MAPK), p44/42 MAPK (ERK1/2), PI3K and NF-κB. However, uptake by non-parenchymal cells in the liver, mediated via scavenging receptors (ie. SR-A), or through bridging interactions with platelets or coagulation factors, also contributes to the induction of innate responses (Di Paolo *et al.*, 2009b; Haisma *et al.*, 2009; Shayakhmetov *et al.*, 2005b; Shayakhmetov *et al.*, 2004b; Stone *et al.*, 2007b). Recently, an Ad5 interaction with the integrin subunit -β3, has been shown to promote the activation of IL-1α in splenic marginal zone macrophages *in vivo* (Di Paolo *et al.*, 2009a).

It is clear that macrophages and dendritic cells play a significant role in the recognition, clearance and subsequent inflammation associated with Ad5 *in vivo* (Di Paolo *et al.*, 2009a; Fejer *et al.*, 2008; Koizumi *et al.*, 2007). Pre-treatment of animals with clodronate liposomes has been shown to limit vector-related toxicity, and selective depletion of Kupffer cells using gadolinium chloride ($GdCl_3$) has been shown to reduce hepatotoxicity through preventing serum TNF-α elevation (Kuzmin *et al.*, 1997; Lieber *et al.*, 1997). TNF-α plays a pivotal role in the clearance of adenoviral vectors (Elkon *et al.*, 1997), and E1A expression can sensitise hepatocytes to TNF-α mediated cell killing (Engler *et al.*, 2004). Additionally, much of the hepatic toxicity induced has also been attributed to neutrophil recruitment following the rapid release of macrophage inflammatory protein-2 (MIP-2) from activated Kupffer cells (Muruve *et al.*, 1999). It was shown in two independent studies that hepatic injury induced by systemic delivery of Ad5 could be prevented either by pre-treatment with anti-MIP-2 antibodies, or by studying the effects of vector-related toxicity in IL-1 receptor knockout mice (Muruve *et al.*, 1999; Shayakhmetov *et al.*, 2005c). These findings were complemented by the fact that MIP-2 expression is dependent on intact IL-1 signalling and activation (Shayakhmetov *et al.*, 2005c).

More recently it has been shown that vectors which have reduced accumulation in the spleen, display attenuated hepatic injury despite extensive hepatocyte transduction (Koizumi *et al.*, 2007). The phenotype of Ad5-pK7, a HSPG retargeted vector, has been attributed to diminished IL-6 signalling, as a direct result of limited uptake by splenic dendritic cells. These data highlight the importance of developing vectors which evade both splenic sequestration and Kupffer cell activation; although it is clear that

multiple mechanisms contribute to the toxicity of Ad5 *in vivo*. Further studies are warranted in order to determine the precise molecular interactions and cellular effectors involved in these processes.

*Section.*1.6.2 Translational Relevance of Pre-Clinical *In Vivo* Studies

A significant proportion of the data regarding the *in vivo* biodistribution, toxicity and efficacy of adenoviral vectors refer to studies performed in small animal models, namely mice. Undoubtedly, these studies have led to increased knowledge in the field and have influenced the future direction of Ad-based therapeutic strategies. However, the translational relevance of many of these findings remains unclear. Several major issues which limit the translational potential of adenoviral vectors, especially when attempting to achieve targeted delivery following systemic delivery, currently exist. Species variations in innate immune responses, permissiveness for viral replication, differences in hepatic micro-anatomy, differential interactions with blood cell populations and with native receptors, in addition to the presence of neutralising immunity (discussed below) all contribute the the broad spectrum of Ad responses observed in pre-clincal animal models. These differences are outlined in *Table*.1.

The liver is the major site for accumulation of Ad5 following systemic delivery in murine models. The fenestrae of the sinusoidal endothelial cells in the livers of mice are relatively large (~140nm) and easily accomodate the smaller Ad5 particle (~100nm). This permits rapid access to hepatocytes and to the space of Disse (Lievens *et al.*, 2004). Conversely, the smaller endothelial fenestrae (~107nm) in humans may be more restrictive to Ad delivery (Wisse *et al.*, 2008). The distinct hepatotropism of Ad5 in murine models is mediated through an interaction between the Ad5 hexon and coagulation factor FX (Kalyuzhniy *et al.*, 2008; Waddington *et al.*, 2008). However, the role of this interaction in determining liver transduction in humans, or in fact other small animal models, has not been well characterised. Murine and human FX display high amino acid sequence homology, and both bind to Ad5 with high affinity (Kalyuzhniy *et al.*, 2008). Evidence supporting the relevance of this functional interaction has been demonstrated *in vivo* using human FX to rescue hepatocyte transduction in warfarinised mice. Whether or not this interaction plays a dominant role in limiting efficacy, or inducing toxicity in humans, remains to be determined. However, it is well established that the coagulation cascade is intrinsically linked with cancer and importantly, elevations in FX are frequently detected in patients with solid tumours (Falanga, 2005; Ferrigno *et al.*, 2001; Iversen *et al.*, 2002). Therefore, it is worth

considering that the Ad5-FX interaction may well be relevant in human patients undergoing oncolytic therapy.

Transient liver toxicities and transaminitis are commonly reported side effects in human clinical trials with Ad5-based vectors (see *Table*.1). Dose-limiting hepatotoxicity is a characteristic effect of systemic Ad5 administration in murine models. However, acute liver toxicity is also observed in non-human primates, rats and hamsters (Brunetti-Pierri *et al.*, 2004; Lichtenstein *et al.*, 2009; Nicol *et al.*, 2004). Additionally, it appears that a similar repertoire of inflammatory cytokines is induced by intravascular delivery of Ad5 in multiple species. Serum elevations of IL-6, TNF-α, IFN-γ and IL-12 have been most frequently reported in humans, non-human primates and mice (see *Table*.1). Systemic activation of IL-6, TNF-α, IFN-γ and IL-12 in mice can pre-dispose to lethal septic shock in response to bacterial LPS or endotoxin (Starnes *et al.*, 1992; Wysocka *et al.*, 1995). Interestingly, septic shock in pediatric patients in response natural adenovirus infection has also been associated with dramatic elevations in IL-6 and TNF-α (Mistchenko *et al.*, 1994).

Although transient thrombocytopenia or leukopenia appears to be a common effect induced by Ad5 in humans, non-human primates and mice, there are vast differences in the interactions of Ad5 with other blood cell populations. Anemia and erythroid asplasia have been reported in humans and more recently, hamsters, although it is worth considering that the former may be related to regular phlebotomy during the course of the clinical trial. Alternatively, these effects may be related to the ability of Ad5 to agglutinate CAR-expressing erythrocytes, an interaction which has now been confirmed using rat and human, but not murine erythrocytes (Carlisle *et al.*, 2009; Nicol *et al.*, 2004). Furthermore, in non-human primate models it appears that the spleen is more efficiently transduced than in murine models (Schnell *et al.*, 2001; Smith *et al.*, 2003a). This may be a reflection of differences in hepatic micro-anatomy, which could lead to increased bioavailability for the spleen. In support of this, increased blood persistence was also been reported in non-human primates (Smith *et al.*, 2003a). Interestingly, data from human clinical trials has shown that input virus is cleared within 6hrs of intravascular delivery (Reid *et al.*, 2001). This is in stark contrast with clearance rates in mice, in which Ad5 has a half-life of less than 2 minutes following intravenous delivery (Alemany *et al.*, 2000b). Nonetheless, it is clear that a great deal of work needs to be done in order to successfully correlate pre-clincial studies with outcome in humans and it is necessary that we adopt a pragmatic attitude when assigning relevance to data obtained from selected animal models.

(Atencio *et al.*, 2006; Au *et al.*, 2007; Reid *et al.*, 2002)

*Section.*1.6.3 Immunogenicity and Pre-Existing Immunity

The use of immunocompetent animal models in which to study oncolytic Ad-mediated effects has greater translational relevance to the clinical setting. However, this is complicated when studying human cancers in murine models, as human xenografts must be grown using immunodeficient mice. Therefore, these models fail to adequately assess the *in vivo* safety profile of oncolytic Ads, and do not factor in the effects of an adaptive immune response, or the existence of neutralising antibodies. Ad5 does not replicate productively in murine cells due to host range restrictions (Duncan *et al.*, 1978; Ginsberg *et al.*, 1991). However, a limited number of Ad5-permissive lines have now been identified which are suitable for developing syngeneic, immunocompetent murine models (Ganly *et al.*, 2000; Guo *et al.*, 2006; Hallden *et al.*, 2003; Wang *et al.*, 2003).

Recently, immunocompetent Syrian hamster models have proven useful in assessing the effects of oncolytic adenoviruses *in vivo* (Bortolanza *et al.*, 2007; Bortolanza *et al.*, 2009; Gros *et al.*, 2008; Spencer *et al.*, 2009; Thomas *et al.*, 2006b). Furthermore, the role of pre-existing immunity and the effects of transient immunosuppression on anti-tumoural efficacy have recently been comparatively assessed (Dhar *et al.*, 2009). Interestingly, pre-existing immunity to Ad5 did not impair the efficacy of an oncolytic Ad5 which was administered intratumourally, and in fact prevented the toxicity induced by vector leakage and dissemination from the tumour to other organs. Analyses of the toxicity and biodistribution of Ad5-based vectors in Syrian hamsters are also currently ongoing (Lichtenstein *et al.*, 2009; Ying *et al.*, 2009). Paralleling the findings in murine models, replicating Ad5-based vectors also display dramatic liver sequestration and hepatotoxicity in hamsters following systemic delivery. Although a direct role for coagulation factors was not demonstrated in these studies, it is possible that FX-dependent hepatocyte transduction may also contribute to the accumulation of Ad5 in these models.

The increased interest in utilising immunocompetent murine or Syrian hamster models has prompted careful considerations when developing vectors. This is due to several reports that the retention of the E3 region of Ad5 is critical in maintaining the longevity of viral transgene expression, and therefore the therapeutic efficacy (Bortolanza *et al.*, 2009; Wang *et al.*, 2003). The E3 region produces viral proteins which function as immunomodulatory agents, counteracting various facets of the innate and adaptive immune response to Ad5 (Bennett *et al.*, 1999; Carmody *et al.*, 2006; Cox *et al.*, 1991; Lichtenstein *et al.*, 2004; Tollefson *et al.*, 2001). In particular, deletions within the E3B

region (10.4/14.5kDa-RID and 14.7kDa) have resulted in accelerated vector clearance from the tumours of immunocompetent mice, which correlated with increased macrophage infiltration and cytokine production (Wang *et al.*, 2003). Interestingly, deletion of E3-gp19kDa led to increased replication and anti-tumoural efficacy in an immunocompetent murine model, however the opposite effect was found in an immunocompetent hamster model (Bortolanza *et al.*, 2009; Wang *et al.*, 2003).

*Section.*1.6.4 Tumour Microenvironment

The heterogenous cellular milieu which constitutes a solid tumour represents a major challenge for the effective spread and lytic effect of oncolytic Ads. Solid tumour masses are composed of neoplastic cells, stromal fibroblasts, myofibroblasts, endothelial cells and immune cells, all of which interact with various components of the extracellular matrix (ECM) to affect migration, proliferation and invasion (Wernert, 1997).

The diffusion of therapeutic agents into the tumour following systemic delivery is enhanced by vascular permeability, a feature which is reportedly found in solid tumours (Hashizume *et al.*, 2000; Yuan *et al.*, 1995). However, poorly distributed vasculature within the tumour mass can impede the uniform distribution and subsequent spread of therapeutic agents. Furthermore, the dysregulation of blood vessel formation or vessel architecture, in addition to the absence of functional lymphatics, contribute to the development of a necrotic and hypoxic microenvironment. The presence of expansive necrotic regions within the tumour mass negates the therapeutic efficacy of oncolytic Ads, which require living cells for replication and progeny production. Furthermore, the physical nature of the tumour stroma and ECM impose barrier-like restrictions on the dissemination of virus throughout the tumour. Additionally, the sequestration of input vector by fibroblasts within the ECM can also limit viral production and spread, as it is well established that productive adenoviral replication is dramatically impaired in fibroblasts (Bazan-Peregrino *et al.*, 2008; Gonzalez *et al.*, 2006). Thus, various Ad-based vector engineering strategies have been employed in an attempt to overcome some of these restrictions.

Angiogenesis is critical for the progression and dissemination of tumours, however under normal conditions in adults the process is strictly regulated (Folkman, 1971; 1995). Therefore, targeting angiogenesis represents a means to retard tumour growth and metastasis, and induce widespread tumour necrosis. Adenoviral vectors can be retargeted efficiently to vascular endothelial cells (Nettelbeck *et al.*, 2001; Nicklin & Baker, 2008; Nicklin *et al.*, 2001; Nicklin *et al.*, 2004; Nicklin *et al.*, 2000; Reynolds *et*

al., 2000; Shinozaki *et al.*, 2006; Trepel *et al.*, 2000; Work *et al.*, 2004a; Work *et al.*, 2004b), where they can be programmed to deliver anti-angiogenic factors or express cytotoxic/proapoptotic agents under the control of endothelial-specific promoter elements (Feldman *et al.*, 2000; Greenberger *et al.*, 2004; Regulier *et al.*, 2001; Song *et al.*, 2005; Varda-Bloom *et al.*, 2001).

Furthermore, the induction of hypoxia as a result of inadequate tumour vasculature is one of the hallmarks of solid cancers (Brown & Giaccia, 1998; Pouyssegur *et al.*, 2006). Again, this can be exploited for therapeutic effect by designing oncolytic Ads which feature hypoxia-inducible gene/cytotoxic transgene expression (Huang *et al.*, 2005; Post *et al.*, 2007; Post & Van Meir, 2003). However, these strategies should also be combined with strategies to enhance the intra-tumoural spread and potency of Ad-based therapies. Recently, dramatic improvements in efficacy have been achieved when delivering oncolytic Ads which exhibit an enhanced release phenotype; through the overexpression of the Adenoviral Death Protein (E3-ADP) or through the viroporin-like activity of a truncated, mutant E3-gp19K protein, expressed by AdT1 (Doronin *et al.*, 2003; Gros *et al.*, 2008). Interestingly, the AdT1 mutant also displayed enhanced release from cancer-associated fibroblasts. Novel Ad-engineering strategies to enhance potency include the incorporation of fusogenic proteins to induce syncytia formation, or enzymatic transgenes which digest/depolymerise components of the extracellular matrix, therefore enhancing viral spread throughout the tumour (Ganesh *et al.*, 2007; Guedan *et al.*, 2008). Alternatively, such agents have also demonstrated efficacy following co-administration with virus (Ganesh *et al.*, 2008).

Other approaches to improving the spread and potency of therapeutic Ads, aim to suppress or subvert the immune response directed towards the virus. Several studies have reported prolonged transgene expression, in addition to successful repetitive administration, when using immunosuppressive treatment regimes (Bouvet *et al.*, 1998; Jooss *et al.*, 1996; Smith *et al.*, 1996). Furthermore, a recent study using an immunocompetent Syrian hamster model, demonstrated enhanced anti-tumoural efficacy following transient immunosuppression with cyclophosphamide (Thomas *et al.*, 2008). In contrast, other studies aim to exploit Ad vectors for immunotherapy applications, by using them to express chemoattractants such as granulocyte-macrophage colony-stimulating factor (GM-CSF), to actively recruit immune effectors to the tumour, or stimulate adaptive anti-tumoural immune responses (Lei *et al.*, 2009).

Section.1.7 Integrins and the Role of αvβ6 in Cancer

Integrins are a diverse family of cell surface adhesion molecules with a range of cell-cell, cell-extracellular matrix (ECM) and signal transduction functions (*Figure*.1.7). Structurally, integrins are obligate heterodimers composed of two distinct non-covalently associated α (alpha) and β (beta) subunits. There exist approximately 25 characterised, ligand-distinct combinations generated from 18 α and 8 β subunits, with further variants created by differential splicing and post-translational modifications. Integrins are transmembrane proteins with a large extracellular domain and short non-catalytic cytoplasmic domain, with the exception of -β4 which has a relatively large cytoplasmic region (Kajiji *et al.*, 1989). Integrins play an essential role in regulating signalling pathways responsible for cytoskeleton reorganisation during adhesion and migration, and their signals promote cell survival and proliferation (Guo & Giancotti, 2004).

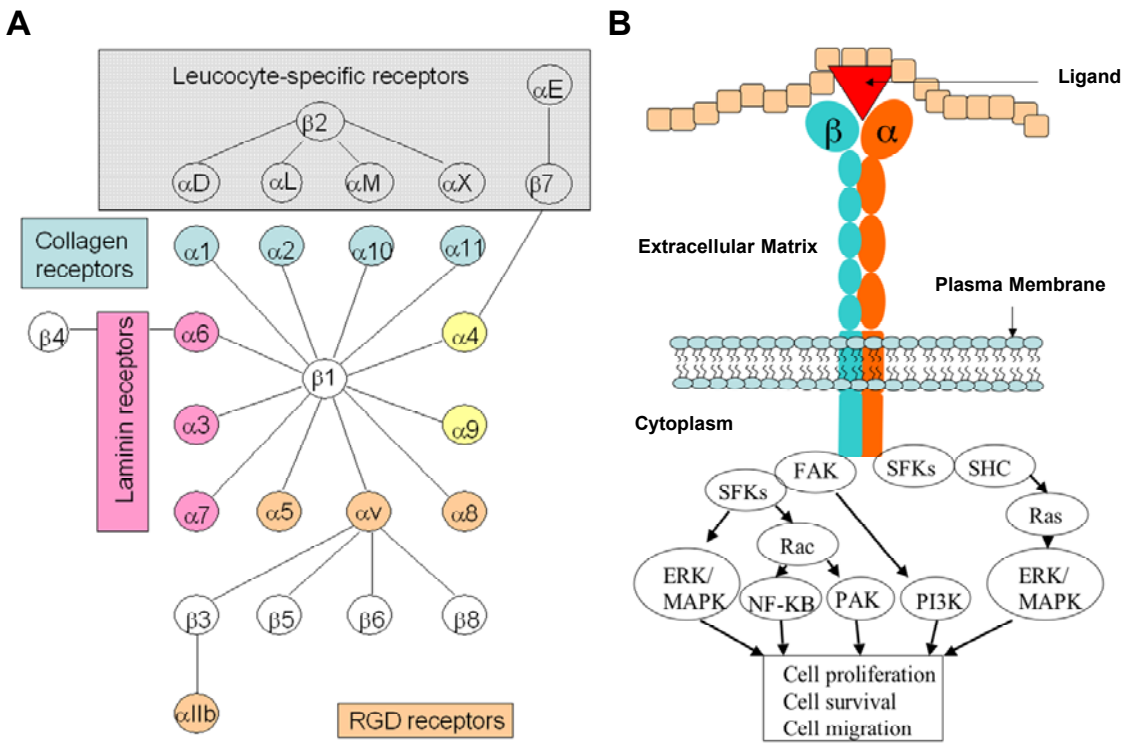

***Figure*.1.7 The Integrin Superfamily, Structure and Signalling (A)** Heterodimeric integrins can be classified into several subfamilies based on ligand specificity. The different subunits show selectivity in their binding partners; for example the αv subunit can pair with multiple β subunits, however the β6 subunit can only bind with αv subunits. **(B)** Integrins are composed of α and β transmembrane subunits with a short cytoplasmic tail (except β4) and an extended extracellular domain. The short cytoplasmic domains of both α and β subunits interact with downstream intracellular effector proteins, activating several signalling pathways, with roles in proliferation, cell survival and migration. Both figures have been taken from Thomas *et al*., 2006a.

Their indirect interactions with microfilament-scaffolding domains are mediated by regulating phosphorylating kinases, such as focal adhesion kinase (FAK) and Src kinase family members, which activate downstream effector substrates. Integrin binding ligands include fibronectin, vitronectin, collagen, laminin and tenascin-C and interactions are often characterised by the recognition of RGD (Arg-Gly-Asp) motifs in their binding domains.

The epithelial-specific integrin αvβ6 remains undetectable on normal adult tissue, but is upregulated by inflammation, tumourigenesis and epithelial re-establishment following wound healing (Breuss *et al.*, 1995; Haapasalmi *et al.*, 1996). Overexpression of αvβ6 is also found in a range of fibrotic conditions including kidney and biliary duct disease (Trevillian *et al.*, 2004; Wang *et al.*, 2007). Additionally, αvβ6 has been shown to play a role in maintaining immunological homeostasis in murine lung, and dysregulated expression of the integrin can lead to pulmonary fibrosis or Acute Lung Injury (Ganter *et al.*, 2008; Horan *et al.*, 2008; Munger *et al.*, 1999; Puthawala *et al.*, 2008). In the neoplastic context, expression of αvβ6 integrin is restricted to carcinomas, and has been reported in pre-malignant oral epithelial dysplasias (Hamidi *et al.*, 2000), oral and dermal carcinomas, as well as carcinomas of the lung, pancreas, stomach, and ovary (*Table*.2). Additionally, αvβ6 recently has been independently identified as a strong prognostic indicator in ovarian, lung, colorectal, cervical and breast cancer (Ahmed *et al.*, 2002b; Bates *et al.*, 2005; Elayadi *et al.*, 2007; Hazelbag *et al.*, 2007). The cell surface localisation of αvβ6, coupled with its prognostic associations in a broad range of human carcinomas highlight its importance as a novel molecular target. However, the expression of αvβ6 in a range of underlying inflammatory or fibrotic conditions in humans warrants consideration when designing therapeutic delivery strategies targeted specifically to αvβ6, as this may impact the success of treatment regimes.

TABLE 2. Expression of αvβ6 in Human Carcinomas[a]

Carcinoma	Reference	Number of carcinomas	% Positive tumours	Evidence	Comment
Oral SCC	Nystrom *et al*., 2006	20	85	IHC	<30% oral dysplasia were also αvβ6+
	Impola *et al*., 2004	11	100	ISH	Expression maintained in LN metastases
	Regezi *et al*., 2002	40	100	IHC	Peri-tumoral dysplasia was also αvβ6+
	Hamidi *et al*., 2000	5	80	IHC	41% OL, Peri-tumoral dysplasia αvβ6+
	Jones *et al*., 1997	17	100	IHC	Absent expression in normal oral mucosa
	Breuss *et al*.,1995	30	90	ISH	Absent expression in normal oral mucosa
HNSCC	Van Aarsen *et al*., 2008	100	64	IHC	Absent/minimal expression in normal tissue
Skin	Van Aarsen *et al*., 2008	49	84	IHC	SCC, not normal tissue was αvβ6+
	Marsh *et al*., 2008	13	77	IHC	Morphoeic BCC αvβ6+
Colon	Yang *et al*., 2008	358	34	TMA	71% expression in liver metastases
	Van Aarsen *et al*., 2008	60	12	IHC	
	Bates *et al*., 2005	488	47	IHC	αvβ6 expression maintained in metastases
Stomach	Kawashima *et al*., 2003	38	84	IHC, RT-PCR	94% αvβ6+ carcinomas had LN metastases
Eosphagus	Van Aarsen *et al*., 2008	56	68	IHC	Absent/minimal expression in normal tissue
Pancreas	Van Aarsen *et al*., 2008	107	57	IHC	
	Sipos *et al*., 2004	34	100	IHC	Expressed in well differentiated tumours
Lung	Van Aarsen *et al*., 2008	54	35	IHC	
	Elayadi *et al*., 2007	289	54	TMA	αvβ6+ correlated with poor prognosis
	Smythe *et al*., 1995	51	50	IHC	αvβ6 determined to be a prognostic marker
Breast	Van Aarsen *et al*., 2008	145	43	IHC	
	Arihiro *et al*., 2000	90	18	IHC, WB	No Grade 1 tumours αvβ6+
Ovarian	Van Aarsen *et al*., 2008	52	33	IHC	
	Ahmed *et al*., 2002 b	45	100	IHC	αvβ6+ expression correlated with grade
Cervical	Hazelbag *et al*., 2007	85	58	IHC	αvβ6+ correlated with poor prognosis
Kidney	Van Aarsen *et al*., 2008	103	21	IHC	
Liver	Van Aarsen *et al*., 2008	59	<2	IHC	

[a] Abbreviations are as follows; SCC = Squamous Cell Carcinoma, HNSCC = Head and Neck SCC, BCC = Basal Cell Carcinoma, IHC = Immunohistochemistry, ISH = In situ hybridisation, LN = lymph node, OL = Oral leukoplakia, TMA = Tissue microarray, RT-PCR = Reverse Transcriptase polymerase chain reaction, WB = Western blot. Table updated from Thomas *et al*., 2006a.

*Section.*1.7.1 Ligand Binding to αvβ6

Ligand binding to αvβ6 is strongly preferential for RGD tripeptide motifs which are followed by +1 and +4 leucine residues. The DLXXL motif was first identified by phage display as the key epitope which conferred strong αvβ6 binding, with minimal interaction with other αvβ3/αvβ5 integrins (Kraft *et al.*, 1999). This was further substantiated by DLXXL peptide inhibition studies on FMDV infection following the confirmation that natural FMDV infection is mediated by αvβ6 (Burman *et al.*, 2006; DiCara *et al.*, 2008; Jackson *et al.*, 2000). Previous work in our laboratory selected a panel of sequence overlapping peptides, all containing the RGDLXXL motif, from known αvβ6 ligands (*Table*.3), which included latency associated peptide (LAP) of TGF-β1 and TGF-β3 (Annes *et al.*, 2002; Munger *et al.*, 1999), the VP1 structural protein of FMDV, Coxsackiesvirus A9 (Heikkila *et al.*, 2009; Williams *et al.*, 2004) and fibronectin (Weinacker *et al.*, 1994).

TABLE 3. Ligands for αvβ6[a]

Ligand	Type of Protein	Reference
Fibronectin	ECM	Busk *et al*., 1992
Tenascin-C	ECM	Prieto *et al*., 1993
Vitronectin	ECM	Huang *et al*., 1998
LAP of TGF-β1	Cytokine	Munger *et al*., 1999
LAP of TGF-β3	Cytokine	Annes *et al*., 2002
FMDV	Virus Capsid Protein	Jackson *et al*., 2000
CAV-9	Virus Capsid Protein	Williams *et al*., 2004

[a] Abbreviations are as follows; ECM = Extracellular matrix, LAP = Latency associated peptide, TGF-β = Transforming growth factor, FMDV = Foot and Mouth Disease Virus, CAV = Coxsackies virus.

Linear peptides were synthesised (CR-UK Peptide Synthesis Laboratory) and assessed for their ability to competitively inhibit αvβ6-dependent adhesion. A candidate peptide, derived from the viral surface protein, VP1, of Foot and Mouth Disease Virus (FMDV), was selected for its high affinity and specificity for αvβ6. Using nuclear magnetic resonance (NMR) analysis it was determined that the efficacy of the peptide was dependent on the inclusion of the DLXXL motif in an extended carboxy α-helical structure, with the RGD motif situated at the apex of a hairpin loop domain (DiCara *et al.*, 2007). Saturation Transfer Difference NMR identified that the highly conserved +1/+4 Leucine or Isoleucine residues, presented adjacently on the surface of the loop, bind closely to the αvβ6 surface (DiCara *et al.*, 2007). The critical function conferred by the formation of this post-RGD, α-helical domain was confirmed by substitution of two L-valine residues for D-valine isoforms. This effectively resulted in the disruption of the helix, without compromising the sequence or overall molecular charge, abrogating binding to the integrin and therefore confirming the importance of the structural conformation of this potential αvβ6 antagonist.

TABLE 4. Functions of αvβ6[a]

Function	Comment	Cell Type	Reference
Promotion of Migration and Invasion	αvβ6-dependent activation of TGF-β1 promotes invasion through inducing the trans-differentiation of fibroblasts into myofibroblasts	OSCC	Marsh *et al*., 2008
	HS1-Associated protein (HAX-1) regulates migration and invasion via clathrin-mediated endocytosis of αvβ6	OSCC	Ramsay *et al*., 2007
	TNF-α-dependent upregulation of αvβ6 associated with increased migration and upregulation of MMP-9	Murine keratinocytes	Scott *et al*., 2004
	αvβ6 promotes invasion through upregulation of MMP-3	OSCC	Li *et al*., 2003 Ramos *et al*., 2002
	Upregulation of uPA	Ovarian carcinoma	Ahmed *et al*., 2002b
	Promotion of migration over fibronectin, vitronectin and LAP	OSCC, Murine keratinocytes	Thomas *et al*., 2002 Huang *et al*., 1998
	αvβ6 promotes invasion through upregulation of MMP-9	OSCC	Thomas *et al*., 2001a, b
Activation of TGF-β	αvβ6-mediated TGF-β1 activation can be induced by "inside-out" signalling to the Protease-Activated Receptor-1 (PAR1) via RhoA and Rho kinase	Murine lung epithelial cells	Jenkins *et al*., 2006
	αvβ6 promotes TGF-β-dependent EMT, risk factor for early stage disease	Colon carcinoma cells	Bates *et al*., 2005
	αvβ6 binds and activates TGF-β3	Colon carcinoma cells	Annes *et al*., 2002
	αvβ6 binds and activates latent TGF-β1, activation dependent upon interaction of αvβ6 with actin cytoskeleton but independent of proteolytic cleavage of the peptide	Colon carcinoma cells, Keratinocytes	Munger *et al*., 1999
Promotion of Proliferation and Generation of Survival Signals	Downregulation of αvβ5 through upregulation of αvβ6 may protect SCCs from anoikis by activation of an Akt survival signal	OSCC	Janes & Watt, 2004
	Identification of the EKXKVDL motif in the C-terminus of the -β6 subunit required for proliferation in 3D-cultures	Colon carcinoma cells	Dixit *et al*., 1996
	αvβ6 promotes proliferation through 11 amino acids in the C-terminus of the -β6 subunit	Colon carcinoma cells	Annes *et al*., 2002

[a] Abbreviations are as follows; TGF-β = Transforming Growth Factor-β, HS-1 = Haematopoietic lineage cell-specific protein-1, TNF-α = Tumour Necrosis Factor-α, MMP = Matrix metalloprotease, uPA = urokinase plasminogen activator , LAP = Latency associated peptide, EMT = Epithelial mesenchymal transition, SCC = Squamous Cell Carcinoma, OSCC = Oral SCC.

*Section.*1.7.2 αvβ6 Promotes Invasion and Migration

The integrin αvβ6 binds to the arginine-glycine-aspartic acid (RGD) motif in its ligands which include fibronectin, tenascin-C, vitronectin and the latency-associated peptide (LAP) of TGF-β1 and TGF-β3 (*Table.*3). Several studies have demonstrated that αvβ6 can promote keratinocyte migration towards fibronectin and vitronectin, in addition to independently upregulating matrix metalloproteinase -9 (MMP-9) expression (Huang *et al.*, 1998; Thomas *et al.*, 2001c). In order for tumour cells to invade and metastasise, they are required to efficiently degrade and traverse the basement membrane, a dense network composed of Type IV collagen, laminins, fibronectin and HSPGs (Yurchenco *et al.*, 2004). It has been shown that αvβ6 integrin initiates an invasive phenotype through the enhanced proteolytic activity of collagenases MMP-9, and, to a lesser extent, MMP-2 (Thomas *et al.*, 2001a; Thomas *et al.*, 2001c). The regulation of MMP-9 expression by αvβ6 has been shown to be modulated through an interaction between the C-terminal cytoplasmic tail of the -β6 subunit and ERK, a member of the Mitogen Activated Protein Kinase family (Ahmed *et al.*, 2002a; Gu *et al.*, 2002; Morgan *et al.*, 2004; Niu *et al.*, 2002). Additionally, clathrin-mediated endocytosis of αvβ6 has been shown to be necessary for carcinoma cell motility and invasion *in vitro* (Ramsay *et al*., 2007). Thus, the functional roles of αvβ6 in growth, progression and migration, doubtlessly underlie its associations with progressive and invasive malignant phenotypes. An outline of αvβ6 functions is presented in *Table*.4.

*Section.*1.7.3 αvβ6 Activates Latent TGF-β

The pleiotropic cytokine, Transforming Growth Factor-β (TGF-β), regulates many biological events, including cell growth, apoptosis and inflammation (Massague *et al.*, 1992; McCartney-Francis & Wahl, 1994; Taipale *et al.*, 1998; Wahl, 1992). Dysregulation of TGF-β expression and activation is associated with a number of pathological conditions including cancer, autoimmune disease, fibrosis and viral infection (Ma *et al.*, 2003; Morris *et al.*, 2003; Munger *et al.*, 1999; Prime *et al.*, 2004a; Prime *et al.*, 2004b; Schultz-Cherry & Hinshaw, 1996; Sharma & Ziyadeh, 1994). During carcinogenesis, TGF-β is thought to exert its effects in a biphasic manner; initially acting as a tumour suppressor, but later stimulating tumour progression (Akhurst & Balmain, 1999; Akhurst & Derynck, 2001; Derynck *et al.*, 2001).

TGF-β is synthesised as an inactive complex, non-covalently associated with is Latency Associated Peptide (LAP). The latent complex is secreted and deposited in the extracellular matrix (ECM), where it can be activated when required by cleavage, or

through conformational changes induced upon ligand binding (Munger *et al.*, 1999). TGF-β1 and TGF-β3, but not TGF-β2, are activated by binding of αvβ6 to LAP (Annes *et al.*, 2002; Munger *et al.*, 1999). Additionally, TGF-β itself has been shown to stimulate *de novo* expression of αvβ6 in keratinocytes (Zambruno *et al.*, 1995). Furthermore, tumour necrosis factor-α (TNF-α) has also been implicated in the upregulation of αvβ6 and MMP-9 (Scott *et al.*, 2004). Interestingly, both TGF-β and TNF-α have been proposed to co-ordinate the induction of αvβ6 through upregulation of the Ets-1 transcription factor (Bates *et al.*, 2005). However, the precise factors which determine the transcriptional upregulation of αvβ6, currently remain unclear.

Section.1.7.4 Strategies to Target αvβ6

The high level cell surface expression of αvβ6 on malignant tissue relative to normal adult tissue, in addition to its roles in invasion and metastasis, make it an attractive target for targeted therapeutics and *in vivo* imaging applications. Indeed several strategies have now been evaluated, for the selective targeting and imaging of αvβ6 positive neoplasms. Successful *in vivo* imaging of αvβ6+ tumours using radiolabelled A20FMDV2 peptide, or radiolabelling combined with PEGylation, has previously been demonstrated (Hausner *et al.*, 2009a; Hausner *et al.*, 2007; Hausner *et al.*, 2009b). In an independent study, Li and colleagues assessed the *in vivo* tumour targeting capacity of an alternative RGDLXXL-containing αvβ6-targeting peptide, H2009.1 (Elayadi *et al.*, 2007; Li *et al.*, 2009). This peptide, synthesised as a tetrameric peptide linked to PEG, displayed a αvβ6 binding affinity in the picomolar range (Li *et al.*, 2009). Furthermore, this group have successfully conjugated doxorubicin to H2009.1 and demonstrated enhanced αvβ6-specific cytotoxicity *in vitro* (Guan *et al.*, 2008).

Alternative strategies include the use of small molecule inhibitors or function blocking antibodies to inhibit αvβ6-dependent migration and invasion (Van Aarsen *et al.*, 2008; Weinreb *et al.*, 2004; Xue *et al.*, 2001). However, the large size of monoclonal antibodies can often preclude efficient penetration into the tumour (Colcher *et al.*, 1998). Additionally, their immunogenicity can also limit their therapeutic utility. More recently, a humanised recombinant scFv antibody to αvβ6 was engineered using the A20FMDV2 peptide, although to date this has only been characterised *in vitro* (Kogelberg *et al.*, 2008). Furthermore, Pameijer and colleagues have described the conversion of an αvβ6-specific peptide, identified by phage display, to a chimeric antigen receptor displayed on T-cells (Pameijer *et al.*, 2007). Subsequently, these αvβ6-directed cytotoxic T-lymphocytes were capable of enhanced killing of αvβ6-expressing primary ovarian carcinoma lines.

Retargeting viral vectors represents another strategy to achieve *in vivo* efficacy or non-invasive imaging. Adenoviruses are one of the best studied viral families for gene therapy applications. To date, adenovirus vectors have been retargeted efficiently through the genetic incorporation of various peptide ligands into the capsid (Dmitriev *et al.*, 1998; Kurachi *et al.*, 2007a; Wickham *et al.*, 1997). Following the elucidation of the crystal structure of Ad5, the HI loop of the fibre protein was identified as a suitable locale for the genetic incorporation of active targeting modalities (Krasnykh *et al.*, 1998; Xia *et al.*, 1994). Therefore, we hypothesised that the insertion of the 20mer peptide A20FMDV2 at this site would permit the retention of its critical structural configuration, within the confines of the HI loop. Success of this strategy would initially confer an expanded viral tropism facilitating enhanced Ad5 transduction to αvβ6-positive cells *in vitro* and, potentially, *in vivo*. Furthermore, following the characterisation of retargeting, we planned to ablate native tropism determinants in order to refine the selectivity of infection.

*Section.*1.8 Aims of this Thesis

General Aim

To generate a recombinant Ad5 vector featuring the previously identified A20FMDV2 peptide in the HI loop of the fibre knob domain. This vector was designated with the nomenclature Ad5-EGFP$_{A20}$ to distinguish from the unmodified vector Ad5-EGFP$_{WT}$ featuring a wildtype fibre protein. Subsequent aims were to test the *in vitro* and *in vivo* characteristics of Ad5-EGFP$_{A20}$ and to demonstrate successful retargeting to αvβ6 integrin.

Objectives

- To generate a replication competent Ad5 vector featuring EGFP under the control of the endogenous E3 promoter in place of E3-6.7K/gp19K (Ad5-EGFP$_{WT}$).
- To genetically engineer the A20FMDV2 peptide into the HI loop of Ad5-EGFP$_{WT}$ to generate Ad5-EGFP$_{A20}$.
- To screen and select a panel of αvβ6-expressing human carcinoma cell lines with varying levels of CAR expression, for subsequent *in vitro* and *in vivo* characterisation of virus constructs.

In Vitro Characterisation of Virus Constructs

- To demonstrate successful expansion of Ad5 tropism to αvβ6, and to confirm that this was mediated through the insertion of A20FMDV2.
- Once efficient retargeting was demonstrated *in vitro*, the subsequent aims were to combine retargeting to αvβ6 with ablation mutations to Ad5 native receptor binding determinants (CAR), and further characterise these constructs.
- Furthermore, these CAR-binding ablated constructs were to be combined with putative blood factor binding ablating mutations (477*dl*TAYT), in an effort to generate a vector retargeted to αvβ6, but detargeted from liver sequestration following systemic delivery. These constructs were again further characterised *in vitro*.

In Vivo Characterisation of Virus Constructs Following Local Delivery in Mice

- To assess the efficacy of Ad5-EGFP$_{WT}$ or Ad5-EGFP$_{A20}$, using the SKOV3ip1 intraperitoneal model of ovarian carcinoma.
- To assess the anti-tumoural efficacy of Ad5-EGFP$_{WT}$ or Ad5-EGFP$_{A20}$ administered intratumourally.
- To demonstrate efficient non-invasive *in vivo* fluorescence imaging of viral replication by detection of EGFP expression.

In Vivo Characterisation of Virus Constructs Following Systemic Delivery in Mice

- To demonstrate superior *in vivo* tumour targeting with Ad5-EGFP$_{A20}$ compared with Ad5-EGFP$_{WT}$, following systemic delivery.
- To investigate and compare the effects of CAR-binding ablation, and putative blood factor binding ablation mutations on the hepatotropism and toxicity of an A20-modified vector Ad5-477*dl*TAYT$_{A20}$, following systemic delivery.

CHAPTER 2. Materials and Methods

Section.2.1 Reagents and Basic Cell Culture Techniques

2.1.1 Cell lines and Growth Media. All human carcinoma cell lines used in this study, along with their growth requirements, are listed alphabetically in *Table*.5. A list of transfected lines used, or generated in this study, can be found in *Table*.6. Dulbecco's Modification of Eagle's Medium (DMEM), α-MEM, Ham's F12, Roswell Park Memorial Institute (RPMI) and isotonic Phosphate Buffered Saline (PBS) were supplied by Cancer Research UK (CR-UK) Media Services (South Mimms, Herts). All culture medium contained 100IU penicillin and 100μg/ml streptomycin. Keratinocyte Growth Media (KGM) was made using α-MEM containing 10% foetal calf serum (Globepharm, Surrey) supplemented with 2.5μg/L amphotericin B (Gibco BRL), 1.8 x 10^{-4}M adenine, 5μg/ml insulin, 1.6 x 10^{-10} M cholera toxin, 0.5μg/ml hydrocortisone and 10ng/ml epidermal growth factor (Sigma). Oral squamous cell carcinoma line SCC25, was grown in 1:1 DMEM:Ham's F12 supplemented with 2.5mM L-glutamine adjusted to contain 15mM HEPES and 1.2g/L sodium bicarbonate with 400ng/ml hydrocortisone. Unless otherwise stated, growth medium consisted of DMEM supplemented with 10% Foetal Calf Serum (FCS; Biowest, Nuaille, France). Cell lines used for the amplification and titration of adenoviruses were HEK293 and JH293, respectively. CAR-binding ablated, αvβ6-retargeted, mutant Ads were amplified using -β6 transfected lines, HEK293-β6 or A549-β6, and were titrated on JH293-β6. Medium used for culture of -β6 transfected cell lines was supplemented additionally with 5μg/ml puromycin dihydrochloride (Sigma, UK).

2.1.2 Maintenance, growth and passage of cell lines. Cells were grown at 37°C in a humidified atmosphere of 5-8% (v/v) carbon dioxide/air, and maintained as adherent monolayers on tissue culture plastic (Falcon, distributed by VWR). Cells were sub-cultured approximately twice weekly by incubation with 33% (v/v) trypsin/PBS (CR-UK Media Services), followed by neutralisation of the trypsin with growth medium and distribution of a single-cell suspension to fresh tissue culture flasks with fresh growth medium. Cells required for frozen stocks were counted prior to being pelleted by centrifugation following trypsin neutralisation. Cells were resuspended in growth medium supplemented with 10% dimethyl sulphoxide (DMSO; BDH, distributed by VWR UK) to a final concentration of $2x10^6$ cells/ml after which they were transferred to 2ml cryovials (Falcon) and stored overnight in insulated polystyrene boxes (Eprak, Scotlab, Scotland) at -80°C. The vials were then transferred to liquid nitrogen for long-term storage. Vials were subsequently defrosted on ice and the cells washed once in warm growth medium before plating. All cells were tested routinely for mycoplasma by scientific officers in the Department of Molecular Oncology and Imaging.

TABLE 5. Human Cell Lines Used in this Study[a]

Cell Name	Cell Type	Medium	Source
A549	Lung Adenocarcinoma	DMEM	CR-UK Cell Services
BICR6	Hypopharynx SCC	KGM	ECACC: 05070501
BICR56	Tongue SCC	KGM	ECACC: 06031002
BT-20	Breast Adenocarcinoma	α-MEM	ATCC: HTB-19
CA1	Breast Adenocarcinoma	DMEM	Dr. I McKenzie, QMUL
CAOV3	Ovarian Adenocarcinoma	DMEM	ATCC: HTB-75
Detroit 562	Pharyngeal Carcinoma	KGM	ATCC: CCL-138
DLD-1*	Colorectal Carcinoma	DMEM	Dr. R Alemany, ICO
H400	Oral SCC	KGM	Dr. S Prime, Uni. of Bristol
HEK293	Human Embryonic Kidney	DMEM	ATCC: CRL-1573
HSC-3	Tongue SCC	KGM	RIKEN Cell Bank, Japan
JH293	Clonal expansion of HEK293	DMEM	CR-UK Cell Services
MCF10CA1a†	Breast Adenocarcinoma	DMEM	Dr. S Statner, KI
NP-9*	Pancreatic Adenocarcinoma	RPMI	Dr. R Alemany, ICO
NP-18*	Pancreatic Adenocarcinoma	RPMI	Dr. R Alemany, ICO
SCC25	Tongue SCC	DMEM:Ham's F12	ATCC: CRL-1628
SiHa	Cervical SCC	DMEM	ATCC: HTB-35
SKOV-3	Ovarian Adenocarcinoma	DMEM	ATCC: HTB-77
SKOV3ip1	Ovarian Carcinoma	DMEM	Dr. J. Price, MD Anderson
TR126	Tongue SCC	RPMI	CR-UK Cell Services
TR138	Laryngeal SCC	RPMI	CR-UK Cell Services

[a] Human cell lines used in this study are listed alphabetically. All cells were grown in media supplemented with 10% Foetal Calf Serum (FCS). Full details of growth requirements can be found in *Section*.2.1. Abbreviations are as follows; SCC = Squamous cell carcinoma, DMEM = Dulbecco's Modification of Eagle's Medium, KGM = Keratinocyte Growth Medium, RPMI = Roswell Park Memorial Institute media, CR-UK = Cancer Research UK Cell Services, ECACC = European Collection of Cell Culture, ATCC = American Type Culture Collection (catalogue numbers listed), QMUL = Queen Mary University of London, ICO = Institut Català d'Oncologia, KI = Karmanos Institute. †MCF10CA1a is abbreviated throughout this study as CA1a. * Selected lines were grown with 5% FCS.

2.1.3 Generation of Stable -β6 Expressing Cell Lines. A number of -β6 expressing cell lines were generated by retroviral cDNA transduction (*Table*.6), using a strategy described previously (Morgenstern & Land, 1990; Thomas *et al.*, 2001b). Briefly, the amphotropic retroviral packaging cell line, AM12-β6, was grown to ~50% confluency. The following day culture medium was removed, and replaced with a smaller volume in order to concentrate the virus. Additionally, the target cell population was seeded to reach ~50% confluency the next day. Retrovirus-containing supernatant was removed from the AM12-β6 cells, 4mg/ml Polybrene hexadimethrine bromide (Sigma, UK) added, and the suspension filtered through a 0.45μm sterile filter. Growth medium was removed from the target cell population, and was replaced with the retrovirus-containing suspension. The following day, cells were washed and medium was replaced with fresh, puromycin-containing medium. Selection in puromycin was carried out for ~10 days, washing and re-feeding every 2-3 days to remove dead cells. Resistant cells expressing -β6 were amplified sufficiently before they were screened for

-β6 surface expression by flow cytometry (see *Section*.2.1.5). When required, high β6-expressing cell populations were obtained by Fluorescence Associated Cell sorting (see *Section*.2.1.6).

TABLE 6. Transfected Cell Lines Used in this Study[a]

Cell Name	Parental Cell Type	Medium	Source/Reference
A549-β6	Lung Adenocarcinoma	DMEM	Generated in this study
A375puro	Melanoma A375 (ATCC; CRL-1619)	DMEM	DiCara *et al*., 2007
A375-β6	Melanoma A375 (ATCC; CRL-1619)	DMEM	DiCara *et al*., 2007
AM12-β6	NIH 3T3 Murine Fibroblasts	DMEM	Thomas *et al*., 2001b
C1	Human Tongue SCC H357	KGM	Thomas *et al*., 2001b
CHO-CAR	Chinese Hamster Ovary	DMEM	Dr. G Santis, KCL
CHO-β6	Chinese Hamster Ovary-K1	DMEM	Generated in this study
DX3puro	Human Melanoma DX-3	RPMI	Hausner *et al*., 2007
DX3-β6	Human Melanoma DX-3	RPMI	Hausner *et al*., 2007
HEK293-β6	Human Embryonic Kidney	DMEM	Generated in this study
JH293-β6	Human Embryonic Kidney	DMEM	Generated in this study
SKOV3ip1-β6	Ovarian Carcinoma	DMEM	Generated in this study
VB6	Derived from C1 (above)	KGM	Thomas *et al*., 2001b

[a] Transfected cell lines used in this study are listed alphabetically. All lines transfected with -β6 cDNA were selected, and grown in media supplemented with 5μg/ml puromycin. Abbreviations are as follows; SCC = Squamous cell carcinoma, DMEM = Dulbecco's Modification of Eagle's Medium, KGM = Keratinocyte Growth Medium, RPMI = Roswell Park Memorial Institute media, KCL = Kings College London.

2.1.4 Antibodies. All antibodies used in this study are listed in *Table*.7. Antibodies used for flow cytometry were as follows; rat monoclonal anti-αvβ6, 53A.2 (generated in-house), mouse anti-αvβ3 antibody LM609 (Chemicon) or 23C6 (Santa Cruz, USA), mouse anti-αvβ5 antibody P1F6 (Chemicon) and mouse anti-CAR antibody RmcB (a kind gift from Dr. Yaohe Wang, CR-UK). Matched isotype controls were rat IgG_{2a} (Abcam) for 53A.2 and mouse IgG_1 (Dako) for all other antibodies. All primary antibodies were used at a final concentration of 10μg/ml. Fluorescently labelled secondary antibodies used were donkey anti-rat, or goat anti-mouse AlexaFluor488 conjugates (Molecular Probes, UK). Antibodies used in function inhibition assays included anti-αvβ6 6.3G9 (generously provided by S. Violette, BiogenIdec, USA), anti-αvβ6 53A.2, anti-αvβ3, anti-αvβ5, as described above, in addition to anti-αvβ8, 14E5 (a kind gift from Dr. S. Nishimura, UCSF) and pan αv inhibitor, L230 (ATCC, hybridoma). Antibodies used for immunostaining procedures were as follows; polyclonal rabbit anti-E1A, 13S-5 (Santa Cruz, USA), was used to detect Ad5 E1A in frozen liver tissue and the fluorescently labelled secondary antibody used was goat anti-rabbit Alexafluor488 (Molecular Probes, UK). Staining for E1A in paraffin-embedded tissue sections was carried out by Pathology Services (Institute of Cancer), using the OmniMap™ kit with mouse anti-Adenovirus [M58] (GeneTex, AutogenBioclear), a rabbit anti-mouse IgG_1 Fc linker (Epitomics, USA) and a secondary anti-rabbit HRP-conjugate (Ventana,

Roche Diagnostics). Detection of αvβ6 integrin in human xenograft tissue was performed using mouse anti-αvβ6 antibody, 6.2G2 (provided by S. Violette, BiogenIdec, USA). Endogenous avidin/biotin or murine IgG activity was blocked using the Avidin/Biotin blocking kit or the MOM kit (both Vector Laboratories, USA). Biotinylated MOM anti-mouse IgG was detected with an avidin/biotin-HRP conjugate, using the Elite ABC kit (Vector Laboratories, USA).

TABLE 7. Antibodies Used in this Study[a]

Primary Ab	Host/Iso.*	Antigen	Application	Source	Reference
10D5	Ms (IgG_{2a})	αvβ6	FB, FC	Chemicon, Millipore,	DiCara *et al*., 2008
14E5	Ms (IgG_1)	αvβ8	FB, FC	Dr. S Nishimura, UCSF	Kogelberg *et al*., 2008
23C6	Ms (IgG_1)	αvβ3	FC	Santa Cruz Antibodies	Jackson *et al*., 1997
53A.2	Rt (IgG_{2a})	αvβ6	FB, FC	CR-UK Antibody Services	Coughlan *et al*., 2009
6.2G2	Ms (IgG_1)	αvβ6	IHC-P	Dr. S Violette, BiogenIdec	Weinreb *et al*., 2004
6.3G9	Ms (IgG_1)	αvβ6	FB, IHC-P	Dr. S Violette, BiogenIdec	Weinreb *et al*., 2004
L230	Ms (IgG_1)	αv subunit	FN, FC	ATCC: HB-8448	Weinacker *et al*., 1996
LM609	Ms (IgG_1)	αvβ3	FB, FC	Chemicon, Millipore	Coughlan *et al*., 2009
M58	Ms (IgG_{2a})	Adenovirus	IHC-P	GeneTex, AutogenBio	Wang *et al*., 2003
M78	Rb (IgG)	Ad2/5 E1A	IHC-Fr	Santa Cruz Antibodies	Cascallo *et al*., 2007
P1F6	Ms (IgG_1)	αvβ5	FB, FC	Chemicon, Millipore	Coughlan *et al*., 2009
RmcB	Ms (IgG_1)	CAR	FB, FC	CR-UK Antibody Services	Bergelson *et al*., 1997
Secondary Ab	**Host/Iso.**	**Antigen**	**Application**	**Source**	**Reference**
AlexaFluor488	Donkey	Rat IgG	FC	Invitrogen	N/A
AlexaFluor488	Goat	Mouse IgG	FC	Invitrogen	N/A
AlexaFluor488	Goat	Rabbit IgG	IHC-Fr	Invitrogen	N/A
HRP†	Goat	Rabbit IgG	IHC-P	Ventana, Roche Diag.	N/A
Avidin/Biotin HRP‡	Goat	Rabbit IgG	IHC-P	Vector Laboratories	N/A

[a] Antibodies used in this study are listed alphabetically, or numerically. Abbreviations are as follows; Ab = antibody, Iso = Isotype, Ms = mouse, Rt = rat, Rb = rabbit, CAR = coxsackie and adenovirus receptor, FB = Function blocking, FC = Flow cytometry, IHC-P = Immunohistochemistry paraffin, IHC-Fr = Immunohistochemistry frozen, HRP = Horseradish peroxidase. *Isotype controls were as follows; Mouse IgG_{2a} (Abcam), Mouse IgG_1 (Dako), Rat IgG_{2a} (Abcam) and Rabbit IgG (Santa Cruz, USA). †Antibody was provided as part of the OmniMap™ detector kit with linkoid™ (Ventana). ‡Antibody was provided as part of the Elite ABC kit (Vector Laboratories).

2.1.5 Flow Cytometry for Surface Receptors. Detection of surface receptors by flow cytometry was carried out as follows; triplicate samples of $1x10^5$ cells in 50µl serum free medium was added to 50µl of antibody at a final concentration of 10µg/ml. Primary antibody incubations were carried out on ice for 45mins after which samples were washed twice in 2ml serum free medium, centrifuging each time at 1200rpm for 3mins. Samples were incubated on ice in the dark for 30mins with the relevant, AlexaFluor488 fluorescently labelled secondary antibody (final dilution of 1:125). Controls included both unstained cells and isotype matched controls, incubated under the same conditions. Labelled cells were scanned on an LSR1 flow cytometer (Becton-Dickinson, CA, USA) acquiring $1x10^4$ gated events, and results analysed using CellQuestPro software. Statistics were collected using single parameter histograms (FL1-H). However, dead cells were excluded by propidium iodide staining (FL3-H) when required. Flow cytometry was also used to determine the ability of the modified

adenoviral $Knob_{A20}$ protein to bind to αvβ6 on BT-20 cells, and to inhibit αvβ6-specific, 53A.2 antibody binding (see *Section*.2.5.3). Furthermore, viral infectivity and competition EGFP gene transfer assays were also quantified by acquisition of EGFP fluorescence in FL1-H (see *Section*.2.8.2).

2.1.6 Fluorescence Activated Cell Sorting (FACS). High -β6 expressing, transfected cells were sorted by Fluorescence Activated Cell Sorting (FACS) on a MoFlo FACS machine (Beckman Coulter) using Summit v4.0 software. Sorting was performed at the FACS laboratory, CR-UK London Research Institute, by Sukhveer Purewal and Carolyn Koh. Target cell lines were pre-screened on an LSR1 flow cytometer (Becton-Dickinson, CA, USA) to determine the percentage of the population which were -β6 positive. The cell number selected for FACS sorting differed from cell line to cell line, but was dependent on the % of positive cells determined by pre-screening, and the desired number of output, FACS-sorted cells. The amount of primary antibody was doubled for every 10-fold increase in cell number. A standard dilution of 1:60 is used for 53A.2 when staining ~$2x10^5$ cells, and so a 1:30 dilution was sufficient for $2x10^6$ cells, and scaled up accordingly. Cells in 500µl volumes were incubated with an equal volume of diluted primary antibody for 45mins on ice. Samples were washed twice in serum free medium, centrifuging at 1200rpm for 3mins each time. The amount of secondary antibody, donkey anti-rat AlexaFluor488, was also doubled for each 10-fold increase in cell number (final dilution 1:62.5). Samples were maintained on ice for 30mins in the dark, washed twice in serum-free medium, centrifuged and resuspended in a final volume of 2ml serum-free DMEM. Unstained and secondary only control samples (in 50µl volumes) were used for setting up parameters on the FACS. Cell suspensions were filtered through a 70µm nylon cell strainer (Becton-Dickinson, USA). Viable cells were identified by DAPI [4',6-diamidino-2-phenylindole] staining, and single cells were selected on the basis of forward and side light scatter characteristics and pulse width. A sample of the sorted population was run on an LSR1 flow cytometer (Becton-Dickinson, CA, USA) immediately following sorting to confirm expression levels. Selected populations were amplified for several weeks and frozen stocks generated.

2.1.7 Quantification of Serum Cytokines/Chemokines Using a Cytometric Bead Assay. Serum was separated from whole blood using Sarstedt CB300 capillary tubes with clot activator (Sarstedt, Germany). Serum levels of IL-6, RANTES, IFN-γ, TNF-α and IL-12(p70) were quantified using a multiplex cytometric bead assay (FlowCytomix™, Bender MedSystems GmbH, Austria). Lyophilised standards for each cytokine/chemokine to be analysed, were centrifuged briefly and reconstituted with 1X

Assay Buffer (PBS and 10% BSA). Two separate standard curves, in the range 0-20,000pg/ml, were prepared by diluting each cytokine stock 1:20, followed by a 3-fold serial dilution. A 1:20 cytometric bead mixture was made up to the required volume using 1X Assay Buffer (25µl per reaction). A 1:20 biotin-conjugate mixture was also made up to the required volume using 1X Assay Buffer (50µl per reaction). A preparation of Streptavadin-Phycoerythrin (PE) was prepared according to the manufacturer's instructions.

A 96-well filter plate was equilibrated using 50µl of 1X Assay Buffer, and medium aspirated using a vacuum Filtration Manifold (Millipore, UK). The bottom of the plate was blotted dry, and 25µl of each standard or serum sample added to the relevant wells. The pre-prepared cytometric bead mixture was added (25µl) to all wells, including the blank wells. 50µl of the Biotin-Conjugate mixture was added to all wells, the plate covered with adhesive film and aluminium foil, and incubated at room temperature (18-25˚C) for 2hrs on a microplate shaker at 500rpm. Following incubation, the adhesive film was removed and wells emptied using the vacuum filtration manifold. Wells were washed twice with 100µl Assay Buffer (1X), medium removed as before, and excess liquid removed from the base of the plate. Streptavidin-PE solution (50µl) was added to all wells, the plate covered with adhesive film and incubated at room temperature for 1hr on a microplate shaker at 500rpm. Following incubation, wells were emptied and washed twice as before. 200µl Assay Buffer (1X) was added to each well and mixed thoroughly by repeated aspiration and ejection. Samples were transferred to flow cytometry tubes (Becton-Dickinson, CA, USA), and made up to a final volume of 500µl. Analysis was performed following acquisition on an LSR1 flow cytometer (Becton-Dickinson, CA, USA). Cytometer set up was established using a detailed protocol provided with the kit (FlowCytomix™, BenderMedSystems GmbH, Austria). Calculations and analysis of results were performed using FlowCytomix Pro 2.2 Software, as directed by the manufacturer. When necessary, CellQuestPro acquisition files were filtered to eliminate debris using FCS Filter v1.0.4 Software (Soft Flow, Hungary).

2.1.8 Bacterial strains, Yeast strains, Medium and Growth Conditions. Bacterial strains used in this study included chemically competent *Escherichia coli* (*E.coli*) DH10B (generated in-house), electrocompetent ElectroMAX™DH10B™ (Invitrogen™), One Shot™ Top10-F (Invitrogen™) and SG13009-pREP4 (Qiagen®). Bacterial strains were cultivated at 37°C in either Luria-Bertani (LB) broth [1% (w/v) tryptone, 0.5% (w/v) yeast extract and 1% (w/v) sodium chloride] or plated onto LB supplemented with 1.5% (w/v) agar. Medium was enriched with relevant antibiotics as required [ampicillin (Amp),

kanamycin (Kan) or chloramphenicol (Chl) at concentrations of 100μg/ml, 25μg/ml and 25μg/ml respectively].

Yeast strain, *Saccharomyces cerevisiae* YPH857 (ATCC 76628): genotype MATalpha ura3-52 lys2-801 ade2-101 trp1-Δ63 his3-Δ200 leu2Δ1, was grown at 30°C in YPD broth [2% (w/v) peptone-Y, 1% (w/v) yeast extract and 2% (w/v) dextrose] or plated onto YPD supplemented with 1.7% (w/v) agar. YPH857 harbouring the Ad5-containing plasmid pMB20 (generously provided by Richard Iggo, UK), were grown in synthetic defined dropout medium, -HIS [0.17% (w/v) yeast nitrogen base, 0.5% (w/v) ammonium sulphate and 2% (w/v) dextrose] or plated onto -HIS supplemented with 1.7% (w/v) agar. Intermediate recombination derivatives (ie. pMB20 incorporating the URA3 integrating shuttle vector) were grown in synthetic dropout media -HIS -URA [0.17% (w/v) yeast nitrogen base, 0.5% (w/v) ammonium sulphate and 2% (w/v) dextrose] or plated onto medium supplemented with 1.7% (w/v) agar. All bacterial medium was supplied by Clare Hall Media Production Services (CR-UK) and yeast medium supplied commercially by Q.Biogene.

Section.2.2 Recombinant DNA and Cloning Techniques

Standard restriction enzymes, T4 DNA *Ligase* and *Antarctic Phosphatase* were supplied by New England Biolabs®Inc and reactions carried out as recommended by the manufacturer. Methylation sensitive, modifying enzyme *Dpn*I was supplied by Promega. Standard Polymerase Chain Reaction (PCR) reactions were optimised with Opti-Prime™ PCR Optimisation Kit (Stratagene) using *Taq* DNA polymerase (Roche). Mutagenic PCR, or strategies using Splicing by Overlap Extension (SOEing) PCR, were carried out using high fidelity Platinum® *Pfx* DNA polymerase (Invitrogen). All PCR primers and sequencing primers used were supplied by Sigma-Genosys (*Table*.8 and *Table*.9, respectively).

2.2.1 Restriction Digestions. Restriction enzyme digestions were set up in 20µl volumes. Samples were digested with 1.0U/µg DNA with the required restriction enzyme(s) in 1X buffer supplied by manufacturer, as directed. 1X Bovine Serum Albumin (BSA) was added when required.

2.2.2 Antarctic Phosphatase Treatment. Digested backbone DNA (1µg) was modified by incubation with 1U *Antarctic Phosphatase* (New England Biolabs) in 1X buffer. Reactions were set up in 20µl reaction volumes and incubated at 37°C for 15mins (for 5' overhangs or blunt end digestions), or for 1hr (for 3' overhangs) before further incubation for 5mins at 65°C to denature the modifying enzyme. Reactions were allowed to cool to room temperature before setting up ligation reactions. The molarities of the linearised backbone and desired insertion were calculated from the formula below, and ligation ratios were adjusted to 2:1, 3:1 or 4:1 for insert:dephosphorylated backbone (50ng).

Picomole Ends per Microgram of Double-Stranded Linear DNA

$$(2 \times 10^6) / (650 \times \text{Number of bases of plasmid}) = \text{pmol ends/µg double-stranded}$$

2.2.3 Ligations. Reactions were set up in 25µl volumes using 1µl T4 DNA *Ligase*, 1X T4 *Ligase* buffer and differential ratios of backbone to insert (described above). Controls included unmodified backbone-no insert, dephosphorylated backbone-no insert and no backbone-insert only. Standard ligation reactions were incubated overnight at 16°C in a PTC-200 Peltier Thermal Cycler (MJ Research), prior to transformation into competent *E.coli* bacteria.

2.2.4 Standard PCR. PCR reactions were set up in 50µl volumes containing; 100-200ng of template DNA, forward and reverse primers at 0.5-1µM each, 1mM dNTPs,

1X Opti-Prime™ buffer (Stratagene) and 1U *Taq* DNA polymerase (Roche). A control lacking DNA was run in parallel. PCR was performed in a PTC-200 Peltier Thermal Cycler (MJ Research) under the following conditions: denaturation at 94°C for 5mins followed by 28 cycles at 94°C for 45s, annealing at 58°C for 45s and elongation at 72°C for 50s followed by a final extension step at 72°C for 10mins. PCR products were confirmed by gel electrophoresis analysis (*Section*.2.2.8.).

2.2.5 Mutagenesis PCR. Site directed mutagenesis was carried out by mutagenic PCR using oligonucleotide primers encoding desired mutations and containing complementary flanking sequences. Reactions were set up in 50µl volumes containing; 200ng of template DNA, forward and reverse primers at 1µM each, 1mM dNTPs, 1mM $MgSO_4$, 1X *Pfx* buffer and 1U *Pfx* DNA polymerase (Invitrogen™). Control reactions lacking DNA polymerase were run in parallel. Mutagenic PCR was performed in a PTC-200 Peltier Thermal Cycler (MJ Research) under the following conditions: denaturation at 94°C for 3mins followed by 20 cycles of 30s denaturing at 94°C, 30s annealing at 60°C and 12mins elongation at 68°C, followed by a final extension step at 70°C for 20mins. 15U of *Dpn*I, a methylation sensitive restriction enzyme (Promega), was added after the PCR to digest the template DNA, leaving newly synthesised and unmethylated DNA intact. The digestion reaction was performed in buffer supplied by the manufacturer at 37˚C for 2hrs. *Dpn*I modified DNA was transformed into DH10B *E.coli* and plasmid DNA extracted (QIAamp DNA mini kit, Qiagen).

2.2.6 Gene Splicing by Overlap Extension (SOEing) PCR. Gene splicing by overlap extension is a PCR based system for generating recombinant or chimeric gene sequences, without the reliance on restriction sites (Horton, 1995; 1997; Horton *et al.*, 1990). A schematic overview of the strategy is presented in *Fig.2.*1. Firstly, fragments to be overlapped were amplified in separate reactions using primers which feature the desired modifications within the 5' region (Step 1). These 5' modified PCR fragments were purified using the QIAquick® Gel Extraction Kit 50 (Qiagen®) after which 5µl of each was added to a single PCR reaction carried out in the absence of primers (Step 2). This step permits hybridisation of the complementary sequences within the primer-introduced, 5' regions. The resulting single PCR product was gel purified, as above, and 5µl subjected to a final round of PCR using forward and reverse primers designed to amplify the entire target sequence (Step 3).

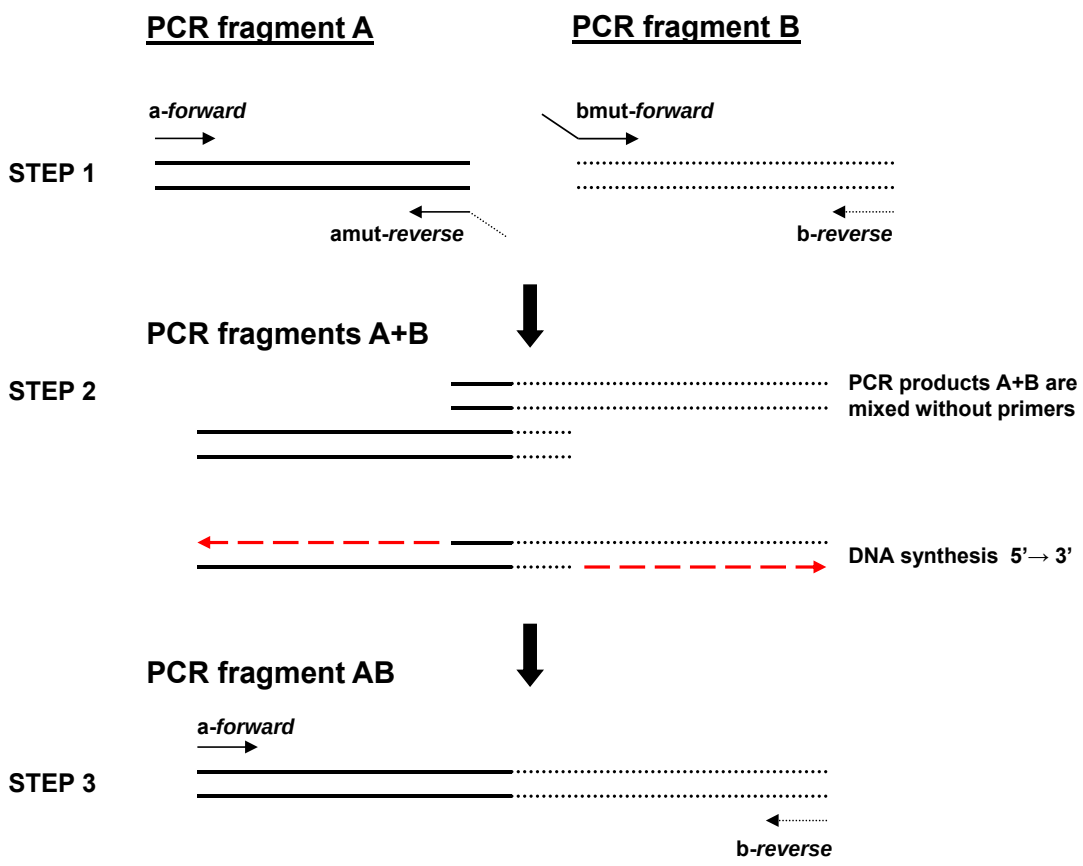

***Figure*.2.1 Schematic Overview of Splicing by Overlap Extension PCR (SOEing PCR).** In Step 1 separate PCR products, PCR A and PCR B, are amplified using primers designed to introduce a specific, mutant sequence into the region of DNA to be overlapped (amut-*reverse* and bmut-*forward*). In Step 2, PCR products generated in Step 1 (PCR A and PCR B) are added to a single PCR reaction, in the absence of primers. This reaction allows the hybridisation of their complementary *mut* regions, producing an overlapped fragment, PCR A+B. In the final reaction, Step 3, PCR A+B is amplified with primers, a-*forward* and b-*reverse*, to generate the target sequence, PCR AB.

Reactions for Step 1 (PCR-A or PCR-B) were set up in 50µl volumes containing; 200ng of template DNA, primers (either a-*forward* and amut-*reverse* or bmut-*forward* and b-*reverse*) at 1µM each, 1mM dNTPs, 0.5-1.0mM $MgSO_4$, 1X *Pfx* buffer and 1U *Pfx* DNA polymerase (Invitrogen™). PCR was performed in a PTC-200 Peltier Thermal Cycler (MJ Research) under the following conditions; denaturation at 94°C for 3mins followed by 25 cycles of 1min denaturing at 94°C, 30s annealing at 60°C and 3mins elongation at 68°C, followed by a final extension step at 68°C for 10mins. Reactions for Step 2 were set up in 25µl volumes containing; 5µl of each PCR product (ie. PCR-A + PCR-B), 1mM dNTPs, 0.5-1.0mM $MgSO_4$, 1X *Pfx* buffer and 1U *Pfx* DNA polymerase using identical conditions, with the exception of the number of cycles, which was reduced to 15. For Step 3, 5µl of the PCR product obtained in Step 2 (PCR-AB) was added to the final PCR reaction (PCR-AB). The final amplification step was set up as described in Step.1, however primers used in this case were a-*forward* and b-*reverse*. In order to

facilitate TA cloning into holding vector pcDNA3.1/V5-HIS©-TOPO® (Invitrogen™) the final product (PCR-AB) was incubated with an excess of dATPs at 72˚C for 10mins. Reactions were set up in 25µl volumes as follows; 14.5µl PCR-AB, 10mM dATP, 1X Buffer [10mM Tris-HCl pH8.8, 3.5mM $MgCl_2$, 75mM KCl and 5nM EDTA] and 1U *Taq* Polymerase. Plasmids were named accordingly (ie. pPCR-AB-TOPO), sequenced to verify the success of the strategy, and vectors used for various subcloning strategies when required.

2.2.7 Quantitative Real Time PCR. Viral and total genomic DNA was obtained from virally infected cells, or murine tissue, using the QIAamp Blood mini kit or QIAamp DNA mini kit (both Qiagen, UK). 20ng of total DNA was subjected to fluorogenic TaqMan Real Time Quantitative PCR (qPCR) using the Applied Biosystems 7500 Real Time PCR system. TaqMan reactions were performed in triplicate, on two separate occasions, using primers for the hexon region of the genome, Forward: 5'-AGCGCGCGAATAAACTGCT-3' and Reverse: 5'-AGGAG ACCACTGCCATGTTGT-3' (Sigma), and a probe from Applied Biosystems (Hexon Probe FAM-CCGCCG CTCCGTCCTGCA-MGB). Negative controls were run to ensure that no amplification occurred in the absence of DNA. Cycling conditions were as follows; 50˚C for 2mins, 95˚C for 10mins, 95˚C for 15sec for 40 cycles followed by 60˚C for 1min. Total adenoviral genomes were calculated using a standard curve of 10^1-10^9 viral genomes (see *Section*.2.8.1), and data were analysed using Sequence Detection Software v1.3 (Applied Biosystems).

2.2.8 DNA Analysis by Gel Electrophoresis. Gel electrophoresis analysis was used to confirm successful cloning, ligation or PCR steps. 5-10µl of restriction digests or PCR products were run on a 1-2% (w/v) agarose gel [1-2g agarose in 1X Tris-Borate-EDTA (TBE) buffer with 5µl ethidium bromide (EtBr) at 0.5µg/ml] for ~30mins @ 100V. Samples were run alongside a 1kb DNA ladder (Invitrogen™). Visualisation of the gel under UV light ensured that inserts were present or that PCR products were the expected size. Digested fragments, or PCR bands required for further cloning and ligation steps, were excised from the gel under UV light using a sterile blade and DNA purified using QIAquick® Gel Extraction Kit 50 (Qiagen®).

2.2.9 Preparation of Chemically Competent *E.coli*. DH10B *E.coli* were made competent by $CaCl_2$ treatment by standard method (Cohen *et al.*, 1972). Briefly; a single colony was inoculated overnight in 10ml LB. 5ml of the overnight starter culture was added to 500ml LB, and bacteria grown with aeration for ~3hrs at 37˚C. Once bacteria had reached a mid-logarithmic phase of growth (OD_{600nm}=0.4), cells were

pelleted by centrifugation at 4000rpm for 10mins at 4˚C. Supernatant was removed and cells resuspended in 10ml ice-cold 0.1M $CaCl_2$. Cells were recovered by centrifugation at 4000rpm for 10mins at 4˚C. Supernatant was removed and the pellet resuspended in 2ml ice-cold 0.1M $CaCl_2$ with 20% (v/v) glycerol, for each 50ml of original culture. Cells were dispensed into 200µl aliquots and were stored for 12-24hrs at 4˚C, after which they were transferred to -80˚C for long term storage. SG13009 *E.coli,* suitable for recombinant protein expression, were made competent as follows; a single bacterial colony harbouring the Kan^R pREP4 which had been freshly grown overnight, was picked from an LB agar plate at 25µg/ml Kan, inoculated into 10ml LB/Kan and grown overnight at 37°C with aeration. The following morning, 1ml of the overnight culture was added to 100ml of pre-warmed selective medium and was incubated with aeration at 37°C until an optical density (OD) of 600nm was reached. The culture was chilled for 5mins on ice and transferred to a sterile round-bottom centrifuge tube. Cells were pelleted by centrifugation at 4000g for 5mins at 4°C. Supernatant was discarded and cells resuspended gently in 30ml cold, sterile, TFB1 buffer pH5.8 [100mM RbCl, 50mM $MnCl_2$, 30mM KAc, 10mM $CaCl_2$ and 15% (v/v) glycerol] and held on ice for 90mins. Cells were collected by centrifugation at 4000g for 5mins at 4°C, after which the supernatant was discarded and cells resuspended in 4ml ice-cold, sterile, TFB2 buffer [10mM MOPS, 10mM RbCl, 75mM $CaCl_2$ and 15% (v/v) glycerol]. Cells were aliquoted into 100µl volumes in sterile eppendorfs before being frozen at -80°C until required for transformation. 5µl of pQE30-based ligation reactions were used to transform, by heat shock, one aliquot of competent SG13009 cells, as recommended by the manufacturer (Qiagen®). Transformants were selected as before on LB/Kan, now supplemented additionally with Amp at 100µg/ml.

2.2.10 Transformations. Chemically competent DH10B *E.coli* were transformed using 5µl of standard ligation reactions. The same strain was used for transformation with 2µl *Dpn*I digested, mutagenic shuttle vectors. Cells were held on ice for 10mins before addition of DNA (~50ng DNA in a volume of 10µl or less) and the cell-DNA suspension was incubated for a further 30mins on ice. Bacteria were subjected to heatshock at 42˚C for 90secs and transferred immediately to ice for 2mins. Cells were resuscitated in 800µl SOC (Invitrogen) medium [2% (w/v) tryptone, 0.5% (w/v) yeast extract, 10mM NaCl, 2.5mM KCl, 10mM $MgCl_2$, 10mM $MgSO_4$, 20mM glucose], and cultures incubated for 45min at 37˚C with aeration. Approximately 200µl of culture was spread onto pre-warmed selective agar and plates incubated overnight at 37˚C. Plasmid DNA constructs resulting from ligation into pcDNA3.1/V5-HIS©-TOPO® (Invitrogen™) were used to transform one vial of One Shot™ Top10-F competent cells (Invitrogen™) as

recommended by the manufacturer, and transformants were selected on LB agar supplemented with 100µg/ml Amp. Competent SG13009 (pREP4) *E.coli* (Qiagen®) were used for transformation with pQE30 derived expression vector constructs prior to protein induction, according to manufacturer protocol. Transformants were plated onto LB agar enriched with Kan and Amp, and plates incubated upside-down overnight at 37°C. Large construct pMB20-derivatives were transformed into ElectroMAX™ DH10B™ (Invitrogen) using a BioRad GenePulser® II electroporator. No more than 100ng of DNA was used to transform cells under the following conditions; 1.8kV, 200Ω and 25µF. Transformants were selected with Chl at 12.5µg/ml. For all transformation protocols, cells were resuscitated in SOC, plated onto relevant selective medium and incubated overnight at 37°C.

2.2.11 Plasmid DNA Extraction. Colonies were picked from overnight selective medium plates, inoculated into 2ml of antibiotic selective LB broth, and were incubated in a shaking 37°C incubator overnight. Bacterial cultures were harvested by centrifugation at 13,000rpm and plasmid DNA extracted from pellet by standard protocol, using QIAprep® Spin Miniprep Kit 250 (Qiagen®). Constructs confirmed by sequencing analysis were amplified by QIAprep® Maxiprep Kit (25). DNA concentration was determined using a NanoDrop® ND-1000 photospectrometer (NanaoDrop Technologies$_{Inc}$). Samples were assessed at 260nm versus a blank control of the elution buffer. DNA from large construct plasmids (ie. pMB20-based) was extracted by alternative means (see *Section*.2.6.5).

2.2.12 Sequencing and Analysis using Bioedit Software. Plasmids were sequenced at the Genome Centre (William Harvey Institute, Barts and The London School of Medicine). Reactions were set up in 12µl volumes and sequencing PCR carried out on a Peltier Thermal Cycler DNA Engine PTC-225 (MJ Research) using BigDye® Terminator v3.1 Cycle Sequencing reaction reagent (Applied Biosystems) in 1X sequencing buffer (Applied Biosystems), with 10pmol primer and ~400ng template DNA. Each clone was sequenced with a minimum of two different primers to generate overlapping readings (*Table*.9). The cycling reaction was: denaturation at 96°C for 30sec followed by 25 cycles of 30s denaturing at 96°C, 15s annealing at 50°C followed by 1 min elongation at 60°C for a final time of ~1.5hours. The PCR products were cleaned up, the plate was sealed and PCR products sequenced on an ABI Prism 3700 DNA Analyzer by capillary electrophoresis (performed by staff at the Genome Centre). Chromatograms were analysed using Bioedit software, and 100% identity confirmed by BLAST analysis comparing against plasmid sequences created and stored in the VectorNTI database by the licence holder (VectorNTI Advance 10, Invitrogen).

TABLE 8. Primers Used for PCR Applications[a]

Primer Name	Sequence 5'→3'	Ad5 Region (nt)
A20-*forward*	CTGTGCCCAACTTGAGAG	N/A
A20-*reverse*	GCCACCTTTTGAGCCAAC	N/A
AdinPCR-*forward*	CCAAAAGTAACATTGTCAGTCAAG	32571-32594
AdinPCR-*reverse*	GCAATGTATGAAAAAGTGTAAGAG	32772-32749
*Bam*HI-*Sfo*I-Left-*reverse*	*GGATCCGGCGCC*AGTTGTGTCTCCTGTTTCCTGTGT	32651-32674
*dl*TAYT-*forward*	CTGAAGGC*AACGCTGTTGGATTTATG	32513-32530
*dl*TAYT477-*reverse*	CAACAGCGTT*GCCTTCAGTAAGATCTC	32513-32522
*dl*TAYT485-*reverse*	CTGAAGGCAACAGCGTT*GCCTTCAG**TTT**TATCTC	32492-32501
EGFP-*forward*	CCCACCATGGTGAGCAAGG	N/A
EGFP-*reverse*	GACTTGTACAGCTCGTCCATG	N/A
F5Knob-*forward*	TTTAAGGATCCGGTGCCATTACAGTAGGAA	32195-32213
F5Knob-*reverse*	TATATAAGCTTATTCTTGGGCAATGTATGA	32762-32782
*Kpn*I-ADP-*reverse*	G*GGTACC*CGAACATGTGTTTCAGTCCGTCCAATC	29723-29748
Mut6XHIS-*forward*	CACCATCACCATCACCCAAGTGCATACTC	32675-32688
Mut6XHIS-*reverse*	GATGGTGATGGTGATGAGTTGTGTCTCCTG	32661-32675
MutY477A-*forward*	TTCCTGGACCCAGAA**GCT**TGGAACTTTAGAAAT	32450-32482
MutY477A-*reverse*	ATTTCTAAAGTTCCA**AGC**TTCTGGGTCCAGGAA	32450-32482
MutL485K-*forward*	CTTTAGAAATGGAGATA**AAA**CTGAAGGCACAGC	32473-32505
MutL485K-*reverse*	GCTGTGCCTTCAG**TTT**TATCTCCATTTCTAAAG	32473-32505
*Not*I-Left-*forward*	*GCGGCCGC*GGCCTAGAATTTGATTCAAACAAG	32126-32149
*Sac*II-12.5K-*forward*	G*CCGCGG*GAGCTCGATCAATTTATTCCTAACTTTG	27795-27816
*Sfo*I-*Right*-*forward*	*GGCGCC*CCAAGTGCATACTCTATGTCATTT	32675-32698
*Xba*I-12.5K-*reverse*	C*TCTAGA*GCTGCGCCTTTGGCCTAATAC	28507-28528
*Xba*I-hNIS-*forward*	C*TCTAGA*GATGGAGGCCGTGGAGACCGGGGAACGG	N/A
*Xho*I-ADP-*forward*	C*CTCGAG*GCAATTGACTCTATGTGGGATATGCTCC	29349-29375
*Xho*I-hNIS-*reverse*	C*CTCGAG*GTCAGAGGTTTGTCTCCTGCTGGTCTCG	N/A
*Xho*I-Right308-*reverse*	*CTCGAG*CCAGCCGGGGAGAAAGGACTGTGT	32959-32983
*Xho*I-Right844-*reverse*	*CTCGAG*CACGTGGGTTCTGTGGTCC	33469-33487

[a] PCR primers are listed alphabetically. Nucleotide (nt) numbers refer to the primer binding region of the Ad5 genome based on Human Adenovirus C serotype 5 (AY:339865.1). Engineered restriction sites are underlined and in italics. Introduced mutations are highlighted in bold and deletions are indicated by an asterisk (*). N/A refers to primers which bind to sequences in shuttle vectors, or modified Ad5 constructs.

TABLE 9. Primers Used for Sequencing[a]

Primer Name	Sequence 5'→3'	Ad5 Region (nt)
Ad5-*reverse*	CCCATGATATGATGCTTTTTAAGG	32983-33006
Ad5.2-*reverse*	CTGCGCTTGTGGTATGATG	33490-33508
Ad5.3-*reverse*	GGCTGGAATGCAGTCTACTTC	29860-29880
AdinPCR-*forward*	CCAAAAGTAACATTGTCAGTCAAG	32571-32594
AdinPCR-*reverse*	GCAATGTATGAAAAAGTGTAAGAG	32749-32772
AdSeq-*forward*	GCCTATACAAACGCTGTTGG	32504-32523
AdSeq-*reverse*	CCAACAGCGTTTGTATAGGC	32504-32523
BGH-*reverse*	TAGAAGGCACAGTCGAGG	pcDNA3.1/V5-HIS-TOPO
E1ASeq-*forward*	CTTGAGTGCCAGCGAGTAGAGTTTTC	502-527
E1ASeq-*reverse*	GTTAACCAAGTCCTCGATACATTCCAC	1471-1497
E3Seq-*forward*	GACCTCAATAACTCTGTTTACCAG	28453-28476
E3Seq-*reverse*	GAGATAGGAGATGGCATAGAAG	28137-28145
EGFP-*forward*	CCCACCATGGTGAGCAAGG	pIP5-EGFP
EGFP-*reverse*	GACTTGTACAGCTCGTCCATG	pIP5-EGFP
FibreUp-*forward*	GCAACGCTGTTGGATTTATG	32513-32530
FibreUp4-*forward*	CATCCGCACCCACTATCTTCA	31005-31025
FibreDown-*reverse*	GTGTAAGAGGATGTGGCAAAT	32737-32757
LC-*forward*	GAATTTGGTTCACCTAATGC	32069-32088
LC-*reverse*	GGTTTAGGATGGTGGTGG	33625-33642
pQE-*forward*	CGGATAACAATTTCACACAG	pQE30 derivatives
pQE-*reverse*	GTTCTGAGGTCATTACTGG	pQE30 derivatives
T3-*forward*	AATTAACCCTCACTAAAGG	pGV1 derivatives
T7-*forward*	TAATACGACTCACTATAGGG	pcDNA3.1/V5-HIS-TOPO
T7-*reverse*	GTAATACGACTCACTATAGGGC	pGV1 derivatives

[a] Sequencing primers used in this study are listed alphabetically. Nucleotide (nt) numbers refer to the primer binding region in the Ad5 genome, based on Human Adenovirus C serotype 5 (AY:339865.1). Alternatively, the vector backbone for various sequencing applications is listed.

Section.2.3 Construction of Shuttle Plasmids for Adenovirus Genome Modifications

Restriction digestion and PCR reactions were carried out by standard molecular biology techniques, as described in *Section*.2.2. PCR primers used in the construction of shuttle vectors are listed in *Table*.8, and sequencing primers listed in *Table*.9. All primers were supplied by Sigma-Genosys. All plasmids constructed were verified by sequencing. DNA was amplified by miniprep following transformation into chemically competent DH10B bacteria, as described previously (*Section*.2.2.10).

2.3.1 URA3 Integrating Shuttle Vector pGV1. All shuttle vectors constructed in this study were assembled using the pGV1 construct as a backbone. A restriction map of pGV1 is presented in *Fig*.2.2A. This construct is a URA3 [Orotidine-5'-phosphate (OMP) decarboxylase] integrating shuttle vector, based on a pRS406 (Accession number: U03446) construct in which the ARS/CEN (Autonomously replicating sequence/Centromere sequence) and yeast replication elements have been removed. In addition, the *Hind*III site within the multicloning site (MCS) was inactivated by mutagenesis and the vector renamed pGV1 (Vassaux *et al.*, 1997).

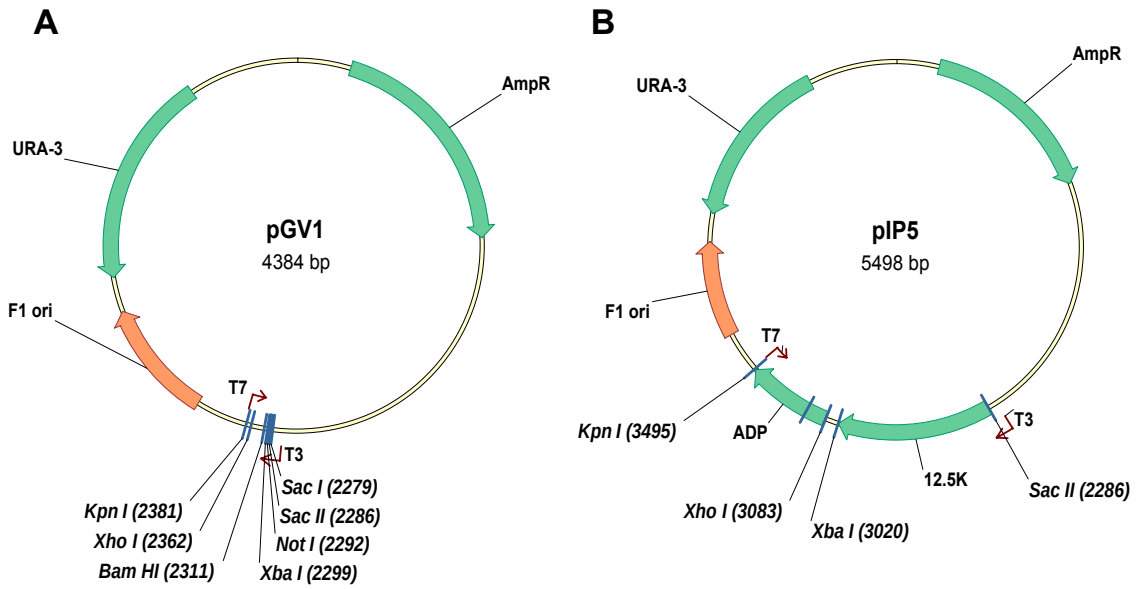

***Figure*.2.2 Restriction Map for URA-integrating Shuttle Vectors. (A)** Restriction map for pGV1 (URA3 integrating shuttle vector). Binding sites for sequencing primers, T3-*forward* and T7-*reverse,* are highlighted as arrows (T3/T7). **(B)** Restriction map of pIP5 showing the sites where Ad5 sequence, corresponding to E3-region genes *12.5K* and *ADP*, was cloned into the pGV1 backbone. Vector maps are to scale and the multi-cloning site (MCS) shows all restriction sites used for cloning strategies described in this study. Restriction maps were generated using VectorNTI Software (VectorNTI Advance 10, Academic Version, Invitrogen) from sequences generated, and stored in the database by the licence holder.

2.3.2 E3 Region Modification; Construction of pIP5. The pIP5 vector was constructed previously in the Vassaux Laboratory (Merron *et al.*, 2007; Peerlinck *et al.*, 2008). A restriction map is presented in *Fig.*2.2B. Homologous Ad5 sequence flanking the non-essential E3 region gene, *gp19K,* was amplified by PCR from Ad5 template DNA (pMB20; provided by Richard Iggo). Sequence spanning the E3 region *12.5K* gene (nt27793-28524) was amplified by primers, *Sac*II-12.5K-*forward* and *Xba*I-12.5K-*reverse*, introducing engineered *Sac*II/*Xba*I restriction sites. Nucleotide sequence spanning E3 *ADP* (nt29349-29750) was amplified using engineered primers, *Xho*I-ADP-*forward* and *Kpn*I-ADP-*reverse*. Nucleotide numbers refer to the sequence location within the Ad5 genome (Accession number: AY339865). The PCR products were gel purified using QIAquick® Gel Extraction Kit 50 (Qiagen®), and DNA eluted in 30µl of H_20. Purified DNA was ligated into pcDNA3.1/V5-HIS©-TOPO® (Invitrogen™), to create p12.5K-TOPO and pADP-TOPO. Both genes were transferred into the multi cloning site (MCS) of pGV1 by sequential rounds of subcloning. Firstly, *Sac*II/*Xba*I restriction digestion of pGV1 and p12.5K-TOPO generated pGV1-12.5K, and subsequently *Xho*I/*Kpn*I digestion of pGV1-12.5K and pADP-TOPO generated pGV1-12.5K-ADP. This E3 integrating shuttle vector was renamed pIP5.

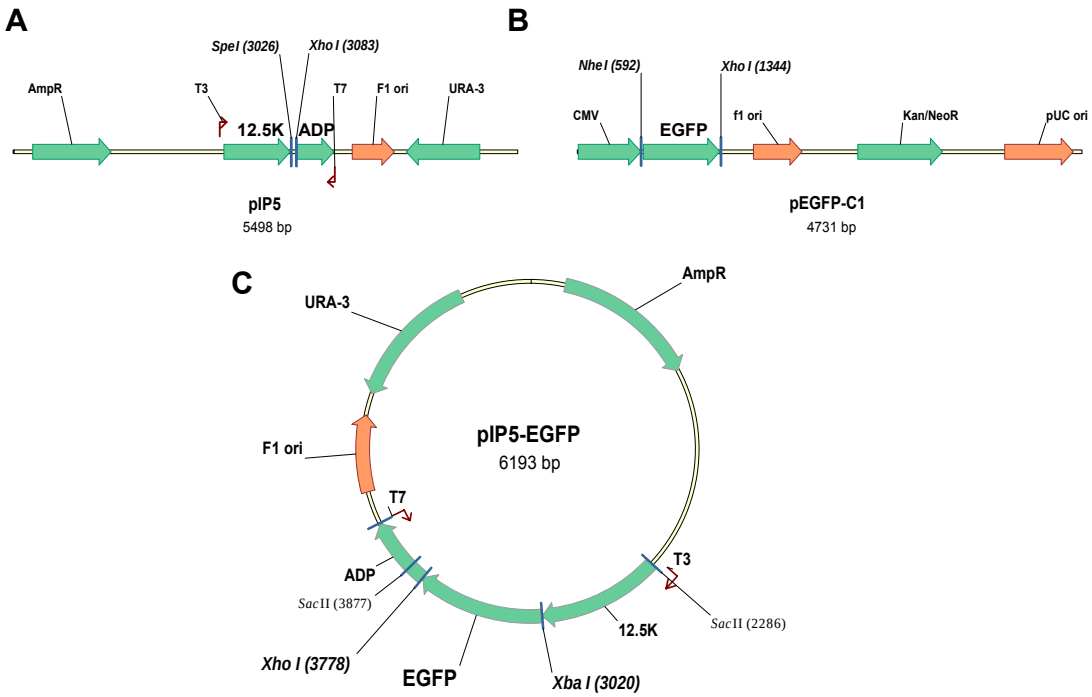

***Figure*.2.3 Cloning Strategy used to Generate Shuttle Vector, pIP5-EGFP. (A)** The pIP5 backbone was digested with *Spe*I/*Xho*I. **(B)** In parallel, pEGFP-C1 was digested with *Nhe*I/*Xho*I to release the EGFP fragment. **(C)** *Spe*I and *Nhe*I digestion created compatible, cohesive ends, permitting their ligation. Therefore, pIP5-EGFP was generated by ligation of *Nhe*I/*Xho*I-digested EGFP into *Spe*I/*Xho*I-digested and dephosphorylated pIP5. Vector maps (linear/circular representation) are to scale and the multi-cloning site (MCS) and restriction sites used in this cloning strategy are displayed. Restriction maps were generated using VectorNTI Software (VectorNTI Advance 10, Academic Version, Invitrogen) from sequences generated, and stored in the database by the licence holder.

2.3.3 E3 Region Modification; Construction of pIP5-EGFP. The gene for Enhanced Green Fluorescent Protein (EGFP) was cloned into *Spe*I/*Xho*I digested pIP5, following compatible *Nhe*I/*Xho*I digestion from pEGFP-C1 (Clontech). A schematic overview of the cloning strategy is shown in *Fig.*2.3. The pIP5 backbone, and *EGFP* insert were purified using the Qiagen QIAquick® Gel Extraction Kit, the backbone dephosphorylated using *Antarctic Phosphatase (*NEB) and overnight ligations transformed into chemically competent DH10B. Plasmid DNA was extracted, purified and successful ligations confirmed by restriction digestion, and sequencing using T3-*forward* and T7-*reverse* primers.

2.3.4 Fibre Region Modification; Construction of p*IV*$_{Sfo\text{I}}$. Adenoviral homologous sequence flanking the site within the *fibre* (*IV*) gene which was selected for heterologous A20FMDV2 DNA insertion, was cloned from pAdEasy-1 adenoviral template DNA (nt32674-32675). A schematic of the cloning strategy used can be found in *Fig.*2.4. The upstream fragment of the *IV* (Left/L), corresponding to nucleotides 32126-32674, was amplified using *Not*I-Left-*forward* and *Bam*HI-*Sfo*I-Left-*reverse* primers which introduced engineered restriction sites, *Not*I and *Bam*HI-*Sfo*I, at the 5' ends, respectively. The downstream *IV* fragment (Right/R), corresponding to nucleotides 32675-32982, was amplified in the same way, using *Sfo*I-Right-*forward* and *Xho*I-Right308-*reverse* primers introducing restriction sites, *Sfo*I and *XhoI,* respectively. PCR products were purified following gel excision and were ligated separately into pcDNA/V5-HIS©-TOPO®, creating p*IV***L**-TOPO and p*IV***R**308-TOPO.

A further post gel excision incubation step for 10mins at 72°C with an excess of dNTPs was required to enhance subsequent TOPO ligation efficiency. These constructs were confirmed by sequencing with T7-*forward* and BGH-*reverse* primers. The final p*IV* shuttle vector was assembled by successive rounds of subcloning. Firstly, sequence confirmed p*IV***L**-TOPO and pGV1 were *Not*I/*Bam*HI digested in parallel and the p*IV***L** fragment ligated into the MCS of the pGV1 shuttle following gel excision purification, dephosphorylation and ligation. This vector was named pGV1-*IV***L** and was again sequenced with T3-*forward*, and T7-*reverse* sequencing primers. The second round of subcloning involved the parallel *Sfo*I/*Xho*I digestion of pGV1-*IV***L** and the previously constructed p*IV***R**308-TOPO. This process resulted in the successful assembly of a shuttle vector, p*IV*$_{Sfo\text{I}}$ containing a unique blunt end restriction site (*Sfo*I) at the site identified for insertion of heterlogous DNA, thus facilitating cloning of any potential oligoduplex ligand, by blunt end ligation. The sequence confirmed final construct was bulked up by QIAprep® Maxiprep DNA extraction.

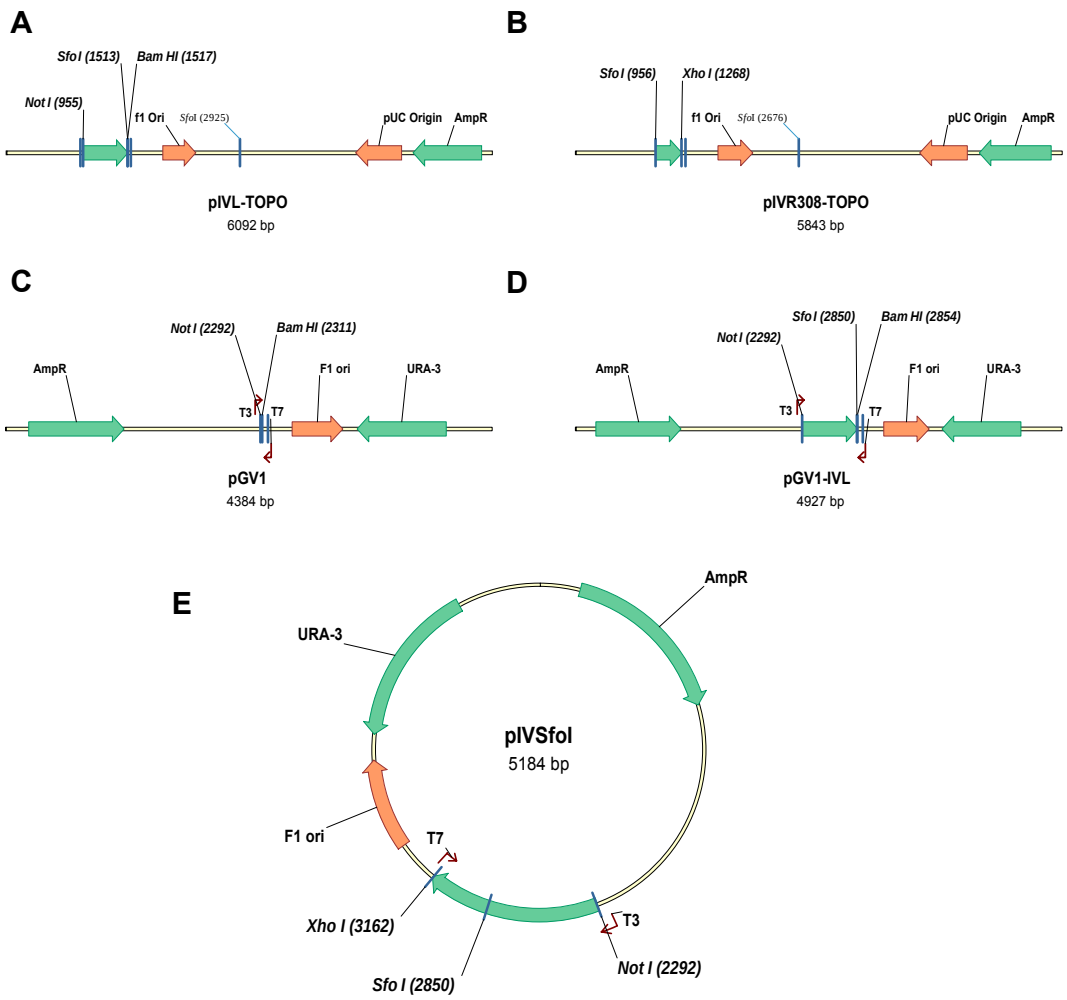

***Figure.*2.4 Cloning Strategy used to Generate HI-loop modifying Shuttle Vector, p*IV*$_{SfoI}$. (A)** Intermediate holding vector p*IV*L-TOPO was created by TA cloning of a 5'-*Not*I, and 3'- *Bam*HI-*Sfo*I engineered PCR product. **(B)** The same strategy was used to create p*IV*R308-TOPO, from a 5'-*Sfo*I, 3'-*Xho*I engineered PCR product. **(C)** The final vector, p*IV*$_{SfoI}$, was assembled by two sequential rounds of subcloning. The pGV1 backbone and the intermediate holding vector, p*IV*L-TOPO, were *Not*I/*Bam*HI digested simultaneously. **(D)** The released fragment, *IV*L, was ligated into pGV1, to create pGV1-*IV*L. This construct was sequenced before the final round of subcloning. The pGV1-*IV*L backbone and the intermediate holding vector, p*IV*R308-TOPO, were *Sfo*I/*Xho*I digested simultaneously. **(E)** The released fragment, *IV*R308, was ligated into pGV1-*IV*L to generate the final construct, p*IV*$_{SfoI}$, creating a unique blunt end restriction site (*Sfo*I) within the fibre sequence. Vector maps (linear/circular representation) are to scale and the multi-cloning site (MCS) and restriction sites used in the cloning strategy are displayed. Restriction maps were generated using VectorNTI Software (VectorNTI Advance 10, Academic Version, Invitrogen).

2.3.5 Fibre Region Modification; Construction of p*IV*$_{A20}$. A strategic overview of the construction of this vector is shown in *Fig.*2.5. Terminally phosphorylated, HPLC purified, complementary oligonucleotides, spanning the RGDLXXL motif within the VP1 viral surface protein of Foot and Mouth Disease Virus (FMDV) were obtained from SIGMA-Genosys (corresponding to nucleotides 3680-3739 of FMDV; AY593816). Sense, and antisense oligonucleotides, 5'-AATGCTGTGCCCAACTTGAGAGGTGACC

TTCAAGTGTTGGCTCAAAAGGTGGCACGGACG-3' and 5'-CGTCCGTGCCACCTTT TGAGCCAACACTTGAAGGTCACCTCTCAAGTTGGGCACAGCATT-3' at 1μM each were annealed together in a 50μl reaction volume with 1X annealing buffer (2X: 200mM Potassium Acetate, 60mM HEPES-KOH pH7.4 and 4mM Magnesium Acetate), and were incubated at 95°C for 4mins followed by 70°C for 10mins. This was followed by subsequent reduction in temperature of 5°C every 5mins until 4°C was reached. The duplex oligonucleotides were diluted 1:20 and 1μl of the dilution ligated to 100ng of *Sfo*I digested, dephosphorylated, pIV_{SfoI} in a final volume of 10μl, by blunt end ligation. The ligation reaction was incubated overnight at 16°C, after which 2μl were used to transform chemically competent DH10B. Bacterial cultures harvested by centrifugation and plasmid DNA extracted from the pellet. Samples were screened by PCR using A20-*forward*/AdinPCR-*reverse* for the presence of the insert, in conjunction with a further PCR screening using AdinPCR-*forward*/AdinPCR-*reverse*, to detect a 60bp size difference when analysed on a 2% agarose gel. Successful constructs were confirmed again by sequencing with T3-*forward*, T7-*reverse*, AdinPCR-*forward* and AdinPCR-*reverse*, and were renamed pIV_{A20}.

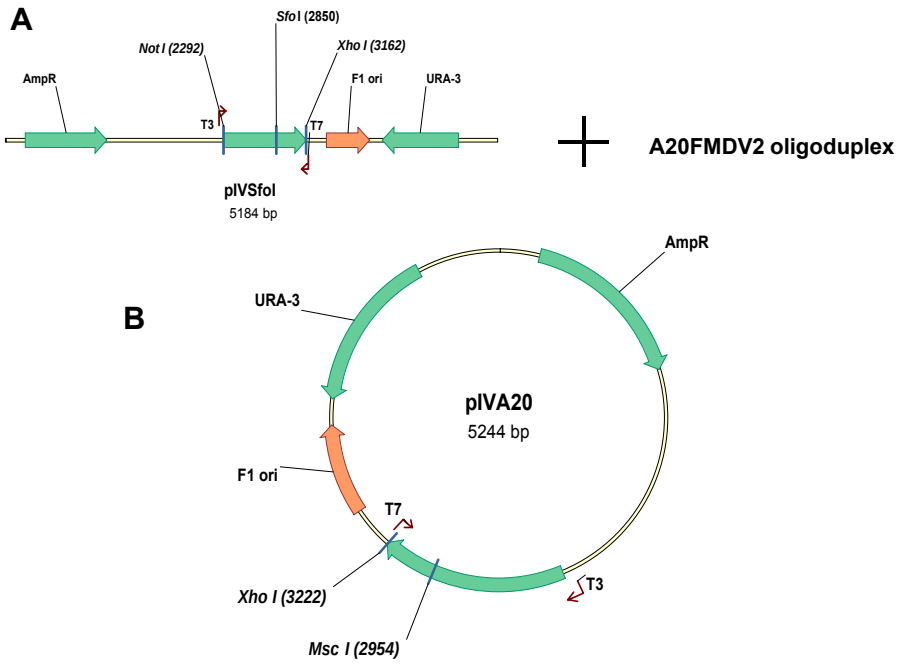

***Figure.*2.5 Cloning Strategy used to Generate the A20FMDV2 Fibre modified Shuttle Vector, pIV_{A20}.** **(A)** Shuttle vector, pIV_{SfoI}, was linearised with a unique blunting restriction enzyme, *Sfo*I, and was dephosphorylated. **(B)** A terminally phosphorylated oligoduplex, with sequence corresponding to the αvβ6-binding RGDLXXL domain from Foot and Mouth Disease Virus (FMDV), was ligated into *Sfo*I digested pIV_{SfoI}, by blunt end ligation to create pIV_{A20}. Vector maps (linear/circular representation) are to scale and the multi-cloning site (MCS) and restriction sites used at each step in the cloning strategy are displayed. Restriction maps were generated using VectorNTI Software (VectorNTI Advance 10, Academic Version, Invitrogen).

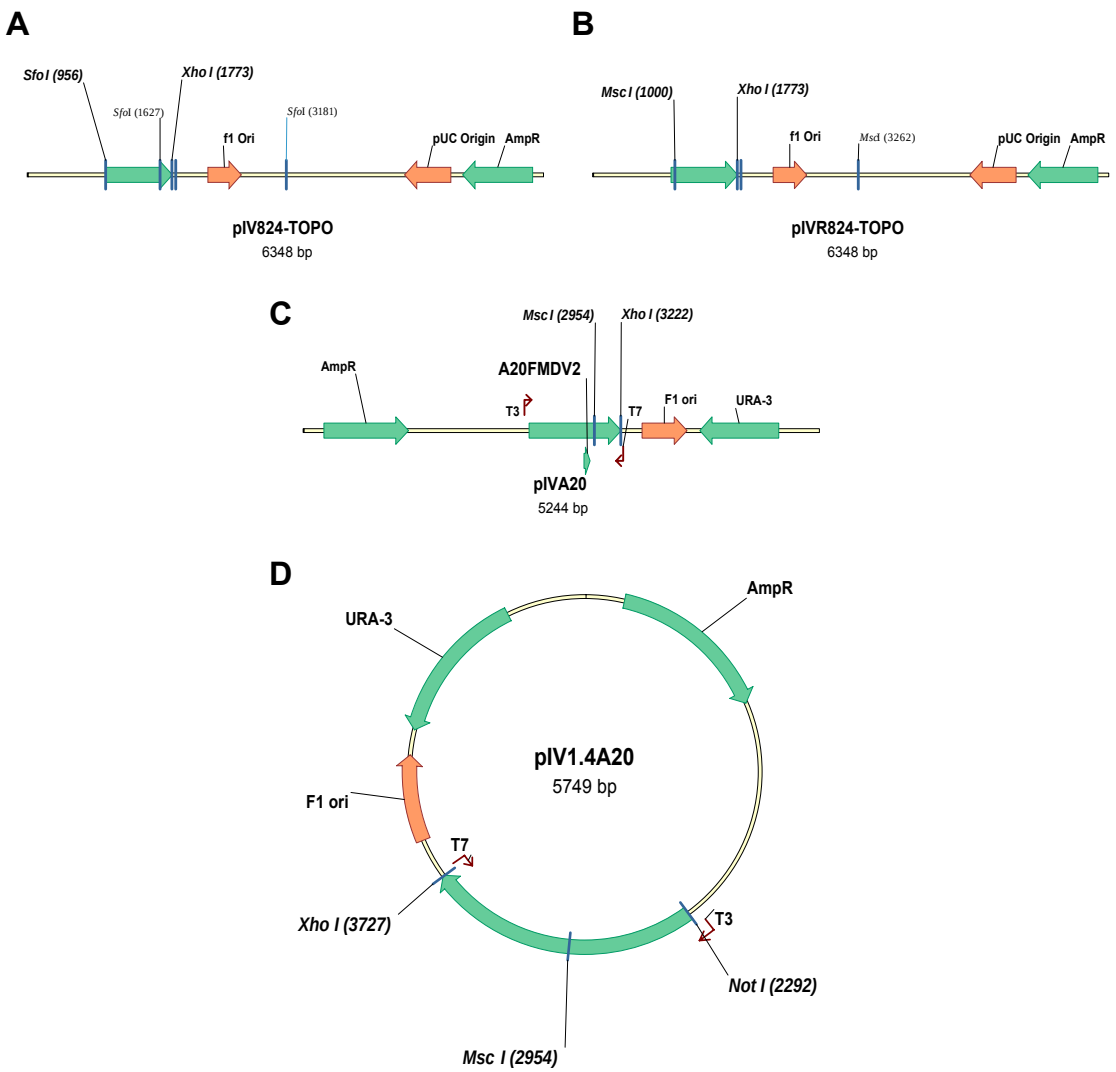

***Figure.*2.6 Cloning Strategy used to Generate the extended A20FMDV2 Fibre modified Shuttle Vector, p*IV*1.4$_{A20}$.(A)** An extended, 1.4kb, *IV*R fragment was generated by PCR using a similar strategy to that used to create p*IV*R308-TOPO. The *Xho*I-reverse primer used in this strategy amplified a larger fragment (844bp instead of 308bp), and therefore this intermediate holding vector was named p*IV*844-TOPO. However, the extended region featured an additional, internal *Sfo*I site, which was not compatible with the downstream cloning strategy. **(B)** An alternative cloning strategy using *Msc*I/*Xho*I was employed. p*IV*$_{A20}$ was *Msc*I/*Xho*I digested in parallel with p*IV*R824-TOPO, and the *IV*R308 fragment substituted for the extended *IV*R844 fragment. **(C)** The final extended version of the p*IV*$_{A20}$ shuttle construct was named p*IV*1.4$_{A20}$. Vector maps (linear/circular representation) are to scale and the multi-cloning site (MCS) and restriction sites used at each step in the cloning strategy are displayed. Restriction maps were generated using VectorNTI Software (VectorNTI Advance 10, Academic Version, Invitrogen).

2.3.6 Fibre Region Modification; Construction of p*IV*1.4$_{A20}$. An extended, downstream *IV*-R fragment (nt32675-33487) was cloned by PCR from pAdEasy-1 template DNA, using the existing primer *Sfo*I-Right-*forward*, in combination with a new reverse primer *Xho*I-Right824-*reverse*, which again introduced engineered restriction sites *Sfo*I and *Xho*I, to facilitate further subcloning into the URA3 integrating shuttle

vector. A schematic overview of the cloning strategy is presented in *Fig.*2.6. The 824bp PCR product was purified following gel excision and ligated into pcDNA/V5-HIS©-TOPO®. Constructs were confirmed by sequencing with T7-*forward*/BGH-*reverse* primers. Successful constructs were named p*IV***R**$_{824}$-TOPO. However, sequencing of p*IV*R$_{824}$-TOPO revealed the presence of a second *Sfo*I site within the fibre sequence, which was not compatible with the planned cloning strategy. Therefore, the final construct, p*IV*1.4$_{A20}$ was assembled by parallel *Msc*I/*Xho*I restriction digestion of p*IV*$_{A20}$/p*IV***R**$_{824}$-TOPO and ligation of the p*IV***R**$_{824}$ fragment into the linearised p*IV*$_{A20}$ shuttle, thus extending it. This newly constructed shuttle was sequenced with primers T3-*forward*, T7-*reverse*, AdSeq-*forward* and -*reverse*, and was renamed p*IV*1.4$_{A20}$.

2.3.7 Fibre Region Modification; Construction of p*IV*-477*dl*TAYT$_{A20}$ and p*IV*-485*dl*TAYT$_{A20}$. In order to introduce CAR-binding ablating mutations, or putative blood factor binding deletions, the p*IV*1.4$_{A20}$ shuttle vector was modified further. A schematic overview of the cloning strategy is presented in *Fig.*2.7. CAR-binding mutations Y477A and L485K were combined with a TAYT deletion (*dl*TAYT) and constructed as follows; pKnob477*dl*TAYT$_{WT/A20}$-TOPO and -485*dl*TAYT$_{WT/A20}$-TOPO constructs (described in *Section*.2.4.4), were used as templates for subcloning, to transfer the respective modifications into p*IV*1.4$_{A20}$. Two single restriction sites were identified within the fibre sequence of p*IV*1.4$_{A20}$, *Pfl*MI and *Msc*I, sites which were common to the fibre sequence contained within the pKnob477*dl*TAYT$_{A20}$-TOPO and -485*dl*TAYT$_{A20}$-TOPO constructs. In addition, these sites flanked the region containing the introduced mutations. Therefore, a *Pfl*MI/*Msc*I subcloning strategy was used to transfer the 388bp, 477*dl*TAYT$_{A20}$ or 485*dl*TAYT$_{A20}$ fragment into p*IV*1.4$_{A20}$ shuttle, in place of the corresponding 400bp fragment. Recognition of the *Pfl*MI site can be blocked by *dcm* methylation. Therefore, the sequence of the *Pfl*MI sites within all vectors to be digested were checked to ensure that they did not contain the internal cytosine residues required for *dcm* methylation. Digested fragments were ligated into *Pfl*MI/*Msc*I digested and dephosphorylated backbone, p*IV*1.4$_{A20}$. Successful clones were verified by sequencing using T3-*forward* and T7-*reverse* sequencing primers.

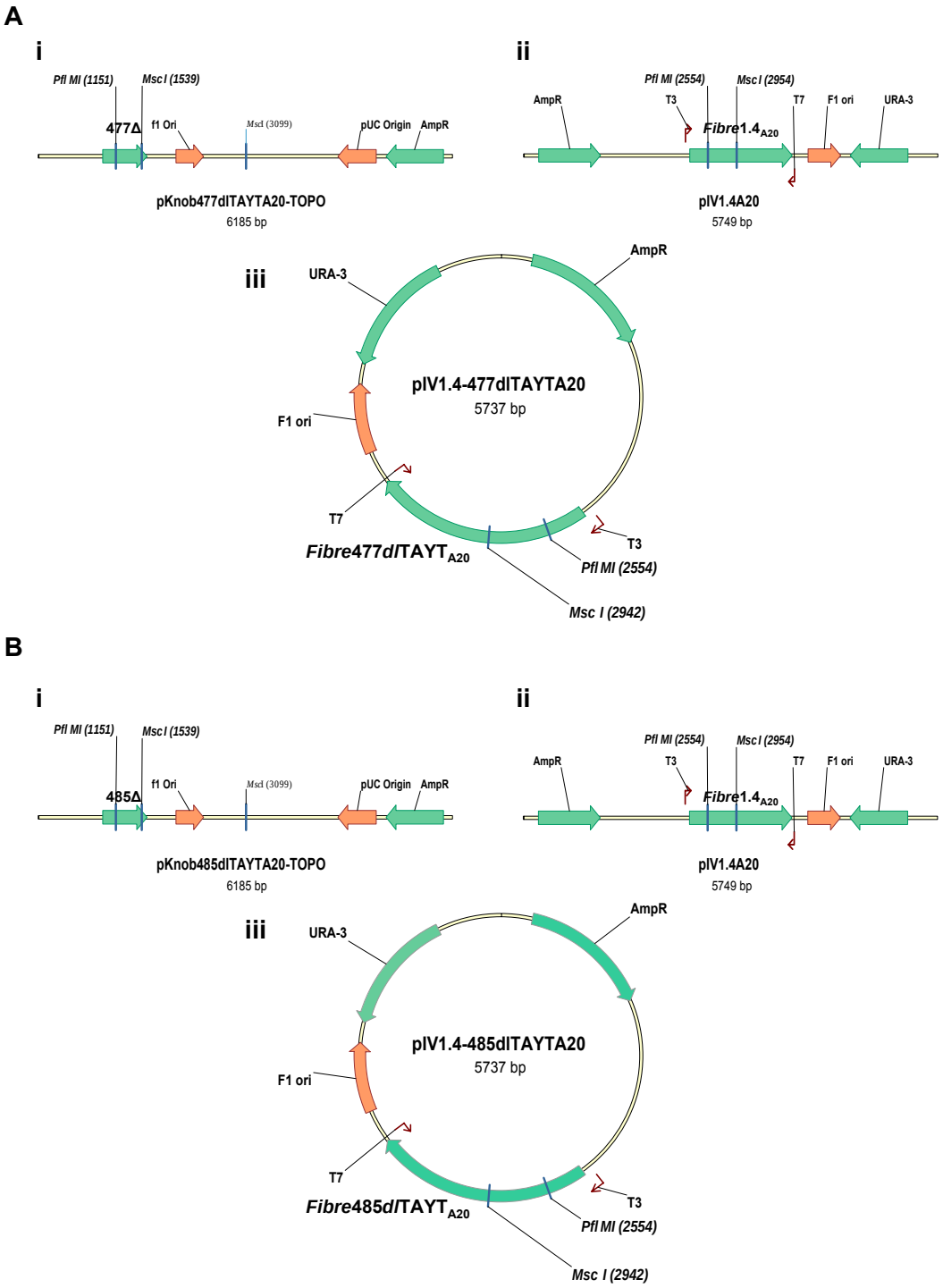

***Figure.*2.7 Cloning Strategy used to Generate Blood Factor Binding Ablated and *Fibre* Modifying Shuttle Vectors, p*IV*477*d*ITAYT$_{A20}$ and p*IV*485*d*ITAYT$_{A20}$. (A) i** Intermediate TA holding vector, pKnob477*d*ITAYT$_{A20}$ was generated previously and is described in *Section*.2.4.4. Two restriction sites, *Pfl*MI/*Msc*I, were identified which were compatible with subcloning of the 477*d*ITAYT mutation into the p*IV*1.4$_{A20}$ shuttle vector. **ii)** Backbone p*IV*1.4$_{A20}$ and pKnob477*d*ITAYT$_{A20}$ were digested simultaneously with *Pfl*MI/*Msc*I. **iii** Ligation of the 477*d*ITAYT fragment into p*IV*1.4$_{A20}$ resulted in a *fibre* modifying shuttle vector which was renamed p*IV*1.4-477*d*ITAYT$_{A20}$. (**B) i** An identical strategy using pKnob485*d*ITAYT$_{A20}$ and **ii** p*IV*1.4$_{A20}$ digested simultaneously with *Pfl*MI/*Msc*I, resulted in the generation of **iii** p*IV*1.4-485*d*ITAYT$_{A20}$. Vector maps (linear/circular representation) are to scale and the multi-cloning site (MCS) and restriction sites used at each step in the cloning strategy are displayed. Restriction maps were generated using VectorNTI Software (VectorNTI Advance 10, Academic Version, Invitrogen).

2.3.8 Fibre Region Modification; Construction of p*IV*-477*dl*TAYT$_{6XHIS}$ and p*IV*-485*dl*TAYT$_{6XHIS}$. In order to construct non-retargeted, but CAR/blood factor binding ablated Ad5 mutants, shuttle vectors were generated which featured a 6XHIS epitope in place of A20FMDV2. The presence of the 6XHIS epitope permits the amplification of these mutant viruses on 293.HissFv.rec cells, HEK293 cells which have been stably transfected with an anti-HIS scFv (Douglas *et al.*, 1999). Once again, SOEing PCR was used to assemble these constructs, using the pKnob477*dl*TAYT$_{A20}$-TOPO and -485*dl*TAYT$_{A20}$-TOPO vectors as template DNA (see *Section*.2.4.4). The PCR-A fragment was amplified using primers, F5Knob-*forward* and Mut6XHIS-*reverse*, and the PCR-B fragment was amplified using Mut6XHIS-*forward* and F5Knob-*reverse*. The Mut6XHIS primers were designed so that they were compatible with both the 477, and 485 templates. The final PCR-AB fragment for each was amplified in Step 3 using F5Knob-*forward* and F5Knob-*reverse*, and products cloned into pcDNA/V5-HIS©-TOPO®(Invitrogen™). Constructs were renamed accordingly (eg. pKnob477*dl*TAYT$_{6XHIS}$-TOPO) and sequenced. Subcloning into the p*IV*1.4$_{A20}$ shuttle was once again achieved by *Pfl*MI/*Msc*I digestion, substituting the A20-containing fragment for the corresponding 6XHIS-containing fragment.

*Section.*2.4 Construction of Expression Vectors and Recombinant Protein Production

Vector constructs were generated using standard molecular biological techniques. Primers used for PCR, and sequencing are listed in *Table*.8 and *Table*.9, respectively. Adenoviral *fibre* sequence corresponding to the knob domain, plus the first seven residues of the polylysine repeat motif (nt32195-32782), was cloned by PCR from pAdEasy-1 adenoviral template DNA for wildtype $Knob_{WT}$, and from p*IV*1.4_{A20} for A20-modified $Knob_{A20}$ using a previously described strategy (Krasnykh *et al.*, 1996). PCR primers, F5Knob-*forward* and F5Knob-*reverse*, were designed to introduce engineered *Bam*HI/*Hind*III restriction sites, facilitating directional cloning into the pQE30 expression vector (Qiagen®). Restriction digestion and ligation reactions were set up as previously described and DNA extracted by standard QIAprep® Spin Miniprep Kit (Qiagen®). All constructs were screened by sequencing with the pQE Sequencing-Primer Set (Qiagen®) using pQE30-SeqIII/IV-*forward* and pQE30-Seq-*reverse* primers to ensure that inserts were in frame with the N-terminal 6XHIS tag.

2.4.1 pQE30$Knob_{WT}$. PCR amplification of the WT knob domain of the Ad5 *fibre* gene resulted in a product of 628bp. The PCR product was purified by QIAquick® Gel Extraction (Qiagen®) and the insert ligated into pcDNA/V5-HIS©-TOPO® (Invitrogen™) by standard protocol, to create pTOPO$Knob_{WT}$. Constructs were sequenced using T7-*forward*/BGH-*reverse* primers supplied by the manufacturer. Subcloning of $Knob_{WT}$ into the pQE30 expression vector was achieved by parallel *Bam*HI/*Hind*III restriction digestion of pQE30/pTOPO$Knob_{WT}$, separation and identification of the ~3.4kbp/628bp bands by gel electrophoresis, and their purification following gel excision. Ligation reactions were set up as described previously, pQE-$Knob_{WT}$ constructs sequence confirmed and transformed into competent SG13009 *E.coli* (Qiagen®), harbouring the pREP4 repressor plasmid, for subsequent protein expression.

2.4.2 pQE30$Knob_{A20}$. PCR amplification of the A20-modified knob of the Ad5 *fibre* (from p*IV*1.4_{A20}) resulted in a product of 694bp, which was purified as described above. The insert was again ligated into pcDNA/V5-HIS©-TOPO® (Invitrogen™), to generate pTOPO$Knob_{A20}$, which was confirmed by sequencing, as above. Subcloning into the pQE30 expression vector was also achieved by parallel *Bam*HI/*Hind*III restriction digestion of pQE30/pTOPO$Knob_{A20}$ and purification of the respective bands following gel excision.

2.4.3 pQE30KnobΔCAR$_{WT}$ and pQE30KnobΔCAR$_{A20}$. Sequence confirmed pQE30Knob$_{WT}$ /pQE30Knob$_{A20}$ constructs were used as templates for mutagenic PCR as described previously (*Section*.2.2.5). Mutagenic primers, MutL485K-*forward* and –*reverse*, or MutY477A-*forward* and –*reverse*, were used to introduce point mutations at sites thought to be critical for CAR binding (Kirby *et al*., 2000). Following *Dpn*I digestion of PCR products, 2µl were used to transform competent DH10B, DNA extracted by standard methods, and samples sequenced and verified. Successful clones were transformed into SG13009 (pREP4) *E.coli*, which had been made chemically competent, in preparation for protein expression. These were selected on LB agar supplemented with Amp/Kan [100µg/ml/25µg/ml]. Constructs were renamed accordingly; pQEKnobY477A$_{WT/A20}$ or pQEKnobL485K$_{WT/A20}$.

2.4.4 pQE30Knob477*dl*TAYT$_{A20}$ and pQE30Knob485*dl*TAYT$_{A20}$. The CAR-binding mutant pQE-Knob constructs described above were further modified to incorporate a 4 amino acid deletion (*dl*TAYT). This modification, in combination with the Y477A mutation and a FLAG peptide insertion, has been reported to reduce binding to serum/coagulation factors, FIX and C4BP (Gaggar *et al.*, 2007; Shayakhmetov *et al.*, 2005b). These constructs were generated using a SOEing PCR strategy (see *Fig*.2.1). In Step 1, the PCR-A fragments were amplified using primers F5Knob-*forward* in combination with either *dl*TAYT477-*reverse*, or *dl*TAYT485-*reverse*, for pQE30Knob$_{WT}$ and pQEKnob$_{A20}$, respectively. The PCR-B fragments were amplified using *dl*TAYT-*forward* and F5Knob-*reverse*, which were designed so that they were suitable for all strategies (ie. 477 or 485, WT or A20). All PCR-AB fragments were amplified in Step 3 using F5Knob-*forward* and F5Knob-*reverse* and the final products cloned individually into pcDNA/V5-HIS©-TOPO® (Invitrogen™). Constructs were renamed accordingly (ie. pKnob477*dl*TAYT$_{A20}$-TOPO) and sequenced.

However, the Y477A mutation resulted in the introduction of an additional *Hind*III site within the Knob477*dl*TAYT$_{A20}$ fragment, and therefore subcloning into pQE30 could not be achieved using the standard *Bam*HI/*Hind*III strategy (*Fig.*2.8A). Conveniently, the desired Knob modifications were flanked on either side by the original, and introduced *Hind*III sites. Therefore, a single *Hind*III digestion strategy was used to subclone the Knob477*dl*TAYT$_{A20}$ fragment from pKnob477*dl*TAYT$_{A20}$–TOPO into the previously constructed pQEKnob477$_{A20}$ vector, which also contained the extra *Hind*III site (see *Section*.2.4.3).

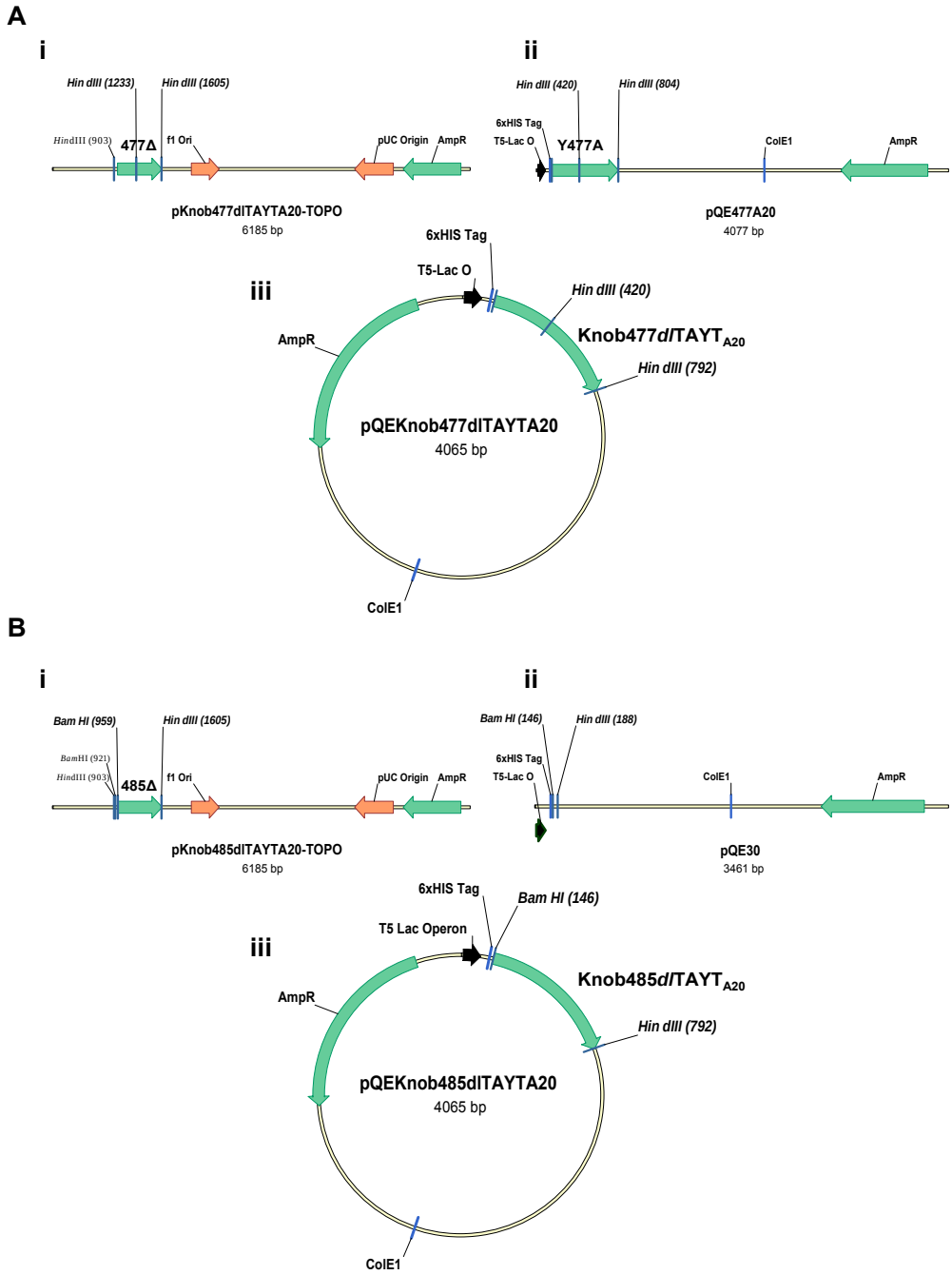

***Figure.*2.8 Cloning Strategy Used to Generate Blood Factor Binding Ablated and Fibre Modifying Expression Vectors, pQEKnob477*d*ITAYT$_{A20}$ and pQEKnob485*d*ITAYT$_{A20}$. (A) i** Intermediate holding vector, pKnob477*d*ITAYT$_{A20}$ was generated previously, and is described in *Section.*2.4.4. The mutagenesis strategy (Y477A) resulted in the generation of an additional, internal *Hind*III site. Therefore a HindIII cloning strategy was used, instead of *Bam*HI/*Hind*III, to transfer the 477*d*ITAYT$_{A20}$-containing fragment to the pQE30 expression vector. **ii** The pQE477$_{A20}$ vector also features the additional *Hind*III site Therefore, this vector was used as a backbone for *Hind*III-mediated ligation of the -477*d*ITAYT$_{A20}$ fragment. **iii** This resulted in the generation of the pQEKnob477*d*ITAYT$_{A20}$. (**B) i** Intermediate holding vector, pKnob485*d*ITAYT$_{A20}$ was generated previously. **ii** Expression vector pQE30 was used as the backbone for the *Bam*HI/*Xho*I subcloning of the -485dITAYT$_{A20}$ fragment. **iii** The final construct was renamed pQEKnob485*d*ITAYT$_{A20}$. Vector maps (linear/circular representation) are to scale and the multi-cloning site (MCS) and restriction sites used at each step in the cloning strategy are displayed. Restriction maps were generated using VectorNTI Software (VectorNTI Advance 10, Academic Version, Invitrogen).

The desired *Hind*III fragment (372bp), released by digestion, was separated from a similarly sized fragment (330bp) by gel electrophoresis on a 2% agarose gel. Subcloning of the Knob485*dl*TAYT$_{A20}$ fragment from the –TOPO holding vector, to the pQE30 expression vector, was achieved by *Bam*HI/*Hind*III digestion (*Fig*.2.8B). Constructs were renamed accordingly; pQEKnob477*dl*TAYT$_{A20}$ or pQEKnob485 *dl*TAYT$_{A20}$. A ClustalW protein alignment highlighting the differences between Knob$_{WT}$, Knob$_{A20}$ and Knob477*dl*TAYT$_{A20}$/Knob485*dl*TAYT$_{A20}$ can be found in *Appendix II.*

2.4.5 Recombinant Protein Expression and Purification. Protein expression and purification was optimised at the Protein Isolation and Cloning Lab at 44 Lincoln Inn Fields (CR-UK). SG13009, pQE30Knob-containing pre-cultures were grown overnight in 1L Terrific Broth [1.2 % (w/v) Tryptone, 2.4 % (w/v) Yeast Extract, 0.4% (v/v) Glycerol], supplemented with 100ml Potassium phosphate salt solution and Amp (100µg/ml) and Kan (25µg/ml). A 10% inoculum was added to a large scale culture which was grown at 37°C until an OD_{600nm}=0.6 was reached (~5hrs). Protein expression was induced for 2-3hrs on addition of Isopropyl β-D-1-thiogalactopyranoside (IPTG) to a final concentration of 0.5-1.0mM. Induced cultures were harvested by centrifugation at 4000rpm for 15mins, pellets frozen and stored at -80˚C. The following day IPTG-induced 1L pellets were resuspended in 50ml of freshly made Lysis buffer pH7.9 [50mM Tris-HCl, 300mM NaCl, 1% (w/v) NP40 (Fluka Biochemika), 10mM Imidazole (Sigma, UK), 1mM β-mercaptoethanol and 0.1% (v/v) Lysozyme (Sigma)], with 1µg/ml DNAse and agitated on a roller at 4°C for 1hr. Cells were pelleted by ultracentrifugation at 30,000g for 20mins using a Beckman 35Tii rotor in an Optima L-80 XP Ultracentrifuge. The cleared cell lysate was transferred to a clean 50ml falcon and agitated on a roller for 1hr at 4˚C with 0.5-1.0ml Ni-NTA Agarose (Qiagen) per 1L of culture. The lysate-matrix suspension was centrifuged at 1000rpm for 10mins, supernatant discarded. Conical Poly-Prep polypropylene columns (Biorad, UK) were pre-equilibrated with 50ml Wash buffer pH7.9 [50mM Tris-HCl, 300mM NaCl, 10mM Imidazole and 1mM β-mercaptoethanol]. The lysate-matrix slurry was mixed with 10ml Wash buffer and loaded into the chromatography column, and washed with 10 column volumes of Wash buffer. Bound protein was eluted by column fractionation under native conditions by eluting fractions in Elution buffer pH7.9 with ascending Imidazole concentration [50mM, 100mM, 200mM or 300mM Imidazole with 10mM Tris-HCl, 300mM NaCl and 1mM β-mercaptoethanol]. An elution profile was generated following analysis by sodium dodecyl sulphate polyacrylamide gel electrophoresis (SDS-PAGE).

2.4.6 SDS-PAGE and Coomassie Staining. Boiled elution fractions (20µl) were run on a 12% SDS-PAGE gel with 5X SDS-PAGE sample buffer [0.225M Tris-HCl pH6.8, 50% (v/v) Glycerol, 5% (w/v), 0.05% (w/v) and 0.25M Dithiothreitol (DTT)], alongside a whole cell lysate or cleared cell lysate fraction. Samples were run at 200V for ~45mins, run against a pre-stained broad range (6-175kDa) protein marker (New England Biolabs, USA). Gels were fixed with a solution containing methanol and glacial acetic acid [50% (v/v) CH_3OH and 10% (v/v) glacial CH_3COOH] followed by staining for 1hr with Coomassie's solution [0.25% (w/v) Coomassie Brilliant Blue R250, 45% (v/v) CH_3OH and 10% (v/v) glacial CH_3COOH]. Gels were de-stained overnight in a solution containing 45% (v/v) CH_3OH and 10% (v/v) glacial CH_3COOH. Suitable elution fractions (>90% purity) were pooled and dialysed overnight in PBS.

Section.2.5 *In Vitro* Characterisation of Recombinant Knob Proteins

2.5.1 Determination of Protein concentration. The concentrations of purified Knob proteins were determined by the Pierce Bicinchoninic acid (BCA) protein assay (Thermo Scientific, USA), carried out according to manufacturer's guidelines. A standard curve of bovine IgG, in the range 20-2000µg/ml, was used to calculate protein concentrations.

2.5.2 Trimerisation Assay. The ability of fibre modified recombinant Knob proteins to form homotrimers, was assessed by SDS-PAGE of boiled and unboiled samples. For each Knob protein, 5µg total protein was either boiled at 95˚C for 5mins, or left at room temperature for 5mins. Immediately prior to loading on the gel, 5X SDS-PAGE loading buffer (without DTT), was added to each sample. Boiled and unboiled samples were run in parallel on a 12% SDS-PAGE gel for ~1hr at 200V. Protein migration was visualised following Coomassie blue staining.

2.5.3 Validation of the Selectivity of Knob$_{A20}$ Mutants for αvβ6. An experiment was carried out to determine the ability of A20-modified, Knob protein derivatives (Knob$_{A20}$, Knob477*dl*TAYT$_{A20}$ or Knob485*dl*TAYT$_{A20}$) to bind to αvβ6, and to inhibit the binding of an αvβ6-specific antibody, 53A.2. Triplicate samples of 1x10^5 BT-20 cells (high levels of αvβ6 but low levels of the CAR receptor) were incubated on ice for 30 minutes, with increasing concentrations of each Knob protein (0.001-10µg/10^5 cells). Cells were washed twice and then incubated with anti- αvβ6 antibody on ice for 45 minutes (53A.2 at 10µg/ml). A rat isotype control IgG$_{2a}$ (Abcam), and Knob$_{WT}$ (at 10µg/ml) were used as negative controls. Preparations were washed twice in DMEM and incubated on ice with secondary antibody for a further 30 minutes (goat anti-mouse IgG AlexaFluor488; 1:250; Invitrogen). Cells were washed twice and resuspended in a final volume of 200µl serum free DMEM. Labelled cells were scanned on an LSR1 flow cytometer (Becton-Dickinson, CA, USA). A gate was set to exclude debris and fluorescence in FL1-H was recorded, acquiring 1x10^4 events. Results were analyzed using CellQuest software. Fluorescence values obtained for untreated control cells were taken to be 100% and fluorescence of Knob-treated cells expressed relative to this. A dose response curve was generated, and IC$_{50}$ values calculated by non-linear regression analysis using GraphPad Prism Version 3.03 (GraphPad Software, San Diego, CA).

2.5.4 Migration Inhibition Assay. Migration assays were carried out to assess the ability of the modified adenoviral Knob proteins (Knob$_{A20}$, Knob477*dl*TAYT$_{A20}$ or Knob485*dl*TAYT$_{A20}$) to inhibit αvβ6-dependent cell motility. Haptotactic cell migration

assays were performed using matrix coated Transwell® filters (8µm pore size, BD Biosciences). The membrane undersurfaces of three wells were coated with protein control BSA, but all other wells were coated with LAP (0.5µg/ml in α-MEM) for 1hr at 37°C. All wells were blocked with migration buffer (0.1% BSA in α-MEM) for 30mins at 37°C. VB6 cells were incubated with an αvβ6 inhibitory antibody (6.3G9; 10µg/ml), isotype control (mouse IgG_1; 10µg/ml), or Knob proteins ($Knob_{WT}$ and $Knob_{A20}$; 10µg/ml) for 30mins at 4°C prior to seeding. Cells were plated in the upper chamber at a density of $5x10^4$ in 100µl of migration buffer, and allowed to migrate for 24hrs. Cells which migrated to the lower chamber (including those attached to the lower surface of the membrane) were trypsinised and counted on a Casy 1 counter (Sharfe System GmbH, Germany). In order to determine IC_{50} values for inhibition of migration a separate experiment was performed using different concentrations of Knob477*dl*$TAYT_{A20}$ or Knob485*dl*$TAYT_{A20}$ (in the range 0.025-25µg/ml).

2.5.5 Validation of CAR-Binding Ablation Mutations. The ability of the A20-modified, or CAR-binding ablated Knob mutants (WT and A20) to bind CAR, was estimated from cell-binding experiments on CHO-CAR cells. The capacity for CAR-binding mutant proteins $KnobL485K_{WT}$, $KnobL485K_{A20}$, Knob485*dl*$TAYT_{WT}$, Knob485*dl*$TAYT_{A20}$, Knob477*dl*$TAYT_{WT}$ and Knob477 *dl*$TAYT_{A20}$, to inhibit Ad5-$EGFP_{WT}$ mediated infection was assessed by flow cytometry. The IC_{50} of $Knob_{WT}$ for inhibition of Ad5-$EGFP_{WT}$ infection of CHO-CAR cells (0.115µg/10^5 cells), has been previously determined (Kirby *et al.*, 1999). Therefore, when characterising the CAR-binding capacity of the mutants, a single concentration (100µg/10^5 cells), in excess of the IC_{50} value was used. Cells were seeded ($1x10^5$ cells/well) in 24-well plates and incubated overnight. Confluent monolayers were washed twice in PBS, and triplicate wells pre-incubated with each of the Knob proteins for 1hr at 4˚C. Without washing, Ad5-$EGFP_{WT}$ was added to cells at a constant multiplicity of infection (MOI) of 10PFU/cell. Incubation was carried out at 4˚C for a further hour to promote virus binding, but not internalisation. Cells were washed twice in cold PBS to remove unbound virus, and cells covered with pre-warmed complete medium. Plates were incubated for ~22hrs, after which EGFP gene transfer was quantified by the detection of fluorescence in FL1-H, by flow cytometry. As adenovirus constructs corresponding to the $Knob_{A20}$ mutant, and putative blood factor binding mutants, Knob485*dl*$TAYT_{A20}$ and Knob477*dl*$TAYT_{A20}$, were being generated simultaneously, we wished to quantify IC_{50} values for these proteins. Serial dilutions of protein were prepared in serum free DMEM, at concentrations ranging from 0.01-100µg/10^5 cells. Without washing, either Ad5-$EGFP_{WT}$, or Ad5-$EGFP_{A20}$ were added to cells, to compete for binding to the CAR receptor. IC_{50} values were calculated from

non-linear regression analysis of sigmoidal dose response curves, using GraphPad Prism v3.0 software (GraphPad Software, San Diego).

Section.2.6 Generation of Recombinant Adenoviral Genomes

The parental yeast vector used in this study, pMB20 (provided by Richard Iggo, UK), contains DNA from human adenovirus type 5 (Ad5), and is maintained in yeast as a low copy Yeast/Bacterial Artificial Chromosome (YAC/BAC). This vector possesses replication origins for both yeast and bacteria. Transformation of the yeast with a relevant URA3 integrating shuttle vector results in part one of a two-step gene replacement event, or "pop-in" event, in which intermediate constructs contain a duplication of the target sequence (*Fig.*2.9). Transformants are selected on -HIS -URA and screened by PCR analysis following extraction of yeast DNA. All primers used for PCR screening and sequence confirmation are listed in *Table*.8 and *Table*.9. Removal of the selective requirement for URA3 results in a second spontaneous recombination event, or "pop-out", which excises the integrated shuttle retaining the target DNA in place of its corresponding region of homology. This is mediated by means of a recombination event between the target Ad5 sequence within the shuttle, and the adenoviral backbone within the YAC/BAC. "Pop-out" recombinants, which have lost the URA3 integrating vector, are selected on -HIS supplemented with 5-Fluro-orotic acid (5-FOA) at 0.1-0.2% (w/v). This compound is converted to a toxic metabolite 5'Fluoro-uracil (5-FU) by the URA3 gene product (orotidine-5'-phosphate decarboxylase), which eliminates intermediate stage recombinants, therefore ensuring the selection of the excisive recombinant clones.

2.6.1 E3 Region Modification; pMB20-EGFP. YPH857 yeast containing the pMB20 wildtype Ad5 backbone, were freshly streaked onto -HIS agar and incubated overnight at 30°C. A fresh colony was inoculated into 100ml -HIS broth and incubated for 12-24 hrs at 30°C with aeration, in preparation for lithium acetate transformation using the Alkali-Cation Yeast Transformation Kit (Q.BIOgene) the following day. The pIP5-EGFP shuttle vector was linearised by *Not*I restriction digestion. 2μg of shuttle DNA was digested in a final volume of 20μl, for 2hrs at 37°C, followed by an enzyme denaturing step at 65°C for 15mins. Meanwhile, yeast cells were made competent by treatment with a Lithium/Caesium Acetate mixture, according to the manufacturer's protocol. During this time, transformation reactions were set up using four different concentrations of DNA from 0.1-1μg, in a maximum volume of 10μl. DNA was combined with 5μl Carrier DNA and 5μl Histamine solution, mixed gently with 100μl competent host cells and yeast transformed by heat shock at 42°C for 10mins. Cells were plated onto -HIS -URA selective agar and incubated at 30°C for 48-72hrs, until colonies appeared. Individual colonies were picked and incubated for 12-24hrs in 10ml

-HIS -URA broth at 30°C with aeration. Each colony selected for "pop-in" screening was recorded and numbered on a reference plate of the same medium. Successful integrative recombinants or "pop-ins", confirmed by PCR analysis on extracted yeast DNA (see below), were inoculated from their reference plate into 10ml -HIS broth and incubated for 12-24hrs at 30°C with aeration. Following this incubation period, 100μl of culture was plated onto -HIS 5-FOA and incubated for 24-48hrs at 30°C, to select for "pop-out" recombinants. Individual colonies were again selected, referenced on -HIS and screened by PCR following yeast DNA extraction (see *Section*.2.6.5). Successful constructs were transformed into commercially available electrocompetent bacteria, ElectroMAX™DH10B™ *E.coli* (Invitrogen™), BAC DNA extracted and constructs sequenced.

2.6.2 Fibre Region Modification; pMB20-EGFP$_{A20}$. YPH857 yeast containing the pMB20-EGFP Ad5 backbone, were freshly streaked onto -HIS agar and incubated overnight at 30°C. Cultures were prepared for transformation the next day, as described above, using the Alkali-Cation Yeast Transformation Kit (Q.BIOgene). The p*IV*$_{A20}$ fibre-modifying shuttle vector was linearised by *Msc*I restriction digestion. However, several attempts to generate A20-modified pMB20 BACS by homologous recombination using this shuttle construct failed. Therefore, a modified derivative of this construct, p*IV*1.4$_{A20}$, was generated. In an attempt to promote the likelihood of a recombination event, the region of homology downstream of the A20-insertion, was extended by ~500bp. 2μg of p*IV*1.4$_{A20}$ was digested in a final volume of 20μl, for 2hrs at 37°C, followed by an enzyme denaturing step at 65°C for 15mins. Recombinants were selected as described previously.

2.6.3 Fibre Region Modification; pMB20-477/485*dl*TAYT$_{A20}$. YPH857 yeast already containing the pMB20-EGFP$_{A20}$ Ad5 backbone, were freshly streaked onto -HIS agar and incubated overnight at 30°C. Cultures were prepared for transformation the next day, as described above, using the Alkali-Cation Yeast Transformation Kit (Q.BIOgene). The p*IV*-477/485*dl*TAYT$_{A20}$ shuttle vectors (see *Section*.2.3.7) were linearised by digestion with *Msc*I (as above), and recombinant selected as described above.

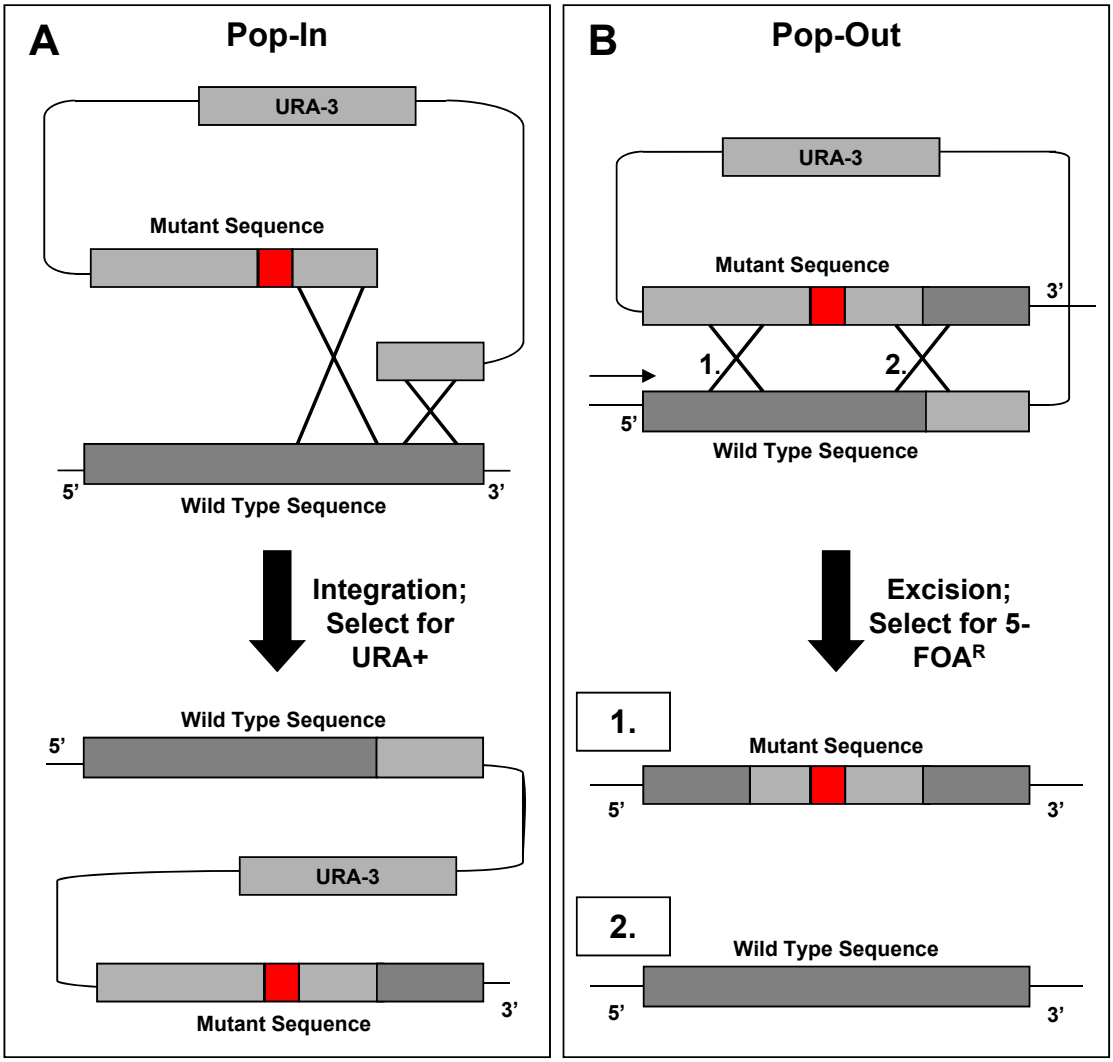

***Figure.*2.9 Schematic Overview of Two-Step Homologous Recombination in Yeast or "Pop-in Pop-out". (A)** Step 1 or "pop-in" results in the integration of a linearised URA3 integrating shuttle vector into a large adenoviral genome containing plasmid (ie. pMB20 and its derivatives). Integration results in the duplication of the target sequence, one wild type and one mutant. Selection of pop-in recombinants is through their ability to metabolise uracil. **(B)** The selective requirement for URA is removed, and so is no longer required for viability. This results in a spontaneous recombination event resulting in the excision of the integrated DNA. Successful excision recombinants are selected using 5'-Fluro-orotic acid. This is converted to the toxic metabolite 5'-Fluro-uracil in the presence of residual URA-containing recombinants which results in their elimination. Two step gene replacement has two resultant events, **1** or **2** (see above), the desired mutation or the wild type reversion, respectively.

2.6.4 Yeast DNA Extraction and Screening PCR. Yeast DNA was extracted from overnight cultures following enzymatic digestion of the cell wall resulting in spheroplast formation. Cultures were centrifuged at 5000g for 5-10mins after which the supernatant was discarded. Pellets were resuspended with 20ml YI solution [36.44% Sorbitol (w/v), 20% (v/v) 0.5M ethylenediaminetetraacetic acid (EDTA)], and centrifuged for a further 10mins at 5000g. Cell pellets were subjected to enzymatic digestion by resuspension in 500μl yeast lytic enzyme solution [36.44% Sorbitol (w/v), 20% (v/v) 0.5M EDTA, 2%

(w/v) Zymolase (MP Biomedical, UK) and 0.1% (v/v) β-mercaptoethanol]. Cells were incubated at 30°C for 1hr, after which the spheroplasting process was observed under a microscope as cell lysis on addition of 1 drop of 10% Sodium Dodecyl Sulphate (SDS). Spheroplasts were pelleted by centrifugation at 5000g for 5mins, and resuspended in 300μl of RNAse solution [10mM Tris, 1mM EDTA and 0.005% RNAse (v/v)]. Spheroplasts were lysed on addition of 30μl 10% SDS and were incubated at 65°C for 1hr. Precipitation of debris, protein and genomic DNA was achieved on addition of 100μl 5M Potassium Acetate (CH_3COOK) followed by centrifugation, in a table top centrifuge, at maximum speed for 30mins at 4°C. Supernatant was transferred to a 2ml eppendorf and the same volume of room temperature isopropanol [$(CH_3)CHOH$] was added before DNA was pelleted by centrifugation at maximum speed for 15mins at at 4°C. Supernatant was discarded and pellet washed gently in 1ml room temperature ethanol (EtOH), ensuring that the pellet floated freely. DNA was precipitated by centrifugation at maximum speed for 10mins at 4°C, the pellet air dried and resuspended in 30-50μl H_20. DNA concentrations were determined using a NanoDrop® ND-1000 photospectrometer (NanaoDrop Technologies$_{Inc}$). Samples were assessed at 260nm versus a blank control.

2.6.5 Transformation of *E.coli* with Yeast DNA and BAC DNA Extraction. PCR confirmed yeast DNA constructs were transformed into ElectroMAX™DH10B™ *E.coli* (Invitrogen™), to facilitate further PCR screening, and confirmation by restriction digestion fingerprinting. No more than 100ng of DNA in a final volume of 1μl was used to transform competent cells by electroporation using a BioRad GenePulser®II Electroporator, under the following conditions; 1.8kV, 200Ω, 25μF. Cells were resuscitated in 1ml SOC (Invitrogen™) medium [0.5% (w/v) Yeast extract, 2.0% (w/v) tryptone, 10mM NaCl, 2.5mM KCl, 10mM $MgCl_2$, 20mM $MgSO_4$ and 20mM glucose], at 37°C with aeration for 1hr. 100μl of this suspension was plated onto prewarmed LB agar plates with Chl (25μg/ml) and incubated overnight at 37°C. The following day individual colonies were picked off and were inoculated in 5-10ml LB/Chl broth (25μg/ml) and incubated overnight at 37°C with aeration. DNA was extracted by a slightly modified, miniprep version of Large Con Kit (Qiagen®), which included a second alkaline lysis step to eliminate bacterial chromosomal DNA. Cultures were centrifuged at 3000g for 10mins at room temperature and the pellets resuspended in 300μl reagent P1 (Qiagen®) supplemented with 50μg/ml RNAse A, followed by transfer into a 1.5ml eppendorf. Suspensions were incubated at room temperature for 5mins following addition of 300μl normal alkaline lysis reagent P2 (Qiagen®). After 5mins, 300μl of pre-chilled alkaline lysis reagent P3 (Qiagen®) was added and the suspension incubated

for 30mins on ice, after which they were centrifuged at maximum speed (15,700g) in a refrigerated tabletop centrifuge for 10mins at 4°C. The supernatant was collected, transferred to a clean eppendorf to which an equal volume of room temperature isopropanol was added, and centrifuged at 15,700g for 10mins at room temperature. Supernatant was removed and the pellet resuspended gently in 50μl sdH_20 before being transferred to another sterile eppendorf, 200μl room temperature ethanol was added and the mixture centrifuged at 15,700g for 10mins at room temperature, using a tabletop centrifuge. Supernatant was discarded and the pellet resuspended in 30μl Elution Buffer (EB). These constructs were further screened analysing their restriction digestion fingerprint profile when compared against wildtype pMB20, following digestion with *Xba*I/*Xho*I. Successful constructs were prepared for large scale DNA extraction using the Large Con MaxiPrep Kit (Qiagen®) after which the pellet was eluted in H_20 if required for sequencing, or in endotoxin-free TE for transfection applications.

*Section.*2.7 Adenovirus Production and Validation Techniques

2.7.1 Ad5 Genome Transfection and Rescue. Virus production by transfection of HEK293 cells with *Pac*I digested pMB20 plasmid, or its derivatives, was carried out in the category 2 tissue culture laboratory. 10µg of pMB20 recombinants were digested overnight at 37°C in a final volume of 50µl, with 1U *Pac*I per µg DNA, to release the Ad5 genome. The 36kbp fragment was purified as follows; 200µl TEN buffer [10mM Tris-HCl pH8.0, 100mM NaCl, 1mM EDTA] was added to the 50µl *Pac*I digest. An equal volume of phenol/chloroform/isoamyl alcohol was added, the sample vortexed briefly and centrifuged at 15,700g for 5mins at room temperature. The upper aqueous layer was collected (~250µl) and an equal volume of chloroform alone added. The sample was transferred to a sterile 1.5ml eppendorf, after which 600µl of ice-cold 100% EtOH and 0.1 volumes of 3M NaAc were added. The suspension was incubated for 30mins on ice and then centrifuged at 15,700g for 15mins at room temperature. The supernatant was removed carefully and the pellet washed in 1ml 70% EtOH. The sample was centrifuged again at 15,700g for 5mins, supernatant removed and the pellet allowed to dry for 5mins, after which it was resuspended in ~25µl of endotoxin-free elution buffer (Qiagen). Purifed viral DNA was transfected into HEK293/HEK293-β6 cells using FuGENE 6 Transfection reagent (Roche) as follows; FuGENE 6 reagent was mixed with viral DNA in ratios of 3:2, 3:1 and 6:1µl/µg, respectively and incubated for 15mins. 2 x 10^5 HEK293/HEK293-β6 cells, in a final volume of 2ml DMEM 10% FCS, were added to each well of a 6-well plate. The FuGENE-DNA suspension was added in a dropwise manner immediately, and the plate swirled to ensure even dispersion. Plates were incubated under standard conditions for 3-11 days during which transfection efficiency and cytopathic effects (CPE) were observed by visualisation of EGFP by UV light under a microscope. Following cell detachment, the cell-medium suspension containing virus was collected and stored in a 15ml falcon at -80°C, until required for further expansion of the virus.

2.7.2 Virus Propagation and Expansion. A frozen virus suspension collected from one of the wells in the initial transfection was used to infect a 10cm^2 dish seeded with HEK293 cells (5x10^5/well) grown in DMEM 10% (v/v) FCS, the previous day. CAR-binding ablated, A20-retargeted viruses were amplified on either HEK293-β6 or A549-β6 cells, in medium supplemented with puromycin (5µg/ml). Prior to infection the medium was removed and replaced with 10-15ml DMEM 2% (v/v) FCS. The viral suspension was subjected to three cycles of freeze-thaw lysis after which the entire contents of the falcon were tipped onto the 10cm^2 plate. Virus/culture medium suspension was collected 3-5 days post infection and frozen at -80°C until required for

infection of a T175 flask at 70-80% confluency. In preparation for further viral amplification, the suspension was again subjected to three cycles of freeze-thaw lysis, after which 3-5ml was used to infect the T175. Full CPE was reached within 48-72hrs, after which the virus/medium suspension was again collected and frozen at -80°C. Freeze thawed virus suspension (6-7ml) was used to infect a confluent CF-10 tower, which was harvested within 48-72hrs. Virus produced was collected by ultracentrifugation following purification on a Caesium Chloride gradient.

2.7.3 Virus Purification Using CsCl Gradient. Once cells were detached from the CF-10 (~48-72hrs post-infection), cells were harvested by centrifugation at 1000g in a Sigma 6K15 Centrifuge for 10mins at 4˚C. The pellet was allowed to settle for 10mins prior to aspiration off of the supernatant. Each pellet was resuspended in 15ml cold PBS. Pellets were centrifuged at 250g for 10mins at 4˚C using a Sigma 6K15 Centrifuge, and the final pellet re-suspended in 12ml sterile, cold 10mM Tris-HCl pH8.0. Pellets were subjected to three rounds of freeze/thaw lysis, and were stored at -80˚C until ready for caesium chloride (CsCl) banding. A CsCl discontinuous density gradient was prepared as follows; 10.4ml of CsCl solution at a density of 1.25g/ml was under-layered with 7.6ml of CsCl solution at a density of 1.4g/ml in a 3.5' ultracentrifuge tube (Beckman-Coulter). The previously freeze-thawed viral lysate was centrifuged at 8000g for 10mins at 4˚C in a Sigma 6K15 Centrifuge, and the supernatant layered carefully on top of the CsCl gradient. Tubes were weighed and balanced to within 0.01g, before being centrifuged at 25,000rpm for 2hrs at 15˚C using a Beckman 55Ti rotor in an Optima L-80 XP Ultracentrifuge. Following ultracentrifugation, functional particles were distinguished from defective particles on the basis of their altered buoyant density in a CsCl gradient. Three bands were visible; an upper band of cellular debris, a central band containing unpackaged virus and a lower band containing successfully encapsulated, functional virus. This fraction was extracted from the gradient as follows; the ultracentrifuge tube was restrained using a clamp and pierced carefully using a 19 gauge needle attached to a 10ml syringe. The band was aspirated carefully in minimal volume of CsCl possible, and transferred to a labelled falcon tube. Bands were pooled and layered onto 3ml of 1.35g/ml CsCl solution in a ½ x 2' ultracentrifuge tube, tubes balanced and centrifuged at 40000rpm for ~15hrs at 15˚C using a Beckman SW32Ti swing out rotor in an Optima L-80 XP Ultracentrifuge. The virus band was collected, as before, and resuspended ~1:2 in buffer [96mM NaCl, 0.5mM Na_2HPO_4, 2.8mM KCl, 0.3mM $MgCl_2$, 0.5mM $CaCl_2$, 30% (v/v) glycerol]. The virus-buffer mixture was injected into a 3000M_W Slide-a-lyzer cassette (Pierce Biotechnology, UK) and dialysed for 24 hours in 2l dialysis solution [10mM Tris-HCl pH 7.4, 1.0mM $MgCl_2$, 150m NaCl, 10% (v/v) glycerol]. The following

day virus was removed from the dialysis cassette, and aliquots of 50-100µl volumes stored at -80°C in cryovials.

2.7.4 Virus Titration ($TCID_{50}$). Ten-fold serial dilutions of viral stocks were titrated on JH293/JH293-β6 cell seeded in 96-well plates the previous day ($1x10^4$cells/well). Titrations were performed on quadruplicate plates. The cells were incubated with virus for ten days at 37°C DMEM with 2% (v/v) FCS, supplemented with puromycin (5µg/ml) when required. Infection was detected by induction of CPE and visualisation of EGFP fluorescence under UV light. Viral Tissue Culture Infectious Dose-50 ($TCID_{50}$) titres were read according to the method of Reed-Muench. Titres were precisely calculated using the Kärber statistical method $T = 10^{1+d(S-0.5)}$ where d is Log_{10} of the dilution and S is the sum of the ratios. $TCID_{50}$ values were adjusted (they have been empirically determined to be 0.7 Log higher than standard plaque assays) to enable viral titres to be expressed as PFU/ml (Kontermann *et al.*, 2003; Wang *et al.*, 2003; Wu & Curiel, 2008; Zhao *et al.*, 2009).

ie. $1x10^x$ $TCID_{50}$/ml is adjusted to $1x10^{X-0.7}$ PFU/ml.

2.7.5 Virus Particle Quantification (OD_{260nm}). For determination of virus particle counts, two 100µl aliquots of purified virus stock were diluted in 100µl 2X Virus Lysis Buffer [1% (w/v) SDS and 0.04M Tris-HCl, pH7.4]. A 1:10 dilution of virus, and an aliquot of TSG alone, was also included. The virus suspension was heated to 56˚C for 10mins, after which 300µl sterile distilled H_2O was added, and the sample transferred to a quartz cuvette. The absorbance constant for Ad5 has been determined previously (Maizel *et al.*, 1968). The absorbance of each sample was read at a fixed wavelength of 260/280nm (typically ~1.2-1.3 after CsCl purification) and viral particles per ml (PPM) calculated from the following formula:

Particles/ml = OD_{260nm} x Dilution factor x 1.12×10^{12} [Absorbance constant for Ad5]

Section.2.8 *In Vitro* Characterisation of Adenovirus Vectors

2.8.1 Purification of Viral DNA for PCR Applications. Viral DNA was extracted from virally infected cells or directly from purified virus stocks using the QIAamp Blood DNA mini Kit (Qiagen), according to manufacturer's instructions. DNA extracted from virally infected cells was used for sequencing applications, to confirm the incorporation of various mutations within the Ad5 mutants. DNA extracted from purified viral DNA was used to create a standard curve (ranging from 10^9-10^1 genomes) for quantitative real-time PCR (qPCR) applications. The concentration of purified vDNA was determined using a NanoDrop® ND-1000 photospectrometer (NanoDrop Technologies). The Ad5 genome is ~36 kilobase pairs (kbp) in size. As the mass of 1bp has been calculated to be ~1.096 x 10^{-21} g/bp we can calculate that the Ad5 genome weighs ~3.95 x 10^{-17} g. Therefore, 1x10^9 genomes would be equivalent to ~39.456ng. The 1x10^9 dilution was calculated and a 10-fold serial dilution performed to obtain the other dilutions for the standard curve. Standard curves consistently had R^2 values of ≥ 0.98, and a slope approaching -3.23.

2.8.2 *In Vitro* Infectivity Assays. Using a panel of αvβ6-expressing human carcinoma cell lines, the infectivity of the αvβ6-retargeted virus Ad5-EGFP$_{A20}$ was compared with its control, Ad5-EGFP$_{WT}$. In separate experiments, characterisation of viral entry was achieved through the use of competition assays, using Knob$_{WT}$ or Knob$_{A20}$, or a function blocking antibody to αvβ6 integrin (53A.2) to inhibit viral infection. Further function blocking experiments were carried out using inhibitors to other integrins (αvβ3/αvβ5/αvβ8) in order to demonstrate that the route of infection with Ad5-EGFP$_{A20}$ was modulated predominantly through αvβ6. Experiments were performed as follows; confluent monolayers were pre-incubated with an excess of Knob$_{WT}$ or Knob$_{A20}$ (20µg/ml), or the relevant antibodies (10µg/ml) in serum free medium for 1hr at 4˚C. Without washing, Ad5-EGFP$_{WT}$ or Ad5-EGFP$_{A20}$ were added to cells at a multiplicity of infection (MOI) of 10PFU/cell (MOI has been used to describe PFU/cell concentrations throughout this thesis). Incubation was carried out at 4˚C for 1 hour to promote virus binding without internalisation, monolayers washed twice in cold PBS to remove unbound virus, cells covered with pre-warmed complete medium and incubated at 37˚C for 22hrs to allow EGFP transgene expression. Viral EGFP gene transfer and competition gene transfer assays were quantified by acquisition of EGFP fluorescence in FL1-H, by flow cytometry.

2.8.3 Cytotoxicity Assays. Cell viability following viral infection was estimated using an MTT (3-2,5-diphenyltetrazolium bromide; Sigma-Aldrich, Poole, UK) assay.

Carcinoma cells ($2x10^5$) were seeded in 24-well plates and infected with 10-fold serial dilutions of virus (MOI 0.0001-100; PFU/cell) in medium with 5% FCS. At 120hrs post-infection 100µl MTT reagent (5mg/ml) was added to each well, and the plate incubated for 2hrs at 37˚C. Supernatant was removed and the MTT crystals dissolved in 500ul DMSO after which absorbance at 560nm was read in a 96-well plate using an Opsys MR microplate reader (Dynex Technologies Ltd, West Sussex, UK). Cell viability assays were carried out in triplicate and repeated on three independent occasions.

2.8.4 Replication Burst Assays. For quantification of viral replication per cell, $1x10^5$ cells were infected with Ad5-$EGFP_{WT}$ or Ad5-$EGFP_{A20}$, at MOI 10. Triplicate samples for each time-point were harvested at 24, 48 and 72hr post-infection by scraping into 0.5ml of 0.1M Tris-HCl pH8.0. Cell suspensions were subjected to three rounds of freeze-thaw lysis, after which virus released was titrated by serial dilution on JH293 cells, again carried out in triplicate.

2.8.5 Infectivity +/- FIX, FX and Heparin. Infectivity experiments were carried out on CHO-K1, CHO-CAR, DX3puro, DX3-β6, TR126, SKOV3ip1 and BT-20 cells, to assess the contribution of coagulation factors human factor IX (FIX), and factor X (FX) on infectivity. Cells ($1x10^5$) were seeded in 24-well plates and allowed to attach overnight. The following day, triplicate wells were infected for 2hrs at 37˚C at MOI 10 with Ad5-$EGFP_{WT}$, Ad5-$EGFP_{A20}$ or Ad5-477*dl*$TAYT_{A20}$ alone, or mixed with physiological concentrations of FIX (3µg/ml, Abcam), FX (1IU/ml, Innovative Research), FX mixed with porcine heparin (1 IU/ml; 10µg/ml, Sigma), or heparin alone (10µg/ml). Following the 2hr incubation, cells were washed twice in PBS, fresh culture medium replaced and the infection allowed to proceed for ~22hrs under standard conditions. The end-point for these assays was the quantification of EGFP fluorescence, quantified by flow cytometry as described previously.

Section.2.9 *In Vivo* Characterisation of Adenovirus Constructs

All *in vivo* experiments were performed at the Biological Support Unit (BSU) by qualified staff and were done under suitable UK Home Office personal, and project licence authority. Dose escalation and hepatotoxicity experiments in immunocompetent mice, were carried out at the facility of the Institut d'Investigació Biomèdica de Bellvitge, IDIBELL (AAALAC unit 1155) at the Institut Català d'Oncologia (ICO), Barcelona, Spain. All animal experiments carried out at this facility were in accordance with the regulations of the IDIBELL Ethical Committee for Animal Experimentation.

2.9.1 *In Vivo* Ovarian Intraperitoneal Xenograft Experiment. This experiment was carried out by Professor I.A. McNeish and Jerome Burnet (technician). CD1 nu/nu female mice were injected intraperitoneally (i.p) with $1x10^7$ SKOV3ip1 ovarian carcinoma cells. Viruses Ad5-$EGFP_{WT}$, Ad5-$EGFP_{A20}$ and non-replicating, E1-deleted control virus, LM-X (McNeish *et al.*, 2001) were injected on days 12-16 inclusive, at a dose of $5x10^9$ particles in 400 µL of 20% icodextrin (Innovata plc, Nottingham, United Kingdom) per injection. Mice were assessed daily and were killed when they reached Home Office morbidity limits (approaching 20% body weight loss, presence of significant ascites and poor well-being, as determined by BSU staff). Survival was assessed for Ad5-$EGFP_{WT}$ and Ad5-$EGFP_{A20}$ however, a comparisson with the non-replicating vehicle control, Ad LM-X was not possible as it was found to be contaminated with replicating Ad5 stock.

2.9.2 Intratumoural Efficacy Experiment Using the Isogeneic DX3puro/DX3-β6 Model. This experiment was carried out by Professor I.A. McNeish and Jerome Burnet (technician). $4x10^6$ DX3puro, or DX3-β6 cells, were implanted subcutaneously onto the right flanks of CD1 nude female mice. Tumours were measured weekly until they reached approximately 8-10mm (~$250mm^3$ volumes). The intratumoural (i.t.) efficacy of both Ad5-$EGFP_{WT}$ and Ad5-$EGFP_{A20}$ was assessed by *in vivo* fluorescence imaging, in addition to estimation of tumour volume variation. Cohorts of up to eight animals received three daily i.t. injections of either Ad5-$EGFP_{WT}$ or Ad5-$EGFP_{A20}$ ($1x10^{10}$vp in 50µl PBS). At fixed time points, including immediately prior to virus administration, mice were anesthetised (2% halothane in O_2 by inhalation) and imaged using a Xenogen IVIS Imaging System 100 system (Xenogen, Alameda, CA), using the fluorescence module. Fluorescence data from defined regions of interest were analysed with Living Image software (Xenogen) and are presented as the fluorescence efficiency. Mice were killed when tumours approached 14mm in diameter. Tumours were excised, and fixed

in formol saline after which the tissue was processed, embedded in paraffin and sectioned by Pathology Services at the Institute of Cancer.

2.9.3 Experiment to Determine Hepatotoxicity in Immunocompetent Mice Following Systemic Delivery. Balb/c immunocompetent mice were used for dose escalation toxicity studies following intravenous administration of PBS, Ad5-EGFP$_{WT}$, Ad5-EGFP$_{A20}$ or Ad5-477*dl*TAYT$_{A20}$. Doses of 2.5x10^{10} and 4x10^{10}vp/mouse were administered by tail vein injection, in separate experiments. Mice were assessed daily for their body weight variation and overall morbidity. At days 6 or 3 post-infection (depending on dose), all cohorts were killed and a blood sample obtained by intra-cardiac puncture immediately post-mortem. Plasma (150µl) was separated from whole blood using Microtainer heparinised tubes (Becton-Dickinson) and samples sent to the Falcultat de Veterinària, Universitat Autònoma de Barcelona for quantification of liver transaminase levels. When possible, whole blood samples were collected in K_2EDTA microcontainer capillary tubes (Becton-Dickinson) and sent for haematological analysis. Serum samples, required for the quantification of cytokines/chemokines, were obtained from whole blood samples using Sarstedt CB300 microvette capillary tubes with clot activator (Sarstedt, Germany). Livers and spleens were harvested for tissue processing, and quantification of viral genomes by quantitative TaqMan Real Time-PCR (see *Section*.2.2.7).

2.9.4 Quantification of Serum Cytokines/Chemokines and Analysis of Haematology in Immunocompetent Mice Following Systemic Delivery (24hrs). Serum cytokine and haematological profiles were obtained from Balb/c immunocompetent mice following systemic administration of PBS, Ad5-EGFP$_{WT}$, Ad5-EGFP$_{A20}$ or Ad5-477*dl*TAYT$_{A20}$ (4x10^{10}vp/mouse). Cytokine/chemokine (IL-6, RANTES, IFN-γ, TNF-α and IL-12p70) levels were quantified 6hrs and 24hrs post-infection, from 25µl serum, using a fluorescent cytometrix bead assay (FlowCytomix™, Bender MedSystems). The protocol is described in detail in *Section*.2.1.7. Results were analysed using FlowCytomix Pro 2.2 Software. Haematological profiles were assessed 24hrs post-infection at the Clinical Veterinary Biochemistry Service at the Faculatat de Veterinària, Universitat Autònoma de Barcelona from 250µl samples of whole blood. Blood samples were obtained by intracardiac puncture immediately post-mortem (performed by Francisca Alcayaga and Alena Gros).

2.9.5 Experiment to Assess Tumour Targeting and Hepatotoxicity in Nude Mice Following Systemic Delivery. Animal work for this study was carried out by Professor Ian. R. Hart, Dr. John F. Marshall and Mr. Arif Mustafa (technician). 4x10^{6} DX3-β6 cells

were implanted subcutaneously onto the shoulder of CD1 nude female mice. Once tumours reached approximately 125mm^3 (~3 weeks), mice were injected with PBS, Ad5-EGFP$_{WT}$ or Ad5-EGFP$_{A20}$ (5x10^{10} viral particles per mouse) by intravenous tail vein injection. Vitamin K-dependent coagulation factors were depleted in identical, but separate, groups by a subcutaneous injection of 133µg warfarin (Sigma) dissolved in peanut oil (Sigma). Warfarin treatment was carried out at days -1 and -3 prior to viral administration. At 1hr post-infection, a 60µl blood sample was obtained from the tail vein of non-warfarinised mice, for titration of virus by TCID$_{50}$. Mice were assessed regularly for their overall morbidity, and their body weight was recorded daily. All cohorts were killed 72hrs post-infection, blood samples obtained immediately post-mortem and tumours/organs harvested for analysis. Liver transaminases, alanine aminotransferase (ALT), and aspartate aminotransferase (AST), were quantified from 150µl of mouse serum by Axiom Veterinary Laboratories (Devon, UK).

Section.2.10 Histopathological Techniques

2.10.1 Tissue Preservation and Processing. Harvested organs/tumours were treated as follows; in preparation for paraffin processing, tissue was fixed overnight in formal saline/4% paraformaldehyde, whereas tissue required for frozen sections was embedded in O.C.T (Tissue-Tek) containing cryomolds (Tissue-Tek), and frozen at -80˚C immediately post-necropsy. Tissue was dehydrated in preparation for paraffin embedding as follows; immersion in 70% EtOH for 1hr, transfer to 96% EtOH for 1hr, 96% EtOH for 1hr, transfer to 96% EtOH overnight followed by immersion in 100% EtOH for 1hr, 100% EtOH for 1.5hrs, 100% EtOH for 1.5hrs and finally tissue transferred to xylene for 1.5hrs after which it was immersed in paraffin (60˚C) for a minimum of 12hrs. Paraffin-embedded tissue sectioning, and Haematoxlin and Eosin (H&E) staining were carried out by Keyur Trivedi and Dr. Mohammed Ikram (Pathology Service, Institute of Cancer). Frozen tissue sections (5µm) were cut using a Cryotom® Electronic cryostat (Thermo Electron Corporation) and two sections loaded onto charged microscope slides (Thermo Scientific, UK).

2.10.2 Immunostaining on Frozen Tissue; E1A. Frozen liver sections were stained for E1A expression using a rabbit anti-Adenovirus E1A polyclonal antibody [M78], 13 S-5 (Santa Cruz) as follows; pre-cut frozen sections were fixed in ice-cold acetone for 10mins, rinsed in deionised H_20 and blocked for 30mins in 10% normal goat serum (Sigma, UK). Primary antibody 13 S-5 (Santa Cruz, USA), or a secondary only (goat anti-rabbit AlexaFluor488, Invitrogen) diluted 1:100 in PBS+Tween 0.05% was added, and sections incubated for 1hr at room temperature. Sections were washed three times in PBS+Tween 0.05%, after which the fluorescent secondary antibody was added for 1hr at a final dilution of 1:200. Sections were washed, mounted with VectaShield+DAPI (Vector Laboratories, UK), coverslips added and slides allowed to dry overnight. Immunofluorescence was captured using either an Olympus BX60 fluorescence microscope and SpotAdvanced™ software, or a Zeiss laser scanning microscope (LSM 510META) and LSM 5 Software, version 3.2 (Zeiss, Germany).

2.10.3 Immunostaining on Paraffin Sections; E1A. Tumour xenografts, murine liver and/or spleen sections were stained for E1A using mouse anti-Adenovirus [M58] antibody (GeneTex, BiogenAutoclear, USA). Automated immunostaining was performed at the Pathology Service, Institute of Cancer.

2.10.4 Immunostaining on Paraffin Sections; αvβ6. Paraffin-embedded, tumour xenograft sections were cut by staff in Pathology Services at the Institute of Cancer.

Two sections were loaded per slide to facilitate αvβ6 staining using mouse anti-human mAb, 6.2G2 (provided by Shelia Violette, BiogenIdec, USA) in parallel with its isotype control, mouse IgG_1 (Dako). Sections (10μm) were de-waxed by immersion in Xylene [$C_6H_4(CH_3)_2$] for 5mins, Xylene for 5mins, 100% EtOH for 2mins, 100% EtOH for 2mins, 95% EtOH for 2mins, 50% EtOH for 2mins, 50% EtOH for 2mins and a final wash in distilled H_2O for 2mins. The optimal antigen retrieval method for 6.2G2 previously was shown to be enzymatic pepsin. Endogenous peroxidase activity was blocked by coating the slide in a solution of methanol/hydrogen peroxidase [0.45% (v/v) H_2O_2 in 400ml CH_3OH] for 15mins at room temperature. Slides were washed twice in PBS for 2mins each time and excess liquid removed. Sections were circled using a PAP pen (Invitrogen, UK) and 200μl pepsin (Invitrogen, UK) added to the sections, which were incubated at 37˚C for 5mins. Slides were washed twice in PBS as before. Some tissues may have endogenous binding activity for avidin, biotinylated HRP or other Biotin/avidin components, and these were blocked using the Avidin/Biotin blocking kit (Vector SP-2001, Vector Laboratories, USA) prior to addition of the biotinylated antibody.

As the primary antibody 6.2G2 was raised in a mouse, internal mouse immunoglobulin (IgG) within the human xenograft tissue was blocked using the MOM kit (Vector BMK-2202, Vector Laboratories, USA). Both kits were used as directed by the manufacturer. One section per slide was incubated overnight at 4˚C with either anti-αvβ6 (6.2G2), at a final concentration of 6μg/ml, or isotype control at 10μg/ml. The following day, sections were washed twice in PBS for 2mins, after which the MOM biotinylated anti-mouse IgG reagent was added for 10mins at room temperature. Sections were rinsed again in PBS as before. Using the Elite ABC kit (Vector PK-6102, Vector Laboratories, USA), the avidin/biotin-HRP conjugate (ABC reagent) was added, and sections incubated at room temperature for 30mins. Slides were washed twice in PBS, after which chromogenic DAB substrate [3,3' Diamino Benzidine Tetrahydrochloride $C_{12}H_{14}N_4N$, $(HCl)_4$] was added for up to 5mins. Slides were rinsed in running tap water for approximately 1min, before counterstaining for nuclei using Mayer's haematoxylin for 1min. Stained sections were dehydrated by carrying out the initial steps in reverse; immersion in distilled H_2O for 2mins, 50% EtOH for 2mins, 50% EtOH for 2mins, 95% EtOH for 2mins, 100% EtOH for 2mins, 100% EtOH for 2mins, immersion in Xylene [$C_6H_4(CH_3)_2$] for 5mins, and finally Xylene for a further 5mins. Sections were allowed to dry after which coverslips were mounted using Permount (Fisher SP15-500,UK). Sections were visualised using a Zeiss AxioCam MRc5 camera and Axiovision Software (Zeiss, Germany).

2.10.5 Pathologic Examination of Immunohistochemistry. Pathologic assessment of H&E stained/immunostained tissue samples was carried out by a qualified pathologist, Prof. Gareth Thomas. Histological analysis was done blindly, without prior knowledge of the specimens.

Section.2.11 Statistical Analysis and Software Used

2.11.1 Statistical Analysis. All dose-response curves and statistical analyses were generated using GraphPad Prism Version 3.03 (GraphPad Software, San Diego, CA). Dose response curves were analysed by non-linear regression analysis, and statistical significance determined by comparing the EC_{50} values of two groups. A two-tailed, unpaired Student's *t*-test was used to compare means between two samples. The Kaplan-Meier curve was analysed using the Mantel-Haenszel, Logrank test to compare two groups. A *p*-value of <0.05 was considered to be statistically significant. Figures show representative examples of independent repeats. *In vitro* data are expressed as the mean +/- SD, and *in vivo* data +/- SEM.

2.11.2 Vector NTI Cloning Software and BioEdit Sequencing Analysis. Vector sequences were stored and restriction maps constructed using Vector NTI Advance™ Software, using the academic licence (Invitrogen). Analysis of sequencing chromatograms was performed using BioEdit Sequence Alignment Editor, version 7.0.5.3.

2.11.3 Protein Alignments and Structural Analysis. Protein alignments were generated using ClustalW multiple sequence alignment programme (EMBL-EBI). Structural predictions of helix formation were obtained using AGADIR software, a freely available alogorithm which predicts the helical content of peptides (Muñoz & Serrano, 1997).

2.11.4 Real-Time qPCR Analysis. Analysis of qPCR data were performed using ABI Sequence Detection Software v1.3 (Applied Biosystems).

2.11.5 Flow Cytometry Software. Standard flow cytometry was analysed using CellQuestPro Software, version 4.0.2 (Becton-Dickinson, CA). Aquisition of cells for FACS sorting was performed using Summit v4.0 software and analysis was carried out using FlowJo v8.8.4, by Sukhveer Purewal and Carolyn Koh (FACS laboratory, London Research Institute). Analysis of serum cytokines/chemokines, quantified using a cytometric bead assay, was performed using FlowCytoMix Pro 2.2 Software (Bender MedSystems). When necessary, CellQuestPro acquisition files were filtered to exclude debris using FCS Filter v1.0.4 Software (Soft Flow, Hungary).

CHAPTER 3. Results

Chapter.3 *In Vitro* Assessment of the Potential for Retargeting Ad5 to αvβ6 Integrin

The clinical use of Ad5 for cancer therapy is hampered by its often inefficient transduction of malignant tissue *in vivo,* mediated in part by the innate hepatotropism of the virus. Additionally, expression levels of the native Ad5 receptor, CAR, have been reported to be down-regulated in cancer, which is in contrast with the expression of CAR on normal tissue. Therefore, it is clear that the development of prototype vectors which exhibit CAR-independent, and high efficiency retargeting to clinically relevant markers, would be highly desirable.

The epithelial-specific integrin, αvβ6, represents an attractive target for directed therapy since it generally is not expressed on normal adult epithelium, but is upregulated in numerous carcinomas, including breast, lung, ovarian, cervical and colorectal, where it often correlates with poor prognosis (Ahmed *et al.*, 2002b; Bates *et al.*, 2005; Elayadi *et al.*, 2007; Hazelbag *et al.*, 2007). In addition, it has been shown previously that over 90% of oral squamous cell carcinomas (OSCC) express αvβ6 strongly (Nystrom *et al.*, 2006; Thomas *et al.*, 2002) and that upregulation of αvβ6 expression is associated with increased tumour cell invasion and metastatic potential *in vivo* (Nystrom *et al*., 2006; Thomas *et al*., 2001b; Van Aarsen *et al*., 2008).

Binding to αvβ6 is via the RGD motif in its ligands which include fibronectin, tenascin, the latency associated peptides (LAP) of transforming growth factors β1 and β3, in addition to the VP1 structural protein of Foot and Mouth Disease Virus (FMDV) for which αvβ6 is a native receptor (Jackson *et al.*, 2000). Recent data have demonstrated that specificity for αvβ6 is dependent on the inclusion of a DLXXL motif in an extended carboxy α-helical loop, with the RGD motif situated at the apex of a hairpin loop domain (DiCara *et al.*, 2007). The DLXXL motif was first identified by phage display as the key epitope that conferred strong αvβ6 binding with minimal interactions with αvβ3/αvβ5 integrins (Kraft *et al.*, 1999). Several groups have now reported the selection of αvβ6-specific peptides containing this motif (Elayadi *et al.*, 2007; Li *et al.*, 2009; Pameijer *et al.*, 2007). We have previously documented the analysis of a panel of linear peptides containing the αvβ6-selective, RGDLXXL motif (DiCara *et al.*, 2007). These peptides were not randomly identified by phage display, but were chosen by rational selection from known αvβ6 ligands all of which contained this sequence motif. Functional studies identified the A20FMDV2 candidate peptide, derived from the VP1 protein of FMDV, as having high affinity and selective binding to αvβ6 (DiCara *et al.*, 2007).

The initial aims of this project were to genetically incorporate this targeting entity into the HI loop of the Ad5 fibre knob domain, in an attempt to subvert the native tropism of Ad5 to αvβ6. It was hoped that a recombinant adenovirus displaying this peptide would allow significant improvements in selective delivery to αvβ6-positive tumour xenografts *in vivo*.

TABLE 10. Surface Receptor Expression

	CAR		αvβ6	
	% Positive Cells	Geometric Mean	% Positive cells	Geometric Mean
A375puro	96.62	39.08	0.87	2.93
A375-β6	82.57	25.76	95.94	51.25
A549‡	97.53	77.27	2.40	13.84
A549-β6	N.D	N.D	98.82	32.69
BICR5	95.82	59.47	N.D	N.D
BICR56	99.72	58.73	N.D	N.D
BT-20	5.26	14.79	97.30	33.08
C1	99.50	82.54	N.D	N.D
CA1	87.70	27.21	N.D	N.D
CAOV3	6.50	7.83	24.90	22.13
CHO-CAR	93.12	354.48	N.D	N.D
CHO-K1	0.63	10.98	0.51	19.06
CHO-β6	N.D	N.D	98.05	153.65
DLD-1*	N.D	N.D	60.92	15.99
DX3puro	12.25	12.85	0.89	20.31
DX3-β6	5.72	12.74	96.06	66.90
H400	84.14	28.88	N.D	N.D
HEK293	99.31	162.72	0.82	61.07
HEK293-β6	N.D	N.D	97.11	135.51
HSC-3	54.37	28.02	63.90	23.71
JH293	N.D	N.D	0.98	31.20
JH293-β6	97.76	96.97	99.17	114.13
MCF10CA1a†	61.21	14.77	99.66	76.12
NP-9*	N.D	N.D	0.71	8.60
NP-18*	N.D	N.D	0.75	9.88
SCC25	91.92	37.22	99.01	72.19
SiHa	95.99	20.28	0.43	13.18
SKOV3	99.21	81.11	N.D	N.D
SKOV3ip1	59.91	37.30	44.88	17.09
SKOV3ip1-β6	N.D	N.D	98.17	44.31
TR126	3.96	46.52	96.28	66.97
TR138	56.53	71.17	95.12	115.86
VB6	99.60	93.94	52.11	115.86

[a] Cell lines used in this study are listed alphabetically. Surface receptor expression profiles were obtained by flow cytometry using an LSR1 (Becton-Dickinson, CA, USA). Geometric mean fluorescence, and percent positive statistics ($1x10^4$ gated events) were collected using single parameter histograms (FL1-H). Negative control isotype IgG fluorescence values were subtracted from the geometric mean fluorescence of the test antibody (RmcB/53A.2). Isotype controls; Mouse IgG_1 for anti-CAR (RmcB) and Rat IgG_{2a} for anti-αvβ6 (53A.2). * Indicates cells provided by Dr. Ramon Alemany, Institut Català d'Oncologia (ICO), Barcelona, Spain. †MCF10CA1a is abbreviated throughout this study as CA1a. ‡ Flow cytometry performed by Marta Gimenez-Alejandre (ICO). ND = Not determined.

Section.3.1 Characterisation of Cell Lines

3.1.1. Screening of Cell Lines for αvβ6 and CAR Expression. A broad panel of human carcinoma cell lines was screened by flow cytometry to determine the levels of αvβ6 and CAR expressed on the surface (*Table*.10). Selected lines were additionally screened for levels of αvβ3, αvβ5 and αvβ8 integrins (*Table*.11); performed by Linda Hammond and Sabari Vallath. The integrin αvβ6 is highly expressed in numerous carcinomas, whereas the native adenovirus receptor, CAR, has been reported to be down-regulated (Anders *et al.*, 2009; Buscarini *et al.*, 2007; Jee *et al.*, 2002; Matsumoto *et al.*, 2005; Mikami *et al.*, 2001). In order to reflect this observation, a panel of cell lines with high αvβ6 expression and varying CAR expression was selected for initial *in vitro* studies. Most carcinoma cell lines expressed αvβ6. However the vast majority of these lines also expressed very high levels of CAR. The BT-20 and TR126 cells lines were the only endogenous, αvβ6-expressing cell lines which were identified as having low CAR. Conveniently, an isogenic matched pair of -β6 transfected, and non-transfected cells (DX3puro/DX3-β6), were identified which also had very low CAR expression.

TABLE 11. Selected Surface Integrin Expression[a]

	αvβ3		αvβ5		αvβ8	
	% Positive	Geo. Mean	% Positive	Geo. Mean	% Positive	Geo. Mean
A375puro	99.31	29.13	2.25	8.20	30.82	9.09
A375-β6	27.19	9.63	3.98	8.86	4.84	8.36
A549	N.D	N.D	N.D	N.D	4.80	22.30
DX3puro	97.90	27.32	93.54	19.11	86.39	20.37
DX3-β6	98.96	29.63	88.97	17.69	78.04	19.26

[a] Cell lines are listed alphabetically. Surface receptor expression profiles were obtained by flow cytometry using an LSR1 (Becton-Dickinson, CA, USA). Geometric mean fluorescence, and percent positive statistics ($1x10^4$ gated events) were collected using single parameter histograms (FL1-H). Negative control isotype IgG fluorescence values were subtracted from the geometric mean fluorescence of the test antibody. Isotype controls; Mouse IgG_1 for anti-αvβ3 (23C6), anti-αvβ5 (P1F6) and anti-αvβ8 (14E5). ND = Not determined. Flow cytometry was performed by Linda Hammond and Sabari Vallath.

3.1.2. Generation of Stable -β6 Expressing Cell Lines. Several -β6 expressing cell lines were generated in this study by retroviral transduction of -β6 cDNA (see *Table*.7). In order to facilitate the amplification and titration of non-CAR binding, but A20-retargeted viral constructs, viral producer cell lines HEK293-β6 and JH293-β6 cells were generated which expressed high levels of αvβ6 on the cell surface (*Fig*.3.1A-D). CHO-αvβ6 cells were generated also (*Fig*.3.2A+B). In an attempt to generate potential *in vivo* models, -β6 cDNA was also introduced into SKOV3ip1 and A549 cells (*Fig*.3.3 and *Fig*.3.4). Several attempts to generate stable -β6-expressing low CAR lines, NP-9 and CAOV3, failed.

3.1.3 FACS Sorting of -β6 Expressing Lines. Transfected cells were selected in puromycin-containing medium, and passaged for several weeks. Once sufficient stocks had been generated, high expressing populations for HEK293-β6, JH293-β6, CHO-αvβ6 and SKOV3ip1-αvβ6 cells were selected by cell sorting (FACS), as described in *Section*.2.1.6. Expression profiles were assessed prior to, and, following cell sorting (see *Fig*.3.1-*Fig*.3.4).

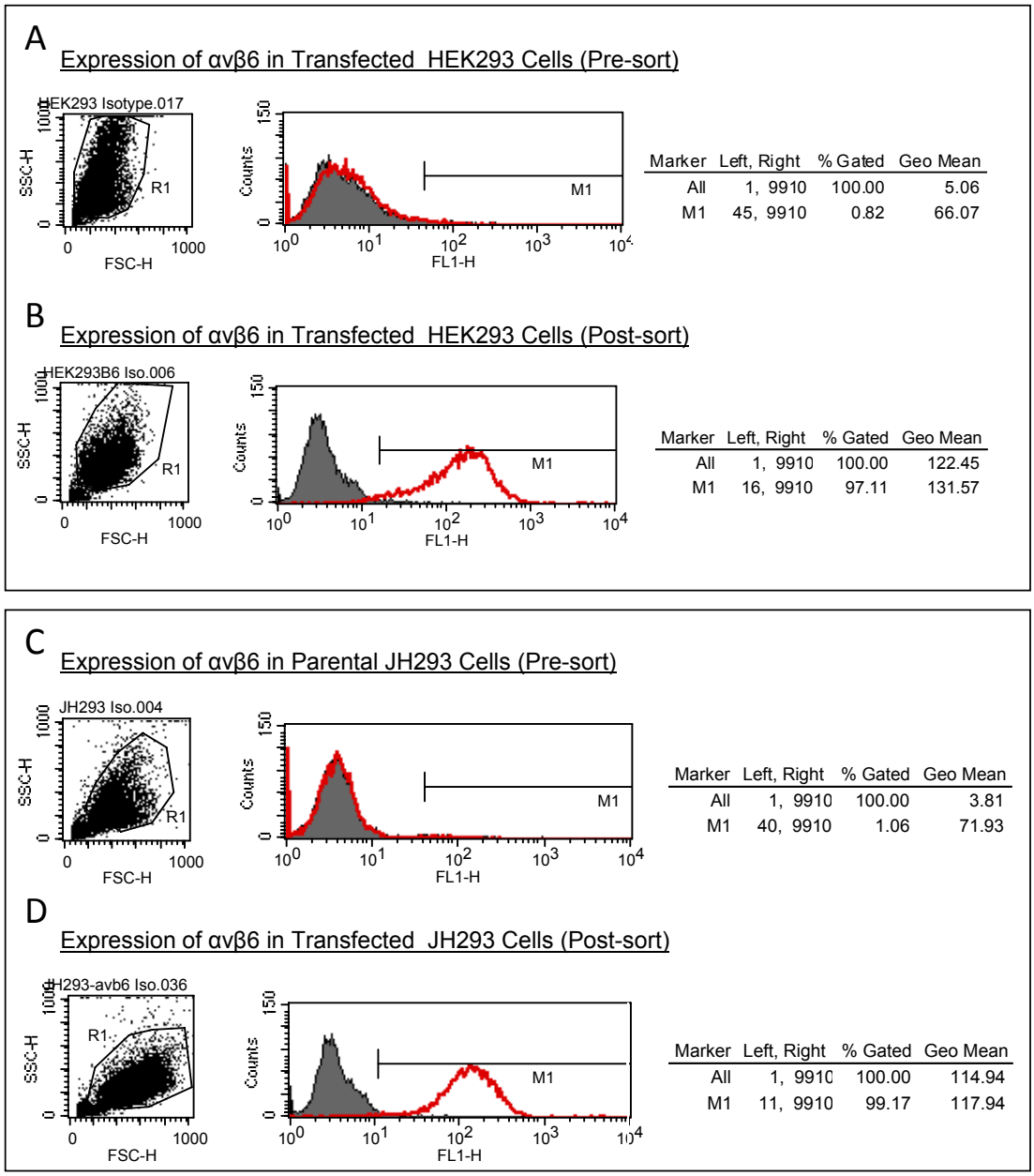

***Figure.*3.1 (A+B) Expression of αvβ6 in HEK293/HEK293-β6 Cells.** HEK293 cells were screened by flow cytometry, pre- and post- retroviral transduction of -β6 cDNA, for surface expression of αvβ6 integrin. Antibodies used were rat, anti-αvβ6 antibody, 53A.2 (IgG_{2a}) and a donkey anti-rat AlexaFluor488 conjugate. **(C+D) Expression of αvβ6 in JH293/JH293-β6 Cells.** Surface levels were determined as before, and a high expressing population of each cell line was further selected by fluorescence activated cell sorting (FACS). Cells were renamed HEK293-β6/JH293-β6. Labelled cells were scanned onto an LSR1 flow cytometer, a gate set to exclude dead cells and debris and $1x10^4$ gated events acquired. Statistics were collected from single parameter histograms.

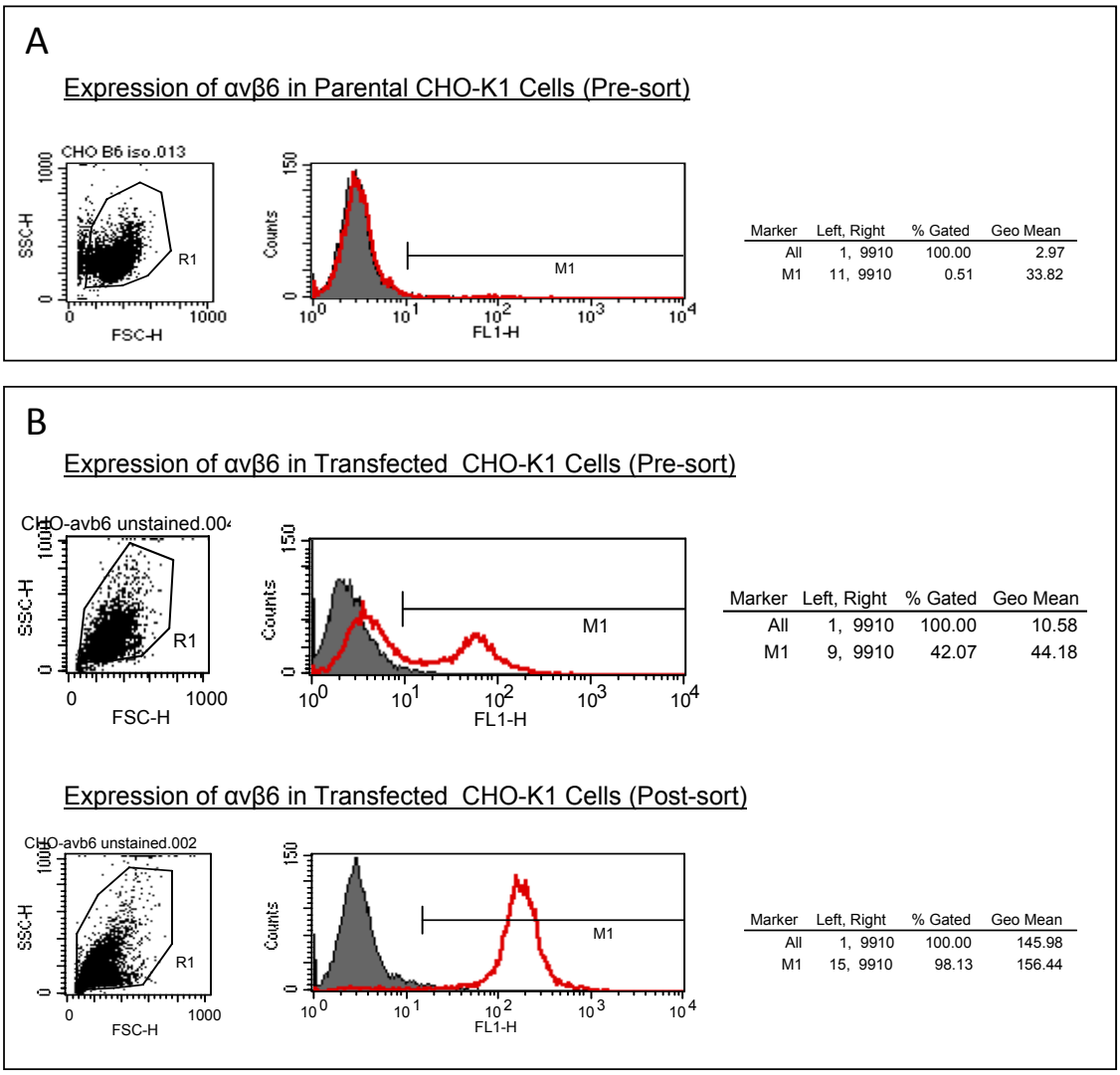

***Figure*.3.2 Expression of αvβ6 in CHO-K1/CHO-β6 Cells. (A)** CHO-K1 cells were screened by flow cytometry, pre- and post- transfection of –β6 cDNA, for surface expression of αvβ6 integrin. Antibodies used were rat, anti-αvβ6 antibody, 53A.2 (IgG_{2a}) and a donkey anti-rat AlexaFluor488 conjugate. **(B) Expression of αvβ6 in CHO-K1 Cells Following Retroviral Transfection of –β6 cDNA.** Parental CHO-K1 cells were retrovirally transduced with -β6 cDNA, and were selected in puromycin containing medium for several weeks following transfection. Surface levels were determined as before, and a high expressing population further selected by fluorescence activated cell sorting (FACS). These cells were renamed CHO-αvβ6. Labelled cells were scanned onto an LSR1 flow cytometer, a gate set to exclude dead cells and debris and $1x10^4$ gated events acquired. Statistics were collected from single parameter histograms.

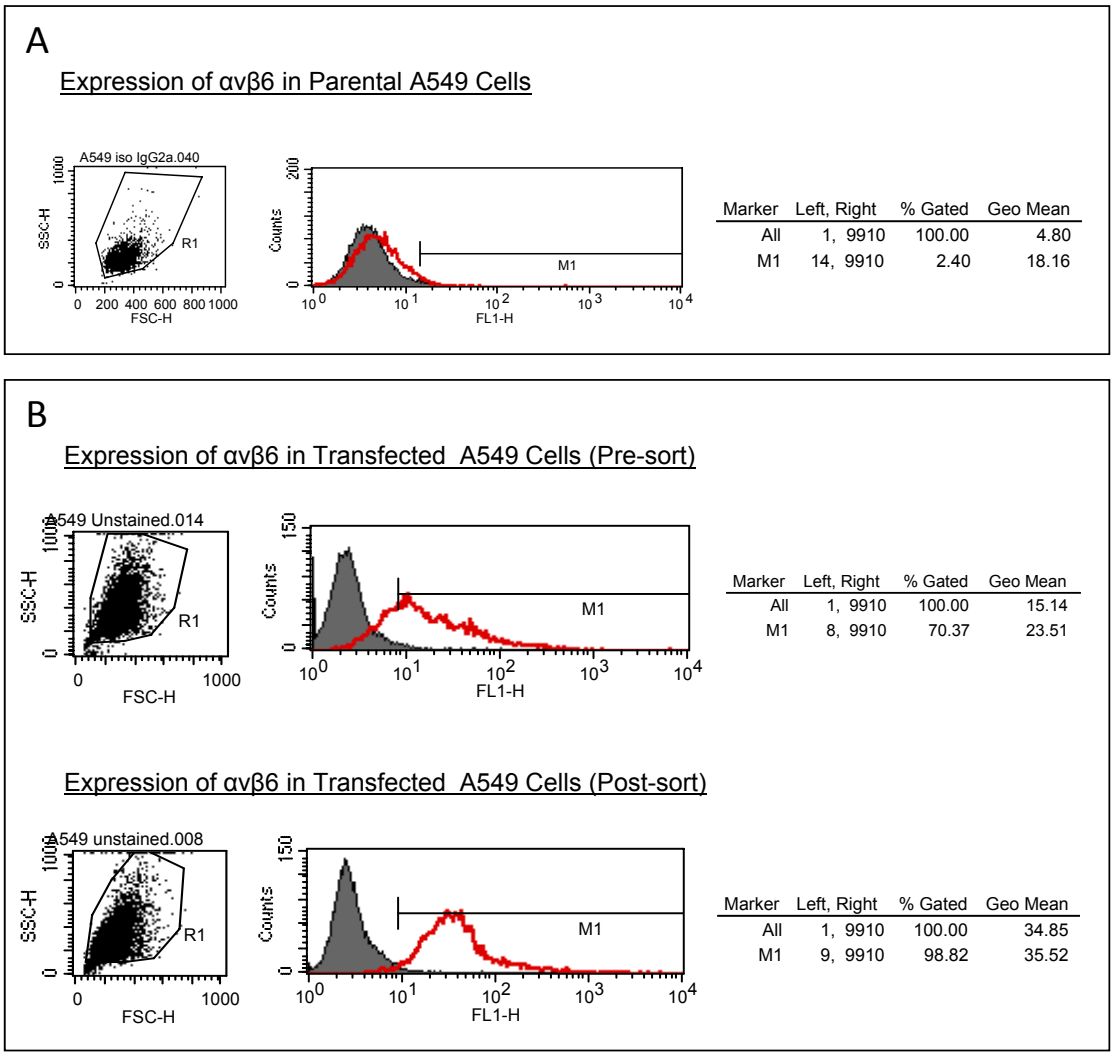

***Figure.*3.3 Expression of αvβ6 in A549/A549-β6 Cells. (A)** A549 cells were screened by flow cytometry, pre- and post- transfection of –β6 cDNA, for surface expression of αvβ6 integrin. Antibodies used were rat, anti-αvβ6 antibody, 53A.2 (IgG_{2a}) and a donkey anti-rat AlexaFluor488 conjugate. **(B) Expression of αvβ6 in A549 Cells Following Retroviral Transfection of –β6 cDNA.** Parental A549 cells were retrovirally transduced with -β6 cDNA, and were selected in puromycin containing medium for several weeks following transfection. Surface levels were determined as before, and a high expressing population further selected by fluorescence activated cell sorting (FACS). These cells were renamed A549-αvβ6. Labelled cells were scanned onto an LSR1 flow cytometer, a gate set to exclude dead cells and debris and $1x10^4$ gated events acquired. Statistics were collected from single parameter histograms.

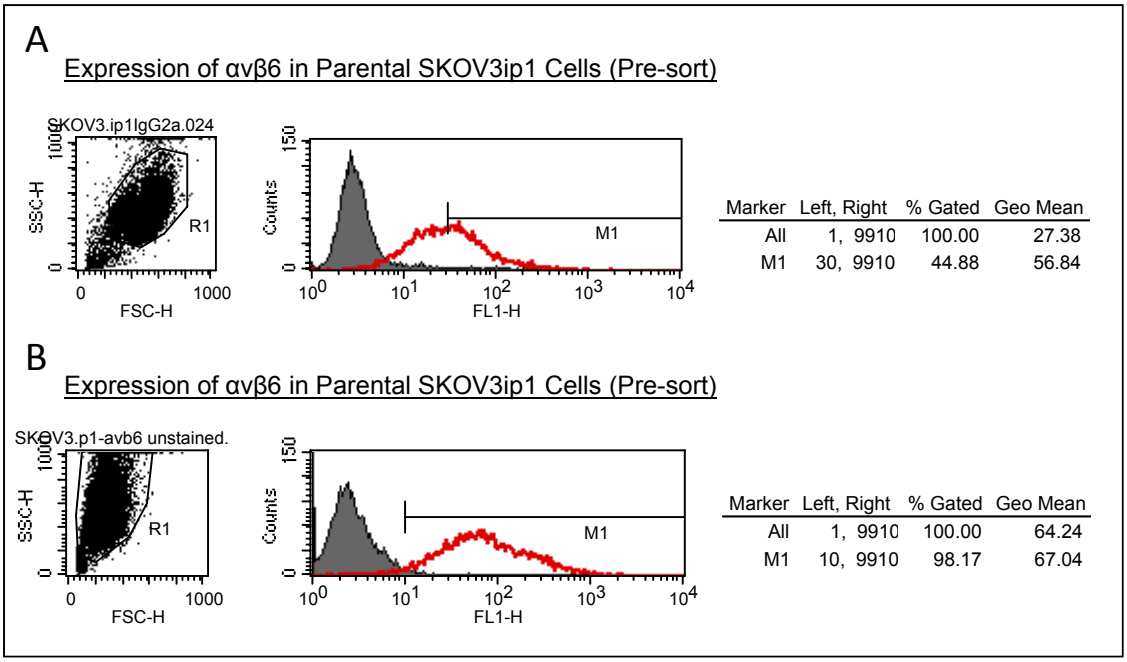

***Figure.*3.4 Expression of αvβ6 in SKOV3ip1/SKOV3ip1-β6 Cells. (A)** Ovarian SKOV3ip1 cells were screened by flow cytometry, pre- and post- transfection with –β6 cDNA, for surface expression of αvβ6 integrin. Antibodies used were rat, anti-αvβ6 antibody, 53A.2 (IgG_{2a}) and a donkey anti-rat AlexaFluor488 conjugate. **(B) Expression of αvβ6 in SKOV3ip1 Cells Following Retroviral Transfection of –β6 cDNA.** Parental SKOV3ip1 cells were retrovirally transduced with -β6 cDNA, and were selected in puromycin containing medium for several weeks following transfection. Surface levels were determined as before, and a high expressing population further selected by fluorescence activated cell sorting (FACS). These cells were renamed SKOV3ip1-αvβ6. Labelled cells were scanned onto an LSR1 flow cytometer, a gate set to exclude dead cells and debris and $1x10^4$ gated events acquired. Statistics were collected from single parameter histograms.

*Section.*3.2 *In Vitro* Characterisation of A20-Modified, Recombinant Ad5 Knob Proteins

We previously identified the A20FMDV2 peptide as having high affinity and specificity for αvβ6 integrin (DiCara *et al.*, 2008; DiCara *et al.*, 2007). Previous attempts to redirect the tropism of adenoviruses through the incorporation of peptide ligands into the HI loop, or C-terminus of the fibre knob domain have been successful. These insertions have included the insertion of the RGD-4C motif (Dmitriev *et al.*, 1998; Krasnykh *et al.*, 1998; Wickham *et al.*, 1997), TAT peptide from HIV-1 (Kurachi *et al.*, 2007b), or the cationic polylysine (pK7) motif (Cripe *et al.*, 2001; Dmitriev *et al.*, 1998; Krasnykh *et al.*, 1998; Wickham *et al.*, 1997), in addition to various other peptides, most of which are identified using phage display strategies (Denby *et al.*, 2007; Nicklin *et al.*, 2001). However, no prior attempts have been made to retarget Ad5 to αvβ6. We proposed that the genetic incorporation of A20FMDV2 into the HI loop of Ad5 would permit high efficiency retargeting to αvβ6.

The insertion of heterologous targeting ligands does not automatically correlate with the retention of their function in the context of the trimeric fibre, and frequently these insertions are incompatible with viral assembly. Therefore, the functionality of the A20FMDV2 peptide within the structural constraints of the adenovirus knob domain was assessed, prior to generating recombinant Ad5 genomes. A20-modified adenoviral knob expression vectors were generated and recombinant $Knob_{A20}$ protein produced and purified. A number of *in vitro* functional experiments were used to validate and characterise these 6XHIS-tagged, A20-modified Knob proteins.

3.2.1 Predictive Modelling of A20 Helix Formation within $Knob_{A20}$. It has been shown previously that the specificity of the A20FMDV2 peptide for αvβ6 is dependent on the formation of a critical post-RGD, C-terminal α-helical loop (DiCara *et al.*, 2007). To model theoretically whether the A20FMDV2 peptide could assume its critical helical conformation within the adenoviral knob protein, Agadir software (http://www.embl-heidelberg.de/Services/serrano/agadir/agadir-start.html) was used to predict the potential helical propensity of A20FMDV2 within $Knob_{A20}$ (*Fig.*3.5). This analysis was based on the A20FMDV2 protein sequence, flanked by ten native Ad5 residues on either side (not shown). The algorithm prediction was favourable; in fact the flanking residues appeared to further enhance the helicity. Therefore, we proceeded with the construction of the $Knob_{A20}$ expression vector for *in vitro* characterisation.

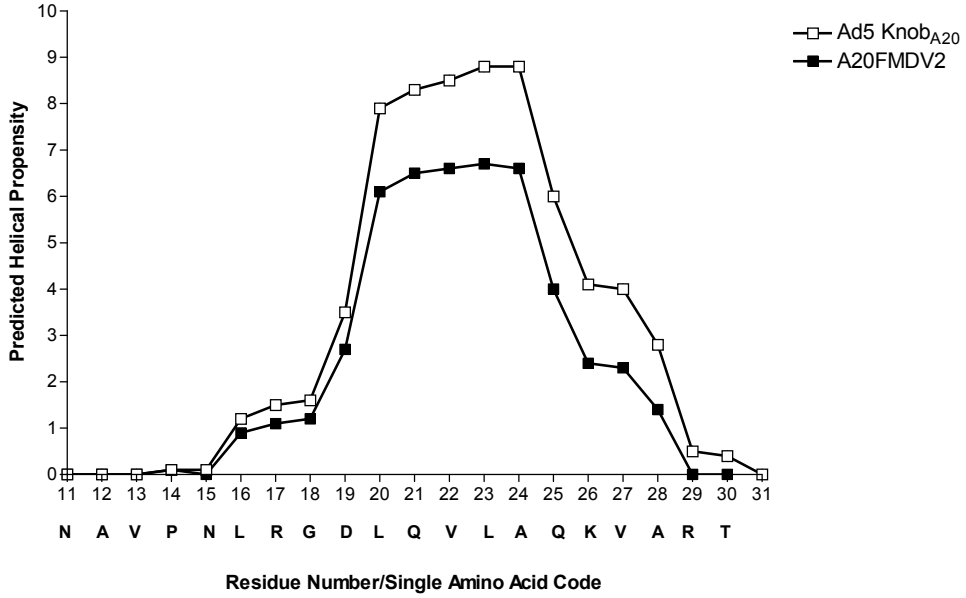

***Figure*.3.5 Predicted Helical Propensity of A20FMDV2 Determined using AGADIR Software.** AGADIR is an algorithm which predicts the helical content of peptides (Munoz & Serrano, 1997). The effect of adenoviral residues flanking the HI loop insertion site, on helix formation in A20FMDV2, was assessed. Ten flanking amino acid residues from Ad5 Knob were included on either side of A20FMDV2 (not shown, but included in the analysis). The service is provided by the Serrano group (http://www.embl.de /Services/serrano/agadir/agadir-start.html).

3.2.2 Sequencing Analysis of pQEKnob Expression Plasmids. Once the pQE30-based expression vectors had been constructed, they were screened by PCR and/or restriction digestion, and positive clones confirmed by sequencing analysis. Sequencing confirmed that the modified Knob sequences were in frame with the N-terminal, 6XHIS-tag. A ClustalW protein alignment of all modified Knob proteins generated in this study can be found in *Appendix I.*

3.2.3 Recombinant Knob Protein Expression and Purification. Optimisation of recombinant protein expression and purification was carried out by Tobias Simmonds at the Protein Cloning and Isolation Laboratory, London Research Institute, CR-UK. A time course for Knob$_{WT}$ protein expression was performed and ~4hrs post-IPTG induction was found to be the adequate time for harvesting cells for protein purification (*Fig*.3.6A). Elution under native conditions was also optimised by Tobias Simmonds who produced the first batch of Knob$_{WT}$ and Knob$_{A20}$. A representative protein expression profile following IPTG-induction is shown in *Fig*.3.6B. Samples were run on a 12% SDS-PAGE gel and the approximate molecular weights (M_w) of the monomers were detected at ~22.1kDa for Knob$_{WT}$ and ~24.4kDa for Knob$_{A20.}$ Approximate M_w values were predicted using VectorNTI software, following translation of the nucleotide sequence of the relevant expression vector into amino acid sequence.

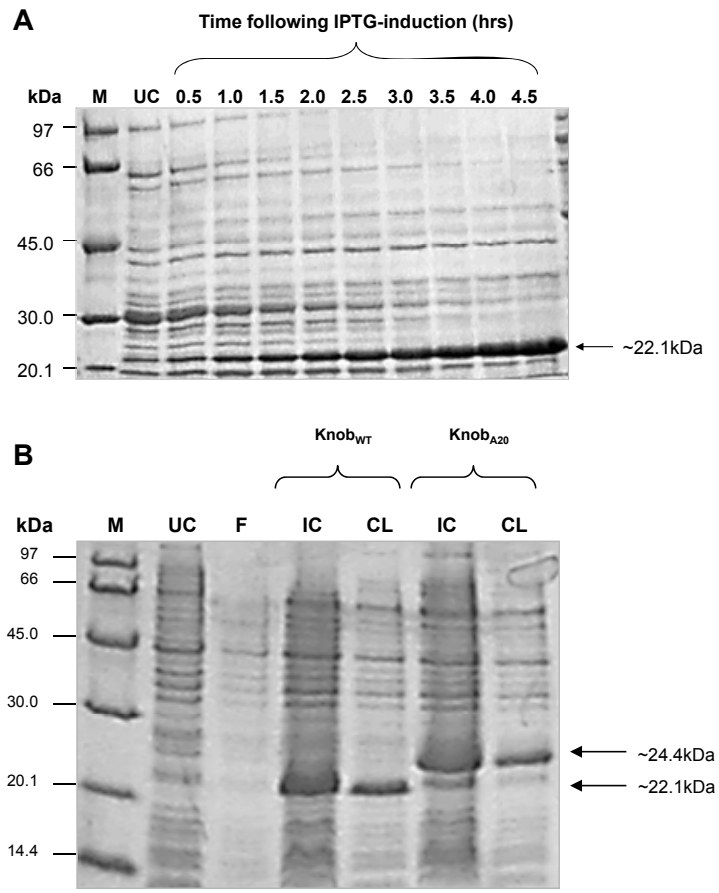

***Figure*.3.6 (A) Time-course of IPTG-induced $Knob_{WT}$ protein expression.** Optimisation of recombinant $Knob_{WT}$ protein expression was carried out by Tobias Simmonds at the Protein Cloning and Isolation Laboratory, London Research Laboratories, CR-UK. Arrow indicates the ~22.1kDa $Knob_{WT}$ monomer. M = Marker (Rainbow Marker, Amersham Biosciences), UC = Uninduced Control. **(B) Expression Profile for $Knob_{WT}$ and $Knob_{A20}$ at ~4hrs post-IPTG Induction.** M = Marker, UC = Uninduced Control, F = Flowthrough, IC = Induced Control, and CL = Cleared Lysate. Arrows indicate the $Knob_{WT}$ monomer (~22.1kDa) and the $Knob_{A20}$ monomer (~24.4kDa).

As expected, uninduced control cells did not over-express Knob protein, whereas, in comparison in the induced fractions for $Knob_{WT}$ and $Knob_{A20}$, the appropriate sized bands were clearly visible. In addition, cleared lysate fractions, which were run in parallel, also retained the appropriate size band, wash or flowthrough fractions did not. Following optimisation of the purification protocol, we performed all subsequent protein expression and purification procedures (*Fig*.3.7). HIS-tagged Knob proteins were isolated using an Ni-NTA Agarose column (see *Section*.2.4.5). $Knob_{A20}$ was eluted under native conditions using a concentration gradient (50mM-300mM Imidazole), and eluate fractions analysed by visualisation on an SDS-PAGE gel. Appropriate fractions which had high purity (ie. no contaminating bands) were pooled, dialysed overnight against PBS, and purified protein concentrations calculated using the Pierce BCA protein assay.

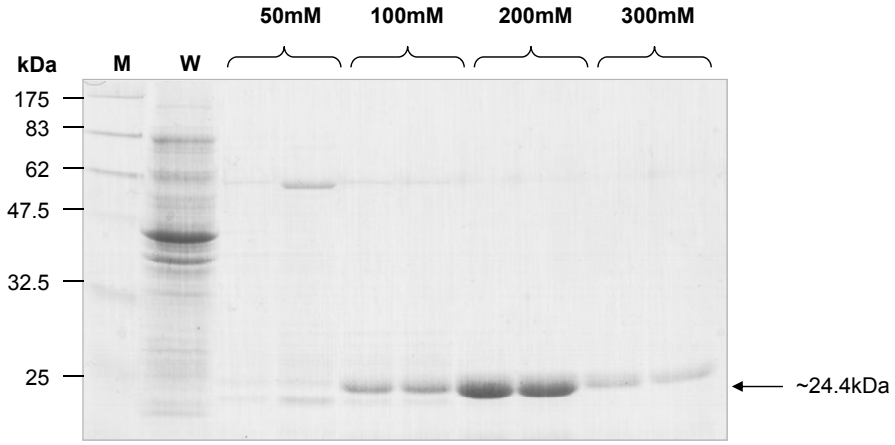

***Figure*.3.7 Elution Profile for Knob$_{A20}$.** Elution fractions were run on a 12% SDS-PAGE gel and bands visualised by Coomassie's staining. Fractions which were determined to have high purity (≥ 200mM), were pooled and dialysed overnight against PBS. M = Marker (NEB Prestained Broad Range 6-175kDa). Imidazole concentrations ranging from 50-300mM were used to elute protein under native conditions. Arrow indicates the band corresponding to the Knob$_{A20}$ monomer (~24.4kDa).

3.2.4 Trimerisation Assay. It has been reported previously that the HI loop can tolerate insertions of up to 83aa with negligible effects on virion integrity, or viral titres obtained (Belousova *et al.*, 2002). However, we wished to confirm that the insertion of the A20FMDV2 peptide sequence at this site would not affect trimerisation of the fibre, prior to amplifying the modified virus. Therefore, the ability of Knob$_{WT}$, and more importantly Knob$_{A20}$, to form a homotrimer was confirmed by SDS-PAGE carried out under semi-denaturing conditions, comparing the migration of boiled and unboiled samples, which were run in parallel (data not shown).

3.2.5 Validation of Knob$_{A20}$ Binding to αvβ6 Integrin. Using a flow cytometry-based competition experiment we confirmed that Knob$_{A20}$ was capable of binding to cells expressing αvβ6 (*Fig*.3.8). It was decided that direct detection of cell-bound Knob$_{A20}$ (via the HIS-tag) was not a suitable approach, since we could not eliminate the possibility that background binding to CAR would affect the results, even on a low CAR-expressing cell line. Therefore, an indirect approach was employed. Using BT-20 cells (high levels of αvβ6 but low levels of CAR) we tested the ability of increasing concentrations of Knob$_{A20}$ (0.0001µg-10µg/10^5 cells) to bind to surface αvβ6, and to competitively inhibit the subsequent binding of an anti-αvβ6 mAb, 53A.2. Levels of bound 53A.2 were detected using a secondary, donkey anti-rat AlexaFluor488-conjugated antibody, and results were analysed by flow cytometry, acquiring fluorescence in FL1-H. BT-20 cells, untreated with recombinant Knob protein, were taken to be 100% (=100% antibody binding), and all other values were expressed relatively, as a % of the untreated cells. Results demonstrated that Knob$_{A20}$ exhibited dose-dependent inhibition of αvβ6-specific antibody binding, with 50% maximal

inhibition at 0.03µg/10^5 cells. $Knob_{WT}$ was included as a control, but was unable to block 53A.2 binding at a high concentration (≥10µg/10^5 cells) and did not differ from untreated cells (*p*=0.498). This experiment confirmed that the A20FMDV2 peptide, within $Knob_{A20}$, was functional with respect to its ability to bind to αvβ6.

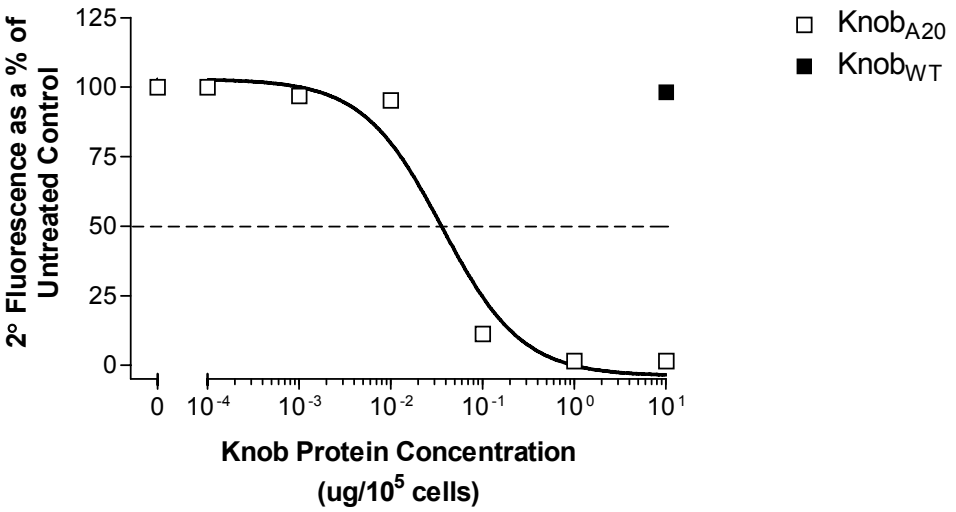

***Figure*.3.8 Competitive Inhibition of 53A.2 Binding to αvβ6 Integrin by $Knob_{A20}$.** BT-20 cells (low CAR, high αvβ6) were incubated n ice with increasing concentrations of $Knob_{A20}$ (0.0001-10µg/10^5 cells), or $Knob_{WT}$ (10µg/10^5 cells). Antibody 53A.2 was added to cells without washing and cells incubated at 4˚C for 1hr. Binding was analysed by flow cytometry following the addition of a secondary donkey anti-rat AlexaFluor488 conjugate. Untreated cells were taken as 100% fluorescence and all other values expressed relative to this (see *Section*.2.5.3). $Knob_{WT}$ produced no significant effect at 10µg/10^5 cells (*p*=0.498), and is indicated by a single point on the graph. The affinity of of $Knob_{A20}$ for αvβ6 has not been detemined directly. Results were analysed by non-linear regression fitted to a sigmoidal curve, using GraphPad Prism Version 3.03 (GraphPad Software, San Diego, USA). Data represent the mean ± SD of triplicate samples (no bars represent SD values smaller than the symbol used).

3.2.6 Functional Inhibition of αvβ6-Dependent Cell Migration by $Knob_{A20}$. The ability of $Knob_{A20}$ to functionally inhibit αvβ6-dependent, VB6 cell migration towards the latency associated peptide (LAP) of TGF-β1 was confirmed using a Transwell migration assay (*Fig.*3.9A+B). VB6 cells have been modified to express high levels of αvβ6, and migrate towards LAP using only αvβ6 (Thomas *et al.*, 2002). A preliminary experiment was carried out in order to titrate the effective concentration required for this assay (*Fig*.3.9A). Knob proteins were used at concentrations of µg/ml instead of µg/10^5 cells to permit comparisons with previously titrated function-blocking antibodies. The ability of $Knob_{A20}$ to inhibit αvβ6-dependent cell migration at concentrations in the range of 5-100µg/ml was assessed over a period of 24hrs. A BSA protein control (no LAP) was included in the experiment to represent the basal level of random αvβ6-independent cell migration, and each value was normalised to this. $Knob_{A20}$ successfully abrogated cell migration at all concentrations used (*p*<0.001), as efficiently as an anti-αvβ6 inhibitory antibody (10D5) even at the lowest concentration used (5µg/ml; *p*=0.982).

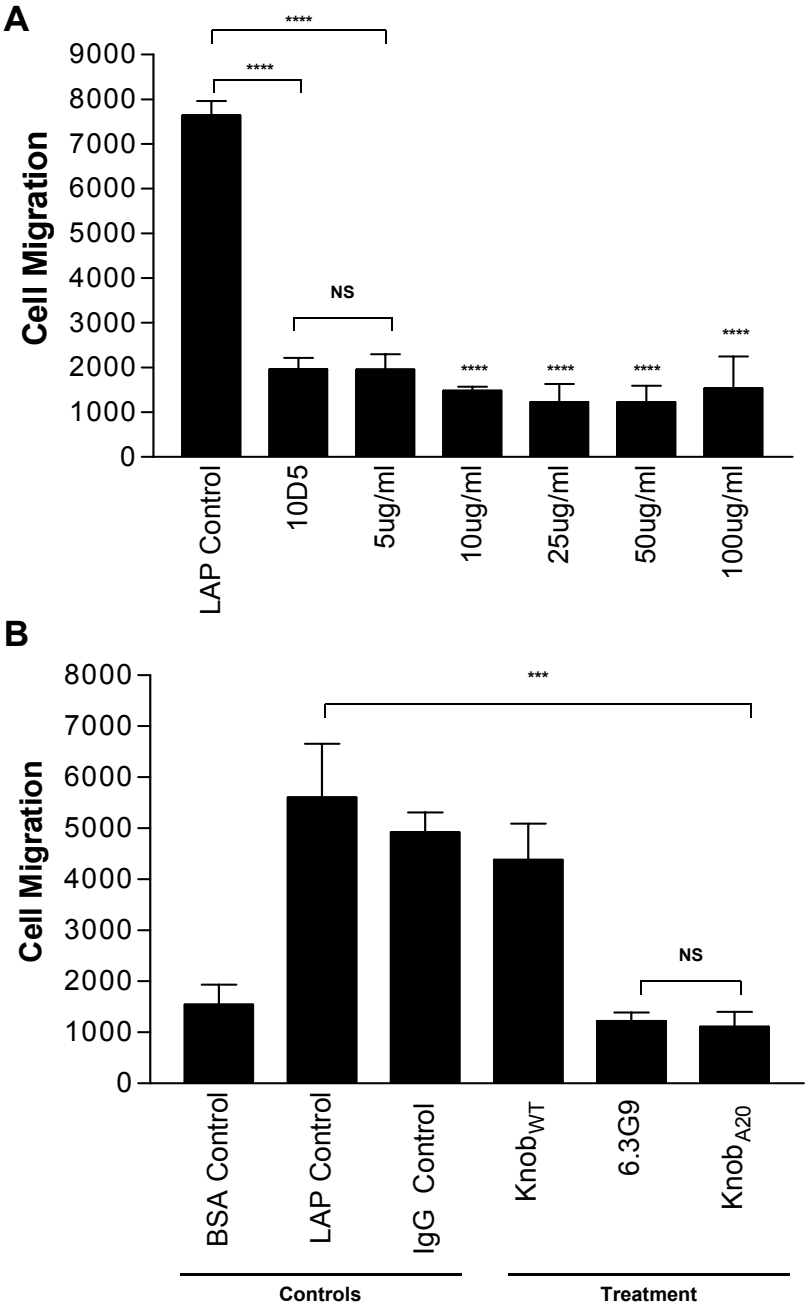

Figure*.3.9 (A) Knob$_{A20}$ Inhibition of αvβ6-Dependent Cell Migration.** Knob$_{A20}$ abrogates the αvβ6-dependent migration of VB6 cells towards Latency Associated Peptide (LAP) of TGF-β1. A BSA protein control was included to represent the basal level of non αvβ6-dependent cell migration, and all results normalised to this control. An αvβ6-specific, function blocking antibody (10D5) was included as a positive control for inhibition of migration. Knob$_{A20}$ inhibited αvβ6-dependent migration at all concentrations used. **(B) Knob$_{A20}$ Inhibition of αvβ6-Dependent Cell Migration.** The migration experiment was repeated to include the relevant controls; BSA protein control, LAP control and IgG$_1$ isotype control. Additionally Knob$_{WT}$ was included at an equivalent concentration to Knob$_{A20}$ and an αvβ6-specific function blocking antibody 63G.9 (all used at 10µg/ml). Data represent the mean ± SD of triplicate samples. Statistical significance was determined using the unpaired Student's *t*-test comparing the means of two samples (* indicates a *P*-value of <0.0001, *** *p*<0.001, NS *p*>0.05). Statistics displayed above the histogram, refer to the difference when compared to the LAP positive control.

In a separate experiment, the migration assay was repeated to include an isotype antibody (IgG_1), and $Knob_{WT}$ as non-inhibitory controls (*Fig*.3.9B). Again, $Knob_{A20}$ significantly inhibited VB6 cell migration towards LAP (p=0.002), functioning as efficiently as 6.3G9, an αvβ6-inhibitory antibody (p=0.595). In contrast, $Knob_{WT}$, used at an equal concentration (10µg/ml), produced no significant effect (p=0.173). In this particular experiment, the background migration (BSA protein control) was not subtracted from the overall migration, but is represented on the graph to show that $Knob_{A20}$ is capable of reducing cell migration to basal levels. These data confirmed that the A20FMDV2 insertion, within the structural constraints of the adenovirus Knob protein, was functional with respect to abrogation of αvβ6 function.

Section.3.3 Generation of αvβ6 Retargeted, Fibre-Modified Adenoviruses

Viral genome-containing YAC/BACs, generated by homologous recombination in yeast, were transformed into bacteria and screened by PCR for the incorporation of the A20FMDV2 sequence. Clones which were positive by PCR screening were sequenced and verified prior to viral production and expansion.

3.3.1 PCR Screening of Shuttle Vectors and A20-Modified, Ad5-containing YACs.

The A20FMDV2 oligoduplex sequence was blunt end ligated into *Sfo*I digested pIV_{SfoI} to generate the A20-modifying shuttle pIV_{A20}. In order to select clones which had a single A20FMDV2 insertion and not a duplication of the sequence, pIV_{A20} plasmid minipreps were screened by PCR using primers AdinPCR-*forward* and AdinPCR-*reverse* (*Fig*.3.10). pIV_{SfoI} was used as a negative control, generating a product of ~184bp. A ~244bp PCR product was generated for positive clones which had incorporated a single A20FMDV2 oligoduplex. Selected clones were further confirmed by sequencing analysis, using T3-*forward* and T7-*reverse* primers. At a later stage, the region of homology within pIV_{A20} was extended to improve the probability of recombination, creating p$IV1.4_{A20}$. This cloning strategy did not affect the A20FMDV2 insertion, and the p$IV1.4_{A20}$ shuttle was created using pIV_{A20} as a template (see *Fig*.2.6). The p$IV1.4_{A20}$ construct was also sequenced using T3-*forward* and T7-*reverse* primers.

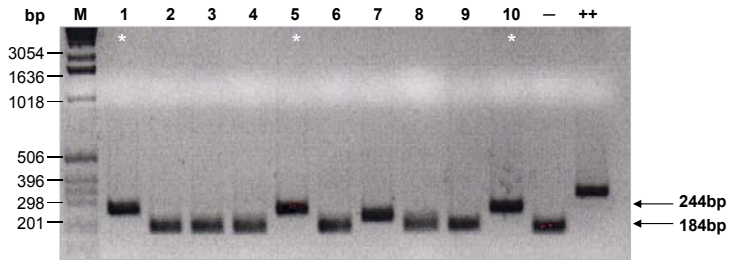

***Figure*.3.10 PCR Screening of A20-modified Shuttle Vectors.** A20FMDV2 modified pIV_{SfoI} clones were selected by PCR screening using primers AdinPCR-f*orward* and AdinPCR-*reverse.* Positive clones were distinguished from negative clones by the presence of a 60bp shift, detected by visualisation under UV light following gel electrophoresis on a 2% agarose gel. M = Marker (1kb DNA Ladder, Invitrogen), #1-10 indicates clone number, – indicates negative control (pIV_{SfoI} vector) and ++ indicates a clone with a duplicate A20FMDV2 insertion. Arrows highlight the size in bp of the negative clones (184bp) and the positive clones (244bp). An asterix highlights the clones selected for sequencing.

A20-modified, Ad5-containing YACs were screened at each stage of recombination. An overview of the "pop-in/pop-out" method of homologous recombination in yeast can be found in *Fig*.2.9. Intermediate stage or "pop-in" recombinants which had incorporated

the integrating shuttle vector were screened by PCR on purified yeast DNA, using primers AdinPCR-*forward* and AdinPCR-*reverse* (*Fig*.3.11A). Clones which were positive for the integrative event, generated either two bands at ~478bp and 418bp, or a single band at ~478bp. Negative clones produced a band at 418bp only. Only positive clones were selected for subsequent recombination (ie. "pop-out" stage). Final stage, or "pop-out" recombinants were screened by PCR using a different strategy (*Fig*.3.11B). Successfully modified Ad5 constructs were screened using a forward primer which had homology to the A20FMDV2 sequence (A20-*forward*), and a reverse primer (Ad5.2-*reverse*) which had homology to Ad5 sequence, external to that which had been cloned into the shuttle vector, p*IV*1.4$_{A20}$. This was to ensure that we did not obtain false positives by PCR (amplified from the intermediate "pop-in" stage of recombination, in which the shuttle vector sequence was integrated into the Ad5-containing YAC/BAC). Clones which failed to incorporate the A20FMDV2 insertion did not generate a PCR product.

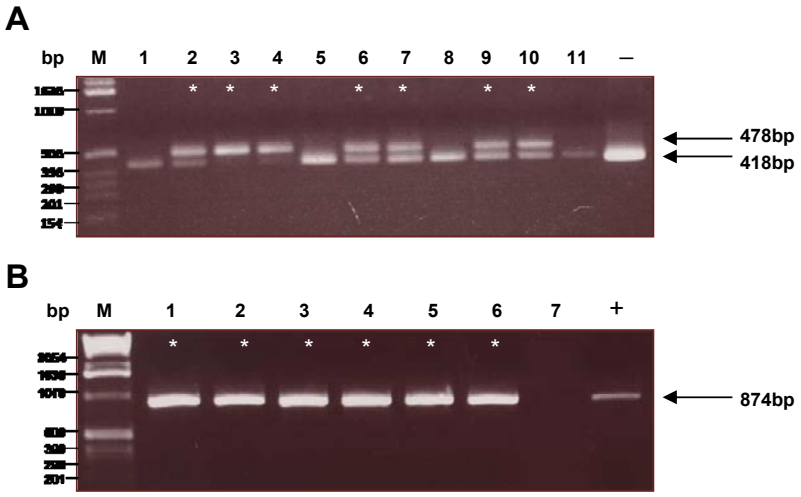

***Figure*.3.11 (A) PCR Screening of "Pop-in" A20-modified Ad5-Containing YACS.** Integrative recombination results in a duplication of the target sequence; the shuttle derived *fibre* sequence containing the mutation, and the YAC DNA containing unmodified Ad5 *fibre* sequence. Positive clones were identified by the presence of a ~60bp shift or by the presence of duplicate PCR products, of ~478bp and ~418bp, corresponding to the integrated p*IV*1.4$_{A20}$ shuttle and the Ad5 backbone DNA, respectively. M = Marker (1kb DNA Ladder, Invitrogen), #1-11 indicates clone number, – indicates negative control (pMB20, unmodifed Ad5-containing YAC DNA). Arrows highlight the size in bp of the positive clones (478bp) and the negative clones (418bp). An asterix highlights the clones selected for subsequent recombination events. **(B) PCR Screening of "Pop-out" A20-modified, Ad5-Containing Yeast Artificial Chromosomes.** Successful "pop-out" clones were screened by PCR using primers A20-*forward* and Ad5.2-*reverse*, so that a PCR product would be observed only when the A20FMDV2 insertion had been incorporated successfully. M = Marker (1kb DNA Ladder, Invitrogen), #1-7 indicates clone number, + indicates positive control (#3 from A). Arrows highlight the size in bp of the positive clones (244bp). An asterix highlights the clones selected for transformation into competent *E.coli*, and subsequent sequencing analysis.

3.3.2 Sequencing Analysis of Modified Ad5 Viral Genomes. An overview of the A20-fibre modification strategy is shown in *Fig*.3.12A. A sequencing chromatogram for the original, unmodified Ad5 fibre sequence is presented, highlighting the insertion site within the HI-loop. Additionally, the sequencing chromatogram obtained following the successful modification of the fibre region, generating Ad5-EGFP$_{A20}$, also is presented (*Fig*.3.12B).

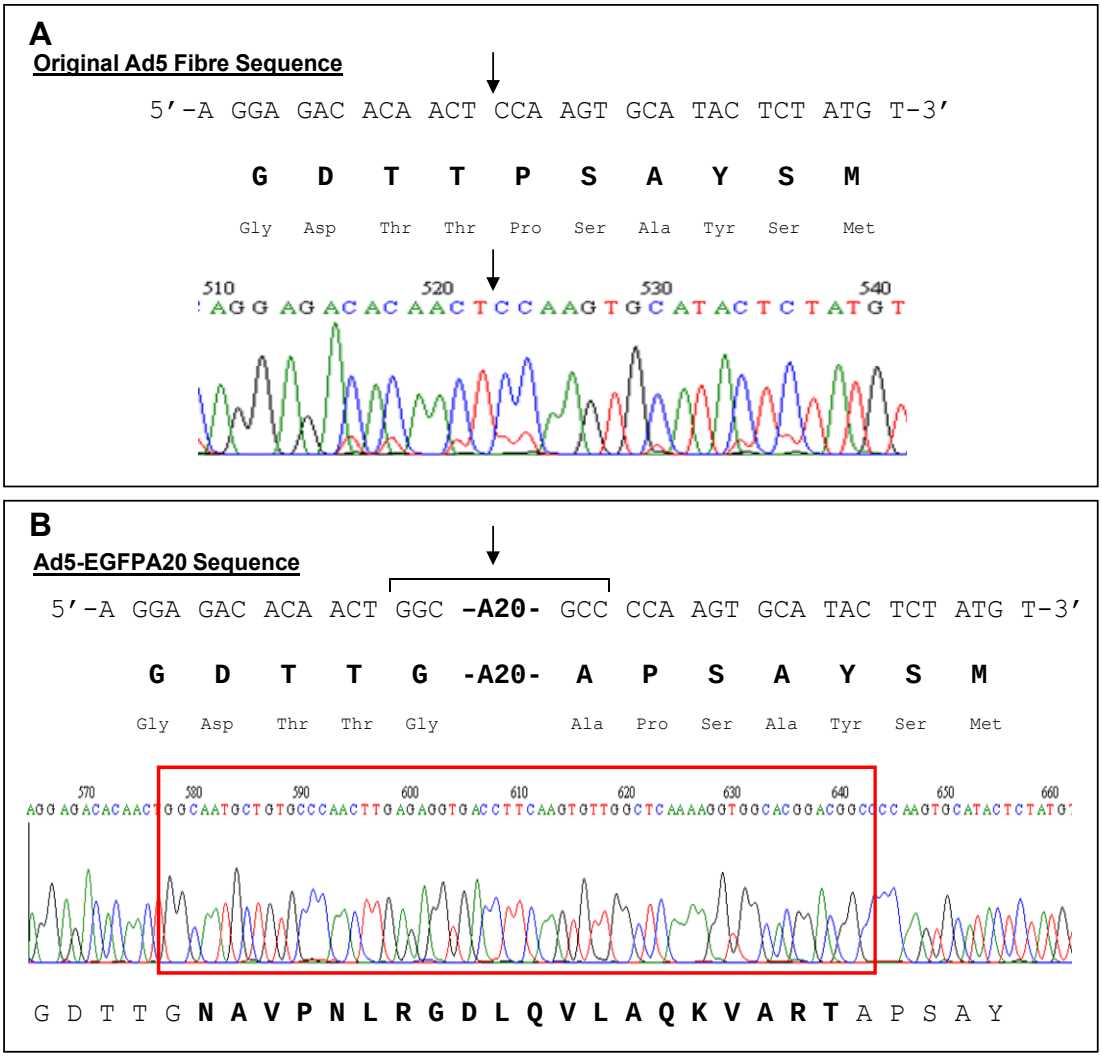

***Figure*.3.12 (A) Sequencing Confirmation of the Native Ad5 Fibre Sequence Prior to Modification.** A schematic showing the original nucleotide and amino acid sequence of the Ad5 fibre. Sequencing chromatogram shows the original, unmodified sequence. The arrow highlights the site selected for the insertion of the A20FMDV2 oligoduplex sequence. **(B) Sequencing Confirmation of the A20-Modified Fibre Sequence.** Nucleotide sequence and amino acid sequence, as before. The sequencing chromatogram confirms the successful insertion of the A20FMDV2 sequence by blunt end ligation into the unique engineered *Sfo*I site (see *Section*.2.3.4 and *Section*.2.3.5). The red box highlights the A20FMDV2 sequence, flanked on either side by wildtype Ad5 fibre sequence. The arrow again indicates the insertion site for A20FMDV2. Sequencing chromatograms were analysed using BioEdit Sequence Alignment Editor, version 7.0.5.3.

3.3.3 Comparative Infectivity on a Panel of αvβ6-Expressing Carcinoma Lines. The ability of the αvβ6-retargeted virus, Ad5-EGFP$_{A20}$, to enhance the infection of a panel of αvβ6-expressing human carcinoma cell lines was assessed relative to its control, Ad5-EGFP$_{WT}$ (*Fig*.3.13). A constant amount of virus (MOI 10) was added to cells for 1hr at 4˚C, to permit virus binding but not internalisation. Cells were incubated at 37˚C for 22hrs after which EGFP transgene expression was quantified by flow cytometry. Ad5-EGFP$_{A20}$ succeeded in enhancing the transduction of all cell lines investigated, even those which expressed high levels of CAR (p<0.0001 for all).

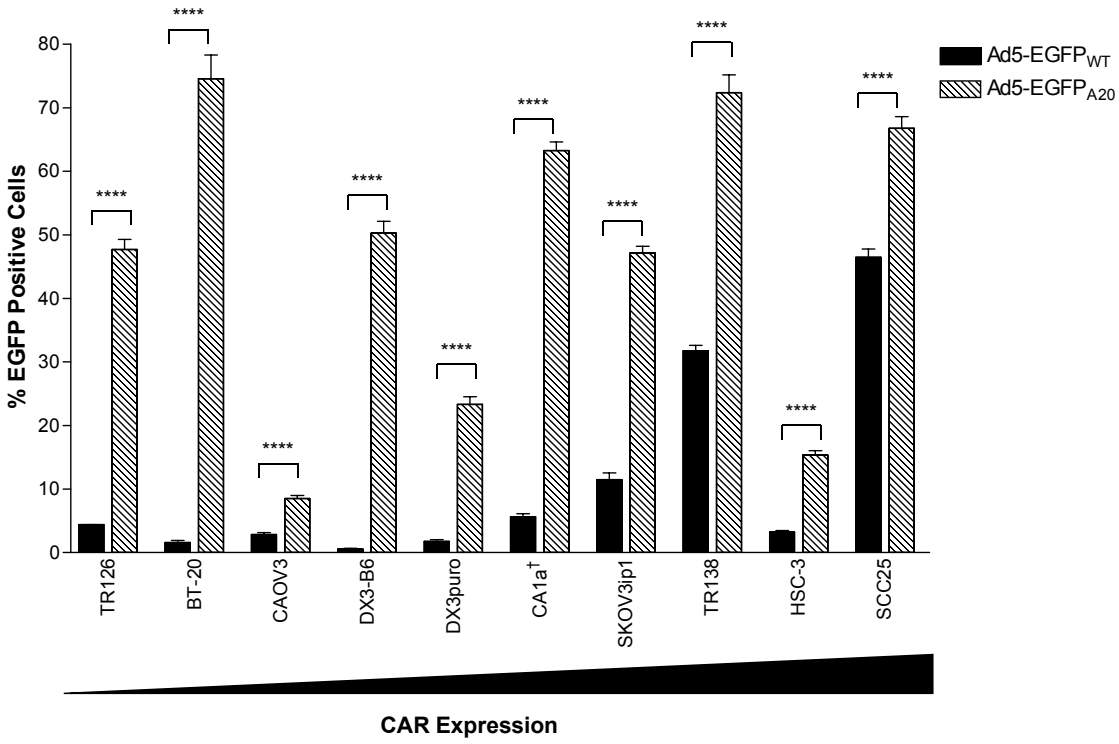

Figure*.3.13 Comparative Infectivity on a Panel of αvβ6-Expressing Human Carcinoma Lines.** A panel of cell lines was selected on the basis of their αvβ6, and CAR expression status (see *Table*.10). The transduction efficiency of Ad5-EGFP$_{A20}$ was compared with Ad5-EGFP$_{WT}$ at an MOI 10 (PFU/cell). Cells were exposed to virus for 1hr at 4˚C, to dissociate virus binding from internalisation, and EGFP gene transfer quantified by flow cytometry ~22hrs post-infection (see *Section*.2.8.2). The histogram represents the % EGFP positive cells and cells arranged are in order of increasing CAR expression levels (ranging from <5-92%, *see Table*.10). Data represent the mean ± SD of triplicate samples and are representative of at least two independent experiments. Statistical significance was determined using the unpaired Student's *t*-test comparing the means of the Ad5-EGFP$_{WT}$ and Ad5-EGFP$_{A20}$ groups for each cell line (* indicates a *P*-value <0.00001, bars indicate SD, no bars represent SD values smaller than the symbol used). †CA1a is abbreviated from MCF10CA1a throughout this study.

Moreover, the high efficiency transduction observed with Ad5-EGFP$_{A20}$ in low CAR cell lines, which were previously refractory or relatively insensitive to Ad5-EGFP$_{WT}$ mediated transduction, suggested that αvβ6 was capable of acting as an efficient

surrogate receptor for attachment/entry. In low CAR-expressing cell lines, a ~50-fold increase in transduction was observed on BT-20 and DX3-β6 cells infected with Ad5-EGFP$_{A20}$, when compared with Ad5-EGFP$_{WT}$. Increases of ~13-fold, ~11-fold, ~10-fold and ~3-fold were also observed for DX3puro, CA1a, TR126 and CAOV3 cells, respectively. On cells which had moderate-to-high levels of CAR-expression, increases in transduction of ~5-fold, ~2-fold and ~1.5-fold were observed for SKOV3ip1/HSC-3, TR138 and SCC25 cells, respectively.

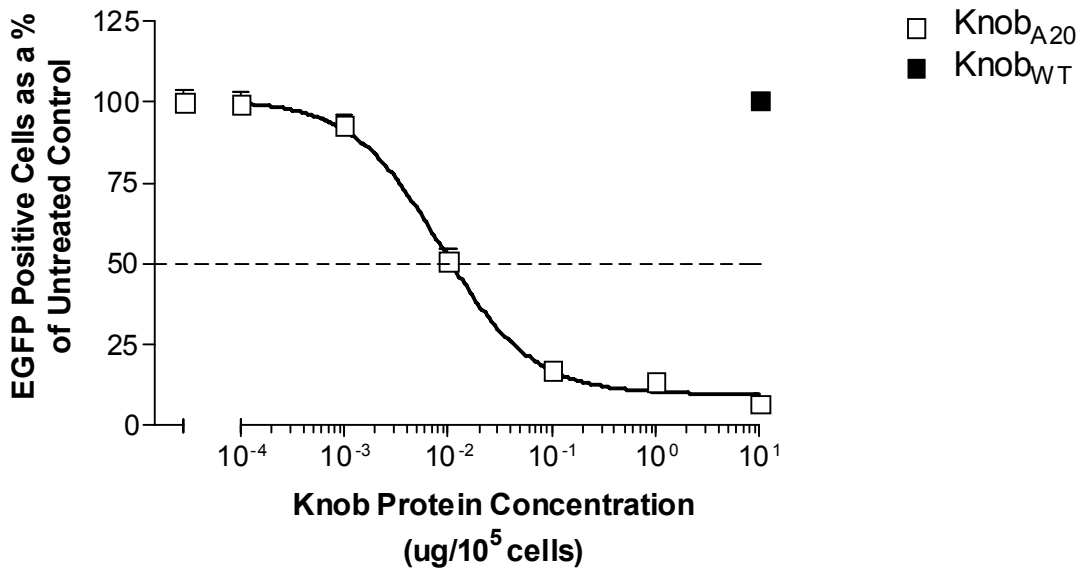

***Figure*.3.14 Competitive Inhibition of Ad5-EGFP$_{A20}$ Mediated Transduction by Knob$_{A20}$.** Knob$_{A20}$ binds to αvβ6 on BT-20 cells and inhibits the binding of, and therefore the transduction of, Ad5-EGFP$_{A20}$ in a dose-dependent manner. BT-20 cells (low CAR, high αvβ6) were incubated with increasing concentrations of Knob$_{A20}$ (0.0001-10μg/10^5 cells), or Knob$_{WT}$ (10μg/10^5 cells). Cells were incubated with Knob proteins for 1hr at 4˚C after which they were infected with a constant MOI of Ad5-EGFP$_{A20}$ (10) for a further hour at 4˚C. Virus was removed and EGFP gene transfer quantified ~22hrs later by flow cytometry. Untreated cells were taken as 100% fluorescence and all other values expressed relative to this (see *Section*.2.8.2). Knob$_{WT}$ produced no significant effect at 10μg/10^5 cells and is indicated as a single point on the graph. Results were analysed by non-linear regression fitted to a sigmoidal curve, using GraphPad Prism Version 3.03 (GraphPad Software, San Diego, USA). Data represent the mean ± SD of triplicate samples (no bars represent SD values smaller than the symbol used).

3.3.4 Calculation of the IC$_{50}$ of Knob$_{A20}$ for Inhibition of Ad5-EGFP$_{A20}$ Infection. Exploiting the fact that exogenously added Ad5 knob protein can inhibit the attachment of the virus from which it is derived (Freimuth *et al.*, 1999; Santis *et al.*, 1999), we compared the ability of Knob$_{WT}$ and Knob$_{A20}$ to inhibit the subsequent infection of Ad5-EGFP$_{A20}$. However, prior to the use of Knob$_{A20}$ in several competition assays, we calculated its IC$_{50}$ value for inhibition of Ad5-EGFP$_{A20}$ mediated infection (*Fig*.3.14). BT-20 cells were chosen for their high αvβ6 expression and low CAR expression. Cells

were pre-incubated with increasing concentrations of $Knob_{A20}$ (0.0001-10µg/10^5 cells), and then super-infected with Ad5-$EGFP_{A20}$ (MOI 10; PFU/cell). The virus-protein mixture was removed by washing, and cells processed for detection of EGFP gene transfer by flow cytometry 22hrs later, as described previously. Cells treated with virus alone were taken as 100% infection, and all other values expressed relative to this. The IC_{50} of $Knob_{A20}$ was calculated to be 0.008µg/10^5 cells. A high concentration of $Knob_{WT}$ (10µg/10^5 cells), which was included as a control in this experiment, produced no significant effect (p=0.969). These data further confirmed that the enhanced infection mediated by Ad5-$EGFP_{A20}$ was modulated through the insertion of the A20FMDV2 peptide into the HI loop region.

3.3.5 Characterisation of the Altered Tropism of Ad5-$EGFP_{A20}$. Data obtained previously confirmed that the enhanced infectivity observed with Ad5-$EGFP_{A20}$, was due to the insertion of the A20FMDV2 peptide sequence. However, we also wanted to demonstrate clearly, that this new tropism was mediated primarily through an interaction with αvβ6 integrin (*Fig*.3.15).

A suitable panel of αvβ6-expressing cell lines was chosen for this experiment; low CAR-expressing lines, BT-20, DX3-β6 and TR126, and moderate-high expressing lines, SKOV3ip1, TR138 and SCC25. To characterise the tropism determinant for Ad5-$EGFP_{A20}$ fully, infectivity experiments were carried out in the presence of the following inhibitors; $Knob_{WT}$, $Knob_{A20}$, or a function-blocking antibody to αvβ6, 53A.2. Ad5-$EGFP_{WT}$ was included as a control (data not shown), producing similar levels of infectivity as shown in *Fig*.3.13. $Knob_{WT}$ successfully inhibited Ad5-$EGFP_{WT}$ infection (data not shown). $Knob_{WT}$ did not affect the entry of Ad5-$EGFP_{A20}$ on any cell line (p>0.200 for all), except in SKOV3ip1 cells (p=0.01). In contrast, pre-incubation of all cell lines with $Knob_{A20}$ resulted in a significant reduction in Ad5-$EGFP_{A20}$ infectivity (p<0.0001 for all). Function blocking of αvβ6, using 53A.2, resulted in the significant reduction of Ad5-$EGFP_{A20}$ mediated infection, over the entire panel of cell lines (p<0.0001 for all). This reduction was most apparent in lines which had low CAR. These data confirmed that αvβ6 was the predominant determinant of Ad5-$EGFP_{A20}$ entry *in vitro*. Additionally, the ability of Ad5-$EGFP_{A20}$ to mediate infection in the presence of an excess of $Knob_{WT}$, confirmed that Ad5-$EGFP_{A20}$ was capable of CAR-independent entry.

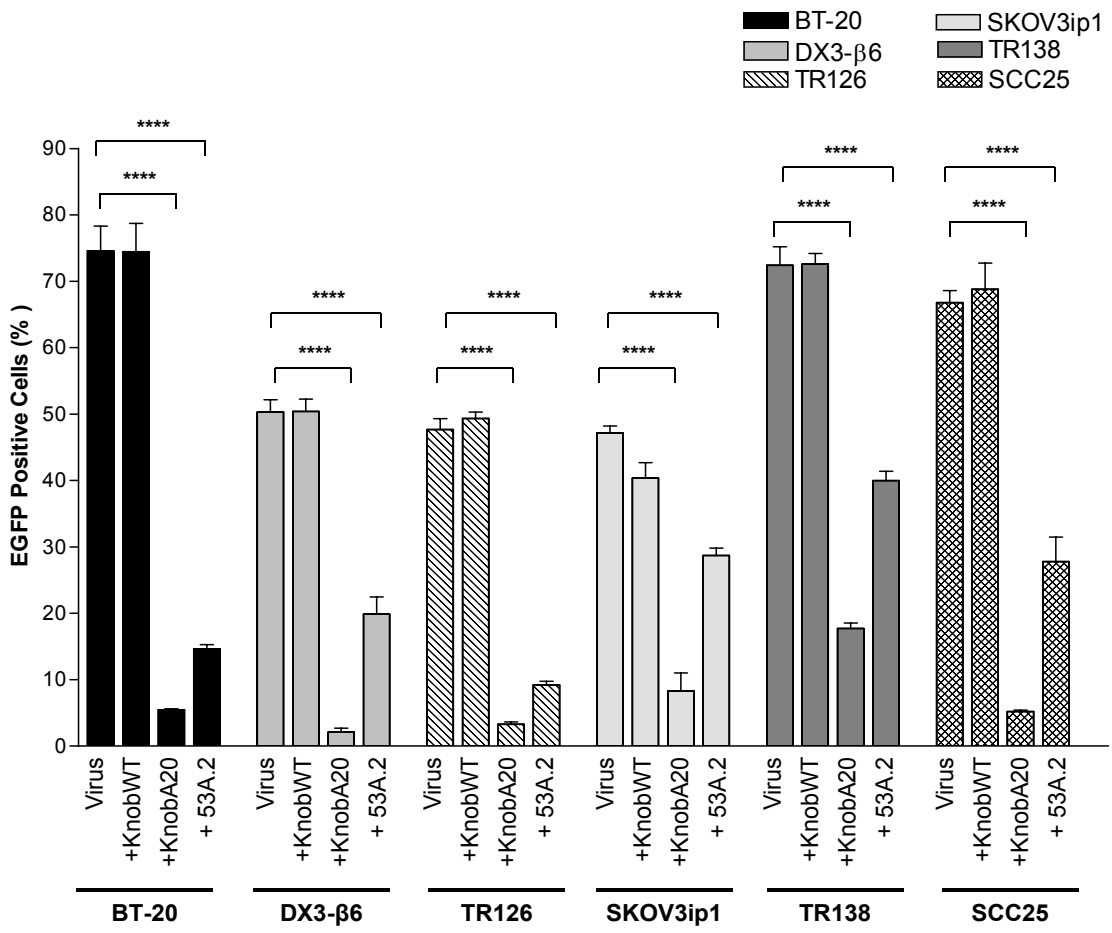

Figure*.3.15 Characterisation of the Tropism Determinants for Ad5-EGFP$_{A20}$.** A panel of cell lines was selected to investigate the determinants of the enhanced tropism seen with Ad5-EGFP$_{A20}$. Cells were pre-incubated for 1hr at 4˚C with 10µg/ml of Knob$_{WT}$, Knob$_{A20}$ or an anti-αvβ6 antibody (53A.2), after which a constant MOI (10) of Ad5-EGFP$_{A20}$ was added for 1hr at 4˚C. The virus-protein mixture was removed and EGFP gene transfer quantified ~22hrs post-infection (see *Section.*2.8.2). Data represent the mean ± SD of triplicate samples and are representative of at least two independent experiments. Statistical significance was determined using the unpaired Student's *t*-test comparing the means of the Ad5-EGFP$_{WT}$ and Ad5-EGFP$_{A20}$ groups for each cell line (* indicates a *P*-value <0.0001, bars indicate SD, no bars represent SD values smaller than the symbol used).

3.3.6 Investigation of the Role of Alternative Integrins in Ad5-EGFP$_{A20}$ Infectivity.

It has been shown previously that the A20FMDV2 peptide does not interact with αvβ3 or αvβ5 integrins (DiCara *et al.*, 2007). However, to ensure that Ad5-EGFP$_{A20}$ infection was independent of an interaction with either of these integrins, further infectivity experiments were carried out in the presence of function blocking antibodies to αvβ6, in parallel with function blocking antibodies to αvβ3/αvβ5/αvβ8 (*Fig*.3.16A+B). Antibodies used are listed in *Table*.7. We obtained some unexpected results when comparing the infectivity of both viruses in DX3puro cells (see *Fig*.3.13). DX3puro cells do not express αvβ6, yet an ~13-fold increase in infectivity with Ad5-EGFP$_{A20}$ was observed when compared with Ad5-EGFP$_{WT}$. Previous characterisation of the A20FMDV2 peptide,

carried out on the same DX3puro/DX3-β6 isogenic cell line pair (DiCara *et al.*, 2007), demonstrated that the peptide had no affinity for the non-β6 expressing line, DX3puro. However, based on these results it seemed possible that the A20FMDV2 insertion, at least within Ad5-EGFP$_{A20}$, had some affinity for an alternative, as yet unknown receptor which was expressed on these cells. As the integrin αvβ8 had been previously implicated in native infection with Foot and Mouth Disease virus (Jackson *et al.*, 2004), we decided to include an anti-αvβ8 antibody (14E5) in the competition experiment.

This experiment was performed as described previously, using EGFP transgene expression as the end-point for the assay. Cells infected with Ad5-EGFP$_{A20}$, but which were untreated with inhibitors, were taken as 100% (% EGFP positive cells), and all other values expressed relative to this. Ad5-EGFP$_{WT}$ was included as a control for both cell lines investigated (DX3puro/DX3-β6), yielding similar transduction efficiencies as seen in *Fig*.3.13. It was clear that neither αvβ3 nor αvβ5 contributed significantly to Ad5-EGFP$_{A20}$ mediated entry in either cell line, as simultaneous inhibition of both of these integrins resulted in only ~12%, and ~9% reductions for DX3puro and DX3-β6, respectively (p>0.05 for both). In DX3puro cells, inhibition with 53A.2 had no effect on Ad5-EGFP$_{A20}$ entry, an expected result as these cells do not express αvβ6. Conversely, inhibition of αvβ6 on the -β6 transfected DX3-β6 line, using 53A.2, resulted in a ~81% reduction in transduction (p<0.0001), supporting its role as the primary tropism determinant for Ad5-EGFP$_{A20}$.

Function blocking of the αv integrin subunit using a pan αv inhibitor (L230) resulted in ~60%, and 50% decreases in transduction in both DX3puro and DX3-β6, respectively (p=0.0013 and p=0.0029). This effect was particularly interesting for the DX3puro cells (-β6 negative) as it indicated that Ad5-EGFP$_{A20}$ was capable of utilising an alternative αv integrin for entry in these cells. This alternative receptor was confirmed to be αvβ8. Using an anti-αvβ8 inhibitor (14E5), an ~75% reduction in transduction in DX3puro cells was observed (p=0.0003). Due to the compensatory effect of αvβ6, transduction in DX3-β6 cells was affected to a lesser extent by inhibition of αvβ8 (~44% reduction), although the effect was significant (p=0.0028). Interestingly, function blocking of both αvβ6 and αvβ8 simultaneously with 53A.2/14E5, almost completely ablated Ad5-EGFP$_{A20}$ transduction, reducing entry by ~95% (p<0.0001). These data confirmed that Ad5-EGFP$_{A20}$ was capable of utilising both αvβ6 and αvβ8 for entry, although this interaction appeared to be more efficient with αvβ6.

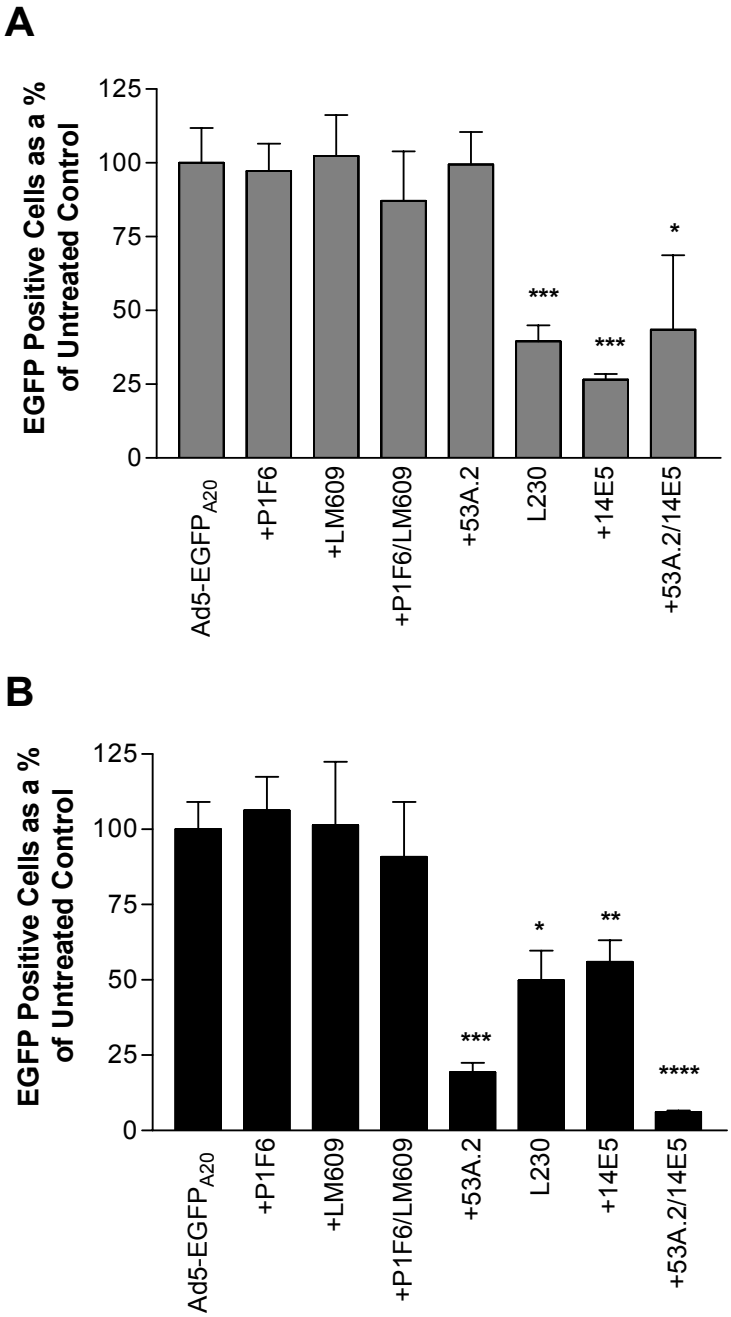

Figure*.3.16 (A) Ad5-EGFP$_{A20}$ Transduction of DX3puro Cells in the Presence of Integrin Inhibitors.** The DX3puro/DX3-β6 cell lines were selected to investigate the role of other integrins (ie. αvβ3, αvβ5 and αvβ8) on the enhanced tropism seen with Ad5-EGFP$_{A20}$. Both cell lines have low CAR expression and high integrin expression, however DX3puro does not express αvβ6 (see *Table*.10 and *Table.*11). Cells were pre-incubated for 1hr at 4˚C with 10µg/ml of a pan-αv inhibitor (L230), anti-αvβ3 (LM609), anti-αvβ5 (P1F6), anti-αvβ8 (14E5), anti-αvβ6 antibody (53A.2) and LM609/P1F6 and 14E5/53A.2 in combination. Ad5-EGFP$_{A20}$ was added at an MOI 10 for 1hr at 4˚C, and EGFP gene transfer quantified ~22hrs post-infection (see *Section*.2.8.2). **(B) Ad5-EGFP$_{A20}$ Transduction of DX3-β6 Cells in the Presence of Integrin Inhibitors.** Experiment was performed exactly as described above. Data represent the mean ± SD of triplicate samples and are representative of two independent experiments. Statistical significance was determined using the unpaired Student's *t*-test comparing the means of each treated Ad5-EGFP$_{A20}$ group (* indicates a *P*-value <0.00001, *** *p*<0.001, ** *p*<0.01, * *p*<0.05, bars indicate SD, no bars represent SD values smaller than the symbol used).

3.3.7 Comparative Replication Kinetics of Ad5-EGFP$_{WT}$ and Ad5-EGFP$_{A20}$.

The replication kinetics of viruses Ad5-EGFP$_{WT}$ and Ad5-EGFP$_{A20}$ were compared at 24, 48

and 72hr time-points for the following cell lines; DX3puro, DX3-β6, TR126, TR138, SCC25, SKOV3ip1, BT-20 and HSC-3 (*Fig*.3.17). All cell lines in the panel were infected at an MOI of 10, and intracellular viral titres per cell (PFU/cell) calculated by $TCID_{50}$ from cells harvested at the relevant time-points.

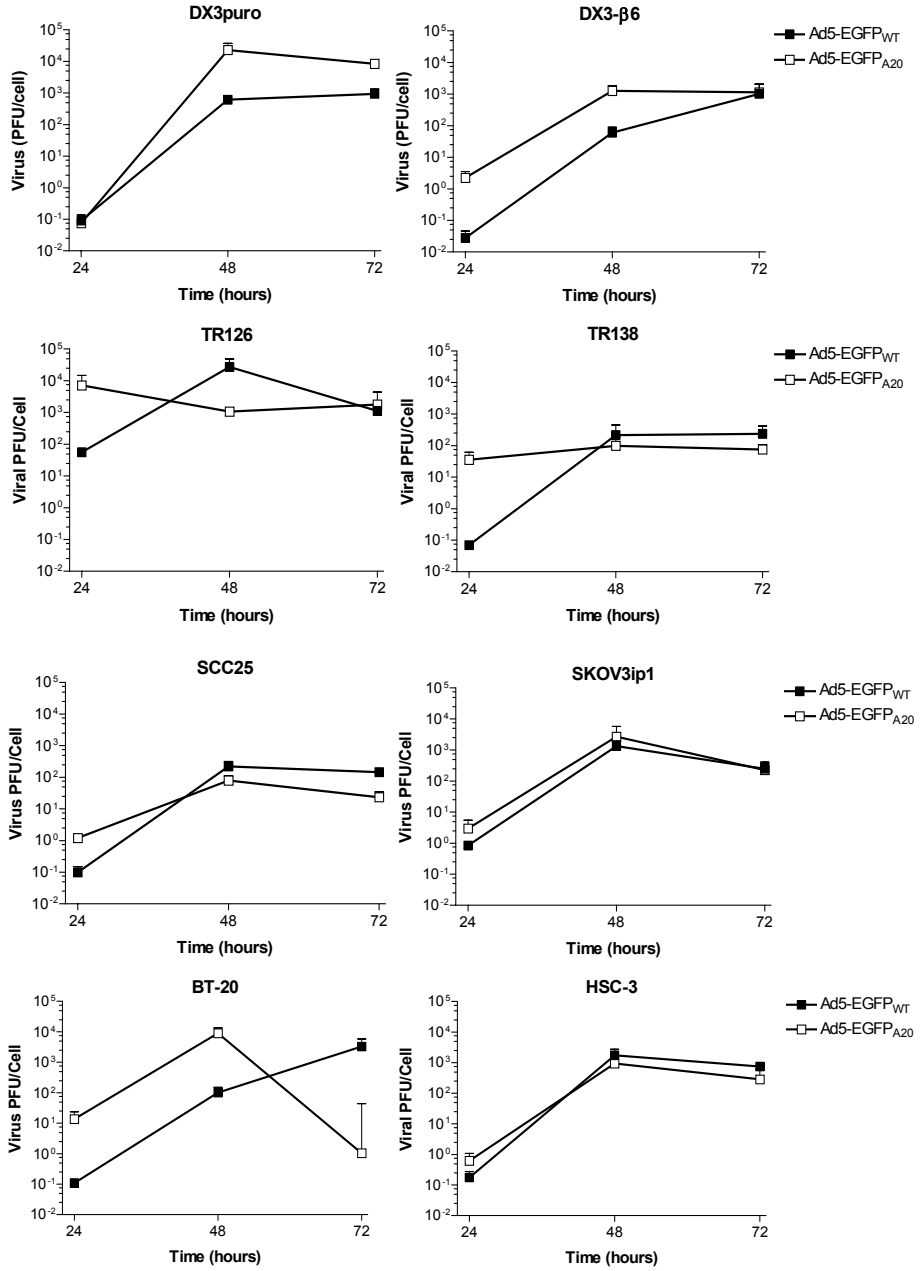

***Figure*.3.17 Comparative Replication Kinetics of Ad5-EGFP$_{WT}$ and Ad5-EGFP$_{A20}$.** Intracellular viral titre production (PFU/cell) was assessed for DX3puro, DX3-β6, TR126, TR138, SCC25, SKOV3ip1, BT-20 and HSC-3 at 24, 48 and 72hrs post-infection with an MOI 10. Cells were harvested at each time-point and titrated on JH293 cells using a standard end point dilution assay ($TCID_{50}$). Data represent the mean ± SD of triplicate samples, titrated on triplicate plates, and are representative of two independent experiments.

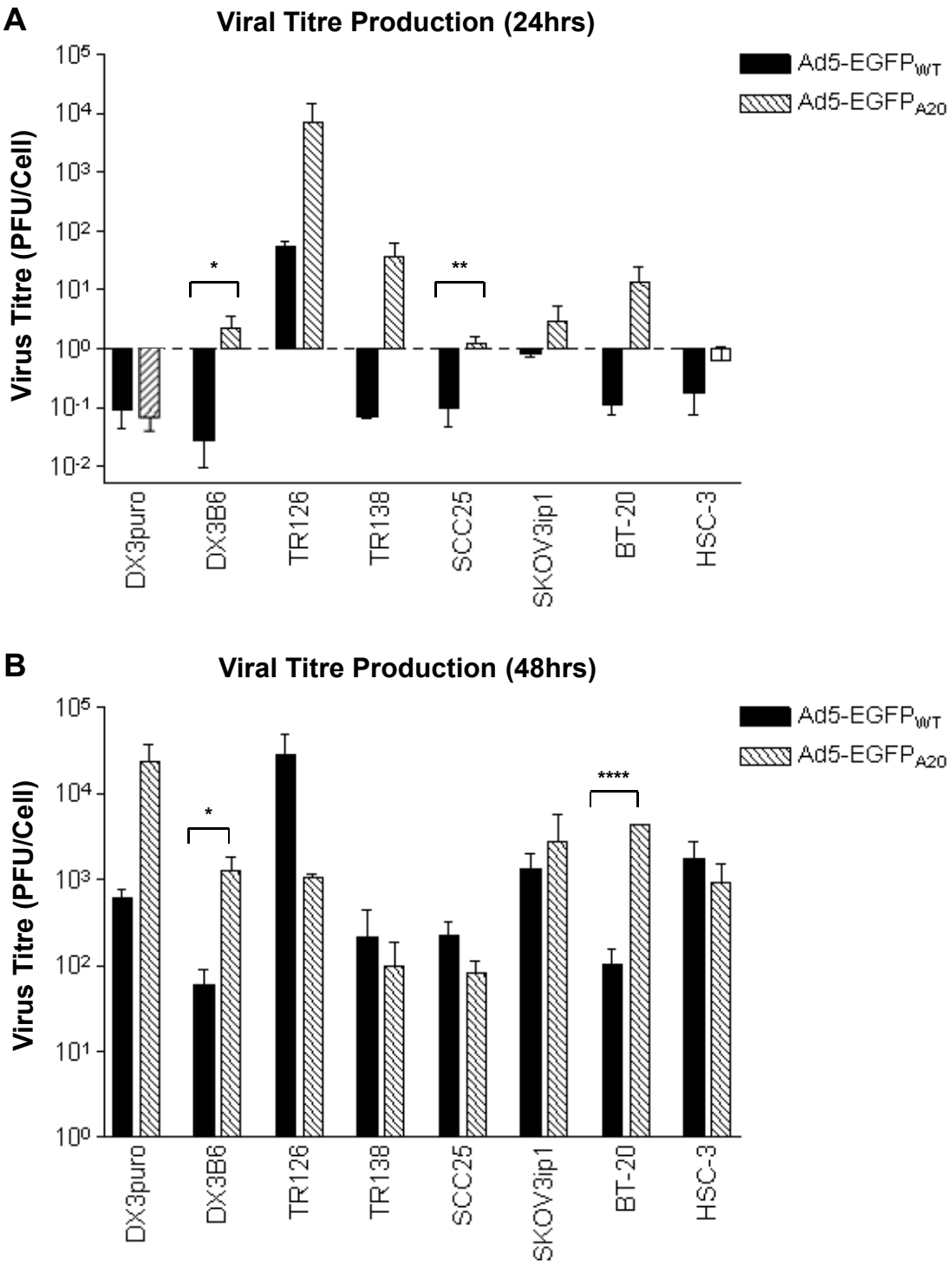

Figure*.3.18 Overview of Intracellular Viral Production (PFU/cell), 24 (A) and 48hrs (B) Post-Infection.** The intracellular viral titres produced by Ad5-EGFP$_{WT}$ and Ad5-EGFP$_{A20}$ (input dose = MOI 10 PFU/cell) on a panel of cell lines was compared by titration (TCID$_{50}$) of virus in cells harvested 24/48hrs post-infection. The unpaired Student's *t*-test was used to compare the means of Ad5-EGFP$_{WT}$ and Ad5-EGFP$_{A20}$ for each cell line (* indicates a *P*-value <0.0001, ** $p<0.01$, * $p<0.05$, $N = 3$, bars indicate SD, no bars represent SD values smaller than the symbol used).

At 24hrs, Ad5-EGFP$_{A20}$ titres were higher than Ad5-EGFP$_{WT}$ for all lines, (except DX3puro which produced equivalent titres). This was presumably a reflection of the high efficiency attachment and infectivity through αvβ6 integrin seen in previous experiments (*Fig*.3.13). Differences in viral titres were most notable in BT-20, TR126, TR138, SCC25 and DX3-β6 cells, where Ad5-EGFP$_{A20}$ production was increased ~10-100-fold compared to Ad5-EGFP$_{WT}$. Viral titres produced with Ad5-EGFP$_{WT}$ at an early time-point (24hrs), did not appear to correspond with CAR expression levels (see *Table.*10). Surprisingly, the highest titres were obtained in TR126 cells which express very low levels of CAR. However, entry/spread in this particular experiment would also be affected by differential levels of integrins involved in internalisation, in addition to interactions with other lower affinity receptors.

Virus yields increased between 24 and 48hrs for both viruses. However, at 48hrs Ad5-EGFP$_{A20}$ viral titres were reduced, or reached a plateau in TR126 and TR138 cells, respectively. This effect was most likely a result of increased virus-induced cytotoxicity due to the high uptake of input dose at early time-points in these cells. At later time-points, 48-72hrs, replication was reduced or reached a plateau in all cell lines infected with Ad5-EGFP$_{A20}$. However, in BT-20 and DX3-β6 cells at 48hr time-points, Ad5-EGFP$_{WT}$ titres were still increasing and were only beginning to reach the 48hr titre of Ad5-EGFP$_{A20}$. A comparative overview of viral titres produced at 24 and 48hr time points is presented in histogram format in *Fig*.3.18A and B.

3.3.8 Comparative Cytotoxicity of Ad5-EGFP$_{WT}$ and Ad5-EGFP$_{A20}$. Comparative cytotoxicity profiles (MTT) for Ad5-EGFP$_{WT}$ and Ad5-EGFP$_{A20}$ were assessed on a selected panel of human carcinoma cell lines (*Fig.*3.19 and *Fig*.3.20). Cells were infected with doses of virus ranging from MOI 0.0001-100PFU/cell and cytotoxicity assessed 120hrs post-infection. Ad5-EGFP$_{A20}$ exhibited significantly increased cytotoxicity on all cell lines which had low-moderate levels of CAR (*Fig*.3.19 and see *Table*.10). Results obtained on the isogenic matched lines DX3puro and DX3-β6, were unusual, although consistent with data described previously (see *Fig*.3.13 and *Fig*.3.16A+B). As expected, Ad5-EGFP$_{A20}$ improved the cytotoxicity in an αvβ6-expressing cell line, DX3-β6, reducing the EC_{50} value ~90-fold when compared with the control, Ad5-EGFP$_{WT}$. However, in the non-β6 expressing line, DX3puro, the EC_{50} values obtained with Ad5-EGFP$_{A20}$, were also reduced ~25-fold relative to Ad5-EGFP$_{WT}$, probably a reflection of its alternate interaction with αvβ8.

Figure*.3.19 Comparative Cytotoxicity Profiles for Ad5-EGFP$_{WT}$ and Ad5-EGFP$_{A20}$ on a panel of Low-Moderate CAR-Expressing Cell Lines.** Cytotoxicity was determined by MTT assay, carried out 120hrs post-infection, with virus concentrations ranging from 0.0001-100 PFU/cell and mean percentage survival was expressed as a percentage of uninfected cells (Uninfected cells are represented on the X-axis as 0, following a break in the logarithmic scale). Cell lines investigated were; isogenic matched pair **(A)** DX3puro and **(B)** DX3-β6, HNSCC lines **(C)** TR126 and **(D)** TR138, Ovarian carcinoma lines **(E)** CAOV3 and **(F)** SKOV3ip1 and Breast carcinoma lines **(G)** BT-20 and **(H)** †CA1a, abbreviated from MCF10CA1a. Dose-response curves were generated by non-linear regression analysis using GraphPad Prism Version 3.03 (GraphPad Software, San Diego, CA). EC_{50} values for the dose response curves are displayed in *Table*.12. Cytotoxicity profiles shown are representative of at least two independent repeat experiments carried out on triplicate samples on different occasions. The unpaired Student's *t*-test was used to demonstrate the significance of the difference in EC_{50} values for each virus (* is indicates a *P*-value <0.0001, NS = not statistically significant, $p>0.05$, $N = 3$, bars indicate SD, no bars represent SD values smaller than the symbol used).

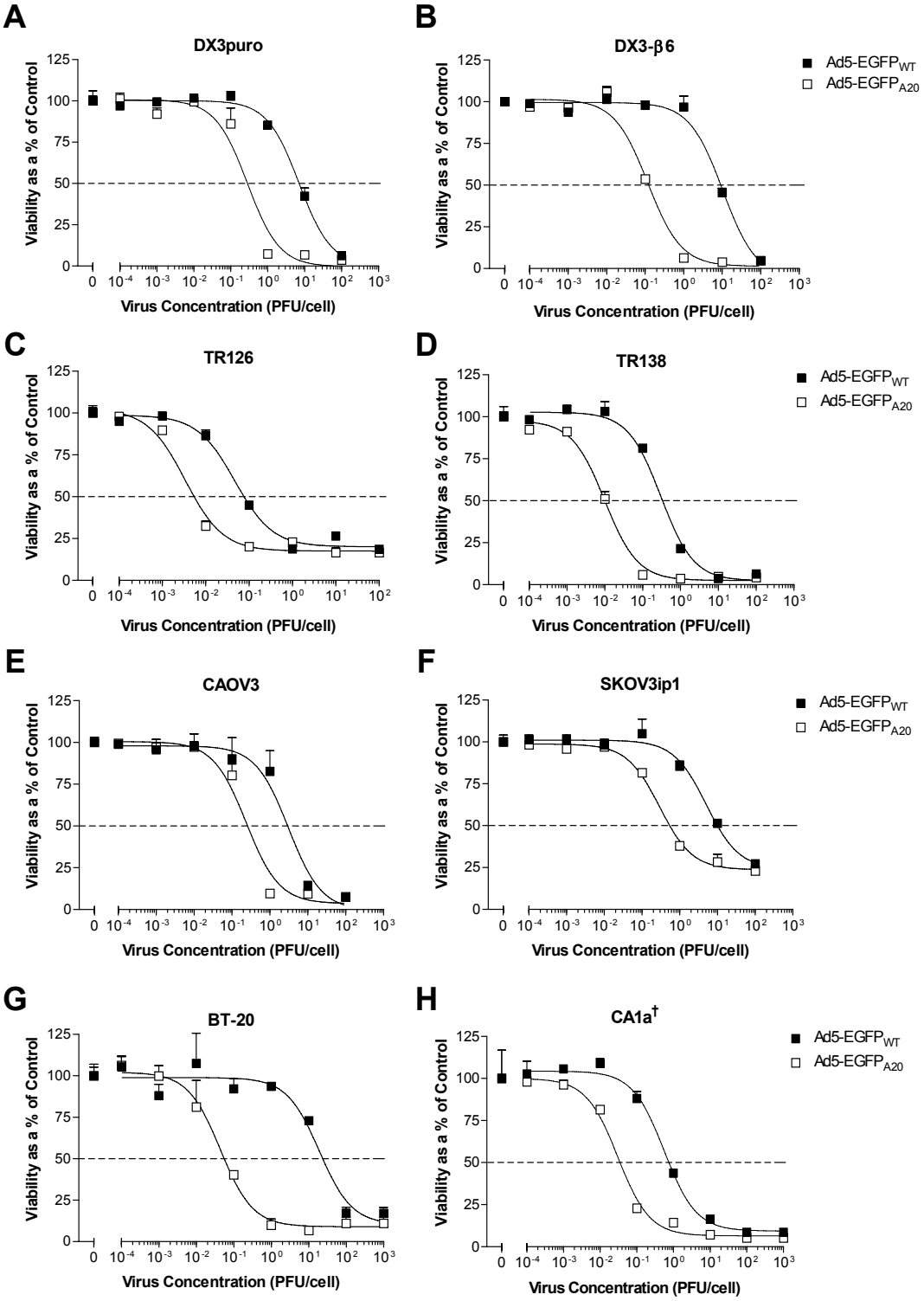

Table 12. EC_{50} Values (PFU/Cell)[a]

	DX3puro	DX3-β6	TR126	TR138	CAOV3	SKOV3ip1	BT-20	CA1a†
Ad5-EGFP$_{WT}$	7.06	10.33	0.05	0.3	3.1	5.02	19.13	0.56
Ad5-EGFP$_{A20}$	0.28	0.12	0.003	0.009	0.24	0.29	0.04	0.03

[a] EC_{50} represents half the maximal effective concentration of virus per cell. Viability was assessed by MTT assay and results analysed by non-linear regression fitted to a sigmoidal curve. Values are expressed in Plaque Forming Units (PFU/Cell). †CA1a is abbreviated from MCF10CA1a.

In HNSCC lines, TR126 and TR138, the EC_{50} values for Ad5-$EGFP_{A20}$ were reduced by ~17-fold and ~33-fold respectively, when compared to Ad5-$EGFP_{WT}$ (p=0.0011 and p<0.0001). Infection of ovarian carcinoma lines CAOV3 and SKOV3ip1 with Ad5-$EGFP_{A20}$ also resulted in reduced EC_{50} values, ~13-fold and ~17-fold, respectively. Similarly, in breast carcinoma lines BT-20 and CA1a (abbreviated from MCF10CA1a), EC_{50} values were reduced ~480-fold and ~18-fold, when compared with Ad5-$EGFP_{WT}$ (p<0.0001 and p=0.0001, respectively).

Several high CAR expressing cell lines were also investigated (*Fig*.3.20 and *Table*.10). These included isogenic matched pairs C1 and VB6, A375puro and A375-β6 and HNSCC lines, Detroit-562 and SCC25, and lung carcinoma lines, H441 and A549. C1 cells were found to be less sensitive to Ad5-$EGFP_{A20}$ than to Ad5-$EGFP_{WT}$, with the EC_{50} value increased ~2.5-fold in this cell line (p=0.025). However, in the -β6 transfected derivative of this line, a slight increase (~1.5-fold) in cytotoxicity was observed, although this was not statistically significant (p=0.450). There was no significant difference in cytotoxicity between Ad5-$EGFP_{WT}$ and Ad5-$EGFP_{A20}$ for either A375puro, or A375-β6 and EC_{50} values obtained were almost identical (p=0.663 and p=0.07, respectively). Similar results were seen in the HNSCC lines, Detroit 562, SCC25 and HSC-3; again no significant changes in EC_{50} values (p=0.552, p=0.318 and p=0.491, respectively). In lung carcinoma line H441, slight differences in EC_{50} values were detected, but again these were not significant (p=0.291).

It is clear that in cell lines which express high levels of CAR, retargeting to αvβ6 does not confer an efficacy advantage, failing to improve cytotoxicity *in vitro*. Therefore, these high CAR cell lines were not considered to be useful for future experiments.

***Figure*.3.20 Comparative Cytotoxicity Profiles for Ad5-EGFP$_{WT}$ and Ad5-EGFP$_{A20}$ on a panel of High CAR-Expressing Cell Lines.** Cytotoxicity was determined by MTT assay, carried out 120hrs post-infection, with virus concentrations ranging from 0.0001-100 PFU/cell and mean percentage survival was expressed as a percentage of uninfected cells (Uninfected cells are represented on the X-axis as 0, following a break in the logarithmic scale). Cell lines investigated were; isogenic matched pairs **(A)** C1 and **(B)** VB6, **(C)** A375puro and **(D)** A375-β6, HNSCC lines **(E)** Detroit 562, **(F)** SCC25 and **(G)** HSC-3 and Lung carcinoma line **(H)** H441. Dose-response curves were generated by non-linear regression analysis using GraphPad Prism Version 3.03 (GraphPad Software, San Diego, CA). EC_{50} values for the dose response curves are displayed in *Table*.13. Cytotoxicity profiles shown are representative of at least two independent repeat experiments carried out on triplicate samples on different occasions. The unpaired Student's *t*-test was used to demonstrate the significance of the difference in EC_{50} values for each virus (NS = not statistically significant, $p>0.05$, $N = 3$, bars indicate SD, no bars represent SD values smaller than the symbol used).

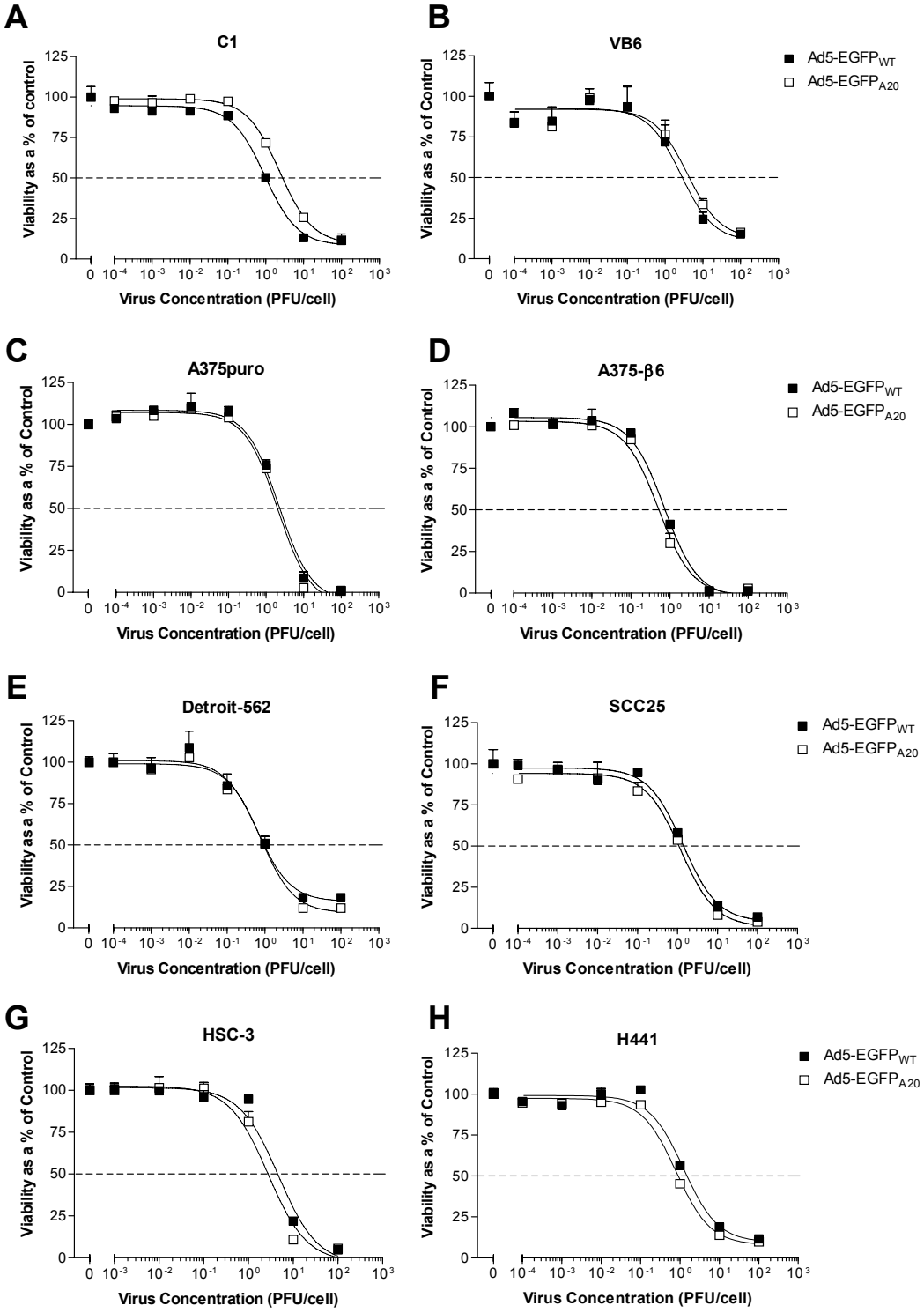

TABLE 13. EC_{50} Values (PFU/Cell)[a]

	C1	VB6	A375puro	A375-β6	Detroit 562	SCC25	HSC-3	H441
Ad5-EGFP$_{WT}$	0.94	2.83	2.19	0.71	6.31	1.37	4.74	1.24
Ad5-EGFP$_{A20}$	2.31	4.25	2.02	0.50	7.69	1.20	2.75	0.79

[a] EC_{50} represents half the maximal effective concentration of virus per cell. Viability was assessed by MTT assay and results analysed by non-linear fitted to a sigmoidal curve. Values are expressed in Plaque Forming Units (PFU/Cell).

Section.3.4 *In Vivo* Assessment of Retargeting to αvβ6 Following Local Delivery

3.4.1 Ovarian Intraperitioneal Xenograft Experiment. Using an ovarian intraperitoneal model, we assessed the median survival of cohorts treated with either non-replicating control virus LM-X, Ad5-EGFP$_{WT}$ or Ad5-EGFP$_{A20}$ (5x10^{9}vp/mouse). 1x10^{7} SKOV3ip1 cells were injected intraperitoneally (i.p) and 12 days later, virus was injected intraperitoneally for 5 consecutive days (days 12-16 inclusive). A Kaplan-Meier curve is presented in *Fig*.3.21. Unfortunately, the LM-X non-replicating control virus was found to be contaminated with wildtype replicating Ad5 and therefore, is not indicated on the graph. Ad5-EGFP$_{A20}$ treated cohorts displayed improved median survival when compared to those treated with Ad5-EGFP$_{WT}$ (61 days compared with 57 days), although this was not statistically significant (p=0.06).

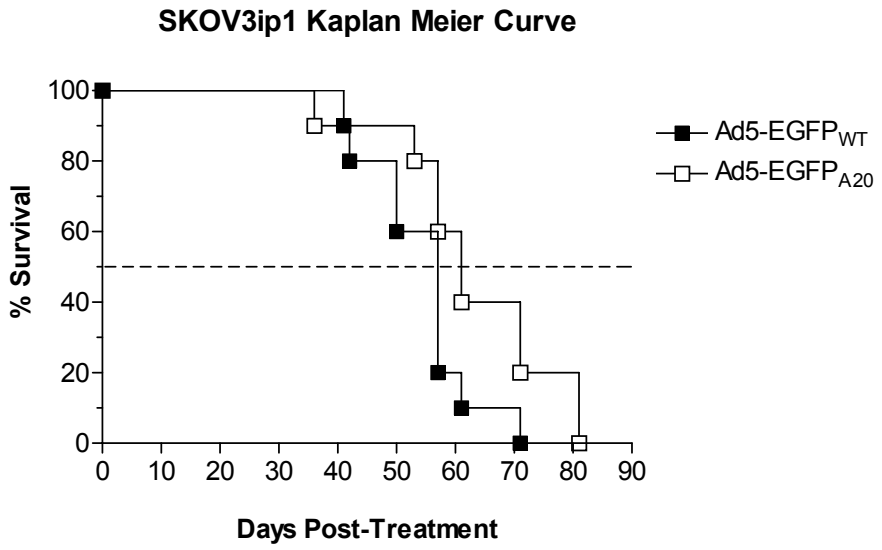

***Figure*.3.21 Kaplan Meier Survival Curve; SKOV3ip1 Intraperitoneal Model.** SKOV3ip1 ovarian carcinoma cells (1x10^{7}) were injected intraperitoneally into 6-8 week old CD1 nu/nu female mice (N=10). Viruses, Ad5-EGFP$_{WT}$ and Ad5-EGFP$_{A20}$ were injected on days 12-16 inclusive (5x10^{9}vp/mouse in 400µl of 20% icodextrin). Animals were killed once they reached Home Office morbidity limits (approaching 20% body weight loss, presence of significant ascites and poor well being, as determined by BSU staff). Kaplan Meier survival curves were generated, and non-parametric log rank analysis performed using GraphPad Prism Version 3.03 (GraphPad Software, San Diego, CA). Median survival for each cohort was calculated to be 57 days for Ad5-EGFP$_{WT}$, and 61 days for Ad5-EGFP$_{A20}$ (p=0.06).

3.4.2 Noninvasive *In Vivo* Fluorescence Imaging of Ad5-EGFP$_{WT}$ and Ad5-EGFP$_{A20}$ Replication Following Local Delivery. In this study, both Ad5-EGFP$_{WT}$ and Ad5-EGFP$_{A20}$ were constructed so that EGFP was under the control of the endogenous E3 promoter, in place of the E3-6.7K/gp19K cassette (Hawkins *et al.*, 2001). Noninvasive fluorescence imaging with EGFP inserted at this site has recently been

evaluated, and was shown to correlate well with viral DNA replication (Ono *et al.*, 2005). In fact, it has been shown previously that strong reporter gene expression from this promoter is dependent on efficient viral genome replication (Mittal *et al.*, 1993). Thus, the *in vivo* viral replication kinetics of Ad5-EGFP$_{WT}$ and Ad5-EGFP$_{A20}$ were assessed indirectly using a noninvasive fluorescence-based optical imaging system (*Fig*.3.22A and *Fig*.3.23A).

Using the isogenic cell line pair DX3puro and DX3-β6 (αvβ6-/αvβ6+), fluorescence efficiency was assessed following local injection (performed by Jerome Burnet and Prof. Iain McNeish). DX3puro/DX3-β6 cells ($4x10^6$) were implanted subcutaneously onto the right flanks of CD1 nude female mice. Once tumours had reached ~250mm^3, $1x10^{10}$vp of either non-replicating control virus LM-X, Ad5-EGFP$_{WT}$ or Ad5-EGFP$_{A20}$, were administered intratumourally.

In the DX3puro xenografts, the fluorescence efficiency detected in the Ad5-EGFP$_{A20}$ groups was dramatically superior to that of the Ad5-EGFP$_{WT}$ treated cohort (*Fig*.3.22A+C). The DX3puro cell line does not express αvβ6 (see *Table.*10), however it does express high levels of αvβ8 (see *Table*.11). Previous data presented in this chapter demonstrated that the Ad5-EGFP$_{A20}$ virus can efficiently utilise αvβ8 as an alternative receptor for entry in the absence of αvβ6 (see *Fig*.3.16A). A statistically significant difference in fluorescence was detected between Ad5-EGFP$_{A20}$ and Ad5-EGFP$_{WT}$ on day 4 (p=0.013). EGFP expression was reduced for both cohorts on days 7 and 11 post-infection and fluorescence detected did not differ (p>0.05). However, a dramatic peak in EGFP expression was observed in the Ad5-EGFP$_{A20}$ treated groups on day 14 post-infection, which differed significantly from Ad5-EGFP$_{WT}$ (p<0.0001). This difference was maintained through to day 21 (p<0.0001 for all time-points). By day 24, the EGFP fluorescence detected from both groups were identical (p>0.05).

Unexpectedly, there were no dramatic differences in EGFP fluorescence detected between Ad5-EGFP$_{WT}$ and Ad5-EGFP$_{A20}$ in the αvβ6-expressing DX3-β6 tumours (*Fig*.3.23A+C). Fluorescence levels for both groups closely mirrored each other and did not differ significantly at any time-points (p>0.05). Interestingly, Ad5-EGFP$_{WT}$ appeared to replicate more efficiently in the DX3-β6 xenograft, than in the DX3puro xenograft (see *Fig*.3.22A and *Fig*.3.23A).

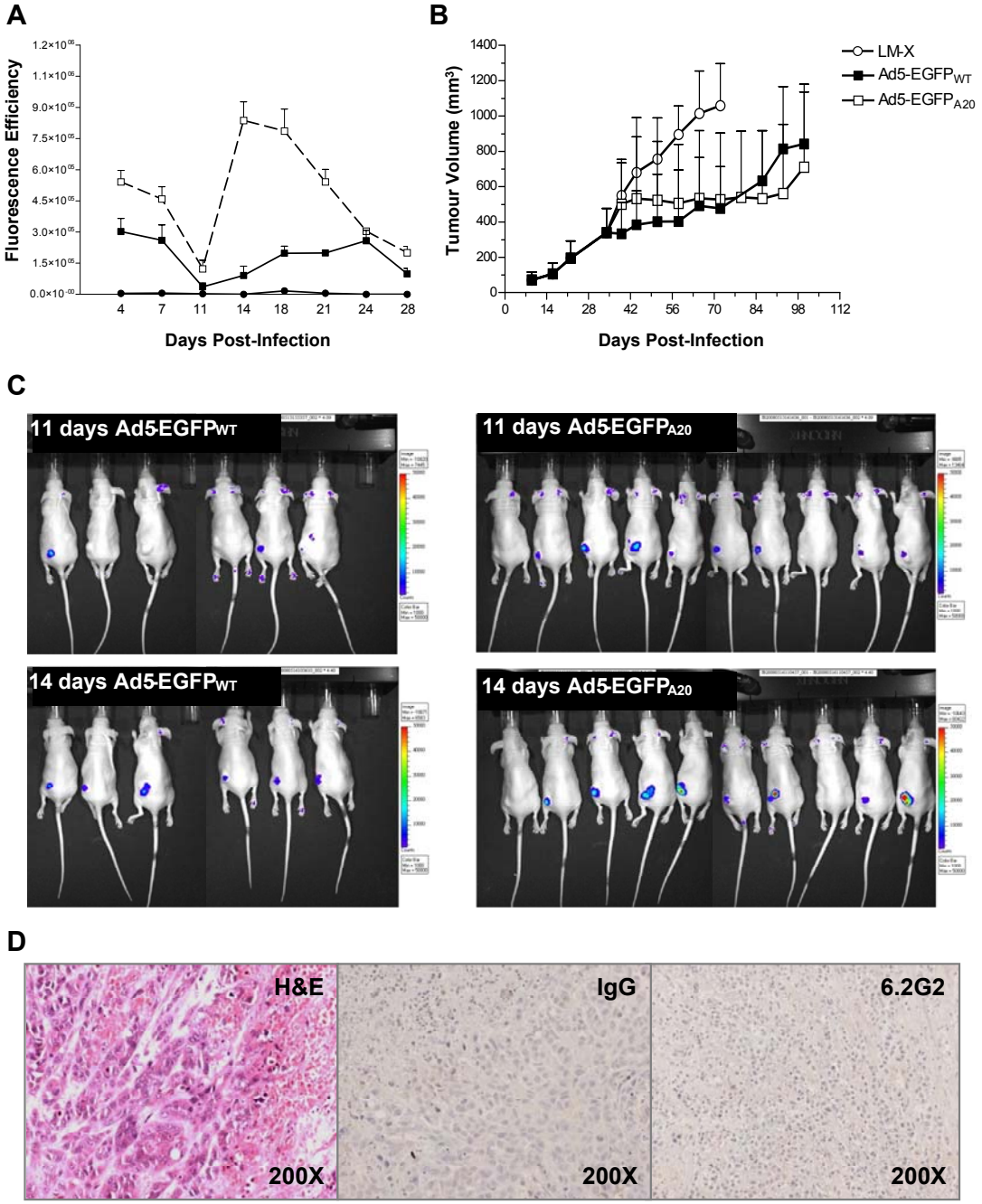

***Figure*.3.22 DX3puro Xenografts; *In Vivo* Fluorescence Imaging and Anti-tumoral Efficacy following Local Delivery of Virus. (A)** DX3puro tumour xenografts were implanted subcutaneously onto the right flanks of 6-8 week old CD1 nude female mice (*N*=6-10). Once the tumours had reached ~250mm^3, 1x10^{10}vp of non-replicating control virus (LM-X), Ad5-EGFP$_{WT}$ or Ad5-EGFP$_{A20}$ was injected intra-tumourally. EGFP fluorescence efficiency was measured on eight separate occasions using an Xenogen IVIS Imaging System 100, using the fluorescence nodule. **(B)** Tumour volume was measured on average three times weekly for the duration of the experiment. Once tumours reached ~8-10mm diameter animals were killed in accordance with Home Office Licence Regulations **(C)** Noninvasive *in vivo* fluorescence imaging was recorded for cohorts treated with Ad5-EGFP$_{WT}$ and Ad5-EGFP$_{A20}$ (days 11 and 14 post-infection). **(D)** Immunohistochemical analysis of DX3puro tumour pathology (control tumours shown). *From left to right*; H&E staining and anti-αvβ6 immunostaining with 6.2G2 which confirmed the absence of αvβ6 expression in these tumours. Sections were photographed at a magnification of 200X using a Zeiss AxioCam Mrc5 camera and Axiovision Software (Zeiss, Germany).

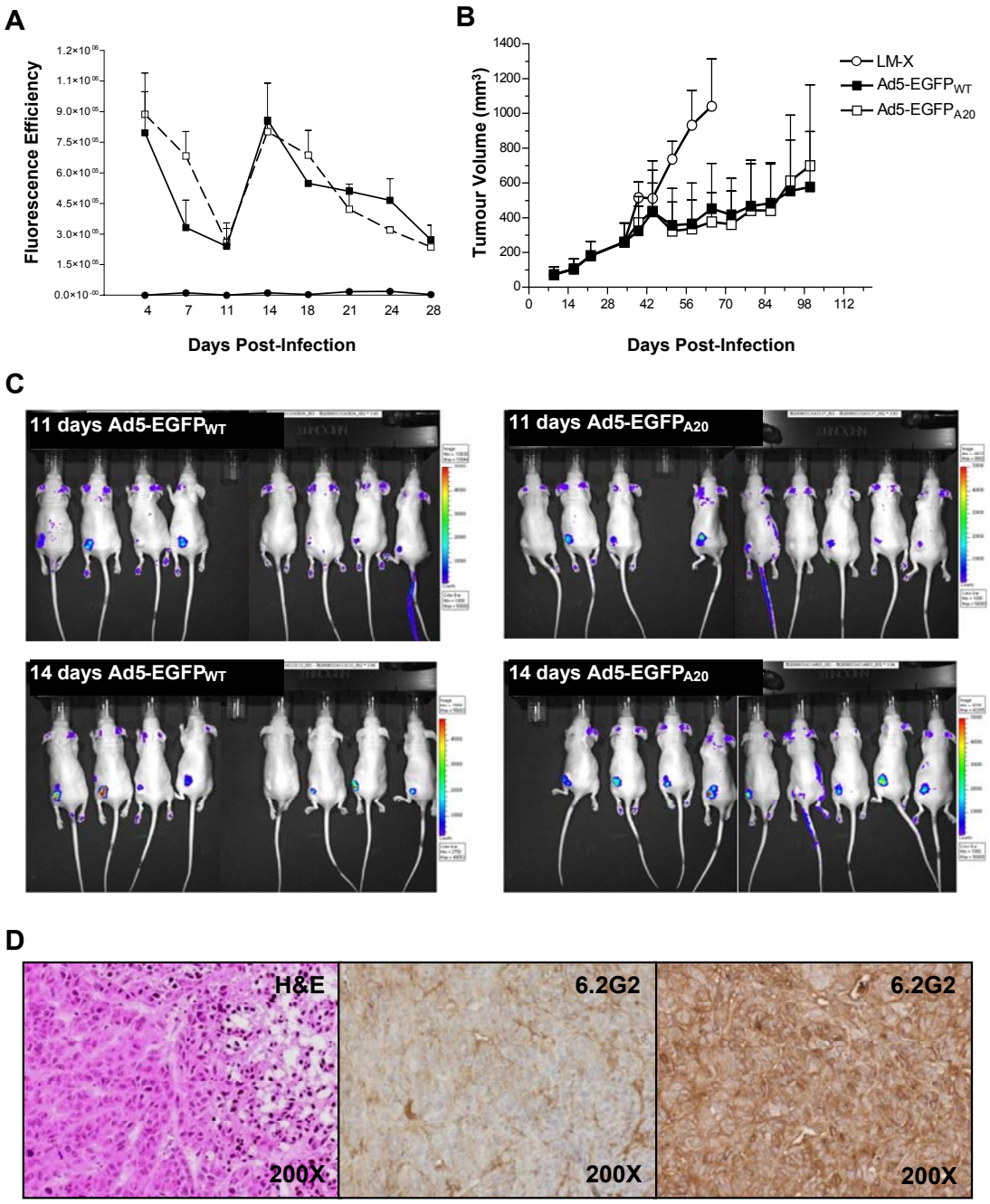

***Figure*.3.23 DX3-β6 Xenografts; *In Vivo* Fluorescence Imaging and Anti-tumoral Efficacy following Local Delivery of Virus. (A)** DX3-β6 tumour xenografts were implanted subcutaneously onto the right flanks of 6-8 week old CD1 nude female mice (*N*=8-10). Once the tumours had reached ~250mm^3, 1x10^{10}vp of non-replicating control virus (LM-X), Ad5-EGFP$_{WT}$ or Ad5-EGFP$_{A20}$ was injected intra-tumourally. EGFP fluorescence efficiency was measured on eight separate occasions using an Xenogen IVIS Imaging System 100, using the fluorescence nodule. **(B)** Tumour volume was measured on average three times weekly for the duration of the experiment. Once tumours reached ~8-10mm diameter animals were sacrificed in accordance with Home Office Licence Regulations **(C)** Noninvasive *in vivo* fluorescence imaging was recorded for cohorts treated with Ad5-EGFP$_{WT}$ and Ad5-EGFP$_{A20}$ (days 11 and 14 post-infection). **(D)** Immunohistochemical analysis of DX3-β6 tumour pathology (control tumours shown). *From left to right*; H&E staining, anti-αvβ6 immunostaining with 6.2G2 showing a region of poor expression taken from a tumour harvested at the end of the experiment and anti-αvβ6 immunostaining with 6.2G2 showing a region of high expression taken from a tumour harvested at an early time-point (~3 weeks). Sections were photographed at a magnification of 200X using a Zeiss AxioCam Mrc5 camera and Axiovision Software (Zeiss, Germany).

3.4.3 Anti-Tumoural Efficacy Following Local Delivery. DX3puro/DX3-β6 tumours were measured three times weekly in order to establish the efficacy of each treatment (*Fig*.3.22B and *Fig*.3.23B). Animals were killed once tumours reached ~8-10mm in diameter. In animals bearing DX3puro xenografts, the tumour volumes of both Ad5-$EGFP_{WT}$ and Ad5-$EGFP_{A20}$ treated groups differed from vehicle control (p=0.005 and p=0.03, respectively), on day 72 post-infection (*Fig*.3.22B). Unfortunately, the dramatic differences in EGFP fluorescence noted between Ad5-$EGFP_{WT}$ and Ad5-$EGFP_{A20}$, which suggested superior viral replication of the latter within the tumour, did not confer an enhanced anti-tumoural effect (*Fig*.3.22B). In animals harbouring DX3-β6 tumours, again, both viruses, Ad5-$EGFP_{WT}$ and Ad5-$EGFP_{A20}$, displayed enhanced anti-tumoural efficacy when compared with vehicle control at day 65 post-infection (p=0.0025 and p=0.0002, respectively), but did not differ significantly from each other (p>0.05).

3.4.4 Histological Examination of Tumour Xenografts; H&E Staining and Immunostaining for αvβ6 Integrin. Tumours were excised at time of death, fixed appropriately and processed for paraffin embedding and sectioning (Pathological Services, Institute of Cancer). All sections were assessed histologically following haematoxylin and eosin (H&E) staining. Additionally, sections from both DX3puro and DX3-β6 tumours were immunostained with an anti-αvβ6 antibody, 6.2G2, in parallel with an isotype control antibody.

As expected the DX3puro tumours did not express αvβ6 (*Fig*.3.22D). Pathological assessment of H&E stained tissue revealed regions of necrosis within the tissue. Additionally, histological analysis of the DX3-β6 tumours also identified large necrotic areas (*Fig*.3.23D). Regions of viable tumour cells (without necrosis) were selected for presention of αvβ6 immunostaining, as necrotic tissue shows high levels of non-specific staining. However, necrotic regions were present in all samples analysed (data not shown). Interestingly, immunohistochemistry identified that there was a loss of αvβ6-expression within the DX3-β6 xenografts over time. Tumours which were harvested at earlier time-points in the experiment, retained high level expression throughout the tumour mass (*far right*), whereas tumours harvested later in the experiments had reduced expression levels (*centre*).

Chapter.3 Discussion

To date, several strategies for the selective targeting of αvβ6, both *in vitro* and *in vivo* have been reported. These have included the generation of a chimeric T-cell antigen receptor expressing a 12mer αvβ6-specific ligand, which successfully redirected cytotoxic T lymphocytes to αvβ6-expressing primary ovarian lines (Pameijer *et al.*, 2007), the administration of αvβ6 blocking antibodies or soluble TGF-β inhibitors in an attempt to functionally inhibit αvβ6 *in vivo* (Van Aarsen *et al.*, 2008; Weinreb *et al.*, 2004; Xue *et al.*, 2001), the generation of a humanised scFv directed to αvβ6 (Kogelberg *et al.*, 2008) or the use of radiolabelled A20FMDV2 or other αvβ6-targeting peptides for non-invasive, *in vivo* imaging of αvβ6-positive tumours (Hausner *et al.*, 2009a; Hausner *et al.*, 2007; Hausner *et al.*, 2009b; Li *et al.*, 2009). However, to date, there have been no attempts to redirect an adenovirus to αvβ6 for therapeutic applications.

*Section.*3.1 Characterisation of Cell Lines

The extensive characterisation of a broad range of human carcinoma lines resulted in the identification of a panel suitable for *in vitro* characterisation of our constructs. Several attempts were made to establish tumour xenograft models for TR126, TR138 and BT-20 cells, but these were unsuccessful. Unfortunately, the established tumour xenograft models used in our laboratory were not considered suitable for *in vivo* applications with Ad5-EGFP$_{A20}$, due to the lack of efficacy *in vitro* (ie. A375puro/A375-β6, and C1/VB6 models).

*Section.*3.2 *In Vitro* Characterisation of A20-Modified Knob$_{A20}$ Proteins

The resolution of the crystal structure of the Ad5 knob domain by X-ray crystallography identified the HI loop region as a locale suitable for peptide incorporation (Xia *et al.*, 1994). The rationale supporting this was that the HI loop was exposed on the surface of the fibre knob structure but had no involvement in cell binding and, importantly, possessed a flexible structure whose length varied greatly between Ad serotypes. To date, the HI loop has been shown to tolerate the insertion of ligands of up to 83aa with negligible effects on the structural integrity of the virus (Belousova *et al.*, 2002). The A20FMDV2 peptide itself has an innate structure which is critical to its function, and it has been found that cysteine-induced cyclicisation attenuates its affinity and specificity

(Dr. Mark Howard, personal communication). Thus, we did not consider the use of a cysteine-constrained A20FMDV2 insertion in this study. Alternatively, we hypothesised that the innate flexibility of the Ad5 HI loop would permit the A20FMDV2 insertion to assume its critical conformation, and result in a retargeted adenovirus with high affinity binding to αvβ6.

Initial *in vitro* experiments with the A20-modified recombinant knob protein were very encouraging. The insertion of the αvβ6-targeting peptide, A20FMDV2, into the HI loop of the Ad5 knob domain, resulted in the successful binding and functional inhibition of αvβ6, in a dose dependent manner. The reduced $Knob_{A20}$ monomer is approximately 24.4kDa inclusive of its 6XHIS tag, and the corresponding homotrimer was consistently observed at ~62kDa by SDS-PAGE. The calculated IC_{50} for $Knob_{A20}$ mediated inhibition of 53A.2 (anti-αvβ6 antibody) binding, corresponded to a concentration of ~2.5nM (IC_{50} = 0.03μg/10^5 cells in a 200μl volume). $Knob_{A20}$ was also capable of completely abrogating αvβ6-dependent cell migration and invasion at a concentration of 80nM (5μg/ml), the lowest concentration tested in these experiments. Importantly, the incorporation of the peptide did not appear to preclude native fibre assembly, as confirmed by the ability of $Knob_{A20}$ to form a homotrimer (data not shown).

Strategies to target αvβ6 for *in vivo* imaging or therapeutic applications (function blocking), currently are being investigated (Hausner *et al.*, 2009a; Hausner *et al.*, 2007; Li *et al.*, 2009; Van Aarsen *et al.*, 2008). Therefore, the functional characteristics of $Knob_{A20}$ reported in this study suggest it may prove useful for similar targeting strategies. The ^{99m}Tc-iodinatation of adenoviral knob proteins has been described previously (Awasthi *et al.*, 2004; Zinn *et al.*, 1998). Consistent with the innate hepatotropic profiles of various Ad serotypes *in vivo*, accumulation of these ^{99m}Tc-Knob proteins predominantly was in the liver. Interestingly, these labelled knobs were proposed to be accumulated and internalised through CAR, independently of integrins (Awasthi *et al.*, 2004). In support of this proposed receptor-mediated entry process, depletion of Kupffer cells using $GdCl_3$ did not affect the liver accumulation of ^{99m}Tc-Knob (Zinn *et al.*, 1998). Therefore, a native CAR-binding ablated $Knob_{A20}$ may prove useful for such imaging applications *in vivo*, limiting the non-specific sequestration in the liver and maximising tumour targeting through αvβ6. In further support for its potential utility, the knob trimer is sufficiently large (~62kDa) such that it could avoid rapid clearance by the renal system, but small enough that it could achieve deeper tumour penetration (Awasthi *et al.*, 2004). Additionally, its size may also permit it to avoid degradation by serum peptidases *in vivo*. Taken together, these qualities suggest it may suffice as an alternative to current peptide/antibody-based imaging strategies.

In summary, the data presented in this section confirmed a high affinity interaction between $Knob_{A20}$ and αvβ6 and supported the possibility that the genetic incorporation of A20FMDV2 into Ad5 would permit efficient retargeting to αvβ6.

Section.3.3 *In Vitro* Characterisation of A20-Modified Ad5-$EGFP_{A20}$

In vitro viral transduction experiments demonstrated the success of the retargeting strategy. Ad5-$EGFP_{A20}$ exhibited superior transduction over Ad5-$EGFP_{WT}$ (p<0.0001 for all cells), and also was capable of enhancing entry in cell lines (BT-20, TR126 and DX3-β6) which were previously refractory to native Ad5-$EGFP_{WT}$ infection. Inhibitory experiments, using anti-αvβ6 53A.2, demonstrated that αvβ6 was the major tropism determinant for Ad5-$EGFP_{A20}$ entry in αvβ6-expressing cells (*Fig*.3.15). Moreover, the finding that $Knob_{A20}$ had an IC_{50} of 0.008μg/10^5 cells (~1.3nM) for inhibition of Ad5-$EGFP_{A20}$, a value approximately 15-fold less than the IC_{50} published previously for $Knob_{WT}$-mediated inhibition of Ad5 infection (Kirby *et al*., 2000), suggested that the interaction between Ad5-$EGFP_{A20}$ and αvβ6 was one of high affinity. In addition to enhancing transduction through αvβ6, the replication kinetics of Ad5-$EGFP_{A20}$ in low CAR, high αvβ6-expressing cells (DX3-β6, TR126, TR138 and BT-20) were superior to Ad5-$EGFP_{WT}$ (*Fig*.3.17 and *Fig*.3.18). However, viral titres obtained did not always correspond with transduction efficiency, an expected finding as intracellular host factors can also determine sensitivity to Ad5 replication (Wang *et al*., 2009). Cytotoxicity was also improved dramatically in low CAR, high αvβ6-expressing cells (*Fig*.3.19), but was not comparably enhanced in high CAR-expressing lines (*Fig*.3.20).

Overall, the interpretation of the *in vitro* data was not difficult. However, there were some unexpected observations which warranted further investigation. In particular, the DX3puro cell line (non αvβ6-expressing) yielded some unusual results which were inconsistent with the hypothesis that αvβ6 was the sole determinant for entry with Ad5-$EGFP_{A20}$ (see *Fig*.3.13 and *Fig*.3.19). The critical DLXXL motif which confers αvβ6 specificity has been reported to have minimal interactions with αvβ3/αvβ5 integrins (DiCara *et al.*, 2007). However, in addition to αvβ6, the integrins αvβ1, αvβ3 and αvβ8 have been implicated in Foot and Mouth Disease Virus (FMDV) infection (Jackson *et al.*, 2004; Jackson *et al.*, 2002; Jackson *et al.*, 1997; Jackson *et al.*, 2000). Therefore, in an attempt to delineate, or indeed to exclude a role for alternative integrins in the infection of Ad5-$EGFP_{A20}$, gene transfer assays were repeated in the presence, and absence of inhibitors to these receptors (*Fig*.3.16). Although a significant proportion of infection with Ad5-$EGFP_{A20}$ could be modulated through αvβ8, it was clear that αvβ6

remained the predominant tropism determinant. However, these data finally offered an explanation as to why DX3puro cells supported significantly higher transduction/ cytotoxicity when compared with Ad5-EGFP$_{WT}$. Interestingly, αvβ8 is expressed to a high level in the lung, central nervous system (CNS) and on dendritic cells (McCarty *et al.*, 2005; Mu *et al.*, 2002; Nishimura *et al.*, 1998; Travis *et al.*, 2007). Therefore, the identification that Ad5-EGFP$_{A20}$ can promote infection through αvβ8 suggests that Ad5-EGFP$_{A20}$ may prove useful for future retargeting strategies, or may have broader experimental applications.

The development of CAR-independent targeting strategies has once again become an important consideration in the design of Ad5-based vectors for applications in human disease. This is due to the discovery that human erythrocytes can aggregate Ad5 through CAR binding and impede targeted delivery (Carlisle *et al.*, 2009; Seiradake *et al.*, 2009), in addition to reports that CAR-binding can activate the inflammatory response to Ad5 in epithelial cells, and in hepatic tissue, following retro-orbital administration (Schoggins *et al.*, 2005; Tamanini *et al.*, 2006). The ability of Ad5-EGFP$_{A20}$ to mediate high efficiency entry, in a CAR-independent manner was promising and suggested that ablation of CAR-binding determinants would not impair the efficacy of Ad5-EGFP$_{A20}$. Therefore, the *in vitro* characteristics of Ad5-EGFP$_{A20}$, suggested that it could potentially have advantages over Ad5-EGFP$_{WT}$ *in vivo*, in terms of its ability to infect, replicate and induce cytotoxicity to a greater extent in CAR-deficient cell lines which express αvβ6.

*Section.*3.4 *In Vivo* Characterisation of A20-Modified Ad5-EGFP$_{A20}$

The results obtained following local delivery of Ad5-EGFP$_{A20}$ compared with Ad5-EGFP$_{WT}$ were, largely, disappointing. Based on extensive *in vitro* characterisation, we had determined that enhanced efficacy with Ad5-EGFP$_{A20}$ was most pronounced in cell lines which had high αvβ6 expression but low CAR expression. Downregulated CAR expression in pathological specimens and primary cell lines derived from human tumours, has been reported extensively (Anders *et al.*, 2009; Buscarini *et al.*, 2007; Jee *et al.*, 2002; Matsumoto *et al.*, 2005; Mikami *et al.*, 2001; Rauen *et al.*, 2002). Additionally, loss of CAR expression is thought to correlate with disease progression (Anders *et al.*, 2009; Mikami *et al.*, 2001; Vincent *et al.*, 2009). In contrast, αvβ6 is significantly upregulated in numerous human carcinomas where it is responsible for conferring a pro-invasive phenotype which correlates with poor prognosis. For these reasons, we wanted to assess comparatively the *in vivo* efficacy of Ad5-EGFP$_{WT}$ and

Ad5-EGFP$_{A20}$ using low CAR, high αvβ6-expressing models, as we believed that this profile may more accurately reflect the scenario *in vivo*. However, we failed to identify a large number of cell lines which displayed this profile (see *Table*.10). Moreover, a large number of those cell lines which we did identify, were not tumourigenic, and several attempts to grow BT-20, TR126 and TR138 cells in nude mice failed.

Ad5-EGFP$_{A20}$ had significantly enhanced cytotoxicity in SKOV3ip1 cells when compared with Ad5-EGFP$_{WT}$, despite having only moderate levels of CAR:αvβ6 expression on the cell surface (see *Table*.10). However, we hypothesised that the enhanced *in vitro* cytotoxicity may confer a survival advantage *in vivo* when using the SKOV3ip1 intraperitoneal xenograft model for ovarian carcinoma. This was not the case. Ad5-EGFP$_{A20}$ treatment improved median survival by only 5 days, and this was not statistically significant (p=0.06).

Subsequently, we decided to perform an *in vivo* fluorescence imaging, and anti-tumoural efficacy experiment using the isogenic matched lines, DX3puro/DX3-β6. The choice of this model was not our first as it is a rapidly growing tumour which becomes extensively necrotic. Therefore, it is not ideal for assessing the *in vivo* replication and spread of adenovirus. Additionally, it had been found during the course of prior experiments using this model, that the DX3-β6 xenografts lost expression of αvβ6 *in vivo* (Dr. Antonio Saha, unpublished observations). Furthermore, we demonstrated in previous *in vitro* experiments that Ad5-EGFP$_{A20}$ could also mediate infection through αvβ8 in the non-αvβ6 expressing DX3puro cells. Indeed, it appeared that this characteristic was retained, if not enhanced *in vivo*, as EGFP fluorescence expressed by Ad5-EGFP$_{A20}$ suggested it was capable of efficient intra-tumoural replication in the DX3puro xenografts, when compared with Ad5-EGFP$_{WT}$. In fact, Ad5-EGFP$_{WT}$ failed to replicate to any great extent within the DX3puro tumour. However, one of the key limitations of fluorescence imaging is the lack of penetration. Therefore, it is possible that the lack of EGFP expression detected with Ad5-EGFP$_{WT}$ may be due to differences in injection site within the tumour. Indeed, despite injecting equal doses of virus on the same day, there was a great deal of variation within each treated cohort. However, it was reassuring that in both tumour models viral replication with both viruses appeared to peak at an early time-point post infection, drop at 11 days, and peak again 14 days post-infection.

Unexpectedly, in the DX3-β6 xenografts, EGFP expression in the Ad5-EGFP$_{WT}$ treated groups effectively mirrored the Ad5-EGFP$_{A20}$ treated cohorts. However, the loss of αvβ6 expression in these tumours may have contributed to the lack of difference

detected between Ad5-EGFP$_{WT}$ and Ad5-EGFP$_{A20}$. Interestingly, the fluorescence efficiency detected in the DX3-β6 xenografts on the first day of imaging (day 4 post-infection), was approximately 2-3 fold higher than detected in the DX3puro xenografts at the same time-point. Thus, it appeared that at early time-points *in vivo*, the DX3-β6 line better supported the replication of both Ad5-EGFP$_{WT}$ and Ad5-EGFP$_{A20}$. Tumour sections from DX3puro and DX3-β6 xenografts displayed extensive regions of necrosis when analysed histologically following sacrifice of the animals. It is possible that differing level of necrosis within the tumours at the time of imaging, affected intratumoural replication and spread at early time-points.

CHAPTER 4. Results

Chapter.4 *In Vitro* Characterisation of Ad5 Detargeting from CAR/ Coagulation Factors Combined with Retargeting to αvβ6 Integrin

Limited adenoviral uptake in malignant tissue, as a result of off-target sequestration in the reticuloendothelial system, remains a major obstacle to the application of therapeutic adenoviruses for the treatment of disseminated metastasis. In addition, the lack of selectivity associated with current retargeting strategies (ie. Ad5-RGD-4C and Ad5-K7), combined with the broad expression of the native CAR receptor, restricts the therapeutic index. The recent finding that human, but not murine, erythrocytes express CAR on their surface supports the importance of developing CAR-independent retargeting strategies, or indeed the use of relevant *in vivo* models for the study of intravenously administered Ad5 vectors (Carlisle *et al.*, 2009; Seiradake *et al.*, 2009). Therefore, it is clear that combining transductionally retargeted, cancer selective Ad5 vectors with primary receptor (CAR) ablation, with strategies for avoidance of the reticuloendothelial system and/or blood components, are key requirements in the development of realistic, systemically administered therapies for cancer.

The molecular determinants critical for CAR binding have been described extensively, as have reports regarding the generation of various CAR-binding ablated Ad5 vectors (Jakubczak *et al.*, 2001; Kirby *et al.*, 1999; 2000; Roelvink *et al.*, 1999; Santis *et al.*, 1999). Substitution mutations at critical residues S408E, P409A, Y477A and L485K have been shown to ablate CAR binding *in vitro*. However, CAR-binding ablation strategies alone have not proven useful in limiting the extensive liver transduction of Ad5 *in vivo,* or in altering the overall biodistribution of the vector (Alemany & Curiel, 2001; Leissner *et al.*, 2001; Martin *et al.*, 2003; Mizuguchi *et al.*, 2002; Nicol *et al.*, 2004; Smith *et al.*, 2002). Recently, it has become clear that various serum factors (FIX, FX, C4BP and Protein C) dictate hepatocyte transduction, and that CAR-mediated entry is redundant *in vivo*, at least in the context of sequestration within the reticuloendothelial system (Alba *et al.*, 2009; Kalyuzhniy *et al.*, 2008; Parker *et al.*, 2006; Shayakhmetov *et al.*, 2005b; Vigant *et al.*, 2008; Waddington *et al.*, 2008). Shayakhmetov and colleagues have described an Ad5 mutant, Ad5*mut*, which featured a set of mutations within the fibre which abrogated binding to FIX and C4BP *in vitro*. This vector displayed significantly reduced liver transduction and toxicity, and a failure to co-localise with Kupffer cells *in vivo* (Shayakhmetov *et al.*, 2005b). Conveniently, the set of incorporated mutations included the Y477A amino acid substitution, at a tyrosine residue described previously to be a critical determinant for CAR-binding (Kirby *et al.*, 2000; Roelvink *et al.*, 1999). This modification was combined with a TAYT deletion

within the FG loop of the fibre, and the insertion of a non-targeting FLAG peptide within the HI loop.

A combination of high affinity tumour-selective targeting in vectors genetically engineered for avoidance of the reticuloendothelial system has not yet been achieved. Therefore, the aim of this part of the project was to generate CAR-binding ablated Ad5 mutants, Ad5-Y477A and Ad5-L485K with both wildtype and A20-modified fibres. Subsequent aims were to incorporate the Y477A*dl*TAYT set of mutations into the Ad5-$EGFP_{A20}$ vector, in an attempt to create a virus which featured tumour targeting (via the interaction between A20FMDV2 and αvβ6), and reduced toxicity *in vivo,* through limiting off-target sequestration of the virus in the liver.

Section.4.1 Validation of ΔCAR/Blood Factor Binding Ablated Knob Mutants

4.1.1 Sequencing Analysis of Modified pQE30Knob Expression Plasmids. Several modified pQE30-based expression vectors were generated to facilitate the expression of, and purification of mutant recombinant proteins. These included CAR-binding mutants; $KnobY477A_{WT}$, $KnobY477A_{A20}$, $KnobL485K_{WT}$ and $KnobL485K_{A20}$ and combination mutants; Knob477*dl*$TAYT_{WT}$, Knob477*dl*$TAYT_{A20}$, Knob485*dl*$TAYT_{WT}$ and Knob485*dl*$TAYT_{A20,}$ which featured CAR-binding mutations (Y477A or L485K) in addition to the putative blood factor binding mutation (*dl*TAYT). Amino acid substitutions were introduced by mutagenic PCR and combination mutants subsequently were assembled using a SOEing PCR approach (see *Fig*.2.1 for an overview of the strategy). All successful modifications were confirmed by sequencing and constructs were checked to ensure that the sequences were in frame with the N-terminal 6X-HIS tag (*Fig*.4.1-*Fig*.4.4). An overview of some of the fibre mutants generated in this study can be found as a ClustalW protein alignment (*Appendix II*).

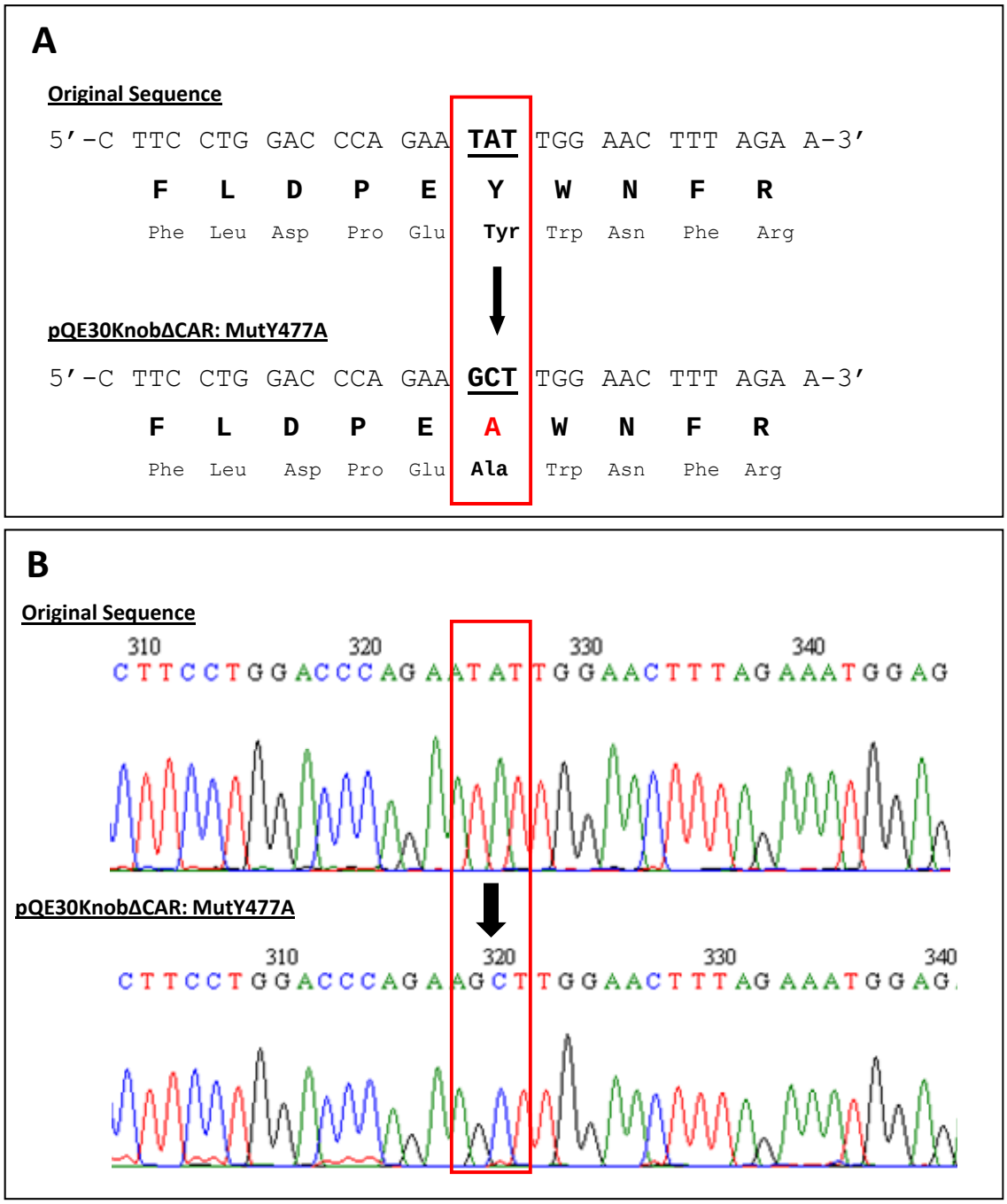

***Figure*.4.1 Generation of pQE30KnobΔCAR$_{WT/A20}$ (Y477A) by Site Directed Mutagenesis. (A)** Original nucleotide and amino acid sequence without mutation (*top*). A schematic showing the desired nucleotide and amino acid sequence, with Y477A to be introduced by mutagenic PCR (*bottom*). The red box highlights the nucleotide changes from TAT to GCT, with the sequence to be mutated, and the resultant amino acid substitution highlighted in bold and underlined in black. **(B)** Sequencing chromatogram showing the original CAR-binding determinant (477Y) within the adenoviral *fibre* gene (*top*), and its conversion to 477A, following successful site directed mutagenesis (*bottom*).

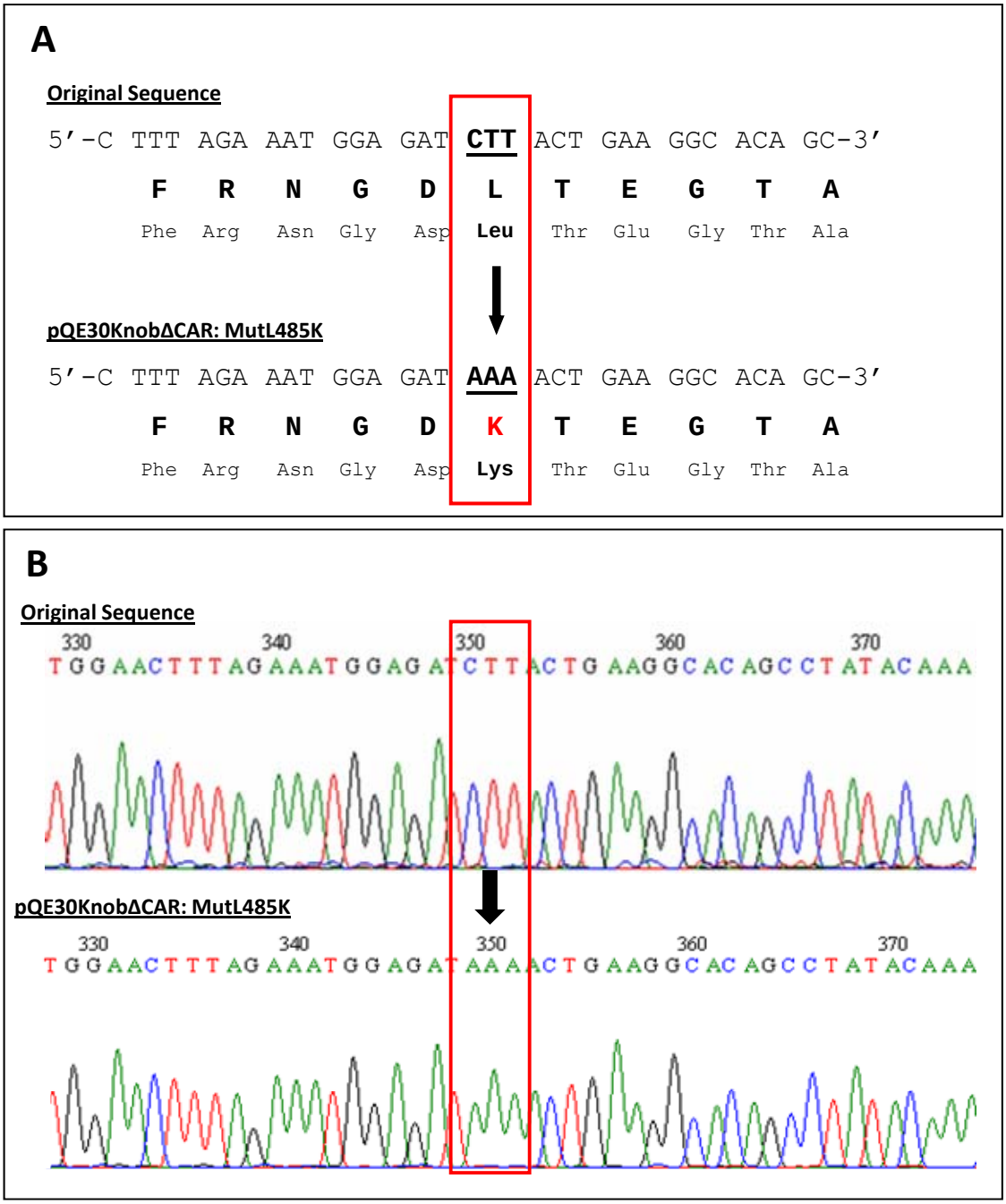

***Figure.*4.2 Generation of pQE30KnobΔCAR$_{WT/A20}$ (L485K) by Site Directed Mutagenesis. (A)** Original nucleotide and amino acid sequence without mutation (*top*). A schematic showing the desired nucleotide and amino acid sequence, with L485K to be introduced by mutagenic PCR (*bottom*). The red box highlights the nucleotide changes from CTT to AAA, with the sequence to be mutated and the resultant amino acid substitution highlighted in bold and underlined in black. **(B)** Sequencing chromatogram showing the original CAR-binding determinant (485L) within the adenoviral *fibre* gene (*top*), and its conversion to 485K, following successful site directed mutagenesis (*bottom*).

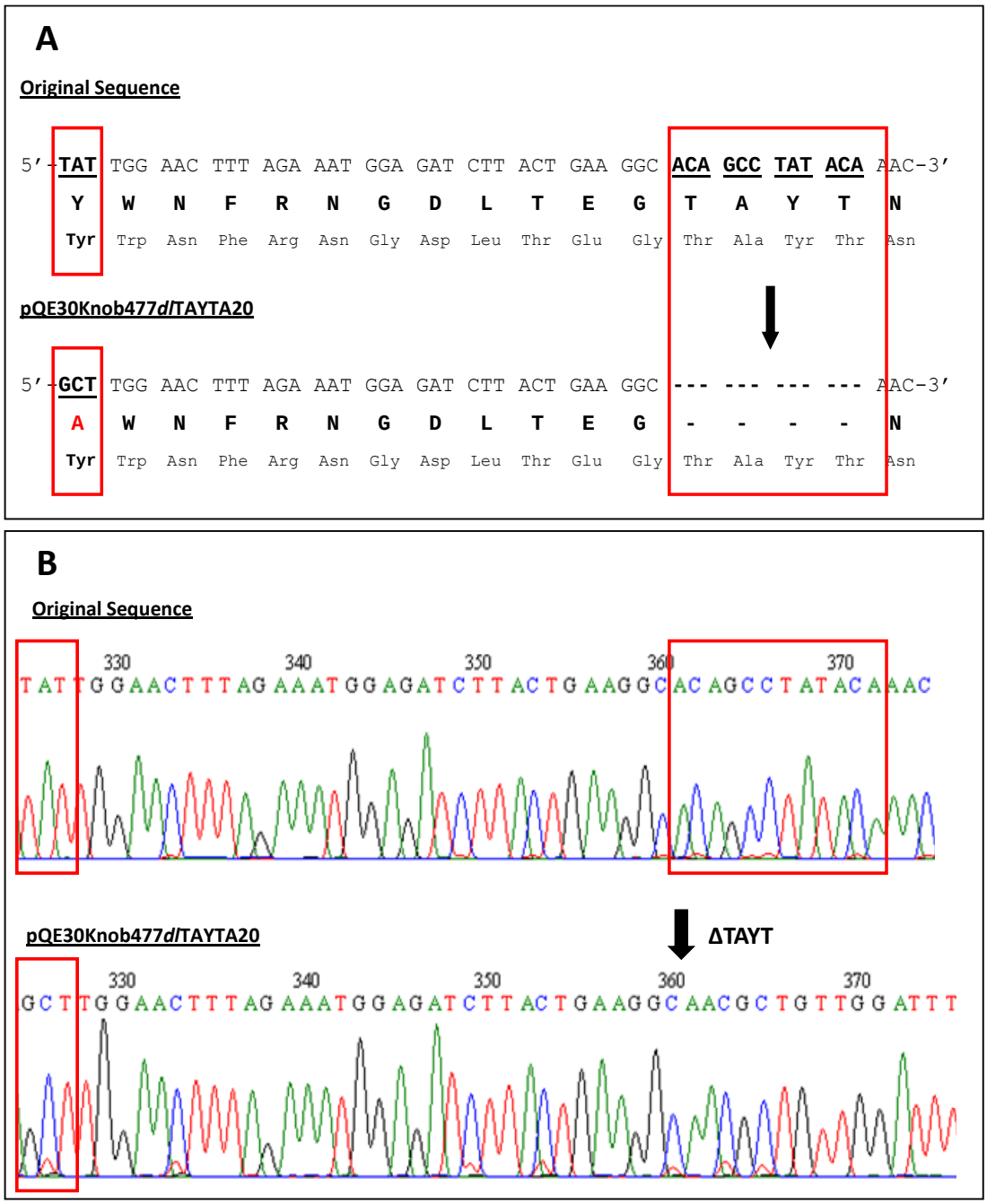

***Figure.*4.3 Results for site directed mutagenesis of pQE30Knob477*d*/TAYT$_{WT}$ and pQE30Knob477*d*/TAYT$_{A20}$. (A)** Original Ad5 nucleotide and amino acid sequence without modification (*top*). A schematic showing the desired nucleotide and amino acid sequence (*bottom*). Mutants were generated using SOEing PCR. The red boxes highlight the nucleotide changes from TAT to GCT, and the TAYT deletion. Nucleotide sequences to be mutated/deleted and the resultant changes are highlighted in bold and underlined in black. **(B)** Sequencing chromatogram showing the original Ad5 sequence (*top*), and the pQEKnob477*d*/TAYT$_{A20}$ sequence following successful assembly of the modified regions by SOEing PCR (*bottom*).

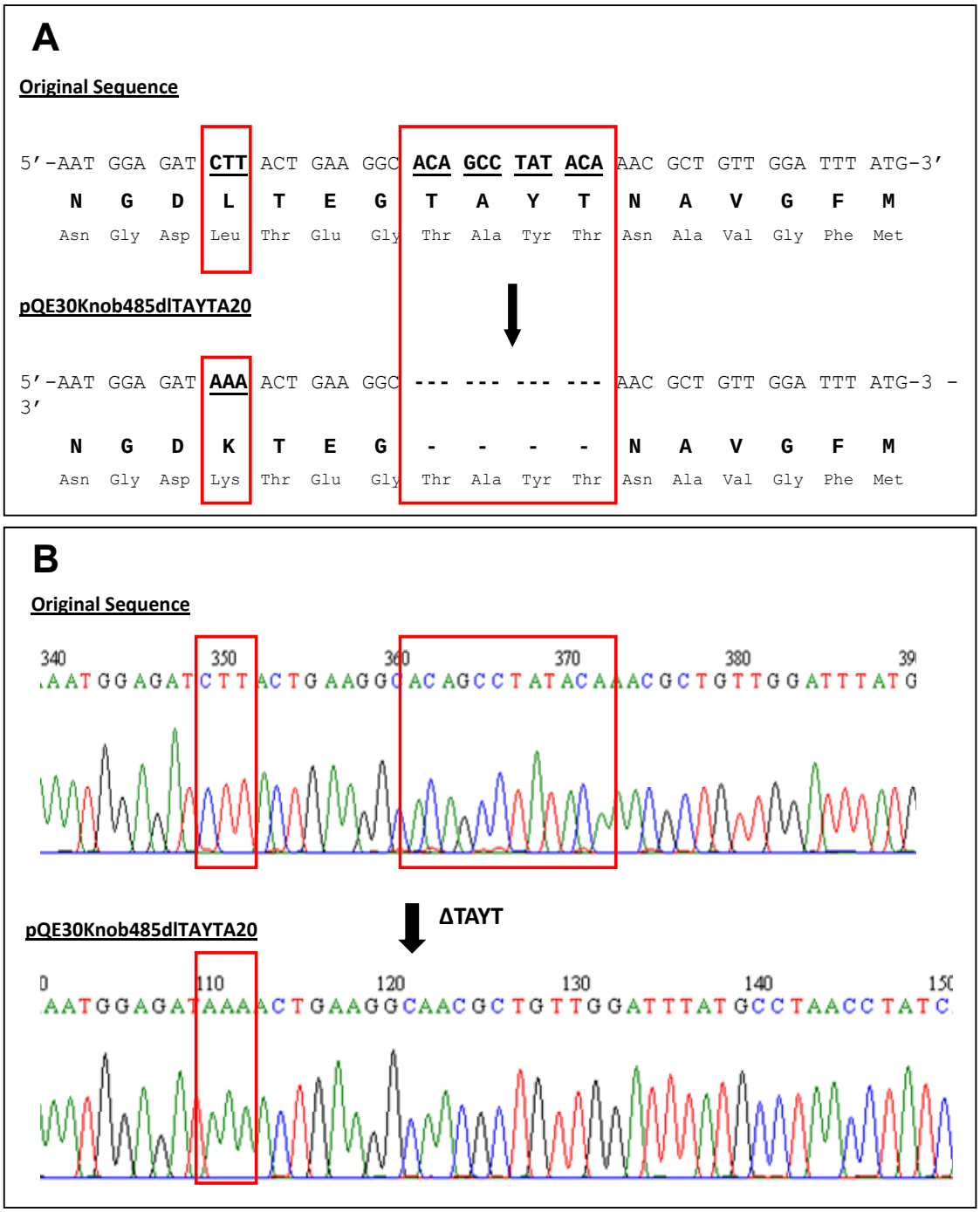

***Figure*.4.4 Results for site directed mutagenesis of pQE30Knob485*dl*TAYT$_{WT}$ and pQE30Knob485*dl*TAYT$_{A20}$. (A)** Original Ad5 nucleotide and amino acid sequence without modification (*top*). A schematic showing the desired nucleotide and amino acid sequence (*bottom*). Mutants were generated using SOEing PCR. The red boxes highlight the nucleotide changes from CTT to AAA, and the TAYT deletion. Nucleotide sequences to be mutated/deleted and the resultant changes are highlighted in bold and underlined in black. **(B)** Sequencing chromatogram showing the original Ad5 sequence (*top*), and the pQEKnob485*dl*TAYT$_{A20}$ sequence following successful assembly of the modified regions by SOEing PCR (*bottom*).

4.1.2 Recombinant Knob Protein Expression and Purification. CAR-binding ablated mutant proteins, KnobL485K$_{WT}$ and KnobL485K$_{A20}$, were produced by Tobias Simmonds, at the Protein Isolation laboratory, CR-UK. The KnobY477A$_{WT}$ and KnobY477A$_{A20}$ pQE-based plasmids were generated, however the corresponding proteins were not expressed or purified. Alternatively, the plasmids were used as templates for the generation of the Knob477*dl*TAYT$_{WT}$ and Knob477*dl*TAYT$_{A20}$ constructs. Using the protocol which had been optimised previously, mutant proteins Knob485*dl*TAYT$_{WT}$, Knob485*dl*TAYT$_{A20}$, Knob477*dl*TAYT$_{WT}$ and Knob477*dl*TAYT$_{A20}$ were expressed and purified.

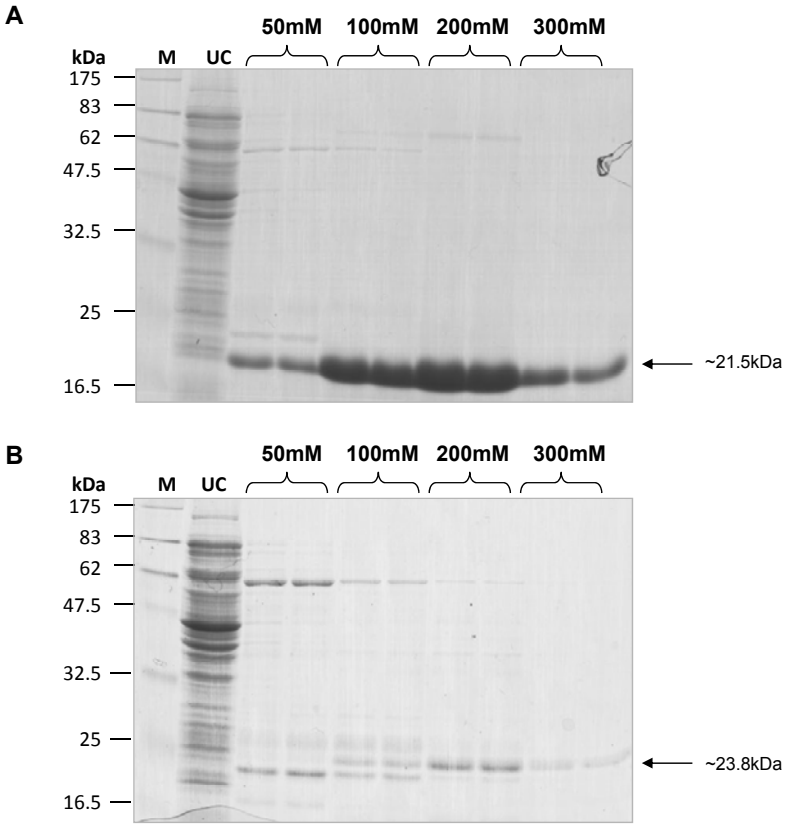

***Figure*.4.5 Elution Profile for Knob477*dl*TAYT$_{WT}$ (A) and Knob477*dl*TAYT$_{A20}$ (B).** Elution fractions (50-300mM imidazole) were run on a 12% SDS-PAGE gel, and bands visualised by Coomassie's staining. Fractions which were determined to have high purity (≥ 100mM for Knob477*dl*TAYT$_{WT}$, or ≥ 200mM for Knob477*dl*TAYT$_{A20}$), were pooled and dialysed overnight against PBS. Abbreviations are as follows; kDa = kilodalton, M = Marker (NEB Prestained Broad Range 6-175kDa) and UC represents uninduced control fraction. Arrows indicate the bands corresponding to the Knob477*dl*TAYT$_{WT}$ (~21.5kDa) and the Knob477*dl*TAYT$_{A20}$ monomer (~23.8kDa).

Elution profiles for Knob477*dl*TAYT$_{WT}$ and Knob477*dl*TAYT$_{A20}$ are shown in *Fig*.4.5A and B. Uninduced control and elution fractions were run in parallel on a 12% SDS-PAGE gel. Columns loaded with cell lysate-matrix slurry, were washed several times prior to elution of protein using imidazole, and a sample of the first wash was run in

parallel with the elution fractions. As expected, the uninduced control fractions did not contain protein, whereas in the elution fractions for both Knob477*dl*TAYT$_{WT}$ and Knob477*dl*TAYT$_{A20}$, the appropriate sized bands were clearly visible. Approximate molecular weights of the monomers were predicted to be ~21.5kDa for Knob477*dl*TAYT$_{WT}$, and ~23.8kDa for Knob477*dl*TAYT$_{A20}$ (using VectorNTI software to translate the nucleotide sequence into protein, inclusive of the 6XHIS Tag).

Elution profiles for Knob485*dl*TAYT$_{WT}$ (data not shown) and Knob485*dl*TAYT$_{A20}$ (*Fig*.4.6), were also obtained. Again, proteins were eluted under native conditions using a concentration gradient in the range of 100mM-300mM imidazole, and fractions analysed following SDS-PAGE. For each protein, appropriate fractions which had high purity (ie. minimal contaminating bands) were pooled, dialysed overnight against PBS and purified protein concentration calculated, as before, using the Pierce BCA protein assay.

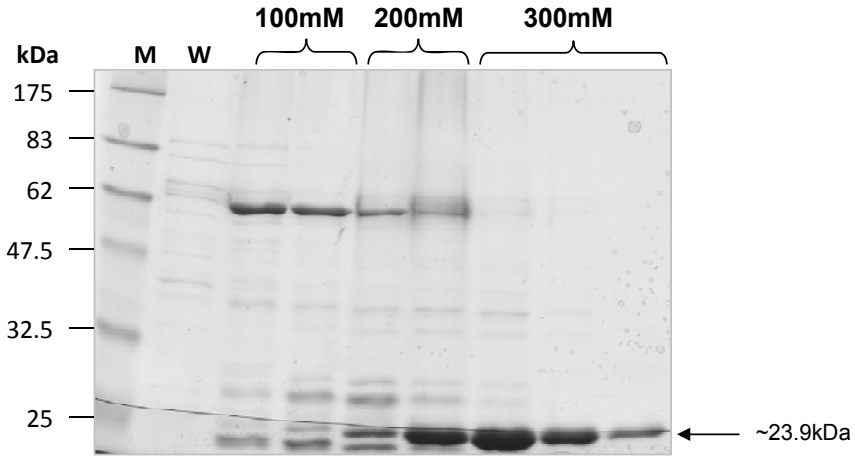

Figure.4.6 Elution Profile for Knob485*dl*TAYT$_{A20}$. Elution fractions (50-300mM imidazole) were run on a 12% SDS-PAGE gel, and bands visualised by Coomassie's staining. Fractions which were determined to have high purity (300mM) were pooled and dialysed overnight against PBS. Abbreviations are as follows; kDa = kilodalton, M = Marker (NEB Prestained Broad Range 6-175kDa) and W represents wash fraction. An arrow indicates the band corresponding to the Knob$_{A20}$ monomer (~23.9kDa). The elution profile for Knob485*dl*TAYT$_{WT}$ was visualised but not recorded.

4.1.3. Trimerisation Assay. We wanted to genetically incorporate the 477*dl*TAYT and 485*dl*TAYT modifications into the Ad5-EGFP$_{A20}$ virus backbone. Therefore the ability of Knob477*dl*TAYT$_{A20}$ (data visualised but not recorded) and Knob485*dl*TAYT$_{A20}$ (*Fig*.4.7) to form a homotrimer was confirmed by SDS-PAGE under semi-denaturing conditions. This was not assessed for the WT counterparts (Knob477*dl*TAYT$_{WT}$ and Knob485*dl*TAYT$_{WT}$), which were generated purely as controls for *in vitro* CAR-binding experiments (see *Fig*.4.11A).

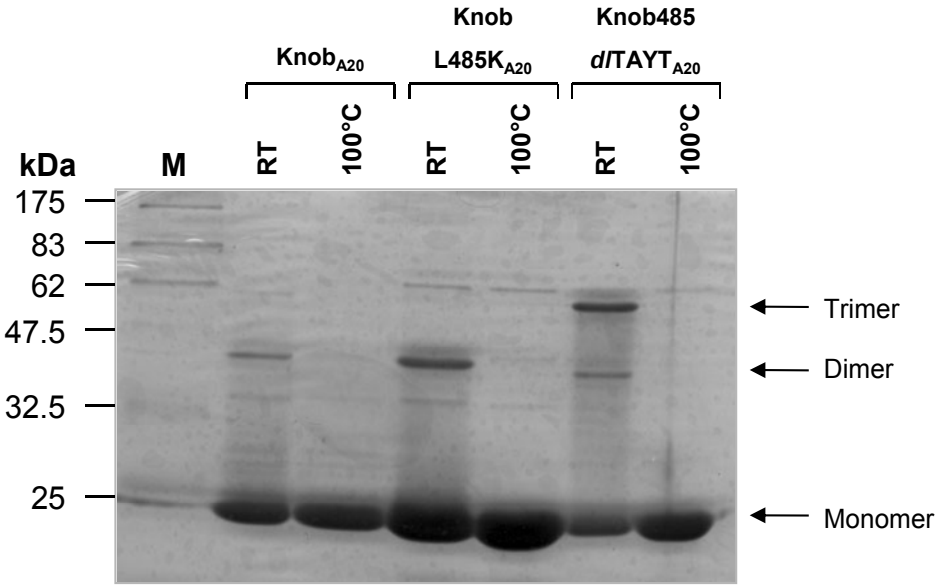

***Figure*.4.7 Trimerisation Assay Knob$_{A20}$, KnobL485K$_{A20}$ and Knob485*d*TAYT$_{A20}$.** Purified Knob$_{A20}$, KnobL485K$_{A20}$ and Knob485*d*TAYT$_{A20}$ protein samples (~5µg) were boiled at 95˚C for 5mins, or left at room temperature. Immediately prior to loading onto a 10% SDS-PAGE gel, 5X SDS-PAGE buffer (without DTT) was added to each sample (1X). Samples were run in parallel under semi-denaturing conditions in order to approximate trimer, dimer and monomer formation (indicated by an arrow). Abbreviations are as follows; kDa = kilodalton, M = Marker (NEB Pre-stained Broad Range 6-175kDa), RT = Room temperature.

4.1.4. Validation of ΔCAR/Blood Factor Knob$_{A20}$ Mutants; Binding to αvβ6. In order to eliminate the possibility that the introduced set of mutations (ΔCAR/Blood factor binding mutations) had altered the ability of the A20FMDV2 insertion to recognise αvβ6, the recombinant Knob477*d*TAYT$_{A20}$ and Knob485*d*TAYT$_{A20}$ mutants were tested for their ability to bind αvβ6 *in vitro* (*Fig.*4.8A+B). This experiment was carried out exactly as described previously for Knob$_{A20}$ (*Section.*3.2.5). BT-20 cells (high levels of αvβ6 but low levels of CAR) were incubated with increasing concentrations of each protein (0.0001µg-10µg/10^5 cells), after which unbound αvβ6 was detected using anti-αvβ6 mAb, 53A.2. Levels of bound 53A.2 were detected using a secondary, donkey anti-rat AlexaFluor488 antibody and results were analysed by flow cytometry, acquiring fluorescence in FL1-H. The fluorescence level for BT-20 cells untreated with recombinant Knob protein was taken to be 100% (or otherwise 100% antibody binding) and all other values were expressed as a % of this untreated control.

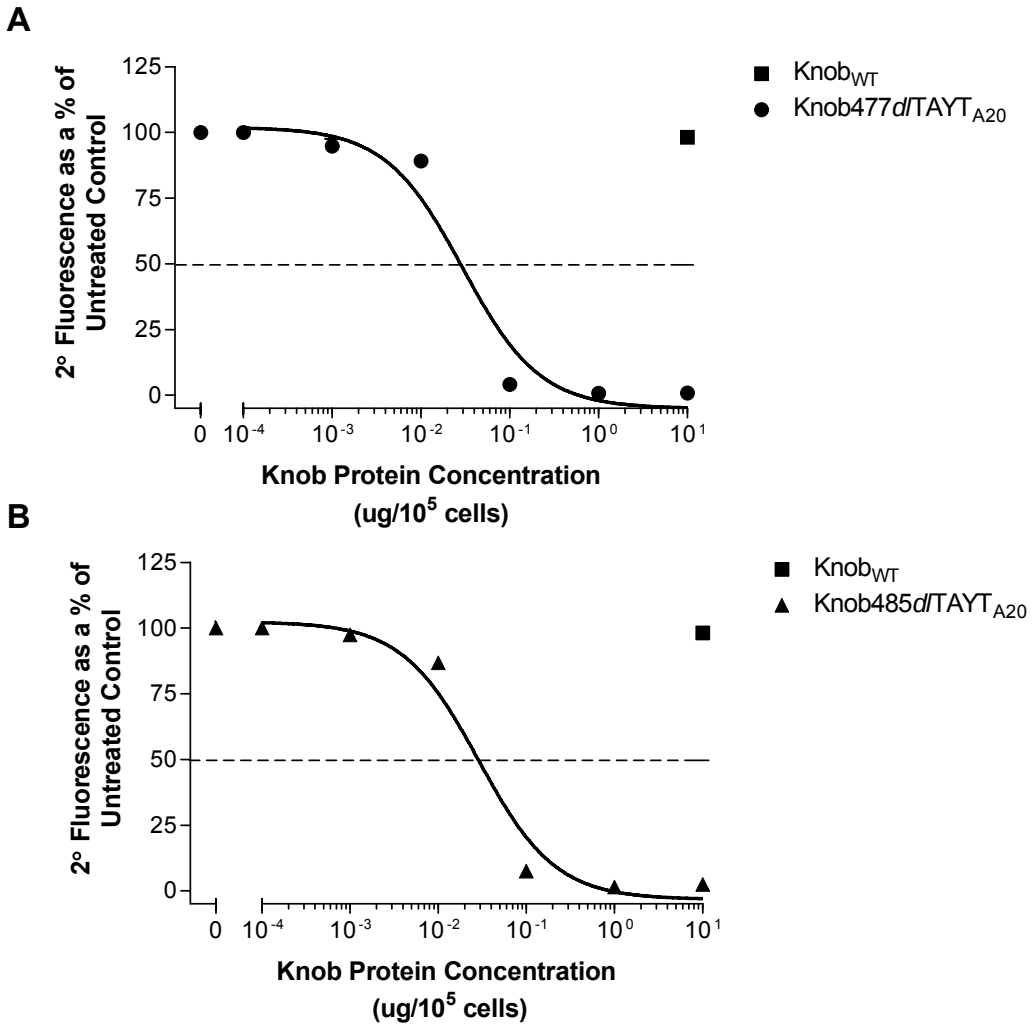

***Figure*.4.8 Competitive Inhibition of 53A.2 Binding to αvβ6 Integrin by Knob477*d*/TAYT$_{A20}$ (A) and Knob485*d*/TAYT$_{A20}$ (B).** Both recombinant knob proteins were capable of blocking αvβ6 on the surface of BT-20 cells, inhibiting the binding of an αvβ6-specific antibody (53A.2) in a dose-dependent manner (see *Section*.2.5.3). BT-20 cells (low CAR, high αvβ6) were incubated on ice with increasing concentrations of A20-modified Knob proteins (0.0001-10μg/10^5 cells), or Knob$_{WT}$ at a single concentration (10μg/10^5 cells). 53A.2 was added to cells, and its binding analysed by flow cytometry following the addition of a secondary donkey anti-rat AlexaFluor488 conjugate. Untreated cells were taken as 100% fluorescence and all other values expressed relative to this (see *Section*.2.5.3). Knob$_{WT}$ produced no significant effect at 10μg/10^5 cells (p=0.168) and is represented as a single point on the graph. The affinity of of Knob477/485*d*/TAYT$_{A20}$ for αvβ6 has not been detemined directly. Results were analysed by non-linear regression fitted to a sigmoidal curve, using GraphPad Prism Version 3.03 (GraphPad Software, San Diego, USA). Data represent the mean ± SD of triplicate samples (no bars represent SD values smaller than the symbol used).

The results confirmed that the incorporation of the various modifications (an amino acid substitution, in addition to a TAYT deletion) did not affect the interaction between the A20FMDV2 insertion and αvβ6 integrin. Each protein (Knob477*d*/TAYT$_{A20}$ and Knob485*d*/TAYT$_{A20}$) exhibited dose-dependent inhibition of an αvβ6-specific antibody binding, with 50% maximal inhibition at an identical concentration to that found for

$Knob_{A20}$ (0.03µg/10^5 cells; see *Fig.*3.8). $Knob_{WT}$, included as a control in the experiment, was unable to block 53A.2 binding at a high concentration (10µg/10^5 cells) and results did not differ from untreated cells (*p*=0.168). These data confirmed that the A20FMDV2 peptide, when combined with the introduced ΔCAR/Blood factor binding mutations, retained a fully functional ability to bind αvβ6.

4.1.5 Validation of ΔCAR/Blood Factor $Knob_{A20}$ Mutants; Functional Inhibition of αvβ6. We wanted to confirm that the modified Knob477*dl*$TAYT_{A20}$ and Knob485*dl*$TAYT_{A20}$ proteins also retained their ability to functionally inhibit αvβ6-dependent, VB6 cell migration towards the latency-associated peptide (LAP) of TGF-β1 (*Fig.*4.9A and B). The ability of increasing concentrations (0.025-25µg/ml) of Knob477*dl*$TAYT_{A20}$ or Knob485*dl*$TAYT_{A20}$ to inhibit αvβ6-dependent cell migration was assessed over a period of 24hrs, using a Transwell migration assay. BSA protein-coated wells were included in the experiment as a control for αvβ6-independent (random) cell migration. $Knob_{WT}$ was also used as a control in both experiments (*Fig.*4.9A and B), but produced no significant effect (*p*=0.489 and *p*=0.548, respectively).

Both Knob477*dl*$TAYT_{A20}$, and Knob485*dl*$TAYT_{A20}$ significantly inhibited VB6 cell migration towards LAP at all concentrations tested 0.025-25µg/ml ($p<0.05$). At a concentration of 0.025µg/ml, Knob477*dl*$TAYT_{A20}$ completely inhibited αvβ6-dependent cell migration towards LAP, reducing it to basal BSA levels (*p*=0.116). In comparison, a concentration of 0.25µg/ml Knob485*dl*$TAYT_{A20}$ was the lowest concentration which effectively reduced migration to basal levels (*p*=0.117). Knob477*dl*$TAYT_{A20}$ was as effective as an anti-αvβ6 inhibitory antibody (6.3G9) at concentrations of 2.5µg/ml (*p*=0.101), whereas Knob485*dl*$TAYT_{A20}$ required the higher concentration of 25µg/ml to produce an equivalent effect (*p*=0.106). In these experiments, the background migration (BSA protein control) was not subtracted from the overall migration, but is represented on the graph to show the level of background, αvβ6-independent cell migration.

An overview of the ability of A20-modified knob proteins $Knob_{A20}$, Knob477*dl*$TAYT_{A20}$ and Knob485*dl*$TAYT_{A20}$ to inhibit αvβ6-dependent migration is presented in *Fig.*4.10. In this experiment, all knob proteins were used at a single concentration of 10µg/ml. These data, combined with those presented in *Fig.*4.8 and *Fig.*4.9, confirmed that the integrity of the A20FMDV2 insertion was not disrupted, but that it retained its function despite the close proximity of the introduced mutations.

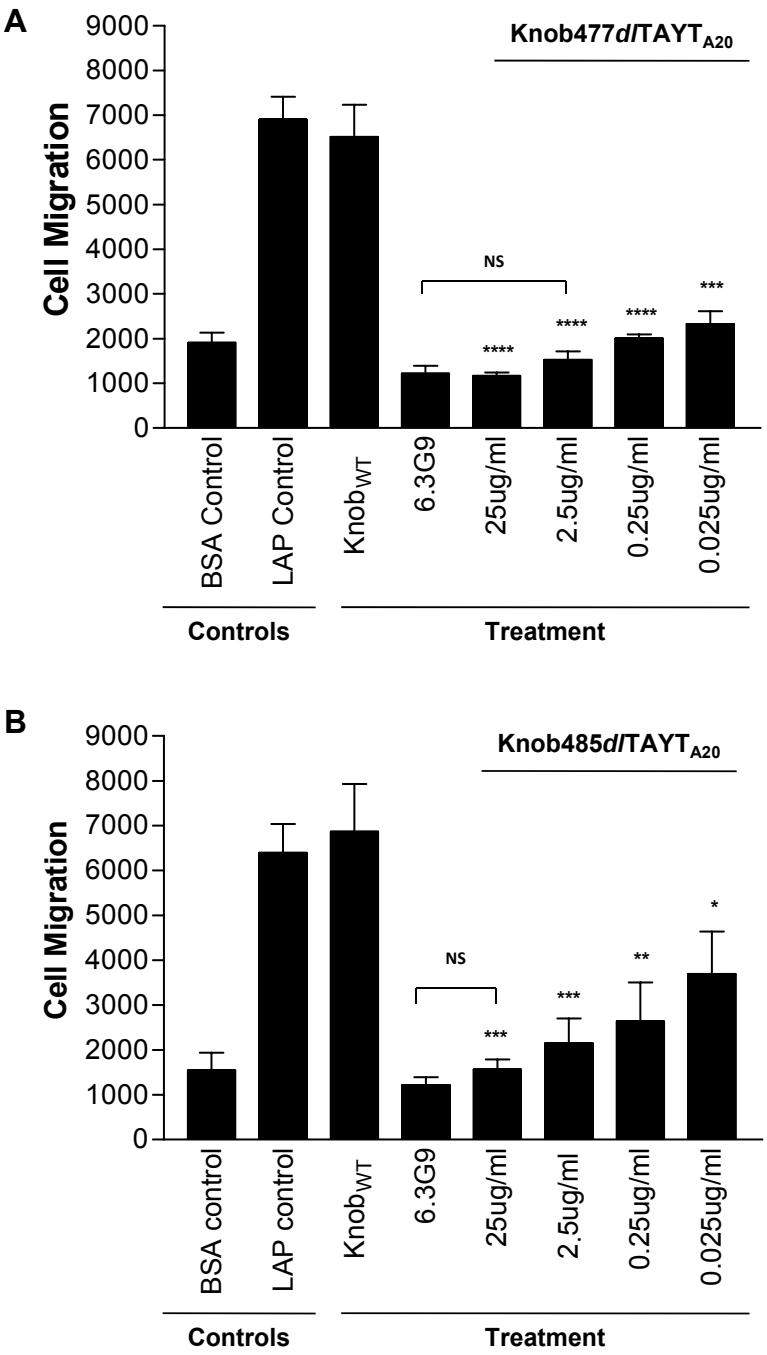

Figure.*4.9 Knob477*dl*TAYT$_{A20}$ Inhibition of αvβ6-Dependent Cell Migration (A), and Knob485*dl*TAYT$_{A20}$ (B).** Both A20-modified, recombinant knob proteins were capable of abrogating the αvβ6-dependent cell migration of VB6 cells towards the Latency Associated Peptide (LAP) of TGF-β1, in a Transwell migration assay (see *Section.*2.5.4). Controls for migration included; a BSA protein negative control (cells untreated with LAP) representing basal, non αvβ6-dependent migration, and a LAP positive control representing the level of αvβ6-dependent migration. Cells were treated with the following; Knob$_{WT}$ (10µg/ml), increasing concentrations of either Knob477*dl*TAYT$_{A20}$ or Knob485*dl*TAYT$_{A20}$ (0.025-25µg/ml), or a function blocking antibody to αvβ6, 6.3G9 (10µg/ml). Data represent the mean ± SD of triplicate samples and are representative of a single experiment carried out within a single plate. Statistical significance was determined using the unpaired Student's t-test comparing the means of each sample when compared with the LAP control, or between treated groups, as indicated on the histogram (* indicates a *P*-value of <0.05, ** *p*<0.01, *** *p*<0.001, * *p*<0.0001, bars indicate SD, NS = not statistically significant, p>0.05).

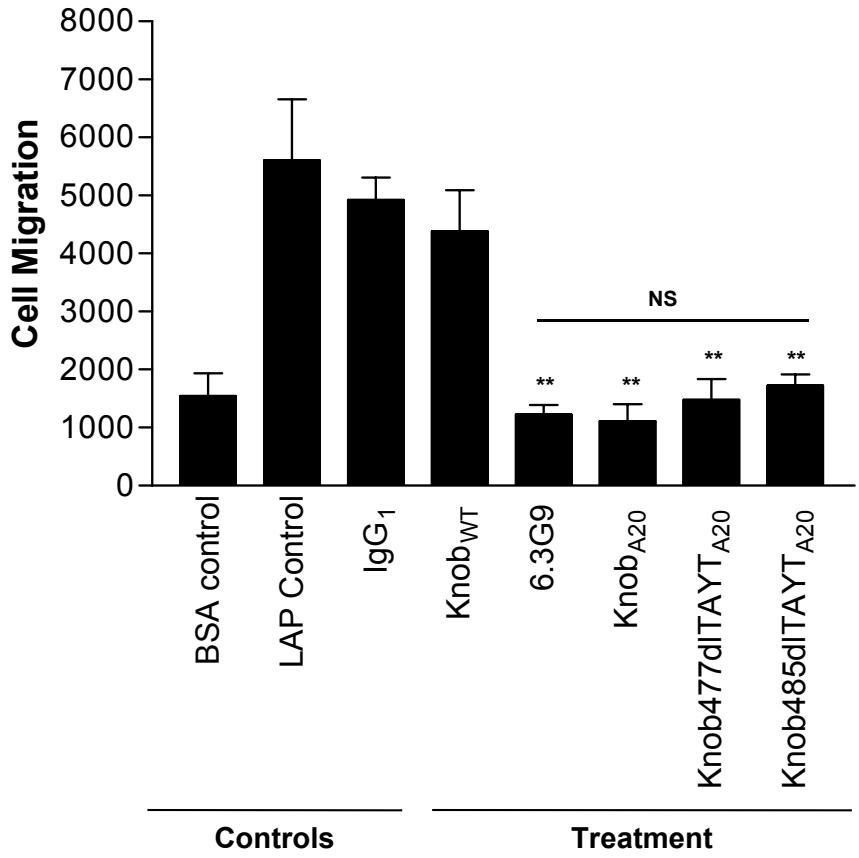

***Figure*.4.10 Overview of Knob$_{A20}$, Knob477*d*/TAYT$_{A20}$ and Knob485*d*/TAYT$_{A20}$ Mediated Inhibition of αvβ6-Dependent Cell Migration.** All A20-modified, recombinant knob proteins were compared in a VB6 cell migration assay (see *Section*.2.5.4). Controls for migration included; a BSA protein negative control (cells untreated with LAP) representing basal, non αvβ6-dependent migration, a LAP positive control representing the level of αvβ6-dependent migration and an isotype control (IgG$_1$) for 6.3G9. All recombinant proteins (Knob$_{WT}$, Knob$_{A20}$, Knob477*d*/TAYT$_{A20}$ and Knob485*d*/TAYT$_{A20}$), and antibodies, IgG$_1$ and 6.3G9, were used at a final concentration of 10µg/ml. Data represent the mean ± SD of triplicate samples and are representative of a single experiment carried out within a single plate. Statistical significance was determined using the unpaired Student's t-test comparing the means of each sample when compared with the LAP control, or between treated groups, as indicated on the histogram (** indicates a *P*-value of <0.01, bars indicate SD, NS = not statistically significant, p>0.05).

4.1.6 Validation of the ΔCAR-Binding Mutant Knob Proteins. The use of recombinant knob or fibre protein to block the infection of a virus from which it was derived, is a well established assay (Freimuth *et al.*, 1999; Santis *et al.*, 1999). Therefore, once the complete panel of CAR-binding and/or blood factor binding mutants had been generated and purified to sufficient quantities, we analysed their CAR-binding capacity in parallel (*Fig*.4.11A). CHO-CAR cells (generously provided by Dr. George Santis) were pre-incubated with a single concentration of each protein (100µg/10^5 cells) for 1hr on ice. This was followed by super-infection with Ad5-EGFP$_{WT}$ (MOI 10) for a further hour under the same conditions, after which the suspension was removed, and infection allowed to proceed for ~22hrs. Successful EGFP gene transfer

was quantified by flow cytometry. Ad5-EGFP$_{WT}$ infected cells which were untreated with recombinant protein were expressed as 100% infectivity, and all other values expressed relative to this.

As expected both Knob$_{WT}$ and Knob$_{A20}$ significantly inhibited Ad5-EGFP$_{WT}$ infection, by ~96% and ~95% respectively (p<0.0001 for both). Recombinant protein, Knob485$_{WT}$, featuring the L485K point mutation at a previously described CAR-binding determinant, was unable to inhibit Ad5-EGFP$_{WT}$ infection, confirming that its native binding had been ablated. However, rather unexpectedly, the A20-modified version of this protein completely inhibited infection (p<0.0001; data not shown), in a manner comparable to CAR-binding Knob$_{WT}$ or Knob$_{A20}$ (p=0.0001, compared to both). This was later explained by the discovery that Protein Production Services had accidentally purified Knob$_{A20}$ instead of KnobL485K$_{A20}$ (personal communication). KnobY477A$_{WT}$ and KnobY477A$_{A20}$ were not expressed as recombinant protein due to time constraints, and therefore not included in the analysis.

CAR-binding mutants which had been combined with the modification of putative blood factor binding sites were also assessed. Knob477*dl*TAYT$_{WT}$ was unable to inhibit the infection of Ad5-EGFP$_{WT}$ (p=0.057). Unexpectedly, Knob477*dl*TAYT$_{A20}$ was capable of inhibiting ~12% of Ad5-EGFP$_{WT}$ infection at 100µg/10^5 cells, not a dramatic result, although it was found to be statistically significant (p=0.02). As expected, both the Knob485*dl*TAYT$_{WT}$, and Knob485*dl*TAYT$_{A20}$ mutants, failed to inhibit Ad5-EGFP$_{WT}$ infection (p=0.233 and p=0.508, respectively), confirming the successful ablation of their CAR-binding ability.

In order to further characterise the unusual result found with Knob477*dl*TAYT$_{A20}$ in *Fig.*4.11A, the experiment was repeated (*Fig*.4.11B), however this time comparing increasing concentrations (0.001-100µg/10^5 cells) of both Knob$_{A20}$ and Knob477*dl*TAYT$_{A20}$. Knob485*dl*TAYT$_{A20}$ was not assessed. The IC$_{50}$ for Knob$_{WT}$ mediated inhibition of native Ad5 infection has been published (Kirby *et al.,* 2000). This value was determined to be 0.115µg/10^5 cells, and was obtained using the same CHO-CAR cells, and a similar experimental approach. Therefore, we chose only to include Knob$_{WT}$ as a control in this experiment at two concentrations, 0.01µg and 0.1µg/10^5 cells (data not shown). As expected, Knob$_{A20}$ was capable of inhibiting Ad5-EGFP$_{WT}$ infection with an IC$_{50}$ of 0.34µg/10^5 cells, confirming that Knob$_{A20}$ retained native CAR binding, albeit with slightly impaired efficiency when compared to Knob$_{WT}$. As shown in *Fig*.4.11B, Knob477*dl*TAYT$_{A20}$ did not substantially inhibit Ad5-EGFP$_{WT}$ infection at concentrations of up to 10µg/10^5 cells, although inhibition was found to be significant at

100µg/10^5 cells (p=0.04), consistent with the result obtained in *Fig*.4.11A. This effect was explained, to an extent, by results obtained in subsequent experiments (see *Fig*.4.14A).

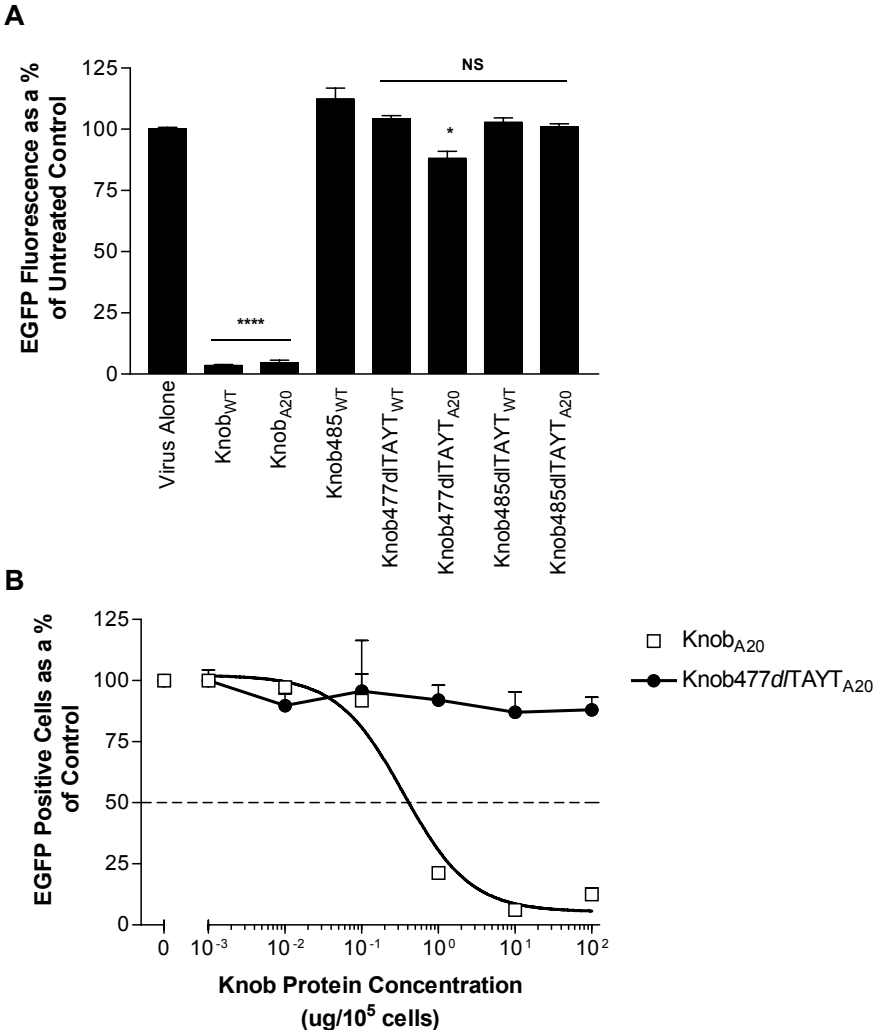

***Figure*.4.11 (A) Comparative Analysis of a Panel of CAR-Binding Mutant Knob Proteins.** All modified Knob proteins generated in this study were compared, in a single experiment, for their ability to inhibit native Ad5-EGFP$_{WT}$ entry to CHO-CAR cells. Cells were incubated with a single concentration of each Knob protein (100µg/10^5 cells) for 1hr at 4˚C after which they were infected with Ad5-EGFP$_{WT}$ (MOI 10: PFU/cell) for a further hour at 4˚C. EGFP gene transfer was quantified ~22hrs later by flow cytometry. Untreated cells were taken as 100% fluorescence and all other values expressed relative to this (see *Section*.2.8.2). **(B) Characterisation of the CAR-binding Capacity of Knob477*dl*TAYT$_{A20}$.** Knob$_{A20}$ and Knob477*dl*TAYT$_{A20}$ were assessed for their ability to inhibit the infection of Ad5-EGFP$_{WT}$. CHO-CAR cells were incubated with increasing concentrations of Knob$_{A20}$ or Knob477*dl*TAYT$_{A20}$ (0.001-100µg/10^5 cells). Knob$_{WT}$ was included as a control at concentrations of 0.01- and 0.1µg/10^5 cells (data not shown), and the experiment performed exactly as described above. Results were analysed by non-linear regression fitted to a sigmoidal curve, using GraphPad Prism Version 3.03 (GraphPad Software, San Diego, USA). Data represent the mean ± SD of triplicate samples and are representative of two independent experiments carried out on different occasions. Statistical significance was determined using the unpaired Student's *t*-test comparing the means of each sample when compared with the virus alone sample, or between treated groups, as indicated on the histogram (* indicates a *P*-value of <0.05, **** p<0.0001, bars indicate SD, NS = not statistically significant, p>0.05).

Section.4.2 Validation of CAR-Binding Ablated Viral Mutants, Infectivity and Cytotoxicity

Once the combination mutation virus, Ad5-477*dl*TAYT$_{A20}$, had been generated and purified to sufficient titres, its *in vitro* characteristics were compared with Ad5-EGFP$_{WT}$ and Ad5-EGFP$_{A20}$. Additionally, the Ad5-485*dl*TAYT$_{A20}$ mutant was generated and purified, although its titres were substantially lower than the other viruses generated in this study (*Table.*14). Therefore, it was not selected for *in vivo* studies and accordingly, *in vitro* characterisation of this construct is limited to date.

Table 14. Titres of Virus Constructs Used in this Study[a]

Virus Name	Modification (E3)	Modification (Fibre)	Titre (VP/ml)	Titre (PFU/ml)	Ratio (VP/PFU)
Ad5-EGFP$_{WT}$	Δ6.7K/gp19K-EGFP	N.A	1.79 x 10^{12}	1.98 x 10^{10}	90
Ad5-EGFP$_{A20}$	Δ6.7K/gp19K-EGFP	A20FMDV2 insertion	1.26 x 10^{12}	1.80 x 10^{10}	70
Ad5-477*dl*TAYT$_{A20}$	Δ6.7K/gp19K-EGFP	A20FMDV2 insertion, Y477A and *dl*TAYT	3.71 x 10^{11}	3.61 x 10^{9}	100
Ad5-485*dl*TAYT$_{A20}$	Δ6.7K/gp19K-EGFP	A20FMDV2 insertion, L485K and *dl*TAYT	4.65 x 10^{11}	9.51 x 10^{8}	480
Ad5-477*dl*TAYT$_{6XHIS}$	Δ6.7K/gp19K-EGFP	A20FMDV2 insertion, Y477A and *dl*TAYT	N.D	N.D	N.D
Ad5-485*dl*TAYT$_{6XHIS}$	Δ6.7K/gp19K-EGFP	A20FMDV2 insertion, L485K and *dl*TAYT	N.D	N.D	N.D
Ad5-Δ24-EGFP$_{A20}$	Δ6.7K/gp19K-EGFP	A20FMDV2 insertion	N.D	N.D	N.D
Ad5-hNIS$_{A20}$	Δ6.7K/gp19K-hNIS	A20FMDV2 insertion	N.D	N.D	N.D

[a] Viruses generated in this study are listed. Viral titres were obtained by TCID$_{50}$ end-point dilution assay (PFU/ml), and spectrophotometrically at an absorbance of OD$_{600nm}$ (VP/ml). Abbreviations are as follows; VP = Viral particle, PFU = Plaque forming unit, EGFP = Enhanced green fluorescent protein, N.A = Not applicable, FMDV = Foot and Mouth Disease Virus, HIS = Histidine, Y = Tyrosine, A = Alanine, L = Leucine, K = Lysine, hNIS = Human sodium iodide symporter, N.D = Not determined.

4.2.1 Comparative Infectivity of Ad5-EGFP$_{WT}$, Ad5-EGFP$_{A20}$ and Ad5-477*dl*TAYT$_{A20}$ on a Panel of αvβ6-Expressing Cell Lines. The transduction efficiency of Ad5-477*dl*TAYT$_{A20}$ was compared with Ad5-EGFP$_{WT}$, and Ad5-EGFP$_{A20}$ using a selected panel of carcinoma lines (*Fig*.4.12). In agreement with results obtained in previous transduction experiments (see *Fig*.3.13), Ad5-EGFP$_{A20}$ displayed significantly improved infectivity in all cell lines tested (p<0.0001). Importantly, the CAR-binding ablated mutant Ad5-477*dl*TAYT$_{A20}$ retained this ability, also significantly enhancing the transduction of all cell lines tested (p<0.0001). In fact, the transduction efficiency of Ad5-477*dl*TAYT$_{A20}$ in CAOV3 and DX3-β6 cells was superior to that of Ad5-EGFP$_{A20}$ (p<0.0001 and p=0.033, respectively). Thus, we concluded that the introduction of the 477*dl*TAYT set of mutations into the fibre did not interfere with the ability of the A20FMDV2 peptide to promote viral entry through αvβ6.

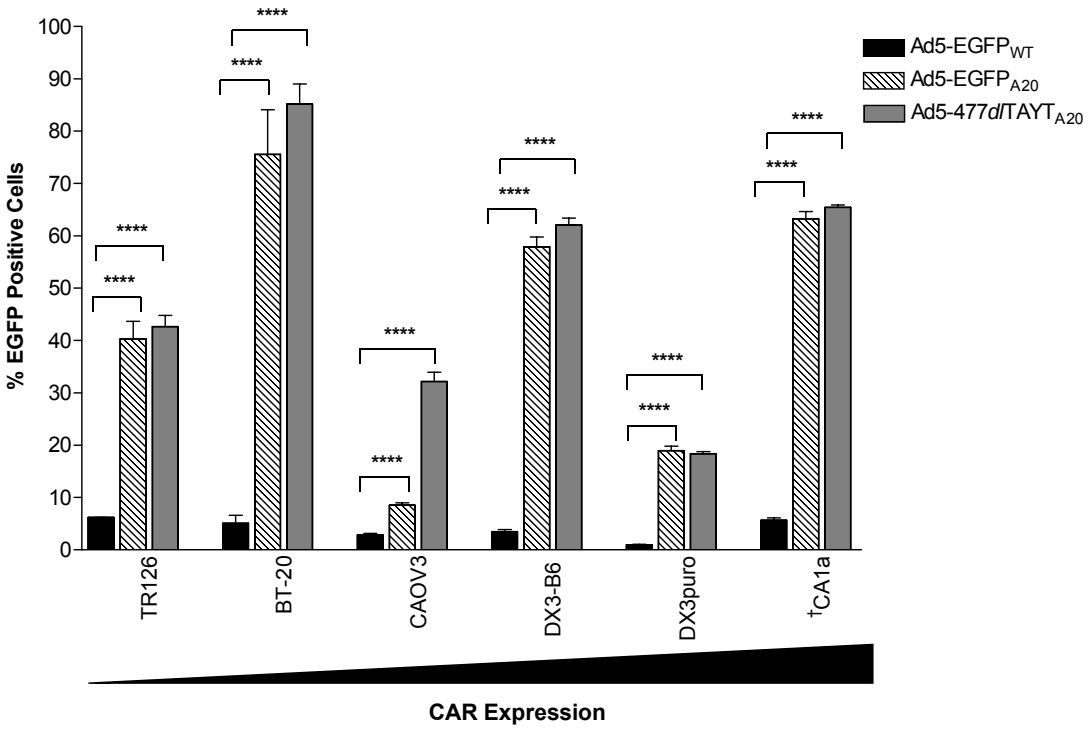

Figure*.4.12 Comparative Infectivity of Ad5-EGFP$_{WT}$, Ad5-EGFP$_{A20}$ and Ad5-477*dl*TAYT$_{A20}$ on a Panel of αvβ6-Expressing Cell Lines.** The transduction efficiency of each virus was assessed following infection at an MOI 10 (PFU/cell). Cells were exposed to virus for 1hr at 4˚C, and EGFP transgene expression quantified by flow cytometry ~22hrs post-infection (see *Section*.2.8.2). Histogram shows the % EGFP positive cells gated in FL1-H, arranged in order of ascending CAR-expression (see *Table*.10). Data represent the mean ± SD of triplicate samples, from a single experiment. Statistical significance was determined using the unpaired Student's *t*-test to compare the means of each group (* indicates a *P*-value <0.0001, NS = not statistically significant, *p*>0.05, bars indicate SD, no bars represent SD values smaller than the symbol used. †CA1a is abbreviated from MCF10CA1a.

4.2.2 Comparative Cytotoxicity of Ad5-EGFP$_{WT}$, Ad5-EGFP$_{A20}$ and Ad5-477*dl*TAYT$_{A20}$ on a Panel of αvβ6-Expressing Lines. A comparative cytotoxicity profile (MTT) was generated using a selected panel of human carcinoma cell lines, comparing Ad5-477*dl*TAYT$_{A20}$, with Ad5-EGFP$_{WT}$ and Ad5-EGFP$_{A20}$ (*Fig.*4.13A-F). Cells (A549, BT-20, CA1a, CAOV3, SKOV3ip1 and TR126), were infected with doses of virus ranging from MOI 0.0001-100 PFU/cell, and cytotoxicity determined 120hrs post-infection.

When compared to Ad5-EGFP$_{WT}$, Ad5-477*dl*TAYT$_{A20}$ exhibited increased cytotoxicity (EC_{50}) in low-moderate CAR-expressing lines; BT-20 (~13-fold, *p*=0.0006), CA1a (~8-fold, *p*=0.002), CAOV3 (~8-fold, *p*=0.049), SKOV3ip1 (~28-fold, *p*<0.0001) and TR126 (~3-fold, *p*>0.05, not significant). Additionally, non-CAR binding virus Ad5-485*dl*TAYT$_{A20}$, also displayed improved cytotoxicity over Ad5-EGFP$_{WT}$ in each of the low-moderate CAR-expressing cell lines tested; CA1a (~14-fold, *p*=0.0001), CAOV3 (~7-fold, *p*=0.151, not significant) and SKOV3ip1 cells (~80-fold, *p*<0.0001).

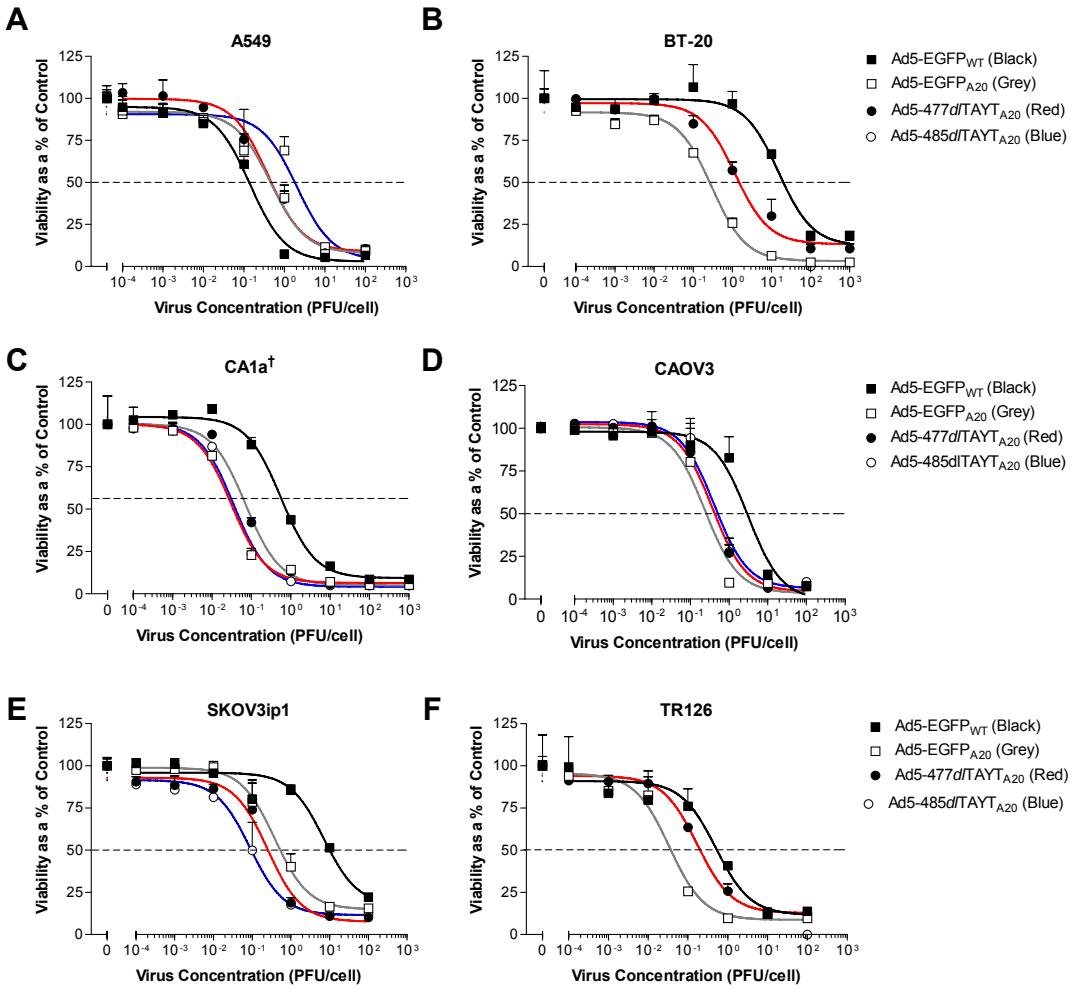

Table 15. EC$_{50}$ Val

Ad5-EGFP$_{WT}$	[redacted]					
Ad5-EGFP$_{A20}$	[redacted]					
Ad5-477*d*/TAYT$_{A20}$	[redacted]					
Ad5-485*d*/TAYT$_{A20}$	2.05	N.D	0.04	0.42	0.09	N.D

[a] EC$_{50}$ values represent half the maximal effective concentration of virus per cell. Viability was assessed by MTT assay and results analysed by non-linear regression fitted to a sigmoidal curve. Values expressed in Plaque Forming Units (PFU/Cell). N.D = Not determined. †CA1a is abbreviated from MCF10CA1a.

***Figure*.4.13 Comparative Cytotoxicity Profiles for Ad5-EGFP$_{WT}$, Ad5-EGFP$_{A20}$, Ad5-477*d*/TAYT$_{A20}$ and Ad5-485*d*/TAYT$_{A20}$ on a Panel of αvβ6-Expressing Cell Lines.** Cytotoxicity was determined by MTT assay, carried out 120hrs post-infection, with virus concentrations ranging from 0.0001-100 PFU/cell and mean percentage survival was expressed as a percentage of uninfected cells (Uninfected cells are represented on the X-axis as 0, following a break in the logarithmic scale). Cell lines investigated were; **(A)** A549 and **(B)** BT-20, **(C)** †CA1a **(D)** CAOV3 **(E)** SKOV3ip1 and **(F)** TR126. Dose-response curves were generated by non-linear regression analysis using GraphPad Prism Version 3.03 (GraphPad Software, San Diego, CA). EC$_{50}$ values for the dose response curves are displayed in *Table*.15. Cytotoxicity profiles shown are representative of a single experiment carried out using triplicate samples. The unpaired Student's *t*-test was used to demonstrate the significance of the difference in EC$_{50}$ values for each virus (N.D = Not Determined, NS = not statistically significant, $p>0.05$, bars indicate SD, no bars represent SD values smaller than the symbol used). †CA1a is abbreviated from MCF10CA1a.

However, both CAR-modified viruses displayed decreased cytotoxicity in high CAR, A549 cells, resulting in ~6-fold decrease for Ad5-477*d*/TAYT$_{A20}$ (p=0.002) and a ~15-

fold decrease for Ad5-485*dl*TAYT$_{A20}$ (p=0.003). However, the latter result was expected, as the native CAR-binding of these vectors is ablated and A549 cells express almost negligible levels of αvβ6 and αvβ8 (<5%, see *Table.*10 and *Table*.11), precluding CAR-independent entry via these surrogate receptors. When compared with Ad5-EGFP$_{A20}$, the CAR-binding ablated viruses also varied in their ability to induce cytotoxicity. The cytotoxic effect of Ad5-477*dl*TAYT$_{A20}$ was impaired in BT-20 cells (~4-fold reduction, p=0.002) and TR126 cells (~6-fold reduction, p=0.024). However, in the majority of the cell lines tested, the cytotoxicity of Ad5-477*dl*TAYT$_{A20}$ was either increased significantly (SKOV3ip1; ~1.5-fold, p=0.034), or did not differ from Ad5-EGFP$_{A20}$ (A549; p=0.255, CA1a; p=0.435 and CAOV3; p=0.366). When compared to Ad5-EGFP$_{A20}$, Ad5-485*dl*TAYT$_{A20}$ displayed a ~4-fold decrease in cytotoxicity in A549 cells, however this was not significant (p=0.124). In fact, EC_{50} values obtained for this virus did not differ significantly from Ad5-EGFP$_{A20}$ in two further cell lines investigated (CA1a; p=0.968 and CAOV3; p=0.166). Moreover, it displayed significantly increased cytotoxicity in SKOV3ip1 cells (p=0.0009).

Section.4.3 Validation of ΔCAR/Blood Factor Binding Ablated A20-Modified Viral Mutants

A fundamental role for serum/coagulation factors (ie. FVII, FIX, FX, Protein C and C4BP) in directing liver uptake of Ad5 following systemic delivery in mice, has been demonstrated in recent years (Alba *et al.*, 2009; Kalyuzhniy *et al.*, 2008; Parker *et al.*, 2006; Shayakhmetov *et al.*, 2005b; Vigant *et al.*, 2008; Waddington *et al.*, 2008). Coagulation factor mediated hepatocyte transduction is thought to result from engagement with heparan sulphate proteoglycans (HSPGs), and/or low-density lipoprotein receptor-related protein, LRP. FX-mediated enhancement of hepatocyte transduction *in vivo* has been reported to occur through a direct interaction between FX and Ad5 hexon (Alba *et al.*, 2009; Kalyuzhniy *et al.*, 2008; Vigant *et al.*, 2008; Waddington *et al.*, 2008). Conversely, FIX and C4BP have been shown to interact with the fibre knob domain (Gaggar *et al.*, 2007; Shayakhmetov *et al.*, 2005b). The 477*dl*TAYT set of mutations which was genetically incorporated into the fibre, to generate Ad5-477*dl*TAYT$_{A20}$, has been reported to ablate binding to FIX and C4BP (the reported vector had a FLAG epitope in place of the A20 peptide). The authors reported that this fibre modified vector had reduced liver transduction, and limited co-localisation with Kupffer cells *in vivo* following intravenous delivery (Shayakhmetov *et al.*, 2005b).

4.3.1 Comparative Infectivity +/- FIX, FX and Heparin on CHO-K1 Cells. Using an *in vitro* assay, we decided to investigate if FIX and/or FX could enhance the Ad5-EGFP$_{WT}$, Ad5-EGFP$_{A20}$ and Ad5-477*dl*TAYT$_{A20}$-mediated infection of HSPG-expressing CHO-K1 cells (*Fig*.4.14A). We did not assess the levels of HSPGs on the surface of CHO-K1 cells for a number of reasons; firstly, suitable antibodies for detection by flow cytometry are limited, and expensive, due to the complexity of the post-translationally modified glycosaminoglycan (GAG) side chains. Additionally, CHO-K1 cells have previously been published as a suitable *in vitro* model for assessing coagulation factor mediated Ad-enhancement (Liu *et al.*, 2009; Parker *et al.*, 2006). C4BP was not assessed as it was not commercially available when these experiments were performed. Cells were co-incubated for 2hrs at 37˚C with each virus (MOI 10), and physiological concentrations of commercially available human FIX, FX, or FX with porcine heparin to inhibit HSPGs. We did not have sufficient stocks of FIX to test in combination with heparin. Indeed, in this study approximately 3.5% infection was observed with Ad5-EGFP$_{WT}$ in the absence of any treatment with blood factors. Treatment with both FIX and FX resulted in enhancing the infectivity of Ad5-EGFP$_{WT}$ ~4-fold and ~6-fold, respectively (p=0.001 and p<0.0001). The effect of FX was completely inhibited in the presence of heparin, confirming that the enhancement was mediated through HSPGs. In addition, the low level infection observed with Ad5-EGFP$_{WT}$ alone was also completely inhibited upon co-incubation with heparin, suggesting that the basal level of infectivity was due to entry via HSPGs. However, this

was not an unusual observation, as HSPGs have previously been reported to act as an alternative, lower affinity receptor for Ad5 in the absence of CAR (Dechecchi *et al*., 2001, 2002). Similarly, Ad5-EGFP$_{A20}$ alone infected CHO-K1 cells to a low level (~3% infected cells). Interestingly, FIX did not appear to enhance the infectivity of Ad5-EGFP$_{A20}$ (p=0.101), despite the fact that this virus does not contain any of the putative blood factor binding mutations which would eliminate an interaction between FIX and the fibre. As expected, FX improved entry very effectively (~11-fold increase, p=0.0004), and again this FX-mediated infectivity enhancement was ablated in the presence of heparin (p=0.0004). In agreement with results obtained for Ad5-EGFP$_{WT}$, heparin alone also inhibited Ad5-EGFP$_{A20}$ infection of these cells (p=0.018). Unexpectedly, the Ad5-477*dl*TAYT$_{A20}$ virus alone infected ~30% of the CHO-K1 cells. No significant infectivity enhancement was observed upon co-incubation of this virus with physiological concentrations of FIX (p=0.052), which was consistent with previously published data for this mutant, which is mutated for binding to FIX and C4BP (Shayakhmetov *et al*., 2005). FX significantly enhanced the infectivity of Ad5-477*dl*TAYT$_{A20}$ (~2-fold, p<0.0001), an effect which was again inhibited by co-incubation with heparin. Interestingly, heparin alone completely inhibited all infection with Ad5-477*dl*TAYT$_{A20}$. This suggested that the Ad5-477*dl*TAYT$_{A20}$ had a greatly enhanced interaction with HSPGs, when compared with the lower level interaction with Ad5-EGFP$_{WT}$ and Ad5-EGFP$_{A20}$. This effect was reproduced in repeat experiments, and in CHO-CAR cells (below, *Fig*.4.14B).

4.3.2 Comparative Infectivity +/- FIX, FX and Heparin on CHO-CAR cells. An identical experiment, to that described above, was carried out using CHO-CAR cells (*Fig*.4.14B). As expected, both Ad5-EGFP$_{WT}$ and Ad5-EGFP$_{A20}$ infected CHO-CAR cells to a high level (~93%), although Ad5-EGFP$_{A20}$ was marginally less efficient at doing so (~86%, p=0.0005). The 2hr incubation with an MOI 10 of both these viruses resulted in infectivity levels which were so high that it was difficult to interpret the effects of FIX or FX-mediated enhancement. However, results mirrored those obtained on CHO-K1 cells (*Fig*.4.14A), demonstrating that FX significantly enhanced the infection of both Ad5-EGFP$_{WT}$ and Ad5-EGFP$_{A20}$ (p=0.019 and p<0.0001, respectively), whereas FIX enhanced only the infection of Ad5-EGFP$_{WT}$ (p=0.004), but not that of Ad5-EGFP$_{A20}$ or Ad5-477*dl*TAYT$_{A20}$ (p=0.057 and p=0.815, respectively). These data, when considered collectively with data obtained in CHO-K1 cells, suggested that these viruses do not interact with FIX *in vitro* to promote enhanced infection.

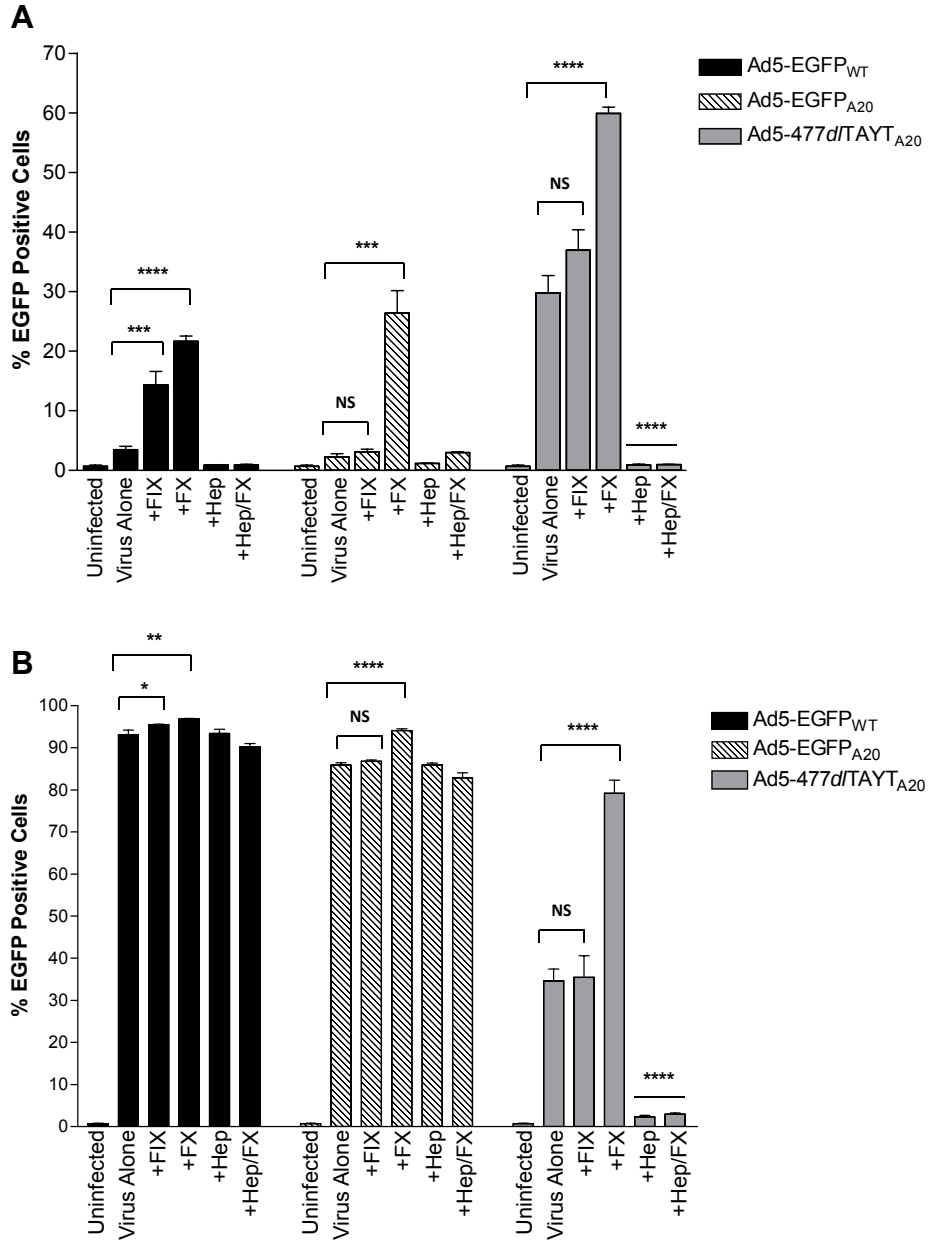

Figure*.4.14 (A) Comparative Infectivity +/- FIX, FX and Heparin on CHO-K1 Cells.** The effect of coagulation factors FIX and FX, on the infectivity of Ad5-EGFP$_{WT}$, Ad5-EGFP$_{A20}$ and Ad5-477*dl*TAYT$_{A20}$, was assessed on CHO-K1 cells. Ad5 interactions with FIX/FX promote entry via engagement with Heparan Sulphate Proteoglycans (HSPGs), therefore porcine heparin was included as an inhibitor for blood factor mediated entry (used at 10µg/ml). Cells were infected for 2hrs at 37˚C with virus alone (MOI 10; PFU/cell), or virus co-incubated with physiological concentrations of blood factors FIX, FX or FX/Heparin. EGFP gene transfer was assessed by flow cytometry (see *Section*.2.8.5). **(B) Comparative Infectivity +/- FIX, FX and Heparin on CHO-CAR Cells.** This experiment was carried out exactly as described above, and in parallel to (A). Data are representative of 2-3 independent repeat experiments, using triplicate samples (*N*=3). The unpaired Student's *t*-test was used to demonstrate the significance of the difference of the mean of each group (indicates a *P*-value of <0.001, **** p<0.0001, NS = not statistically significant, *p*>0.05, bars indicate SD, no bars represent SD values smaller than the symbol used). Statistics displayed above the histogram for Ad5-477*dl*TAYT$_{A20}$ +Hep, and +FX/Hep, in both figures refer to the difference when compared to the corresponding virus+FX sample.

Ad5-477*dl*TAYT$_{A20}$ is a non-CAR binding virus and therefore should not, theoretically, infect CHO-CAR cells. However, as its infectivity profile in CHO-CAR cells was found to be identical to that in CHO-K1 cells, this confirmed that its entry was CAR-independent, and modulated by an alternative receptor, which is expressed on both CHO-K1 and CHO-CAR cells. Results obtained on both cell lines when co-incubating Ad5-477*dl*TAYT$_{A20}$ with heparin confirmed this, demonstrating that this construct efficiently utilises HSPGs as an alternative mode of entry.

4.3.3 Comparative Infectivity +/- FIX, FX and Heparin on Human Carcinoma Lines, BT-20 and TR126. Coagulation factors have been implicated in tumour transduction *in vivo*, in addition to their roles in promoting uptake of Ad5 by the reticuloendothelial system (Coughlan *et al.*, 2009; Gimenez-Alejandre *et al.*, 2008; Koski *et al.*, 2009; Liu *et al.*, 2009; Shashkova *et al.*, 2008). Therefore, it was thought that investigating the effects of FIX and FX on enhancing viral uptake in human carcinoma lines *in vitro* could, potentially, help to predict the success of tumour transduction *in vivo* (personal communication, Dr. Ramon Alemany), particularly if coagulation factors are depleted. The ability of FIX and FX to enhance the infection of human carcinoma cell lines, BT-20 and TR126 was assessed using the same approach as described above.

In BT-20 cells (*Fig*.4.15A), both FIX and FX significantly enhanced the infection of Ad5-EGFP$_{WT}$ (~2.5-fold; p=0.003 and ~4-fold; p=0.0003, respectively) and again, the FX-mediated enhancement through HSPGs was inhibited upon co-incubation of the virus-FX suspension with heparin (p<0.0001). Interestingly, in these cells, neither FIX, nor FX improved the infection of Ad5-EGFP$_{A20}$ or Ad5-477*dl*TAYT$_{A20}$. The inability of FIX to mediate infectivity enhancement of Ad5-EGFP$_{A20}$ (p=0.906), and Ad5-477*dl*TAYT$_{A20}$ (p=0.96) was expected, corroborating results obtained on CHO-K1 and CHO-CAR cells which suggest that the A20-modified viruses do not interact with FIX. However, the lack of enhancement with FX was unexpected. The interaction with FX is modulated through the hexon, and this interaction succeeded in enhancing the infection of both Ad5-EGFP$_{A20}$ and Ad5-477*dl*TAYT$_{A20}$ in previous experiments (*Fig*.4.14A and B). Therefore, the apparent lack of enhancement in BT-20 cells may be due to a saturating effect of the virus, or perhaps as a result of lower level expression of HSPGs (or at least those HSPG forms required for the FX-interaction).

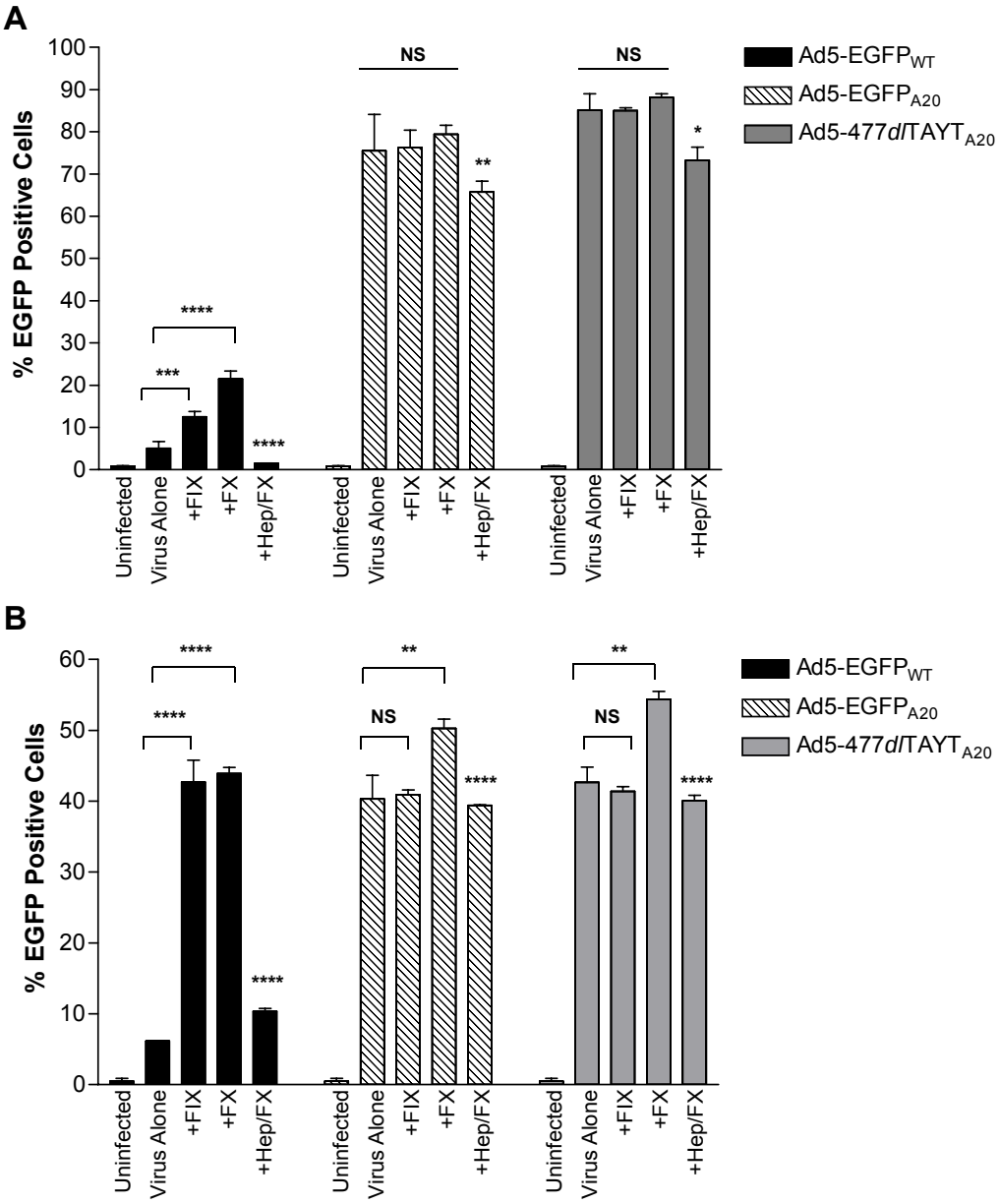

***Figure*.4.15 (A) Comparative Infectivity +/- FIX, FX and Heparin on BT-20 Breast Carcinoma Cells**. The effect of coagulation factors FIX and FX, on the infectivity of Ad5-EGFP$_{WT}$, Ad5-EGFP$_{A20}$ and Ad5-477*d*/TAYT$_{A20}$, was assessed on BT-20 cells. Ad5 interactions with FIX/FX promote entry via engagement with Heparan Sulphate Proteoglycans (HSPGs) therefore porcine heparin was included as an inhibitor for blood factor mediated entry (used at 10µg/ml). Cells were infected for 2hrs at 37˚C with virus alone (MOI 10; PFU/cell), or virus co-incubated with physiological concentrations of blood factors FIX, FX or FX/Heparin. EGFP gene transfer was assessed by flow cytometry (see *Section.*2.8.5). **(B) Comparative Infectivity +/- FIX, FX and Heparin on TR126 HNSCC Cells.** The effect of coagulation factors FIX and FX, on viral infectivity was assessed on TR126 cells. This experiment was carried out exactly as described above. Data are representative of two independent repeat experiments, using triplicate samples (N=3). The unpaired Student's *t*-test was used to demonstrate the significance of the difference of the mean of each group (** indicates a *P*-value of <0.01, *** $p<0.001$, **** $p<0.0001$, NS = not statistically significant, $p>0.05$, bars indicate SD, no bars represent SD values smaller than the symbol used). Statistics displayed above the histogram for +FX/Hep samples refer to the difference when compared to the corresponding virus+FX sample.

In TR126 cells (*Fig*.4.15B), both FIX and FX significantly enhanced the infection of Ad5-EGFP$_{WT}$ (~7-fold increased for both, $p<0.0001$), and FX-mediated enhancement was inhibited with heparin ($p<0.0001$). Consistent with results obtained with CHO-K1, CHO-CAR and BT-20 cells, FIX did not enhance the infection of Ad5-EGFP$_{A20}$ ($p=0.786$). As expected, infection of TR126 cells with Ad5-EGFP$_{A20}$ was enhanced significantly in the presence of FX ($p=0.008$), and this enhancement was ablated by co-incubation with heparin ($p=0.002$). A similar profile was found with Ad5-477*dl*TAYT$_{A20}$; once again FIX did not augment infectivity ($p=0.384$), but FX enhanced infection significantly ($p=0.001$), an effect which was reversed in the presence of heparin ($p=0.0013$).

4.3.4 Comparative Infectivity +/- FIX, FX and Heparin on -β6 Expressing DX3-β6 Cells. As an *in vivo* DX3-β6 xenograft model had already been established in the Tumour Biology Laboratory, we decided to investigate the ability of coagulation factors, FIX and FX, to enhance the infectivity of Ad5-EGFP$_{WT}$, Ad5-EGFP$_{A20}$ and Ad5-477*dl*TAYT$_{A20}$ in these -β6 transfected cells (*Fig*.4.16A and B). At an MOI 10, FIX enhanced the infectivity of Ad5-EGFP$_{WT}$ ($p=0.011$), but had no significant effect on the infectivity of Ad5-EGFP$_{A20}$ or Ad5-477*dl*TAYT$_{A20}$ ($p=0.686$ and $p=0.457$, respectively). FX augmented Ad5-EGFP$_{WT}$ infectivity approximately 20-fold ($p<0.0001$), and also enhanced the entry of Ad5-EGFP$_{A20}$ and Ad5-477*dl*TAYT$_{A20}$, although the effect was not clearly visible due to high level transduction at MOI 10 ($p=0.008$ and $p=0.018$, respectively). FX-induced Ad5-EGFP$_{WT}$ enhancement was completely ablated upon co-incubation with heparin; however inhibition of HSPGs did not completely ablate infection with Ad5-EGFP$_{A20}$ and Ad5-477*dl*TAYT$_{A20}$ which were capable of high efficiency entry through αvβ6 integrin.

This experiment was repeated using an MOI of 1.0, and similar effects were observed (*Fig*.4.16B). However, at this low concentration of virus FIX did not enhance the infectivity of Ad5-EGFP$_{WT}$, Ad5-EGFP$_{A20}$ or Ad-477*dl*TAYT$_{A20}$. Consistent with data obtained previously, FX enhanced the infection of Ad5-EGFP$_{WT}$, Ad5-EGFP$_{A20}$ and Ad5-477*dl*TAYT$_{A20}$ significantly ($p<0.0001$, $p=0.0005$ and $p=0.0008$), and again heparin reversed this effect ($p<0.0001$, for all). Heparin did not impair the transduction of A20-modified viruses, Ad5-EGFP$_{A20}$ and Ad5-477*dl*TAYT$_{A20}$, which maintained high level transduction through alternative receptor, αvβ6.

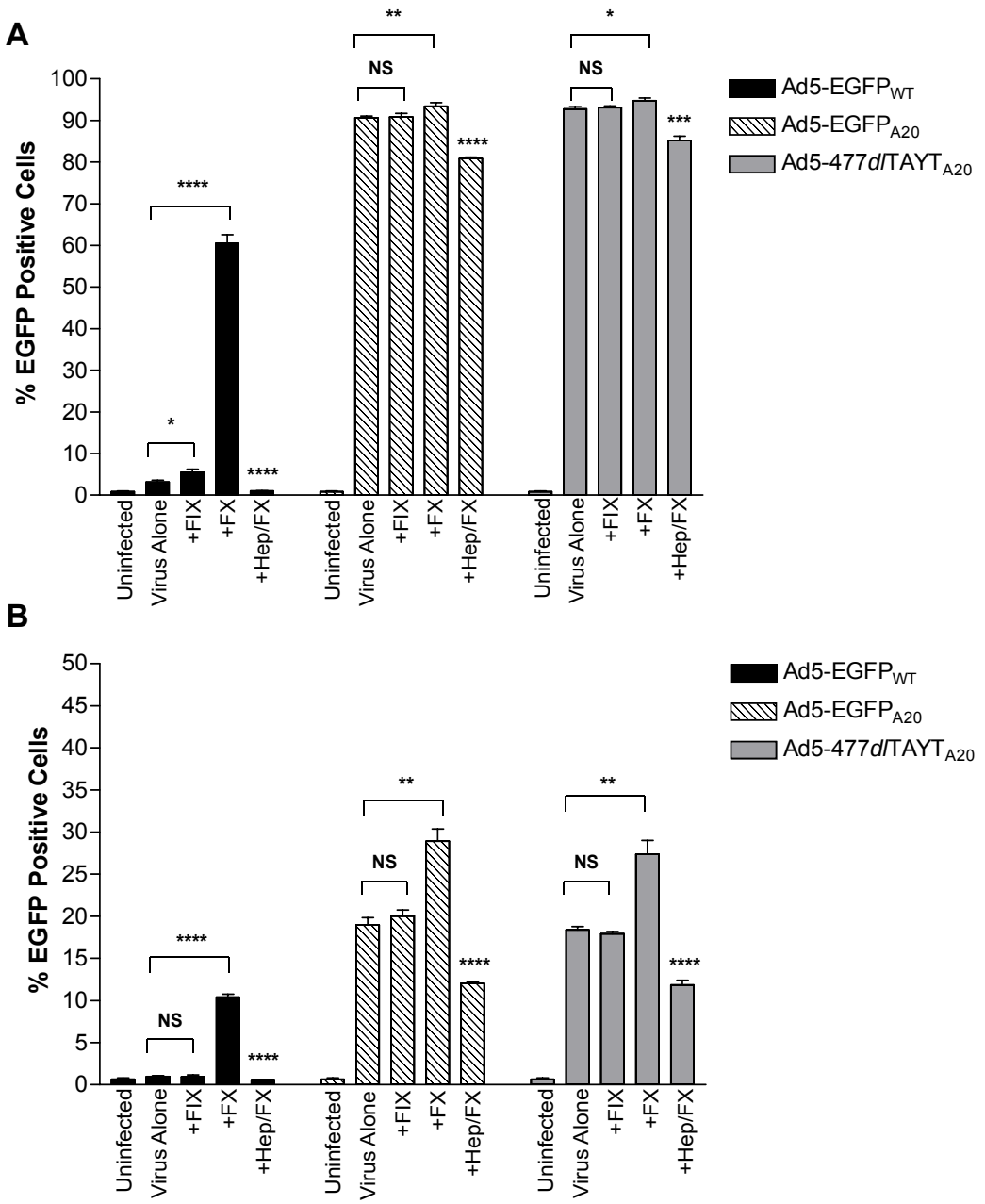

Figure.*4.16 (A) Comparative Infectivity +/- FIX, FX and Heparin on DX3-β6 Transfected Cell Line (MOI 10).** The effect of coagulation factors FIX and FX, on the infectivity of Ad5-EGFP$_{WT}$, Ad5-EGFP$_{A20}$ and Ad5-477*dl*TAYT$_{A20}$, was assessed on DX3-β6 cells. Ad5 interactions with FIX/FX promote entry via engagement with Heparan Sulphate Proteoglycans (HSPGs) therefore porcine heparin was included as an inhibitor for blood factor mediated entry (used at 10µg/ml). Cells were infected for 2hrs at 37˚C with virus alone (MOI 10; PFU/cell), or virus co-incubated with physiological concentrations of blood factors FIX, FX or FX/Heparin. EGFP gene transfer was assessed by flow cytometry (see *Section*.2.8.5). **(B) Comparative Infectivity +/- FIX, FX and Heparin on DX3-β6 Transfected Cell Line (MOI 1).** This experiment was carried out exactly as described above, however cells were infected with a lower MOI (1). Data are representative of two independent repeat experiments, using triplicate samples (*N*=3). The unpaired Student's *t*-test was used to demonstrate the significance of the difference of the mean of each group (* indicates a *P*-value of <0.05, ** *p*<0.01, *** *p*<0.001, * *p*<0.0001, NS = not statistically significant, *p*>0.05, bars indicate SD, no bars represent SD values smaller than the symbol used). Statistics displayed above the histogram for +FX/Hep samples refer to the difference when compared to the corresponding virus+FX sample.

*Chapter.*4 Discussion

In this chapter, we have shown *in vitro* that Ad5-477*dl*TAYT$_{A20}$, a CAR- and blood factor binding ablated Ad5 vector retargeted to αvβ6, retains its high efficiency interaction with its target in a manner comparable to the parental vector, Ad5-EGFP$_{A20}$. We have also verified that the native CAR receptor binding capacity of this virus is ablated, as is its ability to interact with FIX to promote infectivity enhancement through HSPGs. Furthermore, we have observed that the combination of the various introduced mutations (477*dl*TAYT$_{A20}$) in this virus have conferred an unexpected affinity for HSPGs, in excess of the basal level often observed with Ad5-EGFP$_{WT}$. This may have implications for the *in vivo* characteristics of this virus. Additionally, and again unexpectedly, we have verified that the Ad5-EGFP$_{A20}$ vector fails to interact with FIX in promoting infectivity enhancement, an effect presumably mediated indirectly by the insertion of the A20FMDV2 peptide in the HI loop of the fibre knob.

*Section.*4.1 *In Vitro* Characterisation of ΔCAR/FIX-Binding Knob$_{A20}$ Mutants

The recombinant knob proteins generated in this study proved very useful in characterising the functional effects of the various mutations introduced, prior to contemplating their incorporation into the Ad5-EGFP$_{A20}$ background by homologous recombination. Mutant Knob proteins which featured CAR-binding ablation mutations Y477A, or L485K, were generated early in these studies, when the initial objectives were to generate a CAR-binding ablated, A20-retargeted Ad5 vector. In time, increasing evidence reported in the literature highlighted the redundancy of CAR in the hepatotropism and biodistribution of Ad5 (Alemany & Curiel, 2001; Leissner *et al.*, 2001; Martin *et al.*, 2003; Mizuguchi *et al.*, 2002; Nicol *et al.*, 2004; Smith *et al.*, 2002), and emphasised the importance of various blood components in governing successful targeting *in vivo* (Kalyuzhniy *et al.*, 2008; Lyons *et al.*, 2006; Parker *et al.*, 2006; Shayakhmetov *et al.*, 2005b; Vigant *et al.*, 2008; Waddington *et al.*, 2008). Therefore, the focus of the project shifted to the generation of a vector which was retargeted to αvβ6, while simultaneously detargeted from CAR, and coagulation factor binding.

The Y477A and L485K, CAR-binding mutant pQE plasmids had been constructed early in this study but, only KnobL485K$_{WT}$ was produced as recombinant knob protein. However, both plasmids were subsequently used as templates for the construction and generation of Knob477*dl*TAYT$_{A20}$ and Knob485*dl*TAYT$_{A20}$, and their corresponding WT controls. The ability of the A20-modified Knob proteins to form homotrimers was

confirmed to ensure that the introduced mutations were compatible with fibre assembly, which is critical for the formation of a functional Ad5 particle (Hong & Engler, 1996; Novelli & Boulanger, 1991). These constructs were further validated to demonstrate that they retained the high efficiency binding and functional inhibition of αvβ6 observed with $Knob_{A20}$ in earlier experiments (see *Fig*.3.8, *Fig*.3.9 and *Fig*.3.10) and, finally, the relative success of each CAR-binding mutation was assessed for each mutant.

Both Knob477*dl*$TAYT_{A20}$ and Knob485*dl*$TAYT_{A20}$ retained their affinity for binding to αvβ6, in a manner comparable to $Knob_{A20}$ (*Fig*.4.8A and B). In a flow cytometry based competition experiment, using an anti-αvβ6 antibody (53A.2) the IC_{50} values obtained for each protein were found to be identical to the value calculated for $Knob_{A20}$ (IC_{50}=0.03μg/10^5 cells) in a previous experiment (see *Fig*.3.8). Furthermore, both mutant proteins also completely abrogated αvβ6-dependent VB6 cell migration towards LAP, at concentrations equivalent to $Knob_{A20}$ (≤10μg/ml, *Fig*.4.10). Collectively, these data confirmed that the incorporation of the 477/485*dl*TAYT set of mutations had negligible effects on the function of the A20FMDV2 peptide within the structural confines of the Ad5 fibre knob domain.

Next, we wished to validate the success of the CAR/*dl*TAYT mutations in ablating native Ad5 receptor binding (*Fig*.4.11A). The use of recombinant Knob or fibre to inhibit the infection of the virus from which it was derived, is a well established assay (Freimuth *et al.*, 1999; Santis *et al.*, 1999). Competition experiments with Ad5-$EGFP_{WT}$, and each mutant Knob protein were carried out on CHO-CAR cells (generously provided by Dr. George Santis). Parental CHO cells are sufficiently refractory to human adenovirus infection, such that transfection of the CAR receptor facilitates Ad5 infection in a CAR-dependent manner. Thus, in principle, Knob proteins which retained CAR-binding would inhibit Ad5-$EGFP_{WT}$ infection, and those which featured successfully ablated CAR-binding determinants, would be unable to do so.

As expected, CAR-binding intact proteins, $Knob_{WT}$ and $Knob_{A20}$, inhibited >95% of the infection with Ad5-$EGFP_{WT}$ (p<0.0001). With the exception of $KnobL485K_{A20}$ and Knob477*dl*$TAYT_{A20}$, all CAR-binding mutant Knob proteins failed to significantly inhibit Ad5-$EGFP_{WT}$ infection (MOI 10), even at the high concentration of Knob protein used (100μg/10^5 cells), which was ~1000-fold higher than the calculated IC_{50} for $Knob_{WT}$ mediated inhibition of native Ad5 infection (Kirby *et al*., 2000). Knob477*dl*$TAYT_{A20}$ marginally reduced Ad5-$EGFP_{WT}$ infection, although this reduction was statistically significant (p=0.02). This result was unexpected, especially as the corresponding WT control, Knob477*dl*$TAYT_{WT}$ completely failed to inhibit infection with Ad5-$EGFP_{WT}$.

However, this effect was possibly explained by results obtained in later experiments with the Ad5-477*dl*TAYT$_{A20}$ virus construct (see *Fig*.4.14A and B) in which we confirmed, through inhibition with heparin, that this virus has some affinity for HSPGs, found on the surface of both CHO-K1, and CHO-CAR cells. Therefore, it is plausible that the high concentration of Knob477*dl*TAYT$_{A20}$ (100µg/10^5 cells) used in this experiment may have promoted binding of this protein to HSPGs, perhaps creating a steric hindrance to subsequent binding of Ad5-EGFP$_{WT}$, or potentially inhibiting the portion of Ad5-EGFP$_{WT}$ infection which is mediated through HSPGs.

Section.4.2 *In Vitro* Characterisation of ΔCAR/FIX-Binding Ad5-EGFP$_{A20}$ Mutants; Infectivity and Cytotoxicity

In recent years, the importance of removing the CAR-binding capacity of Ad5 vectors lost its critical appeal. This was due, in part, to various conflicting reports regarding the role of CAR in liver transduction (Einfeld *et al.*, 2001; Leissner *et al.*, 2001; Martin *et al.*, 2003; Smith *et al.*, 2002; Smith *et al.*, 2003a), in addition to the lack of altered biodistribution *in vivo* following administration of CAR-binding ablated mutant Ads (Alemany & Curiel, 2001). However, CAR detargeting has once again become an important consideration when designing vectors for clinical applications, as new evidence has shown that human, but not murine erythrocytes express CAR on their surface (Carlisle *et al.*, 2009; Seiradake *et al.*, 2009). This has highlighted yet another challenge to achieving successful tumour targeting *in vivo*, as it has been shown that Ad5-based vectors can be sequestered by erythrocytes in the circulation, failing to reach their target tissue (Carlisle *et al.*, 2009).

Ad5 binding to CAR represents the initial event in cell attachment *in vitro* (Bergelson *et al*., 1998; Kirby *et al*., 2000). However, through the incorporation of targeting ligands at various sites on the capsid, this dependence on CAR can be circumvented, rendering CAR-binding dispensable. Therefore, the relative efficiency of Ad5-477*dl*TAYT$_{A20}$, in promoting high efficiency infection through αvβ6, was compared with that of Ad5-EGFP$_{A20}$ and Ad5-EGFP$_{WT}$ (*Fig*.4.12). In the previous chapter, using a panel of αvβ6-expressing human carcinoma lines, we demonstrated that the entry of Ad5-EGFP$_{A20}$ was superior to that of Ad5-EGFP$_{WT}$, and was dependent on the inclusion of the A20FMDV2 peptide in the HI loop of the fibre (see *Fig*.3.13 and *Fig*.3.15). However, we wanted to absolutely confirm that the introduction of the 477*dl*TAYT set of mutations did not detrimentally affect this interaction with αvβ6. This concern was unfounded, as Ad5-477*dl*TAYT$_{A20}$ successfully mediated infection in a manner almost identical to the

unmodified, CAR-binding intact virus Ad5-EGFP$_{A20}$, retaining superior transduction levels over Ad5-EGFP$_{WT}$.

We also compared the relative cytotoxicity of Ad5-477*dl*TAYT$_{A20}$, and in some cases Ad5-485*dl*TAYT$_{A20}$, with Ad5-EGFP$_{A20}$ and Ad5-EGFP$_{WT}$ (*Fig*.4.13). Overall, the ablation of CAR binding did not appear to impair the ability of Ad5-477*dl*TAYT$_{A20}$ or Ad5-485*dl*TAYT$_{A20}$ to exert cytotoxic effects on the cells investigated. In fact, cytotoxicity was substantially improved when compared with Ad5-EGFP$_{WT}$, and was generally comparable to Ad5-EGFP$_{A20}$. As expected, Ad5-485*dl*TAYT$_{A20}$ performed less efficiently in A549 cells. However, the EC_{50} value obtained for Ad5-477*dl*TAYT$_{A20}$ in A549 cells (0.4 PFU/cell) indicated that these cells were still relatively sensitive to infection with Ad5-477*dl*TAYT$_{A20}$, despite the lack of known receptors for this virus (αvβ6 or αvβ8), and its inability to utilise CAR for attachment. A possible explanation for this can be that entry, and/or intracellular spread, was compensated by its ability to use HSPG as an alternative attachment receptor (see *Fig*.4.14A).

Expression of the CAR receptor is restricted to the tight junctions, where it acts as a cell-adhesion molecule, forming trans-epithelial homodimeric complexes (Cohen *et al.*, 2001; Farmer *et al.*, 2009; Honda *et al.*, 2000; Ito *et al.*, 2000). Recently, Ad5 interactions with CAR have been shown to promote the homodimerisation of the molecule in addition to inducing the activation of -β1 and β3 integrin subunits, through the activation of the p44/42 MAPK signal transduction pathway (Farmer *et al.*, 2009). This may represent a strategy on the part of the virus to enhance its own infection. Interestingly, an alternative function for fibre binding to CAR has been described; in which excess fibre produced by Ad5 competitively inhibits CAR homodimer formation, thus disrupting tight junction integrity and permitting efficient intracellular spread and viral escape (Walters *et al.*, 2002). Therefore, it is important to consider that CAR-binding ablated viruses may be impaired in their ability to spread via paracellular spaces. However, intra-epithelial barriers are often dysregulated in the context of human epithelial cancers, and therefore the aforementioned function of the fibre-CAR interactions may be redundant in tumour cells (Dhawan *et al.*, 2005; Hoover *et al.*, 1998). Indeed, in support of this we did not observe significant loss of cytotoxic efficacy with the CAR-binding ablated constructs, at least in the cell lines tested.

*Section.*4.3 *In Vitro* Characterisation of ΔCAR/FIX-Binding Ad5-EGFP$_{A20}$ Mutants; Interactions with Coagulation Factors

An Ad5 interaction with vitamin K-dependent coagulation factors now has been shown to be critical in directing hepatocyte transduction *in vivo* (Alba *et al.*, 2009; Kalyuzhniy *et al.*, 2008; Parker *et al.*, 2006; Shayakhmetov *et al.*, 2005b; Vigant *et al.*, 2008; Waddington *et al.*, 2008). Additionally, coagulation factors have been shown to enhance the infection of human carcinoma lines *in vitro* and have been also implicated in tumour transduction *in vivo* (Coughlan *et al*., 2009, Liu *et al*., 2009, Gimenez-Alejandre *et al*., 2008, Shaskova *et al*., 2008, Shayakhmetov *et al*., 2005). However, this remains controversial. Depletion of vitamin-K dependent coagulation factors using warfarin has been reported to reduce viral uptake in the tumour following systemic delivery (Coughlan *et al.*, 2009; Gimenez-Alejandre *et al.*, 2008) whereas in contrast, it has also been reported that warfarin pre-treatment can enhance Ad5-mediated, anti-tumoural efficacy (Shashkova *et al.*, 2008). In addition, selective depletion of FX alone using X-bp (Factor X-binding protein) has been shown to improve tumour transduction with an Ad5/35 vector, presumably through its increased bioavailability as a direct result of the liver avoidance strategy employed (Liu *et al.*, 2009). Taken as a whole, it is clear that the precise mechanisms which govern efficient tumour transduction with Ad5 *in vivo* currently are not well characterised, and thus warrant further investigation.

Prior to experiments where we assessed the tumour targeting efficiency of Ad5-EGFP$_{WT}$, Ad5-EGFP$_{A20}$ and Ad5-477*dl*TAYT$_{A20}$ following systemic delivery, we wanted to characterise the differential interactions of these constructs with coagulation factors FIX, and FX. For initial proof of principle studies we chose to use CHO-K1 cells, as they not readily infectable with Ad5 but express HSPGs, and therefore are most suitable for investigating coagulation factor dependent enhancement of infection. Studies on these and other cells (CHO-CAR, BT-20, TR126 and DX3-β6) yielded some interesting, and unexpected results. In all lines tested, except BT-20, FX successfully enhanced the infectivity of Ad5-EGFP$_{WT}$, Ad5-EGFP$_{A20}$ and A5-477*dl*TAYT$_{A20}$ (*Fig*.4.14A+B, *Fig*.4.15B and *Fig*.4.16). In BT-20 cells, FX failed to significantly enhance the infection of Ad5-EGFP$_{A20}$ or Ad5-477*dl*TAYT$_{A20}$, and its enhancement of Ad5-EGFP$_{WT}$ infection was not marked, although significant (*Fig*.4.15A). This suggested that these cells express low levels of HSPGs, or at least those variants required for the FX interaction. However, it is possible that other factors are involved, as the exact mechanisms which facilitate Ad5:FX:HSPG-mediated entry to cells, both *in vitro* and *in vivo*, have not been identified.

FIX enhanced the infectivity of Ad5-EGFP$_{WT}$ in all cell lines tested (except DX3-β6 cells infected at MOI 1.0, see *Fig*.4.16B). Interestingly however, FIX consistently failed to enhance the infection of Ad5-EGFP$_{A20}$ and Ad5-477*dl*TAYT$_{A20}$ in all cell lines investigated (*Fig*.4.14A+B, *Fig*.4.15A+B and *Fig*.4.16A+B). This finding was anticipated for Ad5-477*dl*TAYT$_{A20}$, a viral mutant which features a range of mutations designed to abrogate FIX binding. However, the apparent inability of FIX to interact with unmodified Ad5-EGFP$_{A20}$ was unexpected. The A20FMDV2 insertion within the HI loop is in close proximity to the putative blood factor binding molecular determinants (477*dl*TAYT) described by Shayakhmetov and colleagues (Shayakhmetov *et al.*, 2005b). Therefore it is plausible that the A20FMDV2 modification has conferred a structural or steric hindrance which precludes FIX binding, even in the absence of the specific mutations.

Another unexpected finding was that Ad5-477*dl*TAYT$_{A20}$ appeared to have acquired an affinity for HSPGs, effectively utilising them as an alternative receptor for attachment/entry. HSPG receptors are known to bind to stretches of charged lysine (K) or arginine (R) residues (Fromm *et al.*, 1995). However, analysis of the amino acid sequence of the knob domain of both Ad5-EGFP$_{A20}$ and Ad5-477*dl*TAYT$_{A20}$ did not reveal any differences in their lysine/arginine content, both having 12 and 5 residues, respectively (see *Appendix II*). Therefore, it seems likely that the 477*dl*TAYT set of g (E1A) of Frozen Liver Tissue Following Systemic Delivery of Virus e). Immediately post-necropsy, liver tissue (left lobe) was frozen at -80˚C in OCT-ng cryomolds. Frozen tissue sectionfectivity enhancement of tumour cells *in vitro* (Gimenez-Alejandre *et al.*, 2008; Liu *et al.*, 2009; Shayakhmetov *et al.*, 2005b), and interestingly, dysregulation of HSPGs have been described in various pathophysiological conditions, including cancer (Blackhall *et al.*, 2001). Therefore, it will be important to ascertain if, and to what extent, HSPGs facilitate coagulation factor dependent tumour uptake *in vivo*, and whether the ability of the Ad5-477*dl*TAYT$_{A20}$ vector to utilise HSPGs for entry, will compete with, or complement, this pathway.

The ability of the Ad5-EGFP$_{A20}$ and Ad5-477*dl*TAYT$_{A20}$ viruses alone to achieve infection levels equivalent to, or superseding that of Ad5-EGFP$_{WT}$ +FX in the tumour cell lines tested, suggested that these viruses may overcome the dependency on FX for high efficiency targeting *in vivo*, when delivered intravenously. Therefore, an *in vivo* targeting experiment was designed in which vitamin K-dependent coagulation factors would be depleted, using a previously described warfarin pre-treatment regime (see *Chapter.*6).

CHAPTER.5 Results

Chapter.5 *In Vivo* Assessment of Vector-Induced Toxicity in Immunocompetent Mouse Models

Kupffer cells (KCs), the resident macrophages of the liver, are largely responsible for the rapid clearance of systemically delivered Ad5-based vectors from the circulation in mice (Lieber *et al.*, 1997; Worgall *et al.*, 1997). Depletion, or saturation of KCs, with high doses of Ad5, permits efficient hepatocyte transduction (Kuzmin *et al.*, 1997; Liu *et al.*, 2003; Schiedner *et al.*, 2003b; Tao *et al.*, 2001; Wolff *et al.*, 1997), through a FX-hexon dependent interaction (Alba *et al.*, 2009; Kalyuzhniy *et al.*, 2008; Vigant *et al.*, 2008; Waddington *et al.*, 2008). Haemodynamic responses to Ad5 are causatively associated with the activation of hepatic endothelial cells by Ad-stimulated KCs (Schiedner *et al.*, 2003a). Additionally, interactions between Ad5 and platelets, cause acute thrombocytopenia and can contribute to the development of coagulopathic conditions (Othman *et al.*, 2007; Stone *et al.*, 2007b). These co-ordinate interactions contribute to the extensive hepatocellular damage, and these many of these effects can be attributed to the induction of potent anti-viral innate immune responses. Consequently, these various interactions pose a major challenge to the clinical utility of Ad5.

An Ad5 mutant, featuring a set of mutations (Y477A-*dl*TAYT) to inhibit binding of FIX and C4BP to the fibre knob, has previously been described (Shayakhmetov *et al.*, 2005b). This vector displayed reduced co-localisation with KCs, in addition to significantly reduced hepatotoxicity (ALT) and cytokine (IL-6, IFN-γ) induction *in vivo.* In this study, we incorporated this set of mutations into the Ad5-EGFP$_{A20}$ genetic background to generate Ad5-477*dl*TAYT$_{A20}$. Therefore, we wanted to compare the *in vivo* biodistribution, toxicity and haematological profiles of Ad5-477*dl*TAYT$_{A20}$, Ad5-EGFP$_{WT}$ and Ad5-EGFP$_{A20}$ using different doses (2.5 and 4.0x10^{10}vp/mouse), and different time-points post-infection (6 days, 4 days and 24hrs). Additionally, selected chemokine and cytokine profiles were obtained 6hrs and 24hrs post-infection with 4.0x 10^{10}vp/mouse (see *Section*.2.1.7).

Section.5.1 Dose Escalation Hepatotoxicity Studies in Balb/c Immunocompetent Mice

All animal experiments were carried out at the facility of the Institut d'Investigació Biomèdica de Bellvitge, at the Institut Català d'Oncologia (ICO) in accordance with the regulations of the IDIBELL Ethical Committee for Animal Experimentation. Intravenous administration of virus was performed by Blanca Luena (technical staff). Necropsies were assisted by Dr. Manel Cascalló, Alena Gros, Francisca Alcayaga and Juan José Rojas. Blood samples were obtained immediately post-mortem by intra-cardiac puncture (performed by Francisca Alcayaga and Alena Gros). Quantification of AST/ALT from heparinised plasma and analysis of haematological profiles were carried out by the Clinical Veterinary Biochemistry Service at the Facultat de Veterinària, Universitat Autònoma de Barcelona.

5.1.1 Determination of *In Vivo* Hepatotoxicity and Haematological Profiling (2.5 x 10^{10}vp/mouse). In order to assess comparatively the toxicity induced by Ad5-EGFP$_{WT}$, Ad5-EGFP$_{A20}$ and Ad5-477*dl*TAYT$_{A20}$, immunocompetent Balb/c female mice (6 weeks) were administered intravenously with 2.5x10^{10}vp/mouse. A control vector, Ad5-477*dl*TAYT$_{6XHIS}$ was generated successfully by homologous recombination, but was not amplified, or purified prior to these experiments, due to time constraints. Animals were killed 6 days post-infection, a blood sample obtained by intracardiac puncture immediately post-mortem. Haematological profiles were obtained from whole blood samples and liver transaminase (ALT/AST) levels quantified from heparinised plasma.

Significant loss of body weight can be an indirect indicator of virus-induced toxicity (Cascallo *et al.*, 2007; Duncan *et al.*, 1978). Therefore, body weight variations (%) were assessed for each cohort at various time-points post-infection (*Fig*.5.1A). On day 1 post-virus administration, there was no difference in the percentage weight change of any of the viral groups when compared to the PBS control (p=0.073, p=0.46 and p=0.146 for Ad5-EGFP$_{WT}$, Ad5-EGFP$_{A20}$ and Ad5-477*dl*TAYT$_{A20}$, respectively). However, the Ad5-EGFP$_{WT}$ group (-3.4±3.1%) did differ significantly from the Ad5-EGFP$_{A20}$ (p=0.043), and Ad5-477*dl*TAYT$_{A20}$ (p=0.019) groups, both of which showed overall increases in body weight of +0.5±1.9 and +1.23±1.68%, respectively. On day 4, only the Ad5477*dl*TAYT$_{A20}$ treated group differed significantly from the PBS control (+3.86±1.7%, p=0.022), or from the Ad5-EGFP$_{WT}$ treated group (p=0.073). On day 5, both the Ad5-EGFP$_{A20}$ and Ad5-477dlTAYT$_{A20}$ groups had increased body weights (+3.6±1.5% and +5.72±1.98%), and these groups differed from both the PBS control group (p=0.035 and p=0.007) and the Ad5-EGFP$_{WT}$ group (p=0.032 and p=0.006). At the time of euthanasia (day 6), again only the Ad5-477*dl*TAYT$_{A20}$ group differed significantly from the PBS, or Ad5-EGFP$_{WT}$ groups (p=0.005 and p=0.012,

respectively), with an overall gain in body weight of +5.49±1.71%, compared with -1.2±3.5% and +0.40±3.1% for PBS and Ad5-EGFP$_{WT}$ respectively.

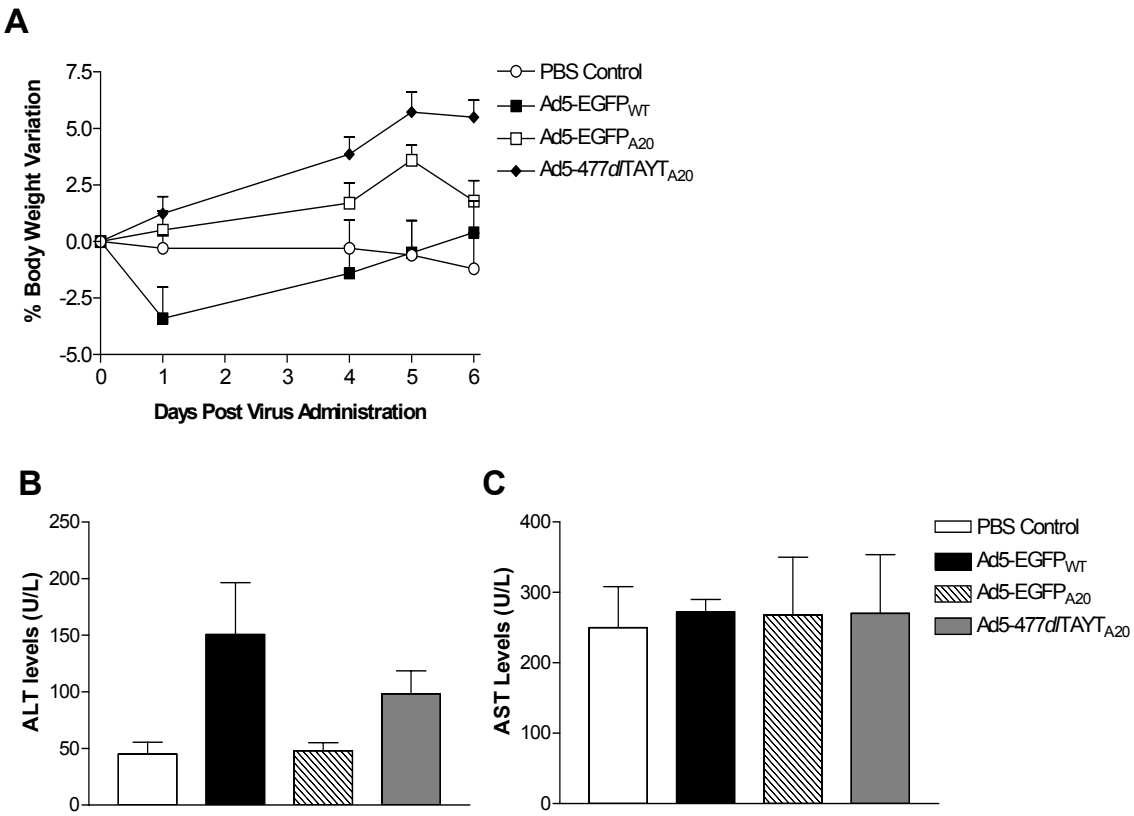

***Figure.*5.1 Determination of Toxicity in Immunocompetent Balb/c Mice Following Systemic Administration of Virus (2.5x10^{10}vp/mouse). (A)** Body weight variation (%) was assessed on a daily basis for cohorts which received intravenous delivery of PBS, Ad5-EGFP$_{WT}$, Ad5-EGFP$_{A20}$ or Ad5-477*d*/TAYT$_{A20}$ (2.5x10^{10}vp/mouse). **(B)** Blood samples were obtained immediately post-mortem by intracardiac puncture (6 days after virus administration) and alanine transaminase (ALT) levels were quantified for each group; PBS, Ad5-EGFP$_{WT}$, Ad5-EGFP$_{A20}$ or Ad5-477*d*/TAYT$_{A20}$. **(C)** Aspartate aminotransferase (AST) levels were also quantified for all groups. Data presented show the mean ± SEM (*N*=5 female mice). Statistical significance was determined using the unpaired Student's *t*-test comparing the means of two samples (differences which were not found to be significant had a *P*-value >0.05; *not marked*, bars indicate SEM).

Transaminase levels were quantified for each cohort (*Fig*.5.1B+C). The Ad5-EGFP$_{WT}$ group had ALT levels which were elevated slightly over baseline, when compared to the Ad5-EGFP$_{A20}$ and Ad5-477*d*/TAYT$_{A20}$ groups, although the differences observed were not significant (p>0.05). This was further supported by the fact that AST levels did not differ significantly for each of the virus groups, nor did the levels differ from those obtained for the PBS control group (p>0.05 for all).

A full haematological profile was obtained for each of the cohorts; including PBS control, Ad5-EGFP$_{WT}$, Ad5-EGFP$_{A20}$ and Ad5-477*dl*TAYT$_{A20}$ groups (*Fig*.5.2). At this dose (2.5x10^{10}vp/mouse) and time-point (day 6), no differences in total lymphocyte numbers were observed for any cohort (p>0.05 for all). Both Ad5-EGFP$_{WT}$ and Ad5-477*dl*TAYT$_{A20}$ showed ~2.5-fold increased neutrophil counts versus PBS control (p=0.004 and p=0.027, respectively). In contrast, total neutrophils remained at a basal level (equivalent to PBS) in cohorts which had been infected with Ad5-EGFP$_{A20}$ (p=0.134). Platelet levels frequently are affected by systemically administered adenovirus, which can induce acute transient thrombocytopenia (Cichon *et al.*, 1999; Othman *et al.*, 2007; Stone *et al.*, 2007b; Wolins *et al.*, 2003). However, no changes to overall platelet levels were observed (p>0.05 for all). In addition, total monocyte levels were not affected significantly, except for the Ad5-477*dl*TAYT$_{A20}$ group, which was increased ~1.5-fold above basal level (p=0.017). There were no significant changes to either total basophil, or eosinophil populations for any group (p>0.05 for all).

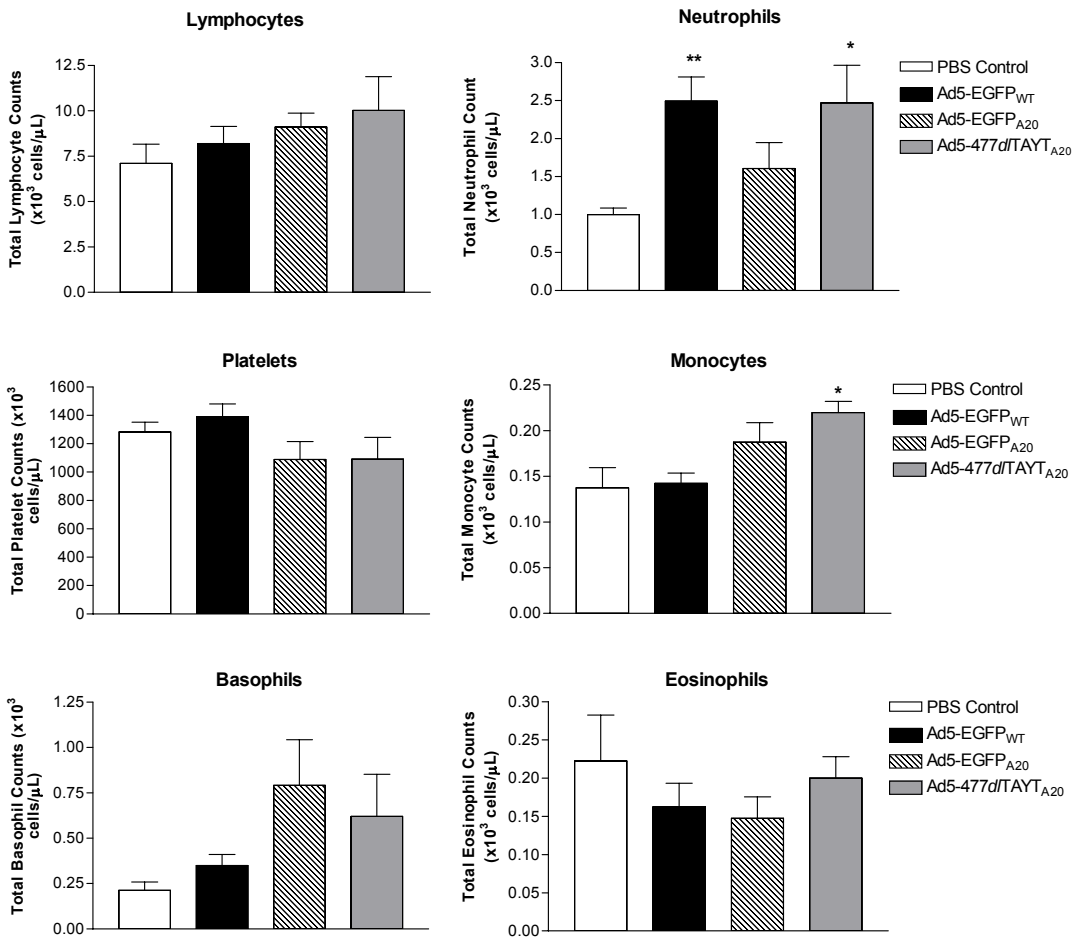

***Figure*.5.2 Haematological Profiles Obtained from Immunocompetent Balb/c Mice Following Systemic Delivery of Virus (2.5x10^{10}vp/mouse**). Whole blood samples (250µl) from each of the treated groups (PBS, Ad5-EGFP$_{WT}$, Ad5-EGFP$_{A20}$ and Ad5-477*dl*TAYT$_{A20}$) were obtained immediately post-mortem by intracardiac puncture (day 6 post-infection). Haematological profiles were assessed at the Clinical Veterinary Biochemistry Service at the Falcultat de Veterinària, Universitat Autònoma de Barcelona. Data presented show the mean ± SEM (N=5 female mice). Statistical significance was determined using the unpaired Student's t-test comparing the means of each group to that of the PBS control group (* indicates a P-value of <0.05, ** p<0.01, differences which were not found to be significant

5.1.2. Determination of *In Vivo* Hepatotoxicity and Haematological Profiling ($4x10^{10}$vp/mouse). A dose of $2.5x10^{10}$vp/mouse did not induce significant toxicity in any cohort, so therefore a higher dose of $4x10^{10}$vp/mouse was used, in a separate experiment, in order to obtain comparative toxicological and haematological profiles for Ad5-EGFP$_{WT}$, Ad5-EGFP$_{A20}$ and Ad5-477*dl*TAYT$_{A20}$. On day 3 post-virus administration, the weight of the Ad5-EGFP$_{WT}$ group (-4.5±1.2%) varied significantly from the PBS control (p=0.0007), which showed increases in overall body weight +3.7±3.4% (*Fig*.5.3A). The A20-modified groups, Ad5-EGFP$_{A20}$ and Ad5-477*dl*TAYT$_{A20}$ did not differ significantly, both displaying increases in body weight, +2.6±1.3% and +1.23±1.68%, respectively. In addition, both of the A20-modified groups, differed significantly from the Ad5-EGFP$_{WT}$ treated animals (p=0.0002 and p<0.0001, respectively). On the day of euthanasia (day 4), both Ad5-EGFP$_{A20}$ and Ad5-477*dl*TAYT$_{A20}$, had body weights comparable to the PBS control group (p=0.437 and p=0.076), whereas the Ad5-EGFP$_{WT}$ cohort differed significantly having lost 6.0±2.4% of its body weight (p=0.0007).

In agreement with these results, transaminase levels were found to be altered significantly between the Ad5-EGFP$_{WT}$ and A20-retargeted groups (*Fig*.5.3B+C). The Ad5-EGFP$_{WT}$ treated group displayed markedly elevated ALT levels, ~35-fold above basal PBS levels (p<0.0001). In comparison, the elevation of ALT in the Ad5-EGFP$_{A20}$ and Ad5-477*dl*TAYT$_{A20}$ treated groups was much less, increased ~4.5-fold (p=0.027) and ~9-fold (p=0.008), respectively. Accordingly, there were significant differences between the levels of ALT induced by the Ad5-EGFP$_{WT}$ and A20-modified groups (p<0.0001 and p=0.0001). AST levels were also similarly affected by each virus. Ad5-EGFP$_{WT}$ treatment induced high levels of AST, ~15-fold above basal level (p<0.0001). However, neither the Ad5-EGFP$_{A20}$ nor Ad5-477*dl*TAYT$_{A20}$ groups succeeded in elevating AST levels above basal PBS levels (p>0.05 for both).

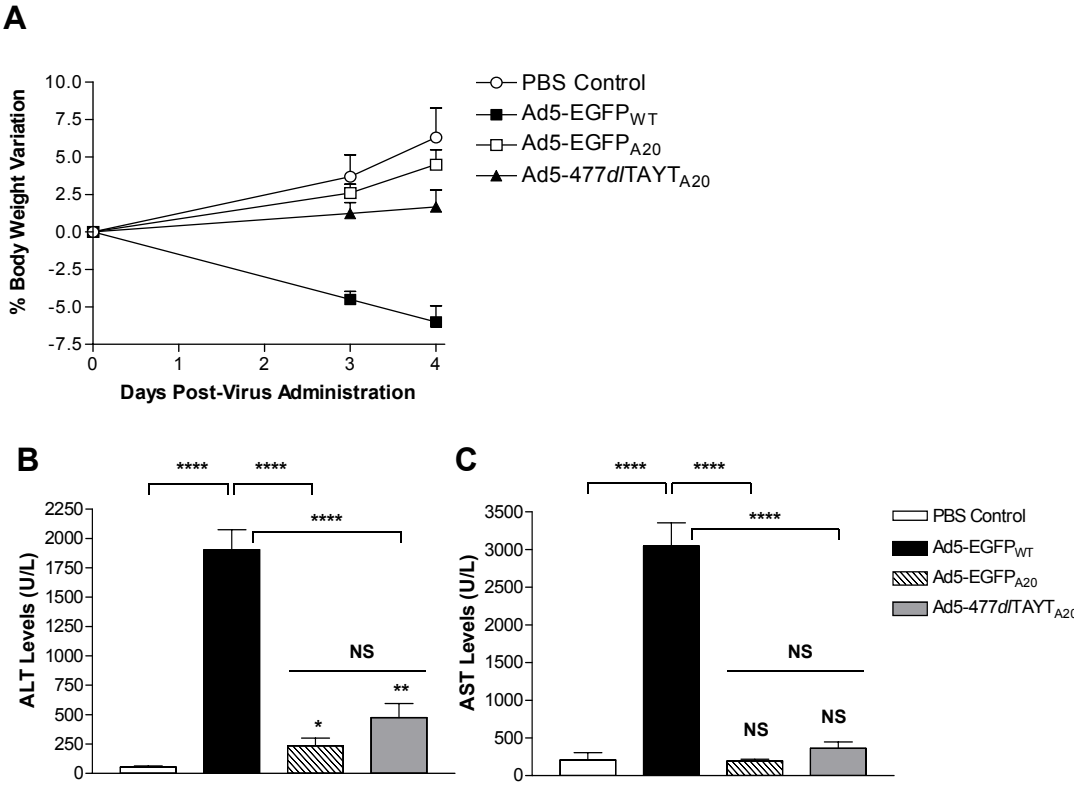

Figure*.5.3 Determination of Toxicity in Immunocompetent Balb/c Mice Following Systemic Administration of Virus (4.0x10^{10}vp/mouse). (A)** Body weight variation (%) was assessed on a daily basis for cohorts which received intravenous delivery of PBS, Ad5-EGFP$_{WT}$, Ad5-EGFP$_{A20}$ or Ad5-477*dl*TAYT$_{A20}$ (2.5x10^{10}vp/mouse). **(B)** Blood samples were obtained immediately post-mortem (4 days after virus administration) and alanine transaminase (ALT) levels were quantified for each group; PBS, Ad5-EGFP$_{WT}$, Ad5-EGFP$_{A20}$ or Ad5-477*dl*TAYT$_{A20}$. **(C)** Aspartate aminotransferase (AST) levels were quantified for all groups; PBS, Ad5-EGFP$_{WT}$, Ad5-EGFP$_{A20}$ or Ad5-477*dl*TAYT$_{A20}$. Data presented show the mean ± SEM (*N*=5 female mice). Statistical significance was determined using the unpaired Student's t-test comparing the means of two samples (* indicates $p<0.0001$, NS indicates $p>0.05$, bars indicate SEM). Statistics displayed directly above the histogram for Ad5-EGFP$_{A20}$/Ad5-477*dl*TAYT$_{A20}$ samples, refer to the difference when compared to the corresponding PBS control sample.

A full haematological profile was obtained for each of the cohorts; PBS control, Ad5-EGFP$_{A20}$ and Ad5-477*dl*TAYT$_{A20}$ (*Fig*.5.4). Unfortunately, only one blood sample was obtained for the Ad5-EGFP$_{WT}$ group, and therefore no statistical analysis can be determined for this group. Furthermore, a large proportion of these blood samples were coagulated prior to analysis. Therefore, the results obtained are not entirely trustworthy, as the basal level cell populations (eg. lymphocytes, monocytes and basophils) are not consistent with results obtained in previous, or subsequent haematological analyses (see *Fig*.5.2 and *Fig*.5.11). At a dose of 4.0x10^{10}vp/mouse, no significant changes in total lymphocyte, neutrophil, platelet or monocyte numbers were observed for any cohort, excluding Ad5-EGFP$_{WT}$ from analysis ($p>0.05$ for all). Total basophil counts were increased in each of the virus treated groups; a ~3-fold, but non-

significant increase in the Ad5-EGFP$_{A20}$ group, and a ~2-fold increase in the Ad5-477*dl*TAYT$_{A20}$ group (p=0.011). No differences were found in total eosinophil counts for any cohort (p>0.05 for all).

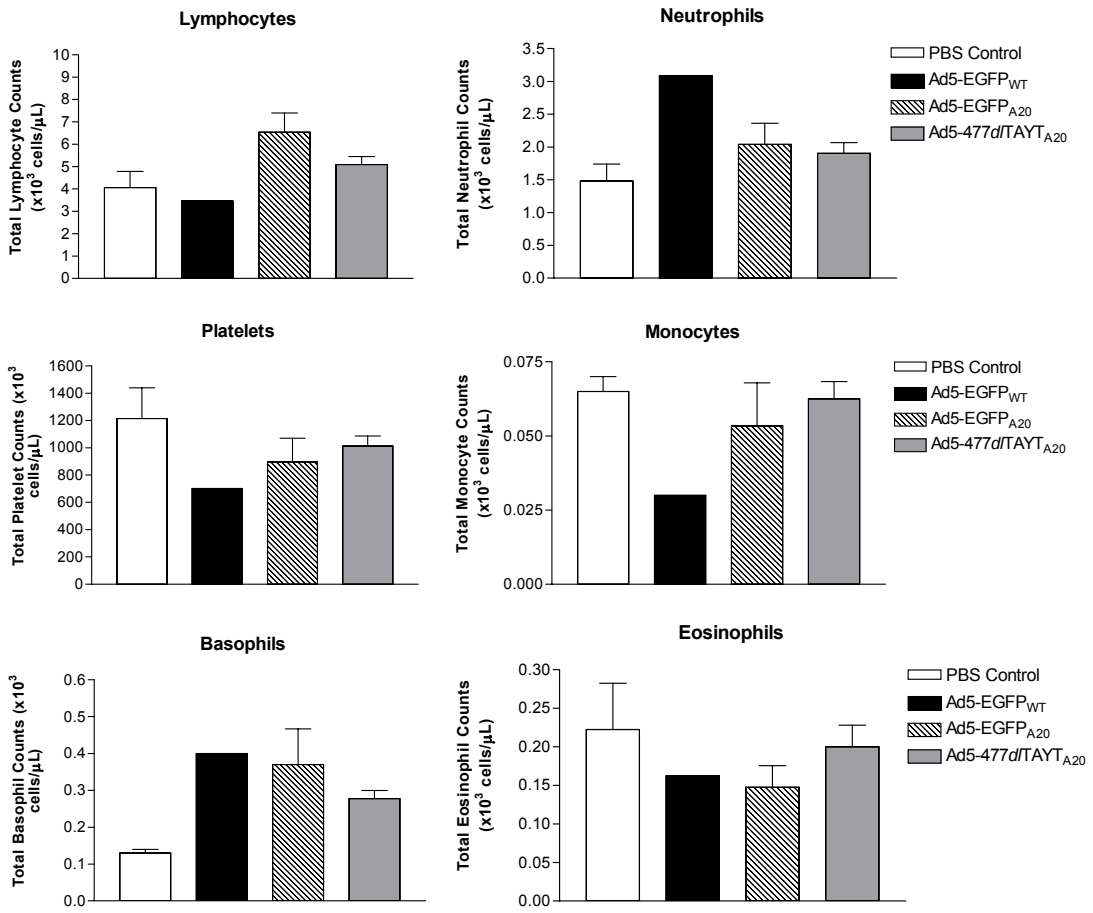

***Figure*.5.4 Haematological Profiles Obtained from Immunocompetent Balb/c Mice Following Systemic Delivery of Virus (4.0x10^{10}vp/mouse).** Whole blood samples (250µl) from each of the treated groups (PBS, Ad5-EGFP$_{WT}$, Ad5-EGFP$_{A20}$ and Ad5-477*dl*TAYT$_{A20}$) were obtained immediately post-mortem by intracardiac puncture (day 4 post-infection). Haematological profiles were assessed at the Clinical Veterinary Biochemistry Service at the Falcultat de Veterinària, Universitat Autònoma de Barcelona. Data presented show the mean ± SEM (N=5 female mice, except Ad5-EGFP$_{WT}$; N=1). Statistical significance was determined using the unpaired Student's t-test comparing the means of two samples (* indicates a P-value of <0.05, differences which were not found to be significant had a P-value >0.05; not marked, bars indicate SEM). Statistics displayed directly above the histogram for the Ad5-477*dl*TAYT$_{A20}$ group (basophils), refer to the difference when compared to the corresponding PBS control sample.

5.1.3 Quantification of Viral Genomes (qPCR) in Murine Liver (4x10^{10}vp/mouse).

Immunocompetent, female Balb/c mice (6 weeks) which had been administered with 4x10^{10}vp/mouse were killed 4 days post-infection, and their livers and spleens harvested for analysis. Absolute viral genome numbers in the liver were quantified by qPCR for each of the Ad5-EGFP$_{WT}$, Ad5-EGFP$_{A20}$ and Ad5-477*dl*TAYT$_{A20}$ treated

groups, using probes and primers to detect the hexon region of the genome (*Fig*.5.5). As expected, a significant amount of Ad5-EGFP$_{WT}$ was detected in the liver. However, in comparison ~7.5-fold fewer Ad5-EGFP$_{A20}$ (p=0.002), and ~5.5-fold fewer Ad-477*dl*TAYT$_{A20}$ (p=0.002) genomes were detected in the liver.

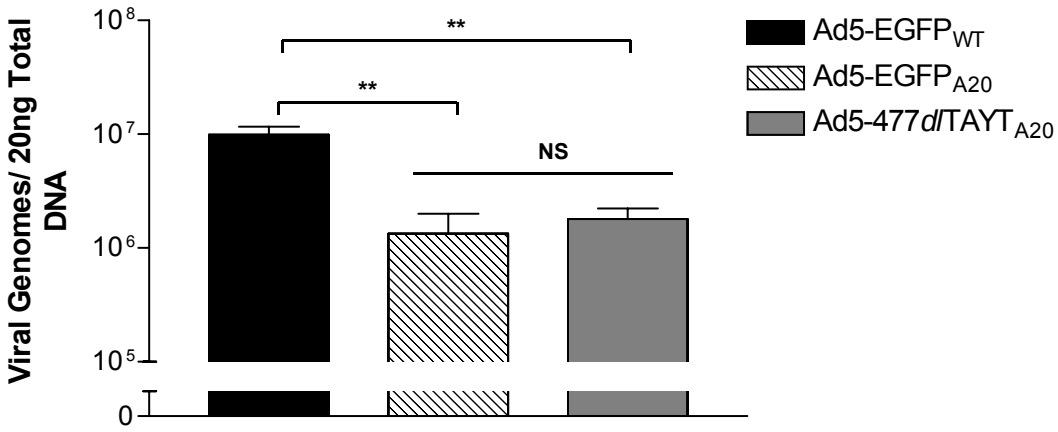

***Figure*.5.5 Quantification of Viral Genomes in Murine Liver Following Systemic Delivery (4.0x10^{10}vp/mouse).** Balb/c immunocompetent, female mice were injected either with PBS, Ad5-EGFP$_{WT}$, Ad5-EGFP$_{A20}$ or Ad5-477*dl*TAYT$_{A20}$ by intravenous tail vein injection (150µl). Mice were killed 4 days post-infection, necropsy performed and total DNA extracted from liver tissue. Absolute viral genomes were quantified by TaqMan Real-Time Quantitative qPCR using a probe to detect the hexon region of the genome (see *Section*.2.2.7). Data presented show the mean ± SEM (N=5 mice). Statistical significance was determined using the unpaired Student's t-test comparing the means of two samples (* indicates a P-value of <0.05, ** p<0.01, NS indicates p>0.05, bars indicate SEM).

5.1.4 Histological Examination of Liver Tissue; H&E Staining and Immunostaining for E1A. Haematoxylin and eosin staining of the liver sections supported these findings, revealing distinct histological differences between Ad5-EGFP$_{WT}$ and Ad5-EGFP$_{A20}$/Ad5-477*dl*TAYT$_{A20}$ treated groups (*Fig*.5.6). The livers from mice administered with Ad5-EGFP$_{WT}$ showed striking hepatocyte atypia; there was evidence of ballooning degeneration of cells and individual cell necrosis. Additionally a prominent peri-portal lymphocytic inflammatory infiltrate was present in the livers of animal which received Ad5-EGFP$_{WT}$. This infiltration was not evident in any fields of view within the liver sections of Ad5-EGFP$_{A20}$ or Ad5-477*dl*TAYT$_{A20}$ treated animals.

The histological appearances we observed in H&E sections were further supported by immunostaining for viral antigen (E1A) in frozen liver sections (*Fig*.5.7). A clear reduction in the level of E1A expression within the hepatocytes of the Ad5-EGFP$_{A20}$ and Ad5-477*dl*TAYT$_{A20}$ treated groups was evident when compared with the Ad5-EGFP$_{WT}$ group (20X magnification). This confirmed that the A20-retargeted viruses

displayed not only reduced accumulation in the liver, but reduced hepatocyte transduction when compared to Ad5-EGFP$_{WT}$.

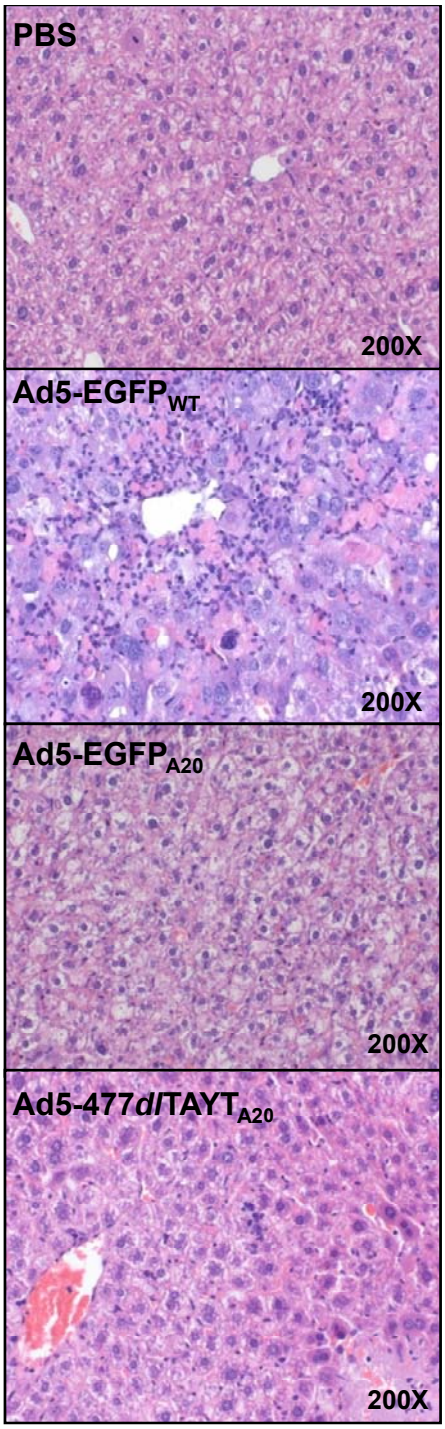

Figure.5.6 Haematoxylin and Eosin Staining of Liver Tissue Following Systemic Delivery of Virus (4.0x10^{10}vp/mouse). Liver sections for each cohort PBS, Ad5-EGFP$_{WT}$, Ad5-EGFP$_{A20}$ or Ad5-477*d*/TAYT$_{A20}$ were cut, stained with H&E (performed by Pathology Services, Institute of Cancer) and assessed histopathologically. Histological analysis was performed blindly by a qualified pathologist (Prof. Gareth Thomas), without prior knowledge of the specimens. Sections were photographed at a magnification of 200X using a Zeiss AxioCam MRc5 camera and Axiovision Software (Zeiss, Germany).

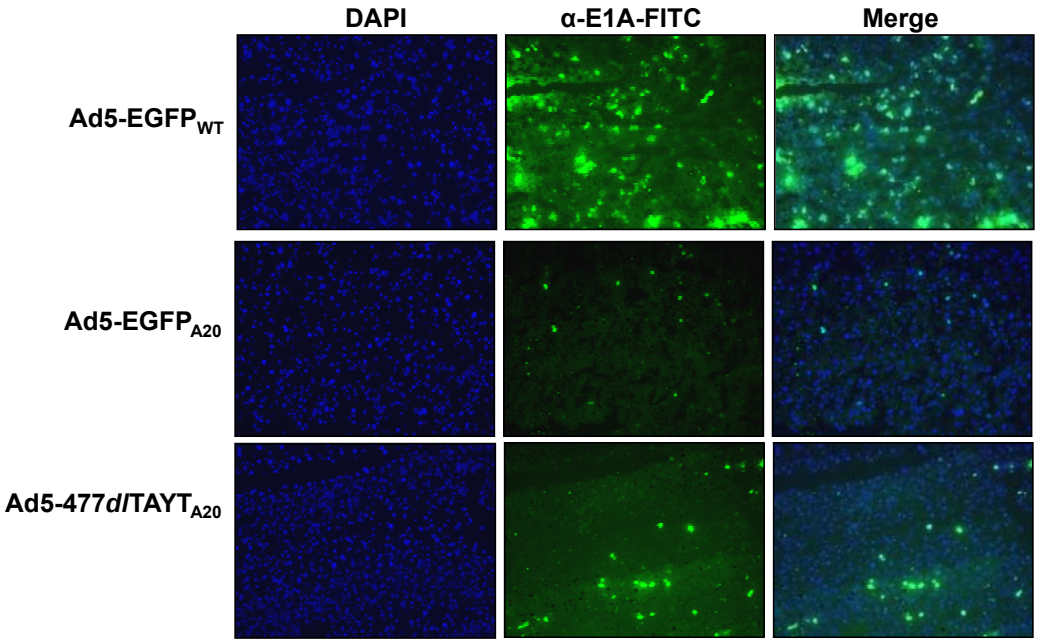

***Figure.*5.7 Immunostaining (E1A) of Frozen Liver Tissue Following Systemic Delivery of Virus (4.0x10^{10}vp/mouse).** Immediately post-necropsy, liver tissue (left lobe) was frozen at -80˚C in OCT-containing cryomolds. Frozen tissue sections (5μm) were stained with an anti-E1A antibody (13 S-5) followed by a goat anti-rabbit AlexaFluor488 conjugated secondary antibody. Sections were counterstained for DAPI using VectaShield reagent. Sections were visualised at a magnification of 20X using an Olympus BX60 fluorescence microscope and images were acquired using SpotAdvanced™ software.

5.1.5 Quantification of Viral Genomes (qPCR) in Murine Spleen ($4x10^{10}$ vp/mouse). Total DNA was extracted from the spleens of the same animals (Balb/c immunocompetent female mice) and absolute viral genome copy numbers quantified as before. The A20-modified viruses (Ad5-EGFP$_{A20}$/Ad5-477*dl*TAYT$_{A20}$) also displayed a significantly altered accumulation in the spleen when compared to Ad5-EGFP$_{WT}$ (*Fig*.5.8). Absolute Ad5-EGFP$_{A20}$ and Ad5477*dl*TAYT$_{A20}$ genome levels in the spleen were found to be ~2.6-fold lower than Ad5-EGFP$_{WT}$ (p=0.0008 and p=0.007, respectively). No differences were noted between Ad5-EGFP$_{A20}$ and Ad5-477*dl*TAYT$_{A20}$ treated cohorts (p=0.929).

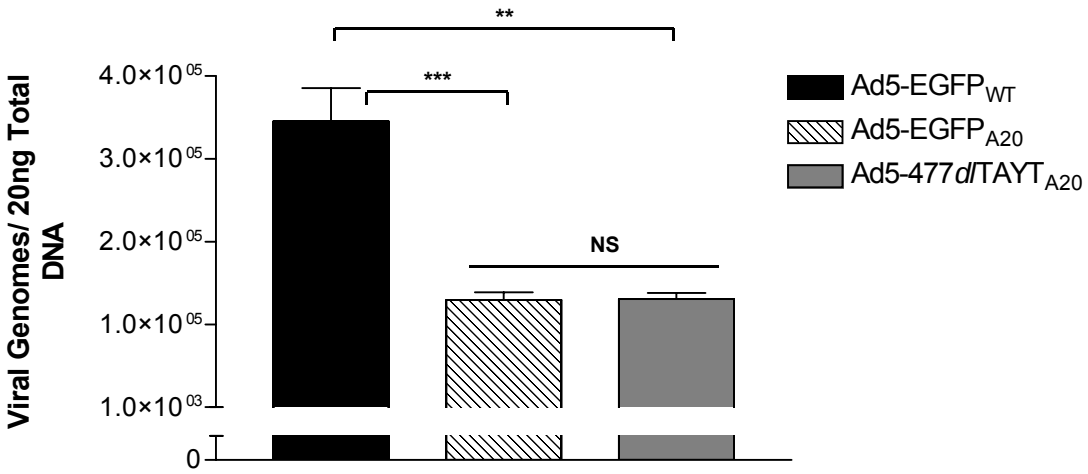

***Figure*.5.8 Quantification of Viral Genomes in Murine Spleen Following Systemic Delivery ($4.0x10^{10}$vp/mouse).** Balb/c immunocompetent, female mice were injected either with PBS, Ad5-EGFP$_{WT}$, Ad5-EGFP$_{A20}$ or Ad5-477*dl*TAYT$_{A20}$ by intravenous tail vein injection (150µl). Mice were killed 4 days post-infection, necropsy performed and total DNA extracted from spleen tissue. Absolute viral genomes were quantified by TaqMan Real-Time Quantitative qPCR using a probe to detect the hexon region of the genome (see *Section*.2.2.7). Data presented show the mean ± SEM (N=5 mice). Statistical significance was determined using the unpaired Student's t-test comparing the means of two samples (** indicates a P-value of <0.01, *** p<0.001, NS indicates p>0.05, bars indicate SEM).

5.1.6 Histological Examination of Spleen Tissue; H&E Staining. Histological examination of H&E stained sections of spleen tissue, again suggested differences between the Ad5-EGFP$_{WT}$ and A20-groups (*Fig*.5.9). In the Ad5-EGFP$_{WT}$ treated animals, the white pulp region appeared enlarged, and there was evidence of follicular hyperplasia when compared with the control PBS group. This effect was not as dramatic in the Ad5-EGFP$_{A20}$ or Ad5-477*dl*TAYT$_{A20}$ groups.

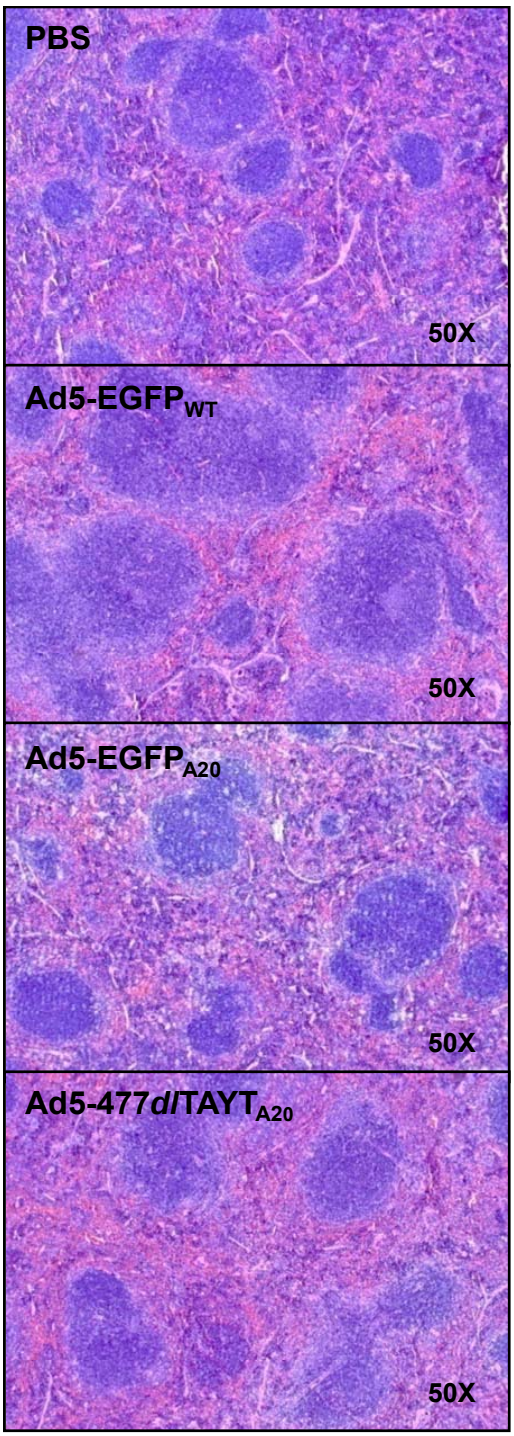

***Figure*.5.9 Haematoxylin and Eosin Staining of Spleen Tissue Following Systemic Delivery of Virus (4.0x10^{10}vp/mouse).** Spleen sections for each cohort PBS, Ad5-EGFP$_{WT}$, Ad5-EGFP$_{A20}$ or Ad5-477*d*/TAYT$_{A20}$ were cut, stained with H&E (performed by Pathology Services, Institute of Cancer) and assessed histopathologically. Histological analysis was performed blindly by a qualified pathologist (Prof. Gareth Thomas), without prior knowledge of the specimens. Sections were photographed at a magnification of 50X using a Zeiss AxioCam MRc5 camera and Axiovision Software. (Zeiss, Germany).

Section.5.2 Biodistribution, Haematology and Cytokine/Chemokine Profiling at Early Time-Points Post-Infection

Intravenous delivery of Ad5 induces rapid innate immune responses, which are characterised by the release of various pro-inflammatory cytokines and chemokines (Di Paolo *et al.*, 2009a; Lieber *et al.*, 1997; Liu *et al.*, 2003; Shayakhmetov *et al.*, 2005c; Zhang *et al.*, 2001). Several studies have shown previously that Ad5-induced cytokine and chemokine responses peak 6-12hrs post-infection and return to near basal levels by 24hrs. Therefore, we also chose these time-points for analysis. In order to investigate the effects of each virus at an earlier time-point (24hrs), additional experiments were carried out at the laboratory of Dr. Ramon Alemany (ICO, Barcelona). An identical dose ($4.0x10^{10}$vp/mouse) and mouse strain (6 week old, Balb/c immunocompetent female mice) were again chosen in order to permit as much comparison to previous studies as possible. *In vivo* biodistribution was assessed by qPCR quantification of absolute viral genomes in the liver, spleen, lung, kidney and heart. Serum cytokine/chemokine levels (IL-6, RANTES, IFN-γ, TNF-α, IL-12p70) were quantified 6hrs, and 24hrs post-infection using a cytometric bead assay, and full haematological profiles were obtained at time of death (24hrs).

5.2.1 Quantification of Serum Cytokines/Chemokines 6hrs and 24hrs Following Systemic Delivery of Virus ($4.0x10^{10}$vp/mouse). Ad5-$EGFP_{WT}$ administration resulted in significant elevations in serum cytokine/chemokine concentrations [pg/ml] 6hrs post-infection (*Fig*.5.10A-C). IL-6 levels in mice treated with Ad5-$EGFP_{WT}$ or Ad5-477*dl*$TAYT_{A20}$ were elevated ~22-fold (p<0.0001) and ~7-fold (p=0.021) over baseline PBS levels (*Fig*.5.10A). However, Ad5-$EGFP_{A20}$ did not increase IL-6 levels at this time-point (p=0.063). Moreover, both A20-retargeted viruses differed significantly from Ad5-$EGFP_{WT}$, inducing substantially lower serum IL-6 levels (p<0.0001 and p=0.0006, respectively). There were no differences observed between Ad5-$EGFP_{A20}$ and Ad5-477*dl*$TAYT_{A20}$ (p=0.358).

RANTES and IFN-γ levels were also elevated above baseline in all virus treated cohorts (p<0.01), however there were significant differences between the Ad5-$EGFP_{WT}$ treated group and the A20-retargeted groups (*Fig*.5.10B and C). When compared to the PBS control group, Ad5-$EGFP_{WT}$ induced high levels of RANTES (~13-fold elevation, p<0.0001), whereas Ad5-$EGFP_{A20}$ and Ad5-477*dl*$TAYT_{A20}$ induced markedly lower levels (~4-fold elevation, p<0.004 and ~7-fold elevation, p=0.001, respectively).

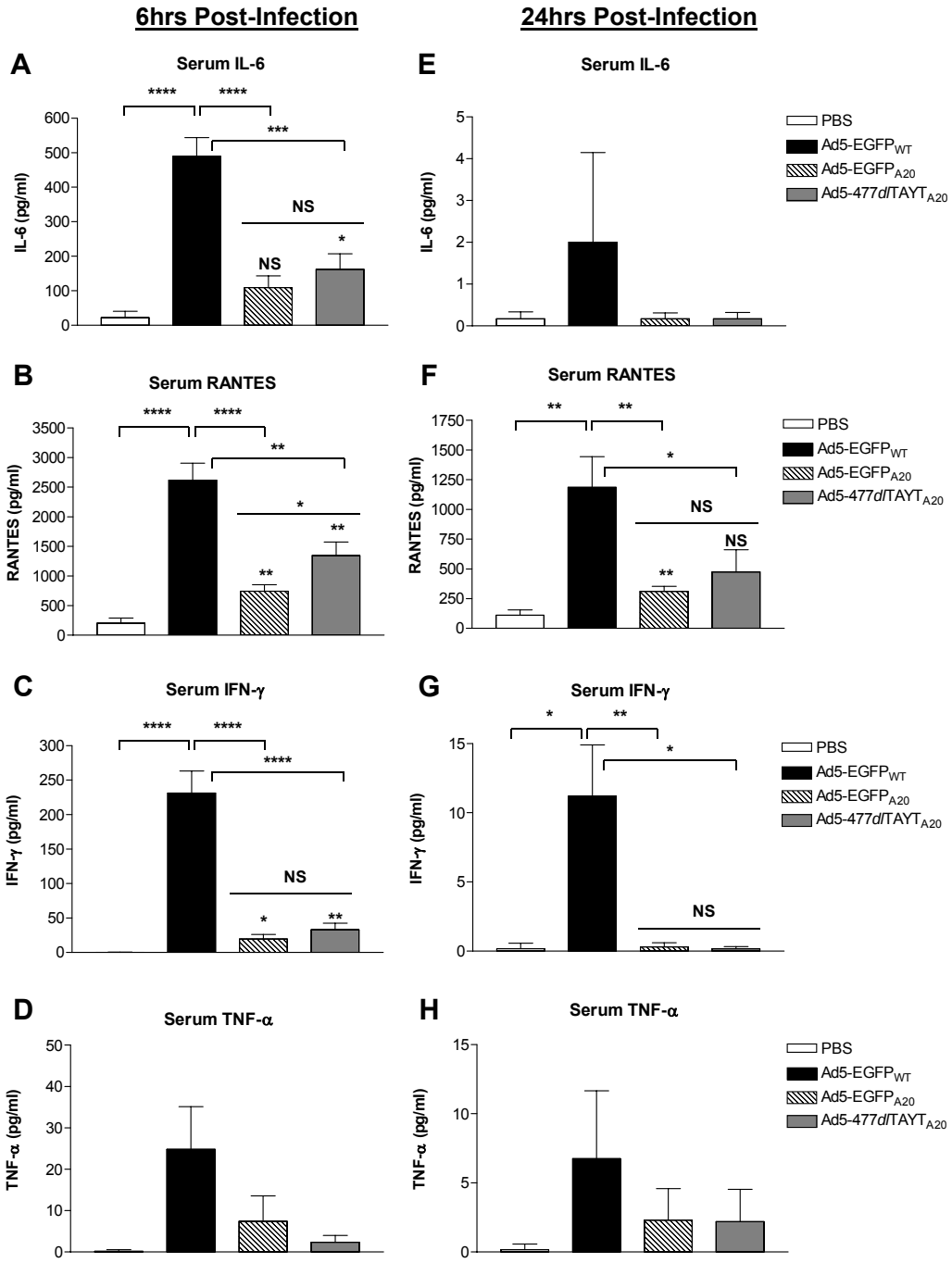

***Figure*.5.10 Quantification of Serum Cytokines/Chemokines from Immunocompetent Balb/c Mice Following Systemic Delivery of Virus (4.0x10^{10}vp/mouse).** Balb/c immunocompetent, female mice were injected either with PBS, Ad5-EGFP$_{WT}$, Ad5-EGFP$_{A20}$ or Ad5-477*dl*TAYT$_{A20}$ by intravenous tail vein injection (150µl). Serum cytokines were quantified at 6hrs (A-D) and 24hrs (E-H) post-injection. Approximately 200µl of whole blood was collected using capillary tubes following a tail snip procedure. Serum was separated, and 25µl used for quantification of cytokines/chemokines (IL-6, RANTES, IFN-γ, TNF-α, and IL-12p70†) using a fluorescent bead, sandwich ELISA-based technology (FlowCytomix™, Bender MedSystems). Samples were acquired by flow cytometry, and analysed using FlowCytomix Pro 2.2 Software (see *Section*.2.1.7). Data presented show the mean ± SEM (*N*=6/8 female mice). Statistical significance was determined using the unpaired Student's t-test comparing the means of two samples (* indicates a *P*-value of <0.05, ** *p*<0.01, NS indicates *p*>0.05, bars indicate SEM). Statistics displayed directly above the histogram for the Ad5-EGFP$_{A20}$/Ad5-477*dl*TAYT$_{A20}$ groups, refer to the difference when compared to the corresponding PBS control sample. †No elevations in serum IL-12(p70) were detected at either time-point (data not shown).

Both Ad5-EGFP$_{A20}$ and Ad-477*dl*TAYT$_{A20}$ differed significantly from Ad5-EGFP$_{WT}$ (p<0.0001 and p=0.005, respectively). Additionally, Ad5-EGFP$_{A20}$ induced less RANTES than Ad5-477*dl*TAYT$_{A20}$ (p=0.028). Similarly, serum IFN-γ concentrations were dramatically elevated above baseline by Ad5-EGFP$_{WT}$ (~1400-fold, p<0.0001), but to a lesser extent by Ad5-EGFP$_{A20}$ and Ad5-477*dl*TAYT$_{A20}$ (~120-fold elevation, p=0.023 and ~200-fold elevation, p=0.009, respectively). Again, both Ad5-EGFP$_{A20}$ and Ad5-477*dl*TAYT$_{A20}$ differed significantly from Ad5-EGFP$_{WT}$ (p<0.0001 for both), however did not differ from each other (p=0.258). There was no significant elevation of TNF-α at this time-point for any virus (p>0.05 for all), which was consistent with a previous study (Zhang *et al.*, 2001). IL-12(p70) levels were unaffected and remained at baseline level (data not shown). However, this is possibly due to poor sensitivity of the assay, as elevations have been reported at this time-point, albeit at a significantly higher dose (Zhang *et al.*, 2001). Additionally, IL-12 exists as two isoforms (p40 and p70), so it is possible that IL-12(p40), and not necessarily IL-12(p70), is differentially regulated in response to Ad5 administration.

With the exception of RANTES, all cytokine/chemokine concentrations [pg/ml] returned approximately to basal levels by 24hrs (*Fig*.5.10E-H). The sustained upregulation of RANTES we observed is consistent with previous studies (Liu *et al*., 2003). At this time-point, serum IL-6 levels were not increased over baseline for any virus-treated group (p>0.05). RANTES levels were reduced when compared with the 6hr time-point, however they remained elevated over basal levels in Ad5-EGFP$_{WT}$ (~11-fold, p=0.003) and Ad5-EGFP$_{A20}$ (~3-fold, p=0.007) treated cohorts, but not in those treated with Ad5-477*dl*TAYT$_{A20}$ (p=0.104). Again, at this time-point both Ad5-EGFP$_{A20}$ and Ad5-477*dl*TAYT$_{A20}$ differed significantly from Ad5-EGFP$_{WT}$ (p=0.003 and p=0.045, respectively), but not from each other (p=0.376). IFN-γ levels had also returned to basal levels 24hrs post-infection, however serum concentrations remained elevated in Ad5-EGFP$_{WT}$ treated cohorts (~70-fold, p=0.019). There were no significant elevations of TNF-α for any virus at this time-point and dose (p>0.05 for all) and as before, IL-12(p70) levels remained unaffected (data not shown).

5.2.2 Haematological Profiles Obtained 24hrs Following Systemic Delivery of Virus (4.0x10^{10}vp/mouse). A full haematological profile was obtained, 24hrs post-infection, for each of the cohorts; PBS control, Ad5-EGFP$_{WT}$, Ad5-EGFP$_{A20}$ and Ad5-477*dl*TAYT$_{A20}$ (*Fig*.5.11). There were significant reductions (>2-fold) in total lymphocytes for all virus treated groups when compared with the PBS control group (p<0.0001 for all). Additionally, there were clear differences between the Ad5-EGFP$_{WT}$ group and the A20-retargeted groups, Ad5-EGFP$_{A20}$ and Ad5-477*dl*TAYT$_{A20}$ (p<0.0001

and p=0.048, respectively). Total neutrophil levels were not affected when comparing virus treated groups with the PBS control cohort (p>0.05). However, there was a difference between the Ad5-EGFP$_{WT}$ and Ad5-477*dl*TAYT$_{A20}$ treated group at this time-point (p=0.03).

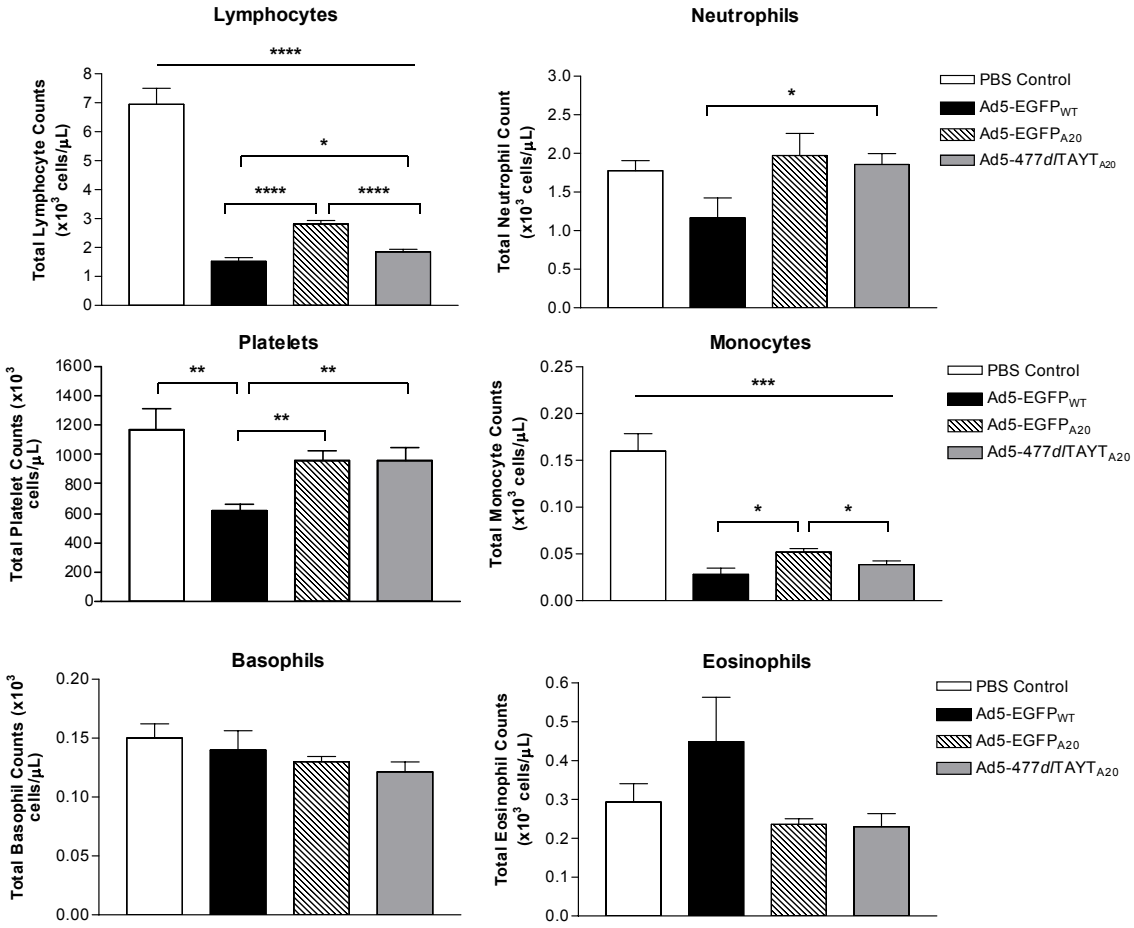

Figure.5.11 Haematological Profiles Obtained from Immunocompetent Balb/c Mice 24hrs Following Systemic Delivery of Virus (4x10^{10}vp/mouse). Whole blood samples (250µl) from each of the treated groups (PBS, Ad5-EGFP$_{WT}$, Ad5-EGFP$_{A20}$ and Ad5-477*dl*TAYT$_{A20}$) were obtained immediately post-mortem by intracardiac puncture (24hrs post-infection). Haematological profiles were assessed at the Clinical Veterinary Biochemistry Service at the Facultat de Veterinària, Universitat Autònoma de Barcelona. Data represent the mean ± SEM (N=6/8 mice). Statistical significance was determined using the unpaired Student's t-test comparing the means of two samples (* indicates a P-value of <0.05, ** p<0.01, *** p<0.001, **** p<0.0001, differences which were not found to be significant had a P-value >0.05; not marked, bars indicate SEM).

Systemic administration of Ad5 has been associated with acute transient thrombocytopenia in various species (Varnavski *et al.*, 2005), and has been reported to occur between 5mins and 24hrs post-infection in mice (Othman *et al.*, 2007). Interestingly, only Ad5-EGFP$_{WT}$ induced thrombocytopenia (~2-fold reduction, p=0.003), whereas neither of the A20-retargeted viruses, Ad5-EGFP$_{A20}$ or Ad5-

477*dl*TAYT$_{A20}$, differed significantly from the PBS control group (p=0.228 and p=0.213, respectively). The thrombocytopenia induced by Ad5-EGFP$_{WT}$ was also found to be significant when compared directly with Ad5-EGFP$_{A20}$ and Ad5-477*dl*TAYT$_{A20}$ treated groups (p=0.011 and p=0.005). Overall platelet levels in Ad5-EGFP$_{A20}$ and Ad5-477*dl*TAYT$_{A20}$ treated cohorts were almost identical (p=0.956). Total monocyte levels were also affected significantly in all virus treated cohorts when compared to the PBS group (>3-fold reductions, p<0.001 for all). Again, Ad5-EGFP$_{WT}$ differed from Ad5-EGFP$_{A20}$, but not from Ad5-477*dl*TAYT$_{A20}$ (p=0.016 and p=0.196, respectively). No significant differences were observed in overall basophil or eosinophil populations (p>0.05).

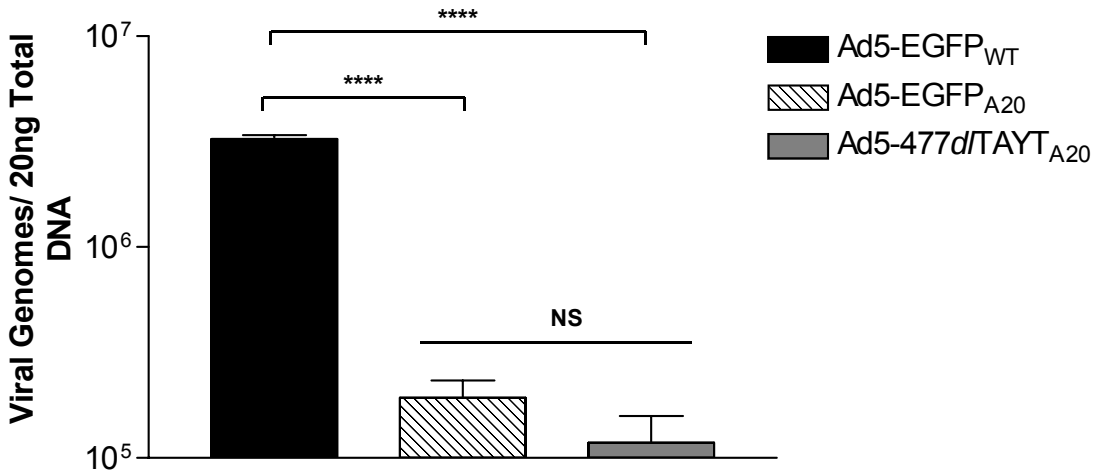

Figure*.5.12 Quantification of Viral Genomes in Murine Liver 24hrs Following Systemic Delivery (4.0x10^{10}vp/mouse).** Balb/c immunocompetent, female mice were injected either with PBS, Ad5-EGFP$_{WT}$, Ad5-EGFP$_{A20}$ or Ad5-477*dl*TAYT$_{A20}$ by intravenous tail vein injection (150µl). Mice were killed 24hrs post-infection, necropsy performed and total DNA extracted from liver tissue. Absolute viral genomes were quantified by TaqMan Real-Time Quantitative qPCR using a probe to detect the hexon region of the genome (see *Section*.2.2.7). Data presented show the mean ± SEM (N=6/8 mice). Statistical significance was determined using the unpaired Student's t-test comparing the means of two samples (* indicates a P-value of <0.0001, NS indicates p>0.05, bars indicate SEM).

5.2.3 Quantification of Viral Genomes (qPCR) in Murine Liver 24hrs Post-Infection (4.0x10^{10}vp/mouse). Immunocompetent Balb/c mice which had been administered systemically with 4x10^{10}vp/mouse were killed 24hrs post-infection, and their livers harvested for analysis. Absolute genome copy numbers in the liver were quantified by quantitative real time PCR (qPCR) for each of the virus treated cohorts; Ad5-EGFP$_{WT}$, Ad5-EGFP$_{A20}$ and Ad5-477*dl*TAYT$_{A20}$ (*Fig*.5.12). Approximately 17-fold fewer Ad5-EGFP$_{A20}$ genomes, and ~27-fold fewer Ad5-477*dl*TAYT$_{A20}$ genomes were detected in the liver when compared with Ad5-EGFP$_{WT}$ (p<0.0001 for both). No differences were found between the A20-retargeted groups (p=0.207).

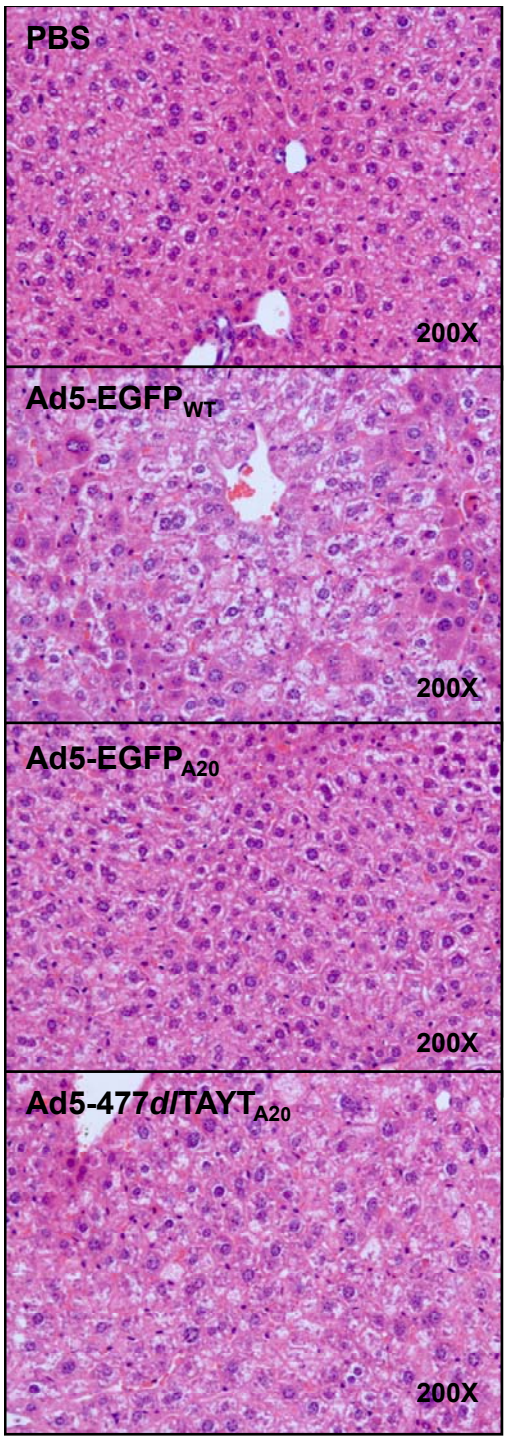

***Figure.*5.13 Haematoxylin and Eosin Staining of Liver Tissue 24hrs Following Systemic Delivery of Virus (4.0x10^{10}vp/mouse).** Liver sections for each cohort PBS, Ad5-EGFP$_{WT}$, Ad5-EGFP$_{A20}$ or Ad5-477*d*/TAYT$_{A20}$ were cut, stained with H&E (performed by Pathology Services, Institute of Cancer) and assessed histopathologically. Histological analysis was performed blindly by a qualified pathologist (Prof. Gareth Thomas), without prior knowledge of the specimens. Sections were photographed at a magnification of 200X using a Zeiss AxioCam MRc5 camera and Axiovision Software (Zeiss, Germany).

5.2.4 Histological Examination of Liver Tissue; Haematoxylin and Eosin Staining and Immunostaining for E1A. Liver tissue was assessed histopathologically following H&E staining (*Fig*.5.13). We observed slight, but not dramatic differences between the

Ad5-EGFP$_{WT}$ and Ad5-EGFP$_{A20}$/Ad5-477*dl*TAYT$_{A20}$ treated cohorts at this time-point (24hrs). The hepatocytes in animals treated with Ad5-EGFP$_{WT}$ appeared swollen, with some nuclear abnormalities evident. In comparison, the Ad5-EGFP$_{A20}$/Ad5-477*dl*TAYT$_{A20}$ groups retained an appearance more similar to the PBS control group.

Immunostaining of frozen liver sections for viral antigen (E1A), again highlighted the dramatic differences between the Ad5-EGFP$_{WT}$, and Ad5-EGFP$_{A20}$/Ad5-477*dl*TAYT$_{A20}$ treated groups (*Fig*.5.14). Substantially less E1A expression was detected in the livers of cohorts which received the A20-retargeted viruses. These findings further supported the significantly reduced levels of viral genomes detected in the livers of these animals by qPCR (*see Fig*.5.12).

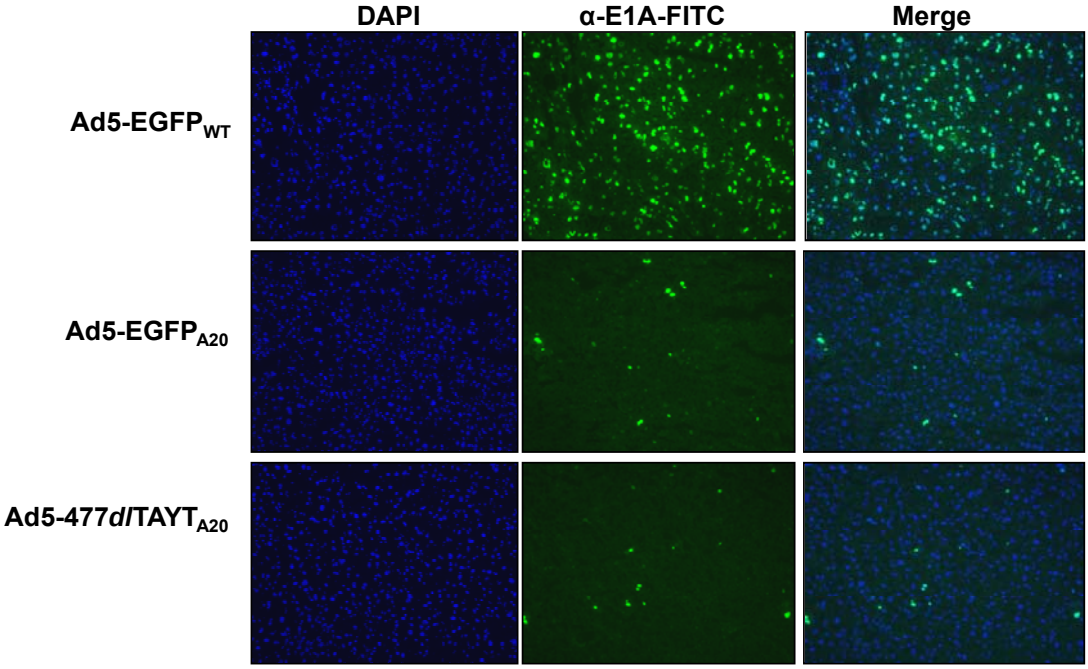

***Figure*.5.14 Immunostaining (E1A) of Frozen Liver Tissue 24hrs Following Systemic Delivery of Virus (4.0x10^{10}vp/mouse).** Immediately post-necropsy, liver tissue (left lobe) was frozen at -80˚C in OCT-containing cryomolds. Frozen tissue sections (5µm) were stained with an anti-E1A antibody (13 S-5) followed by a goat anti-rabbit AlexaFluor488 conjugated secondary antibody. Sections were counterstained for DAPI using VectaShield reagent. Sections were visualised at a magnification of 20X using an Olympus BX60 fluorescence microscope and images acquired using SpotAdvanced™ software.

5.2.5 Quantification of Viral Genomes (qPCR) in Murine Spleen 24hrs Post-Infection (4.0x10^{10}vp/mouse). Absolute genome copy numbers in the spleen were quantified, as before, for each of the virus treated cohorts; Ad5-EGFP$_{WT}$, Ad5-EGFP$_{A20}$ and Ad5-477*dl*TAYT$_{A20}$ (*Fig*.5.15). Approximately 2-fold fewer Ad5-EGFP$_{A20}$, and Ad5-477*dl*TAYT$_{A20}$ genomes, were detected in the spleen when compared with Ad5-

$EGFP_{WT}$ (p=0.013 and p=0.007, respectively). No differences were found between the A20-retargeted groups (p=0.627).

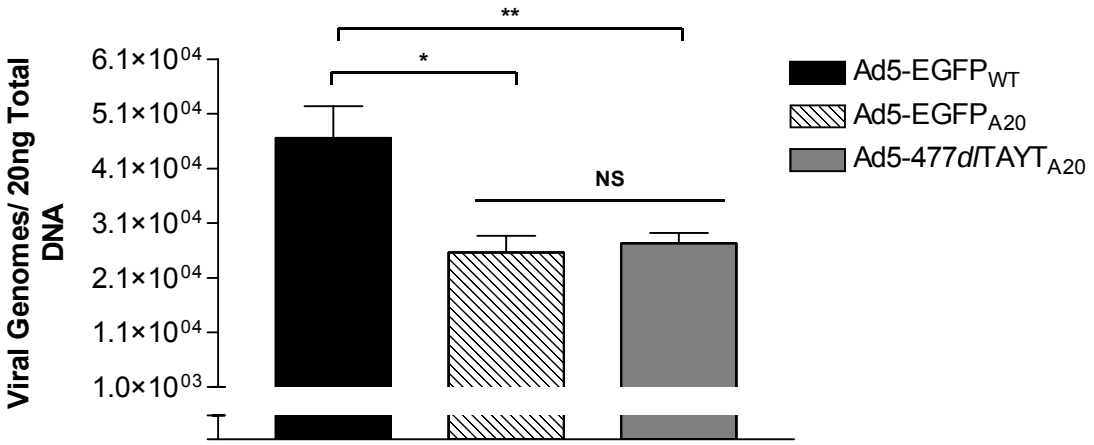

***Figure*.5.15 Quantification of Viral Genomes in Murine Spleen 24hrs Following Systemic Delivery ($4.0x10^{10}$vp/mouse).** Balb/c immunocompetent mice were injected either with PBS, Ad5-$EGFP_{WT}$, Ad5-$EGFP_{A20}$ or Ad5-477*dl*$TAYT_{A20}$ by intravenous tail vein injection (150µl). Mice were killed 24hrs post-infection, necropsy performed and total DNA extracted from spleen tissue. Absolute viral genomes were quantified by TaqMan Real-Time Quantitative qPCR using a probe to detect the hexon region of the genome (see *Section*.2.2.7). Data presented show the mean ± SEM (N=6/8 mice). Statistical significance was determined using the unpaired Student's t-test comparing the means of two samples (* indicates a P-value of <0.05, ** p<0.001, NS indicates p>0.05, bars indicate SEM).

5.2.6 Histological Examination of Spleen Tissue; Haematoxylin and Eosin Staining. Spleen tissue was assessed histopathologically following H&E staining (*Fig*.5.16). Lymphoid follicles were prominent in all viral treated groups. No other differences were noted.

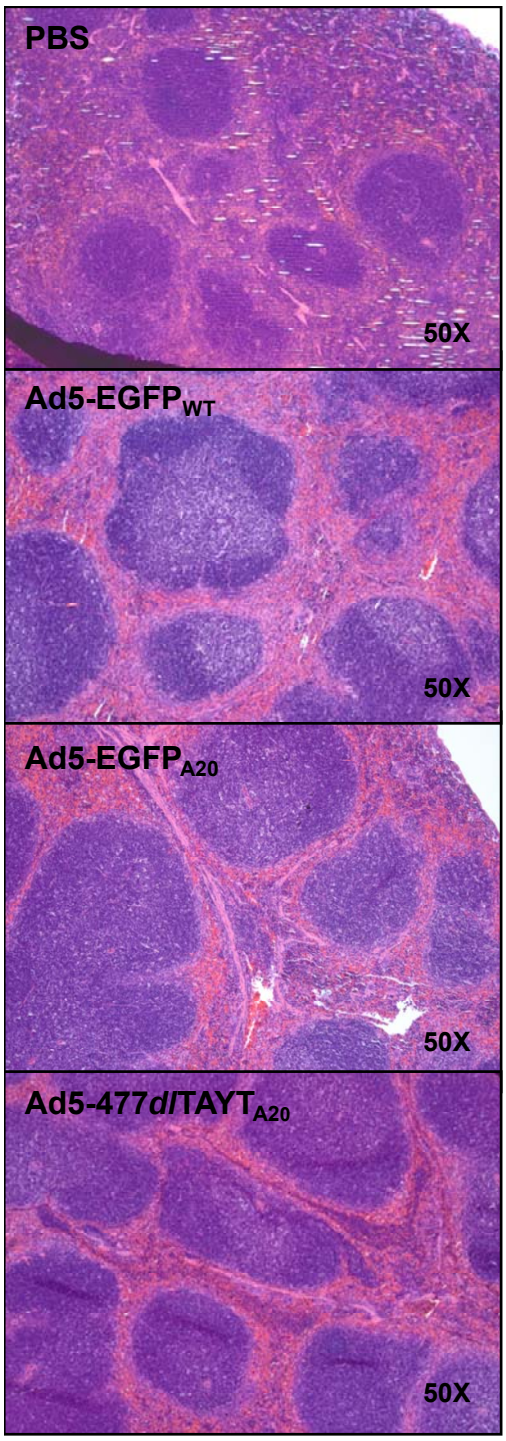

***Figure*.5.16 Haematoxylin and Eosin Staining of Spleen Tissue 24hrs Following Systemic Delivery of Virus (4.0x10^{10}vp/mouse).** Spleen sections for each cohort PBS, Ad5-EGFP$_{WT}$, Ad5-EGFP$_{A20}$ or Ad5-477*dl*TAYT$_{A20}$ were cut, stained with H&E (performed by Pathology Services, Institute of Cancer) and assessed histopathologically. Histological analysis was performed blindly by a qualified pathologist (Prof. Gareth Thomas), without prior knowledge of the specimens. Sections were photographed at a magnification of 50X using a Zeiss AxioCam MRc5 camera and Axiovision Software (Zeiss, Germany)

5.2.7 Quantification of Viral Genomes (qPCR) in Murine Lung, Kidney and Heart 24hrs Post-Infection ($4.0x10^{10}$vp/mouse). In the same experiment, the lung, kidney and heart of each animal was harvested for a comparative biodistribution analysis of viral genomes (*Fig*.5.17A-C). Again, absolute viral genome copy numbers were quantified by qPCR following extraction of total DNA from each respective tissue, using primers and probes to detect the hexon region of the genome.

Approximately ~3-fold, and ~2-fold fewer Ad5-$EGFP_{A20}$ and Ad5-477*dl*$TAYT_{A20}$ genomes were detected in the lung than Ad5-$EGFP_{WT}$ (p=0.0024 and p=0.015, respectively). Ad5-477*dl*$TAYT_{A20}$ displayed a slightly enhanced uptake in the lung when compared with Ad5-$EGFP_{A20}$ (p=0.045). In addition, ~2-fold less Ad5-$EGFP_{A20}$ and Ad5-477*dl*$TAYT_{A20}$ genomes were detected in the kidney, when compared with Ad5-$EGFP_{WT}$ (p=0.012 and p=0.019, respectively). There were no differences between Ad5-$EGFP_{A20}$ and Ad5-477*dl*$TAYT_{A20}$ in this organ (p=0.995). In the heart, the levels of Ad5-$EGFP_{WT}$ and Ad5-$EGFP_{A20}$ were similar (p=0.425). However, the levels of Ad5-477*dl*$TAYT_{A20}$ appeared to be elevated ~6-fold, although this was not found to be significant (p=0.09).

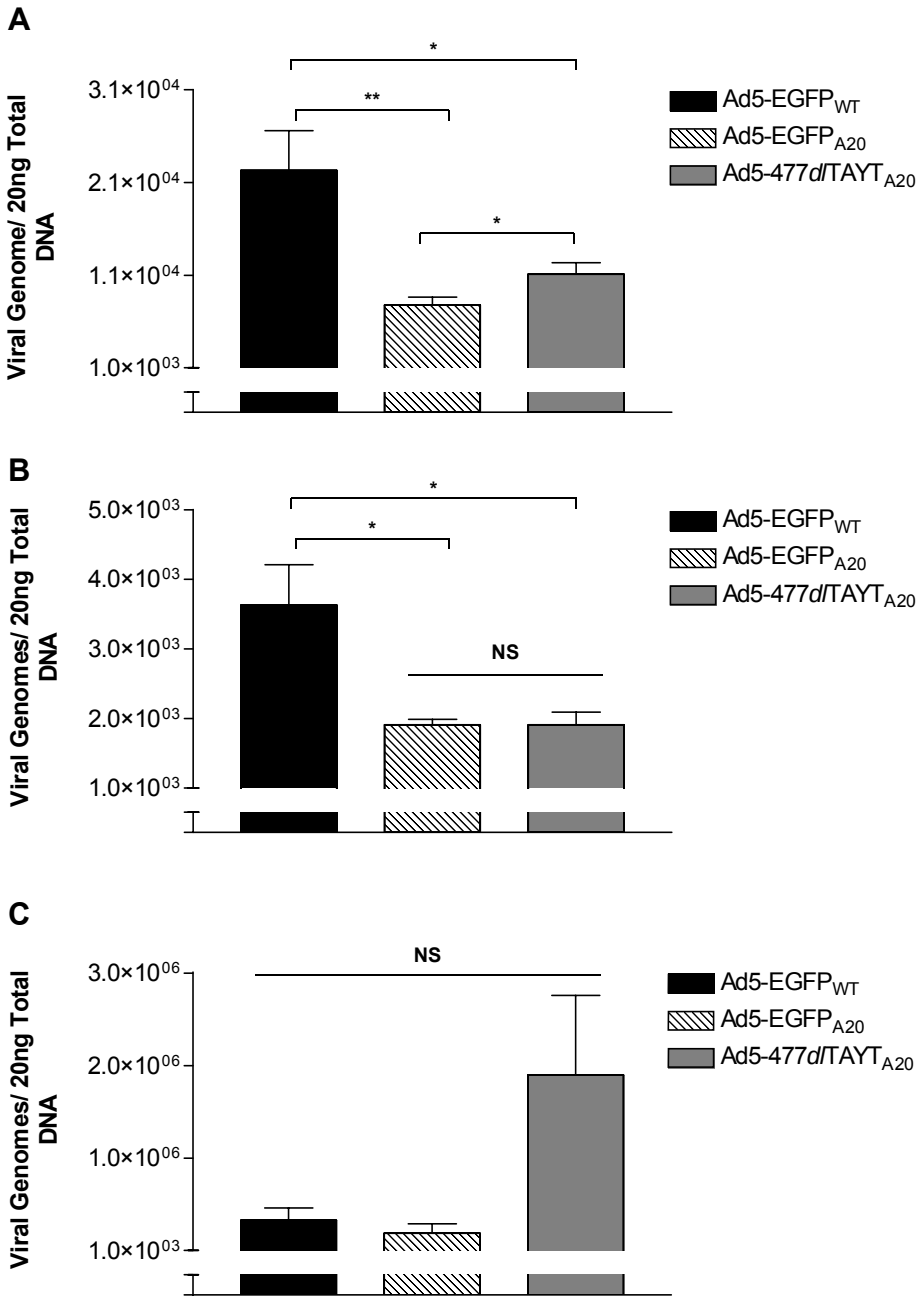

Figure.5.17 (A) Quantification of Viral Genomes in Murine Lung 24hrs Following Systemic Delivery ($4.0x10^{10}$vp/mouse). Balb/c immunocompetent, female mice were injected either with PBS, Ad5-EGFP$_{WT}$, Ad5-EGFP$_{A20}$ or Ad5-477*dl*TAYT$_{A20}$ by intravenous tail vein injection (150µl). Mice were killed 24hrs post-infection, necropsy performed and total DNA extracted from lung tissue. **(B) Quantification of Viral Genomes in Murine Kidney 24hrs Following Systemic Delivery ($4.0x10^{10}$vp/mouse).** Total DNA was extracted from the kidneys of the cohorts described above. **(C) Quantification of Viral Genomes in Murine Heart 24hrs Following Systemic Delivery ($4.0x10^{10}$vp/mouse).** Absolute viral genomes were quantified by TaqMan Real-Time Quantitative qPCR using a probe to detect the hexon region of the genome (see *Section*.2.2.7). Data presented show the mean ± SEM (N=6/8 mice). Statistical significance was determined using the unpaired Student's t-test comparing the means of two samples (* indicates a *P*-value of <0.05, ** *p*<0.001, NS indicates *p*>0.05, bars indicate SEM).

Chapter.5 Discussion

The systemic delivery of Ad5 in many pre-clinical animal models elicits a robust inflammatory response directed against both the viral particle, and its expressed genes (Elkon *et al.*, 1997; Wolins *et al.*, 2003; Zhang *et al.*, 2001). Consequently, heterologous transgene expression can be short-lived, serving to limit the therapeutic effect. The rapid induction of innate immune responses to Ad5 also contributes significantly to the characteristic liver pathology (hepatocyte necrosis, elevation of liver transaminases and a monocytic/lymphocytic infiltrate). These effects are mediated primarily through the action of pro-inflammatory cytokines/chemokines (Koizumi *et al.*, 2007; Liu & Muruve, 2003; Muruve *et al.*, 1999; Shayakhmetov *et al.*, 2005c; Zhang *et al.*, 2001). Recent evidence also suggests that Ad5-induced complement activation *in vivo* may also contribute to these effects, heightening the inflammatory response (Kiang *et al.*, 2006; Tian *et al.*, 2009).

In addition to inducing pro-inflammatory cascades, systemically delivered adenoviral vectors can cause haemodynamic changes and induce acute transient thrombocytopenia, which potentially exacerbates pre-existing coagulopathic conditions (Othman *et al.*, 2007; Schiedner *et al.*, 2003a; Stone *et al.*, 2007b; Wolins *et al.*, 2003). The precise mechanisms by which Ad5 induces thrombocytopenia are complex, and currently unclear, although several hypotheses have been proposed. It has been shown previously that direct binding of the Ad5 particle to platelets results in the formation of platelet-leukocyte aggregates which are cleared by the reticuloendothelial system (Stone *et al.*, 2007b). Subsequently, it was found that formation of the Ad5-platelet-leukocyte complex was dependent on P-selectin and von Willebrand factor (Othman *et al.*, 2007). In another study, it was proposed that complement C3 activation, in response to Ad5-mediated cell damage, also contributes significantly to the induction of acute thrombocytopenia (Kiang *et al.*, 2006).

Murine models currently are the most commonly used for assessing the *in vivo* effects of Ad delivery. Many of the cellular interactions which contribute to the toxicity of systemically delivered Ad5s in murine models are applicable to humans (Herman *et al.*, 1999; Klinger *et al.*, 1998; Mistchenko *et al.*, 1994; Schnell *et al.*, 2001) however many are not relevant, or remain controversial (Carlisle *et al.*, 2009; Eggerman *et al.*, 2002; Seiradake *et al.*, 2009). Clearly, significant hurdles remain which hamper the efficacy, and subsequently the development of adenoviral vectors for therapeutic applications. Therefore, understanding the underlying mechanisms which result in the induction of

innate immune responses is critical to the development of vectors with improved safety profiles, and extended therapeutic duration *in vivo*.

*Section.*5.1 *In Vivo* Biodistribution and Hepatotoxicity in Immunocompetent Mice

Non-specific sequestration of systemically delivered Ad5 vectors in KCs leads to a nonlinear dose response of hepatocyte transduction (Tao *et al.*, 2001). The threshold dose for saturation of KCs ranges from 10^{10}-10^{11}vp/kg (Manickan *et al.*, 2006). Therefore, we performed dose escalation studies in immunocompetent Balb/c mice to assess the *in vivo* hepatotropism and toxicity of Ad5-EGFP$_{WT}$, Ad5-EGFP$_{A20}$ and the putative liver de-targeted vector, Ad5-477*dl*TAYT$_{A20}$. Initial experiments using a dose of 2.5x10^{10}vp/mouse (~10^{11}vp/kg) failed to induce significant toxicity in any cohort. The experiment was repeated using a higher dose (4.0x10^{10}vp/mouse) in order to comparatively analyse transaminase levels, haematological profiles, vector biodistribution and histopathology (liver/spleen) for each group, 4 days post-infection.

In agreement with previously published data, the Ad5-477*dl*TAYT$_{A20}$ vector had significantly reduced hepatotropism and toxicity *in vivo* (Shayakhmetov *et al.*, 2005b). Unexpectedly, Ad5-EGFP$_{A20}$ also displayed this profile, despite the absence of the putative blood factor binding ablating mutations. Animals administered with Ad5-EGFP$_{A20}$ or Ad5-477*dl*TAYT$_{A20}$, displayed overall well-being throughout the duration of the experiment, with limited serum transaminase elevations and a dramatically reduced accumulation of virion DNA in the liver at time of death, which correlated with reduced E1A expression in hepatocytes. In comparison, the Ad5-EGFP$_{WT}$ treated groups were showing signs of cachexia, and had significantly elevated serum transaminases, with higher levels of viral DNA and extensive E1A expression within their livers, at the time of death. Additionally, histological examination of H&E sections of liver tissue revealed distinct differences between the groups. In addition to the lack of hepatocellular dysregulation in Ad5-EGFP$_{A20}$ and Ad5-477*dl*TAYT$_{A20}$ treated groups, the absence of an inflammatory infiltrate was obvious when compared to Ad5-EGFP$_{WT}$ treated cohorts.

The dramatic reductions in liver accumulation and hepatotoxicity with Ad5-EGFP$_{A20}$ were not anticipated. However, these initial *in vivo* studies were performed prior to extensively characterising the interactions of these viruses with FIX/FX *in vitro* (described in *Chapter*.4). In these subsequent experiments, it was confirmed that both A20-modified vectors, Ad5-EGFP$_{A20}$ and Ad5-477*dl*TAYT$_{A20}$, failed to interact with FIX to promote infectivity enhancement in various cell lines (CHO-K1, CHO-CAR, BT-20, TR126 and DX3-β6). Unfortunately, we were unable to investigate the potential role of

C4BP in these *in vitro* studies as it was commercially unavailable at the time. Based on these *in vitro* findings, we hypothesised that the insertion of the A20FMDV2 peptide into the HI loop of the fibre was inducing a conformational change, or steric hindrance which disrupted binding of FIX and/or C4BP to the fibre. However, evidence provided in recent years has confirmed that a FX-hexon interaction is the predominant determinant of hepatocyte transduction *in vivo* following systemic delivery of Ad5 (Alba *et al.*, 2009; Kalyuzhniy *et al.*, 2008; Vigant *et al.*, 2008; Waddington *et al.*, 2008). Therefore, it was unexpected that these fibre modified viruses, both of which retain a fully functional capacity for FX-mediated infectivity enhancement *in vitro*, should display such an altered hepatotropism *in vivo*.

Several other vectors (Ad9, Ad11, Ad35, Ad40) which display reduced transduction of hepatocytes *in vivo* have been described previously, however these effects are thought to be due to inefficient vector trafficking, or the lack of available functional receptors on the surface of liver cells (Liu *et al.*, 2009; Nakamura *et al.*, 2003; Sakurai *et al.*, 2003; Shayakhmetov *et al.*, 2004a; Shayakhmetov *et al.*, 2004b; Stone *et al.*, 2005). Despite their limited hepatocyte transduction, many of these vectors have been shown to accumulate in the liver at levels equivalent to Ad5 at early time-points (Sakurai *et al.*, 2003; Shayakhmetov *et al.*, 2004b; Stone *et al.*, 2005). In contrast, we have shown that the lack of hepatocyte transduction observed with Ad5-EGFP$_{A20}$ and Ad5-477*dl*TAYT$_{A20}$, is accompanied by significant reductions in genome accumulation in the liver (4 days post-infection). This was further substantiated in later experiments which demonstrated that these vectors also displayed reduced liver accumulation 24hrs post-infection. *In vitro* data presented in *Chapter*.4 demonstrated that both Ad5-EGFP$_{A20}$ and Ad5-477*dl*TAYT$_{A20}$ possess an ability to utilise either CAR, or HSPGs (in addition to αvβ6), as receptors for efficient infection. Additionally, *in vitro* infectivity experiments using numerous cell lines confirmed that the intracellular trafficking of these fibre-modified vectors is not impaired as a result of the A20FMDV2 insertion. Therefore, we can eliminate the possibility that the factors described above which result in limiting the hepatotropism of other Ad serotypes (Ad9, Ad11, Ad35, Ad40), are responsible for the effects observed with Ad5-EGFP$_{A20}$ and Ad5-477*dl*TAYT$_{A20}$.

Recent evidence has highlighted the importance of the spleen as a major site for the induction of innate immune responses directed towards intravenously delivered Ads, and it has been proposed that vectors which have limited splenic accumulation would be safer vehicles for gene therapy applications (Di Paolo *et al.*, 2009b; Fejer *et al.*, 2008; Koizumi *et al.*, 2007; Zhang *et al.*, 2001). Therefore, it was reassuring that both Ad5-EGFP$_{A20}$ and Ad5-477*dl*TAYT$_{A20}$ also displayed a reduced tropism for the spleen.

This is in contrast with Ad35-based vectors, currently being investigated for their tumour targeting potential via CD46, which display enhanced splenic sequestration when compared to Ad5 (Liu *et al.*, 2009; Stone *et al.*, 2007a). Interestingly, another fibre modified virus (Ad5-K7 featuring a polylysine motif in the C-terminus of the fibre knob) which displays a biodistribution profile similar to the A20-modified viruses, has been described previously (Koizumi *et al.*, 2007). In this study, the authors also reported reductions in liver toxicity, as measured by serum AST levels and histological examination when compared with the conventional Ad5 control vector. This profile was partially attributed to reduced serum IL-6 levels, which they believed to be a direct result of lower level vector uptake in the spleen (Koizumi *et al.*, 2007). It was argued that IL-6 signalling from splenic dendritic cells plays a critical role in liver toxicity *in vivo*, due to the fact that administration of an anti-IL-6R antibody partially reduced Ad5-induced hepatopathology and serum AST levels (Koizumi *et al.*, 2007). Based on these data, we hypothesised that the reduced toxicity (lower AST/ALT and minimal liver damage histologically) we observed with Ad5-EGFP$_{A20}$ and Ad5-477*dl*TAYT$_{A20}$ in this study, may also be due in part to limited splenic sequestration, and consequently diminished IL-6 signalling.

In order to address this, and the possibility that the reduced hepatotropism was due to increased uptake in alternative organs, we decided to repeat these experiments at an earlier time-point (24hrs), expanding our biodistribution analysis (liver, spleen, lung, heart, kidney), in addition to quantifying a panel of cytokines/chemokines (IL-6, RANTES, IFN-γ, TNF-α and IL-12).

*Section.*5.2 *In Vivo* Biodistribution and Induction of Innate Immunity at Early Time-Points Post-Infection (6-24hrs)

The early phase of the innate response to Ad5 is dose-dependent and occurs independently of viral gene expression (Liu & Muruve, 2003; Liu *et al.*, 2003; Muruve *et al.*, 1999; Zhang *et al.*, 2001). Characteristic elevations in serum chemokines and cytokines [IL-1α, IL-1-β, IL-5, IL-6, IL-12, TNF-α, IFN-γ, GM-CSF, IP-10, MIP-1β and RANTES] are frequently observed, especially when high doses of vector are administered intravenously (Di Paolo *et al.*, 2009a; Kiang *et al.*, 2006; Koizumi *et al.*, 2007; Lieber *et al.*, 1997; Liu *et al.*, 2003; Lozier *et al.*, 2002; Muruve *et al.*, 1999; Muruve *et al.*, 2004; Shayakhmetov *et al.*, 2005c; Zhang *et al.*, 2001). These responses can be triggered by interactions with pattern recognition receptors, including TLR9, and can involve the activation of Type I IFNs (Appledorn *et al.*, 2008; Cerullo *et al.*, 2007;

Fejer *et al.*, 2008; Muruve *et al.*, 2008; Zhu *et al.*, 2007). Recently, an alternative activation pathway has been described, which is independent of TLRs and IFNs (Di Paolo *et al.*, 2009a). The authors demonstrated the importance of a penton-RGD interaction with -β3 integrin expressed on macrophages, in triggering the activation of IL-1α. The activation of pro-inflammatory effectors contributes to vector related toxicity, and to the extensive liver pathology observed with Ad5 (Koizumi *et al.*, 2007; Lieber *et al.*, 1997; Stone *et al.*, 2007a). However, the precise cellular sources of these immune effectors remain unclear, although KCs, splenic marginal zone macrophages and dendritic cells have been implicated (Di Paolo *et al.*, 2009a; Fejer *et al.*, 2008; Koizumi *et al.*, 2007; Zhang *et al.*, 2001).

Compared to Ad5-EGFP$_{WT}$, Ad5-EGFP$_{A20}$ and Ad5-477*dl*TAYT$_{A20}$ once again displayed a reduced accumulation in the liver and spleen, 24hrs post-infection. Unexpectedly, absolute viral genome levels detected 24hrs post-infection (*Fig*.5.5 and *Fig*.5.8), were lower than those than those detected 4 days post-infection (*Fig*.5.12 and *Fig*.5.15). It has previously been shown that >90% Ad5 is eliminated from the liver by approximately 24hrs (Lieber *et al.*, 1997; Worgall *et al.*, 1997). However, as all the vectors used in this study are replicating viruses it is possible that genome replication (but not productive virion production) may explain this discordance. Alternatively, although identical virus stocks, mouse strain and doses were used, these experiments were performed a year apart and genomes were quantified using a different Real Time PCR system (ABI 7300). These factors may also have contributed to the differences observed.

In addition to displaying a reduced hepatotropsim (reduced accumulation of viral genomes, limited E1A expression and low level transaminase elevations), the A20-retargeted viruses, Ad5-EGFP$_{A20}$ and Ad5-477*dl*TAYT$_{A20}$, induced distinctly altered cytokine/chemokine profiles to Ad5-EGFP$_{WT}$, characterised by significantly reduced serum concentrations of IL-6, RANTES and IFN-γ. With respect to Ad5-477*dl*TAYT$_{A20}$, these findings are in agreement with previously published data for Ad5*mut* (an Ad5-477*dl*TAYT-based vector), and provide support for the hypothesis that abrogation of FIX/C4BP binding to the fibre results in a vector with reduced cytokine induction and hepatotoxicity (Shayakhmetov *et al.*, 2005b). However, the precise mechanism which results in this phenotype is currently unclear, and is complicated by the interactions of Ad5 with multiple cell types and blood components following systemic delivery.

In addition to the mechanisms outlined previously (inefficient vector trafficking/lack of functional receptors), rapid vector clearance from the liver has also been shown to limit

hepatocyte transduction. This can occur either through displacement to/successful retargeting to other organs (ie. Ad5Luc-OvF), or through increased vector degradation (ie. Ad35) by non-parenchymal cells (Nakayama *et al.*, 2006; Sakurai *et al.*, 2003; Stone *et al.*, 2007a). The originally described 477*dl*TAYT fibre mutated virus, Ad5*mut*, was shown to have reduced co-localisation with KCs *in vivo* (Shayakhmetov *et al.*, 2005b). In support of this, subsequent studies have demonstrated that Ad5 uptake by KCs via scavenging receptor A (SR-A) can be inhibited by soluble Ad5 knob protein, although this remains to be investigated *in vivo* (Haisma *et al.*, 2009). The A20-modified vectors appear to retain all other characteristics of Ad5*mut in vivo*, therefore it appears unlikely that they would be increasingly degraded by KCs. Microbe scavenging by KCs induces the release of pro-inflammatory mediators which contribute to the destruction of neighbouring hepatocytes, in addition to functioning as chemo-attractants for infiltrating neutrophils (Lieber *et al.*, 1997). Interestingly, Ad5-induced neutrophil recruitment (via MIP-2 induction) has been directly associated with acute hepatic injury and elevation of serum transaminases, ALT/AST (Muruve *et al.*, 1999). Therefore, the limited induction of pro-inflammatory effectors IL-6, RANTES and IFN-γ, reduced ALT/AST levels, minimal hepatic injury (histopathologically) and the distinct absence of an inflammatory infiltrate observed with Ad5-EGFP$_{A20}$ and Ad5-477*dl*TAYT$_{A20}$, again does not reconcile with the hypothesis that the A20-modified vectors could be scavenged more rapidly by KCs. However, we do not currently possess any evidence to confirm a differential interaction between Ad5-EGFP$_{A20}$/Ad5-477*dl*TAYT$_{A20}$ and KCs, and so we cannot eliminate this possibility. Alternatively, it is possible that redirecting the tropism of these vectors could, potentially, lead to divergent endosomal or lysosomal trafficking in KCs, with a differential outcome (eg. viral degradation, without the activation of KCs and subsequent release of cytokines). Nonetheless, it is important to note that increased vector degradation does not necessarily preclude efficient tumour targeting *in vivo*, if the affinity for the target receptor is sufficiently high (Liu *et al.*, 2009).

In addition to a reduced accumulation of A20-modified vectors in the liver, these viruses were also deposited in the spleen to a lesser extent than Ad5-EGFP$_{WT}$. KC depletion with $GdCl_3$ has been shown to reduce TNF-α levels, but increase IL-6 levels (Lieber *et al.*, 1997). It is possible that the selective depletion of KCs, increases vector availability for uptake in the spleen, and contributes to the subsequent increase in IL-6. Broader depletion of tissue macrophages and dendritic cells using clodronate liposomes (Cl_2MBP) has been shown to limit the production of IL-6, IL-12 and TNF-α (Liu & Muruve, 2003; Zhang *et al.*, 2001). This is consistent with the theory that splenic dendritic cells are a major source of IL-6 following intravenous delivery of Ad5 (Koizumi

et al., 2007). Therefore, it is likely that the reduced IL-6 levels associated with Ad5-EGFP$_{A20}$ and Ad5-477*dl*TAYT$_{A20}$ are a direct reflection of the reduced splenic sequestration of these vectors.

In addition to interacting directly with innate immune cells, Ad5 has been shown to interact with complement, natural antibodies, platelets and various other blood components (Kiang *et al.*, 2006; Lyons *et al.*, 2006; Othman *et al.*, 2007; Shayakhmetov *et al.*, 2005b; Stone *et al.*, 2007b; Tian *et al.*, 2009; Waddington *et al.*, 2008; Xu *et al.*, 2008). Moreover, several of these interactions have been shown to, or at least suggested to, contribute to KC-mediated vector clearance; either through opsonisation of the Ad5 particle with complement and/or natural antibodies (Kiang *et al.*, 2006; Xu *et al.*, 2008), or by platelet-mediated sequestration in the liver and subsequent phagocytosis of the Ad5-platelet-leukocyte aggregates by KCs (Stone *et al.*, 2007b). Ad5-induced thrombocytopenia following intravenous delivery is a well reported effect, and although not dangerous in itself, can exacerbate coagulopathic conditions (Othman *et al.*, 2007; Raper *et al.*, 2002; Stone *et al.*, 2007b). Interestingly, we did not observe any induction of thrombocytopenia at 24hrs upon infection with Ad5-EGFP$_{A20}$ or Ad5-477*dl*TAYT$_{A20}$, whereas in comparison Ad5-EGFP$_{WT}$ treated animals had significantly reduced circulating platelet levels. This can possibly be explained to some extent by the lack of hepatic transduction observed with Ad5-EGFP$_{A20}$ and Ad5-477*dl*TAYT$_{A20}$, and the recent finding that C3 activation by damaged hepatocytes, contributes to the development of acute thrombocytopenia (Kiang *et al.*, 2006; Tian *et al.*, 2009).

Lymphopenia was observed in all virally treated groups at the 24-hour time-point, but not at later time-points (in a previous, but separate experiment assessed 4 days post-infection). Type I IFN is induced during the acute phase of viral infections, including following systemic administration of Ad5 (Fejer *et al.*, 2008). Interestingly, induction of Type I IFN is causatively associated with the development of transient lymphopenia (Kamphuis *et al.*, 2006). In addition to lymphocytes, monocytic populations were also dramatically reduced in all virally infected cohorts. It is evident that distinct differences exist between the interactions of Ad5 with murine, and with human blood cells (Carlisle *et al.*, 2009; Lyons *et al.*, 2006; Nicol *et al.*, 2004). This has fundamental relevance to future clinical applications with Ad5, especially the discovery that Ad5 can bind to human erythrocytes through CAR (Carlisle *et al.*, 2009; Seiradake *et al.*, 2009), potentially impairing efficient tumour transduction. It will be interesting to determine whether or not the CAR-binding ablated virus, Ad5-477*dl*TAYT$_{A20}$, proves useful in

avoiding the agglutination of human erythrocytes, especially as this vector retains all of the liver avoidance, and tumour targeting efficiency of Ad5-EGFP$_{A20}$ (see *Chapter.*6).

Finally, the restricted tissue distribution of αvβ6 in humans is well defined, where it is associated with epithelial remodelling events such as embryogenesis, wound healing and carcinogenesis (Breuss *et al.*, 1995). Conversely, its biodistribution in murine models is not established. The integrin, αvβ6, has been shown previously to be constitutively expressed at low levels in the lung, where it is retained in a complex with TGF-β and plays a role in maintaining immunological homeostasis (Munger *et al.*, 1999). We did not detect an increased accumulation of Ad5-EGFP$_{A20}$ or Ad5-477*dl*TAYT$_{A20}$ relative to Ad5-EGFP$_{WT}$ in the lung, or indeed in any other organs analysed in this study (liver/spleen/kidney/heart). Clearly, factors other than receptor availability play a definitive role in the biodistribution of systemically delivered Ad5-based vectors. The anatomical accessibility of the organ, in addition to direct interactions between the virus and various components within the circulation, contribute to the distribution of Ad vectors (Carlisle *et al.*, 2009; Manickan *et al.*, 2006; Waddington *et al.*, 2008). Furthermore, it is difficult to propose a mechanism which underlies the altered tissue distribution of the A20-modified vectors, as the factors which determine non-retargeted Ad5 vectors are currently not well understood.

In summary, in our analysis of Ad5-EGFP$_{A20}$ and Ad5-477*dl*TAYT$_{A20}$, we have uncovered some very interesting and potentially exploitable characteristics. However, it is currently unclear whether the attributes of these A20-modifed viruses are a direct result of abrogating an interaction with FIX/C4BP *in vivo*, or whether their characteristics are solely associated with the biological effects of the A20FMDV2 targeting ligand. We previously generated, by homologous recombination, a non-retargeted control for the 477*dl*TAYT$_{A20}$ virus, pMB20-477*dl*TAYT$_{6XHIS}$, which features a 6XHIS epitope within the HI loop. This construct was never been produced, or purified as virus due to time constraints. However, it may be interesting in the future to confirm if the unusual effects observed, at least in relation to Ad5-477*dl*TAYT$_{A20}$, can be attributed to the 477*dl*TAYT mutation, or in fact to the A20FMDV2 insertion. Nonetheless, minimising vector related toxicity and off target sequestration are highly desirable qualities which need to be considered in the design of therapeutic Ads, as they can permit the use of higher doses, maximising efficacy. Therefore, a vector which displays a reduced tropism for the reticuloendothelial system, coupled with an improved safety profile following systemic delivery, may represent a means of overcoming some of the limitations of current Ad5 therapy.

CHAPTER 6. Results

Chapter.6 *In Vivo* Characterisation of Viruses; Analysis of Tumour Targeting by A20-Modified Adenoviruses Following Systemic Delivery

High efficiency retargeting to cancer-specific markers is highly desirable if adenoviral vectors are to have realistic clinical applications, particularly for the treatment of disseminated disease. However, the off-target sequestration of Ad5 in the liver remains a major obstacle to achieving this goal. A role for coagulation factors in directing liver uptake following systemic delivery has been demonstrated in recent years, and has prompted the experimental use of anti-coagulants, such as warfarin, in an attempt to increase the bioavailability of the virus (Coughlan *et al.*, 2009; Gimenez-Alejandre *et al.*, 2008; Koski *et al.*, 2009; Shashkova *et al.*, 2008; Shashkova *et al.*, 2009; Waddington *et al.*, 2007). However, the development of approaches based on this strategy remain in their infancy. To date, a genetically modified vector which combines high efficiency tumour-selective targeting combined with liver avoidance strategies and/or reduced hepatotoxicity has not been reported.

We obtained convincing *in vitro* data to support the possibility that high affinity targeting to αvβ6 *in vivo*, could supersede the dramatic enhancement conferred by the presence of coagulation factors. Therefore, an assessment of how these modified vectors performed *in vivo* in the presence of, and absence of, coagulation factors was pertinent and critical to these studies. An *in vivo* tumour targeting experiment was designed in which separate cohorts of mice (*N*=5) were administered with each virus, with or without warfarin pre-treatment to deplete vitamin-K dependent coagulation factors. A subcutaneous injection of warfarin, dissolved in peanut oil, was administered at days -3 and -1 prior to virus administration by Mr. Arif Mustafa and Dr. John Marshall, respectively. The following procedures were performed by Professor Ian R. Hart; intravenous injection of virus, extraction of blood from the tail vein, extraction of blood from the cardiac cavity immediately post-mortem, and necropsy. Liver transaminase levels were quantified from mouse serum (Axiom Veterinary Laboratories, Devon, UK).

Section.6.1 Tumour Targeting, Hepatotoxicity and Biodistribution

6.1.1. Quantification of Viral Genomes (qPCR) in DX3-β6 Xenografts. The *in vivo* tumour targeting efficiency of Ad5-EGFP$_{WT}$, Ad5-EGFP$_{A20}$ and Ad5-477*dl*TAYT$_{A20}$ was assessed following systemic delivery. Using a previously established xenograft model, $4x10^6$ DX3-β6 cells (low CAR, high αvβ6) were implanted into the right shoulder of CD1 nude female mice. A single dose of each virus ($5x10^{10}$vp/mouse) was administered by tail vein injection to separate cohorts which had, or had not, received a warfarin pre-

treatment at days -3 and -1 prior to virus administration. Mice were killed 72hrs later, tumours excised and absolute viral genome levels determined by fluorogenic quantitative real-time PCR (*Fig*.6.1). In non-warfarin treated cohorts, both Ad5-EGFP$_{A20}$ and Ad5-477*dl*TAYT$_{A20}$ displayed enhanced tumour uptake when compared with Ad5-EGFP$_{WT}$, improving delivery ~2-fold (p>0.05, *not significant*) and ~3-fold (p=0.019), respectively. Pre-treatment with warfarin, marginally improved tumour uptake of Ad5-EGFP$_{WT}$, although not significantly (p=0.395). Interestingly, warfarin pre-treatment reduced uptake of Ad5-EGFP$_{A20}$ (~1.6-fold decrease; *not significant*) and Ad5-477*dl*TAYT$_{A20}$ (~3-fold decrease; p=0.004) when compared with the corresponding non-warfarinised groups.

6.1.2 Histological Examination of DX3-β6 Tumour Xenografts; H&E Staining and Immunostaining for αvβ6 Integrin. Previous attempts to demonstrate anti-tumoural efficacy using the DX3-β6 xenograft model had failed (see *Chapter*.3). This possibly was due to a combination of factors, including the fact that the -β6 expression in these cells *in vivo* appeared to be lost over time. In addition, this model is a poorly vascularised tumour which rapidly becomes necrotic. Therefore, it is not ideal for studying the effects of Ad5, especially in longer term experiments. However, we had observed in previous experiments that the tumours which were harvested from animals sacrificed at early time points (~3 weeks), retained high level expression of -β6 (see *Fig*.3.23D). Several attempts to develop other low CAR, high αvβ6 expressing xenograft models were not successful (TR126, TR138 and BT-20 cells injected into CD1 nude mice did not result in tumours). Therefore, we had no alternative but to use the DX3-β6 model for this short term targeting experiment (~3 weeks).

$4x10^6$ DX3-β6 cells were implanted subcutaneously into the right shoulder of CD1 nude female mice. When tumours reached approximately 125mm^3 (~3 weeks) animals were subjected to various treatments (see *Section.*6.1.1). Animals were killed 3 days after virus delivery, and tumours harvested for analysis and histological examination. Fortunately, large areas of the DX3-β6 tumours stained strongly positive for -β6 expression, despite extensive necrosis throughout the tissue (*Fig*.6.1B). An IgG control antibody was used to confirm that the -β6 immunostaining was specific. Immunostaining of warfarinised tumours yielded some unexpected results. All sections were processed on the same day, using identical reagents, (antibody dilutions, blocking kits) however the warfarin pre-treated tumours showed extensive staining even in the IgG controls (*Fig*.6.1C). Therefore, we cannot determine the -β6 expression status of these tumours, and indeed whether or not warfarin pre-treatment affects or down-regulates surface expression of αvβ6 *in vivo*.

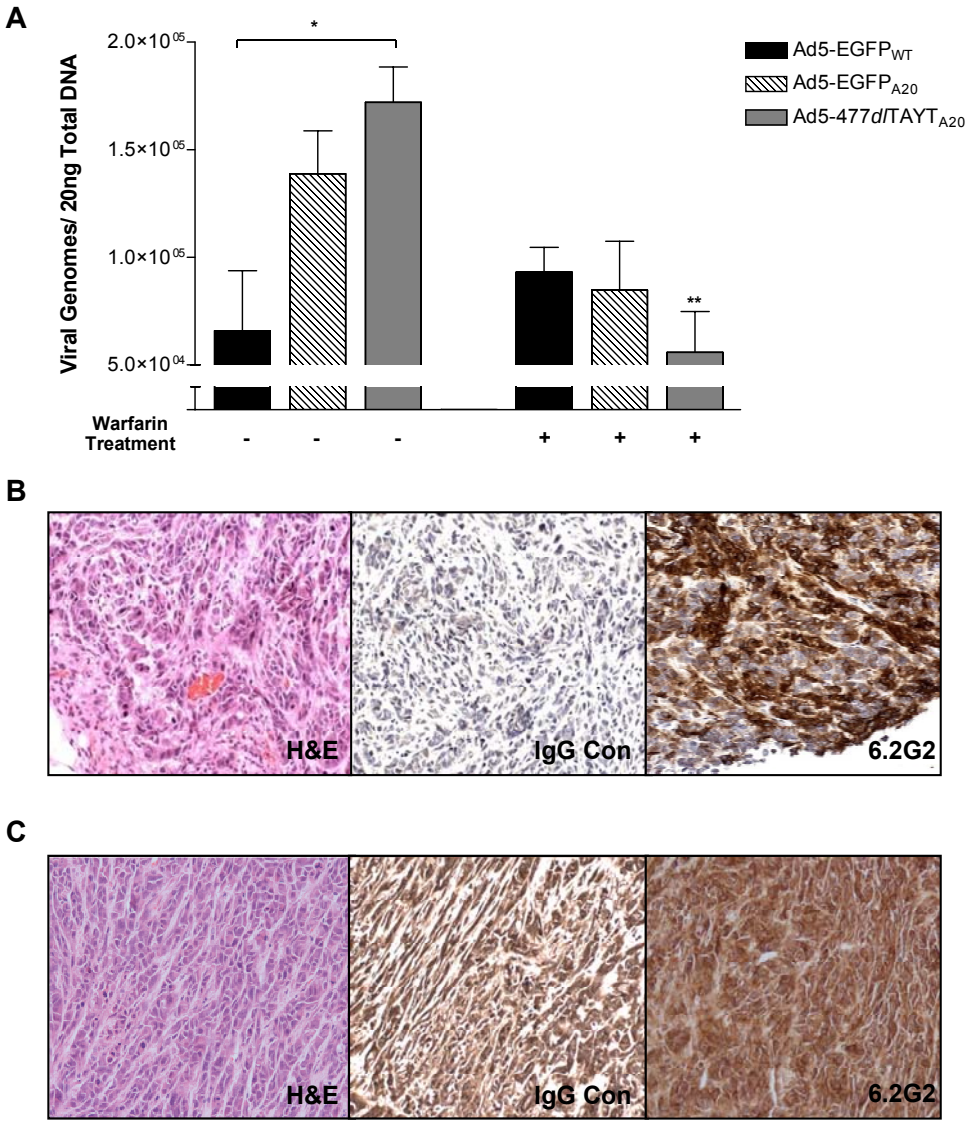

***Figure*.6.1 (A) Quantification of Viral Genomes in DX3-β6 Tumour Xenografts Following Systemic Delivery.** CD1 nude female mice, bearing DX3-β6 xenografts, were injected either with PBS, Ad5-EGFP$_{WT}$, Ad5-EGFP$_{A20}$ or Ad5-477*dl*TAYT$_{A20}$ (5x10^{10}vp/mouse) by intravenous tail vein injection, without (-) or with (+) a pre-dose of warfarin (133µg) at days -3 and -1 prior to virus administration (day 0). Mice were killed after 72hrs, necropsy performed and DNA extracted from tumours. Absolute viral genomes were quantified by TaqMan Real-Time Quantitative PCR (qPCR) using a probe to detect the hexon region of the genome (see *Section.*2.2.7). Data presented represent the mean ± SEM (*N*=4/5 mice) of triplicate qPCR samples and are representative of two independent qPCR experiments. Statistical significance was determined using the unpaired Student's t-test to compare the means of two samples (* indicates a *P*-value of <0.05, ** *p*<0.01, bars indicate SEM). Statistics displayed above the histograms for warfarin pre-treated cohorts refer to the difference when compared to the corresponding untreated cohort. **(B) Histology and Immunohistochemical Analysis of DX3-β6 Tumours (Non-warfarinised).** *From left to right*; Haematoxylin and Eosin staining showing a region of necrosis within a DX3-β6 tumour section, IgG$_1$ control antibody staining, and immunostaining for αvβ6 using 6.2G2. Sections were photographed at a magnification of 200X using a Zeiss AxioCam MRc5 camera and Axiovision Software (Zeiss, Germany). **(C) Histology and Immunohistochemical Analysis of DX3-β6 Tumours (Warfarinised).** *From left to right*; Haematoxylin and Eosin staining of DX3-β6 tumour section, IgG$_1$ control antibody staining, and immunostaining for αvβ6 using 6.2G2. Sections were photographed at a magnification of 200X using a Zeiss AxioCam MRc5 camera and Axiovision Software (Zeiss, Germany).

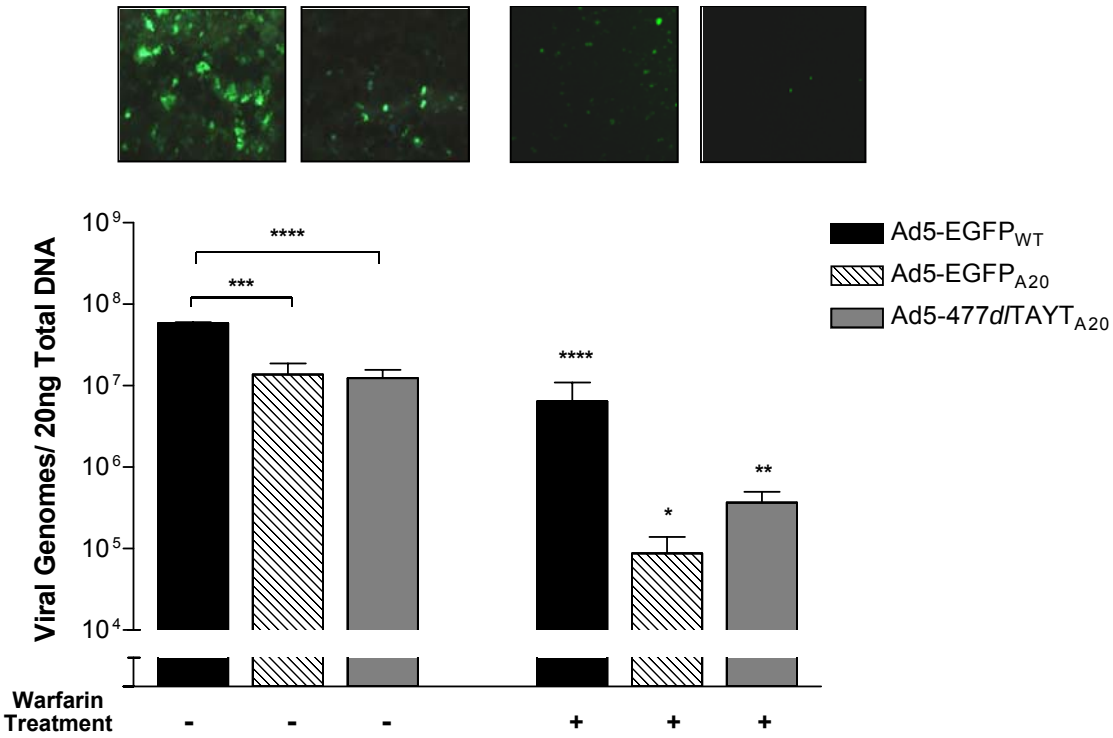

Figure.*6.2 Quantification of Viral Genomes in Murine Liver Following Systemic Delivery.** CD1 nude female mice, bearing DX3-β6 xenografts, were injected either with PBS, Ad5-EGFP$_{WT}$, Ad5-EGFP$_{A20}$ or Ad5-477*dl*TAYT$_{A20}$ (5x10^{10}vp/mouse) by intravenous tail vein injection, without (-) or with (+) a pre-dose of warfarin (133µg) at days -3 and -1 prior to virus administration (day 0). Mice were killed after 72hrs, necropsy performed and DNA extracted from liver tissue. Absolute viral genomes were quantified by TaqMan Real-Time Quantitative PCR (qPCR) using a probe to detect the hexon region of the genome (see *Section*.2.2.7). Data presented represent the mean ± SEM (*N*=4/5 mice) of triplicate qPCR samples and are representative of two independent qPCR experiments. Statistical significance was determined using the unpaired Student's *t*-test to compare the means of two samples (* indicates a *P*-value of <0.05, ** *p*<0.01, *** *p*<0.001, * *p*<0.0001, bars indicate SEM). Statistics displayed above the histograms for warfarin pre-treated cohorts refer to the difference when compared to the corresponding untreated cohort. Inset: Frozen liver sections (5µm) were immunostained with anti-E1A antibody (13 S-5) for Ad5-EGFP$_{WT}$ and Ad5-EGFP$_{A20}$ groups only, with/without warfarin pre-treatment. Immunofluorescence was visualised using a Zeiss laser scanning microscope (LSM 510META) and pictures captured using LSM 5 Software, version 3.2 (Zeiss, Germany).

6.1.3 Quantification of Viral Genomes (qPCR) in Murine Liver. Absolute numbers of viral genomes in the liver, for both non-warfarinised and warfarinised groups, were measured by quantitative real time PCR (*Fig*.6.2). As expected for this dose (5x10^{10}vp/mouse), there was significant sequestration of Ad5-EGFP$_{WT}$ in the livers of non-warfarinised animals. In agreement with our results (*see Chapter*.5), and data published by Shayakhmetov and colleagues, the putative FIX/C4BP-binding ablated vector, Ad5-477*dl*TAYT$_{A20}$, displayed a significantly reduced liver tropism with ~5-fold fewer genomes detected (*p*<0.0001) when compared to Ad5-EGFP$_{WT}$ (Shayakhmetov *et al.*, 2005b). Again, in agreement with data presented in *Chapter*.5, Ad5-EGFP$_{A20}$

displayed an identical profile (p=0.0002). Additionally, this profile was consistent with *in vitro* results presented in *Chapter*.4, where we observed that Ad5-EGFP$_{A20}$, in addition to Ad5-477*dl*TAYT$_{A20}$, failed to interact with FIX to promote infectivity enhancement. These differences were further supported by immunostaining for viral antigen, E1A (*Fig.* 6.2;*inset* and *Fig*.6.3A). In animals subjected to warfarin pre-treatment, a significant reduction in E1A expression (*Fig*.6.2;*inset* and *Fig*.6.4A), in addition to an overall reduction in viral genome levels (~9-fold, p<0.0001), was found in the Ad5-EGFP$_{WT}$ group. However, warfarin had a more striking effect on the liver sequestration of the A20-modified vectors, Ad5-EGFP$_{A20}$ and Ad5-477*dl*TAYT$_{A20}$, with viral genomes reduced by ~160-fold (p=0.035), and ~34-fold (p=0.006) respectively, when compared with the untreated Ad5-EGFP$_{A20}$/Ad5-477*dl*TAYT$_{A20}$ groups.

6.1.4 Histological Examination of Murine Liver Tissue; H&E Staining and Immunostaining for E1A. Immunostaining of paraffin embedded liver tissue demonstrated a clear reduction in the extent of E1A expression in the Ad5-EGFP$_{A20}$ and Ad5-477*dl*TAYT$_{A20}$ groups, when compared to the Ad5-EGFP$_{WT}$ group (*Fig*.6.3A). Moreover, haematoxylin and eosin staining of non-warfarinised liver sections also revealed distinct histological differences between the non-warfarinised Ad5-EGFP$_{WT}$ group, and the Ad5-EGFP$_{A20}$/Ad5-477*dl*TAYT$_{A20}$ groups (*Fig*.6.3B+C), supporting the data shown in *Fig*.6.3A and *Fig*.6.2;*inset*. At a magnification of 200X, the livers of the Ad5-EGFP$_{WT}$ treated mice showed prominent hepatocyte atypia, with loss of cellular and nuclear definition, in addition to widespread hepatocyte necrosis (*Fig*.6.3B). In contrast, the hepatocytes of mice which had been treated with Ad5-EGFP$_{A20}$ or Ad5-477*dl*TAYT$_{A20}$ more closely resembled the untreated PBS control group, with intact cellular junctions and nuclei. These irregularities were more evident at higher magnifications (400X), where several enlarged, hyperchromatic nuclei could be observed in the Ad5-EGFP$_{WT}$ group (*Fig*.6.3C). Moreover, the lack of cellular integrity in the tissue of this group was dramatic, especially when compared with tissue obtained from the Ad5-EGFP$_{A20}$ and Ad5-477*dl*TAYT$_{A20}$ treated cohorts.

In warfarin pre-treated animals, no E1A expression was detected in the livers of any cohort (*Fig*.6.4A). This was consistent with the significantly reduced levels of viral genomes sequestered in the livers of these animals (see *Fig*.6.2). Furthermore, histological assessment of this tissue (H&E) did not show any major differences between the PBS, and virus treated groups although, again, the Ad5-EGFP$_{WT}$ treated groups appeared to display slight abnormalities (enlarged cells and slightly swollen nuclei were visible).

***Figure*.6.3 (A) E1A Immunostaining of Non-Warfarinised Murine Liver Sections (100X Magnification).** CD1 nude female mice, bearing DX3-β6 xenografts, were injected either with PBS, Ad5-$EGFP_{WT}$, Ad5-$EGFP_{A20}$, or Ad5-477*dl*$TAYT_{A20}$ ($5x10^{10}$vp/mouse) by intravenous tail vein injection (day 0). Mice were killed after 72hrs, livers harvested and tissue processed for paraffin embedding. Tissue sectioning and E1A immunostaining, using anti-Adenovirus/E1A [M58], was performed by Keyur Trivedi (Pathology Services) at the Institute of Cancer. **(B) Haematoxylin and Eosin (H&E) Staining of Non-Warfarinised Murine Liver Sections (200X Magnification).** Liver sections for each cohort; PBS control, Ad5-$EGFP_{WT}$, Ad5-$EGFP_{A20}$ and Ad5-477*dl*$TAYT_{A20}$ were stained with H&E (performed by Keyur Trivedi, as above), and tissue assessed histopathologically. Histological analysis was performed blindly by a qualified pathologist (Prof. Gareth Thomas), without prior knowledge of the specimens. **(C) Haematoxylin and Eosin (H&E) Staining of Non-Warfarinised Murine Liver Sections (400X Magnification).** Sections from PBS, Ad5-$EGFP_{WT}$, Ad5-$EGFP_{A20}$ and Ad5-477*dl*$TAYT_{A20}$ cohorts were also examined histopathologically. All sections were photographed using a Zeiss AxioCam MRc5 camera and Axiovision Software (Zeiss, Germany).

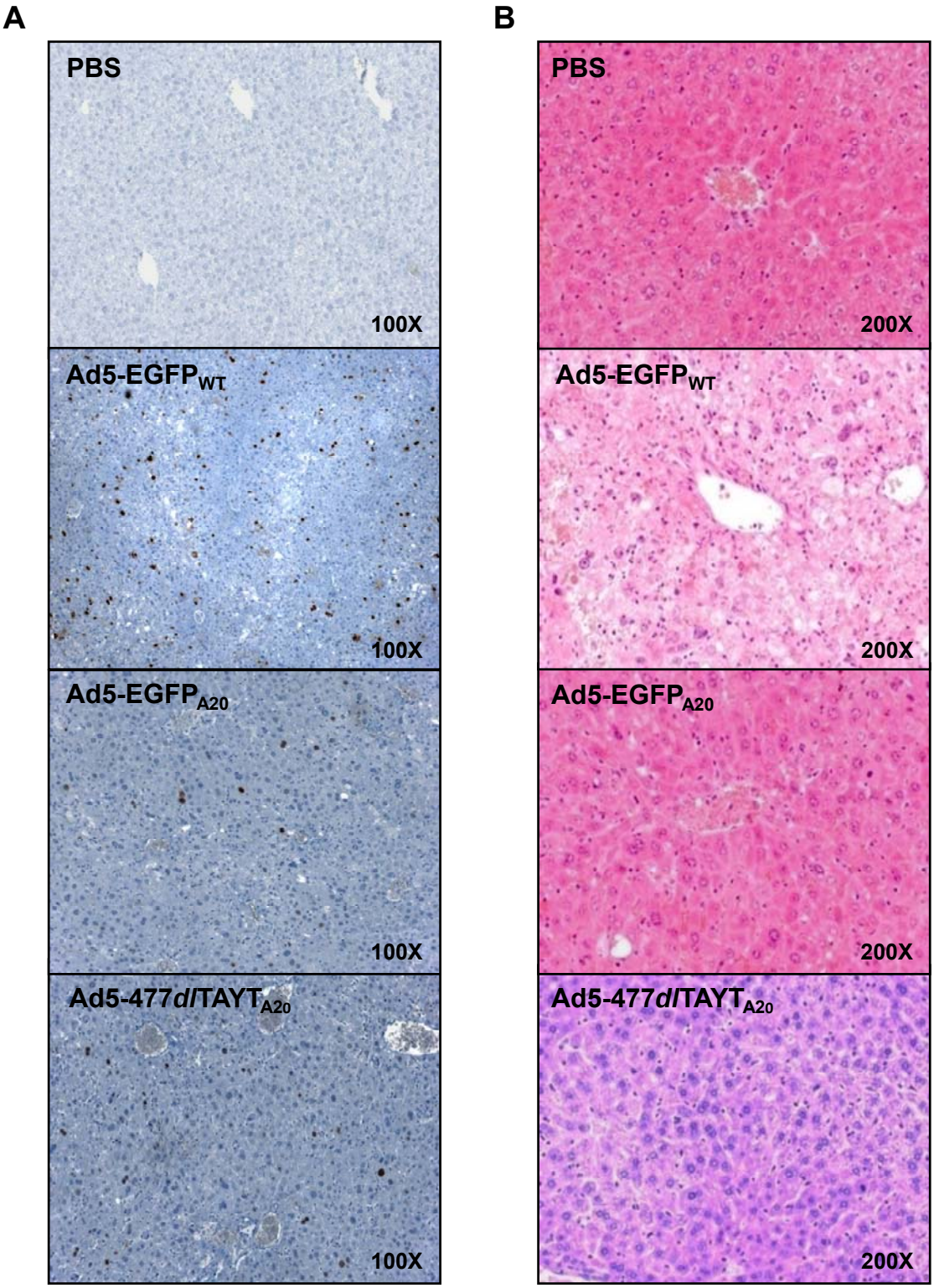
A
PBS
100X
Ad5-EGFP$_{WT}$
100X
Ad5-EGFP$_{A20}$
100X
Ad5-477*d*/TAYT$_{A20}$
100X
B
PBS
200X
Ad5-EGFP$_{WT}$
200X
Ad5-EGFP$_{A20}$
200X
Ad5-477*d*/TAYT$_{A20}$
200X

C

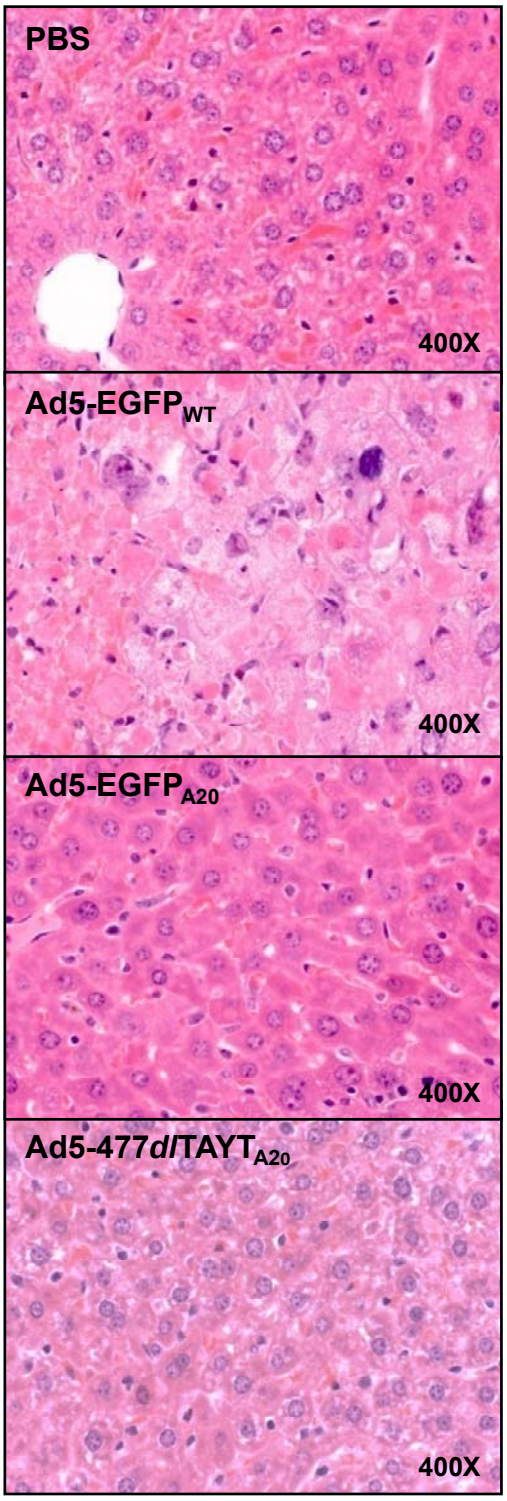
PBS
400X
Ad5-EGFP$_{WT}$
400X
Ad5-EGFP$_{A20}$
400X
Ad5-477*dl*TAYT$_{A20}$
400X

***Figure*.6.4 (A) E1A Immunostaining of Warfarinised Murine Liver Sections (100X Magnification).** CD1 nude female mice, bearing DX3-β6 xenografts, were pre-treated with warfarin (133µg) on days -3, and -1 after which they were injected either with PBS, Ad5-EGFP$_{WT}$, Ad5-EGFP$_{A20}$, or Ad5-477*dl*TAYT$_{A20}$ (5x10^{10}vp/mouse) by intravenous tail vein injection (day 0). Mice were killed after 72hrs, livers harvested and tissue processed for paraffin embedding. Tissue sectioning and E1A immunostaining, using anti-Adenovirus/E1A [M78], was performed by Keyur Trivedi (Pathology Service), at the Institute of Cancer. **(B) Haematoxylin and Eosin (H&E) Staining of Warfarinised Murine Liver Sections (200X Magnification).** Liver sections for each warfarin pre-treated cohort; PBS control, Ad5-EGFP$_{WT}$, Ad5-EGFP$_{A20}$ and Ad5-477*dl*TAYT$_{A20}$ were stained with H&E (performed by Keyur Trivedi, as above), and tissue assessed histopathologically. Histological analysis was performed blindly by a qualified pathologist (Prof. Gareth Thomas), without prior knowledge of the specimens. Sections were photographed at a magnification of 200X using a Zeiss AxioCam MRc5 camera and Axiovision Software (Zeiss, Germany).

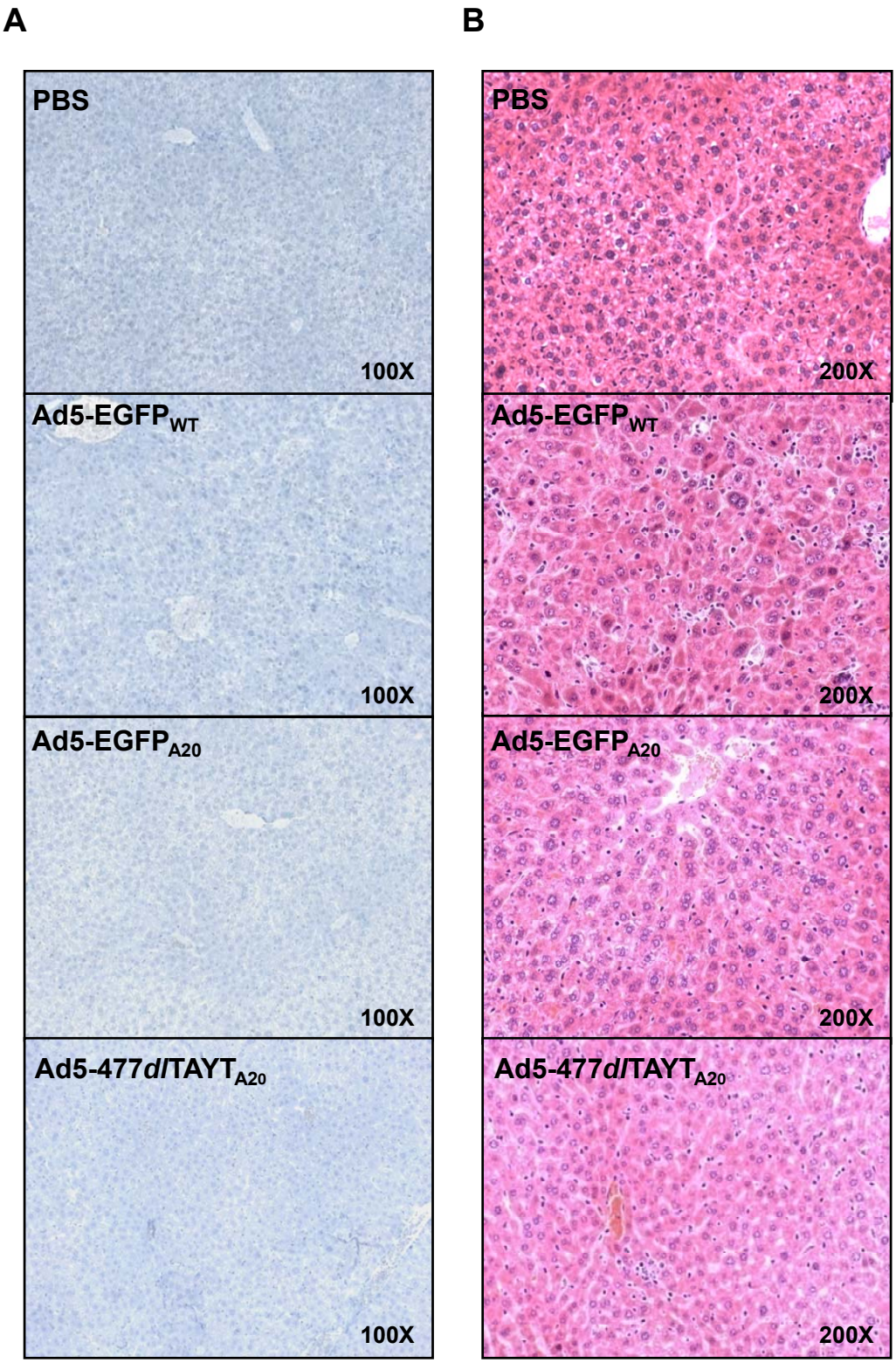
A
B
PBS
100X
PBS
200X
Ad5-EGFP$_{WT}$
100X
Ad5-EGFP$_{WT}$
200X
Ad5-EGFP$_{A20}$
100X
Ad5-EGFP$_{A20}$
200X
Ad5-477*d*/TAYT$_{A20}$
100X
Ad5-477*d*/TAYT$_{A20}$
200X

6.1.5 Determination of Toxicity. The hepatotoxicity induced following systemic delivery of replicating adenoviruses in murine models is dose-limiting (Cascallo *et al.*, 2007; Engler *et al.*, 2004). Therefore, we compared the toxicity induced upon systemic delivery of Ad5-EGFP$_{WT}$, Ad5-EGFP$_{A20}$ and Ad5-477*dl*TAYT$_{A20}$ (5x10^{10}vp/mouse), assessing % body weight variation on a daily basis and in addition, serum transaminase (ALT and AST) levels in serum, obtained at the time of death (Axiom Veterinary Laboratories, Devon, UK).

In non-warfarinised mice, there were significant variations in body weight (%) between the Ad5-EGFP$_{WT}$ group, and the A20-modified groups Ad5-EGFP$_{A20}$/Ad5-477*dl*TAYT$_{A20}$ (*Fig*.6.5A). Variation in the Ad5-EGFP$_{WT}$ group on day 2 was -8.2±1.3%. There were significant differences between the Ad5-EGFP$_{WT}$ group and the Ad5-EGFP$_{A20}$ (-4.0±1.4%, p=0.003), and Ad5-477*dl*TAYT$_{A20}$ (-1.98±2.17%, p=0.002) treated groups, which more closely resembled the PBS control cohort (p>0.05). At this time-point only Ad5-EGFP$_{WT}$ differed statistically from the PBS control group (p=0.0006). On day 3, the percentage weight variation in the Ad5-EGFP$_{WT}$ group was -11.7±2.2%, differing significantly from the Ad5-EGFP$_{A20}$ group (p=0.004), which remained largely unchanged from day 2 at -3.8±3.2%. In addition, no significant variation in the Ad5-477*dl*TAYT$_{A20}$ group (-1.83±1.72%) from day 2-3 was observed, which differed significantly when compared to Ad5-EGFP$_{WT}$ (p=0.0001) on day 3. In warfarin treated groups no significant weight variation was observed at any time point (*Fig*.6.5B), except for Ad5-EGFP$_{WT}$ on day 1 when compared with PBS control (p=0.031).

In the non-warfarinised Ad5-EGFP$_{WT}$ group, there were significant elevations in both serum ALT (*Fig*.6.5C) and AST (*Fig*.6.5E) levels, which were substantially lower in both of the A20-modified virus groups. ALT levels in Ad5-EGFP$_{A20}$ and Ad5-477*dl*TAYT$_{A20}$ treated groups were ~3-fold (p=0.025), and ~10-fold (p=0.009) lower than Ad5-EGFP$_{WT}$. In addition, when compared to Ad5-EGFP$_{WT}$, AST levels were ~3-fold (p=0.0003), and ~10-fold (p<0.0001) lower in Ad5-EGFP$_{A20}$ and Ad5-477*dl*TAYT$_{A20}$ treated groups, respectively. These data corroborated previous results (*Fig*.6.3B+C and *Chapter.*5), confirming that the A20-modifed viruses have reduced hepatotoxicity *in vivo*.

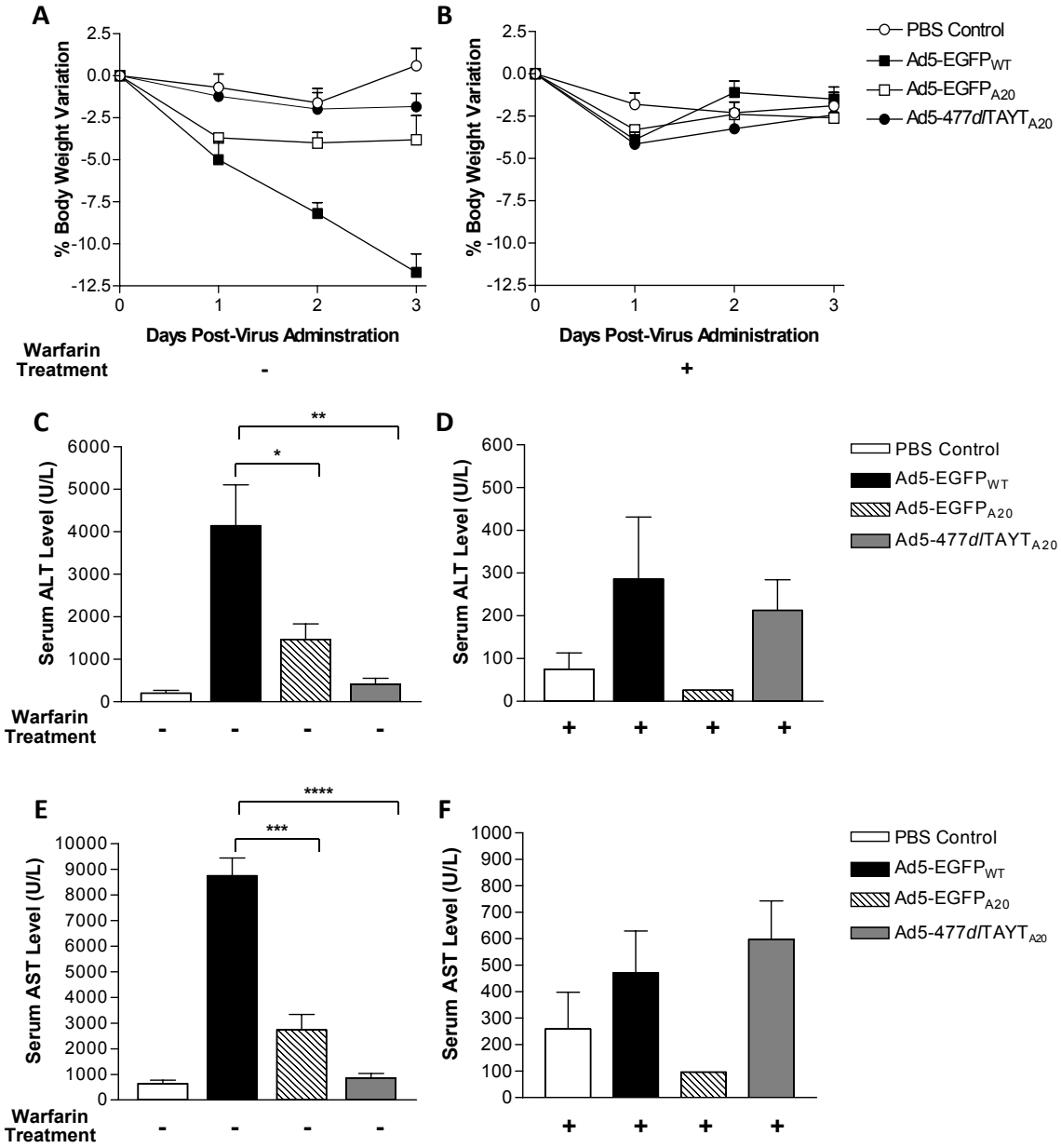

Figure*.6.5 Determination of Toxicity Following Systemic Administration of Virus. (A)** Body weight variation (%) was assessed on a daily basis for CD1 nude cohorts which received intravenous delivery of PBS, Ad5-EGFP$_{WT}$, Ad5-EGFP$_{A20}$ or Ad5-477*dl*TAYT$_{A20}$ (5x10^{10}vp/mouse). **(B)** Percentage body weight variation was assessed for each cohort as described in (A), which had also received a warfarin pre-dose at days -1 and -3, prior to virus administration (day 0). **(C)** Blood samples were obtained immediately post-mortem (72hrs after virus administration) and serum alanine transaminase (ALT) levels were quantified for each of the non-warfarinised groups; PBS, Ad5-EGFP$_{WT}$, Ad5-EGFP$_{A20}$ or Ad5-477*dl*TAYT$_{A20}$. **(D)** Serum ALT levels were quantified for warfarin pre-treated cohorts, as described in (C). **(E)** Serum aspartate aminotransferase (AST) levels were quantified for all non-warfarinised groups; PBS, Ad5-EGFP$_{WT}$, Ad5-EGFP$_{A20}$ or Ad5-477*dl*TAYT$_{A20}$. **(F)** Serum AST levels were quantified for all groups which received a warfarin pre-dose, as described in (E). Data represent the mean ± SEM (*N*=4/5 mice), with the exception of the Ad5-EGFP$_{A20}$ warfarin pre-treated group in (D) and (F), for which only one blood sample was obtained (*N*=1). Statistical significance was determined using the unpaired Student's *t*-test comparing the means of two samples (* indicates a *P*-value of <0.05, ** *p*<0.01, *** *p*<0.001, * *p*<0.0001, bars indicate SD).

As warfarin pre-treatment can reduce the hepatic uptake of wild-type Ad5 significantly, serum levels of ALT (*Fig*.6.5D) and AST (*Fig*.6.5F) were also analysed for Ad5-$EGFP_{WT}$, Ad5-$EGFP_{A20}$ and Ad5-477*dl*$TAYT_{A20}$ warfarin pre-treated groups. Compared with untreated groups, pre-treatment with warfarin significantly reduced ALT and AST levels for Ad5-$EGFP_{WT}$ (ALT ~15-fold reduction; p=0.007 and AST ~20-fold; p<0.0001). Unfortunately, only one blood sample was obtained for the warfarinised Ad5-$EGFP_{A20}$ group, therefore we were unable to perform statistical analysis on this group. However, warfarin pre-treatment did not further reduce the already low levels of ALT induced by Ad5-477*dl*$TAYT_{A20}$ when compared to the corresponding, untreated control group (p=0.263). Similarly, AST levels were not reduced significantly upon warfarin pre-treatment (p=0.29).

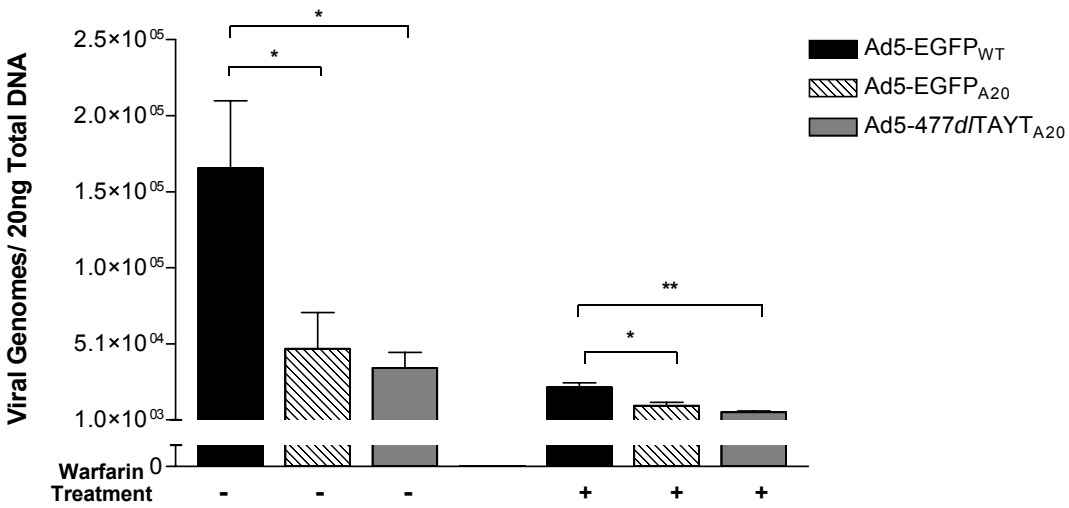

***Figure*.6.6 Quantification of Viral Genomes in Spleen Following Systemic Delivery.** CD1 nude female mice, bearing DX3-β6 xenografts, were injected either with PBS, Ad5-$EGFP_{WT}$, Ad5-$EGFP_{A20}$ or Ad5-477*dl*$TAYT_{A20}$ ($5x10^{10}$vp/mouse) by intravenous tail vein injection, without (-) or with (+) a pre-dose of warfarin (133µg) at days -3 and -1 prior to virus administration (day 0). Mice were killed after 72hrs, necropsy performed and DNA extracted from spleen tissue. Absolute viral genomes were quantified by TaqMan Real-Time Quantitative PCR (qPCR) using a probe to detect the hexon region of the genome (see *Section*.2.2.7). Data presented represent the mean ± SEM (N=4/5 mice) of triplicate qPCR samples and are representative of two independent qPCR experiments. Statistical significance was determined using the unpaired Student's t-test to compare the means of two samples (* indicates a P-value of <0.05, ** p<0.01, bars indicate SEM). Statistics displayed above the histograms for warfarin pre-treated cohorts refer to the difference when compared to the corresponding untreated cohort.

6.1.6 Quantification of Viral Genomes (qPCR) in Murine Spleen. In addition to differences in liver sequestration, the splenic uptake of Ad5-$EGFP_{A20}$ and Ad5-477*dl*$TAYT_{A20}$ was significantly altered when compared with Ad5-$EGFP_{WT.}$ In non-warfarinised groups, absolute Ad5-$EGFP_{WT}$ genome levels in the spleen (*Fig*.6.6) were

significantly higher than the Ad5-EGFP$_{A20}$ (~3-fold, p=0.046), and Ad5-477*dl*TAYT$_{A20}$ groups (~5-fold, p=0.037). Warfarin pre-treatment reduced Ad5-EGFP$_{WT}$ accumulation in the spleen (~7-fold, p=0.012), albeit only to a level equivalent to Ad5-EGFP$_{A20}$ (p=0.316), or Ad5-477*dl*TAYT$_{A20}$ alone (p=0.224). Warfarin pre-treatment did not further enhance the splenic detargeting already observed with the Ad5-EGFP$_{A20}$ (p=0.206), however it did reduce the sequestration of Ad5-477*dl*TAYT$_{A20}$ in the spleen significantly (p=0.03).

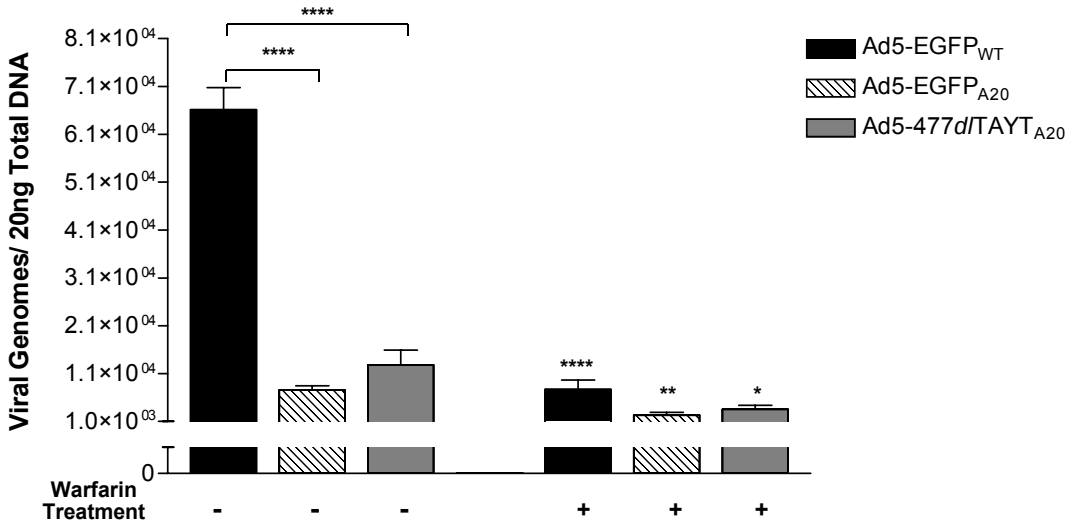

***Figure*.6.7 Quantification of Viral Genomes in Murine Lung Following Systemic Delivery.** CD1 nude female mice, bearing DX3-β6 xenografts, were injected either with PBS, Ad5-EGFP$_{WT}$, Ad5-EGFP$_{A20}$ or Ad5-477*dl*TAYT$_{A20}$ (5x10^{10}vp/mouse) by intravenous tail vein injection, without (-) or with (+) a pre-dose of warfarin (133µg) at days -3 and -1 prior to virus administration (day 0). Mice were killed after 72hrs, necropsy performed and DNA extracted from lung tissue. Absolute viral genomes were quantified by TaqMan Real-Time Quantitative PCR (qPCR) using a probe to detect the hexon region of the genome (see *Section*.2.2.7). Data presented represent the mean ± SEM (N=4/5 mice) of triplicate qPCR samples and are representative of two independent qPCR experiments. Statistical significance was determined using the unpaired Student's t-test to compare the means of two groups (* indicates a P-value of <0.05, ** p<0.01, **** p<0.0001, bars indicate SEM). Statistics displayed above the histogram for warfarin pre-treated cohorts refer to the difference when compared to the corresponding untreated cohort.

6.1.7 Quantification of Viral Genomes (qPCR) in Murine Lung. In non-warfarinised animals, the A20-modified viruses, Ad5-EGFP$_{A20}$ and Ad5-477*dl*TAYT$_{A20}$, were also differentially distributed in the lung when compared to Ad5-EGFP$_{WT}$ (*Fig*.6.7). Ad5-EGFP$_{A20}$ and Ad5-477*dl*TAYT$_{A20}$ appear to naturally be detargeted from murine lung tissue (~9-fold reduction, p<0.0001), and (~5-fold reduction, p<0.0001), when compared with Ad5-EGFP$_{WT}$. Warfarin pre-treatment reduced significantly the pulmonary accumulation of all viruses, Ad5-EGFP$_{WT}$ (~9-fold, p<0.0001), Ad5-EGFP$_{A20}$ (~3-fold, p=0.003) and Ad5-477*dl*TAYT$_{A20}$ (~4-fold, p=0.02). However, the Ad5-EGFP$_{WT}$

treated with warfarin did not differ significantly from the untreated Ad5-EGFP$_{A20}$ (p=0.948), or Ad5-477*dl*TAYT$_{A20}$ cohorts (p=0.205).

6.1.8 Quantification of Viral Genomes (qPCR) in Murine Stomach. Prior studies have identified that murine stomach tissue expresses αvβ6 (Dr. Antonio Saha, unpublished data with permission). Immunostaining for αvβ6 integrin in murine stomach tissue was performed using 6.2G2 (*Fig*.6.8B). We also quantified the levels of viral genomes, for each cohort, in the stomach (*Fig*.6.8A). No significant differences in viral genome numbers were detected between the αvβ6-retargeted viruses, Ad5-EGFP$_{A20}$ and Ad5-477*dl*TAYT$_{A20}$, and the non-retargeted virus, Ad5-EGFP$_{WT}$ (p=0.100, p=0.136, respectively). When compared with untreated, warfarin pre-treatment did not alter Ad5-EGFP$_{WT}$ genome levels in the stomach (p=0.706), however it did alter significantly the accumulation of Ad5-EGFP$_{A20}$ and Ad5-477*dl*TAYT$_{A20}$ (both ~2-fold reduction, p=0.025 and p=0.069, respectively).

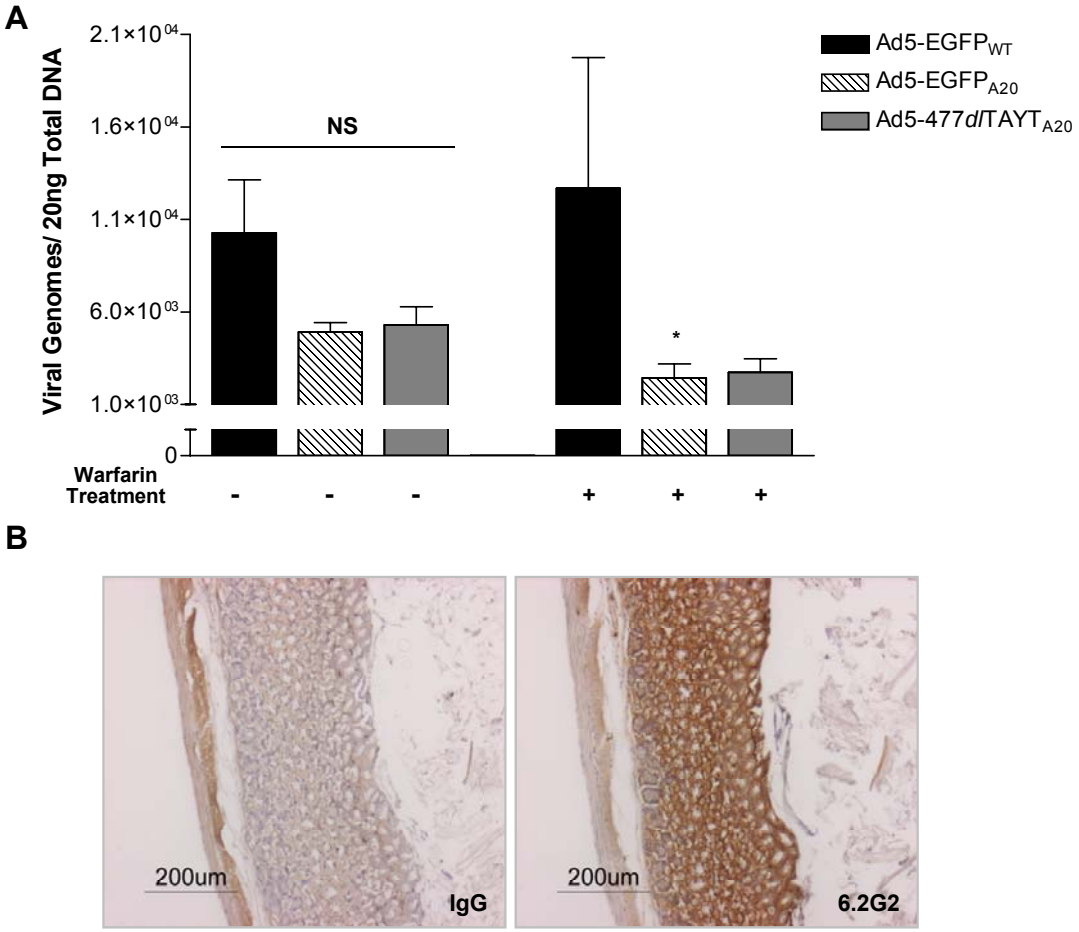

***Figure.*6.8 (A) Quantification of Viral Genomes in Murine Stomach Following Systemic Delivery. CD1** nude female mice, bearing DX3-β6 xenografts, were injected either with PBS, Ad5-EGFP$_{WT}$, Ad5-EGFP$_{A20}$ or Ad5-477*dl*TAYT$_{A20}$ (5x10^{10}vp/mouse) by intravenous tail vein injection, without (-) or with (+) a pre-dose of warfarin (133μg) at days -3 and -1 prior to virus administration (day 0). Mice were killed after 72hrs, necropsy performed and DNA extracted from stomach tissue. Absolute viral genomes were quantified by TaqMan Real-Time Quantitative PCR (qPCR) using a probe to detect the hexon region of the genome (see *Section.*2.2.7). Data presented represent the mean ± SEM (*N*=4/5 mice) of triplicate qPCR samples and are representative of two independent qPCR experiments. Statistical significance was determined using the unpaired Student's *t*-test to compare the means of two groups (* indicates a *P*-value of <0.05, NS *p*>0.05, bars indicate SEM). Statistics displayed on the histogram for warfarin pre-treated cohorts refer to the difference when compared to the corresponding untreated cohort. **(B) Immunostaining of Stomach Tissue for Murine αvβ6 Integrin.** Immunostaining was performed by Dr. Antonio Saha using anti-αvβ6 antibody, 6.2G2 (unpublished data, with permission).

Hepatotoxicity is a dose-limiting factor for the systemic delivery of many adenoviral vectors (Alemany *et al.*, 2000a; Alemany & Curiel, 2001; Lieber *et al.*, 1997). Therefore, high efficiency, tumour-specific targeting with Ad5 is desirable as it can permit the reduction of vector dose administered *in vivo*, and ultimately limit vector-related toxicity (Engler *et al.*, 2004). The overexpression of αvβ6 in a wide range of epithelial malignancies and fibrotic conditions, coupled with its prognostic associations in common cancers such as breast, ovarian, pancreatic, lung and colorectal carcinoma, make it an attractive target for engineered adenoviruses (Ahmed *et al.*, 2002b; Bates *et al.*, 2005; Elayadi *et al.*, 2007; Sipos *et al.*, 2004). However, despite extensive evidence supporting the potential for αvβ6 as a molecular target (Ahmed *et al.*, 2002b; Bates *et al.*, 2005; Breuss *et al.*, 1995; Elayadi *et al.*, 2007; Hazelbag *et al.*, 2007; Marsh *et al.*, 2008; Thomas *et al.*, 2001a; Thomas *et al.*, 2001b; Thomas *et al.*, 2006a; Van Aarsen *et al.*, 2008), there have been no previous attempts to design an adenoviral vector redirected to αvβ6 for therapeutic applications.

Section.6.1 *In Vivo* Effects of Coagulation Factor Depletion on Tumour/Liver Targeting and Biodistribution Following Systemic Delivery

We used the DX3-β6 xenograft model (low CAR, high αvβ6) to compare the tumour targeting efficiency of Ad5-EGFP$_{WT}$, Ad5-EGFP$_{A20}$ and Ad5-477*dl*TAYT$_{A20}$ following systemic delivery and, in a parallel experiment, assessed the effects of coagulation factor depletion on uptake of each vector in the tumour and the liver. Vector induced hepatotoxicity was determined by observing the daily body weight variation of the animals, and was detected post-mortem by histological examination of liver tissue, and quantification of serum transaminases (AST/ALT). In addition, a limited biodistribution was carried out for each virus, quantifying viral genome DNA levels in the liver, spleen, lung, and stomach by real time quantitative PCR.

The biodistribution profiles of the A20-retargeted vectors, Ad5-EGFP$_{A20}$ and Ad5-477*dl*TAYT$_{A20}$, were altered distinctly from that of Ad5-EGFP$_{WT}$. Most importantly however, both retargeted viruses displayed an increased accumulation of genomes in the tumour relative to Ad5-EGFP$_{WT}$, although this difference was not as dramatic as initially hoped. The Ad5-477*dl*TAYT$_{A20}$ vector appeared to perform slightly more efficiently than Ad5-EGFP$_{A20}$ in its ability to reach the tumour, possibly due to its auxiliary affinity for HSPGs (see *Chapter*.4). It is possible that this produced an additive

targeting effect when combined with the ability of Ad5-477*dl*TAYT$_{A20}$ to interact with αvβ6 through the A20-insertion.

In agreement with a previous study, which demonstrated that the 477*dl*TAYT modification was sufficient to significantly reduce the hepatic sequestration of the corresponding vector (Shayakhmetov *et al.*, 2005b), reductions in both the hepatocyte transduction, and liver accumulation, of Ad5-477*dl*TAYT$_{A20}$ genomes, were observed. Interestingly, there was also a significant reduction in the level of absolute genomes detected in the liver with Ad5-EGFP$_{A20}$ (~5-fold, p=0.0002) when compared with Ad5-EGFP$_{WT}$. These findings were paralleled by the significantly reduced hepatotoxicity and lack of transaminitis induced by both A20-modified vectors. Furthermore, these data supported the hypothesis that the Ad5-EGFP$_{A20}$ vector, which failed to interact with FIX *in vitro* to promote infectivity enhancement, was phenotypically similar to Ad5-477*dl*TAYT$_{A20}$, despite lacking the genetic modification of the putative blood factor binding determinants. This strengthened our hypothesis that the insertion of A20FMDV2 conferred a conformational or steric alteration which precluded FIX binding to the fibre. Collectively, these data accurately reflected our previous findings where we assessed biodistribution and toxicity in immunocompetent, non-tumour bearing animals (see *Chapter.*5).

Warfarin mediated depletion of various coagulation factors has been employed as a liver avoidance strategy, with the aim of increasing the blood persistence and bioavailability for the tumour. The level of success of this strategy has been controversial, with some reports of enhanced tumour uptake (Shashkova *et al.*, 2008), and others describing negligible effects or even reductions in tumour uptake (Coughlan *et al.*, 2009; Gimenez-Alejandre *et al.*, 2008; Koski *et al.*, 2009). Despite observing a slight, but non-significant, increase in the quantity of Ad5-EGFP$_{WT}$ viral genomes delivered to the tumour in warfarin pre-treated groups, tumour uptake in both A20-retargeted groups was impaired relative to the corresponding untreated groups. The similarities between our results and those of Gimenez-Alejandre and colleagues (who compared a virus with wildtype capsid, with the corresponding RGD-4C integrin-retargeted construct) may suggest that integrin-directed retargeting might be sensitive to the anti-coagulative effects of warfarin *in vivo*.

However, it is also becoming increasingly evident that the mechanism of action of warfarin is not restricted to its function as an anti-coagulative agent. Thus, it is worth considering that warfarin may affect the tumour uptake of systemically delivery adenoviruses, independently of its direct effects on vitamin K-dependent coagulation

factors. For example, warfarin has been described to have pleiotropic, immuno-modulatory effects, and has been shown to be anti-inflammatory, directly influencing the signal transduction of various cytokines, including IL-6 (Kater *et al.*, 2002). Warfarin also has been shown to inhibit the replication of Human Immunodeficiency Virus (HIV-1) through the modification of cysteine residues in its protease, thus preventing viral polyprotein processing (Bourinbaiar *et al.*, 1993; Davis *et al.*, 1996; Tummino *et al.*, 1994). Interestingly, the Ad5 protease, adenain (L3-23K), which is required for efficient viral entry, disassembly and mature virion processing, also features conserved cysteine residues (Cotten & Weber, 1995; Greber, 1998; Rancourt *et al.*, 1994; Ruzindana-Umunyana *et al.*, 2002), and it has been shown previously that various protease inhibitors can inhibit Ad5 entry *in vitro* (Cotten & Weber, 1995). Therefore, warfarin also may be capable of modifying cysteine residues in adenain, affecting its function. Alternatively, warfarin has been shown to inhibit p44/p42 (ERK1/2) phosphorylation and activation (Nagai *et al.*, 2003). Recent research has shown that the binding of Ad5 to CAR triggers the activation of this signalling pathway, resulting in the homodimerisation of CAR and the activation of -β1 and -β3 integrins (Farmer *et al.*, 2009). As CAR, αvβ1 and αvβ3 are known receptors for Ad5 infection, inhibition of p44/p42 may therefore affect viral entry (Davison *et al.*, 2001; Li *et al.*, 2001; Santis *et al.*, 1999; Wickham *et al.*, 1993). Finally, warfarin has also been reported to inhibit clathrin-mediated endocytosis, by impairing actin polymerisation as a result of inducing epithelial to fibroblastoid conversion (Murata & Sakamoto, 2008). Classical adenovirus internalisation is via clathrin-mediated endocytosis (Leopold & Crystal, 2007; Meier *et al.*, 2002; Meier & Greber, 2003; Worgall *et al.*, 2000). Internalisation of αvβ6 is clathrin-dependent (Ramsay *et al.*, 2007). Therefore, warfarin-mediated inhibition of endocytosis may also have contributed to the impaired tumour transduction we observed in this study.

As reported in many published studies, warfarin significantly reduced the liver uptake and hepatic toxicity induced by Ad5-EGFP$_{WT}$, along with all other viruses used in this study (Di Paolo *et al.*, 2009b; Gimenez-Alejandre *et al.*, 2008; Shashkova *et al.*, 2008; Waddington *et al.*, 2007). Serum transaminase levels in all warfarin pre-treated animals were reduced to basal levels when compared with the corresponding untreated groups (p>0.05; excluding the Ad5-EGFP$_{A20}$ group for which statistical analysis cannot be performed). Interestingly, there were dramatic differences in the levels of virions accumulated in the livers of the A20-modifed groups (~160-fold, p=0.035, and ~34-fold, p<0.0001, respectively), which contrasted with the modest reduction observed in the warfarinised Ad5-EGFP$_{WT}$ group (~9-fold, p<0.0001). The reason for this remains unclear.

Through its function as a vitamin K antagonist, warfarin abrogates Ad5:FX-opsonisation, predominantly affecting transduction of hepatocytes (Parker *et al.*, 2006; Waddington *et al.*, 2007). Interestingly, it has been shown previously that in warfarin treated animals, total virion accumulation in the liver is not altered drastically at early time-points post-infection (Di Paolo *et al.*, 2009b; Kalyuzhniy *et al.*, 2008; Waddington *et al.*, 2007). This suggests that viral uptake by KCs and/or other non-parenchymal cells, is not mediated by coagulation factors (Di Paolo *et al.*, 2009b; Shashkova *et al.*, 2008). It has been shown that systemically administered Ad vectors can accumulate in the hepatic sinusoid endothelial cells of the liver, and can be retained in the space of Disse by redundant mechanisms (Di Paolo *et al.*, 2009b; Shayakhmetov *et al.*, 2005b). Therefore, it also is possible that the A20-retargeted viruses are sequestered to a lesser extent at these alternative sites. This may account for the dramatic differences in genome levels detected in livers of warfarin pre-treated animals. Additionally, warfarin actually has been shown to increase the sequestration of Ad5 virions in Kupffer cells *in vivo* (Xu *et al.*, 2008). Therefore, it is possible that increased, warfarin-induced accumulation of viruses Ad5-EGFP$_{A20}$ and Ad5-477*dl*TAYT$_{A20}$ in KCs, contributed to the loss of tumour targeting efficiency seen in this study.

In the absence of warfarin, Ad5-EGFP$_{A20}$ and Ad5-477*dl*TAYT$_{A20}$ displayed an altered biodistribution when compared with Ad5-EGFP$_{WT}$, resulting in significantly reduced splenic and pulmonary uptake of virus. We detected approximately 3-fold, and ~9-fold less Ad5-EGFP$_{A20}$ genomes in the spleens, and lungs of non-warfarinised animals (p=0.046 and p<0.0001, respectively). Almost identical reductions were observed with Ad5-477*dl*TAYT$_{A20}$ (p=0.037 and p<0.0001, respectively). Interestingly, the distribution in the untreated Ad5-EGFP$_{A20}$ and Ad5-477*dl*TAYT$_{A20}$ groups effectively paralleled the profile seen for the warfarin pre-treated Ad5-EGFP$_{WT}$ group, in terms of accumulation in the spleen and lung. These organs have previously been described as auxiliary sites for Ad5 accumulation *in vivo* (Manickan *et al.*, 2006), although the precise factors which determine uptake at these sites have not been identified. A recent study has suggested that Ad-loaded dying KCs are displaced from the liver within 24hrs of intravenous delivery, and relocate to the lung where they can be detected co-localised together (Manickan *et al.*, 2006). Therefore, the reduced pulmonary sequestration of the A20-retargeted viruses could be a reflection of their reduced accumulation in KCs, conferred by their failure to interact with FIX *in vivo*.

As stated in the previous chapter, vectors which have reduced accumulation in the spleen have been shown to have reduced toxicity, and therefore improved safety profiles *in vivo* (Koizumi *et al.*, 2007; Zhang *et al.*, 2001). The mechanisms which

govern the accumulation of Ad5 in the spleen currently are under-characterised, although uptake appears to have an element of coagulation factor dependency. Thus, warfarin can reduce sequestration significantly, and FX-complementation can reverse this effect (Parker *et al.*, 2006; Waddington *et al.*, 2007). Alternatively, warfarin has been shown to induce increases in KC-mediated accumulation of Ads, which may act to preclude efficient dissemination to other sites, such as the spleen (Xu *et al.*, 2008). However, how FX-complementation in warfarinised mice could reverse KC-mediated accumulation, and restore splenic sequestration, remains unclear.

An altered *in vivo* biodistribution has already been described for RGD-modified adenoviruses; where modest increases in gene expression are often detected in the liver, spleen, lung or heart (Kanerva *et al.*, 2002b; Rein *et al.*, 2004; Reynolds *et al.*, 1999). This tropism *in vivo* would be consistent with the broad tissue distribution of αvβ3 and αvβ5 integrins, the target receptors for Ad5-RGD-4C (Lord *et al.*, 2006; Nagel *et al.*, 2003). The tissue expression of αvβ6 in murine models is not well characterised, however it is known to be expressed constitutively in the lung (Munger *et al.*, 1999). Recent work in our laboratory has also identified that αvβ6 is expressed to high levels in the stomach and intestine of mice (Dr. Antonio Saha, unpublished data). Therefore, we included these organs in our analysis of vector biodistribution, but did not detect an increased accumulation of A20-retargeted vectors at these sites, or in fact any other organs assessed in this study (liver, spleen, lung, stomach, kidney and heart).

It is becoming increasingly clear that receptor-dependent entry may not necessarily effectively determine the localisation and biodistribution of systemically delivered Ads. Clearly, the interactions between Ad5 and various components of the circulatory system play a critical role in dictating the outcome and efficacy of Ads as therapeutic vehicles (Carlisle *et al.*, 2009; Gimenez-Alejandre *et al.*, 2008; Lyons *et al.*, 2006; Parker *et al.*, 2006; Seiradake *et al.*, 2009; Waddington *et al.*, 2008). We currently are unable to confirm the exact mechanism which underlies the reduced hepatotropism and altered biodistribution associated with Ad5-EGFP$_{A20}$ and Ad5-477*dl*TAYT$_{A20}$. Therefore, in the future it will be important to perform a full biodistribution analysis for the A20-modifed vectors, to confirm whether or not their reduced tropism for the reticuloendothelial system is a result of effective retargeting to another murine organ. However, what is clear is that these retargeted vectors are capable of locating to αvβ6-positive tumours *in vivo* following systemic delivery with increased efficiency relative to the wildtype control, and do so with reduced toxicity and impaired induction of pro-inflammatory responses.

CHAPTER 7. Final Discussion

Chapter.7 Final Discussion and Future Directions

In this study, we describe the successful *in vitro* retargeting of Ad5 to αvβ6 through the introduction of a previously characterised αvβ6-selective peptide, A20FMDV2. We have demonstrated that the resultant vector, Ad5-EGFP$_{A20}$, is capable of dramatically enhancing the infection of a panel of αvβ6-expressing human carcinoma cell lines in a CAR-independent manner. Combining this retargeting strategy with CAR-binding, and FIX-binding ablation mutations (Ad5-477*dl*TAYT$_{A20}$), did not impair the interaction with αvβ6. *In vivo*, the retargeting efficiency was improved, although not dramatic. However, *in vivo* assessment of the Ad5-EGFP$_{A20}$ and Ad5-477*dl*TAYT$_{A20}$ constructs, uncovered some interesting features which highlight their potential for future therapeutic applications.

Achieving tumour selective delivery is an important goal for cancer gene therapy. The integrin αvβ6 represents a highly attractive target, due to its restricted expression on normal tissue but high level expression in numerous human carcinomas (Ahmed *et al.*, 2002b; Bates *et al.*, 2005; Breuss *et al.*, 1995; Elayadi *et al.*, 2007; Hazelbag *et al.*, 2007; Marsh *et al.*, 2008; Nystrom *et al.*, 2006; Thomas *et al.*, 2001b; Van Aarsen *et al.*, 2008). Other Ad5-integrin retargeting strategies (eg.Ad5-RGD-4C) have resulted in the RGD-dependent enhancement of CAR-negative cell lines which express αvβ3/5 integrins (Dmitriev *et al.*, 1998; Nagel *et al.*, 2003). Likewise, retargeting through HSPGs using Ad5-pK7 has been shown to enhance the CAR-independent infection of myeloma, glioma, rhabdosacrcoma and various carcinoma cells *in vitro* and *in vivo* (Gonzalez *et al.*, 1999; Ranki *et al.*, 2007; Rein *et al.*, 2004; Staba *et al.*, 2000; Wu *et al.*, 2002). CD40 over-expression also has been identified as a potential target for Ad5 delivery in ovarian carcinoma cells and Hakkarainen *et al* have reported *in vitro* infectivity enhancements of up to 40-fold when using Ad5 pre-complexed with a CD40-targeting molecule (Hakkarainen *et al.*, 2003). More recently, vectors which target CD46 (eg. Ad35 or Ad5/35) are being investigated for tumour targeting applications *in vivo* (Liu *et al.*, 2009; Sakurai *et al.*, 2003; Sakurai *et al.*, 2008; Seshidhar Reddy *et al.*, 2003; Vogels *et al.*, 2003). However, the disadvantage of current retargeting strategies is that these vectors do not necessarily exhibit cancer selective transduction as, αvβ3/5, HSPGs, CD46 and CD40 expression *in vivo* is not limited to malignant tissue (Alderson *et al.*, 1993; Galy & Spits, 1992; Hsu *et al.*, 1997; Ni *et al.*, 2005; Sasisekharan *et al.*, 2002; Tsujimura *et al.*, 1998). It could also be argued the translational relevance of some of these vectors has been impaired by the relatively poor choice of *in vivo* model systems. The restricted tissue distribution of αvβ6 in humans and non-human primates is well established (Breuss *et al.*, 1995; Breuss *et al.*,

1993). This is in contrast with CD46, which displays a broad tissue distribution in humans and non-human primates, though not in rodent species where it is restricted to the testis (Ni *et al.*, 2005). Therefore, pre-clinical *in vivo* studies performed in non-human primates with vectors retargeted to αvβ6 may have more translational relevance for human cancer therapy applications.

The interaction of the A20FMDV2 peptide with αvβ6 is one of high affinity, displaying a dose-dependent inhibition of adhesion of biotinylated peptide (to immobilised recombinant αvβ6) with an IC_{50} of ~0.15nM, and a dose-dependent inhibition of αvβ6-dependent cell adhesion in the order of 1.2nM (DiCara *et al.*, 2007). Additionally, the affinity of binding (K_d) of A20FMDV2 to cellular αvβ6 has been determined to be ~1.7nM (Dr. Antonio Saha; unpublished data with permission). However, the precise binding affinity of A20FMDV2, within the trimeric Ad5 knob domain ($Knob_{A20}$/Ad5-$EGFP_{A20}$), has never formally been determined. This will be important in order to comparatively assess its potential as a high affinity *in vivo* targeting ligand when compared with other Ad-based tumour-selective targeting strategies. For example, Ad35 is currently undergoing investigation for tumour targeting studies, due to its high affinity interaction with CD46. The binding affinity of Ad35 for CD46 (K_d = 14.64nM) has been shown to be comparable to that of Ad5 for CAR, which was shown previously to be ~14.8nM (Kirby *et al.*, 2000; Wang *et al.*, 2008). Furthermore, Wang and colleagues generated Ad35 knob mutants with point mutations which resulted in affinities for CD46 almost 23-fold higher (K_d = 0.63nM) than wildtype Ad35. Interestingly, these mutants did not result in enhanced transduction *in vitro*, however did result in improved uptake *in vivo* in $CD46^{high}$ liver metastases. Thus, it will be important to ascertain whether or not the A20FMDV2-engineered Ad5 fibre could achieve comparable affinities. This would further strengthen its potential for clinical use, especially when considered with the restricted expression profile of αvβ6 in humans.

Achieving successful tumour targeting following systemic delivery of adenoviral vectors is complicated by the sequestration of the virus in off-target locations, as a result of virus interactions with various blood components (Carlisle *et al.*, 2009; Kalyuzhniy *et al.*, 2008; Lyons *et al.*, 2006; Parker *et al.*, 2006; Seiradake *et al.*, 2009; Shayakhmetov *et al.*, 2005b; Stone *et al.*, 2007b; Waddington *et al.*, 2008; Xu *et al.*, 2008). Local delivery strategies can help to avoid, or minimise, some of these limitations. Unfortunately, using our chosen *in vivo* models, we did not observe any significant improvements in efficacy when comparing Ad5-$EGFP_{WT}$ and Ad5-$EGFP_{A20}$ following intraperitoneal, or intratumoural delivery. However, *in vitro*, we observed significant improvements in Ad5-$EGFP_{A20}$-mediated transduction efficiency when using several

Head and Neck Squamous Cell Carcinoma (HNSCC) lines (TR126, TR138, HSC-3 and SCC25). Interestingly, several Ad-based vectors currently are undergoing clinical investigation for the management and treatment of HNSCC (Vattemi & Claudio, 2009). For example, a non-replicating Ad5 vector expressing functional p53 (Gendicine), recently has been licenced in China for the treatment of HNSCC (Peng, 2005). Furthermore, ONYX-*dl*1520 is in use as a mouthwash preparation for the prophylactic treatment of malignant oral dysplasia (Rudin *et al.*, 2003). Expression of αvβ6 is found at high levels in oral dysplasia and HNSCC and expression is maintained throughout disease progression where it correlates with poor prognosis, invasion and metastasis (Nystrom *et al.*, 2006; Thomas *et al.*, 2001a; Thomas *et al.*, 2001b; Van Aarsen *et al.*, 2008). Conversely, CAR expression has been reported to be downregulated in HNSCC (Jee *et al.*, 2002). Moreover, as CAR expression is restricted to tight membrane junctions, it is perhaps limited in its accessibility for infection by Ad5 (Walters *et al.*, 2002). Therefore, it seems possible that an A20-retargeted Ad5 could help to maximise local transduction, especially when using an oral preparation treatment similar to that of ONYX-*dl*1520.

One of the ultimate goals of cancer therapy is to achieve successful delivery to solid tumours and disseminated metastases. This requires the use of systemically delivered treatment modalities. However, efficient retargeting *in vitro* does not always correlate with successful delivery and/or efficacy *in vivo*. In this study, we investigated the effects of introducing the 477*dl*TAYT modification (CAR/FIX-binding ablation mutations) into a vector which simultaneously was retargeted to αvβ6. The introduction of this set of mutations has previously been described to reduce the hepatotropism and toxicity of a similar vector, Ad5*mut*, following intravenous delivery (Shayakhmetov *et al.*, 2005b). Indeed, these findings were reproduced with Ad5-477*dl*TAYT$_{A20}$. However, rather unexpectedly, Ad5-EGFP$_{A20}$, which lacked these mutations, also mirrored this profile *in vivo*.

We can now propose a number of possible explanations for the altered biodistribution of Ad5-EGFP$_{A20}$, particularly with regard to the reticuloendothelial system. It is well established that Ad interactions with serum factors play a more significant role *in vivo* than conventional *in vitro* interactions with CAR and αvβ3/αvβ5 integrins (Shayakhmetov *et al.*, 2005b; Waddington *et al.*, 2008; Xu *et al.*, 2008). The sole structural modification within the Ad5-EGFP$_{A20}$ vector is the insertion of 20aa into the HI loop of the fibre knob, such that the altered hepatotropism observed is unlikely to be due to interference with FX-hexon binding. However, FIX and C4BP previously have been described to bind to the knob domain of Ad5 (Gaggar *et al.*, 2007; Shayakhmetov

et al., 2005b). Interestingly, the 477*dl*TAYT set of mutations described are in close proximity to the site of insertion of A20FMDV2, and so it is plausible that this modification has conferred a conformational change or steric hindrance which may abrogate FIX and/or C4BP binding to Ad5-EGFP$_{A20}$. Indeed, *in vitro* infectivity experiments performed in the presence, and absence, of FIX support this hypothesis. However, it currently remains unclear whether the phenotype of the A20-viruses is a direct (ie. biological function of the peptide), or indirect (structural disruption) result of the insertion of A20FMDV2, into the HI loop of the Ad5 fibre. Structural disruptions to the overall 3D structure of the knob domain could be confirmed, or at least predicted in the future using protein modelling algorithms in combination with published crystallographic data. Functional *in vivo* comparisons between Ad5-477*dl*TAYT$_{6XHIS}$ (non-αvβ6 retargeted 477*dl*TAYT control) and Ad5-477*dl*TAYT$_{A20}$ may also prove interesting. Furthermore, *in vivo* relevance of a differential Ad5-FIX/C4BP interaction warrants further investigation, especially as FX now has been identified as the dominant determinant of hepatocyte transduction (Alba *et al.*, 2009; Kalyuzhniy *et al.*, 2008; Vigant *et al.*, 2008; Waddington *et al.*, 2008).

Alternatively, it is worth considering that the insertion of the strongly cationic A20FMDV2 peptide (pI=11.32) has altered the overall electrostatic properties of the predominantly negative Ad5 particle *in vivo* (Alemany *et al.*, 2000b). This may preclude uptake by scavenging receptors on KC, which preferentially recognise negatively charged materials (Alemany *et al.*, 2000b; Furumoto *et al.*, 2004; Haisma *et al.*, 2008). More recently, opsonisation by complement (C3 and C4), in combination with natural IgM antibodies, has been proposed as an alternative mechanism for the uptake of Ads by scavenging receptors on Kupffer cells *in vivo* (Xu *et al.*, 2008). Interestingly, the electrostatic characteristics of Ad5 can also dictate the extent of recognition by serum proteins, including complement (Chonn *et al.*, 1991; Furumoto *et al.*, 2004). It will be important to investigate whether or not, like Ad5*mut*, Ad5-EGFP$_{A20}$ and Ad5-477*dl*TAYT$_{A20}$ exhibit a reduced co-localisation with Kupffer cells. Selective depletion of Kupffer cells at early time-points, using $GdCl_3$ or broader depletion of tissue macrophages with clodronate liposomes may help to delineate the differential hepatic interactions of the A20-retargeted constructs when compared to Ad5-EGFP$_{WT}$. This may also permit more legitimate comparisons to published FX studies, in which Kupffer cells often are depleted (Alba *et al.*, 2009; Waddington *et al.*, 2008). Furthermore, it would be interesting to assess whether or not the A20-retargeted viruses have a differential interaction with sinusoidal endothelial cells, at early time-points post-infection.

With regard to the efficiency of tumour targeting following systemic delivery, both Ad5-EGFP$_{A20}$ and Ad5-477*dl*TAYT$_{A20}$ achieved superior delivery over Ad5-EGFP$_{WT}$, although only Ad5-477*dl*TAYT$_{A20}$ was found to be statistically significantly different. In addition to their role in hepatocyte transduction, coagulation factors have been implicated previously in directing Ad5 tumour transduction (Gimenez-Alejandre *et al.*, 2008; Liu *et al.*, 2009; Shashkova *et al.*, 2008). In agreement with other studies, *in vivo* depletion of coagulation factors using warfarin pre-treatment did not enhance tumour targeting (Gimenez-Alejandre *et al.*, 2008; Koski *et al.*, 2009). In fact tumour uptake was reduced in the warfarinised, A20-retargeted cohorts. The reason for this remains unclear. However, it would be interesting to see if complementation with FX could rescue tumour uptake, as it is capable of restoring Ad5 accumulation in the liver and spleen in warfarin treated animals (Parker *et al.*, 2006; Waddington *et al.*, 2007). Likewise, it may be useful to combine the A20FMDV2 retargeting entity with hexon modified vectors, which are ablated for FX-binding.

We are aware that the *in vitro* findings, which demonstrate that Ad5-EGFP$_{A20}$, and Ad5-477*dl*TAYT$_{A20}$ can also utilise αvβ8 and/or HSPGs, limits the specificity of the current retargeting approach. The auxiliary affinity of Ad5-EGFP$_{A20}$ for αvβ8 was unexpected, as extensive prior characterisation of the A20FMDV2 peptide, using the same DX3/DX3-β6 cell lines, demonstrated that its specificity was for αvβ6 integrin (DiCara *et al.*, 2007). However, natural Foot and Mouth disease virus (FMDV) infection has been shown to utilise both αvβ6 and αvβ8 (Berryman *et al.*, 2005; Burman *et al.*, 2006; DiCara *et al.*, 2008; Jackson *et al.*, 2004). Therefore, the conformation of the A20FMDV2 peptide within the Ad5 fibre knob domain may be structurally, and biologically more similar to FMDV. Interestingly, mutation of the RGDLXXL motif to RGDRXXL has been shown to inhibit binding to αvβ8, without compromising binding to αvβ6 (Burman *et al.*, 2006). Therefore, the selectivity of the A20-retargeted vectors may be refined further for future studies, if required. However, it is important to note that neither Ad5-EGFP$_{A20}$ nor Ad5-477*dl*TAYT$_{A20}$ displayed an expanded tissue tropism *in vivo*, and in fact exhibited a more restricted biodistribution profile than Ad5-EGFP$_{WT}$. Furthermore, the HSPG-binding capacity of Ad5-477*dl*TAYT$_{A20}$ did not result in augmented hepatocyte transduction, a feature which is observed with the Ad5-K7 vector, which is retargeted specifically to HSPGs (Koizumi *et al.*, 2007).

In the limited biodistribution analysis performed with these vectors (liver, spleen, lung, heart, kidney and stomach) we did not detect any increased genome accumulation with the A20-retargeted vectors when compared to control Ad5-EGFP$_{WT}$. This was reassuring, however warrants further investigation in future studies. It will be important

to determine the blood persistence kinetics of each of the viruses, and to confirm whether or not the enhanced tumour uptake observed with Ad5-EGFP$_{A20}$ and Ad5-477*dl*TAYT$_{A20}$ is a reflection of increased bioavailability. Furthermore, it will be necessary to expand the range of organs analysed, to obtain a full biodistribution and to assess the relative distribution of virus when adjusted for size of organs.

The A20-retargeted viruses displayed dramatically reduced toxicity, and limited induction of pro-inflammatory mediators *in vivo*. These features may permit their use at a higher dose, which could enhance anti-tumoural efficacy *in vivo*. Furthermore, these vectors may permit prolonged transgene expression *in vivo*, as a result of reduced clearance by the immune cells which are actively recruited by various Ad-induced pro-inflammatory effectors. It may also be interesting to investigate whether or not the A20-retargeted vectors have differential interactions with human/rodent blood cell fractions, when compared with Ad5-EGFP$_{WT}$. Vectors which are devoid of CAR-binding determinants may prove useful in preventing agglutinating interactions with human erythrocytes (Carlisle *et al.*, 2009; Nicol *et al.*, 2004; Seiradake *et al.*, 2009). Alternatively, as expression of the integrin αvβ8 has been detected in total splenocytes, CD4^{+} T-cells and dendritic cells, it may be worth investigating any possible increased interaction with these cells (Travis *et al.*, 2007). However, the lack of splenic accumulation, the similarity of our results in immunocompetent and nude mice and the lack of inflammation induced by Ad5-EGFP$_{A20}$/Ad5-477*dl*TAYT$_{A20}$ *in vivo* do not provide much support for this possibility.

In summary, using Ad5-EGFP$_{A20}$ and Ad5-477*dl*TAYT$_{A20}$ in the absence of warfarin pre-treatment, we improved liver-tumour-ratios significantly when compared to Ad5-EGFP$_{WT}$ (100:1 and 72:1, respectively, compared with 900:1). Warfarin pre-treatment further improved these ratios, resulting in ratios of 1:1 and 7:1 for Ad5-EGFP$_{A20}$ and Ad5-477*dl*TAYT$_{A20}$, compared with 70:1 for Ad5-EGFP$_{WT}$. Thus, we believe that the vectors generated in this study may have potential for future clinical applications. To our knowledge, the data presented within this thesis comprise the first report of successful retargeting of Ad5 to αvβ6 (Coughlan *et al.*, 2009). However, in the future further *in vivo* validation of these constructs is warranted. The characterisation of the precise mechanisms underlying the reduced hepatotropism, the limited biodistribution and lack of immune activation, will be important. Additionally, we recently have identified two suitable *in vivo* models (ie. A431 and CA1a) in which to compare the anti-tumoural efficacy of Ad5-EGFP$_{WT}$, Ad5-EGFP$_{A20}$ and Ad5-477*dl*TAYT$_{A20}$. If these experiments are successful, combining the A20/477*dl*TAYT$_{A20}$ fibre mutations with a vector backbone featuring transcriptional selectivity will help to further refine the

therapeutic index, permit dose escalation and enhance potency. Furthermore, an assessment of vector performance, in terms of targeting and efficacy, in immunocompetent, and/or pre-immunised and permissive models will also be required. Much of these future experiments will be performed by Marta Gimenez-Alejandre, under the supervision of Dr. Ramon Alemany, at the Institut Català d'Oncologia, Barcelona, Spain as part of our ongoing collaborative agreement.

Appendix I-II

```
CLUSTAL 2.0.10 multiple sequence alignment

Ad5_WT          MKRARPSEDTFNPVYPYDTETGPPTVPFLTPPFVSPNGFQESPPGVLSLRLSEPLVTSNG 60
Ad5_A20         MKRARPSEDTFNPVYPYDTETGPPTVPFLTPPFVSPNGFQESPPGVLSLRLSEPLVTSNG 60
                ************************************************************

Ad5_WT          MLALKMGNGLSLDEAGNLTSQNVTTVSPPLKKTKSNINLEISAPLTVTSEALTVAAAAPL 120
Ad5_A20         MLALKMGNGLSLDEAGNLTSQNVTTVSPPLKKTKSNINLEISAPLTVTSEALTVAAAAPL 120
                ************************************************************

Ad5_WT          MVAGNTLTMQSQAPLTVHDSKLSIATQGPLTVSEGKLALQTSGPLTTTDSSTLTITASPP 180
Ad5_A20         MVAGNTLTMQSQAPLTVHDSKLSIATQGPLTVSEGKLALQTSGPLTTTDSSTLTITASPP 180
                ************************************************************

Ad5_WT          LTTATGSLGIDLKEPIYTQNGKLGLKYGAPLHVTDDLNTLTVATGPGVTINNTSLQTKVT 240
Ad5_A20         LTTATGSLGIDLKEPIYTQNGKLGLKYGAPLHVTDDLNTLTVATGPGVTINNTSLQTKVT 240
                ************************************************************

Ad5_WT          GALGFDSQGNMQLNVAGGLRIDSQNRRLILDVSYPFDAQNQLNLRLGQGPLFINSAHNLD 300
Ad5_A20         GALGFDSQGNMQLNVAGGLRIDSQNRRLILDVSYPFDAQNQLNLRLGQGPLFINSAHNLD 300
                ************************************************************

Ad5_WT          INYNKGLYLFTASNNSKKLEVNLSTAKGLMFDATAIAINAGDGLEFGSPNAPNTNPLKTK 360
Ad5_A20         INYNKGLYLFTASNNSKKLEVNLSTAKGLMFDATAIAINAGDGLEFGSPNAPNTNPLKTK 360
                ************************************************************

                                                  AB Loop (402-419)
                                                A
Ad5_WT          IGHGLEFDSNKAMVPKLGTGLSFDSTGAITVGNKNNDKLTLWTTPAPSPNCRLNAEKDAK 420
Ad5_A20         IGHGLEFDSNKAMVPKLGTGLSFDSTGAITVGNKNNDKLTLWTTPAPSPNCRLNAEKDAK 420
                ************************************************************

                 B         C   CD Loop (440-454) D   *DG Loop (463-515)
Ad5_WT          LTLVLTKGGSQILATVSVLAVKGSLAPISGTVQSAHLIIREDENGVLLNNSFLDPEYWNF 480
Ad5_A20         LTLVLTKGGSQILATVSVLAVKGSLAPISGTVQSAHLIIREDENGVLLNNSFLDPEYWNF 480
                ************************************************************

                E  F   Ψ                          GH Loop (521-529)
                                                G         H
Ad5_WT          RNGDLTEGTAYTNAVGFMPNLSAYPKSHGKTAKSNIVSQVYLNGDKTKPVTLTITLNGTQ 540
Ad5_A20         RNGDLTEGTAYTNAVGFMPNLSAYPKSHGKTAKSNIVSQVYLNGDKTKPVTLTITLNGTQ 540
                ************************************************************

                        HI Loop (536-550)          IJ Loop (557-573)
                                                I                   J
Ad5_WT          ETGDTT----------------------PSAYSMSFSWDWSGHNYINEIFATSSYTFSYI 578
Ad5_A20         ETGDTTGNAVPNLRGDLQVLAQKVARTAPSAYSMSFSWDWSGHNYINEIFATSSYTFSYI 600
                ******                      *********************************

Ad5_WT          AQE 581
Ad5_A20         AQE 603
                ***
```

Appendix I. **Structural Alignment of WT and A20-Modified Ad5 Fibre with Major Structural Regions Highlighted.** ClustalW protein alignment highlighting the structural domains of the fibre region of Ad5-EGFP$_{WT}$ and modified Ad5-EGFP$_{A20}$ (A20FMDV2 peptide sequence in red). Block yellow indicates the A-J strand regions of the monomeric structure, and boxed sequence represents the loop domains, with approximated nucleotide numbers (Adapted from Xia *et al*., 1994). *The small β-sheets E and F are considered to be part of the DG Loop. Amino acids highlighted in bold and underlined indicate Ser408, Pro409, Tyr477 and Leu485, all identified as critical residues involved in CAR binding (Kirby *et al*., 2000). Ψ highlights the TAYT epitope which is thought to confer binding to FIX/C4BP (Shayakhmetov *et al*., 2005b).

```
CLUSTAL 2.0.10 multiple sequence alignment

                                        A      AB Loop                B        C
KnobWT              HHHHHHGSGAITVGNKNNDKLTLWTTPAPSPNCRLNAEKDAKLTLVLTKCGSQILATVSV 60
KnobA20             HHHHHHGSGAITVGNKNNDKLTLWTTPAPSPNCRLNAEKDAKLTLVLTKCGSQILATVSV 60
Knob485dlTAYTA20    HHHHHHGSGAITVGNKNNDKLTLWTTPAPSPNCRLNAEKDAKLTLVLTKCGSQILATVSV 60
Knob477dlTAYTA20    HHHHHHGSGAITVGNKNNDKLTLWTTPAPSPNCRLNAEKDAKLTLVLTKCGSQILATVSV 60
                    ************************************************************

                        CD Loop        D                  *DG Loop        Ψ
KnobWT              LAVKGSLAPISGTVQSAHLIIRFDENGVLLNNSFLDPEYWNFRNGDLTEGTAYTNAVGFM 120
KnobA20             LAVKGSLAPISGTVQSAHLIIRFDENGVLLNNSFLDPEYWNFRNGDLTEGTAYTNAVGFM 120
Knob485dlTAYTA20    LAVKGSLAPISGTVQSAHLIIRFDENGVLLNNSFLDPEYWNFRNGDKTEG----NAVGFM 116
Knob477dlTAYTA20    LAVKGSLAPISGTVQSAHLIIRFDENGVLLNNSFLDPEAWNFRNGDLTEG----NAVGFM 116
                    ***************************************************************

                                      GH Loop        G        H        HI Loop
KnobWT              PNLSAYPKSHGKTAKSNIVSQVYLNGDKTKPVTLTITLNGTQETGDTT------------ 168
KnobA20             PNLSAYPKSHGKTAKSNIVSQVYLNGDKTKPVTLTITLNGTQETGDTTGNAVPNLRGDLQ 180
Knob485dlTAYTA20    PNLSAYPKSHGKTAKSNIVSQVYLNGDKTKPVTLTITLNGTQETGDTTGNAVPNLRGDLQ 176
Knob477dlTAYTA20    PNLSAYPKSHGKTAKSNIVSQVYLNGDKTKPVTLTITLNGTQETGDTTGNAVPNLRGDLQ 176
                    ***************************************************************

                                I        IJ Loop        J
KnobWT              ----------PSAYSMSFSWDWSGHNYINEIFATSSYTFSYIAQE 203
KnobA20             VLAQKVARTAPSAYSMSFSWDWSGHNYINEIFATSSYTFSYIAQE 225
Knob485dlTAYTA20    VLAQKVARTAPSAYSMSFSWDWSGHNYINEIFATSSYTFSYIAQE 221
Knob477dlTAYTA20    VLAQKVARTAPSAYSMSFSWDWSGHNYINEIFATSSYTFSYIAQE 221
                              ***********************************
```

Appendix II. **Structural Alignment of Knob$_{WT}$, Knob$_{A20}$, Knob485*dl*TAYT$_{A20}$ and Knob477*dl*TAYT$_{A20}$.** ClustalW protein alignment highlighting the sequence differences between the modified Knob proteins (A20FMDV2 peptide sequence in red). Block yellow indicates the A-J strand regions of the monomeric structure, and boxed sequence represent the loop domains, with approximated nucleotide numbers (Adapted from Xia *et al*., 1994). *The small β-sheets E and F are considered to be part of the DG Loop. Amino acids highlighted in bold and underlined indicate Ser408, Pro409, Tyr477 and Leu485, all identified as critical residues involved in CAR binding (Kirby *et al*., 2000). Ψ highlights the TAYT epitope which is thought to confer binding to FIX/C4BP (Shayakhmetov *et al*., 2005b). * identifies sequence identity.

References

Ahmed, N., Niu, J., Dorahy, D. J., Gu, X., Andrews, S., Meldrum, C. J., Scott, R. J., Baker, M. S., Macreadie, I. G. & Agrez, M. V. (2002a). Direct integrin alphavbeta6-ERK binding: implications for tumour growth. *Oncogene* **21**, 1370-1380.

Ahmed, N., Riley, C., Rice, G. E., Quinn, M. A. & Baker, M. S. (2002b). Alpha(v)beta(6) integrin-A marker for the malignant potential of epithelial ovarian cancer. *J Histochem Cytochem* **50**, 1371-1380.

Akhurst, R. J. & Balmain, A. (1999). Genetic events and the role of TGF beta in epithelial tumour progression. *J Pathol* **187**, 82-90.

Akhurst, R. J. & Derynck, R. (2001). TGF-beta signaling in cancer--a double-edged sword. *Trends Cell Biol* **11**, S44-51.

Alba, R., Bradshaw, A. C., Parker, A. L., Bhella, D., Waddington, S. N., Nicklin, S. A., van Rooijen, N., Custers, J., Goudsmit, J., Barouch, D. H., McVey, J. H. & Baker, A. H. (2009). Identification of coagulation factor (F)X binding sites on the adenovirus serotype 5 hexon: effect of mutagenesis on FX interactions and gene transfer. *Blood*.

Alderson, M. R., Armitage, R. J., Tough, T. W., Strockbine, L., Fanslow, W. C. & Spriggs, M. K. (1993). CD40 expression by human monocytes: regulation by cytokines and activation of monocytes by the ligand for CD40. *J Exp Med* **178**, 669-674.

Alemany, R., Balague, C. & Curiel, D. T. (2000a). Replicative adenoviruses for cancer therapy. *Nat Biotechnol* **18**, 723-727.

Alemany, R. & Curiel, D. T. (2001). CAR-binding ablation does not change biodistribution and toxicity of adenoviral vectors. *Gene Ther* **8**, 1347-1353.

Alemany, R., Suzuki, K. & Curiel, D. T. (2000b). Blood clearance rates of adenovirus type 5 in mice. *J Gen Virol* **81**, 2605-2609.

Anders, M., Vieth, M., Rocken, C., Ebert, M., Pross, M., Gretschel, S., Schlag, P. M., Wiedenmann, B., Kemmner, W. & Hocker, M. (2009). Loss of the coxsackie and adenovirus receptor contributes to gastric cancer progression. *Br J Cancer* **100**, 352-359.

Annes, J. P., Rifkin, D. B. & Munger, J. S. (2002). The integrin alphaVbeta6 binds and activates latent TGFbeta3. *FEBS Lett* **511**, 65-68.

Appledorn, D. M., Patial, S., McBride, A., Godbehere, S., Van Rooijen, N., Parameswaran, N. & Amalfitano, A. (2008). Adenovirus vector-induced innate inflammatory mediators, MAPK signaling, as well as adaptive immune

responses are dependent upon both TLR2 and TLR9 in vivo. *J Immunol* **181**, 2134-2144.

Arihiro, K., Kaneko, M., Fujii, S., Inai, K. & Yokosaki, Y. (2000). Significance of alpha 9 beta 1 and alpha v beta 6 integrin expression in breast carcinoma. *Breast Cancer* **7**, 19-26.

Arnberg, N., Edlund, K., Kidd, A. H. & Wadell, G. (2000a). Adenovirus type 37 uses sialic acid as a cellular receptor. *J Virol* **74**, 42-48.

Arnberg, N., Kidd, A. H., Edlund, K., Olfat, F. & Wadell, G. (2000b). Initial interactions of subgenus D adenoviruses with A549 cellular receptors: sialic acid versus alpha(v) integrins. *J Virol* **74**, 7691-7693.

Atencio, I. A., Grace, M., Bordens, R., Fritz, M., Horowitz, J. A., Hutchins, B., Indelicato, S., Jacobs, S., Kolz, K., Maneval, D., Musco, M. L., Shinoda, J., Venook, A., Wen, S. & Warren, R. (2006). Biological activities of a recombinant adenovirus p53 (SCH 58500) administered by hepatic arterial infusion in a Phase 1 colorectal cancer trial. *Cancer Gene Ther* **13**, 169-181.

Au, T., Thorne, S., Korn, W. M., Sze, D., Kirn, D. & Reid, T. R. (2007). Minimal hepatic toxicity of Onyx-015: spatial restriction of coxsackie-adenoviral receptor in normal liver. *Cancer Gene Ther* **14**, 139-150.

Awasthi, V., Meinken, G., Springer, K., Srivastava, S. C. & Freimuth, P. (2004). Biodistribution of radioiodinated adenovirus fiber protein knob domain after intravenous injection in mice. *J Virol* **78**, 6431-6438.

Babiss, L. E., Ginsberg, H. S. & Darnell, J. E., Jr. (1985). Adenovirus E1B proteins are required for accumulation of late viral mRNA and for effects on cellular mRNA translation and transport. *Mol Cell Biol* **5**, 2552-2558.

Bandara, L. R. & La Thangue, N. B. (1991). Adenovirus E1a prevents the retinoblastoma gene product from complexing with a cellular transcription factor. *Nature* **351**, 494-497.

Barnett, B. G., Crews, C. J. & Douglas, J. T. (2002). Targeted adenoviral vectors. *Biochim Biophys Acta* **1575**, 1-14.

Barton, E. S., Forrest, J. C., Connolly, J. L., Chappell, J. D., Liu, Y., Schnell, F. J., Nusrat, A., Parkos, C. A. & Dermody, T. S. (2001). Junction adhesion molecule is a receptor for reovirus. *Cell* **104**, 441-451.

Bates, R. C., Bellovin, D. I., Brown, C., Maynard, E., Wu, B., Kawakatsu, H., Sheppard, D., Oettgen, P. & Mercurio, A. M. (2005). Transcriptional activation of integrin beta6 during the epithelial-mesenchymal transition defines a novel prognostic indicator of aggressive colon carcinoma. *J Clin Invest* **115**, 339-347.

Bauerschmitz, G. J., Guse, K., Kanerva, A., Menzel, A., Herrmann, I., Desmond, R. A., Yamamoto, M., Nettelbeck, D. M., Hakkarainen, T., Dall, P., Curiel, D. T.

& Hemminki, A. (2006). Triple-targeted oncolytic adenoviruses featuring the cox2 promoter, E1A transcomplementation, and serotype chimerism for enhanced selectivity for ovarian cancer cells. *Mol Ther* **14**, 164-174.

Bayo-Puxan, N., Cascallo, M., Gros, A., Huch, M., Fillat, C. & Alemany, R. (2006). Role of the putative heparan sulfate glycosaminoglycan-binding site of the adenovirus type 5 fiber shaft on liver detargeting and knob-mediated retargeting. *J Gen Virol* **87**, 2487-2495.

Bazan-Peregrino, M., Carlisle, R. C., Hernandez-Alcoceba, R., Iggo, R., Homicsko, K., Fisher, K. D., Hallden, G., Mautner, V., Shen, Y. & Seymour, L. W. (2008). Comparison of molecular strategies for breast cancer virotherapy using oncolytic adenovirus. *Hum Gene Ther* **19**, 873-886.

Belousova, N., Krendelchtchikova, V., Curiel, D. T. & Krasnykh, V. (2002). Modulation of adenovirus vector tropism via incorporation of polypeptide ligands into the fiber protein. *J Virol* **76**, 8621-8631.

Belousova, N., Mikheeva, G., Gelovani, J. & Krasnykh, V. (2008). Modification of adenovirus capsid with a designed protein ligand yields a gene vector targeted to a major molecular marker of cancer. *J Virol* **82**, 630-637.

Bennett, E. M., Bennink, J. R., Yewdell, J. W. & Brodsky, F. M. (1999). Cutting edge: adenovirus E19 has two mechanisms for affecting class I MHC expression. *J Immunol* **162**, 5049-5052.

Bergelson, J. M., Cunningham, J. A., Droguett, G., Kurt-Jones, E. A., Krithivas, A., Hong, J. S., Horwitz, M. S., Crowell, R. L. & Finberg, R. W. (1997). Isolation of a common receptor for Coxsackie B viruses and adenoviruses 2 and 5. *Science* **275**, 1320-1323.

Bergelson, J. M., Krithivas, A., Celi, L., Droguett, G., Horwitz, M. S., Wickham, T., Crowell, R. L. & Finberg, R. W. (1998). The murine CAR homolog is a receptor for coxsackie B viruses and adenoviruses. *J Virol* **72**, 415-419.

Berget, S. M., Moore, C. & Sharp, P. A. (1977). Spliced segments at the 5' terminus of adenovirus 2 late mRNA. *Proc Natl Acad Sci U S A* **74**, 3171-3175.

Berget, S. M. & Sharp, P. A. (1977). A spliced sequence at the 5'-terminus of adenovirus late mRNA. *Brookhaven Symp Biol*, 332-344.

Berk, A. J. (1986a). Adenovirus promoters and E1A transactivation. *Annu Rev Genet* **20**, 45-79.

Berk, A. J. (1986b). Functions of adenovirus E1A. *Cancer Surv* **5**, 367-387.

Berk, A. J., Lee, F., Harrison, T., Williams, J. & Sharp, P. A. (1979). Pre-early adenovirus 5 gene product regulates synthesis of early viral messenger RNAs. *Cell* **17**, 935-944.

Berryman, S., Clark, S., Monaghan, P. & Jackson, T. (2005). Early events in integrin alphavbeta6-mediated cell entry of foot-and-mouth disease virus. *J Virol* **79**, 8519-8534.

Bhat, N. R. & Fan, F. (2002). Adenovirus infection induces microglial activation: involvement of mitogen-activated protein kinase pathways. *Brain Res* **948**, 93-101.

Bierman, H. R., Crile, D. M., Dod, K. S., Kelly, K. H., Petrakis, N. L., White, L. P. & Shimkin, M. B. (1953). Remissions in leukemia of childhood following acute infectious disease: staphylococcus and streptococcus, varicella, and feline panleukopenia. *Cancer* **6**, 591-605.

Bischoff, J. R., Kirn, D. H., Williams, A., Heise, C., Horn, S., Muna, M., Ng, L., Nye, J. A., Sampson-Johannes, A., Fattaey, A. & McCormick, F. (1996). An adenovirus mutant that replicates selectively in p53-deficient human tumor cells. *Science* **274**, 373-376.

Blackhall, F. H., Merry, C. L., Davies, E. J. & Jayson, G. C. (2001). Heparan sulfate proteoglycans and cancer. *Br J Cancer* **85**, 1094-1098.

Bluming, A. Z. & Ziegler, J. L. (1971). Regression of Burkitt's lymphoma in association with measles infection. *Lancet* **2**, 105-106.

Bortolanza, S., Alzuguren, P., Bunuales, M., Qian, C., Prieto, J. & Hernandez-Alcoceba, R. (2007). Human adenovirus replicates in immunocompetent models of pancreatic cancer in Syrian hamsters. *Hum Gene Ther* **18**, 681-690.

Bortolanza, S., Bunuales, M., Alzuguren, P., Lamas, O., Aldabe, R., Prieto, J. & Hernandez-Alcoceba, R. (2009). Deletion of the E3-6.7K/gp19K region reduces the persistence of wild-type adenovirus in a permissive tumor model in Syrian hamsters. *Cancer Gene Ther*.

Bosher, J., Robinson, E. C. & Hay, R. T. (1990). Interactions between the adenovirus type 2 DNA polymerase and the DNA binding domain of nuclear factor I. *New Biol* **2**, 1083-1090.

Bourinbaiar, A. S., Tan, X. & Nagorny, R. (1993). Effect of the oral anticoagulant, warfarin, on HIV-1 replication and spread. *Aids* **7**, 129-130.

Bouvet, M., Fang, B., Ekmekcioglu, S., Ji, L., Bucana, C. D., Hamada, K., Grimm, E. A. & Roth, J. A. (1998). Suppression of the immune response to an adenovirus vector and enhancement of intratumoral transgene expression by low-dose etoposide. *Gene Ther* **5**, 189-195.

Branton, P. E. & Rowe, D. T. (1985). Stabilities and interrelations of multiple species of human adenovirus type 5 early region 1 proteins in infected and transformed cells. *J Virol* **56**, 633-638.

Bray, F., Sankila, R., Ferlay, J. & Parkin, D. M. (2002). Estimates of cancer incidence and mortality in Europe in 1995. *Eur J Cancer* **38**, 99-166.

Breuss, J. M., Gallo, J., DeLisser, H. M., Klimanskaya, I. V., Folkesson, H. G., Pittet, J. F., Nishimura, S. L., Aldape, K., Landers, D. V., Carpenter, W. & et al. (1995). Expression of the beta 6 integrin subunit in development, neoplasia and tissue repair suggests a role in epithelial remodeling. *J Cell Sci* **108 (Pt 6)**, 2241-2251.

Breuss, J. M., Gillett, N., Lu, L., Sheppard, D. & Pytela, R. (1993). Restricted distribution of integrin beta 6 mRNA in primate epithelial tissues. *J Histochem Cytochem* **41**, 1521-1527.

Brown, J. M. & Giaccia, A. J. (1998). The unique physiology of solid tumors: opportunities (and problems) for cancer therapy. *Cancer Res* **58**, 1408-1416.

Brunetti-Pierri, N., Palmer, D. J., Beaudet, A. L., Carey, K. D., Finegold, M. & Ng, P. (2004). Acute toxicity after high-dose systemic injection of helper-dependent adenoviral vectors into nonhuman primates. *Hum Gene Ther* **15**, 35-46.

Burman, A., Clark, S., Abrescia, N. G., Fry, E. E., Stuart, D. I. & Jackson, T. (2006). Specificity of the VP1 GH loop of Foot-and-Mouth Disease virus for alphav integrins. *J Virol* **80**, 9798-9810.

Buscarini, M., Quek, M. L., Gilliam-Hegarich, S., Kasahara, N. & Bochner, B. (2007). Adenoviral receptor expression of normal bladder and transitional cell carcinoma of the bladder. *Urol Int* **78**, 160-166.

Campos, S. K., Parrott, M. B. & Barry, M. A. (2004). Avidin-based targeting and purification of a protein IX-modified, metabolically biotinylated adenoviral vector. *Mol Ther* **9**, 942-954.

Carlisle, R. C., Di, Y., Cerny, A. M., Sonnen, A. F., Sim, R. B., Green, N. K., Subr, V., Ulbrich, K., Gilbert, R. J., Fisher, K. D., Finberg, R. W. & Seymour, L. W. (2009). Human erythrocytes bind and inactivate type 5 adenovirus by presenting Coxsackie virus-adenovirus receptor and complement receptor 1. *Blood* **113**, 1909-1918.

Carmody, R. J., Maguschak, K. & Chen, Y. H. (2006). A novel mechanism of nuclear factor-kappaB regulation by adenoviral protein 14.7K. *Immunology* **117**, 188-195.

Cascallo, M., Alonso, M. M., Rojas, J. J., Perez-Gimenez, A., Fueyo, J. & Alemany, R. (2007). Systemic toxicity-efficacy profile of ICOVIR-5, a potent and selective oncolytic adenovirus based on the pRB pathway. *Mol Ther* **15**, 1607-1615.

Cepko, C. L. & Sharp, P. A. (1982). Assembly of adenovirus major capsid protein is mediated by a nonvirion protein. *Cell* **31**, 407-415.

Cerullo, V., Seiler, M. P., Mane, V., Brunetti-Pierri, N., Clarke, C., Bertin, T. K., Rodgers, J. R. & Lee, B. (2007). Toll-like receptor 9 triggers an innate immune response to helper-dependent adenoviral vectors. *Mol Ther* **15**, 378-385.

Chappell, J. D., Gunn, V. L., Wetzel, J. D., Baer, G. S. & Dermody, T. S. (1997). Mutations in type 3 reovirus that determine binding to sialic acid are contained in the fibrous tail domain of viral attachment protein sigma1. *J Virol* **71**, 1834-1841.

Chen, M., Mermod, N. & Horwitz, M. S. (1990). Protein-protein interactions between adenovirus DNA polymerase and nuclear factor I mediate formation of the DNA replication preinitiation complex. *J Biol Chem* **265**, 18634-18642.

Cheng, C. Y., Blanchette, P. & Branton, P. E. (2007). The adenovirus E4orf6 E3 ubiquitin ligase complex assembles in a novel fashion. *Virology* **364**, 36-44.

Chillon, M., Lee, J. H., Fasbender, A. & Welsh, M. J. (1998). Adenovirus complexed with polyethylene glycol and cationic lipid is shielded from neutralizing antibodies in vitro. *Gene Ther* **5**, 995-1002.

Chiu, C. Y., Wu, E., Brown, S. L., Von Seggern, D. J., Nemerow, G. R. & Stewart, P. L. (2001). Structural analysis of a fiber-pseudotyped adenovirus with ocular tropism suggests differential modes of cell receptor interactions. *J Virol* **75**, 5375-5380.

Cho, W. K., Seong, Y. R., Lee, Y. H., Kim, M. J., Hwang, K. S., Yoo, J., Choi, S., Jung, C. R. & Im, D. S. (2004). Oncolytic effects of adenovirus mutant capable of replicating in hypoxic and normoxic regions of solid tumor. *Mol Ther* **10**, 938-949.

Chonn, A., Cullis, P. R. & Devine, D. V. (1991). The role of surface charge in the activation of the classical and alternative pathways of complement by liposomes. *J Immunol* **146**, 4234-4241.

Chow, L. T., Gelinas, R. E., Broker, T. R. & Roberts, R. J. (1977). An amazing sequence arrangement at the 5' ends of adenovirus 2 messenger RNA. *Cell* **12**, 1-8.

Christensen, J. B., Byrd, S. A., Walker, A. K., Strahler, J. R., Andrews, P. C. & Imperiale, M. J. (2008). Presence of the adenovirus IVa2 protein at a single vertex of the mature virion. *J Virol* **82**, 9086-9093.

Chroboczek, J., Ruigrok, R. W. & Cusack, S. (1995). Adenovirus fiber. *Curr Top Microbiol Immunol* **199 (Pt 1)**, 163-200.

Chu, Y., Heistad, D., Cybulsky, M. I. & Davidson, B. L. (2001). Vascular cell adhesion molecule-1 augments adenovirus-mediated gene transfer. *Arterioscler Thromb Vasc Biol* **21**, 238-242.

Cichon, G., Schmidt, H. H., Benhidjeb, T., Loser, P., Ziemer, S., Haas, R., Grewe, N., Schnieders, F., Heeren, J., Manns, M. P., Schlag, P. M. & Strauss, M. (1999). Intravenous administration of recombinant adenoviruses causes thrombocytopenia, anemia and erythroblastosis in rabbits. *J Gene Med* **1**, 360-371.

Cohen, C. J., Shieh, J. T., Pickles, R. J., Okegawa, T., Hsieh, J. T. & Bergelson, J. M. (2001). The coxsackievirus and adenovirus receptor is a transmembrane component of the tight junction. *Proc Natl Acad Sci U S A* **98**, 15191-15196.

Cohen, S. N., Chang, A. C. & Hsu, L. (1972). Nonchromosomal antibiotic resistance in bacteria: genetic transformation of Escherichia coli by R-factor DNA. *Proc Natl Acad Sci U S A* **69**, 2110-2114.

Colcher, D., Pavlinkova, G., Beresford, G., Booth, B. J., Choudhury, A. & Batra, S. K. (1998). Pharmacokinetics and biodistribution of genetically-engineered antibodies. *Q J Nucl Med* **42**, 225-241.

Cotten, M. & Weber, J. M. (1995). The adenovirus protease is required for virus entry into host cells. *Virology* **213**, 494-502.

Coughlan, L., Vallath, S., Saha, A., Flak, M., McNeish, I. A., Vassaux, G., Marshall, J. F., Hart, I. R. & Thomas, G. J. (2009). In vivo retargeting of adenovirus type 5 to alphavbeta6 integrin results in reduced hepatotoxicity and improved tumor uptake following systemic delivery. *J Virol* **83**, 6416-6428.

Cox, J. H., Bennink, J. R. & Yewdell, J. W. (1991). Retention of adenovirus E19 glycoprotein in the endoplasmic reticulum is essential to its ability to block antigen presentation. *J Exp Med* **174**, 1629-1637.

Crawford-Miksza, L. & Schnurr, D. P. (1996). Analysis of 15 adenovirus hexon proteins reveals the location and structure of seven hypervariable regions containing serotype-specific residues. *J Virol* **70**, 1836-1844.

Cripe, T. P., Dunphy, E. J., Holub, A. D., Saini, A., Vasi, N. H., Mahller, Y. Y., Collins, M. H., Snyder, J. D., Krasnykh, V., Curiel, D. T., Wickham, T. J., DeGregori, J., Bergelson, J. M. & Currier, M. A. (2001). Fiber knob modifications overcome low, heterogeneous expression of the coxsackievirus-adenovirus receptor that limits adenovirus gene transfer and oncolysis for human rhabdomyosarcoma cells. *Cancer Res* **61**, 2953-2960.

Crompton, J., Toogood, C. I., Wallis, N. & Hay, R. T. (1994). Expression of a foreign epitope on the surface of the adenovirus hexon. *J Gen Virol* **75 (Pt 1)**, 133-139.

Cuesta, R., Xi, Q. & Schneider, R. J. (2000). Adenovirus-specific translation by displacement of kinase Mnk1 from cap-initiation complex eIF4F. *Embo J* **19**, 3465-3474.

Cuesta, R., Xi, Q. & Schneider, R. J. (2004). Structural basis for competitive inhibition of eIF4G-Mnk1 interaction by the adenovirus 100-kilodalton protein. *J Virol* **78**, 7707-7716.

Curiel, D. T. (1999). Strategies to adapt adenoviral vectors for targeted delivery. *Ann N Y Acad Sci* **886**, 158-171.

Dales, S. & Chardonnet, Y. (1973). Early events in the interaction of adenoviruses with HeLa cells. IV. Association with microtubules and the nuclear pore complex during vectorial movement of the inoculum. *Virology* **56**, 465-483.

Davis, D. A., Dorsey, K., Wingfield, P. T., Stahl, S. J., Kaufman, J., Fales, H. M. & Levine, R. L. (1996). Regulation of HIV-1 protease activity through cysteine modification. *Biochemistry* **35**, 2482-2488.

Davison, E., Diaz, R. M., Hart, I. R., Santis, G. & Marshall, J. F. (1997). Integrin alpha5beta1-mediated adenovirus infection is enhanced by the integrin-activating antibody TS2/16. *J Virol* **71**, 6204-6207.

Davison, E., Kirby, I., Elliott, T. & Santis, G. (1999). The human HLA-A*0201 allele, expressed in hamster cells, is not a high-affinity receptor for adenovirus type 5 fiber. *J Virol* **73**, 4513-4517.

Davison, E., Kirby, I., Whitehouse, J., Hart, I., Marshall, J. F. & Santis, G. (2001). Adenovirus type 5 uptake by lung adenocarcinoma cells in culture correlates with Ad5 fibre binding is mediated by alpha(v)beta1 integrin and can be modulated by changes in beta1 integrin function. *J Gene Med* **3**, 550-559.

De Geest, B., Snoeys, J., Van Linthout, S., Lievens, J. & Collen, D. (2005). Elimination of innate immune responses and liver inflammation by PEGylation of adenoviral vectors and methylprednisolone. *Hum Gene Ther* **16**, 1439-1451.

Debbas, M. & White, E. (1993). Wild-type p53 mediates apoptosis by E1A, which is inhibited by E1B. *Genes Dev* **7**, 546-554.

Dechecchi, M. C., Melotti, P., Bonizzato, A., Santacatterina, M., Chilosi, M. & Cabrini, G. (2001). Heparan sulfate glycosaminoglycans are receptors sufficient to mediate the initial binding of adenovirus types 2 and 5. *J Virol* **75**, 8772-8780.

Dechecchi, M. C., Tamanini, A., Bonizzato, A. & Cabrini, G. (2000). Heparan sulfate glycosaminoglycans are involved in adenovirus type 5 and 2-host cell interactions. *Virology* **268**, 382-390.

Denby, L., Work, L. M., Seggern, D. J., Wu, E., McVey, J. H., Nicklin, S. A. & Baker, A. H. (2007). Development of renal-targeted vectors through combined in vivo phage display and capsid engineering of adenoviral fibers from serotype 19p. *Mol Ther* **15**, 1647-1654.

Derynck, R., Akhurst, R. J. & Balmain, A. (2001). TGF-beta signaling in tumor suppression and cancer progression. *Nat Genet* **29**, 117-129.

Dhar, D., Spencer, J. F., Toth, K. & Wold, W. S. (2009). Effect of preexisting immunity on oncolytic adenovirus vector INGN 007 antitumor efficacy in immunocompetent and immunosuppressed Syrian hamsters. *J Virol* **83**, 2130-2139.

Dhawan, P., Singh, A. B., Deane, N. G., No, Y., Shiou, S. R., Schmidt, C., Neff, J., Washington, M. K. & Beauchamp, R. D. (2005). Claudin-1 regulates cellular transformation and metastatic behavior in colon cancer. *J Clin Invest* **115**, 1765-1776.

Di Paolo, N. C., Kalyuzhniy, O. & Shayakhmetov, D. M. (2007). Fiber shaft-chimeric adenovirus vectors lacking the KKTK motif efficiently infect liver cells in vivo. *J Virol* **81**, 12249-12259.

Di Paolo, N. C., Miao, E. A., Iwakura, Y., Murali-Krishna, K., Aderem, A., Flavell, R. A., Papayannopoulou, T. & Shayakhmetov, D. M. (2009a). Virus Binding to a Plasma Membrane Receptor Triggers Interleukin-1alpha-Mediated Proinflammatory Macrophage Response In Vivo. *Immunity*.

Di Paolo, N. C., van Rooijen, N. & Shayakhmetov, D. M. (2009b). Redundant and synergistic mechanisms control the sequestration of blood-born adenovirus in the liver. *Mol Ther* **17**, 675-684.

Diaconu, I., Denby, L., Pesonen, S., Cerullo, V., Bauerschmitz, G. J., Guse, K., Rajecki, M., Dias, J. D., Taari, K., Kanerva, A., Baker, A. H. & Hemminki, A. (2009). Serotype chimeric and fiber-mutated adenovirus Ad5/19p-HIT for targeting renal cancer and untargeting the liver. *Hum Gene Ther* **20**, 611-620.

DiCara, D., Burman, A., Clark, S., Berryman, S., Howard, M. J., Hart, I. R., Marshall, J. F. & Jackson, T. (2008). Foot-and-mouth disease virus forms a highly stable, EDTA-resistant complex with its principal receptor, integrin alphavbeta6: implications for infectiousness. *J Virol* **82**, 1537-1546.

DiCara, D., Rapisarda, C., Sutcliffe, J. L., Violette, S. M., Weinreb, P. H., Hart, I. R., Howard, M. J. & Marshall, J. F. (2007). Structure-function analysis of Arg-Gly-Asp helix motifs in alpha v beta 6 integrin ligands. *J Biol Chem* **282**, 9657-9665.

Ding, J., McGrath, W. J., Sweet, R. M. & Mangel, W. F. (1996). Crystal structure of the human adenovirus proteinase with its 11 amino acid cofactor. *Embo J* **15**, 1778-1783.

Dixit, R. B., Chen, A., Chen, J. & Sheppard, D. (1996). Identification of a sequence within the integrin beta6 subunit cytoplasmic domain that is required to support the specific effect of alphavbeta6 on proliferation in three-dimensional culture. *J Biol Chem* **271**, 25976-25980.

Dmitriev, I., Kashentseva, E., Rogers, B. E., Krasnykh, V. & Curiel, D. T. (2000). Ectodomain of coxsackievirus and adenovirus receptor genetically fused to epidermal growth factor mediates adenovirus targeting to epidermal growth factor receptor-positive cells. *J Virol* **74**, 6875-6884.

Dmitriev, I., Krasnykh, V., Miller, C. R., Wang, M., Kashentseva, E., Mikheeva, G., Belousova, N. & Curiel, D. T. (1998). An adenovirus vector with genetically modified fibers demonstrates expanded tropism via utilization of a coxsackievirus and adenovirus receptor-independent cell entry mechanism. *J Virol* **72**, 9706-9713.

Dorner, A. A., Wegmann, F., Butz, S., Wolburg-Buchholz, K., Wolburg, H., Mack, A., Nasdala, I., August, B., Westermann, J., Rathjen, F. G. & Vestweber, D. (2005). Coxsackievirus-adenovirus receptor (CAR) is essential for early embryonic cardiac development. *J Cell Sci* **118**, 3509-3521.

Doronin, K., Toth, K., Kuppuswamy, M., Krajcsi, P., Tollefson, A. E. & Wold, W. S. (2003). Overexpression of the ADP (E3-11.6K) protein increases cell lysis and spread of adenovirus. *Virology* **305**, 378-387.

Douglas, J. T., Kim, M., Sumerel, L. A., Carey, D. E. & Curiel, D. T. (2001). Efficient oncolysis by a replicating adenovirus (ad) in vivo is critically dependent on tumor expression of primary ad receptors. *Cancer Res* **61**, 813-817.

Douglas, J. T., Miller, C. R., Kim, M., Dmitriev, I., Mikheeva, G., Krasnykh, V. & Curiel, D. T. (1999). A system for the propagation of adenoviral vectors with genetically modified receptor specificities. *Nat Biotechnol* **17**, 470-475.

Duncan, S. J., Gordon, F. C., Gregory, D. W., McPhie, J. L., Postlethwaite, R., White, R. & Willcox, H. N. (1978). Infection of mouse liver by human adenovirus type 5. *J Gen Virol* **40**, 45-61.

Eggerman, T. L., Mondoro, T. H., Lozier, J. N. & Vostal, J. G. (2002). Adenoviral vectors do not induce, inhibit, or potentiate human platelet aggregation. *Hum Gene Ther* **13**, 125-128.

Einfeld, D. A., Schroeder, R., Roelvink, P. W., Lizonova, A., King, C. R., Kovesdi, I. & Wickham, T. J. (2001). Reducing the native tropism of adenovirus vectors requires removal of both CAR and integrin interactions. *J Virol* **75**, 11284-11291.

Elayadi, A. N., Samli, K. N., Prudkin, L., Liu, Y. H., Bian, A., Xie, X. J., Wistuba, II, Roth, J. A., McGuire, M. J. & Brown, K. C. (2007). A peptide selected by biopanning identifies the integrin alphavbeta6 as a prognostic biomarker for nonsmall cell lung cancer. *Cancer Res* **67**, 5889-5895.

Elkon, K. B., Liu, C. C., Gall, J. G., Trevejo, J., Marino, M. W., Abrahamsen, K. A., Song, X., Zhou, J. L., Old, L. J., Crystal, R. G. & Falck-Pedersen, E. (1997).

Tumor necrosis factor alpha plays a central role in immune-mediated clearance of adenoviral vectors. *Proc Natl Acad Sci U S A* **94**, 9814-9819.

Engler, H., Machemer, T., Philopena, J., Wen, S. F., Quijano, E., Ramachandra, M., Tsai, V. & Ralston, R. (2004). Acute hepatotoxicity of oncolytic adenoviruses in mouse models is associated with expression of wild-type E1a and induction of TNF-alpha. *Virology* **328**, 52-61.

Eto, Y., Yoshioka, Y., Mukai, Y., Okada, N. & Nakagawa, S. (2008). Development of PEGylated adenovirus vector with targeting ligand. *Int J Pharm* **354**, 3-8.

Evans, J. D. & Hearing, P. (2003). Distinct roles of the Adenovirus E4 ORF3 protein in viral DNA replication and inhibition of genome concatenation. *J Virol* **77**, 5295-5304.

Evans, J. D. & Hearing, P. (2005). Relocalization of the Mre11-Rad50-Nbs1 complex by the adenovirus E4 ORF3 protein is required for viral replication. *J Virol* **79**, 6207-6215.

Everitt, E., Lutter, L. & Philipson, L. (1975). Structural proteins of adenoviruses. XII. Location and neighbor relationship among proteins of adenovirion type 2 as revealed by enzymatic iodination, immunoprecipitation and chemical cross-linking. *Virology* **67**, 197-208.

Everitt, E., Sundquist, B., Pettersson, U. & Philipson, L. (1973). Structural proteins of adenoviruses. X. Isolation and topography of low molecular weight antigens from the virion of adenovirus type 2. *Virology* **52**, 130-147.

Ewing, S. G., Byrd, S. A., Christensen, J. B., Tyler, R. E. & Imperiale, M. J. (2007). Ternary complex formation on the adenovirus packaging sequence by the IVa2 and L4 22-kilodalton proteins. *J Virol* **81**, 12450-12457.

Falanga, A. (2005). Thrombophilia in cancer. *Semin Thromb Hemost* **31**, 104-110.

Farmer, C., Morton, P. E., Snippe, M., Santis, G. & Parsons, M. (2009). Coxsackie adenovirus receptor (CAR) regulates integrin function through activation of p44/42 MAPK. *Exp Cell Res*.

Fauquet, C. M., Mayo, M. A., Maniloff, J., Desselberger, U. & Ball, L. A. (2005). Virus Taxonomy; Seventh Report of the International Committee of Viruses. *San Diego: Academic Press*.

Fechner, H., Haack, A., Wang, H., Wang, X., Eizema, K., Pauschinger, M., Schoemaker, R., Veghel, R., Houtsmuller, A., Schultheiss, H. P., Lamers, J. & Poller, W. (1999). Expression of coxsackie adenovirus receptor and alphav-integrin does not correlate with adenovector targeting in vivo indicating anatomical vector barriers. *Gene Ther* **6**, 1520-1535.

Fejer, G., Drechsel, L., Liese, J., Schleicher, U., Ruzsics, Z., Imelli, N., Greber, U. F., Keck, S., Hildenbrand, B., Krug, A., Bogdan, C. & Freudenberg, M. A.

(2008). Key role of splenic myeloid DCs in the IFN-alphabeta response to adenoviruses in vivo. *PLoS Pathog* **4**, e1000208.

Feldman, A. L., Restifo, N. P., Alexander, H. R., Bartlett, D. L., Hwu, P., Seth, P. & Libutti, S. K. (2000). Antiangiogenic gene therapy of cancer utilizing a recombinant adenovirus to elevate systemic endostatin levels in mice. *Cancer Res* **60**, 1503-1506.

Ferrigno, D., Buccheri, G. & Ricca, I. (2001). Prognostic significance of blood coagulation tests in lung cancer. *Eur Respir J* **17**, 667-673.

Fisher, K. D., Stallwood, Y., Green, N. K., Ulbrich, K., Mautner, V. & Seymour, L. W. (2001). Polymer-coated adenovirus permits efficient retargeting and evades neutralising antibodies. *Gene Ther* **8**, 341-348.

Folkman, J. (1971). Tumor angiogenesis: therapeutic implications. *N Engl J Med* **285**, 1182-1186.

Folkman, J. (1995). Angiogenesis in cancer, vascular, rheumatoid and other disease. *Nat Med* **1**, 27-31.

Freimuth, P., Springer, K., Berard, C., Hainfeld, J., Bewley, M. & Flanagan, J. (1999). Coxsackievirus and adenovirus receptor amino-terminal immunoglobulin V-related domain binds adenovirus type 2 and fiber knob from adenovirus type 12. *J Virol* **73**, 1392-1398.

Fromm, J. R., Hileman, R. E., Caldwell, E. E., Weiler, J. M. & Linhardt, R. J. (1995). Differences in the interaction of heparin with arginine and lysine and the importance of these basic amino acids in the binding of heparin to acidic fibroblast growth factor. *Arch Biochem Biophys* **323**, 279-287.

Fueyo, J., Gomez-Manzano, C., Alemany, R., Lee, P. S., McDonnell, T. J., Mitlianga, P., Shi, Y. X., Levin, V. A., Yung, W. K. & Kyritsis, A. P. (2000). A mutant oncolytic adenovirus targeting the Rb pathway produces anti-glioma effect in vivo. *Oncogene* **19**, 2-12.

Furumoto, K., Nagayama, S., Ogawara, K., Takakura, Y., Hashida, M., Higaki, K. & Kimura, T. (2004). Hepatic uptake of negatively charged particles in rats: possible involvement of serum proteins in recognition by scavenger receptor. *J Control Release* **97**, 133-141.

Gaggar, A., Shayakhmetov, D. & Lieber, A. (2007). Identifying functional adenovirus-host interactions using tandem mass spectrometry. *Methods Mol Med* **131**, 141-155.

Gaggar, A., Shayakhmetov, D. M. & Lieber, A. (2003). CD46 is a cellular receptor for group B adenoviruses. *Nat Med* **9**, 1408-1412.

Gahery-Segard, H., Farace, F., Godfrin, D., Gaston, J., Lengagne, R., Tursz, T., Boulanger, P. & Guillet, J. G. (1998). Immune response to recombinant capsid

proteins of adenovirus in humans: antifiber and anti-penton base antibodies have a synergistic effect on neutralizing activity. *J Virol* **72**, 2388-2397.

Gahery-Segard, H., Juillard, V., Gaston, J., Lengagne, R., Pavirani, A., Boulanger, P. & Guillet, J. G. (1997). Humoral immune response to the capsid components of recombinant adenoviruses: routes of immunization modulate virus-induced Ig subclass shifts. *Eur J Immunol* **27**, 653-659.

Galy, A. H. & Spits, H. (1992). CD40 is functionally expressed on human thymic epithelial cells. *J Immunol* **149**, 775-782.

Ganesh, S., Gonzalez-Edick, M., Gibbons, D., Van Roey, M. & Jooss, K. (2008). Intratumoral coadministration of hyaluronidase enzyme and oncolytic adenoviruses enhances virus potency in metastatic tumor models. *Clin Cancer Res* **14**, 3933-3941.

Ganesh, S., Gonzalez Edick, M., Idamakanti, N., Abramova, M., Vanroey, M., Robinson, M., Yun, C. O. & Jooss, K. (2007). Relaxin-expressing, fiber chimeric oncolytic adenovirus prolongs survival of tumor-bearing mice. *Cancer Res* **67**, 4399-4407.

Ganly, I., Mautner, V. & Balmain, A. (2000). Productive replication of human adenoviruses in mouse epidermal cells. *J Virol* **74**, 2895-2899.

Ganter, M. T., Roux, J., Miyazawa, B., Howard, M., Frank, J. A., Su, G., Sheppard, D., Violette, S. M., Weinreb, P. H., Horan, G. S., Matthay, M. A. & Pittet, J. F. (2008). Interleukin-1beta causes acute lung injury via alphavbeta5 and alphavbeta6 integrin-dependent mechanisms. *Circ Res* **102**, 804-812.

Gimenez-Alejandre, M., Cascallo, M., Bayo-Puxan, N. & Alemany, R. (2008). Coagulation factors determine tumor transduction in vivo. *Hum Gene Ther*.

Ginsberg, H. S., Moldawer, L. L., Sehgal, P. B., Redington, M., Kilian, P. L., Chanock, R. M. & Prince, G. A. (1991). A mouse model for investigating the molecular pathogenesis of adenovirus pneumonia. *Proc Natl Acad Sci U S A* **88**, 1651-1655.

Glasgow, J. N., Everts, M. & Curiel, D. T. (2006). Transductional targeting of adenovirus vectors for gene therapy. *Cancer Gene Ther* **13**, 830-844.

Gonzalez, R., Huang, W., Finnen, R., Bragg, C. & Flint, S. J. (2006). Adenovirus E1B 55-kilodalton protein is required for both regulation of mRNA export and efficient entry into the late phase of infection in normal human fibroblasts. *J Virol* **80**, 964-974.

Gonzalez, R., Vereecque, R., Wickham, T. J., Facon, T., Hetuin, D., Kovesdi, I., Bauters, F., Fenaux, P. & Quesnel, B. (1999). Transduction of bone marrow cells by the AdZ.F(pK7) modified adenovirus demonstrates preferential gene transfer in myeloma cells. *Hum Gene Ther* **10**, 2709-2717.

Grable, M. & Hearing, P. (1992). cis and trans requirements for the selective packaging of adenovirus type 5 DNA. *J Virol* **66**, 723-731.

Grandien, M., Pettersson, C. A., Svensson, L. & Uhnoo, I. (1987). Latex agglutination test for adenovirus diagnosis in diarrheal disease. *J Med Virol* **23**, 311-316.

Greber, U. F. (1998). Virus assembly and disassembly: the adenovirus cysteine protease as a trigger factor. *Rev Med Virol* **8**, 213-222.

Greber, U. F., Suomalainen, M., Stidwill, R. P., Boucke, K., Ebersold, M. W. & Helenius, A. (1997). The role of the nuclear pore complex in adenovirus DNA entry. *Embo J* **16**, 5998-6007.

Greber, U. F., Willetts, M., Webster, P. & Helenius, A. (1993). Stepwise dismantling of adenovirus 2 during entry into cells. *Cell* **75**, 477-486.

Green, N. K., Morrison, J., Hale, S., Briggs, S. S., Stevenson, M., Subr, V., Ulbrich, K., Chandler, L., Mautner, V., Seymour, L. W. & Fisher, K. D. (2008). Retargeting polymer-coated adenovirus to the FGF receptor allows productive infection and mediates efficacy in a peritoneal model of human ovarian cancer. *J Gene Med* **10**, 280-289.

Greenberger, S., Shaish, A., Varda-Bloom, N., Levanon, K., Breitbart, E., Goldberg, I., Barshack, I., Hodish, I., Yaacov, N., Bangio, L., Goncharov, T., Wallach, D. & Harats, D. (2004). Transcription-controlled gene therapy against tumor angiogenesis. *J Clin Invest* **113**, 1017-1024.

Gros, A., Martinez-Quintanilla, J., Puig, C., Guedan, S., Mollevi, D. G., Alemany, R. & Cascallo, M. (2008). Bioselection of a gain of function mutation that enhances adenovirus 5 release and improves its antitumoral potency. *Cancer Res* **68**, 8928-8937.

Gu, X., Niu, J., Dorahy, D. J., Scott, R. & Agrez, M. V. (2002). Integrin alpha(v)beta6-associated ERK2 mediates MMP-9 secretion in colon cancer cells. *Br J Cancer* **87**, 348-351.

Guan, H., McGuire, M. J., Li, S. & Brown, K. C. (2008). Peptide-targeted polyglutamic acid doxorubicin conjugates for the treatment of alpha(v)beta(6)-positive cancers. *Bioconjug Chem* **19**, 1813-1821.

Guedan, S., Gros, A., Cascallo, M., Vile, R., Mercade, E. & Alemany, R. (2008). Syncytia formation affects the yield and cytotoxicity of an adenovirus expressing a fusogenic glycoprotein at a late stage of replication. *Gene Ther* **15**, 1240-1245.

Guo, W. & Giancotti, F. G. (2004). Integrin signalling during tumour progression. *Nat Rev Mol Cell Biol* **5**, 816-826.

Guo, W., Zhu, H., Zhang, L., Davis, J., Teraishi, F., Roth, J. A., Stephens, C., Fueyo, J., Jiang, H., Conrad, C. & Fang, B. (2006). Combination effect of oncolytic adenovirotherapy and TRAIL gene therapy in syngeneic murine breast cancer models. *Cancer Gene Ther* **13**, 82-90.

Guse, K., Diaconu, I., Rajecki, M., Sloniecka, M., Hakkarainen, T., Ristimaki, A., Kanerva, A., Pesonen, S. & Hemminki, A. (2009). Ad5/3-9HIF-Delta24-VEGFR-1-Ig, an infectivity enhanced, dual-targeted and antiangiogenic oncolytic adenovirus for kidney cancer treatment. *Gene Ther*.

Gustin, K. E. & Imperiale, M. J. (1998). Encapsidation of viral DNA requires the adenovirus L1 52/55-kilodalton protein. *J Virol* **72**, 7860-7870.

Haapasalmi, K., Zhang, K., Tonnesen, M., Olerud, J., Sheppard, D., Salo, T., Kramer, R., Clark, R. A., Uitto, V. J. & Larjava, H. (1996). Keratinocytes in human wounds express alpha v beta 6 integrin. *J Invest Dermatol* **106**, 42-48.

Haisma, H. J., Boesjes, M., Beerens, A. M., van der Strate, B. W., Curiel, D. T., Pluddemann, A., Gordon, S. & Bellu, A. R. (2009). Scavenger Receptor A: A New Route for Adenovirus 5. *Mol Pharm* **6**, 366-374.

Haisma, H. J., Kamps, J. A., Kamps, G. K., Plantinga, J. A., Rots, M. G. & Bellu, A. R. (2008). Polyinosinic acid enhances delivery of adenovirus vectors in vivo by preventing sequestration in liver macrophages. *J Gen Virol* **89**, 1097-1105.

Hakkarainen, T., Hemminki, A., Pereboev, A. V., Barker, S. D., Asiedu, C. K., Strong, T. V., Kanerva, A., Wahlfors, J. & Curiel, D. T. (2003). CD40 is expressed on ovarian cancer cells and can be utilized for targeting adenoviruses. *Clin Cancer Res* **9**, 619-624.

Hallden, G., Hill, R., Wang, Y., Anand, A., Liu, T. C., Lemoine, N. R., Francis, J., Hawkins, L. & Kirn, D. (2003). Novel immunocompetent murine tumor models for the assessment of replication-competent oncolytic adenovirus efficacy. *Mol Ther* **8**, 412-424.

Hamidi, S., Salo, T., Kainulainen, T., Epstein, J., Lerner, K. & Larjava, H. (2000). Expression of alpha(v)beta6 integrin in oral leukoplakia. *Br J Cancer* **82**, 1433-1440.

Harada, J. N., Shevchenko, A., Shevchenko, A., Pallas, D. C. & Berk, A. J. (2002). Analysis of the adenovirus E1B-55K-anchored proteome reveals its link to ubiquitination machinery. *J Virol* **76**, 9194-9206.

Harlow, E., Whyte, P., Franza, B. R., Jr. & Schley, C. (1986). Association of adenovirus early-region 1A proteins with cellular polypeptides. *Mol Cell Biol* **6**, 1579-1589.

Hashizume, H., Baluk, P., Morikawa, S., McLean, J. W., Thurston, G., Roberge, S., Jain, R. K. & McDonald, D. M. (2000). Openings between defective endothelial cells explain tumor vessel leakiness. *Am J Pathol* **156**, 1363-1380.

Hasson, T. B., Ornelles, D. A. & Shenk, T. (1992). Adenovirus L1 52- and 55-kilodalton proteins are present within assembling virions and colocalize with nuclear structures distinct from replication centers. *J Virol* **66**, 6133-6142.

Hasson, T. B., Soloway, P. D., Ornelles, D. A., Doerfler, W. & Shenk, T. (1989). Adenovirus L1 52- and 55-kilodalton proteins are required for assembly of virions. *J Virol* **63**, 3612-3621.

Hausner, S. H., Abbey, C. K., Bold, R. J., Gagnon, M. K., Marik, J., Marshall, J. F., Stanecki, C. E. & Sutcliffe, J. L. (2009a). Targeted In vivo Imaging of Integrin {alpha} v{beta}6 with an Improved Radiotracer and Its Relevance in a Pancreatic Tumor Model. *Cancer Res*.

Hausner, S. H., DiCara, D., Marik, J., Marshall, J. F. & Sutcliffe, J. L. (2007). Use of a peptide derived from foot-and-mouth disease virus for the noninvasive imaging of human cancer: generation and evaluation of 4-[18F]fluorobenzoyl A20FMDV2 for in vivo imaging of integrin alphavbeta6 expression with positron emission tomography. *Cancer Res* **67**, 7833-7840.

Hausner, S. H., Kukis, D. L., Gagnon, M. K., Stanecki, C. E., Ferdani, R., Marshall, J. F., Anderson, C. J. & Sutcliffe, J. L. (2009b). Evaluation of [64Cu]Cu-DOTA and [64Cu]Cu-CB-TE2A chelates for targeted positron emission tomography with an alphavbeta6-specific peptide. *Mol Imaging* **8**, 111-121.

Hawkins, L. K., Johnson, L., Bauzon, M., Nye, J. A., Castro, D., Kitzes, G. A., Young, M. D., Holt, J. K., Trown, P. & Hermiston, T. W. (2001). Gene delivery from the E3 region of replicating human adenovirus: evaluation of the 6.7 K/gp19 K region. *Gene Ther* **8**, 1123-1131.

Hayes, B. W., Telling, G. C., Myat, M. M., Williams, J. F. & Flint, S. J. (1990). The adenovirus L4 100-kilodalton protein is necessary for efficient translation of viral late mRNA species. *J Virol* **64**, 2732-2742.

Hazelbag, S., Kenter, G. G., Gorter, A., Dreef, E. J., Koopman, L. A., Violette, S. M., Weinreb, P. H. & Fleuren, G. J. (2007). Overexpression of the alpha v beta 6 integrin in cervical squamous cell carcinoma is a prognostic factor for decreased survival. *J Pathol* **212**, 316-324.

Hearing, P., Samulski, R. J., Wishart, W. L. & Shenk, T. (1987). Identification of a repeated sequence element required for efficient encapsidation of the adenovirus type 5 chromosome. *J Virol* **61**, 2555-2558.

Heikkila, O., Susi, P., Stanway, G. & Hyypia, T. (2009). Integrin alphaVbeta6 is a high-affinity receptor for coxsackievirus A9. *J Gen Virol* **90**, 197-204.

Henning, P., Magnusson, M. K., Gunneriusson, E., Hong, S. S., Boulanger, P., Nygren, P. A. & Lindholm, L. (2002). Genetic modification of adenovirus 5 tropism by a novel class of ligands based on a three-helix bundle scaffold derived from staphylococcal protein A. *Hum Gene Ther* **13**, 1427-1439.

Herman, J. R., Adler, H. L., Aguilar-Cordova, E., Rojas-Martinez, A., Woo, S., Timme, T. L., Wheeler, T. M., Thompson, T. C. & Scardino, P. T. (1999). In situ gene therapy for adenocarcinoma of the prostate: a phase I clinical trial. *Hum Gene Ther* **10**, 1239-1249.

Hernandez-Alcoceba, R., Pihalja, M., Wicha, M. S. & Clarke, M. F. (2000). A novel, conditionally replicative adenovirus for the treatment of breast cancer that allows controlled replication of E1a-deleted adenoviral vectors. *Hum Gene Ther* **11**, 2009-2024.

Hilleman, M. R. & Werner, J. H. (1954). Recovery of new agent from patients with acute respiratory illness. *Proc Soc Exp Biol Med* **85**, 183-188.

Honda, T., Saitoh, H., Masuko, M., Katagiri-Abe, T., Tominaga, K., Kozakai, I., Kobayashi, K., Kumanishi, T., Watanabe, Y. G., Odani, S. & Kuwano, R. (2000). The coxsackievirus-adenovirus receptor protein as a cell adhesion molecule in the developing mouse brain. *Brain Res Mol Brain Res* **77**, 19-28.

Hong, J. S. & Engler, J. A. (1996). Domains required for assembly of adenovirus type 2 fiber trimers. *J Virol* **70**, 7071-7078.

Hong, S. S., Karayan, L., Tournier, J., Curiel, D. T. & Boulanger, P. A. (1997). Adenovirus type 5 fiber knob binds to MHC class I alpha2 domain at the surface of human epithelial and B lymphoblastoid cells. *Embo J* **16**, 2294-2306.

Hong, S. S., Szolajska, E., Schoehn, G., Franqueville, L., Myhre, S., Lindholm, L., Ruigrok, R. W., Boulanger, P. & Chroboczek, J. (2005). The 100K-chaperone protein from adenovirus serotype 2 (Subgroup C) assists in trimerization and nuclear localization of hexons from subgroups C and B adenoviruses. *J Mol Biol* **352**, 125-138.

Honkavuori, K. S., Pollard, B. D., Rodriguez, M. S., Hay, R. T. & Kemp, G. D. (2004). Dual role of the adenovirus pVI C terminus as a nuclear localization signal and activator of the viral protease. *J Gen Virol* **85**, 3367-3376.

Hoover, K. B., Liao, S. Y. & Bryant, P. J. (1998). Loss of the tight junction MAGUK ZO-1 in breast cancer: relationship to glandular differentiation and loss of heterozygosity. *Am J Pathol* **153**, 1767-1773.

Horan, G. S., Wood, S., Ona, V., Li, D. J., Lukashev, M. E., Weinreb, P. H., Simon, K. J., Hahm, K., Allaire, N. E., Rinaldi, N. J., Goyal, J., Feghali-Bostwick, C. A., Matteson, E. L., O'Hara, C., Lafyatis, R., Davis, G. S., Huang, X., Sheppard, D. & Violette, S. M. (2008). Partial inhibition of integrin

alpha(v)beta6 prevents pulmonary fibrosis without exacerbating inflammation. *Am J Respir Crit Care Med* **177**, 56-65.

Horton, R. M. (1995). PCR-mediated recombination and mutagenesis. SOEing together tailor-made genes. *Mol Biotechnol* **3**, 93-99.

Horton, R. M. (1997). In vitro recombination and mutagenesis of DNA. SOEing together tailor-made genes. *Methods Mol Biol* **67**, 141-149.

Horton, R. M., Cai, Z. L., Ho, S. N. & Pease, L. R. (1990). Gene splicing by overlap extension: tailor-made genes using the polymerase chain reaction. *Biotechniques* **8**, 528-535.

Horwitz, M. S., Scharff, M. D. & Maizel, J. V., Jr. (1969). Synthesis and assembly of adenovirus 2. I. Polypeptide synthesis, assembly of capsomeres, and morphogenesis of the virion. *Virology* **39**, 682-694.

Horwood, N. J., Smith, C., Andreakos, E., Quattrocchi, E., Brennan, F. M., Feldmann, M. & Foxwell, B. M. (2002). High-efficiency gene transfer into nontransformed cells: utility for studying gene regulation and analysis of potential therapeutic targets. *Arthritis Res* **4 Suppl 3**, S215-225.

Hotta, Y., Honda, T., Naito, M. & Kuwano, R. (2003). Developmental distribution of coxsackie virus and adenovirus receptor localized in the nervous system. *Brain Res Dev Brain Res* **143**, 1-13.

Hsu, C., Boysen, M., Gritton, L. D., Frosst, P. D., Nemerow, G. R. & Von Seggern, D. J. (2005). In vitro dendritic cell infection by pseudotyped adenoviral vectors does not correlate with their in vivo immunogenicity. *Virology* **332**, 1-7.

Hsu, Y. M., Lucci, J., Su, L., Ehrenfels, B., Garber, E. & Thomas, D. (1997). Heteromultimeric complexes of CD40 ligand are present on the cell surface of human T lymphocytes. *J Biol Chem* **272**, 911-915.

Huang, D., Desbois, A. & Hou, S. T. (2005). A novel adenoviral vector which mediates hypoxia-inducible gene expression selectively in neurons. *Gene Ther* **12**, 1369-1376.

Huang, S., Kamata, T., Takada, Y., Ruggeri, Z. M. & Nemerow, G. R. (1996). Adenovirus interaction with distinct integrins mediates separate events in cell entry and gene delivery to hematopoietic cells. *J Virol* **70**, 4502-4508.

Huang, T. G., Savontaus, M. J., Shinozaki, K., Sauter, B. V. & Woo, S. L. (2003). Telomerase-dependent oncolytic adenovirus for cancer treatment. *Gene Ther* **10**, 1241-1247.

Huang, X., Wu, J., Spong, S. & Sheppard, D. (1998). The integrin alphavbeta6 is critical for keratinocyte migration on both its known ligand, fibronectin, and on vitronectin. *J Cell Sci* **111 (Pt 15)**, 2189-2195.

Huebner, R. J., Rowe, W. P., Schatten, W. E., Smith, R. R. & Thomas, L. B. (1956). Studies on the use of viruses in the treatment of carcinoma of the cervix. *Cancer* **9**, 1211-1218.

Impola, U., Uitto, V. J., Hietanen, J., Hakkinen, L., Zhang, L., Larjava, H., Isaka, K. & Saarialho-Kere, U. (2004). Differential expression of matrilysin-1 (MMP-7), 92 kD gelatinase (MMP-9), and metalloelastase (MMP-12) in oral verrucous and squamous cell cancer. *J Pathol* **202**, 14-22.

Ito, M., Kodama, M., Masuko, M., Yamaura, M., Fuse, K., Uesugi, Y., Hirono, S., Okura, Y., Kato, K., Hotta, Y., Honda, T., Kuwano, R. & Aizawa, Y. (2000). Expression of coxsackievirus and adenovirus receptor in hearts of rats with experimental autoimmune myocarditis. *Circ Res* **86**, 275-280.

Iversen, N., Lindahl, A. K. & Abildgaard, U. (2002). Elevated plasma levels of the factor Xa-TFPI complex in cancer patients. *Thromb Res* **105**, 33-36.

Jackson, T., Clark, S., Berryman, S., Burman, A., Cambier, S., Mu, D., Nishimura, S. & King, A. M. (2004). Integrin alphavbeta8 functions as a receptor for foot-and-mouth disease virus: role of the beta-chain cytodomain in integrin-mediated infection. *J Virol* **78**, 4533-4540.

Jackson, T., Mould, A. P., Sheppard, D. & King, A. M. (2002). Integrin alphavbeta1 is a receptor for foot-and-mouth disease virus. *J Virol* **76**, 935-941.

Jackson, T., Sharma, A., Ghazaleh, R. A., Blakemore, W. E., Ellard, F. M., Simmons, D. L., Newman, J. W., Stuart, D. I. & King, A. M. (1997). Arginine-glycine-aspartic acid-specific binding by foot-and-mouth disease viruses to the purified integrin alpha(v)beta3 in vitro. *J Virol* **71**, 8357-8361.

Jackson, T., Sheppard, D., Denyer, M., Blakemore, W. & King, A. M. (2000). The epithelial integrin alphavbeta6 is a receptor for foot-and-mouth disease virus. *J Virol* **74**, 4949-4956.

Jakubczak, J. L., Rollence, M. L., Stewart, D. A., Jafari, J. D., Von Seggern, D. J., Nemerow, G. R., Stevenson, S. C. & Hallenbeck, P. L. (2001). Adenovirus type 5 viral particles pseudotyped with mutagenized fiber proteins show diminished infectivity of coxsackie B-adenovirus receptor-bearing cells. *J Virol* **75**, 2972-2981.

Janes, S. M. & Watt, F. M. (2004). Switch from alphavbeta5 to alphavbeta6 integrin expression protects squamous cell carcinomas from anoikis. *J Cell Biol* **166**, 419-431.

Jee, Y. S., Lee, S. G., Lee, J. C., Kim, M. J., Lee, J. J., Kim, D. Y., Park, S. W., Sung, M. W. & Heo, D. S. (2002). Reduced expression of coxsackievirus and adenovirus receptor (CAR) in tumor tissue compared to normal epithelium in

head and neck squamous cell carcinoma patients. *Anticancer Res* **22**, 2629-2634.

Jelsma, T. N., Howe, J. A., Mymryk, J. S., Evelegh, C. M., Cunniff, N. F. & Bayley, S. T. (1989). Sequences in E1A proteins of human adenovirus 5 required for cell transformation, repression of a transcriptional enhancer, and induction of proliferating cell nuclear antigen. *Virology* **171**, 120-130.

Jenkins, R. G., Su, X., Su, G., Scotton, C. J., Camerer, E., Laurent, G. J., Davis, G. E., Chambers, R. C., Matthay, M. A. & Sheppard, D. (2006). Ligation of protease-activated receptor 1 enhances alpha(v)beta6 integrin-dependent TGF-beta activation and promotes acute lung injury. *J Clin Invest* **116**, 1606-1614.

Jones, J., Watt, F. M. & Speight, P. M. (1997). Changes in the expression of alpha v integrins in oral squamous cell carcinomas. *J Oral Pathol Med* **26**, 63-68.

Jones, N. & Shenk, T. (1979). An adenovirus type 5 early gene function regulates expression of other early viral genes. *Proc Natl Acad Sci U S A* **76**, 3665-3669.

Jooss, K., Yang, Y. & Wilson, J. M. (1996). Cyclophosphamide diminishes inflammation and prolongs transgene expression following delivery of adenoviral vectors to mouse liver and lung. *Hum Gene Ther* **7**, 1555-1566.

Kajiji, S., Tamura, R. N. & Quaranta, V. (1989). A novel integrin (alpha E beta 4) from human epithelial cells suggests a fourth family of integrin adhesion receptors. *Embo J* **8**, 673-680.

Kallewaard, N. L., Zhang, L., Chen, J. W., Guttenberg, M., Sanchez, M. D. & Bergelson, J. M. (2009). Tissue-specific deletion of the coxsackievirus and adenovirus receptor protects mice from virus-induced pancreatitis and myocarditis. *Cell Host Microbe* **6**, 91-98.

Kalyuzhniy, O., Di Paolo, N. C., Silvestry, M., Hofherr, S. E., Barry, M. A., Stewart, P. L. & Shayakhmetov, D. M. (2008). Adenovirus serotype 5 hexon is critical for virus infection of hepatocytes in vivo. *Proc Natl Acad Sci U S A* **105**, 5483-5488.

Kamphuis, E., Junt, T., Waibler, Z., Forster, R. & Kalinke, U. (2006). Type I interferons directly regulate lymphocyte recirculation and cause transient blood lymphopenia. *Blood* **108**, 3253-3261.

Kanerva, A., Mikheeva, G. V., Krasnykh, V., Coolidge, C. J., Lam, J. T., Mahasreshti, P. J., Barker, S. D., Straughn, M., Barnes, M. N., Alvarez, R. D., Hemminki, A. & Curiel, D. T. (2002a). Targeting adenovirus to the serotype 3 receptor increases gene transfer efficiency to ovarian cancer cells. *Clin Cancer Res* **8**, 275-280.

Kanerva, A., Wang, M., Bauerschmitz, G. J., Lam, J. T., Desmond, R. A., Bhoola, S. M., Barnes, M. N., Alvarez, R. D., Siegal, G. P., Curiel, D. T. & Hemminki,

A. (2002b). Gene transfer to ovarian cancer versus normal tissues with fiber-modified adenoviruses. *Mol Ther* **5**, 695-704.

Kater, A. P., Peppelenbosch, M. P., Brandjes, D. P. & Lumbantobing, M. (2002). Dichotomal effect of the coumadin derivative warfarin on inflammatory signal transduction. *Clin Diagn Lab Immunol* **9**, 1396-1397.

Katze, M. G., DeCorato, D., Safer, B., Galabru, J. & Hovanessian, A. G. (1987). Adenovirus VAI RNA complexes with the 68 000 Mr protein kinase to regulate its autophosphorylation and activity. *Embo J* **6**, 689-697.

Kawashima, A., Tsugawa, S., Boku, A., Kobayashi, M., Minamoto, T., Nakanishi, I. & Oda, Y. (2003). Expression of alphav integrin family in gastric carcinomas: increased alphavbeta6 is associated with lymph node metastasis. *Pathol Res Pract* **199**, 57-64.

Kelkar, S. A., Pfister, K. K., Crystal, R. G. & Leopold, P. L. (2004). Cytoplasmic dynein mediates adenovirus binding to microtubules. *J Virol* **78**, 10122-10132.

Kiang, A., Hartman, Z. C., Everett, R. S., Serra, D., Jiang, H., Frank, M. M. & Amalfitano, A. (2006). Multiple innate inflammatory responses induced after systemic adenovirus vector delivery depend on a functional complement system. *Mol Ther* **14**, 588-598.

Kirby, I., Davison, E., Beavil, A. J., Soh, C. P., Wickham, T. J., Roelvink, P. W., Kovesdi, I., Sutton, B. J. & Santis, G. (1999). Mutations in the DG loop of adenovirus type 5 fiber knob protein abolish high-affinity binding to its cellular receptor CAR. *J Virol* **73**, 9508-9514.

Kirby, I., Davison, E., Beavil, A. J., Soh, C. P., Wickham, T. J., Roelvink, P. W., Kovesdi, I., Sutton, B. J. & Santis, G. (2000). Identification of contact residues and definition of the CAR-binding site of adenovirus type 5 fiber protein. *J Virol* **74**, 2804-2813.

Klinger, J. R., Sanchez, M. P., Curtin, L. A., Durkin, M. & Matyas, B. (1998). Multiple cases of life-threatening adenovirus pneumonia in a mental health care center. *Am J Respir Crit Care Med* **157**, 645-649.

Kogelberg, H., Tolner, B., Thomas, G. J., Di Cara, D., Minogue, S., Ramesh, B., Sodha, S., Marsh, D., Lowdell, M. W., Meyer, T., Begent, R. H., Hart, I., Marshall, J. F. & Chester, K. (2008). Engineering a single-chain Fv antibody to alpha v beta 6 integrin using the specificity-determining loop of a foot-and-mouth disease virus. *J Mol Biol* **382**, 385-401.

Koizumi, N., Kawabata, K., Sakurai, F., Watanabe, Y., Hayakawa, T. & Mizuguchi, H. (2006). Modified adenoviral vectors ablated for coxsackievirus-adenovirus receptor, alphav integrin, and heparan sulfate binding reduce in vivo tissue transduction and toxicity. *Hum Gene Ther* **17**, 264-279.

Koizumi, N., Mizuguchi, H., Utoguchi, N., Watanabe, Y. & Hayakawa, T. (2003). Generation of fiber-modified adenovirus vectors containing heterologous peptides in both the HI loop and C terminus of the fiber knob. *J Gene Med* **5**, 267-276.

Koizumi, N., Yamaguchi, T., Kawabata, K., Sakurai, F., Sasaki, T., Watanabe, Y., Hayakawa, T. & Mizuguchi, H. (2007). Fiber-modified adenovirus vectors decrease liver toxicity through reduced IL-6 production. *J Immunol* **178**, 1767-1773.

Kontermann, R. E., Korn, T. & Jerome, V. (2003). Recombinant adenoviruses for in vivo expression of antibody fragments. *Methods Mol Biol* **207**, 421-433.

Koski, A., Rajecki, M., Guse, K., Kanerva, A., Ristimaki, A., Pesonen, S., Escutenaire, S. & Hemminki, A. (2009). Systemic adenoviral gene delivery to orthotopic murine breast tumors with ablation of coagulation factors, thrombocytes and Kupffer cells. *J Gene Med*.

Kraft, S., Diefenbach, B., Mehta, R., Jonczyk, A., Luckenbach, G. A. & Goodman, S. L. (1999). Definition of an unexpected ligand recognition motif for alphav beta6 integrin. *J Biol Chem* **274**, 1979-1985.

Krasnykh, V., Belousova, N., Korokhov, N., Mikheeva, G. & Curiel, D. T. (2001). Genetic targeting of an adenovirus vector via replacement of the fiber protein with the phage T4 fibritin. *J Virol* **75**, 4176-4183.

Krasnykh, V., Dmitriev, I., Mikheeva, G., Miller, C. R., Belousova, N. & Curiel, D. T. (1998). Characterization of an adenovirus vector containing a heterologous peptide epitope in the HI loop of the fiber knob. *J Virol* **72**, 1844-1852.

Krasnykh, V. N., Mikheeva, G. V., Douglas, J. T. & Curiel, D. T. (1996). Generation of recombinant adenovirus vectors with modified fibers for altering viral tropism. *J Virol* **70**, 6839-6846.

Kreppel, F., Gackowski, J., Schmidt, E. & Kochanek, S. (2005). Combined genetic and chemical capsid modifications enable flexible and efficient de- and retargeting of adenovirus vectors. *Mol Ther* **12**, 107-117.

Kritz, A. B., Nicol, C. G., Dishart, K. L., Nelson, R., Holbeck, S., Von Seggern, D. J., Work, L. M., McVey, J. H., Nicklin, S. A. & Baker, A. H. (2007). Adenovirus 5 fibers mutated at the putative HSPG-binding site show restricted retargeting with targeting peptides in the HI loop. *Mol Ther* **15**, 741-749.

Kurachi, S., Koizumi, N., Sakurai, F., Kawabata, K., Sakurai, H., Nakagawa, S., Hayakawa, T. & Mizuguchi, H. (2007a). Characterization of capsid-modified adenovirus vectors containing heterologous peptides in the fiber knob, protein IX, or hexon. *Gene Ther* **14**, 266-274.

Kurachi, S., Tashiro, K., Sakurai, F., Sakurai, H., Kawabata, K., Yayama, K., Okamoto, H., Nakagawa, S. & Mizuguchi, H. (2007b). Fiber-modified adenovirus vectors containing the TAT peptide derived from HIV-1 in the fiber knob have efficient gene transfer activity. *Gene Ther* **14**, 1160-1165.

Kuzmin, A. I., Finegold, M. J. & Eisensmith, R. C. (1997). Macrophage depletion increases the safety, efficacy and persistence of adenovirus-mediated gene transfer in vivo. *Gene Ther* **4**, 309-316.

Le, L. P., Everts, M., Dmitriev, I. P., Davydova, J. G., Yamamoto, M. & Curiel, D. T. (2004). Fluorescently labeled adenovirus with pIX-EGFP for vector detection. *Mol Imaging* **3**, 105-116.

Le, L. P., Li, J., Ternovoi, V. V., Siegal, G. P. & Curiel, D. T. (2005). Fluorescently tagged canine adenovirus via modification with protein IX-enhanced green fluorescent protein. *J Gen Virol* **86**, 3201-3208.

Lechner, R. L. & Kelly, T. J., Jr. (1977). The structure of replicating adenovirus 2 DNA molecules. *Cell* **12**, 1007-1020.

Lei, N., Shen, F. B., Chang, J. H., Wang, L., Li, H., Yang, C., Li, J. & Yu, D. C. (2009). An oncolytic adenovirus expressing granulocyte macrophage colony-stimulating factor shows improved specificity and efficacy for treating human solid tumors. *Cancer Gene Ther* **16**, 33-43.

Leissner, P., Legrand, V., Schlesinger, Y., Hadji, D. A., van Raaij, M., Cusack, S., Pavirani, A. & Mehtali, M. (2001). Influence of adenoviral fiber mutations on viral encapsidation, infectivity and in vivo tropism. *Gene Ther* **8**, 49-57.

Leopold, P. L. & Crystal, R. G. (2007). Intracellular trafficking of adenovirus: many means to many ends. *Adv Drug Deliv Rev* **59**, 810-821.

Leopold, P. L., Kreitzer, G., Miyazawa, N., Rempel, S., Pfister, K. K., Rodriguez-Boulan, E. & Crystal, R. G. (2000). Dynein- and microtubule-mediated translocation of adenovirus serotype 5 occurs after endosomal lysis. *Hum Gene Ther* **11**, 151-165.

Li, D., Duan, L., Freimuth, P. & O'Malley, B. W., Jr. (1999a). Variability of adenovirus receptor density influences gene transfer efficiency and therapeutic response in head and neck cancer. *Clin Cancer Res* **5**, 4175-4181.

Li, E., Brown, S. L., Stupack, D. G., Puente, X. S., Cheresh, D. A. & Nemerow, G. R. (2001). Integrin alpha(v)beta1 is an adenovirus coreceptor. *J Virol* **75**, 5405-5409.

Li, E., Stupack, D., Bokoch, G. M. & Nemerow, G. R. (1998a). Adenovirus endocytosis requires actin cytoskeleton reorganization mediated by Rho family GTPases. *J Virol* **72**, 8806-8812.

Li, E., Stupack, D., Klemke, R., Cheresh, D. A. & Nemerow, G. R. (1998b). Adenovirus endocytosis via alpha(v) integrins requires phosphoinositide-3-OH kinase. *J Virol* **72**, 2055-2061.

Li, H. J., Everts, M., Pereboeva, L., Komarova, S., Idan, A., Curiel, D. T. & Herschman, H. R. (2007). Adenovirus tumor targeting and hepatic untargeting by a coxsackie/adenovirus receptor ectodomain anti-carcinoembryonic antigen bispecific adapter. *Cancer Res* **67**, 5354-5361.

Li, S., McGuire, M. J., Lin, M., Liu, Y. H., Oyama, T., Sun, X. & Brown, K. C. (2009). Synthesis and characterization of a high-affinity {alpha}v{beta}6-specific ligand for in vitro and in vivo applications. *Mol Cancer Ther*.

Li, X., Yang, Y., Hu, Y., Dang, D., Regezi, J., Schmidt, B. L., Atakilit, A., Chen, B., Ellis, D. & Ramos, D. M. (2003). Alphavbeta6-Fyn signaling promotes oral cancer progression. *J Biol Chem* **278**, 41646-41653.

Li, Y., Pong, R. C., Bergelson, J. M., Hall, M. C., Sagalowsky, A. I., Tseng, C. P., Wang, Z. & Hsieh, J. T. (1999b). Loss of adenoviral receptor expression in human bladder cancer cells: a potential impact on the efficacy of gene therapy. *Cancer Res* **59**, 325-330.

Lichtenstein, D. L., Doronin, K., Toth, K., Kuppuswamy, M., Wold, W. S. & Tollefson, A. E. (2004). Adenovirus E3-6.7K protein is required in conjunction with the E3-RID protein complex for the internalization and degradation of TRAIL receptor 2. *J Virol* **78**, 12297-12307.

Lichtenstein, D. L., Spencer, J. F., Doronin, K., Patra, D., Meyer, J. M., Shashkova, E. V., Kuppuswamy, M., Dhar, D., Thomas, M. A., Tollefson, A. E., Zumstein, L. A., Wold, W. S. & Toth, K. (2009). An acute toxicology study with INGN 007, an oncolytic adenovirus vector, in mice and permissive Syrian hamsters; comparisons with wild-type Ad5 and a replication-defective adenovirus vector. *Cancer Gene Ther*.

Lieber, A., He, C. Y., Meuse, L., Schowalter, D., Kirillova, I., Winther, B. & Kay, M. A. (1997). The role of Kupffer cell activation and viral gene expression in early liver toxicity after infusion of recombinant adenovirus vectors. *J Virol* **71**, 8798-8807.

Lievens, J., Snoeys, J., Vekemans, K., Van Linthout, S., de Zanger, R., Collen, D., Wisse, E. & De Geest, B. (2004). The size of sinusoidal fenestrae is a critical determinant of hepatocyte transduction after adenoviral gene transfer. *Gene Ther* **11**, 1523-1531.

Lim, B. K., Xiong, D., Dorner, A., Youn, T. J., Yung, A., Liu, T. I., Gu, Y., Dalton, N. D., Wright, A. T., Evans, S. M., Chen, J., Peterson, K. L., McCulloch, A. D., Yajima, T. & Knowlton, K. U. (2008). Coxsackievirus and adenovirus receptor

(CAR) mediates atrioventricular-node function and connexin 45 localization in the murine heart. *J Clin Invest* **118**, 2758-2770.

Lisewski, U., Shi, Y., Wrackmeyer, U., Fischer, R., Chen, C., Schirdewan, A., Juttner, R., Rathjen, F., Poller, W., Radke, M. H. & Gotthardt, M. (2008). The tight junction protein CAR regulates cardiac conduction and cell-cell communication. *J Exp Med* **205**, 2369-2379.

Liu, Q. & Muruve, D. A. (2003). Molecular basis of the inflammatory response to adenovirus vectors. *Gene Ther* **10**, 935-940.

Liu, Q., Zaiss, A. K., Colarusso, P., Patel, K., Haljan, G., Wickham, T. J. & Muruve, D. A. (2003). The role of capsid-endothelial interactions in the innate immune response to adenovirus vectors. *Hum Gene Ther* **14**, 627-643.

Liu, Y., Wang, H., Yumul, R., Gao, W., Gambotto, A., Morita, T., Baker, A., Shayakhmetov, D. & Lieber, A. (2009). Transduction of liver metastases after intravenous injection of Ad5/35 or Ad35 vectors with and without factor X-binding protein pretreatment. *Hum Gene Ther* **20**, 621-629.

Lord, R., Parsons, M., Kirby, I., Beavil, A., Hunt, J., Sutton, B. & Santis, G. (2006). Analysis of the interaction between RGD-expressing adenovirus type 5 fiber knob domains and alphavbeta3 integrin reveals distinct binding profiles and intracellular trafficking. *J Gen Virol* **87**, 2497-2505.

Louie, J. K., Kajon, A. E., Holodniy, M., Guardia-LaBar, L., Lee, B., Petru, A. M., Hacker, J. K. & Schnurr, D. P. (2008). Severe pneumonia due to adenovirus serotype 14: a new respiratory threat? *Clin Infect Dis* **46**, 421-425.

Lowe, S. W. & Ruley, H. E. (1993). Stabilization of the p53 tumor suppressor is induced by adenovirus 5 E1A and accompanies apoptosis. *Genes Dev* **7**, 535-545.

Lozier, J. N., Csako, G., Mondoro, T. H., Krizek, D. M., Metzger, M. E., Costello, R., Vostal, J. G., Rick, M. E., Donahue, R. E. & Morgan, R. A. (2002). Toxicity of a first-generation adenoviral vector in rhesus macaques. *Hum Gene Ther* **13**, 113-124.

Lutz, P. & Kedinger, C. (1996). Properties of the adenovirus IVa2 gene product, an effector of late-phase-dependent activation of the major late promoter. *J Virol* **70**, 1396-1405.

Lyon, M., Deakin, J. A., Mizuno, K., Nakamura, T. & Gallagher, J. T. (1994). Interaction of hepatocyte growth factor with heparan sulfate. Elucidation of the major heparan sulfate structural determinants. *J Biol Chem* **269**, 11216-11223.

Lyons, M., Onion, D., Green, N. K., Aslan, K., Rajaratnam, R., Bazan-Peregrino, M., Phipps, S., Hale, S., Mautner, V., Seymour, L. W. & Fisher, K. D. (2006).

Adenovirus type 5 interactions with human blood cells may compromise systemic delivery. *Mol Ther* **14**, 118-128.

Ma, L. J., Yang, H., Gaspert, A., Carlesso, G., Barty, M. M., Davidson, J. M., Sheppard, D. & Fogo, A. B. (2003). Transforming growth factor-beta-dependent and -independent pathways of induction of tubulointerstitial fibrosis in beta6(-/-) mice. *Am J Pathol* **163**, 1261-1273.

Magnusson, M. K., Henning, P., Myhre, S., Wikman, M., Uil, T. G., Friedman, M., Andersson, K. M., Hong, S. S., Hoeben, R. C., Habib, N. A., Stahl, S., Boulanger, P. & Lindholm, L. (2007). Adenovirus 5 vector genetically re-targeted by an Affibody molecule with specificity for tumor antigen HER2/neu. *Cancer Gene Ther* **14**, 468-479.

Magnusson, M. K., Hong, S. S., Henning, P., Boulanger, P. & Lindholm, L. (2002). Genetic retargeting of adenovirus vectors: functionality of targeting ligands and their influence on virus viability. *J Gene Med* **4**, 356-370.

Maizel, J. V., Jr., White, D. O. & Scharff, M. D. (1968). The polypeptides of adenovirus. I. Evidence for multiple protein components in the virion and a comparison of types 2, 7A, and 12. *Virology* **36**, 115-125.

Majem, M., Cascallo, M., Bayo-Puxan, N., Mesia, R., Germa, J. R. & Alemany, R. (2006). Control of E1A under an E2F-1 promoter insulated with the myotonic dystrophy locus insulator reduces the toxicity of oncolytic adenovirus Ad-Delta24RGD. *Cancer Gene Ther* **13**, 696-705.

Mal, A., Piotrkowski, A. & Harter, M. L. (1996). Cyclin-dependent kinases phosphorylate the adenovirus E1A protein, enhancing its ability to bind pRb and disrupt pRb-E2F complexes. *J Virol* **70**, 2911-2921.

Mangel, W. F., McGrath, W. J., Toledo, D. L. & Anderson, C. W. (1993). Viral DNA and a viral peptide can act as cofactors of adenovirus virion proteinase activity. *Nature* **361**, 274-275.

Manickan, E., Smith, J. S., Tian, J., Eggerman, T. L., Lozier, J. N., Muller, J. & Byrnes, A. P. (2006). Rapid Kupffer cell death after intravenous injection of adenovirus vectors. *Mol Ther* **13**, 108-117.

Maran, A. & Mathews, M. B. (1988). Characterization of the double-stranded RNA implicated in the inhibition of protein synthesis in cells infected with a mutant adenovirus defective for VA RNA. *Virology* **164**, 106-113.

Marsh, D., Dickinson, S., Neill, G. W., Marshall, J. F., Hart, I. R. & Thomas, G. J. (2008). alpha vbeta 6 Integrin promotes the invasion of morphoeic basal cell carcinoma through stromal modulation. *Cancer Res* **68**, 3295-3303.

Martin, K., Brie, A., Saulnier, P., Perricaudet, M., Yeh, P. & Vigne, E. (2003). Simultaneous CAR- and alpha V integrin-binding ablation fails to reduce Ad5 liver tropism. *Mol Ther* **8**, 485-494.

Massague, J., Cheifetz, S., Laiho, M., Ralph, D. A., Weis, F. M. & Zentella, A. (1992). Transforming growth factor-beta. *Cancer Surv* **12**, 81-103.

Mathis, J. M., Stoff-Khalili, M. A. & Curiel, D. T. (2005). Oncolytic adenoviruses - selective retargeting to tumor cells. *Oncogene* **24**, 7775-7791.

Matsumoto, K., Shariat, S. F., Ayala, G. E., Rauen, K. A. & Lerner, S. P. (2005). Loss of coxsackie and adenovirus receptor expression is associated with features of aggressive bladder cancer. *Urology* **66**, 441-446.

Mautner, V. & Pereira, H. G. (1971). Crystallization of a second adenovirus protein (the fibre). *Nature* **230**, 456-457.

McCartney-Francis, N. L. & Wahl, S. M. (1994). Transforming growth factor beta: a matter of life and death. *J Leukoc Biol* **55**, 401-409.

McCarty, J. H., Cook, A. A. & Hynes, R. O. (2005). An interaction between {alpha}v{beta}8 integrin and Band 4.1B via a highly conserved region of the Band 4.1 C-terminal domain. *Proc Natl Acad Sci U S A* **102**, 13479-13483.

McConnell, M. J., Danthinne, X. & Imperiale, M. J. (2006). Characterization of a permissive epitope insertion site in adenovirus hexon. *J Virol* **80**, 5361-5370.

McDonald, D., Stockwin, L., Matzow, T., Blair Zajdel, M. E. & Blair, G. E. (1999). Coxsackie and adenovirus receptor (CAR)-dependent and major histocompatibility complex (MHC) class I-independent uptake of recombinant adenoviruses into human tumour cells. *Gene Ther* **6**, 1512-1519.

McNeish, I. A., Tenev, T., Bell, S., Marani, M., Vassaux, G. & Lemoine, N. (2001). Herpes simplex virus thymidine kinase/ganciclovir-induced cell death is enhanced by co-expression of caspase-3 in ovarian carcinoma cells. *Cancer Gene Ther* **8**, 308-319.

Meier, O., Boucke, K., Hammer, S. V., Keller, S., Stidwill, R. P., Hemmi, S. & Greber, U. F. (2002). Adenovirus triggers macropinocytosis and endosomal leakage together with its clathrin-mediated uptake. *J Cell Biol* **158**, 1119-1131.

Meier, O. & Greber, U. F. (2003). Adenovirus endocytosis. *J Gene Med* **5**, 451-462.

Merron, A., Peerlinck, I., Martin-Duque, P., Burnet, J., Quintanilla, M., Mather, S., Hingorani, M., Harrington, K., Iggo, R. & Vassaux, G. (2007). SPECT/CT imaging of oncolytic adenovirus propagation in tumours in vivo using the Na/I symporter as a reporter gene. *Gene Ther* **14**, 1731-1738.

Meulenbroek, R. A., Sargent, K. L., Lunde, J., Jasmin, B. J. & Parks, R. J. (2004). Use of adenovirus protein IX (pIX) to display large polypeptides on the virion--

generation of fluorescent virus through the incorporation of pIX-GFP. *Mol Ther* **9**, 617-624.

Michael, S. I., Hong, J. S., Curiel, D. T. & Engler, J. A. (1995). Addition of a short peptide ligand to the adenovirus fiber protein. *Gene Ther* **2**, 660-668.

Mikami, T., Ookawa, K., Shimoyama, T., Fukuda, S., Saito, H. & Munakata, A. (2001). KAI1, CAR, and Smad4 expression in the progression of colorectal tumor. *J Gastroenterol* **36**, 465-469.

Miller, C. R., Buchsbaum, D. J., Reynolds, P. N., Douglas, J. T., Gillespie, G. Y., Mayo, M. S., Raben, D. & Curiel, D. T. (1998). Differential susceptibility of primary and established human glioma cells to adenovirus infection: targeting via the epidermal growth factor receptor achieves fiber receptor-independent gene transfer. *Cancer Res* **58**, 5738-5748.

Mistchenko, A. S., Diez, R. A., Mariani, A. L., Robaldo, J., Maffey, A. F., Bayley-Bustamante, G. & Grinstein, S. (1994). Cytokines in adenoviral disease in children: association of interleukin-6, interleukin-8, and tumor necrosis factor alpha levels with clinical outcome. *J Pediatr* **124**, 714-720.

Mittal, S. K., McDermott, M. R., Johnson, D. C., Prevec, L. & Graham, F. L. (1993). Monitoring foreign gene expression by a human adenovirus-based vector using the firefly luciferase gene as a reporter. *Virus Res* **28**, 67-90.

Miyazawa, N., Crystal, R. G. & Leopold, P. L. (2001). Adenovirus serotype 7 retention in a late endosomal compartment prior to cytosol escape is modulated by fiber protein. *J Virol* **75**, 1387-1400.

Miyazawa, N., Leopold, P. L., Hackett, N. R., Ferris, B., Worgall, S., Falck-Pedersen, E. & Crystal, R. G. (1999). Fiber swap between adenovirus subgroups B and C alters intracellular trafficking of adenovirus gene transfer vectors. *J Virol* **73**, 6056-6065.

Mizuguchi, H., Koizumi, N., Hosono, T., Ishii-Watabe, A., Uchida, E., Utoguchi, N., Watanabe, Y. & Hayakawa, T. (2002). CAR- or alphav integrin-binding ablated adenovirus vectors, but not fiber-modified vectors containing RGD peptide, do not change the systemic gene transfer properties in mice. *Gene Ther* **9**, 769-776.

Moran, E., Zerler, B., Harrison, T. M. & Mathews, M. B. (1986). Identification of separate domains in the adenovirus E1A gene for immortalization activity and the activation of virus early genes. *Mol Cell Biol* **6**, 3470-3480.

Morgan, M. R., Thomas, G. J., Russell, A., Hart, I. R. & Marshall, J. F. (2004). The integrin cytoplasmic-tail motif EKQKVDLSTDC is sufficient to promote tumor cell invasion mediated by matrix metalloproteinase (MMP)-2 or MMP-9. *J Biol Chem* **279**, 26533-26539.

Morgenstern, J. P. & Land, H. (1990). Advanced mammalian gene transfer: high titre retroviral vectors with multiple drug selection markers and a complementary helper-free packaging cell line. *Nucleic Acids Res* **18**, 3587-3596.

Morris, D. G., Huang, X., Kaminski, N., Wang, Y., Shapiro, S. D., Dolganov, G., Glick, A. & Sheppard, D. (2003). Loss of integrin alpha(v)beta6-mediated TGF-beta activation causes Mmp12-dependent emphysema. *Nature* **422**, 169-173.

Morrison, J., Briggs, S. S., Green, N., Fisher, K., Subr, V., Ulbrich, K., Kehoe, S. & Seymour, L. W. (2008). Virotherapy of ovarian cancer with polymer-cloaked adenovirus retargeted to the epidermal growth factor receptor. *Mol Ther* **16**, 244-251.

Mu, D., Cambier, S., Fjellbirkeland, L., Baron, J. L., Munger, J. S., Kawakatsu, H., Sheppard, D., Broaddus, V. C. & Nishimura, S. L. (2002). The integrin alpha(v)beta8 mediates epithelial homeostasis through MT1-MMP-dependent activation of TGF-beta1. *J Cell Biol* **157**, 493-507.

Mul, Y. M., Verrijzer, C. P. & van der Vliet, P. C. (1990). Transcription factors NFI and NFIII/oct-1 function independently, employing different mechanisms to enhance adenovirus DNA replication. *J Virol* **64**, 5510-5518.

Munger, J. S., Huang, X., Kawakatsu, H., Griffiths, M. J., Dalton, S. L., Wu, J., Pittet, J. F., Kaminski, N., Garat, C., Matthay, M. A., Rifkin, D. B. & Sheppard, D. (1999). The integrin alpha v beta 6 binds and activates latent TGF beta 1: a mechanism for regulating pulmonary inflammation and fibrosis. *Cell* **96**, 319-328.

Munoz, V. & Serrano, L. (1997). Development of the multiple sequence approximation within the AGADIR model of alpha-helix formation: comparison with Zimm-Bragg and Lifson-Roig formalisms. *Biopolymers* **41**, 495-509.

Murata, K. & Sakamoto, A. (2008). Impairment of clathrin-mediated endocytosis via cytoskeletal change by epithelial to fibroblastoid conversion in HepG2 cells: a possible mechanism of des-gamma-carboxy prothrombin production in hepatocellular carcinoma. *Int J Oncol* **33**, 1149-1155.

Muruve, D. A., Barnes, M. J., Stillman, I. E. & Libermann, T. A. (1999). Adenoviral gene therapy leads to rapid induction of multiple chemokines and acute neutrophil-dependent hepatic injury in vivo. *Hum Gene Ther* **10**, 965-976.

Muruve, D. A., Cotter, M. J., Zaiss, A. K., White, L. R., Liu, Q., Chan, T., Clark, S. A., Ross, P. J., Meulenbroek, R. A., Maelandsmo, G. M. & Parks, R. J. (2004). Helper-dependent adenovirus vectors elicit intact innate but attenuated adaptive host immune responses in vivo. *J Virol* **78**, 5966-5972.

Muruve, D. A., Petrilli, V., Zaiss, A. K., White, L. R., Clark, S. A., Ross, P. J., Parks, R. J. & Tschopp, J. (2008). The inflammasome recognizes cytosolic microbial and host DNA and triggers an innate immune response. *Nature* **452**, 103-107.

Myhre, S., Henning, P., Friedman, M., Stahl, S., Lindholm, L. & Magnusson, M. K. (2009). Re-targeted adenovirus vectors with dual specificity; binding specificities conferred by two different Affibody molecules in the fiber. *Gene Ther* **16**, 252-261.

Nagai, K., Arai, H., Yanagita, M., Matsubara, T., Kanamori, H., Nakano, T., Iehara, N., Fukatsu, A., Kita, T. & Doi, T. (2003). Growth arrest-specific gene 6 is involved in glomerular hypertrophy in the early stage of diabetic nephropathy. *J Biol Chem* **278**, 18229-18234.

Nagata, K., Guggenheimer, R. A. & Hurwitz, J. (1983). Specific binding of a cellular DNA replication protein to the origin of replication of adenovirus DNA. *Proc Natl Acad Sci U S A* **80**, 6177-6181.

Nagel, H., Maag, S., Tassis, A., Nestle, F. O., Greber, U. F. & Hemmi, S. (2003). The alphavbeta5 integrin of hematopoietic and nonhematopoietic cells is a transduction receptor of RGD-4C fiber-modified adenoviruses. *Gene Ther* **10**, 1643-1653.

Nakamura, T., Sato, K. & Hamada, H. (2003). Reduction of natural adenovirus tropism to the liver by both ablation of fiber-coxsackievirus and adenovirus receptor interaction and use of replaceable short fiber. *J Virol* **77**, 2512-2521.

Nakayama, M., Both, G. W., Banizs, B., Tsuruta, Y., Yamamoto, S., Kawakami, Y., Douglas, J. T., Tani, K., Curiel, D. T. & Glasgow, J. N. (2006). An adenovirus serotype 5 vector with fibers derived from ovine atadenovirus demonstrates CAR-independent tropism and unique biodistribution in mice. *Virology* **350**, 103-115.

Nettelbeck, D. M., Miller, D. W., Jerome, V., Zuzarte, M., Watkins, S. J., Hawkins, R. E., Muller, R. & Kontermann, R. E. (2001). Targeting of adenovirus to endothelial cells by a bispecific single-chain diabody directed against the adenovirus fiber knob domain and human endoglin (CD105). *Mol Ther* **3**, 882-891.

Ni, S., Bernt, K., Gaggar, A., Li, Z. Y., Kiem, H. P. & Lieber, A. (2005). Evaluation of biodistribution and safety of adenovirus vectors containing group B fibers after intravenous injection into baboons. *Hum Gene Ther* **16**, 664-677.

Nicklin, S. A. & Baker, A. H. (2008). Efficient vascular endothelial gene transfer following intravenous adenovirus delivery. *Mol Ther* **16**, 1904-1905.

Nicklin, S. A., Von Seggern, D. J., Work, L. M., Pek, D. C., Dominiczak, A. F., Nemerow, G. R. & Baker, A. H. (2001). Ablating adenovirus type 5 fiber-CAR

binding and HI loop insertion of the SIGYPLP peptide generate an endothelial cell-selective adenovirus. *Mol Ther* **4**, 534-542.

Nicklin, S. A., White, S. J., Nicol, C. G., Von Seggern, D. J. & Baker, A. H. (2004). In vitro and in vivo characterisation of endothelial cell selective adenoviral vectors. *J Gene Med* **6**, 300-308.

Nicklin, S. A., White, S. J., Watkins, S. J., Hawkins, R. E. & Baker, A. H. (2000). Selective targeting of gene transfer to vascular endothelial cells by use of peptides isolated by phage display. *Circulation* **102**, 231-237.

Nicklin, S. A., Wu, E., Nemerow, G. R. & Baker, A. H. (2005). The influence of adenovirus fiber structure and function on vector development for gene therapy. *Mol Ther* **12**, 384-393.

Nicol, C. G., Graham, D., Miller, W. H., White, S. J., Smith, T. A., Nicklin, S. A., Stevenson, S. C. & Baker, A. H. (2004). Effect of adenovirus serotype 5 fiber and penton modifications on in vivo tropism in rats. *Mol Ther* **10**, 344-354.

Nishimura, S. L., Boylen, K. P., Einheber, S., Milner, T. A., Ramos, D. M. & Pytela, R. (1998). Synaptic and glial localization of the integrin alphavbeta8 in mouse and rat brain. *Brain Res* **791**, 271-282.

Niu, J., Dorahy, D. J., Gu, X., Scott, R. J., Draganic, B., Ahmed, N. & Agrez, M. V. (2002). Integrin expression in colon cancer cells is regulated by the cytoplasmic domain of the beta6 integrin subunit. *Int J Cancer* **99**, 529-537.

Novelli, A. & Boulanger, P. A. (1991). Deletion analysis of functional domains in baculovirus-expressed adenovirus type 2 fiber. *Virology* **185**, 365-376.

Nystrom, M. L., McCulloch, D., Weinreb, P. H., Violette, S. M., Speight, P. M., Marshall, J. F., Hart, I. R. & Thomas, G. J. (2006). Cyclooxygenase-2 inhibition suppresses alphavbeta6 integrin-dependent oral squamous carcinoma invasion. *Cancer Res* **66**, 10833-10842.

O'Riordan, C. R., Lachapelle, A., Delgado, C., Parkes, V., Wadsworth, S. C., Smith, A. E. & Francis, G. E. (1999). PEGylation of adenovirus with retention of infectivity and protection from neutralizing antibody in vitro and in vivo. *Hum Gene Ther* **10**, 1349-1358.

O'Shea, C. C., Johnson, L., Bagus, B., Choi, S., Nicholas, C., Shen, A., Boyle, L., Pandey, K., Soria, C., Kunich, J., Shen, Y., Habets, G., Ginzinger, D. & McCormick, F. (2004). Late viral RNA export, rather than p53 inactivation, determines ONYX-015 tumor selectivity. *Cancer Cell* **6**, 611-623.

Onion, D., Crompton, L. J., Milligan, D. W., Moss, P. A., Lee, S. P. & Mautner, V. (2007). The CD4+ T-cell response to adenovirus is focused against conserved residues within the hexon protein. *J Gen Virol* **88**, 2417-2425.

Ono, H. A., Le, L. P., Davydova, J. G., Gavrikova, T. & Yamamoto, M. (2005). Noninvasive visualization of adenovirus replication with a fluorescent reporter in the E3 region. *Cancer Res* **65**, 10154-10158.

Othman, M., Labelle, A., Mazzetti, I., Elbatarny, H. S. & Lillicrap, D. (2007). Adenovirus-induced thrombocytopenia: the role of von Willebrand factor and P-selectin in mediating accelerated platelet clearance. *Blood* **109**, 2832-2839.

Pameijer, C. R., Navanjo, A., Meechoovet, B., Wagner, J. R., Aguilar, B., Wright, C. L., Chang, W. C., Brown, C. E. & Jensen, M. C. (2007). Conversion of a tumor-binding peptide identified by phage display to a functional chimeric T cell antigen receptor. *Cancer Gene Ther* **14**, 91-97.

Pang, S., Dannull, J., Kaboo, R., Xie, Y., Tso, C. L., Michel, K., deKernion, J. B. & Belldegrun, A. S. (1997). Identification of a positive regulatory element responsible for tissue-specific expression of prostate-specific antigen. *Cancer Res* **57**, 495-499.

Parker, A. L., McVey, J. H., Doctor, J. H., Lopez-Franco, O., Waddington, S. N., Havenga, M. J., Nicklin, S. A. & Baker, A. H. (2007). Influence of coagulation factor zymogens on the infectivity of adenoviruses pseudotyped with fibers from subgroup D. *J Virol* **81**, 3627-3631.

Parker, A. L., Waddington, S. N., Buckley, S. M., Custers, J., Havenga, M. J., van Rooijen, N., Goudsmit, J., McVey, J. H., Nicklin, S. A. & Baker, A. H. (2009). Effect of neutralizing sera on factor x-mediated adenovirus serotype 5 gene transfer. *J Virol* **83**, 479-483.

Parker, A. L., Waddington, S. N., Nicol, C. G., Shayakhmetov, D. M., Buckley, S. M., Denby, L., Kemball-Cook, G., Ni, S., Lieber, A., McVey, J. H., Nicklin, S. A. & Baker, A. H. (2006). Multiple vitamin K-dependent coagulation zymogens promote adenovirus-mediated gene delivery to hepatocytes. *Blood* **108**, 2554-2561.

Parks, C. L. & Shenk, T. (1997). Activation of the adenovirus major late promoter by transcription factors MAZ and Sp1. *J Virol* **71**, 9600-9607.

Pasquinucci, G. (1971). Possible effect of measles on leukaemia. *Lancet* **1**, 136.

Peerlinck, I., Amini-Nik, S., Phillips, R. K., Iggo, R., Lemoine, N. R., Tejpar, S. & Vassaux, G. (2008). Therapeutic potential of replication-selective oncolytic adenoviruses on cells from familial and sporadic desmoid tumors. *Clin Cancer Res* **14**, 6187-6192.

Pelner, L., Fowler, G. A. & Nauts, H. C. (1958). Effects of concurrent infections and their toxins on the course of leukemia. *Acta Med Scand Suppl* **338**, 1-47.

Peng, Z. (2005). Current status of gendicine in China: recombinant human Ad-p53 agent for treatment of cancers. *Hum Gene Ther* **16**, 1016-1027.

Pereboev, A. V., Asiedu, C. K., Kawakami, Y., Dong, S. S., Blackwell, J. L., Kashentseva, E. A., Triozzi, P. L., Aldrich, W. A., Curiel, D. T., Thomas, J. M. & Dmitriev, I. P. (2002). Coxsackievirus-adenovirus receptor genetically fused to anti-human CD40 scFv enhances adenoviral transduction of dendritic cells. *Gene Ther* **9**, 1189-1193.

Perez-Romero, P., Gustin, K. E. & Imperiale, M. J. (2006). Dependence of the encapsidation function of the adenovirus L1 52/55-kilodalton protein on its ability to bind the packaging sequence. *J Virol* **80**, 1965-1971.

Post, D. E., Sandberg, E. M., Kyle, M. M., Devi, N. S., Brat, D. J., Xu, Z., Tighiouart, M. & Van Meir, E. G. (2007). Targeted cancer gene therapy using a hypoxia inducible factor dependent oncolytic adenovirus armed with interleukin-4. *Cancer Res* **67**, 6872-6881.

Post, D. E. & Van Meir, E. G. (2003). A novel hypoxia-inducible factor (HIF) activated oncolytic adenovirus for cancer therapy. *Oncogene* **22**, 2065-2072.

Pouyssegur, J., Dayan, F. & Mazure, N. M. (2006). Hypoxia signalling in cancer and approaches to enforce tumour regression. *Nature* **441**, 437-443.

Prime, S. S., Davies, M., Pring, M. & Paterson, I. C. (2004a). The role of TGF-beta in epithelial malignancy and its relevance to the pathogenesis of oral cancer (part II). *Crit Rev Oral Biol Med* **15**, 337-347.

Prime, S. S., Pring, M., Davies, M. & Paterson, I. C. (2004b). TGF-beta signal transduction in oro-facial health and non-malignant disease (part I). *Crit Rev Oral Biol Med* **15**, 324-336.

Prudencio, M., Rodriguez, A. & Mota, M. M. (2006). The silent path to thousands of merozoites: the Plasmodium liver stage. *Nat Rev Microbiol* **4**, 849-856.

Puthawala, K., Hadjiangelis, N., Jacoby, S. C., Bayongan, E., Zhao, Z., Yang, Z., Devitt, M. L., Horan, G. S., Weinreb, P. H., Lukashev, M. E., Violette, S. M., Grant, K. S., Colarossi, C., Formenti, S. C. & Munger, J. S. (2008). Inhibition of integrin alpha(v)beta6, an activator of latent transforming growth factor-beta, prevents radiation-induced lung fibrosis. *Am J Respir Crit Care Med* **177**, 82-90.

Querido, E., Blanchette, P., Yan, Q., Kamura, T., Morrison, M., Boivin, D., Kaelin, W. G., Conaway, R. C., Conaway, J. W. & Branton, P. E. (2001a). Degradation of p53 by adenovirus E4orf6 and E1B55K proteins occurs via a novel mechanism involving a Cullin-containing complex. *Genes Dev* **15**, 3104-3117.

Querido, E., Marcellus, R. C., Lai, A., Charbonneau, R., Teodoro, J. G., Ketner, G. & Branton, P. E. (1997). Regulation of p53 levels by the E1B 55-kilodalton protein and E4orf6 in adenovirus-infected cells. *J Virol* **71**, 3788-3798.

Querido, E., Morrison, M. R., Chu-Pham-Dang, H., Thirlwell, S. W., Boivin, D. & Branton, P. E. (2001b). Identification of three functions of the adenovirus e4orf6 protein that mediate p53 degradation by the E4orf6-E1B55K complex. *J Virol* **75**, 699-709.

Ramos, D. M., But, M., Regezi, J., Schmidt, B. L., Atakilit, A., Dang, D., Ellis, D., Jordan, R. & Li, X. (2002). Expression of integrin beta 6 enhances invasive behavior in oral squamous cell carcinoma. *Matrix Biol* **21**, 297-307.

Ramsay, A. G., Keppler, M. D., Jazayeri, M., Thomas, G. J., Parsons, M., Violette, S., Weinreb, P., Hart, I. R. & Marshall, J. F. (2007). HS1-associated protein X-1 regulates carcinoma cell migration and invasion via clathrin-mediated endocytosis of integrin alphavbeta6. *Cancer Res* **67**, 5275-5284.

Rancourt, C., Tihanyi, K., Bourbonniere, M. & Weber, J. M. (1994). Identification of active-site residues of the adenovirus endopeptidase. *Proc Natl Acad Sci U S A* **91**, 844-847.

Ranki, T., Kanerva, A., Ristimaki, A., Hakkarainen, T., Sarkioja, M., Kangasniemi, L., Raki, M., Laakkonen, P., Goodison, S. & Hemminki, A. (2007). A heparan sulfate-targeted conditionally replicative adenovirus, Ad5.pk7-Delta24, for the treatment of advanced breast cancer. *Gene Ther* **14**, 58-67.

Rao, L., Debbas, M., Sabbatini, P., Hockenbery, D., Korsmeyer, S. & White, E. (1992). The adenovirus E1A proteins induce apoptosis, which is inhibited by the E1B 19-kDa and Bcl-2 proteins. *Proc Natl Acad Sci U S A* **89**, 7742-7746.

Raper, S. E., Chirmule, N., Lee, F. S., Wivel, N. A., Bagg, A., Gao, G. P., Wilson, J. M. & Batshaw, M. L. (2003). Fatal systemic inflammatory response syndrome in a ornithine transcarbamylase deficient patient following adenoviral gene transfer. *Mol Genet Metab* **80**, 148-158.

Raper, S. E., Yudkoff, M., Chirmule, N., Gao, G. P., Nunes, F., Haskal, Z. J., Furth, E. E., Propert, K. J., Robinson, M. B., Magosin, S., Simoes, H., Speicher, L., Hughes, J., Tazelaar, J., Wivel, N. A., Wilson, J. M. & Batshaw, M. L. (2002). A pilot study of in vivo liver-directed gene transfer with an adenoviral vector in partial ornithine transcarbamylase deficiency. *Hum Gene Ther* **13**, 163-175.

Rauen, K. A., Sudilovsky, D., Le, J. L., Chew, K. L., Hann, B., Weinberg, V., Schmitt, L. D. & McCormick, F. (2002). Expression of the coxsackie adenovirus receptor in normal prostate and in primary and metastatic prostate carcinoma: potential relevance to gene therapy. *Cancer Res* **62**, 3812-3818.

Rea, D., Havenga, M. J., van Den Assem, M., Sutmuller, R. P., Lemckert, A., Hoeben, R. C., Bout, A., Melief, C. J. & Offringa, R. (2001). Highly efficient transduction of human monocyte-derived dendritic cells with subgroup B fiber-

modified adenovirus vectors enhances transgene-encoded antigen presentation to cytotoxic T cells. *J Immunol* **166**, 5236-5244.

Regezi, J. A., Ramos, D. M., Pytela, R., Dekker, N. P. & Jordan, R. C. (2002). Tenascin and beta 6 integrin are overexpressed in floor of mouth in situ carcinomas and invasive squamous cell carcinomas. *Oral Oncol* **38**, 332-336.

Regulier, E., Paul, S., Marigliano, M., Kintz, J., Poitevin, Y., Ledoux, C., Roecklin, D., Cauet, G., Calenda, V. & Homann, H. E. (2001). Adenovirus-mediated delivery of antiangiogenic genes as an antitumor approach. *Cancer Gene Ther* **8**, 45-54.

Reid, T., Galanis, E., Abbruzzese, J., Sze, D., Andrews, J., Romel, L., Hatfield, M., Rubin, J. & Kirn, D. (2001). Intra-arterial administration of a replication-selective adenovirus (dl1520) in patients with colorectal carcinoma metastatic to the liver: a phase I trial. *Gene Ther* **8**, 1618-1626.

Reid, T., Galanis, E., Abbruzzese, J., Sze, D., Wein, L. M., Andrews, J., Randlev, B., Heise, C., Uprichard, M., Hatfield, M., Rome, L., Rubin, J. & Kirn, D. (2002). Hepatic arterial infusion of a replication-selective oncolytic adenovirus (dl1520): phase II viral, immunologic, and clinical endpoints. *Cancer Res* **62**, 6070-6079.

Rein, D. T., Breidenbach, M., Wu, H., Han, T., Haviv, Y. S., Wang, M., Kirby, T. O., Kawakami, Y., Dall, P., Alvarez, R. D. & Curiel, D. T. (2004). Gene transfer to cervical cancer with fiber-modified adenoviruses. *Int J Cancer* **111**, 698-704.

Rekosh, D. M., Russell, W. C., Bellet, A. J. & Robinson, A. J. (1977). Identification of a protein linked to the ends of adenovirus DNA. *Cell* **11**, 283-295.

Reynolds, P., Dmitriev, I. & Curiel, D. (1999). Insertion of an RGD motif into the HI loop of adenovirus fiber protein alters the distribution of transgene expression of the systemically administered vector. *Gene Ther* **6**, 1336-1339.

Reynolds, P. N., Zinn, K. R., Gavrilyuk, V. D., Balyasnikova, I. V., Rogers, B. E., Buchsbaum, D. J., Wang, M. H., Miletich, D. J., Grizzle, W. E., Douglas, J. T., Danilov, S. M. & Curiel, D. T. (2000). A targetable, injectable adenoviral vector for selective gene delivery to pulmonary endothelium in vivo. *Mol Ther* **2**, 562-578.

Roberts, D. M., Nanda, A., Havenga, M. J., Abbink, P., Lynch, D. M., Ewald, B. A., Liu, J., Thorner, A. R., Swanson, P. E., Gorgone, D. A., Lifton, M. A., Lemckert, A. A., Holterman, L., Chen, B., Dilraj, A., Carville, A., Mansfield, K. G., Goudsmit, J. & Barouch, D. H. (2006). Hexon-chimaeric adenovirus serotype 5 vectors circumvent pre-existing anti-vector immunity. *Nature* **441**, 239-243.

Robinson, A. J., Younghusband, H. B. & Bellett, A. J. (1973). A circula DNA-protein complex from adenoviruses. *Virology* **56**, 54-69.

Roelvink, P. W., Lizonova, A., Lee, J. G., Li, Y., Bergelson, J. M., Finberg, R. W., Brough, D. E., Kovesdi, I. & Wickham, T. J. (1998). The coxsackievirus-adenovirus receptor protein can function as a cellular attachment protein for adenovirus serotypes from subgroups A, C, D, E, and F. *J Virol* **72**, 7909-7915.

Roelvink, P. W., Mi Lee, G., Einfeld, D. A., Kovesdi, I. & Wickham, T. J. (1999). Identification of a conserved receptor-binding site on the fiber proteins of CAR-recognizing adenoviridae. *Science* **286**, 1568-1571.

Rosen, L. (1960). A hemagglutination-inhibition technique for typing adenoviruses. *Am J Hyg* **71**, 120-128.

Rowe, W. P., Huebner, R. J., Gilmore, L. K., Parrott, R. H. & Ward, T. G. (1953). Isolation of a cytopathogenic agent from human adenoids undergoing spontaneous degeneration in tissue culture. *Proc Soc Exp Biol Med* **84**, 570-573.

Rudin, C. M., Cohen, E. E., Papadimitrakopoulou, V. A., Silverman, S., Jr., Recant, W., El-Naggar, A. K., Stenson, K., Lippman, S. M., Hong, W. K. & Vokes, E. E. (2003). An attenuated adenovirus, ONYX-015, as mouthwash therapy for premalignant oral dysplasia. *J Clin Oncol* **21**, 4546-4552.

Russell, W. C. (2000). Update on adenovirus and its vectors. *J Gen Virol* **81**, 2573-2604.

Russell, W. C. (2009). Adenoviruses: update on structure and function. *J Gen Virol* **90**, 1-20.

Ruzindana-Umunyana, A., Imbeault, L. & Weber, J. M. (2002). Substrate specificity of adenovirus protease. *Virus Res* **89**, 41-52.

Sachs, M. D., Rauen, K. A., Ramamurthy, M., Dodson, J. L., De Marzo, A. M., Putzi, M. J., Schoenberg, M. P. & Rodriguez, R. (2002). Integrin alpha(v) and coxsackie adenovirus receptor expression in clinical bladder cancer. *Urology* **60**, 531-536.

Sakurai, F., Mizuguchi, H., Yamaguchi, T. & Hayakawa, T. (2003). Characterization of in vitro and in vivo gene transfer properties of adenovirus serotype 35 vector. *Mol Ther* **8**, 813-821.

Sakurai, F., Nakamura, S., Akitomo, K., Shibata, H., Terao, K., Kawabata, K., Hayakawa, T. & Mizuguchi, H. (2008). Transduction properties of adenovirus serotype 35 vectors after intravenous administration into nonhuman primates. *Mol Ther* **16**, 726-733.

Salone, B., Martina, Y., Piersanti, S., Cundari, E., Cherubini, G., Franqueville, L., Failla, C. M., Boulanger, P. & Saggio, I. (2003). Integrin alpha3beta1 is an alternative cellular receptor for adenovirus serotype 5. *J Virol* **77**, 13448-13454.

Santis, G., Legrand, V., Hong, S. S., Davison, E., Kirby, I., Imler, J. L., Finberg, R. W., Bergelson, J. M., Mehtali, M. & Boulanger, P. (1999). Molecular determinants of adenovirus serotype 5 fibre binding to its cellular receptor CAR. *J Gen Virol* **80 (Pt 6)**, 1519-1527.

Sarnow, P., Hearing, P., Anderson, C. W., Halbert, D. N., Shenk, T. & Levine, A. J. (1984). Adenovirus early region 1B 58,000-dalton tumor antigen is physically associated with an early region 4 25,000-dalton protein in productively infected cells. *J Virol* **49**, 692-700.

Sasisekharan, R., Shriver, Z., Venkataraman, G. & Narayanasami, U. (2002). Roles of heparan-sulphate glycosaminoglycans in cancer. *Nat Rev Cancer* **2**, 521-528.

Schiedner, G., Bloch, W., Hertel, S., Johnston, M., Molojavyi, A., Dries, V., Varga, G., Van Rooijen, N. & Kochanek, S. (2003a). A hemodynamic response to intravenous adenovirus vector particles is caused by systemic Kupffer cell-mediated activation of endothelial cells. *Hum Gene Ther* **14**, 1631-1641.

Schiedner, G., Hertel, S., Johnston, M., Dries, V., van Rooijen, N. & Kochanek, S. (2003b). Selective depletion or blockade of Kupffer cells leads to enhanced and prolonged hepatic transgene expression using high-capacity adenoviral vectors. *Mol Ther* **7**, 35-43.

Schnell, M. A., Zhang, Y., Tazelaar, J., Gao, G. P., Yu, Q. C., Qian, R., Chen, S. J., Varnavski, A. N., LeClair, C., Raper, S. E. & Wilson, J. M. (2001). Activation of innate immunity in nonhuman primates following intraportal administration of adenoviral vectors. *Mol Ther* **3**, 708-722.

Schoggins, J. W., Nociari, M., Philpott, N. & Falck-Pedersen, E. (2005). Influence of fiber detargeting on adenovirus-mediated innate and adaptive immune activation. *J Virol* **79**, 11627-11637.

Schultz-Cherry, S. & Hinshaw, V. S. (1996). Influenza virus neuraminidase activates latent transforming growth factor beta. *J Virol* **70**, 8624-8629.

Scott, K. A., Arnott, C. H., Robinson, S. C., Moore, R. J., Thompson, R. G., Marshall, J. F. & Balkwill, F. R. (2004). TNF-alpha regulates epithelial expression of MMP-9 and integrin alphavbeta6 during tumour promotion. A role for TNF-alpha in keratinocyte migration? *Oncogene* **23**, 6954-6966.

Segerman, A., Atkinson, J. P., Marttila, M., Dennerquist, V., Wadell, G. & Arnberg, N. (2003). Adenovirus type 11 uses CD46 as a cellular receptor. *J Virol* **77**, 9183-9191.

Seiradake, E., Henaff, D., Wodrich, H., Billet, O., Perreau, M., Hippert, C., Mennechet, F., Schoehn, G., Lortat-Jacob, H., Dreja, H., Ibanes, S., Kalatzis, V., Wang, J. P., Finberg, R. W., Cusack, S. & Kremer, E. J. (2009). The cell adhesion molecule "CAR" and sialic acid on human erythrocytes influence adenovirus in vivo biodistribution. *PLoS Pathog* **5**, e1000277.

Seshidhar Reddy, P., Ganesh, S., Limbach, M. P., Brann, T., Pinkstaff, A., Kaloss, M., Kaleko, M. & Connelly, S. (2003). Development of adenovirus serotype 35 as a gene transfer vector. *Virology* **311**, 384-393.

Sharma, K. & Ziyadeh, F. N. (1994). The emerging role of transforming growth factor-beta in kidney diseases. *Am J Physiol* **266**, F829-842.

Shashkova, E. V., Doronin, K., Senac, J. S. & Barry, M. A. (2008). Macrophage depletion combined with anticoagulant therapy increases therapeutic window of systemic treatment with oncolytic adenovirus. *Cancer Res* **68**, 5896-5904.

Shashkova, E. V., May, S. M., Doronin, K. & Barry, M. A. (2009). Expanded Anticancer Therapeutic Window of Hexon-modified Oncolytic Adenovirus. *Mol Ther*.

Shaw, C. A., Holland, P. C., Sinnreich, M., Allen, C., Sollerbrant, K., Karpati, G. & Nalbantoglu, J. (2004). Isoform-specific expression of the Coxsackie and adenovirus receptor (CAR) in neuromuscular junction and cardiac intercalated discs. *BMC Cell Biol* **5**, 42.

Shayakhmetov, D. M., Carlson, C. A., Stecher, H., Li, Q., Stamatoyannopoulos, G. & Lieber, A. (2002). A high-capacity, capsid-modified hybrid adenovirus/adeno-associated virus vector for stable transduction of human hematopoietic cells. *J Virol* **76**, 1135-1143.

Shayakhmetov, D. M., Eberly, A. M., Li, Z. Y. & Lieber, A. (2005a). Deletion of penton RGD motifs affects the efficiency of both the internalization and the endosome escape of viral particles containing adenovirus serotype 5 or 35 fiber knobs. *J Virol* **79**, 1053-1061.

Shayakhmetov, D. M., Gaggar, A., Ni, S., Li, Z. Y. & Lieber, A. (2005b). Adenovirus binding to blood factors results in liver cell infection and hepatotoxicity. *J Virol* **79**, 7478-7491.

Shayakhmetov, D. M., Li, Z. Y., Gaggar, A., Gharwan, H., Ternovoi, V., Sandig, V. & Lieber, A. (2004a). Genome size and structure determine efficiency of postinternalization steps and gene transfer of capsid-modified adenovirus vectors in a cell-type-specific manner. *J Virol* **78**, 10009-10022.

Shayakhmetov, D. M., Li, Z. Y., Ni, S. & Lieber, A. (2004b). Analysis of adenovirus sequestration in the liver, transduction of hepatic cells, and innate toxicity after injection of fiber-modified vectors. *J Virol* **78**, 5368-5381.

Shayakhmetov, D. M., Li, Z. Y., Ni, S. & Lieber, A. (2005c). Interference with the IL-1-signaling pathway improves the toxicity profile of systemically applied adenovirus vectors. *J Immunol* **174**, 7310-7319.

Shayakhmetov, D. M., Li, Z. Y., Ternovoi, V., Gaggar, A., Gharwan, H. & Lieber, A. (2003). The interaction between the fiber knob domain and the cellular attachment receptor determines the intracellular trafficking route of adenoviruses. *J Virol* **77**, 3712-3723.

Sherr, C. J. & McCormick, F. (2002). The RB and p53 pathways in cancer. *Cancer Cell* **2**, 103-112.

Shinozaki, K., Suominen, E., Carrick, F., Sauter, B., Kahari, V. M., Lieber, A., Woo, S. L. & Savontaus, M. (2006). Efficient infection of tumor endothelial cells by a capsid-modified adenovirus. *Gene Ther* **13**, 52-59.

Silvestry, M., Lindert, S., Smith, J. G., Maier, O., Wiethoff, C. M., Nemerow, G. R. & Stewart, P. L. (2009). Cryo-electron microscopy structure of adenovirus type 2 temperature-sensitive mutant 1 reveals insight into the cell entry defect. *J Virol* **83**, 7375-7383.

Sipos, B., Hahn, D., Carceller, A., Piulats, J., Hedderich, J., Kalthoff, H., Goodman, S. L., Kosmahl, M. & Kloppel, G. (2004). Immunohistochemical screening for beta6-integrin subunit expression in adenocarcinomas using a novel monoclonal antibody reveals strong up-regulation in pancreatic ductal adenocarcinomas in vivo and in vitro. *Histopathology* **45**, 226-236.

Smith, T., Idamakanti, N., Kylefjord, H., Rollence, M., King, L., Kaloss, M., Kaleko, M. & Stevenson, S. C. (2002). In vivo hepatic adenoviral gene delivery occurs independently of the coxsackievirus-adenovirus receptor. *Mol Ther* **5**, 770-779.

Smith, T. A., Idamakanti, N., Marshall-Neff, J., Rollence, M. L., Wright, P., Kaloss, M., King, L., Mech, C., Dinges, L., Iverson, W. O., Sherer, A. D., Markovits, J. E., Lyons, R. M., Kaleko, M. & Stevenson, S. C. (2003a). Receptor interactions involved in adenoviral-mediated gene delivery after systemic administration in non-human primates. *Hum Gene Ther* **14**, 1595-1604.

Smith, T. A., Idamakanti, N., Rollence, M. L., Marshall-Neff, J., Kim, J., Mulgrew, K., Nemerow, G. R., Kaleko, M. & Stevenson, S. C. (2003b). Adenovirus serotype 5 fiber shaft influences in vivo gene transfer in mice. *Hum Gene Ther* **14**, 777-787.

Smith, T. A., White, B. D., Gardner, J. M., Kaleko, M. & McClelland, A. (1996). Transient immunosuppression permits successful repetitive intravenous administration of an adenovirus vector. *Gene Ther* **3**, 496-502.

Smythe, W. R., LeBel, E., Bavaria, J. E., Kaiser, L. R. & Albelda, S. M. (1995). Integrin expression in non-small cell carcinoma of the lung. *Cancer Metastasis Rev* **14**, 229-239.

Song, W., Sun, Q., Dong, Z., Spencer, D. M., Nunez, G. & Nor, J. E. (2005). Antiangiogenic gene therapy: disruption of neovascular networks mediated by inducible caspase-9 delivered with a transcriptionally targeted adenoviral vector. *Gene Ther* **12**, 320-329.

Spencer, J. F., Sagartz, J. E., Wold, W. S. & Toth, K. (2009). New pancreatic carcinoma model for studying oncolytic adenoviruses in the permissive Syrian hamster. *Cancer Gene Ther*.

Sprangers, M. C., Lakhai, W., Koudstaal, W., Verhoeven, M., Koel, B. F., Vogels, R., Goudsmit, J., Havenga, M. J. & Kostense, S. (2003). Quantifying adenovirus-neutralizing antibodies by luciferase transgene detection: addressing preexisting immunity to vaccine and gene therapy vectors. *J Clin Microbiol* **41**, 5046-5052.

Staba, M. J., Wickham, T. J., Kovesdi, I. & Hallahan, D. E. (2000). Modifications of the fiber in adenovirus vectors increase tropism for malignant glioma models. *Cancer Gene Ther* **7**, 13-19.

Stallwood, Y., Fisher, K. D., Gallimore, P. H. & Mautner, V. (2000). Neutralisation of adenovirus infectivity by ascitic fluid from ovarian cancer patients. *Gene Ther* **7**, 637-643.

Starnes, H. F., Pearce, M., Yim, J., Abrams, J., Tewari, A. & Zou, J. (1992). Anti-IL-6 monoclonal antibodies protect against lethal Escherichia coli infection and lethal tumor necrosis factor-alpha challenge in mice. *J Immunol* **148**, 1968.

Stevenson, M., Hale, A. B., Hale, S. J., Green, N. K., Black, G., Fisher, K. D., Ulbrich, K., Fabra, A. & Seymour, L. W. (2007). Incorporation of a laminin-derived peptide (SIKVAV) on polymer-modified adenovirus permits tumor-specific targeting via alpha6-integrins. *Cancer Gene Ther* **14**, 335-345.

Stoff-Khalili, M. A., Rivera, A. A., Glasgow, J. N., Le, L. P., Stoff, A., Everts, M., Tsuruta, Y., Kawakami, Y., Bauerschmitz, G. J., Mathis, J. M., Pereboeva, L., Seigal, G. P., Dall, P. & Curiel, D. T. (2005). A human adenoviral vector with a chimeric fiber from canine adenovirus type 1 results in novel expanded tropism for cancer gene therapy. *Gene Ther* **12**, 1696-1706.

Stone, D., Liu, Y., Li, Z. Y., Tuve, S., Strauss, R. & Lieber, A. (2007a). Comparison of adenoviruses from species B, C, E, and F after intravenous delivery. *Mol Ther* **15**, 2146-2153.

Stone, D., Liu, Y., Shayakhmetov, D., Li, Z. Y., Ni, S. & Lieber, A. (2007b). Adenovirus-platelet interaction in blood causes virus sequestration to the reticuloendothelial system of the liver. *J Virol* **81**, 4866-4871.

Stone, D., Ni, S., Li, Z. Y., Gaggar, A., DiPaolo, N., Feng, Q., Sandig, V. & Lieber, A. (2005). Development and assessment of human adenovirus type 11 as a gene transfer vector. *J Virol* **79**, 5090-5104.

Stracker, T. H., Carson, C. T. & Weitzman, M. D. (2002). Adenovirus oncoproteins inactivate the Mre11-Rad50-NBS1 DNA repair complex. *Nature* **418**, 348-352.

Sumida, S. M., Truitt, D. M., Lemckert, A. A., Vogels, R., Custers, J. H., Addo, M. M., Lockman, S., Peter, T., Peyerl, F. W., Kishko, M. G., Jackson, S. S., Gorgone, D. A., Lifton, M. A., Essex, M., Walker, B. D., Goudsmit, J., Havenga, M. J. & Barouch, D. H. (2005). Neutralizing antibodies to adenovirus serotype 5 vaccine vectors are directed primarily against the adenovirus hexon protein. *J Immunol* **174**, 7179-7185.

Sundquist, B., Everitt, E., Philipson, L. & Hoglund, S. (1973). Assembly of adenoviruses. *J Virol* **11**, 449-459.

Suomalainen, M., Nakano, M. Y., Boucke, K., Keller, S. & Greber, U. F. (2001). Adenovirus-activated PKA and p38/MAPK pathways boost microtubule-mediated nuclear targeting of virus. *Embo J* **20**, 1310-1319.

Suomalainen, M., Nakano, M. Y., Keller, S., Boucke, K., Stidwill, R. P. & Greber, U. F. (1999). Microtubule-dependent plus- and minus end-directed motilities are competing processes for nuclear targeting of adenovirus. *J Cell Biol* **144**, 657-672.

Suzuki, K., Fueyo, J., Krasnykh, V., Reynolds, P. N., Curiel, D. T. & Alemany, R. (2001). A conditionally replicative adenovirus with enhanced infectivity shows improved oncolytic potency. *Clin Cancer Res* **7**, 120-126.

Taipale, J., Saharinen, J. & Keski-Oja, J. (1998). Extracellular matrix-associated transforming growth factor-beta: role in cancer cell growth and invasion. *Adv Cancer Res* **75**, 87-134.

Tamanini, A., Nicolis, E., Bonizzato, A., Bezzerri, V., Melotti, P., Assael, B. M. & Cabrini, G. (2006). Interaction of adenovirus type 5 fiber with the coxsackievirus and adenovirus receptor activates inflammatory response in human respiratory cells. *J Virol* **80**, 11241-11254.

Tao, N., Gao, G. P., Parr, M., Johnston, J., Baradet, T., Wilson, J. M., Barsoum, J. & Fawell, S. E. (2001). Sequestration of adenoviral vector by Kupffer cells leads to a nonlinear dose response of transduction in liver. *Mol Ther* **3**, 28-35.

Taqi, A. M., Abdurrahman, M. B., Yakubu, A. M. & Fleming, A. F. (1981). Regression of Hodgkin's disease after measles. *Lancet* **1**, 1112.

Tarassishin, L., Szawlowski, P., Kidd, A. H. & Russell, W. C. (2000). An epitope on the adenovirus fibre tail is common to all human subgroups. *Arch Virol* **145**, 805-811.

Taylor, A. W. (1953). Effects of glandular fever infection in acute leukaemia. *Br Med J* **1**, 589-593.

Thomas, G. J., Hart, I. R., Speight, P. M. & Marshall, J. F. (2002). Binding of TGF-beta1 latency-associated peptide (LAP) to alpha(v)beta6 integrin modulates behaviour of squamous carcinoma cells. *Br J Cancer* **87**, 859-867.

Thomas, G. J., Lewis, M. P., Hart, I. R., Marshall, J. F. & Speight, P. M. (2001a). AlphaVbeta6 integrin promotes invasion of squamous carcinoma cells through up-regulation of matrix metalloproteinase-9. *Int J Cancer* **92**, 641-650.

Thomas, G. J., Lewis, M. P., Whawell, S. A., Russell, A., Sheppard, D., Hart, I. R., Speight, P. M. & Marshall, J. F. (2001b). Expression of the alphavbeta6 integrin promotes migration and invasion in squamous carcinoma cells. *J Invest Dermatol* **117**, 67-73.

Thomas, G. J., Nystrom, M. L. & Marshall, J. F. (2006a). Alphavbeta6 integrin in wound healing and cancer of the oral cavity. *J Oral Pathol Med* **35**, 1-10.

Thomas, G. J., Poomsawat, S., Lewis, M. P., Hart, I. R., Speight, P. M. & Marshall, J. F. (2001c). alpha v beta 6 Integrin upregulates matrix metalloproteinase 9 and promotes migration of normal oral keratinocytes. *J Invest Dermatol* **116**, 898-904.

Thomas, M. A., Spencer, J. F., La Regina, M. C., Dhar, D., Tollefson, A. E., Toth, K. & Wold, W. S. (2006b). Syrian hamster as a permissive immunocompetent animal model for the study of oncolytic adenovirus vectors. *Cancer Res* **66**, 1270-1276.

Thomas, M. A., Spencer, J. F., Toth, K., Sagartz, J. E., Phillips, N. J. & Wold, W. S. (2008). Immunosuppression enhances oncolytic adenovirus replication and antitumor efficacy in the Syrian hamster model. *Mol Ther* **16**, 1665-1673.

Tian, J., Xu, Z., Smith, J. S., Hofherr, S. E., Barry, M. A. & Byrnes, A. P. (2009). Adenovirus activates complement by distinctly different mechanisms in vitro and in vivo: indirect complement activation by virions in vivo. *J Virol* **83**, 5648-5658.

Tibbles, L. A., Spurrell, J. C., Bowen, G. P., Liu, Q., Lam, M., Zaiss, A. K., Robbins, S. M., Hollenberg, M. D., Wickham, T. J. & Muruve, D. A. (2002). Activation of p38 and ERK signaling during adenovirus vector cell entry lead to expression of the C-X-C chemokine IP-10. *J Virol* **76**, 1559-1568.

Tollefson, A. E., Scaria, A., Hermiston, T. W., Ryerse, J. S., Wold, L. J. & Wold, W. S. (1996). The adenovirus death protein (E3-11.6K) is required at very late

stages of infection for efficient cell lysis and release of adenovirus from infected cells. *J Virol* **70**, 2296-2306.

Tollefson, A. E., Toth, K., Doronin, K., Kuppuswamy, M., Doronina, O. A., Lichtenstein, D. L., Hermiston, T. W., Smith, C. A. & Wold, W. S. (2001). Inhibition of TRAIL-induced apoptosis and forced internalization of TRAIL receptor 1 by adenovirus proteins. *J Virol* **75**, 8875-8887.

Tollefson, A. E., Ying, B., Doronin, K., Sidor, P. D. & Wold, W. S. (2007). Identification of a new human adenovirus protein encoded by a novel late l-strand transcription unit. *J Virol* **81**, 12918-12926.

Tomko, R. P., Xu, R. & Philipson, L. (1997). HCAR and MCAR: the human and mouse cellular receptors for subgroup C adenoviruses and group B coxsackieviruses. *Proc Natl Acad Sci U S A* **94**, 3352-3356.

Toth, K., Spencer, J. F. & Wold, W. S. (2007). Immunocompetent, semi-permissive cotton rat tumor model for the evaluation of oncolytic adenoviruses. *Methods Mol Med* **130**, 157-168.

Travis, M. A., Reizis, B., Melton, A. C., Masteller, E., Tang, Q., Proctor, J. M., Wang, Y., Bernstein, X., Huang, X., Reichardt, L. F., Bluestone, J. A. & Sheppard, D. (2007). Loss of integrin alpha(v)beta8 on dendritic cells causes autoimmunity and colitis in mice. *Nature* **449**, 361-365.

Trepel, M., Grifman, M., Weitzman, M. D. & Pasqualini, R. (2000). Molecular adaptors for vascular-targeted adenoviral gene delivery. *Hum Gene Ther* **11**, 1971-1981.

Trevillian, P., Paul, H., Millar, E., Hibberd, A. & Agrez, M. V. (2004). alpha(v)beta(6) Integrin expression in diseased and transplanted kidneys. *Kidney Int* **66**, 1423-1433.

Tsujimura, A., Shida, K., Kitamura, M., Nomura, M., Takeda, J., Tanaka, H., Matsumoto, M., Matsumiya, K., Okuyama, A., Nishimune, Y., Okabe, M. & Seya, T. (1998). Molecular cloning of a murine homologue of membrane cofactor protein (CD46): preferential expression in testicular germ cells. *Biochem J* **330 (Pt 1)**, 163-168.

Tsukuda, K., Wiewrodt, R., Molnar-Kimber, K., Jovanovic, V. P. & Amin, K. M. (2002). An E2F-responsive replication-selective adenovirus targeted to the defective cell cycle in cancer cells: potent antitumoral efficacy but no toxicity to normal cell. *Cancer Res* **62**, 3438-3447.

Tsuruta, Y., Pereboeva, L., Glasgow, J. N., Luongo, C. L., Komarova, S., Kawakami, Y. & Curiel, D. T. (2005). Reovirus sigma1 fiber incorporated into adenovirus serotype 5 enhances infectivity via a CAR-independent pathway. *Biochem Biophys Res Commun* **335**, 205-214.

Tummino, P. J., Ferguson, D. & Hupe, D. (1994). Competitive inhibition of HIV-1 protease by warfarin derivatives. *Biochem Biophys Res Commun* **201**, 290-294.

Tyler, R. E., Ewing, S. G. & Imperiale, M. J. (2007). Formation of a multiple protein complex on the adenovirus packaging sequence by the IVa2 protein. *J Virol* **81**, 3447-3454.

Ulasov, I. V., Rivera, A. A., Han, Y., Curiel, D. T., Zhu, Z. B. & Lesniak, M. S. (2007). Targeting adenovirus to CD80 and CD86 receptors increases gene transfer efficiency to malignant glioma cells. *J Neurosurg* **107**, 617-627.

Van Aarsen, L. A., Leone, D. R., Ho, S., Dolinski, B. M., McCoon, P. E., LePage, D. J., Kelly, R., Heaney, G., Rayhorn, P., Reid, C., Simon, K. J., Horan, G. S., Tao, N., Gardner, H. A., Skelly, M. M., Gown, A. M., Thomas, G. J., Weinreb, P. H., Fawell, S. E. & Violette, S. M. (2008). Antibody-mediated blockade of integrin alpha v beta 6 inhibits tumor progression in vivo by a transforming growth factor-beta-regulated mechanism. *Cancer Res* **68**, 561-570.

van Oostrum, J. & Burnett, R. M. (1985). Molecular composition of the adenovirus type 2 virion. *J Virol* **56**, 439-448.

van Raaij, M. J., Chouin, E., van der Zandt, H., Bergelson, J. M. & Cusack, S. (2000). Dimeric structure of the coxsackievirus and adenovirus receptor D1 domain at 1.7 A resolution. *Structure* **8**, 1147-1155.

van Raaij, M. J., Mitraki, A., Lavigne, G. & Cusack, S. (1999). A triple beta-spiral in the adenovirus fibre shaft reveals a new structural motif for a fibrous protein. *Nature* **401**, 935-938.

Varda-Bloom, N., Shaish, A., Gonen, A., Levanon, K., Greenbereger, S., Ferber, S., Levkovitz, H., Castel, D., Goldberg, I., Afek, A., Kopolovitc, Y. & Harats, D. (2001). Tissue-specific gene therapy directed to tumor angiogenesis. *Gene Ther* **8**, 819-827.

Varnavski, A. N., Calcedo, R., Bove, M., Gao, G. & Wilson, J. M. (2005). Evaluation of toxicity from high-dose systemic administration of recombinant adenovirus vector in vector-naive and pre-immunized mice. *Gene Ther* **12**, 427-436.

Vassaux, G., Manson, A. L. & Huxley, C. (1997). Copy number-dependent expression of a YAC-cloned human CFTR gene in a human epithelial cell line. *Gene Ther* **4**, 618-623.

Vattemi, E. & Claudio, P. P. (2009). The feasibility of gene therapy in the treatment of head and neck cancer. *Head Neck Oncol* **1**, 3.

Vigant, F., Descamps, D., Jullienne, B., Esselin, S., Connault, E., Opolon, P., Tordjmann, T., Vigne, E., Perricaudet, M. & Benihoud, K. (2008). Substitution of hexon hypervariable region 5 of adenovirus serotype 5

abrogates blood factor binding and limits gene transfer to liver. *Mol Ther* **16**, 1474-1480.

Vincent, T., Neve, E. P., Johnson, J. R., Kukalev, A., Rojo, F., Albanell, J., Pietras, K., Virtanen, I., Philipson, L., Leopold, P. L., Crystal, R. G., de Herreros, A. G., Moustakas, A., Pettersson, R. F. & Fuxe, J. (2009). A SNAIL1-SMAD3/4 transcriptional repressor complex promotes TGF-beta mediated epithelial-mesenchymal transition. *Nat Cell Biol* **11**, 943-950.

Vogels, R., Zuijdgeest, D., van Rijnsoever, R., Hartkoorn, E., Damen, I., de Bethune, M. P., Kostense, S., Penders, G., Helmus, N., Koudstaal, W., Cecchini, M., Wetterwald, A., Sprangers, M., Lemckert, A., Ophorst, O., Koel, B., van Meerendonk, M., Quax, P., Panitti, L., Grimbergen, J., Bout, A., Goudsmit, J. & Havenga, M. (2003). Replication-deficient human adenovirus type 35 vectors for gene transfer and vaccination: efficient human cell infection and bypass of preexisting adenovirus immunity. *J Virol* **77**, 8263-8271.

Von Seggern, D. J., Huang, S., Fleck, S. K., Stevenson, S. C. & Nemerow, G. R. (2000). Adenovirus vector pseudotyping in fiber-expressing cell lines: improved transduction of Epstein-Barr virus-transformed B cells. *J Virol* **74**, 354-362.

Waddington, S. N., McVey, J. H., Bhella, D., Parker, A. L., Barker, K., Atoda, H., Pink, R., Buckley, S. M., Greig, J. A., Denby, L., Custers, J., Morita, T., Francischetti, I. M., Monteiro, R. Q., Barouch, D. H., van Rooijen, N., Napoli, C., Havenga, M. J., Nicklin, S. A. & Baker, A. H. (2008). Adenovirus serotype 5 hexon mediates liver gene transfer. *Cell* **132**, 397-409.

Waddington, S. N., Parker, A. L., Havenga, M., Nicklin, S. A., Buckley, S. M., McVey, J. H. & Baker, A. H. (2007). Targeting of adenovirus serotype 5 (Ad5) and 5/47 pseudotyped vectors in vivo: fundamental involvement of coagulation factors and redundancy of CAR binding by Ad5. *J Virol* **81**, 9568-9571.

Wahl, S. M. (1992). Transforming growth factor beta (TGF-beta) in inflammation: a cause and a cure. *J Clin Immunol* **12**, 61-74.

Walters, R. W., Freimuth, P., Moninger, T. O., Ganske, I., Zabner, J. & Welsh, M. J. (2002). Adenovirus fiber disrupts CAR-mediated intercellular adhesion allowing virus escape. *Cell* **110**, 789-799.

Wang, B., Dolinski, B. M., Kikuchi, N., Leone, D. R., Peters, M. G., Weinreb, P. H., Violette, S. M. & Bissell, D. M. (2007). Role of alphavbeta6 integrin in acute biliary fibrosis. *Hepatology* **46**, 1404-1412.

Wang, H., Liu, Y., Li, Z., Tuve, S., Stone, D., Kalyushniy, O., Shayakhmetov, D., Verlinde, C. L., Stehle, T., McVey, J., Baker, A., Peng, K. W., Roffler, S. &

Lieber, A. (2008). In vitro and in vivo properties of adenovirus vectors with increased affinity to CD46. *J Virol* **82**, 10567-10579.

Wang, K., Huang, S., Kapoor-Munshi, A. & Nemerow, G. (1998). Adenovirus internalization and infection require dynamin. *J Virol* **72**, 3455-3458.

Wang, Y., Hallden, G., Hill, R., Anand, A., Liu, T. C., Francis, J., Brooks, G., Lemoine, N. & Kirn, D. (2003). E3 gene manipulations affect oncolytic adenovirus activity in immunocompetent tumor models. *Nat Biotechnol* **21**, 1328-1335.

Watkins, S. J., Mesyanzhinov, V. V., Kurochkina, L. P. & Hawkins, R. E. (1997). The 'adenobody' approach to viral targeting: specific and enhanced adenoviral gene delivery. *Gene Ther* **4**, 1004-1012.

Weinacker, A., Chen, A., Agrez, M., Cone, R. I., Nishimura, S., Wayner, E., Pytela, R. & Sheppard, D. (1994). Role of the integrin alpha v beta 6 in cell attachment to fibronectin. Heterologous expression of intact and secreted forms of the receptor. *J Biol Chem* **269**, 6940-6948.

Weinreb, P. H., Simon, K. J., Rayhorn, P., Yang, W. J., Leone, D. R., Dolinski, B. M., Pearse, B. R., Yokota, Y., Kawakatsu, H., Atakilit, A., Sheppard, D. & Violette, S. M. (2004). Function-blocking integrin alphavbeta6 monoclonal antibodies: distinct ligand-mimetic and nonligand-mimetic classes. *J Biol Chem* **279**, 17875-17887.

Wernert, N. (1997). The multiple roles of tumour stroma. *Virchows Arch* **430**, 433-443.

Whalen, S. G., Marcellus, R. C., Whalen, A., Ahn, N. G., Ricciardi, R. P. & Branton, P. E. (1997). Phosphorylation within the transactivation domain of adenovirus E1A protein by mitogen-activated protein kinase regulates expression of early region 4. *J Virol* **71**, 3545-3553.

White, E., Cipriani, R., Sabbatini, P. & Denton, A. (1991). Adenovirus E1B 19-kilodalton protein overcomes the cytotoxicity of E1A proteins. *J Virol* **65**, 2968-2978.

White, E., Sabbatini, P., Debbas, M., Wold, W. S., Kusher, D. I. & Gooding, L. R. (1992). The 19-kilodalton adenovirus E1B transforming protein inhibits programmed cell death and prevents cytolysis by tumor necrosis factor alpha. *Mol Cell Biol* **12**, 2570-2580.

Whyte, P., Williamson, N. M. & Harlow, E. (1989). Cellular targets for transformation by the adenovirus E1A proteins. *Cell* **56**, 67-75.

Wickham, T. J., Mathias, P., Cheresh, D. A. & Nemerow, G. R. (1993). Integrins alpha v beta 3 and alpha v beta 5 promote adenovirus internalization but not virus attachment. *Cell* **73**, 309-319.

Wickham, T. J., Roelvink, P. W., Brough, D. E. & Kovesdi, I. (1996). Adenovirus targeted to heparan-containing receptors increases its gene delivery efficiency to multiple cell types. *Nat Biotechnol* **14**, 1570-1573.

Wickham, T. J., Tzeng, E., Shears, L. L., 2nd, Roelvink, P. W., Li, Y., Lee, G. M., Brough, D. E., Lizonova, A. & Kovesdi, I. (1997). Increased in vitro and in vivo gene transfer by adenovirus vectors containing chimeric fiber proteins. *J Virol* **71**, 8221-8229.

Wiethoff, C. M., Wodrich, H., Gerace, L. & Nemerow, G. R. (2005). Adenovirus protein VI mediates membrane disruption following capsid disassembly. *J Virol* **79**, 1992-2000.

Willcox, N. & Mautner, V. (1976). Antigenic determinants of adenovirus capsids. I. Measurement of antibody cross-reactivity. *J Immunol* **116**, 19-24.

Williams, C. H., Kajander, T., Hyypia, T., Jackson, T., Sheppard, D. & Stanway, G. (2004). Integrin alpha v beta 6 is an RGD-dependent receptor for coxsackievirus A9. *J Virol* **78**, 6967-6973.

Wisse, E., Jacobs, F., Topal, B., Frederik, P. & De Geest, B. (2008). The size of endothelial fenestrae in human liver sinusoids: implications for hepatocyte-directed gene transfer. *Gene Ther* **15**, 1193-1199.

Wold, W. S. & Gooding, L. R. (1991). Region E3 of adenovirus: a cassette of genes involved in host immunosurveillance and virus-cell interactions. *Virology* **184**, 1-8.

Wolff, G., Worgall, S., van Rooijen, N., Song, W. R., Harvey, B. G. & Crystal, R. G. (1997). Enhancement of in vivo adenovirus-mediated gene transfer and expression by prior depletion of tissue macrophages in the target organ. *J Virol* **71**, 624-629.

Wolins, N., Lozier, J., Eggerman, T. L., Jones, E., Aguilar-Cordova, E. & Vostal, J. G. (2003). Intravenous administration of replication-incompetent adenovirus to rhesus monkeys induces thrombocytopenia by increasing in vivo platelet clearance. *Br J Haematol* **123**, 903-905.

Worgall, S., Wolff, G., Falck-Pedersen, E. & Crystal, R. G. (1997). Innate immune mechanisms dominate elimination of adenoviral vectors following in vivo administration. *Hum Gene Ther* **8**, 37-44.

Worgall, S., Worgall, T. S., Kostarelos, K., Singh, R., Leopold, P. L., Hackett, N. R. & Crystal, R. G. (2000). Free cholesterol enhances adenoviral vector gene transfer and expression in CAR-deficient cells. *Mol Ther* **1**, 39-48.

Work, L. M., Nicklin, S. A., Brain, N. J., Dishart, K. L., Von Seggern, D. J., Hallek, M., Buning, H. & Baker, A. H. (2004a). Development of efficient viral vectors selective for vascular smooth muscle cells. *Mol Ther* **9**, 198-208.

Work, L. M., Reynolds, P. N. & Baker, A. H. (2004b). Improved gene delivery to human saphenous vein cells and tissue using a peptide-modified adenoviral vector. *Genet Vaccines Ther* **2**, 14.

Wortmann, A., Vohringer, S., Engler, T., Corjon, S., Schirmbeck, R., Reimann, J., Kochanek, S. & Kreppel, F. (2008). Fully detargeted polyethylene glycol-coated adenovirus vectors are potent genetic vaccines and escape from pre-existing anti-adenovirus antibodies. *Mol Ther* **16**, 154-162.

Wu, E., Pache, L., Von Seggern, D. J., Mullen, T. M., Mikyas, Y., Stewart, P. L. & Nemerow, G. R. (2003). Flexibility of the adenovirus fiber is required for efficient receptor interaction. *J Virol* **77**, 7225-7235.

Wu, H. & Curiel, D. T. (2008). Fiber-modified adenoviruses for targeted gene therapy. *Methods Mol Biol* **434**, 113-132.

Wu, H., Seki, T., Dmitriev, I., Uil, T., Kashentseva, E., Han, T. & Curiel, D. T. (2002). Double modification of adenovirus fiber with RGD and polylysine motifs improves coxsackievirus-adenovirus receptor-independent gene transfer efficiency. *Hum Gene Ther* **13**, 1647-1653.

Wysocka, M., Kubin, M., Vieira, L. Q., Ozmen, L., Garotta, G., Scott, P. & Trinchieri, G. (1995). Interleukin-12 is required for interferon-gamma production and lethality in lipopolysaccharide-induced shock in mice. *Eur J Immunol* **25**, 672-676.

Xi, Q., Cuesta, R. & Schneider, R. J. (2004). Tethering of eIF4G to adenoviral mRNAs by viral 100k protein drives ribosome shunting. *Genes Dev* **18**, 1997-2009.

Xia, D., Henry, L. J., Gerard, R. D. & Deisenhofer, J. (1994). Crystal structure of the receptor-binding domain of adenovirus type 5 fiber protein at 1.7 A resolution. *Structure* **2**, 1259-1270.

Xia, H., Anderson, B., Mao, Q. & Davidson, B. L. (2000). Recombinant human adenovirus: targeting to the human transferrin receptor improves gene transfer to brain microcapillary endothelium. *J Virol* **74**, 11359-11366.

Xu, Z., Tian, J., Smith, J. S. & Byrnes, A. P. (2008). Clearance of adenovirus by Kupffer cells is mediated by scavenger receptors, natural antibodies, and complement. *J Virol* **82**, 11705-11713.

Xue, H., Atakilit, A., Zhu, W., Li, X., Ramos, D. M. & Pytela, R. (2001). Role of the alpha(v)beta6 integrin in human oral squamous cell carcinoma growth in vivo and in vitro. *Biochem Biophys Res Commun* **288**, 610-618.

Yang, G. Y., Xu, K. S., Pan, Z. Q., Zhang, Z. Y., Mi, Y. T., Wang, J. S., Chen, R. & Niu, J. (2008). Integrin alpha v beta 6 mediates the potential for colon cancer cells to colonize in and metastasize to the liver. *Cancer Sci* **99**, 879-887.

Yee, S. P. & Branton, P. E. (1985). Detection of cellular proteins associated with human adenovirus type 5 early region 1A polypeptides. *Virology* **147**, 142-153.

Ying, B., Toth, K., Spencer, J. F., Meyer, J., Tollefson, A. E., Patra, D., Dhar, D., Shashkova, E. V., Kuppuswamy, M., Doronin, K., Thomas, M. A., Zumstein, L. A., Wold, W. S. & Lichtenstein, D. L. (2009). INGN 007, an oncolytic adenovirus vector, replicates in Syrian hamsters but not mice: comparison of biodistribution studies. *Cancer Gene Ther*.

Ying, B. & Wold, W. S. (2003). Adenovirus ADP protein (E3-11.6K), which is required for efficient cell lysis and virus release, interacts with human MAD2B. *Virology* **313**, 224-234.

Yolken, R. H., Lawrence, F., Leister, F., Takiff, H. E. & Strauss, S. E. (1982). Gastroenteritis associated with enteric type adenovirus in hospitalized infants. *J Pediatr* **101**, 21-26.

Yoshioka, Y., Asavatanabodee, R., Eto, Y., Watanabe, H., Morishige, T., Yao, X., Kida, S., Maeda, M., Mukai, Y., Mizuguchi, H., Kawasaki, K., Okada, N. & Nakagawa, S. (2008). Tat conjugation of adenovirus vector broadens tropism and enhances transduction efficiency. *Life Sci* **83**, 747-755.

Youil, R., Toner, T. J., Su, Q., Chen, M., Tang, A., Bett, A. J. & Casimiro, D. (2002). Hexon gene switch strategy for the generation of chimeric recombinant adenovirus. *Hum Gene Ther* **13**, 311-320.

Yuan, F., Dellian, M., Fukumura, D., Leunig, M., Berk, D. A., Torchilin, V. P. & Jain, R. K. (1995). Vascular permeability in a human tumor xenograft: molecular size dependence and cutoff size. *Cancer Res* **55**, 3752-3756.

Yun, C. O., Kim, E., Koo, T., Kim, H., Lee, Y. S. & Kim, J. H. (2005). ADP-overexpressing adenovirus elicits enhanced cytopathic effect by induction of apoptosis. *Cancer Gene Ther* **12**, 61-71.

Yurchenco, P. D., Amenta, P. S. & Patton, B. L. (2004). Basement membrane assembly, stability and activities observed through a developmental lens. *Matrix Biol* **22**, 521-538.

Zambruno, G., Marchisio, P. C., Marconi, A., Vaschieri, C., Melchiori, A., Giannetti, A. & De Luca, M. (1995). Transforming growth factor-beta 1 modulates beta 1 and beta 5 integrin receptors and induces the de novo expression of the alpha v beta 6 heterodimer in normal human keratinocytes: implications for wound healing. *J Cell Biol* **129**, 853-865.

Zhang, Y. & Bergelson, J. M. (2005). Adenovirus receptors. *J Virol* **79**, 12125-12131.

Zhang, Y., Chirmule, N., Gao, G. P., Qian, R., Croyle, M., Joshi, B., Tazelaar, J. & Wilson, J. M. (2001). Acute cytokine response to systemic adenoviral vectors in mice is mediated by dendritic cells and macrophages. *Mol Ther* **3**, 697-707.

Zhao, C., Crews, C. J., Derdeyn, C. A. & Blackwell, J. L. (2009). Lac-regulated system for generating adenovirus 5 vaccine vectors expressing cytolytic human immunodeficiency virus 1 genes. *J Virol Methods* **160**, 101-110.

Zhu, J., Huang, X. & Yang, Y. (2007). Innate immune response to adenoviral vectors is mediated by both Toll-like receptor-dependent and -independent pathways. *J Virol* **81**, 3170-3180.

Zinn, K. R., Douglas, J. T., Smyth, C. A., Liu, H. G., Wu, Q., Krasnykh, V. N., Mountz, J. D., Curiel, D. T. & Mountz, J. M. (1998). Imaging and tissue biodistribution of 99mTc-labeled adenovirus knob (serotype 5). *Gene Ther* **5**, 798-808.

Zygiert, Z. (1971). Hodgkin's disease: remissions after measles. *Lancet* **1**, 593.